

DISSERTATION

DUAL NICKEL- AND PHOTOREDOX-CATALYZED ENANTIOSELECTIVE
DESYMMETRIZATION OF MESO ANHYDRIDES AND C–O BOND ACTIVATION VIA
PHOSPHINES AND PHOTOREDOX CATALYSIS

Submitted by

Erin Elizabeth Stache

Department of Chemistry

In partial fulfillment of the requirements

For the Degree of Doctor of Philosophy

Colorado State University

Fort Collins, Colorado

Summer 2018

Doctoral Committee:

Advisor: Tomislav Rovis

Co-Advisor: Abigail G. Doyle

Eugene Chen

Andy McNally

Melissa Reynolds

Matt Kipper

Copyright by Erin Elizabeth Stache 2018

All Rights Reserved

ABSTRACT

DUAL NICKEL- AND PHOTOREDOX-CATALYZED ENANTIOSELECTIVE DESYMMETRIZATION OF MESO ANHYDRIDES AND C–O BOND ACTIVATION VIA PHOSPHINES AND PHOTOREDOX CATALYSIS

Described herein is the application of photoredox catalysis in the development of new synthetic methods. A dual nickel- and photoredox catalyzed desymmetrization of *meso* succinic anhydrides was developed to generate stereodefined *cis* keto-acids in high enantioselectivity and diastereoselectivity. The approach employed benzylic radicals as a coupling partner, generated from a photoredox catalyzed single-electron oxidation of benzylic trifluoroborates using an inexpensive organic dye. A unique epimerization event was discovered and the degree of epimerization was rendered tunable by changing catalyst loadings to ultimately form the *trans* diastereomer preferentially in high enantioselectivity.

A method for the C–O bond activation of aliphatic alcohols and carboxylic acids was developed using phosphines and photoredox catalysis. This novel reaction platform was used to generate aliphatic or acyl radicals directly from benzylic alcohols and aliphatic and aromatic acids, and with terminal hydrogen atom transfer, afforded the desired deoxygenated alkanes and aldehydes. Additionally, the intermediate acyl radicals could be intercepted in an intramolecular cyclization reaction to generate new lactones, amides and ketones.

ACKNOWLEDGEMENTS

It has been a long journey and I have many people to thank for helping me along the way. First I want to thank my two excellent advisors, Abby and Tom, who are two of the best advisors anyone could ask for. Abby accepted me into her lab at Princeton with no questions asked and gave me the freedom to pursue whatever research interested me, including a little work on polymers. She has served as an excellent scientific mentor and female role model for me, and because of that, I have developed more on a personal level, as well as on a scientific level. I want to thank Tom for being such an important mentor and role model for the last ten years. He has been supportive of me as a graduate student in a different lab, as an outside member and as my own graduate mentor. He believed in me when I didn't believe in myself and ultimately convinced me that I was wrong. Because of that support and guidance, I was able to finish my degree and I will be forever grateful for all that he has done for me.

I'd like to thank the Doyle Lab for being such a welcoming and wonderful group of people to work with. I need to especially acknowledge Brian for being a fantastic deskmate and good friend – I miss listening to Adele all day! I also need to thank Eric and Mia for being such wonderful labmates and friends. All three of us started the same day in the lab and have been somewhat of a trio for the last three years – really going to miss you guys! I would also like to thank Alyssa for joining me on the phosphine project and being so willing to just dive in and start working so hard as a first year. I'd like to thank the Rovis group, both past and present for being such great colleagues and friends. They were a great group of people to work down the hall from at CSU and have remained close friends. I've also really enjoyed my visits to Columbia to interact with a fantastic new group of colleagues and friends.

I'd like to thank my family for being so supportive of me throughout this whole experience mostly for letting me leave Wisconsin so I could pursue a degree in chemistry. Also for visiting me in all the different places we've lived and continuing to be a huge part of my life even though we now live far apart.

Lastly, I'd like to thank Todd for many, many things. We met ten years ago at the start of this whole journey, and have gone through so much together. He has been incredibly supportive of every decision I've made, whether he agreed with it or not. I can't imagine having accomplished any of this without his constant encouragement. I do not have the words to possibly express my gratitude or importance in my life.

TABLE OF CONTENTS

ABSTRACT.....	ii
ACKNOWLEDGEMENTS.....	iii
Chapter 1: Transition metal catalyzed desymmetrization of cyclic <i>meso</i> -anhydrides.....	1
1.1 Introduction.....	1
1.2 First examples of anhydride activation with transition metals.....	2
1.3 Mechanism of nickel catalyzed desymmetrization of anhydrides.....	7
1.3.1 Ni-bpy catalytic system for succinic anhydrides.....	7
1.3.2 Ni-PHOX catalytic system for glutaric anhydrides.....	10
1.4 Regioselective olefin-directed anhydride desymmetrization.....	13
1.5 Nickel mediated decarboxylative cross-coupling of cyclic anhydrides.....	15
1.6 Enantioselective desymmetrization of cyclic <i>meso</i> -anhydrides.....	17
1.6.1 Palladium catalyzed desymmetrization of succinic anhydrides.....	17
1.6.2 Rhodium catalyzed desymmetrization of <i>meso</i> anhydrides.....	19
1.7 Cross-electrophile couplings of <i>meso</i> -anhydrides.....	24
1.8 Conclusion and outlook.....	26
References.....	27
Chapter 2: Nickel- and photoredox-catalyzed enantioselective desymmetrization of cyclic <i>meso</i> -anhydrides.....	29
2.1 Introduction.....	29
2.1.1 Principles of photoredox catalysis.....	29
2.1.2 Merging transition metal catalysis and photoredox catalysis.....	33

2.2	Reaction design and initial results.....	37
2.3	Chiral ligand screening.....	41
2.4	Optimization of the asymmetric reaction.....	44
2.4.1	Iridium photocatalyst system.....	44
2.4.2	4CzIPN and final optimizations.....	50
2.4.3	Control reactions and initial mechanistic hypothesis.....	53
2.5	Scope of enantioselective desymmetrization reaction.....	56
2.5.1	Anhydride scope.....	56
2.5.2	Trifluoroborate scope.....	58
2.5.3	Unsuccessful substrates.....	59
2.6	Discussion of trifluoroborate scope and mechanistic implications.....	62
2.6.1	Evaluation of racemic background.....	62
2.6.2	Discovery of trifluoroborate impurities.....	64
2.7	Oxidative addition experiments.....	67
2.8	Evaluation of epimerization event.....	73
2.9	Structure determination and derivatization of enantioenriched keto-acids.....	78
2.10	Additional radical coupling partners.....	80
2.11	Conclusion.....	83
	References.....	84
Chapter 3: Single-electron chemistry of phosphines: phosphine radical cations and phosphoranyl radicals—their generation and synthetic applications.....		
3.1	Introduction.....	87
3.2	Generation of phosphine radical cations.....	89

3.2.1	Stereochemical inversion.....	89
3.2.2	Phosphine radical cations via photocatalysis.....	91
3.3	Synthesis of phosphoranyl radicals.....	93
3.3.1	Identification and structure.....	93
3.3.2	Possible reaction pathways.....	95
3.3.3	α - versus β -scission.....	96
3.4	Synthetic applications of phosphoranyl radicals.....	99
3.4.1	By β -scission pathways.....	99
3.4.2	Phosphinoyl radicals.....	104
3.5	Synthetic applications of phosphine radical cations.....	105
3.5.1	Radical additions.....	105
3.5.2	Cationic trapping.....	108
3.6	Conclusion.....	113
	References.....	114
	Chapter 4: Phosphine mediated C–O bond activation via photoredox catalysis.....	117
4.1	Introduction.....	117
4.2	Reaction design and initial results.....	118
4.3	Alcohol deoxygenation reaction.....	120
4.3.1	Mechanistic studies.....	120
4.3.2	Alcohol deoxygenation and further studies.....	123
4.3.3	Final optimizations and additional mechanistic studies.....	128
4.3.4	Substrate scope of other alcohols.....	131
4.3.5	Radical additions beyond terminal HAT.....	133

4.4	Carboxylic acid C–O bond activation.....	133
4.4.1	Introduction.....	133
4.4.2	Initial results.....	136
4.4.3	Aromatic acid reduction optimization.....	138
4.4.4	Stern-Volmer quenching studies.....	141
4.4.5	Aromatic acid substrate scope.....	143
4.5	Extension to aliphatic carboxylic acids.....	147
4.5.1	Optimization	147
4.5.2	Aliphatic acid reduction scope.....	153
4.6	Cyclization reactions.....	156
4.7	Over-reduction of carboxylic acids.....	158
4.8	Conclusion and outlook.....	161
4.8.1	Intermolecular C–C bond formation.....	162
4.8.2	C–N bond activation.....	163
4.8.3	α -Scission for radical generation.....	164
	References.....	166
	Appendix I.....	168
	References.....	273
	Appendix II	274
	References.....	364
	List of abbreviations.....	365

Chapter 1

Transition metal catalyzed desymmetrization of cyclic *meso*-anhydrides

1.1 Introduction

Constructing complex molecules efficiently from simple, abundant starting materials is a longstanding goal of synthetic chemists given the increasing demand and cost of production of synthetic compounds, including pharmaceuticals as well as fragrances, agrochemicals, etc. As such, new methods are continually developed to forge new C–C and C–X bonds—one such strategy to build new architectures employs transition metal catalysis. Transition metal catalyzed cross-coupling reactions have been transformative and are now an industry standard for forming C–C, C–O and C–N bonds, among others. The field was recognized with the 2010 Nobel Prize in Chemistry—awarded to transition metal catalyzed cross-coupling reactions.^{1,2} A wealth of classical nucleophiles include zinc reagents (Negishi coupling), boron reagents (Suzuki-Miyura coupling), stannanes (Stille coupling), Grignard reagents (Kumada coupling) and olefins (Heck reaction).

Classical electrophiles for transition metal catalyzed cross-coupling reactions include aryl and alkyl halides and pseudohalides. These functional groups are generally quite stable, easy to access and undergo oxidative addition with transition metals for further substrate elaboration. Generally, the halide is lost as stoichiometric waste after the reaction and is not further incorporated to build molecular complexity. Non-classical electrophiles represent a different class of functional groups that commonly, upon oxidative addition, afford atom economy and incorporate more complex functionality in the product.³ Cyclic anhydrides represent one such example of non-classical electrophile.⁴ These species can undergo nucleophilic attack to generate new carbonyl-acid containing compounds (Figure 1).^{5,6} Combining transition metal catalysis with anhydride

desymmetrizations represents a power tool to build complex, stereodefined structures in rapid fashion. Additionally, the 1,4-dicarbonyl or 1,5-dicarbonyl motif that arises from opening succinic or glutaric anhydrides, respectively, are commonly found in polyketide secondary metabolites (Figure 1.1).⁷ This chapter will specifically detail the activation of the C–O bonds of cyclic anhydrides via transition metal catalysis.

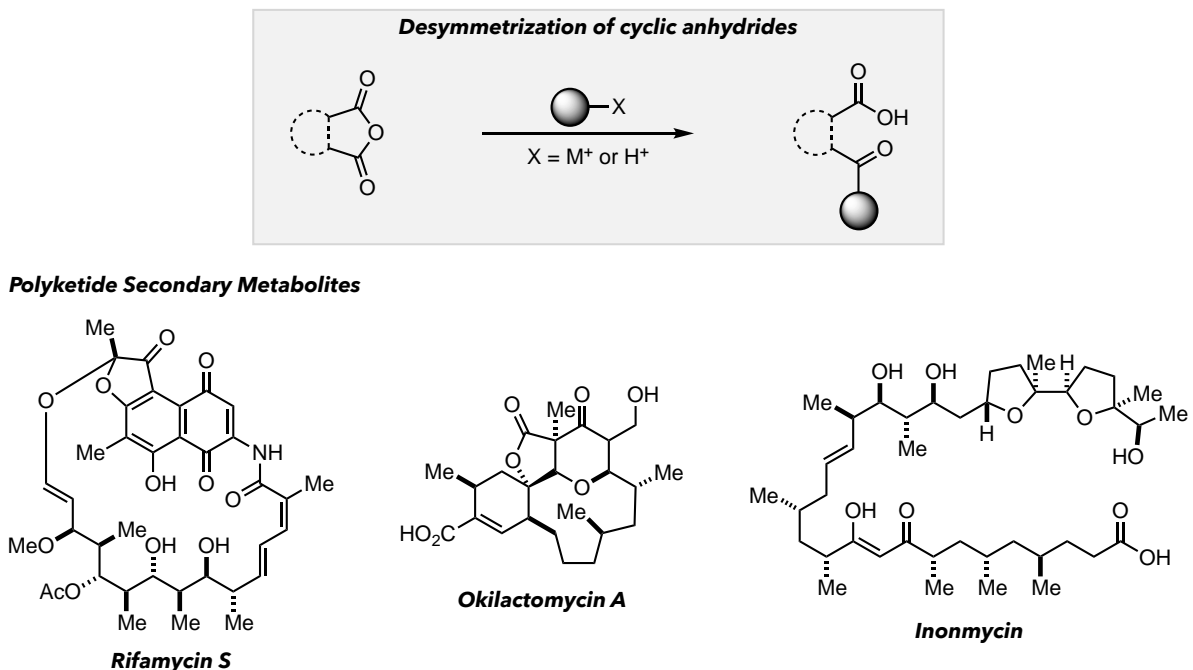
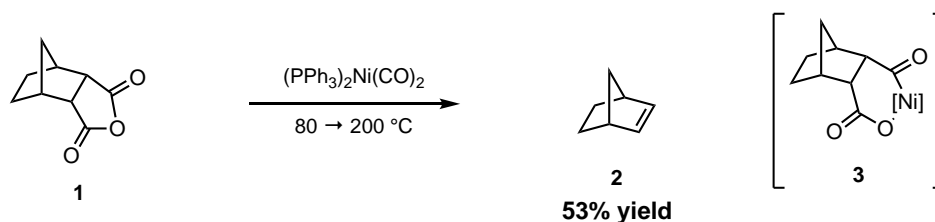


Figure 1.1

1.2 First examples of anhydride activation with transition metals

Transition metal catalyzed activation of anhydrides was first observed in 1973 by Trost and coworkers (Scheme 1.1).⁸ In the presence of a stoichiometric nickel complex, they observed the decomposition of **1** to norbornene (**2**). They proposed that upon oxidative addition to the anhydride, intermediate **3** would be generated. Decarbonylation and β -hydride elimination, followed by decarboxylation and protodemetalation would afford the olefin product, which was driven out of the reaction with heat. They observed similar reactivity with 2,3-dimethyl succinic

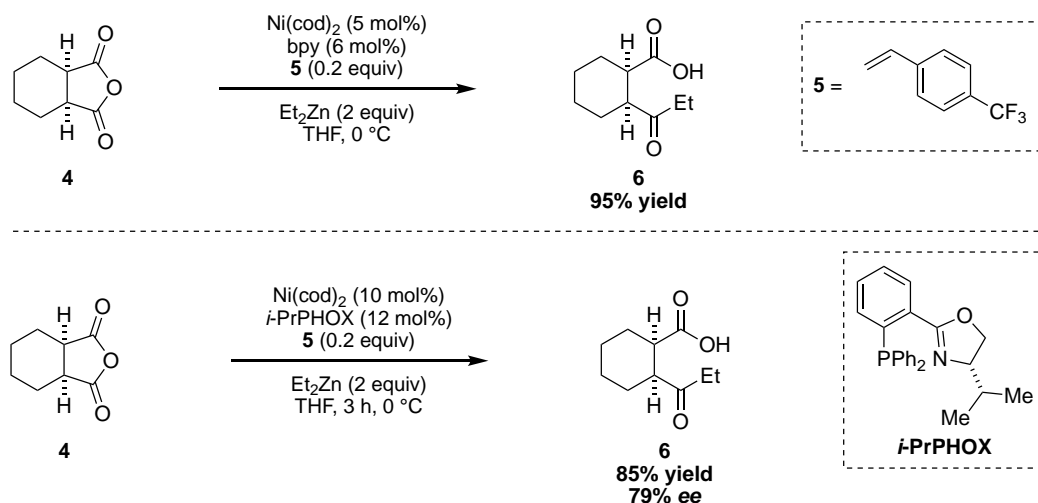
anhydrides, as well as thioanhydrides. This report represents the first example of activation of cyclic anhydrides with a transition metal, via oxidative addition.



Scheme 1.1

Despite the potential of intercepting anhydride oxidative addition adducts with other cross-coupling partners, no further examples appeared until 2001, when Gooßen demonstrated a palladium catalyzed cross-coupling of acyclic anhydrides with boronic acid derivatives to access aryl ketones.⁹ Then, in 2002, the Rovis group presented the first example of a transition metal catalyzed desymmetrization of cyclic anhydrides to access keto-acid products (Scheme 1.2).¹⁰ In the presence of $\text{Ni}(\text{cod})_2$, 2,2'-bipyridyl (bpy) and diethyl zinc, they observed the conversion of *meso* anhydride **4** to keto-acid **6** in excellent yield. Essential for productive reactivity was the addition of electron-deficient olefin (EDO) (**5**). The application of EDOs in nickel catalysis had been previously disclosed by Knochel and coworkers;^{11,12} in this instance, the Rovis group proposed that the EDO accelerated reductive elimination over counterproductive β -hydride elimination. Mechanistically, they envisioned oxidative addition of nickel into the anhydride, would generate the 6-membered metallacycle. Transmetallation with an alkyl zinc reagent followed by reductive elimination could generate the keto-acid as well as regenerates the nickel catalyst. To further exploit the advantages of desymmetrizing *meso* anhydrides, they investigated the formation of enantioenriched keto-acids by employing a chiral ligand. They observed that the reaction is very sensitive to the type of ligand used, with bidentate phosphines proving ineffective

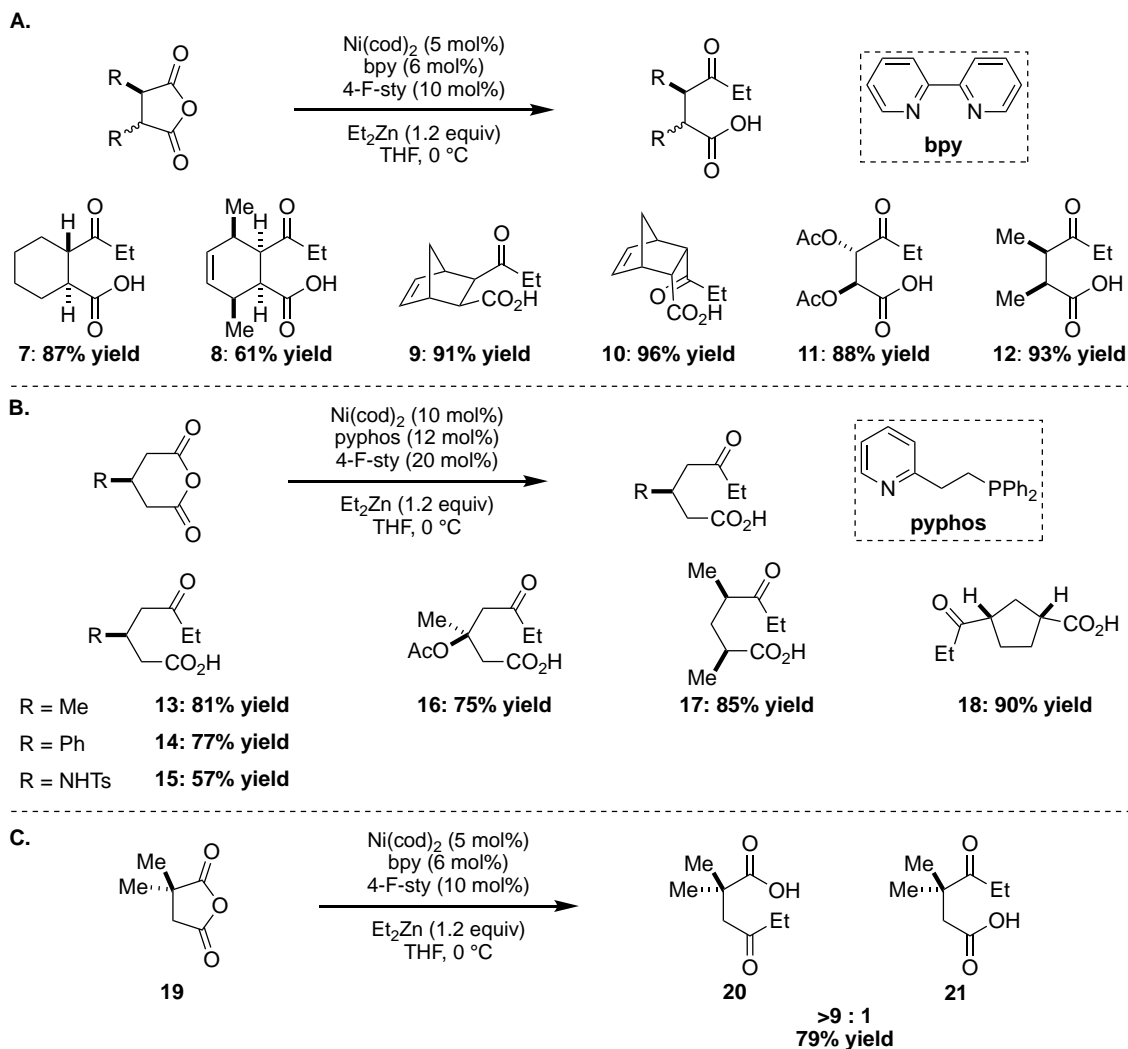
for productive chemistry. Ultimately, this transformation was realized by employing a chiral PHOX ligand, affording the product in good yield and selectivity (85% yield, 79% *ee*).



Scheme 1.2

In 2005, the Rovis group further developed this methodology in a comprehensive study of the nickel-catalyzed desymmetrization of succinic and glutaric anhydrides.¹³ Numerous succinic anhydrides were converted to the corresponding keto-acids (Scheme 1.3A). *Trans* substitution as well as β -substitution were well tolerated (**7** and **8**). Additionally, both *endo*- and *exo*-norbornene derived anhydrides reacted to give products **9** and **10**. Furthermore, acyclic succinic anhydrides, of both *trans* and *cis* substitution, gave the keto-acids in excellent yield (**11** and **12**). Glutaric anhydrides, however, did not proceed to the desired keto-acid products under the standard reaction conditions, but substituting the *bpy* ligand for *pyphos*, restored the desired reactivity. As a general reactivity trend, they observed that *bpy* worked well for succinic anhydrides, while *pyphos* was complementary for a variety of substituted glutaric anhydrides (Scheme 1.3B). Mono- and di-substitution at the 4-position was well-tolerated (**13-16**). Furthermore, 3,5-substituted anhydrides were effectively transformed into corresponding keto-acids **17** and **18** in excellent yield. They also

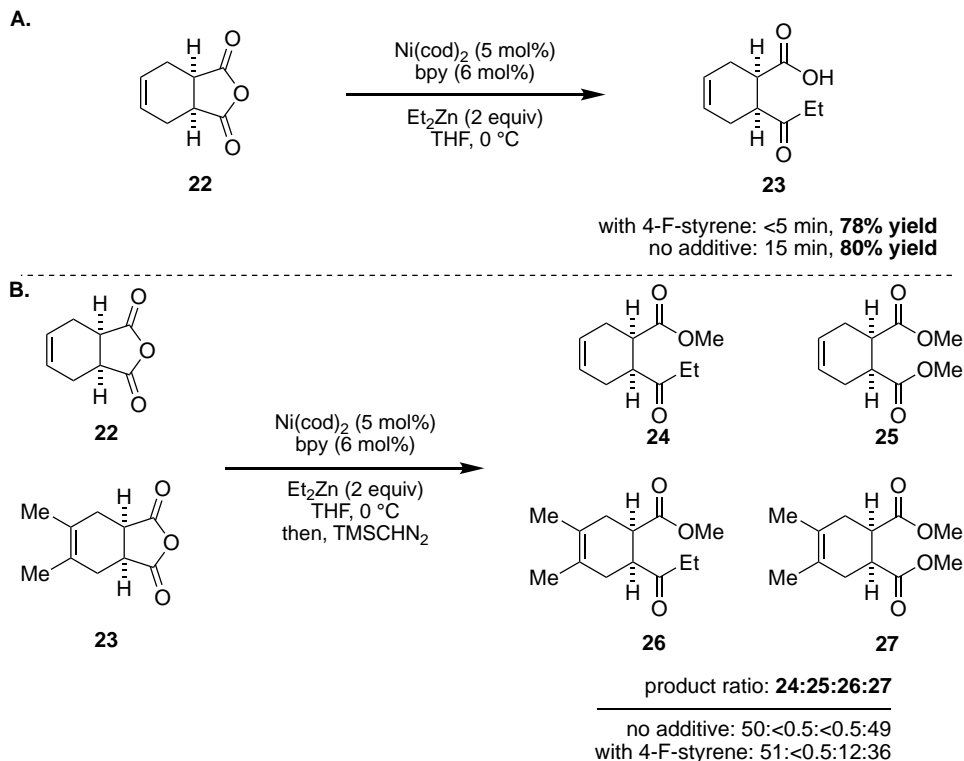
observed that a variety of alkyl and aryl zinc reagents, as well as zinc mixtures, with aryl Grignard or lithium reagents, were competent in the alkylation reaction. Interestingly, a regioselective alkylation reaction occurred when they used structurally biased anhydride **19**, where product **20** was formed preferentially over **21** (Scheme 1.3C). This can be rationalized by a regioselective nickel oxidative addition, away from the α -dimethyl substitution.



Scheme 1.3

The olefin additive had a considerable effect on the rate of the reaction, with styrene additives at just 10 mol% promoting the reaction in 30 min or less, compared to a reaction with no additive (21 h). It was initially hypothesized that the olefin promotes β -hydride elimination by either

withdrawing electron density from the metal center, or by inducing a conformational change. In addition, this rate acceleration was observed when substrates bearing an internal olefin were used. When anhydride **22** was subjected to the reaction conditions with 4-fluorostyrene (4-F-sty) as an additive, the product was afforded in 78% yield in less than 5 minutes (Scheme 1.4A). Interestingly, in the absence of the styrene additive, the product was formed in 80% yield in 15 min, still a significant rate enhancement relative to the reaction of parent anhydride **4**. The addition of cyclohexene to the reaction of **4**, however, did not result in a rate enhancement, suggesting that the olefin in the backbone of anhydride **22**, is likely accelerating the rate through an intramolecular binding of the nickel catalyst. To further probe this effect, they conducted competition experiments between anhydrides **22** and **23** (Scheme 1.4B). In the absence of a 4-fluorostyrene, only anhydride



Scheme 1.4

22 is converted to the desired product. Presumably, the methyl substitution on anhydride **23** prevents coordination of the olefin to nickel relative to **22**, again suggesting that an internal

coordination of the backbone olefin to nickel is promoting the reaction of **22**. When 4-fluorostyrene is added, product **26** is now observed, although **24** is still formed preferentially. Products **25** and **27** represent unreacted anhydride that is opened upon workup and converted to the diesters.

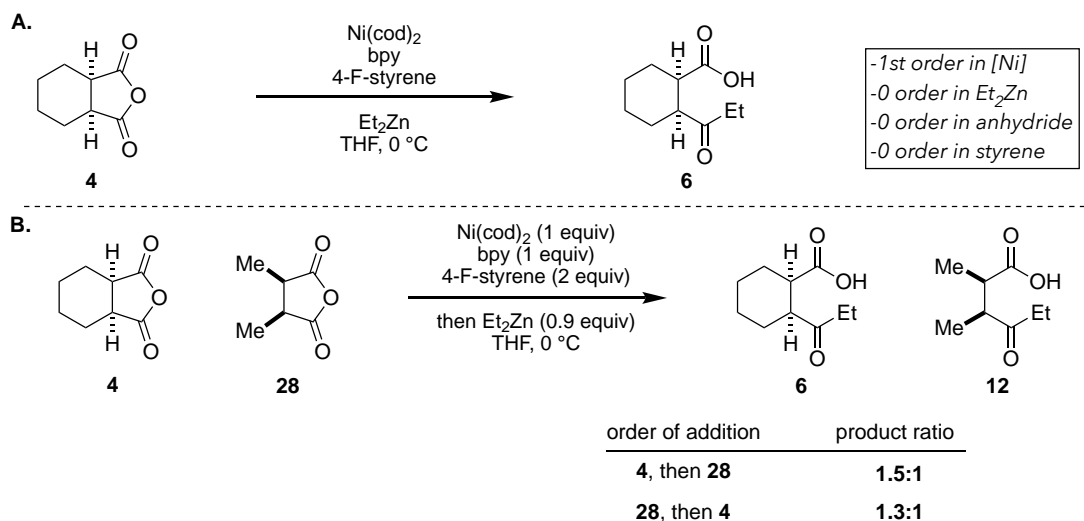
1.3 Mechanism of nickel catalyzed desymmetrization of anhydrides

In 2007, the Rovis group conducted a full mechanistic investigation of the nickel catalyzed desymmetrization of cyclic anhydrides both in a racemic and asymmetric fashion.¹⁴ Though the role of the styrene (or olefin) additive had been reported before, they wanted to understand its function in this catalytic system and its possible impact on the enantioselective variant. Thus far, they had not attained a highly asymmetric desymmetrization using nickel catalysis, which a more complete understanding of the mechanism might engender. They first studied succinic anhydrides under racemic conditions using bpy as a ligand. Secondly, they examined glutaric anhydrides under asymmetric conditions, using PHOX ligands. Ultimately, they disclosed the first report of rate-limiting reductive elimination of C–C bonds from a nickel catalyst, supported by mechanistic evidence.

1.3.1 Ni-bpy catalytic system for succinic anhydrides

The first system they studied was that of succinic anhydrides, using a nickel catalyst and bpy as the ligand for the alkylation of **4** to form keto-acid **6** (Scheme 1.5A). Using initial rate studies by *in situ* IR spectroscopy, they observed a 1st order dependence on nickel catalyst, and a 0th order dependence on anhydride, as well as 4-F-styrene. Diethyl zinc displayed 1st order kinetics at low concentration, but saturation at higher concentrations. They hypothesized that the saturation behavior of diethyl zinc concentration may be indicative of a change in the rate-limiting step; at low concentrations, transmetallation may be rate-limiting, but at higher concentrations the kinetic

data suggests a rate-limiting reductive elimination. The catalytic reaction is carried out under super-stoichiometric zinc loadings, so is likely mimics high zinc concentrations. Based on these data, they formulated a rate law that is 1st order in nickel catalyst, and 0th order in diethyl zinc and **4**.

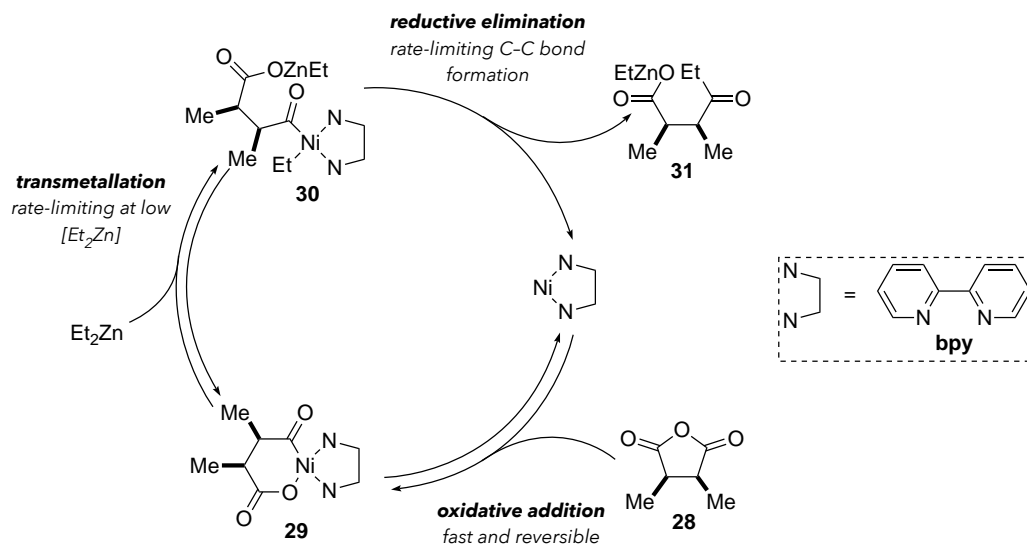


Scheme 1.5

To further interrogate the mechanism, they conducted ¹³C NMR studies, using anhydride **28** to probe the resting state of the catalyst, and observed the oxidative addition adduct **29** (Scheme 1.6) as a possible catalyst resting state. The observation of adduct **29** by NMR and 0th dependence of the reaction on anhydride concentration led to further examination of the oxidative addition step. To probe the reversibility of this step, they conducted a competition experiment between anhydride **4** and **28** (Scheme 1.5B). After first mixing **4** and the nickel/bpy catalyst in a 1:1 ratio with 4-fluorostyrene (2 equiv), they added **28** (1 equiv) and allowed the system to equilibrate, before adding diethyl zinc (0.9 equiv). After analyzing the product mixture, they observed a 1.5:1 mixture of **6** and **12**, results consistent with a fast and reversible oxidative addition. To rule out the possibility of different rates of oxidative addition between the two anhydrides, they conducted the

experiment in the reverse, and observed a 1.3:1 ratio of **6** to **12**, supporting the hypothesis of a fast and reversible oxidative addition step.

The full catalytic cycle is depicted in Scheme 1.6. Based on experimental data, oxidative addition of **28** to form metallacycle **29** is proposed to be fast and reversible. Transmetalation with diethyl zinc to give **30** would be fast and reversible, except at low zinc concentrations, where transmetalation becomes rate-limiting. Finally, reductive elimination of intermediate **30** could give keto-zinc carboxylate **31**, which represents the first evidence-supported rate-limiting C–C bond forming reductive elimination. While these elementary steps hold for alkyl zinc reagents, changes in kinetics were observed when diphenylzinc was used. In this case, a slower initial rate was observed and increasing the concentration of diphenylzinc increased the rate of reaction. This observation is consistent with a rate-determining transmetalation with an easier sp^2 - sp^2 C–C bond forming reductive elimination.



Scheme 1.6

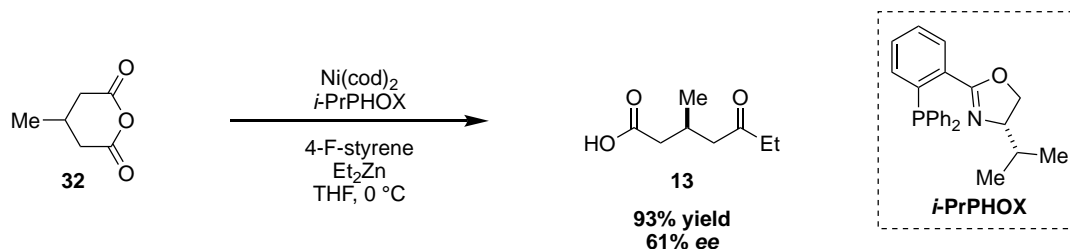
Interestingly, the role of styrene was not elucidated through these mechanistic studies. Its importance in the reaction was clearly demonstrated experimentally with faster reaction times and higher yields, yet it had a 0th order dependence in the rate law. The initial rates in the presence and

absence of styrene were nearly identical through 15% conversion. However, as the reaction progressed, there was an obvious decrease in the rate over time in the absence of styrene. To test the hypothesis of product inhibition, keto-zinc carboxylate was added to the standard reaction conditions, with no loss of productive reactivity. While it does not appear that styrene is influencing the rate of reductive elimination, as has been previously suggested,^{11,12} it is necessary in the reaction, likely for catalyst stability.

1.3.1 Ni-PHOX catalytic system for glutaric anhydrides

The Rovis group next sought to investigate the mechanism of the asymmetric desymmetrization of glutaric anhydrides. As previously reported, the desymmetrization of succinic anhydride **4** to enantioenriched keto acid **6** (Scheme 1.2) proceeded in excellent yield and good enantioselectivity. Despite considerable effort, however, more synthetically useful selectivities were unattainable. Keto-acid **13** derived from glutaric anhydride **32**, was also isolated under similar conditions in 93% yield and 61% *ee* (Scheme 1.7). A full study of this system was undertaken to investigate the role of the olefin additive, as well as elucidate the mechanism. Interestingly, during optimization of the nickel-PHOX system with glutaric anhydrides, they observed changes in selectivity, depending on the identity of the olefin additive. *p*-Substituted styrenes afforded the product in consistent yield, with selectivities ranging from 44-63% *ee*. 1,2-Dihydronaphthlene, however, afforded the product in 70% yield, but only 18% *ee*. In contrast, use of *trans*-stilbene or vinyl cyclohexane afforded low yields and selectivities (<10% *ee*). In the absence of an olefin additive, keto acid **13** is formed in 77% yield, but only 4% *ee*. It should be noted that in the nickel-bpy system, it was hypothesized that the role of the olefin is to stabilize the catalyst, and it appeared to have little effect on the elementary steps of the reaction. In this

case, the reaction proceeds to high yield in the absence of an olefin promoter, and the olefin is influencing the selectivity-determining step.

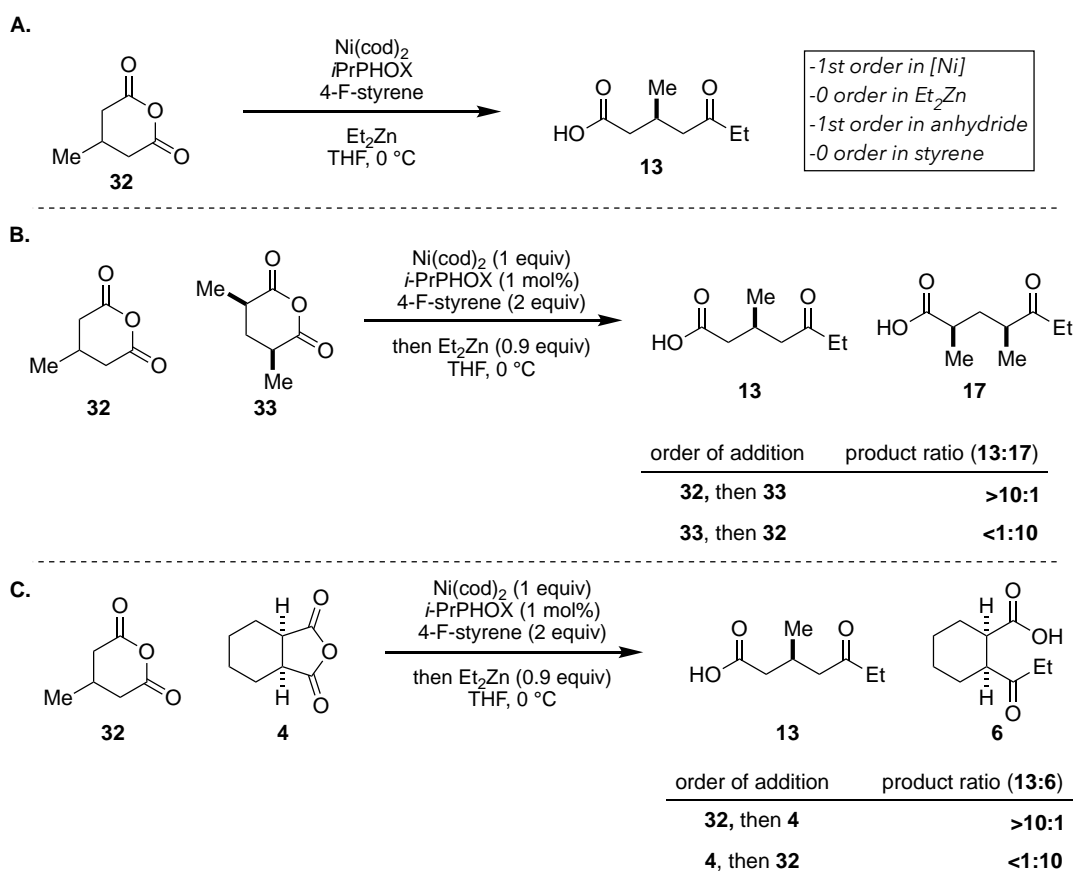


Scheme 1.7

The same experimental techniques were used as in the nickel-bpy system to gather mechanistic information. A 1st order dependence on nickel catalyst and anhydride was observed. Additionally, a 0th order dependence on diethyl zinc concentration and saturation behavior was observed with 4-fluorostyrene concentration (Scheme 1.8A). Furthermore, they observed that enantioselectivity was also dependent on styrene concentration, also demonstrating saturation behavior. The 1st order dependence on anhydride concentration suggests that oxidative addition is rate-limiting in this system, compared to the fast and reversible step observed with nickel-bpy. Additionally, the influence of styrene concentration on selectivity, suggests that the olefin is playing a role in the selectivity-determining step—oxidative addition.

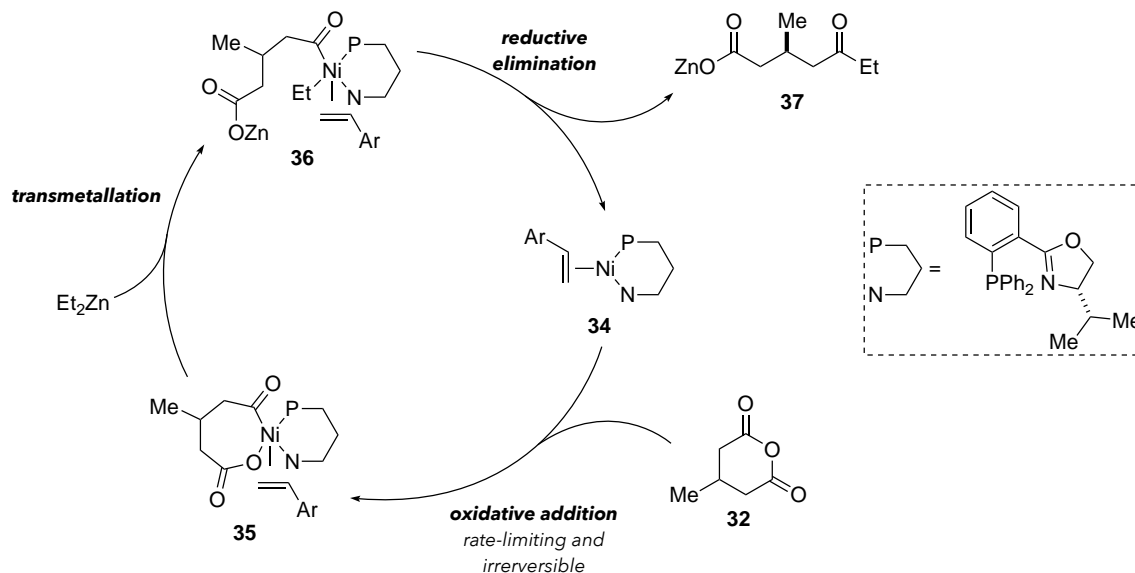
To further probe the nature of oxidative addition, they conducted competition experiments, like that of the nickel-bpy system (Scheme 1.8B). After anhydride **32** was mixed and equilibrated with a stoichiometric amount of the nickel catalyst system, in the presence of stoichiometric 4-fluorostyrene, anhydride **33** was added, and the system was equilibrated. They observed a >10:1 ratio of products **13** and **17**, suggesting that under these conditions, oxidative addition is irreversible. To ensure that the product ratio was not an effect of anhydride identity, they conducted the reverse experiment, adding anhydride **33** first and then adding **32**. In this case, they observed the formation of **17** in >10:1 ratio, supporting the hypothesis of an irreversible oxidative addition.

Aside from the catalyst, the major difference in this system is the use of glutaric anhydrides rather than succinic anhydrides. To confirm that the change in mechanism was due to the ligand, and not the anhydride, they conducted a similar competition experiment between anhydrides **32** and **4**. In this case, they observed results consistent with irreversible oxidative addition, observing no equilibration of oxidative addition adducts. While they did not conduct a full study of anhydride **4** with the PHOX ligand, the observation of irreversible oxidation in Scheme 1.8 suggests that the modest enantioselectivity observed is not the result of reversible oxidative addition, and that oxidative addition is likely the selectivity-determining step for succinic anhydrides with PHOX ligands.



Scheme 1.8

The full catalytic cycle is depicted in Scheme 1.9. Given the saturation dependence of styrene and its effect on the selectivity of the transformation, it was proposed that the catalytic cycle starts with complex **34**, where the PHOX ligated nickel complex is also coordinated to an equivalent of styrene. Oxidative addition, proposed to be the rate-limiting and selectivity-determining step, into anhydride **32** affords complex **35**. Transmetalation with diethyl zinc, followed by reductive elimination would release the product and regenerate complex **34**. In the absence of styrene, it was proposed that a slower catalytic cycle is operative, providing the product in only 4% ee. Despite these mechanistic studies, a more complete understanding of role of the olefin additive and how it impacts selectivity in the Ni-PHOX system, particularly in regards to succinic anhydrides, was not realized.

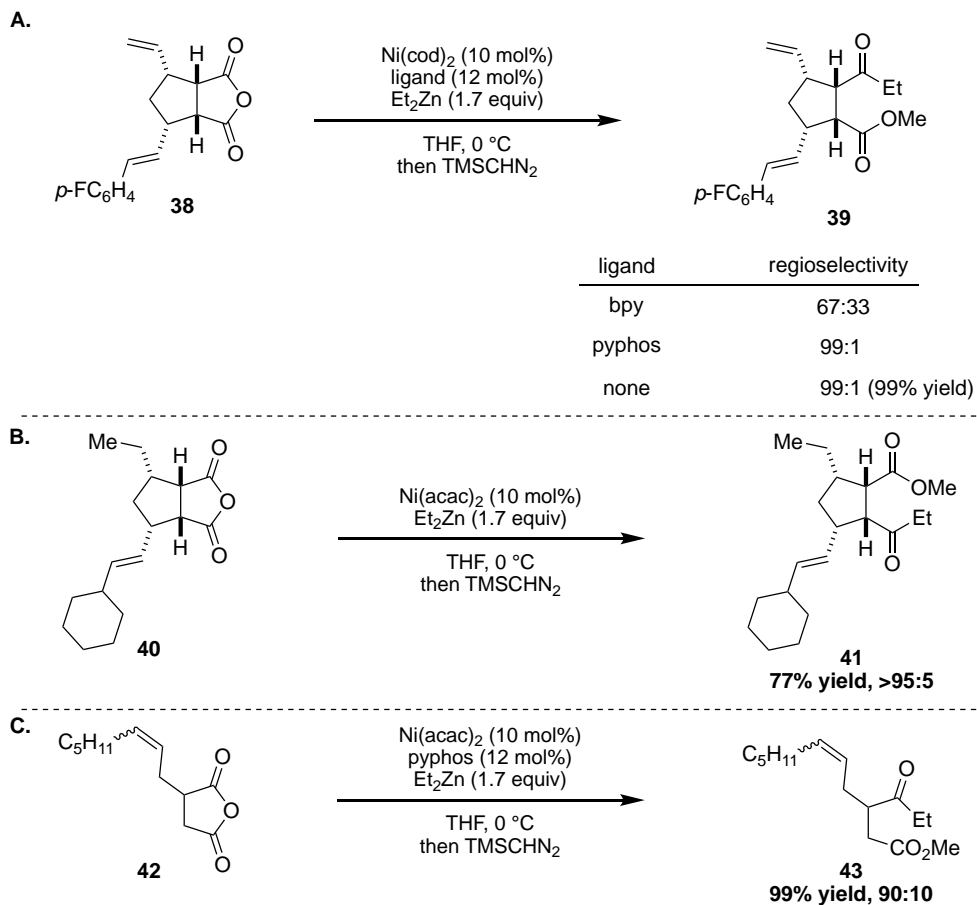


Scheme 1.9

1.4 Regioselective olefin-directed anhydride desymmetrization

Given the important effect of olefins on the reactivity of nickel-catalyzed anhydride desymmetrizations already demonstrated through synthetic and mechanistic studies, this effect could be exploited to conduct regioselective anhydride openings. After studying the mechanism

of these reactions, the Rovis group explored this idea further using anhydrides with tethered olefins.¹⁵ When they subjected anhydride **38** to standard reaction conditions from previous reports, they observed a 2:1 mixture of regioisomers, with the terminal olefin directing preferentially to form **39** (Scheme 1.10A). When pyphos was used in place of bpy as a ligand, the regioselectivity was increased to 99:1, with **39** being formed preferentially. Interestingly, in the absence of ligand,



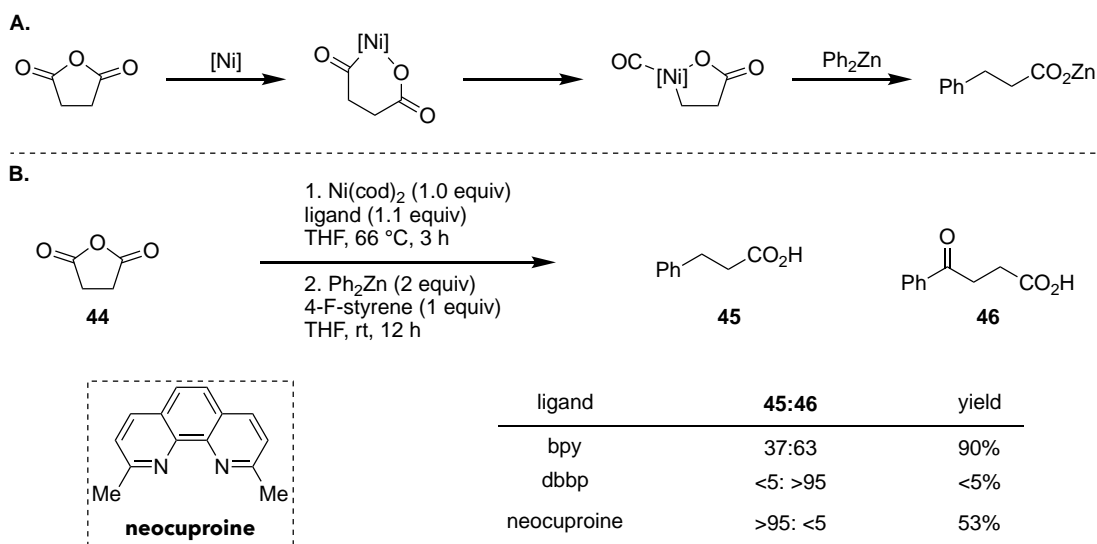
Scheme 1.10

the product is still formed in excellent yield and regioselectivity, demonstrating a ligand-less cross-coupling of cyclic anhydrides using nickel catalysis. Numerous substituents (in place of *p*-FC₆H₄) were also well tolerated in the reaction and provided high regioselectivities and product yields. In control reactions, substrates lacking an olefin directing group did not proceed to product in the absence of an exogenous ligand. To determine whether the substrate olefin could also serve as a

regioselective directing group, they prepared the mono-reduced anhydride **40** (Scheme 1.10B). When subjected to the reaction conditions, they observed the keto-acid product (**41**) in good yield and excellent regioselectivity, this time favoring the complementary regioisomer to **39**. Anhydride **42** was also competent in the reaction, providing the regioselective alkylation in excellent yield and a 90:10 ratio of regioisomers. However, while this reaction did require the use of an exogenous ligand to promote reactivity, the high regioselectivity suggests that the olefin is still involved in the regioselective oxidative addition.

1.5 Nickel mediated decarbonylative cross-coupling of cyclic anhydrides

Concurrent with the initial reports on a nickel catalyzed desymmetrization of cyclic anhydrides, the Rovis group reported a related transformation—a decarbonylative cross-coupling of succinic anhydrides and diphenyl zinc.¹⁶ The transformation could be accomplished if the proposed oxidative addition adduct would undergo decarbonylation prior to transmetallation

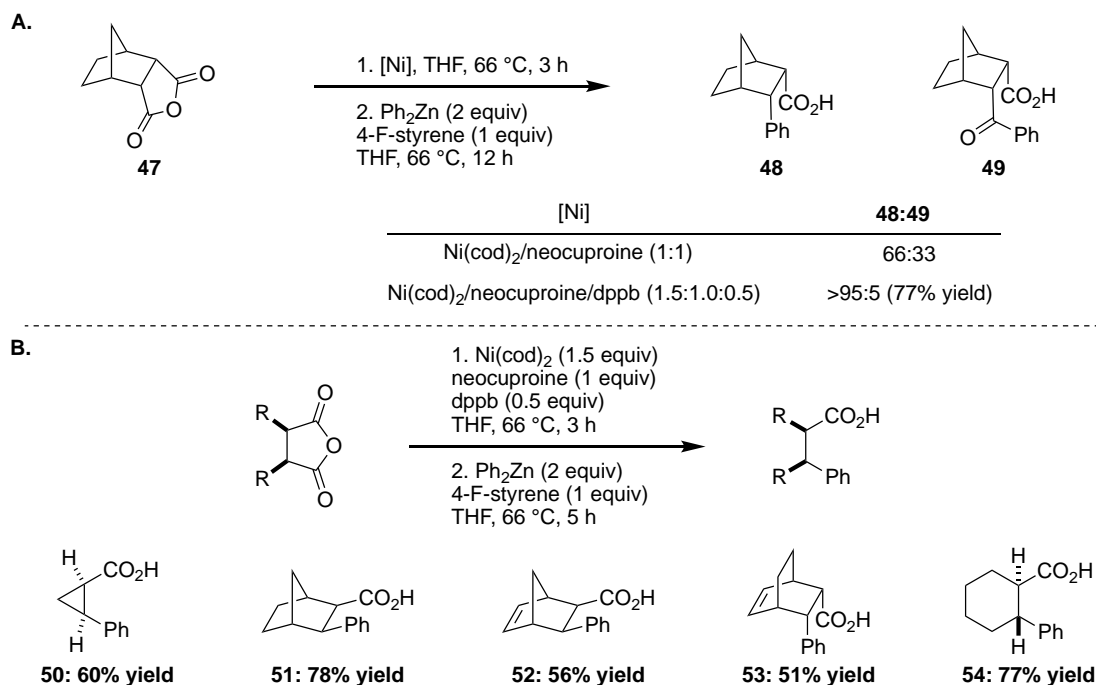


Scheme 1.11

(Scheme 1.11A). This would form a nickel-*sp*³ carbon bond, to ultimately form an *sp*²-*sp*³ C–C bond. They found that the proposed transformation was highly dependent on the ligand used. Succinic anhydride (**44**), in the presence of a stoichiometric nickel-bpy complex, followed by the

addition of diphenyl zinc afforded carboxylic acid **45** and the corresponding keto-acid **46** in a 37:63 ratio and 90% overall yield (Scheme 1.11B). Interestingly, exchanging bpy for 1,4-Bis(diphenylphosphino)butane (dppb) promoted the sp^2-sp^2 C–C bond forming reaction, but in <5% yield. Using neocuproine as a ligand, however, gave the decarbonylated product **45** preferentially in 53% yield.

Despite the high selectivity with succinic anhydride, more complex anhydrides proved more difficult to convert to the decarbonylated product, providing a mixture of acid and keto-acid. They proposed that CO, upon decarbonylation, remained coordinated to nickel and may reinsert prior to transmetallation. They hypothesized that the use of a dppb ligated nickel might sequester CO and provide improved selectivity for the decarbonylated product. When they subjected anhydride **47** to the standard reaction conditions, they observed only a 2:1 ratio of decarbonylation to keto-acid



Scheme 1.12

(**48:49**) (Scheme 1.12A). However, when they employed a mixture of neocuproine and dppb as ligands, they observed preferential formation of **48** in 77% yield. Numerous cyclic anhydrides are

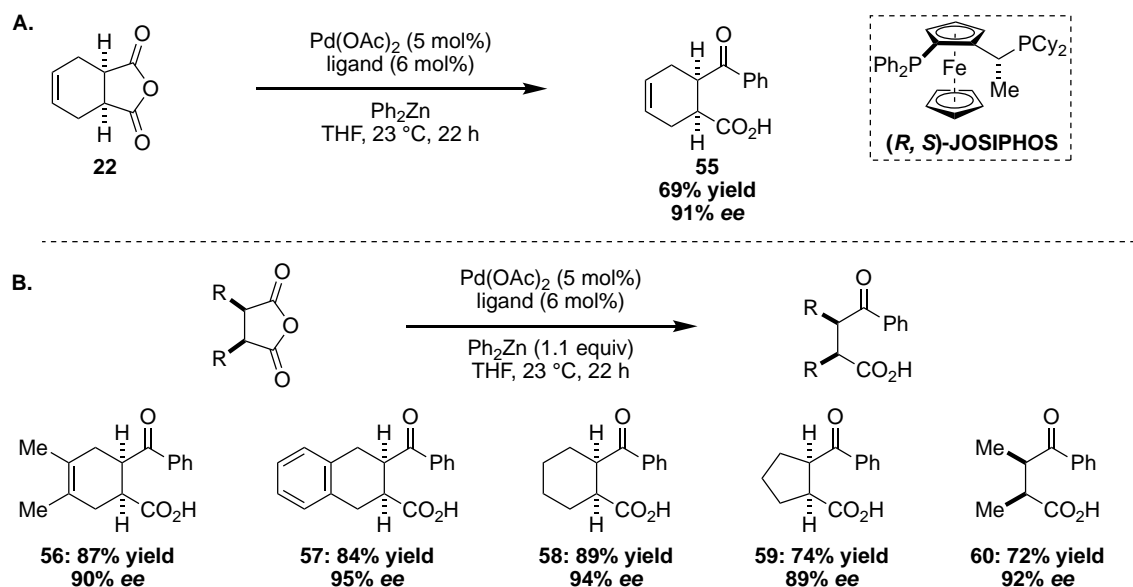
competent under these reaction conditions to form the corresponding acid products in good yield (1.12B). Cyclopropane product **50**, as well as *exo* **51** were formed in good yield. Additionally, alkene functionality was well tolerated, affording **52** in good yield. *Trans* product **54** was also afforded upon subjecting the racemic anhydride to the reaction conditions. Interestingly, stereochemical information is retained, ultimately suggesting this strategy may be used to form stereodefined sp^2 - sp^3 C–C bonds.

1.6 Enantioselective desymmetrization of cyclic *meso*-anhydrides

1.6.1 Palladium catalyzed desymmetrization of succinic anhydrides

Despite the success of using nickel in the cross-coupling of *meso* anhydrides with alkyl and aryl zinc reagents, a highly enantioselective variant was not realized. Enantioselective desymmetrizations of *meso* anhydrides have been realized with other nucleophiles; however, a transition-metal catalyzed variant would be extremely valuable due to the wealth of available nucleophiles. In 2004, the Rovis group realized a highly enantioselective cross-coupling of *meso* succinic anhydrides employing palladium catalysis.¹⁷ A racemic variant of the reaction was accomplished with Pd(PPh₃)₄ and diphenylzinc. The success of phosphine ligands offered a wealth of available chiral ligands that could enable a highly selective transformation. They discovered that (*R,S*)-JOSIPHOS afforded the product (**55**) in 67% yield and 90% *ee* at 80 °C. This is contrast to the nickel/PHOX system, which afforded the cross-coupled product in 79% *ee* (Scheme 1.2). The transformation tolerated a disubstituted olefin in product **56**, as well as a larger phenyl ring in the backbone (**57**) (Scheme 1.13B). Fully saturated **58** was isolated in excellent yield and selectivity, with no change in selectivity observed—under nickel catalyzed conditions, the olefin had influenced the selectivity determining step. Smaller ring sizes, such as cyclopentane were also

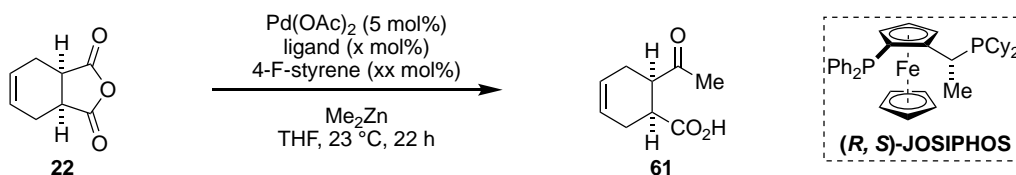
tolerated under the reaction conditions (**59**). Acyclic succinic anhydrides were also converted to **60** in good yield and excellent selectivity, although this reaction required 80 °C to complete.



Scheme 1.13

To expand the nucleophile scope of this transformation, they examined other zinc reagents, and found that dimethyl zinc was competent in the reaction, providing the desired product in 78% yield but reduced selectivity at 64% *ee* (Table 1.1). Utilizing the observations from the nickel catalyzed cross-coupling reactions, 4-fluorostyrene was added to promote the transformation to provide **61** in improved yield and restored enantioselectivity. Increasing the ligand to nickel ratio completely shut down the reaction, but decreasing the ligand loading restored reactivity and selectivity. Decreasing the ligand loading further, however, decreased reactivity and slightly decreased the selectivity of the transformation. This disclosure represented the first highly enantioselective desymmetrization of *meso* anhydrides to form keto-acids.

Table 1.1

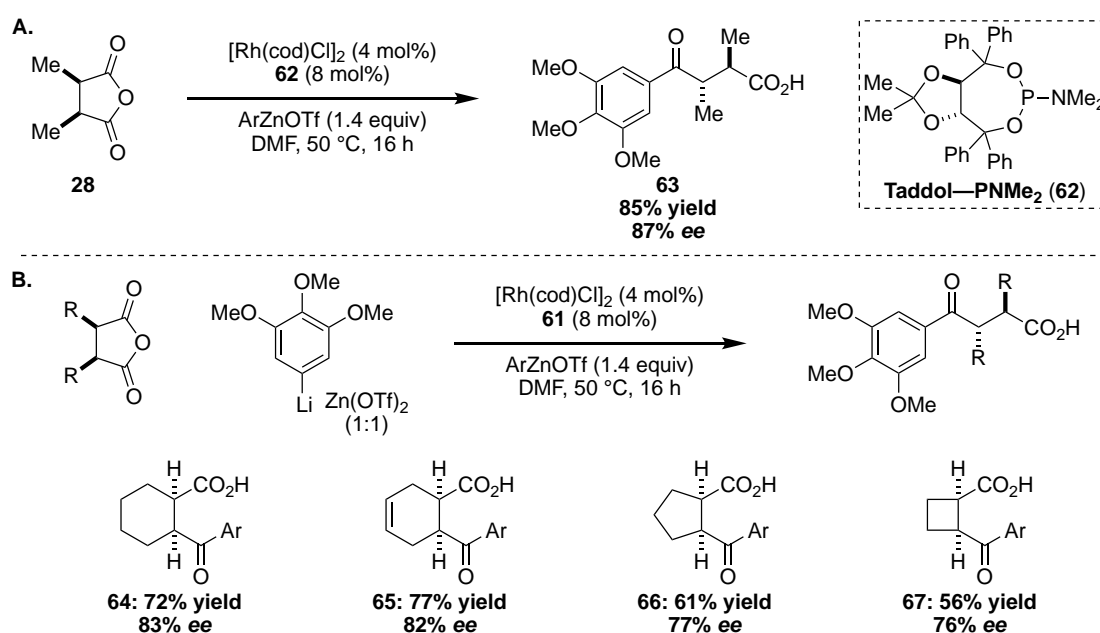
			
Pd:ligand	4-F-styrene	Yield (%)	ee (%)
1:1.0	0	78%	64%
1:1.0	25 mol%	80%	91%
1:1.2	25 mol%	NR	n/a
1:0.8	25 mol%	60%	90%
1:0.5	25 mol%	<25%	84%

1.6.2 Rhodium catalyzed desymmetrization of *meso* anhydrides

Although the palladium-catalyzed enantioselective desymmetrization had been successful for succinic anhydrides, it was limited to diaryl and dialkyl zinc reagents, only a few of which are commercially available.¹⁸ This limitation undermines the power of the cross-coupling reactions and the wealth of available nucleophiles. Additionally, under palladium catalysis, a similar transformation for glutaric anhydrides remained elusive. These substrates are particularly attractive as they map on well to numerous polyketide secondary metabolites and generation of these stereodefined products represents a powerful method to generate molecular complexity from simple starting materials.

In 2007, the Rovis group sought to expand the asymmetric desymmetrization of both succinic and glutaric anhydrides by extending to rhodium catalysis.¹⁹ In the presence of [Rh(cod)Cl]₂, a Taddol-derived ligand (**62**) and a mixed zinc nucleophile in DMF, anhydride **28** was converted to enantioenriched keto-acid **63** in good yield and selectivity (Scheme 1.14A). The mixed zinc nucleophile was prepared from mixing a 1:1 ratio of Zn(OTf)₂ and the aryl lithiate. Previously, THF had been the optimal solvent for these anhydride cross-coupling reactions, but under these conditions, THF afforded reduced yield and markedly reduced selectivity (68% yield, 47% *ee*).

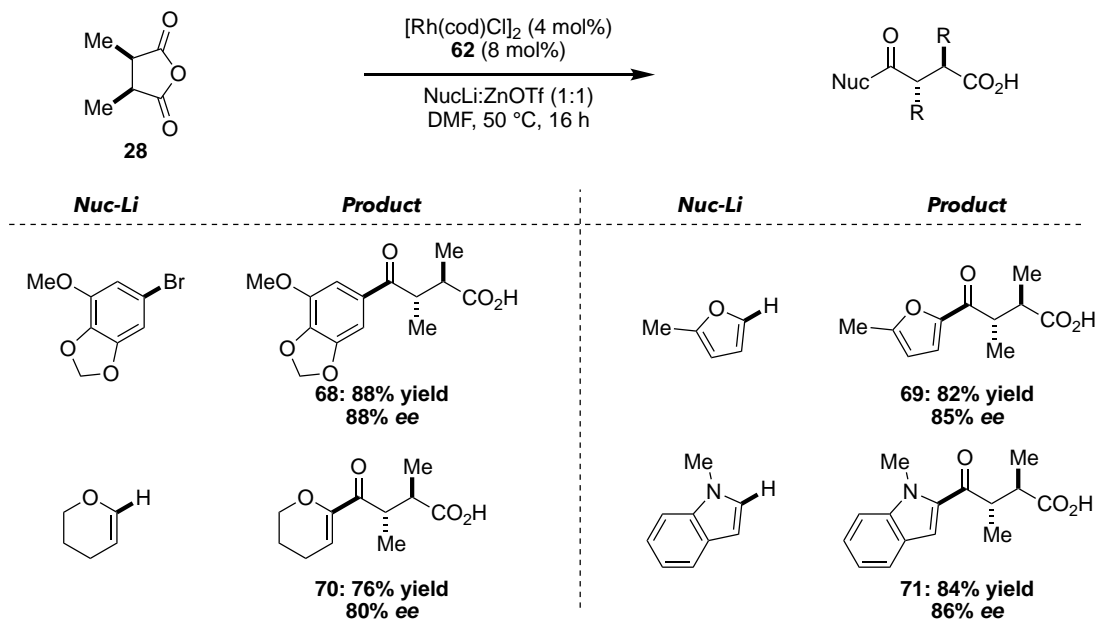
Additionally, use of the *i*-PrPHOX ligand, which had been demonstrated as the most successful ligand in the nickel catalyzed system, provided low yield and selectivity (23% yield, 32% *ee*). The reaction conditions were amenable for numerous *meso* succinic anhydrides including bicyclic anhydride to form product **64** and the unsaturated version (product **65**), with no change in selectivity—again demonstrating a reactivity departure from the nickel-catalyzed system (Scheme 1.14B). Furthermore, smaller ring sizes were well tolerated, with anhydrides **66** and **67** providing products in good yield and selectivity.



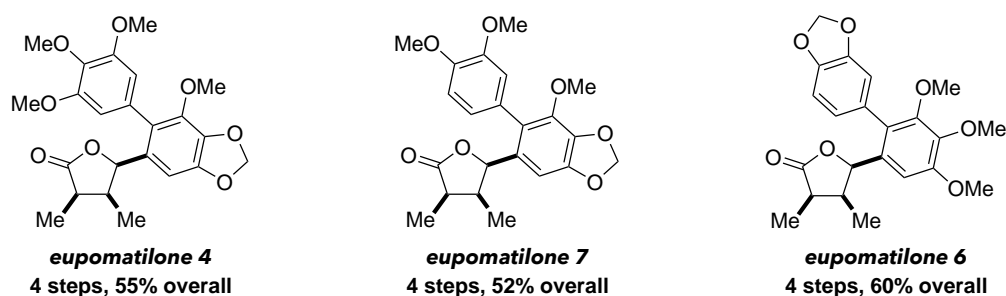
Scheme 1.14

They next sought to examine the available nucleophile scope, employing anhydride **28**. Numerous aryl bromides were lithiated and when mixed with Zn(OTf)_2 , gave the desired cross-coupled product (**68**) in high yield and selectivity (Scheme 1.15). Additionally, 2-methylfuran underwent ortho-lithiation and under the reaction conditions formed product **69** and dihydropyran was converted to product **70** in 76% yield and 80% *ee*. Lastly, *N*-methylindole underwent ortho-lithiation followed by formation of the mixed zinc reagent and cross-coupling to form product **71** in just one step. The ability to use mixed zinc reagents which are generated from nucleophilic

lithiates broadly expands the scope of the anhydride desymmetrization. They further demonstrated the power of this methodology by synthesizing several secondary metabolites in a few steps, starting from anhydride **28**, the appropriate lithiate precursor and employing the rhodium-catalyzed desymmetrization conditions (Scheme 1.16). All anhydride cross-couplings proceeded in >85% yield and >85% *ee*.



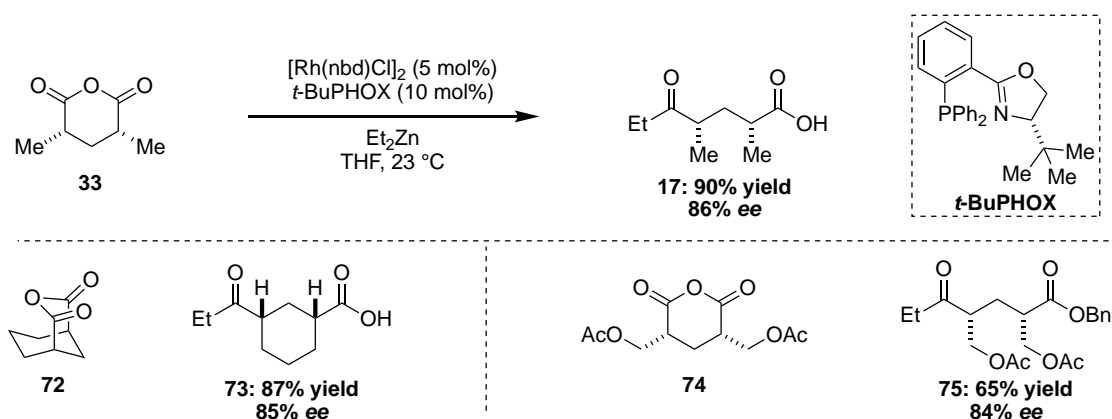
Scheme 1.15



Scheme 1.16

The Rovis group next sought to extend this powerful methodology to the asymmetric desymmetrization of glutaric anhydrides using rhodium catalysis.²⁰ Employing 3,5-dimethyl glutaric anhydride (**33**) under the conditions used for succinic anhydrides and dimethyl zinc, they

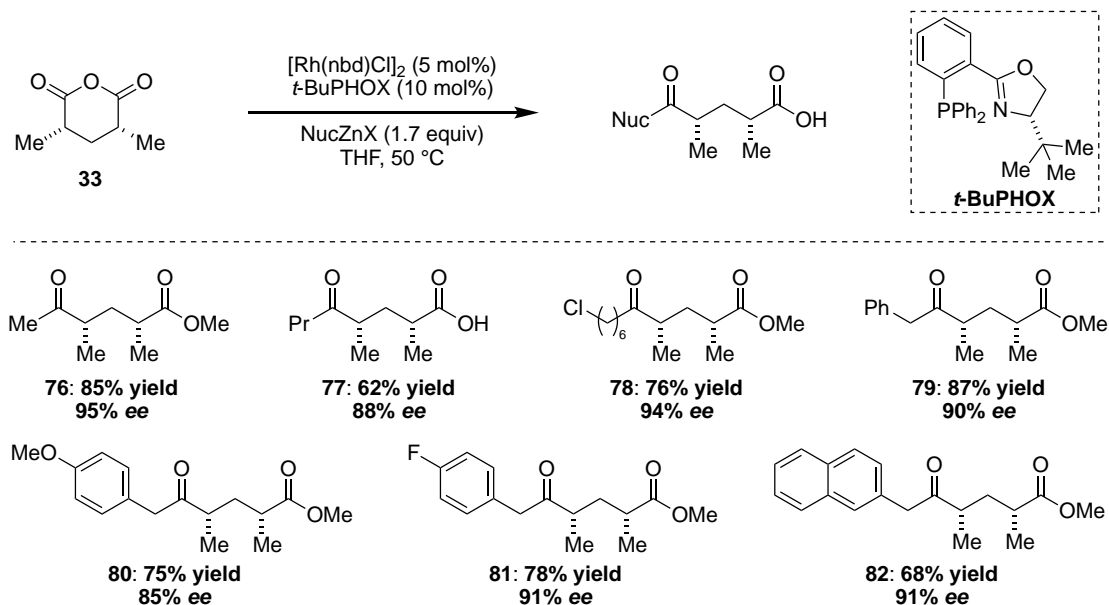
observed no reaction. However, by switching to PHOX type ligands, product **17** was isolated in good yield and selectivity. After exchanging the rhodium catalyst and using *t*-BuPHOX, they formed the cross-coupled product in 90% yield and 86% *ee* (Scheme 1.17). Diethyl zinc nucleophiles provided slightly higher yields and product selectivities, relative to dimethyl zinc; however, diphenyl zinc afforded lower yields and markedly lower selectivities (76% yield, 56% *ee*). By employing TADDOL-PNMe₂ (**62**), they improved the selectivity to 82% *ee*. Other glutaric anhydrides were also competent under the reaction conditions, affording **73** and **75** in good yield and selectivity.



Scheme 1.17

With the highly selective reaction conditions, they wanted to examine the nucleophile scope for this transformation (Scheme 1.18). Under the standard reaction conditions, at 50 °C with dimethylzinc as a nucleophile, product **76** was isolated in high yield and excellent enantioselectivity. Extending the nucleophilic chain to propyl resulted in reduced yield and slightly reduced selectivity. Primary alkyl chlorides were tolerated under the reaction conditions providing **78** in high yield and 94% *ee* (note: the dialkyl zinc reagent was used). Additionally, benzyl substitution was well tolerated, with electron neutral and electron rich benzyl zinc reagents providing the corresponding products in consistent yield and selectivity (**79-82**). Furthermore,

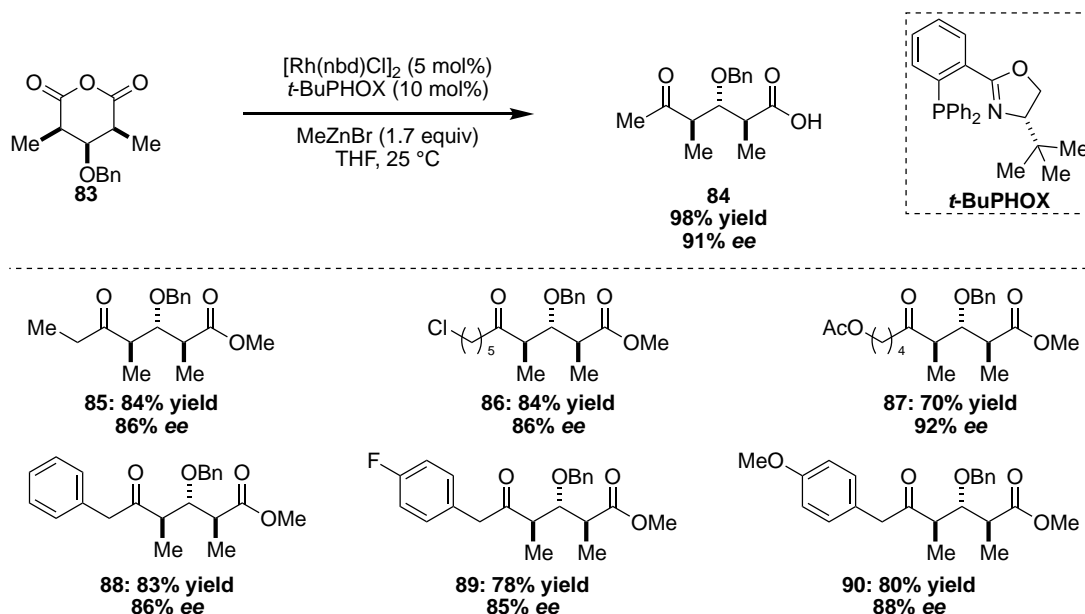
larger 2-naphthylbenzyl was a competent nucleophile, providing the product in 68% yield and 91% *ee*. The small variance in selectivity between zinc nucleophiles suggests that the selectivity determining step is independent of nucleophile. Interestingly, while 3,5-disubstituted glutaric anhydrides worked well in this chemistry, 4-substitution was not tolerated and gave significantly lower enantioselectivity (9% to 53% *ee*).



Scheme 1.18

Many polyketide secondary metabolites contain a 1,3-dimethyl-2-hydroxy motif—the desymmetrization of such substituted glutaric anhydrides represents a powerful strategy to access these structural motifs. The Rovis group recently disclosed a modified strategy to enable the desymmetrization of these compounds in high yield and selectivity.²¹ Employing similar reaction conditions to their previous report and using methylzinc bromide as a nucleophile, benzyl protected 3,5-dimethyl-4-hydroxy glutaric acid (**83**) was converted to keto-acid **84**, in 98% yield and 91% *ee* (Scheme 1.19). They utilized a variety of mixed zinc nucleophiles, with a primary alkyl chloride and acetate being well tolerated (**86** and **87**). Benzyl substituted zinc nucleophiles, both electron neutral and electron rich, also provided the desired products in good yield and

selectivity (**88-90**). The consistency of selectivity among varying nucleophiles suggests that the nucleophile does not play a role in the selectivity determining step.

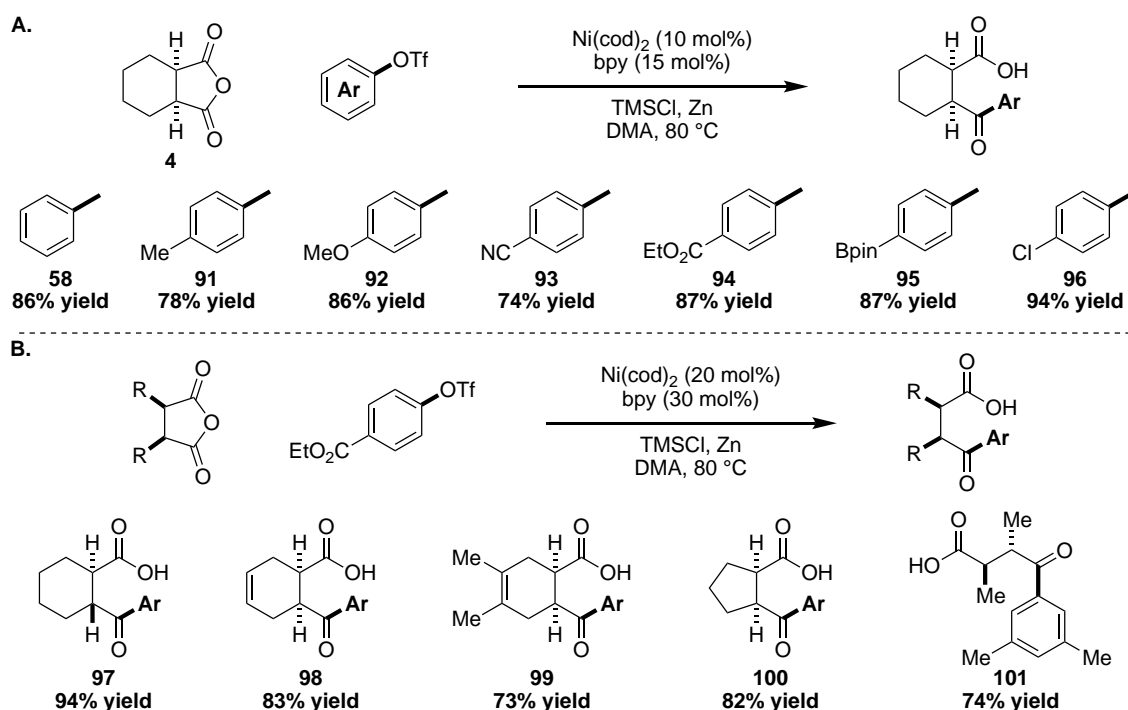


Scheme 1.19

1.7 Cross-electrophile couplings of *meso*-anhydrides

The significant advantage to using transition metals to desymmetrize and cross-couple *meso* anhydrides is the wealth of nucleophiles that are amenable to cross-coupling to form new C–C bonds. Classical nucleophiles include those already disclosed here (zinc reagents–Negishi coupling), but also boron nucleophiles (Suzuki–Miyura coupling), stannanes (Stille coupling), Grignard nucleophiles (Kumada coupling) and olefins (Heck reaction). Despite the expanse of nucleophile classes used in cross-coupling, zinc reagents have appeared privileged in the desymmetrization of *meso* anhydrides. Very recently, a method disclosing a cross-electrophile coupling was reported by the Walsh group.²² Cross-electrophile couplings have gained prominence over the last decade as a strategy to utilize bench stable, commercially available reagents to construct carbon–carbon bonds.²³

The Walsh group observed that aryl triflates could be coupled to succinic anhydrides under reducing conditions, with zinc as a stoichiometric reductant. In the presence of a $\text{Ni}(\text{cod})_2$ -bpy complex, TMSCl and zinc dust, anhydride **4** was coupled to phenyl triflate to provide keto acid **58** in 86% yield (Scheme 1.20A). Aryl bromides and iodides provided product in this reaction, but suffered from homocoupling and decarbonylation side pathways. They examined the scope of aryl triflates with anhydride **4** and found that electron rich to electron poor substrates functioned well in the transformation (**91-94**). Additionally, they found that aryl triflates bearing boronic esters or



Scheme 1.20

chlorides were also competent in this reaction (**95** and **96**). These substrates are particularly attractive as they contain functional group handles for further cross-coupling reactions and further manipulation. They also investigated the scope with respect to anhydride coupling partner and found that the *trans* anhydride also proceeded to product under the standard reaction conditions (Scheme 1.20B). Furthermore, unsaturation in the cyclohexane backbone was tolerated, with

products **98** and **99** formed in good yield. Smaller ring sizes like cyclopentane, as well as acyclic anhydrides afforded the desired products in excellent yield (**100** and **101**).

1.8 Conclusion and outlook

Transition metal catalyzed cross-coupling remains one of the most valuable strategies for building carbon–carbon bonds. The Rovis group and others have demonstrated that cyclic anhydrides are important non-classical electrophiles for cross-coupling reactions. The desymmetrization of *meso* anhydrides represents a valuable synthetic strategy for synthesizing stereodefined 1,4-dicarbonyl and 1,5-dicarbonyl motifs, common structural features found in polyketide metabolites. Furthermore, recent advances in photoredox catalysis (to be discussed in the next chapter) offer new ways to diversify these products into synthetic building blocks that are not immediately obvious based on the starting materials. Although significant advances in the cross-couplings of anhydrides have been achieved, limitations remain. First, despite the effort to increase the nucleophile scope to build more complex keto-acids, the chemistry is still limited to zinc nucleophiles or zinc as a heterogeneous stoichiometric reductant. Typical cross-coupling nucleophiles are either not compatible, or have not shown success under typical reactions conditions. Second, to achieve a highly selective desymmetrization, precious metals such as palladium or rhodium must be used. Third, while nickel catalysis offers the most diversity in terms of substrate scope, the use of an olefin additive is necessary to impart this reactivity, and limits the ability to use this methodology for asymmetric transformations. In the next chapter, I will discuss how photoredox catalysis can address these limitations and our efforts to realize these advances.

References

- (1) Seechurn, C. C. C. J.; Kitching, M. O.; Colacot, T. J.; Snieckus, V. *Angew. Chem. Int. Ed. Engl.* **2012**, *51* (21), 5062.
- (2) Tasker, S. Z.; Standley, E. A.; Jamison, T. F. *Nature* **2014**, *509* (7500), 299.
- (3) Huang, C. Y.; Doyle, A. G. *Chem. Rev.* **2014**, *114* (16), 8153.
- (4) Johnson, J. B.; Rovis, T. *Acc. Chem. Res.* **2008**, *41* (2), 327.
- (5) Shintani, R.; Fu, G. C. *Angew. Chem. Int. Ed. Engl.* **2002**, *41* (6), 1057.
- (6) Atodiresei, I.; Schiffrers, I.; Bolm, C. *Chem. Rev.* **2007**, *107* (12), 5683.
- (7) Zapf, C. W.; Harrison, B. A.; Drahl, C.; Sorensen, E. J. *Angew. Chem. Int. Ed. Engl.* **2005**, *44* (40), 6533.
- (8) Trost, B. M.; Chen, F. *Tetrahedron Letters* **1971**, *12* (28), 2603.
- (9) Gooßen, L. J.; Ghosh, K. *Angew. Chem. Int. Ed. Engl.* **2001**, *40* (18), 3458.
- (10) Bercot, E. A.; Rovis, T. *J. Am. Chem. Soc.* **2002**, *124* (2), 174.
- (11) Giovannini, R.; Stüdemann, T.; Dussin, G.; Knochel, P. *Angew. Chem. Int. Ed. Engl.* **1998**, *37* (17), 2387.
- (12) Giovannini, R.; Stüdemann, T.; Devasagayaraj, A.; Dussin, G.; Knochel, P. *J. Org. Chem.* **1999**, *64* (10), 3544.
- (13) Bercot, E. A.; Rovis, T. *J. Am. Chem. Soc.* **2005**, *127* (1), 247.
- (14) Johnson, J. B.; Bercot, E. A.; Rowley, J. M.; Coates, G. W.; Rovis, T. *J. Am. Chem. Soc.* **2007**, *129* (9), 2718.
- (15) Rogers, R. L.; Moore, J. L.; Rovis, T. *Angew. Chem. Int. Ed.* **2007**, *46* (48), 9301.
- (16) O'Brien, E. M.; Bercot, E. A.; Rovis, T. *J. Am. Chem. Soc.* **2003**, *125* (35), 10498.

- (17) Bercot, E. A.; Rovis, T. *J. Am. Chem. Soc.* **2004**, *126* (33), 10248.
- (18) Johnson, J. B.; Yu, R. T.; Fink, P.; Bercot, E. A.; Rovis, T. *Org. Lett.* **2006**, *8* (19), 4307.
- (19) Johnson, J. B.; Bercot, E. A.; Williams, C. M.; Rovis, T. *Angew. Chem. Int. Ed.* **2007**, *46* (24), 4514.
- (20) Cook, M. J.; Rovis, T. *J. Am. Chem. Soc.* **2007**, *129* (30), 9302.
- (21) Cochran, B. M.; Henderson, D. D.; Thullen, S. M.; Rovis, T. *Synlett* **2017**, *29* (03), 306.
- (22) Lin, T.; Mi, J.; Song, L.; Gan, J.; Luo, P.; Mao, J.; Walsh, P. J. *Org. Lett.* **2018**, *20* (4), 1191.
- (23) Weix, D. J. *Acc. Chem. Res.* **2015**, *48* (6), 1767.

Chapter 2

Nickel- and photoredox-catalyzed enantioselective desymmetrization of cyclic *meso*-anhydrides

2.1 Introduction

Photoredox catalysis is a transformative synthetic tool that has been rapidly developed over the past decade.^{1,2} Generally, a photoredox catalyst, when excited by visible light, can engage in electron transfer or energy transfer to generate new radical species or excited state complex.^{3,4} Radicals are highly reactive species that engage in one-electron pathways, as opposed to two-electron pathways, which can often offer complementary reactivity. Furthermore, use of photoredox catalysis has engendered atypical retrosynthetic bond disconnections. This approach often employs ubiquitous and inexpensive reagents to build new bonds in one step, rather than multiple step pathways. In this introduction, I will give a brief overview and highlight major advances of photoredox catalysis that underscore its utility in a nickel catalyzed anhydride desymmetrization.

2.1.1 Principles of photoredox catalysis

A general schematic of photocatalyst excitation and subsequent electron transfer is depicted in Figure 2.1.⁵ $\text{Ru}(\text{bpy})_3^{2+}$, a commonly used photoredox catalyst, when excited with blue light ($\lambda_{\text{max}} = 452 \text{ nm}$) undergoes a metal to ligand charge transfer (MLCT) into a singlet excited state (S_1). Intersystem crossing (ISC) occurs to transition the singlet excited state complex into a longer-lived triplet excited state ($T_1 = 1100 \text{ ns}$). From this triplet excited state, the catalyst can act as a single-electron oxidant ($E_{\text{red}}^{T1} = + 0.77 \text{ V vs. SCE}$) where it accepts an electron from a donor species to generate a reduced form, $\text{Ru}(\text{bpy})_3^+$. This represents a reductive quenching cycle, where the photocatalyst is reduced and a substrate or reductant is oxidized (Scheme 2.1A). To close the

photocatalytic cycle, a substrate or oxidant must be reduced by the photocatalyst. Alternatively, the photoexcited triplet state catalyst can donate an electron ($E^{T1}_{ox} = -0.81$ V vs. SCE) to an organic

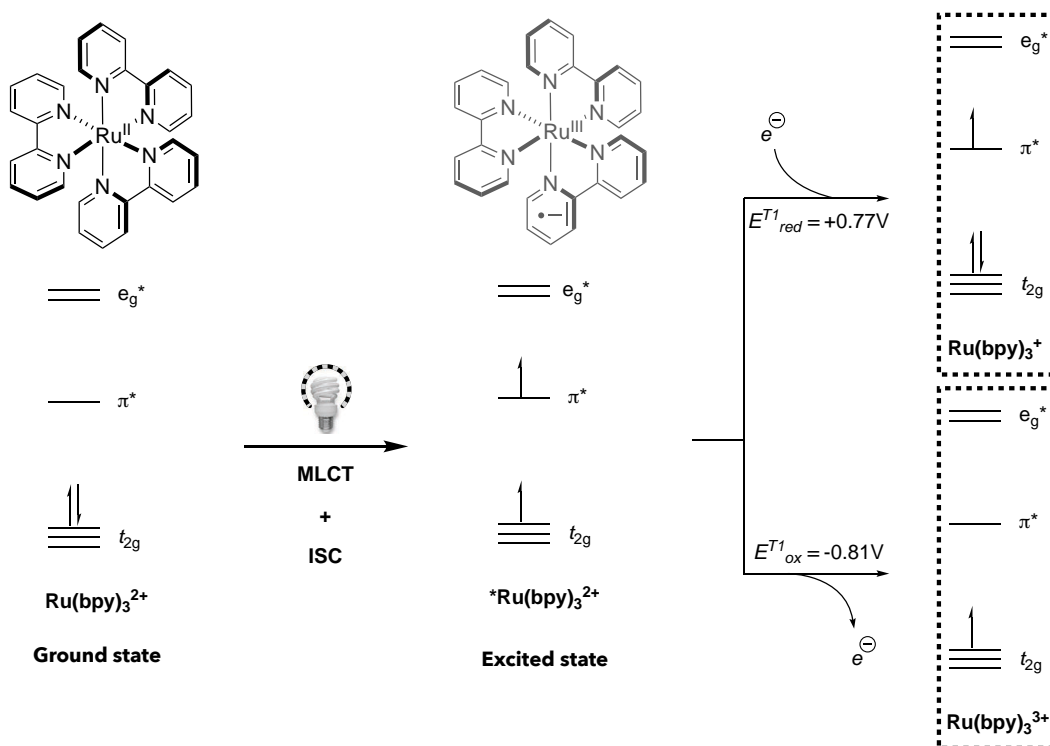
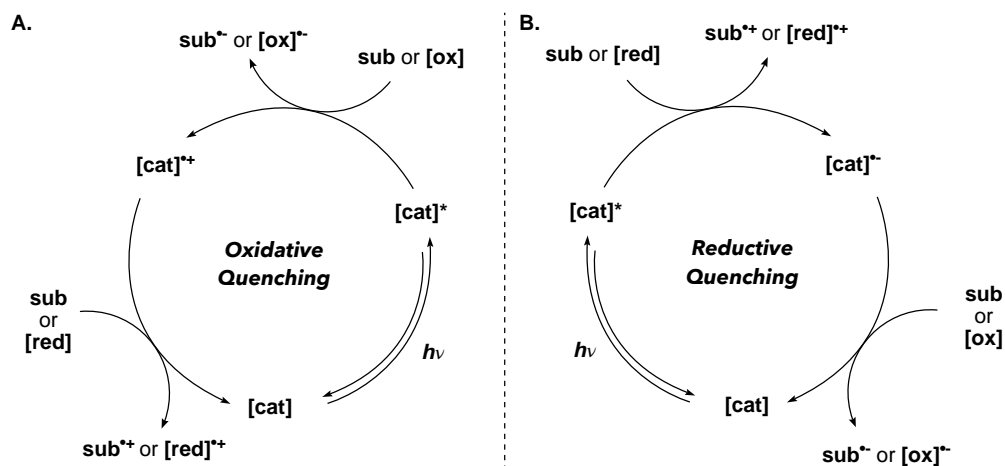


Figure 2.1

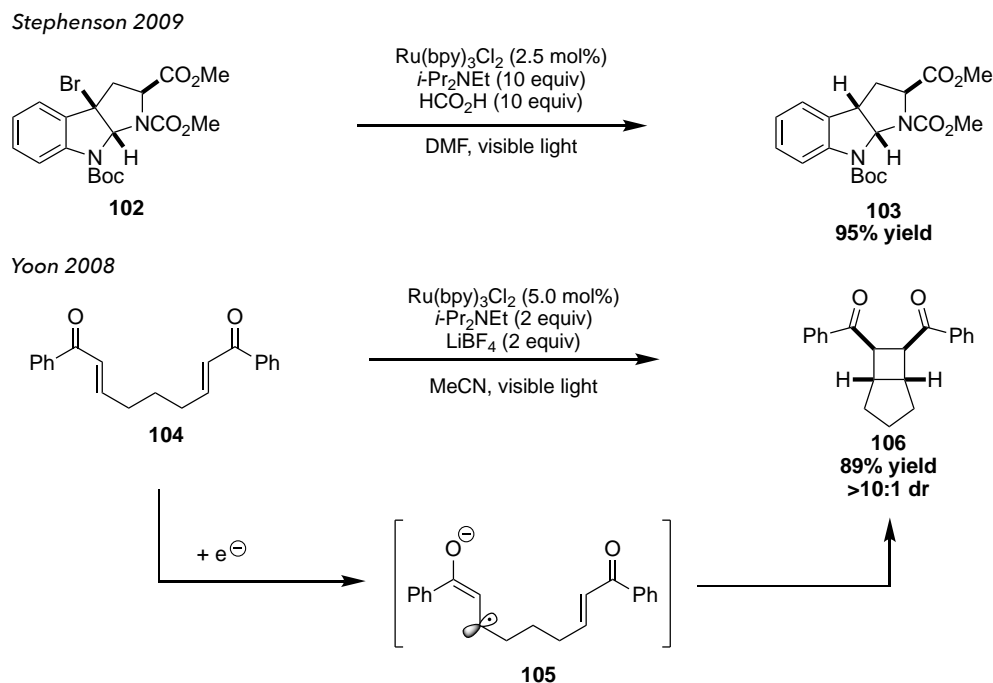
acceptor to convert into an oxidized form, $\text{Ru}(\text{bpy})_3^{3+}$. This is oxidative quenching, where the photocatalyst is oxidized and the organic substrate or an oxidant is reduced (Scheme 2.1B). To close the catalytic cycle, a substrate or reductant is oxidized by the oxidized photocatalyst.

The marked advantage of utilizing photoredox catalysis stems from the ability to have a catalytic amount of an oxidant or reductant in a reaction mixture at the same time, turned on by an external stimulus—visible light. In harnessing photoredox catalysis to generate these radicals in a catalytic, controlled fashion, new bond disconnections may be realized in the construction of valuable new C–H, C–C and C–X bonds. In 2009, the Stephenson group demonstrated a “tin-free” reduction of alkyl bromides to the corresponding C–H bond (Scheme 2.2).⁶ Bromide **102**, in the presence of $\text{Ru}(\text{bpy})_3\text{Cl}_2$, Hünig’s base, formic acid and visible light, undergoes reduction to form

103 in high yield. From a mechanistic perspective, the excited state photocatalyst $[\text{Ru}(\text{bpy})_3]^*$ is not a potent enough reductant to undergo oxidative quenching with **102**, but instead undergoes



Scheme 2.1



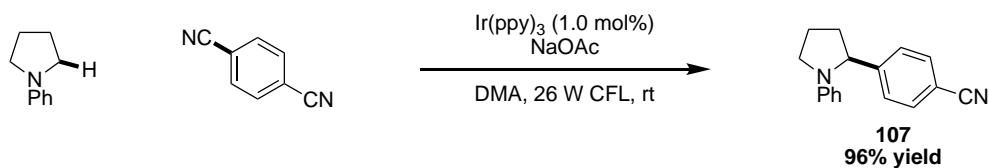
Scheme 2.2

reductive quenching with Hünig's base to form the reduced form of the photocatalyst. This $\text{Ru}(\text{bpy})_3^+$ species can now reduce the substrate to the radical anion, which quickly fragments to the alkyl radical and bromide anion. Abstraction of an H-atom from the resultant radical cation of

the amine base affords the desired product. Concurrently, the Yoon group demonstrated a photocatalyzed intramolecular [2+2] reaction of enones (Scheme 2.2).⁷ Also employing $\text{Ru}(\text{bpy})_3^{2+}$, they similarly use Hünig's base as a sacrificial reductant to access the more reducing $\text{Ru}(\text{bpy})_3^+$ species. This potent reductant can facilitate the formation of radical anion **105** from enone **104**, which undergoes cyclization to form product **106**.

An oxidative quenching cycle is also a common pathway that has been exploited to generate alkyl radicals. In 2011, the MacMillan group, who had previously employed photoredox catalysis in concert with organocatalysis⁸, reported a radical α -arylation of amines (Scheme 2.3).⁹ In the presence of a photoredox catalyst and light, *N*-phenylpyrrolidine is coupled to 1,4-dicyanobenzene in excellent yield. Mechanistically, the highly reducing iridium photocatalyst is proposed to reduce dicyanobenzene to the radical anion. The $[\text{Ir}]^{*+}$ species can then oxidize pyrrolidine to the amine radical cation, which acidifies the α -proton. Deprotonation affords the α -amino radical, which then undergoes radical-radical coupling to afford product **107**. The same product class can be accessed via a decarboxylative coupling of amino acids with arenes, also reported by the MacMillan group in 2014.¹⁰ Similarly, under these conditions, 1,4-dicyanobenzene is first reduced by the photoexcited iridium catalyst. The $[\text{Ir}]^{*+}$ species oxidizes the cesium carboxylate of proline to form a carboxy radical, which undergoes a rapid decarboxylation to afford the α -amino radical. Radical-radical coupling affords the arylated product (**108**). These examples highlight only two complementary methods for accessing similar reactive alkyl radicals. However, this arylation method relies on the reduction potential of the arene, thereby limiting applicable scope to electron deficient arenes or heteroarenes.

MacMillan 2011



MacMillan 2014

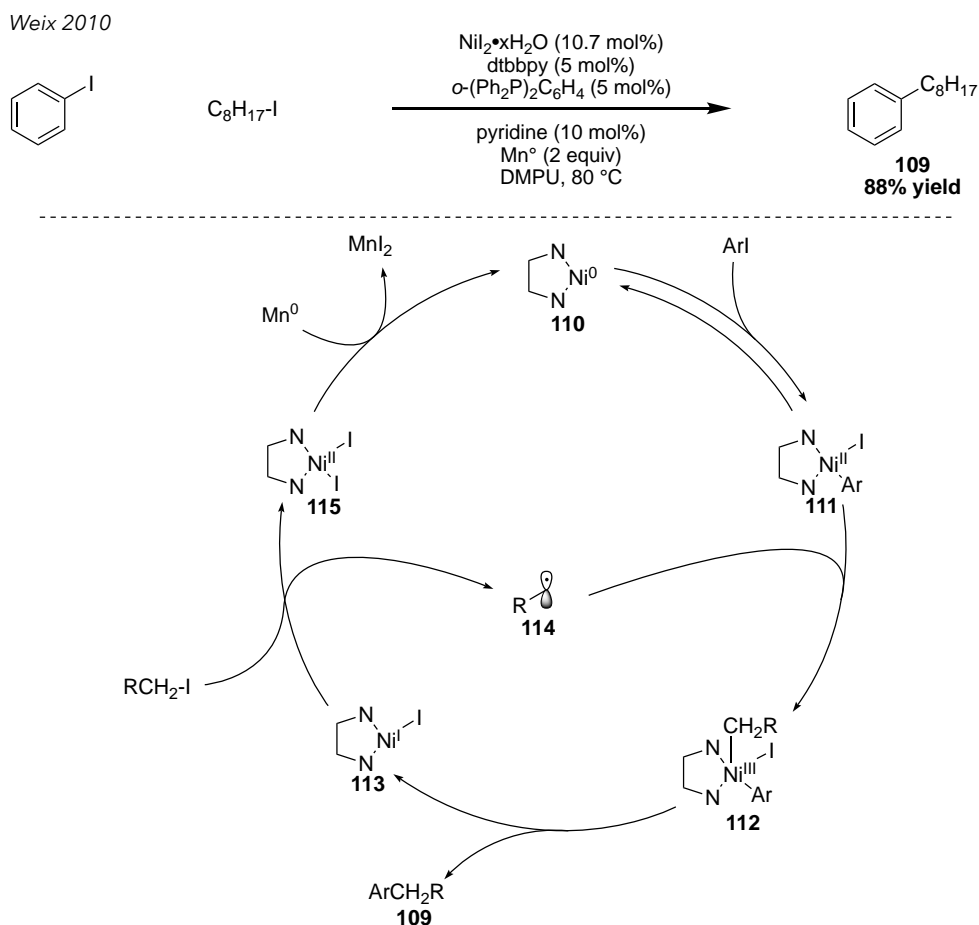


Scheme 2.3

2.1.2 Merging transition metal catalysis and photoredox catalysis

Transition metal catalysis offers a solution to the above challenge, having demonstrated generality with respect to aryl halide electrophile and various classes of two-electron nucleophiles. To push the boundaries beyond typical nucleophiles (such as boron, zinc, tin, and magnesium reagents), cross-electrophile couplings have been developed by the Weix and Fu groups, among others.¹¹ In 2010, the Weix group disclosed a nickel catalyzed cross-coupling of aryl and alkyl halides (Scheme 2.4). They envision a mechanism that commences with an oxidative addition into an aryl halide that would afford a nickel(II) adduct (**111**).¹² This nickel(II) adduct can be intercepted by an alkyl radical (generated by single-electron reduction of an alkyl iodide) to form nickel(III) adduct **112**. Reductive elimination from the high valent nickel species would forge the carbon–carbon bond of the product and a nickel(I) intermediate (**113**). This nickel(I) can reduce another equivalent of alkyl iodide to form the alkyl radical (**114**) and a nickel(II) iodide complex (**115**). Under reductive conditions with manganese, nickel(II) can be reduced to nickel(0) to restart the catalytic cycle. The key feature of this mechanism is the generation of an alkyl radical that can intercept a nickel(II) oxidative adduct. Presumably, this chemistry would be amenable to an array of different radical nucleophiles, that may be generated independently of the nickel catalytic cycle.

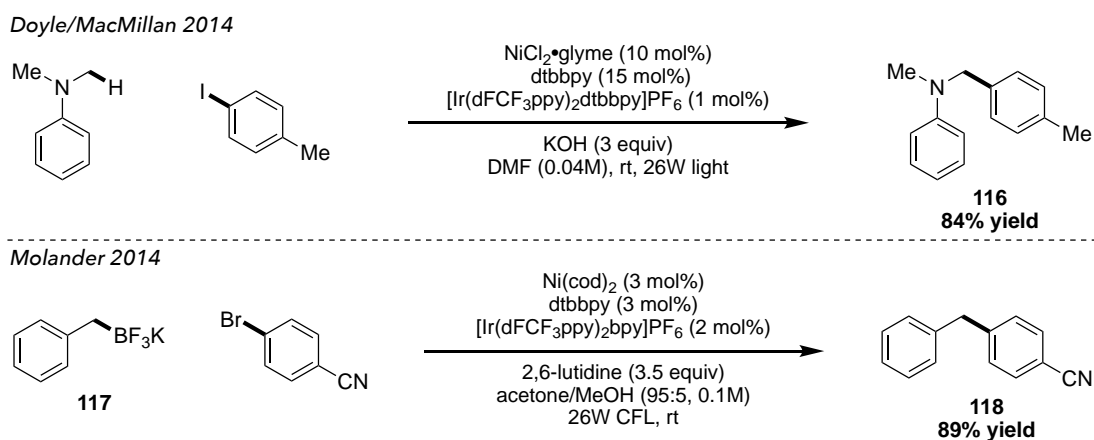
If alkyl radicals could be generated via a different route other than alkyl halides, it would expand the utility of this approach.



Scheme 2.4

In 2014, the Doyle group, in collaboration with the MacMillan group published a report merging the two concepts—photoredox and transition metal catalysis.¹³ In the report by Doyle/MacMillan, they first demonstrated a decarboxylative nickel catalyzed cross-coupling between amino acids and aryl bromides and iodides. Additionally, they disclosed the C–H nickel catalyzed cross-coupling of dimethyl aniline with aryl iodides (Scheme 2.5). In the latter example, it is proposed that the amine undergoes single-electron oxidation, followed by deprotonation to generate the α -amino radical. This radical is then merged into the nickel catalytic cycle to give the

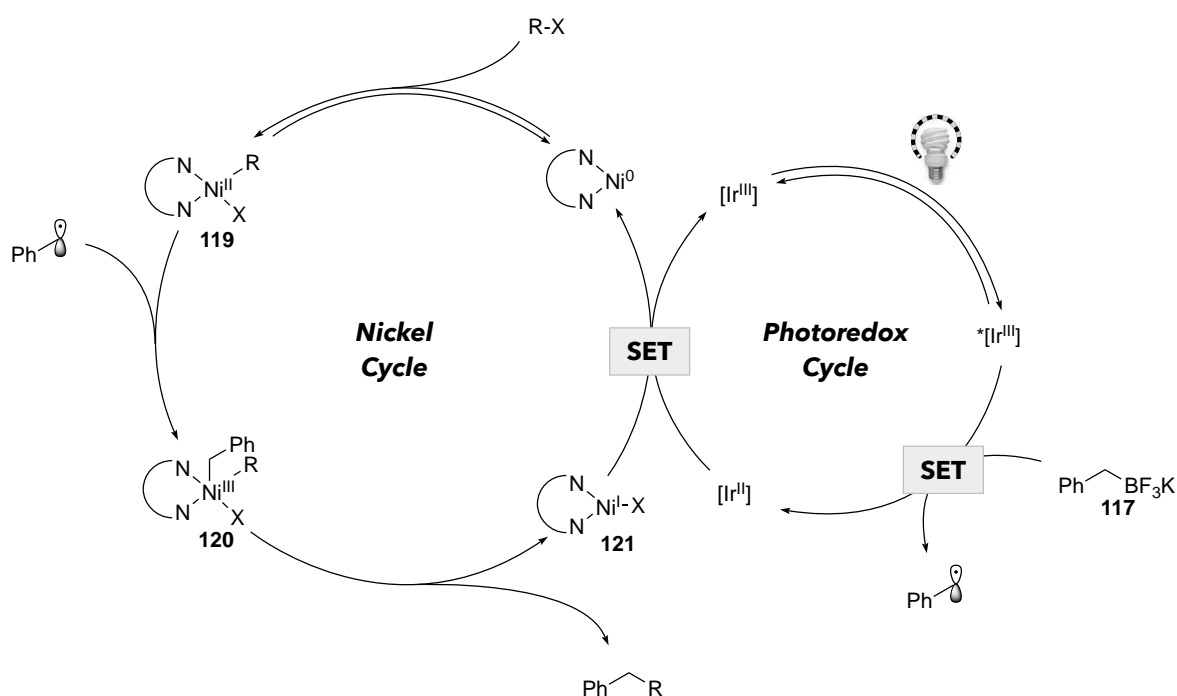
benzyl amine product (**116**). Concurrently, the Molander group developed a similar transformation utilizing benzylic trifluoroborates.¹⁴ Under their reaction conditions, they found that **117** could undergo single-electron oxidation with the photocatalyst to generate a benzylic radical, which was then coupled to the nickel catalytic cycle to produce the cross-coupled product (**118**). It is important to note the use of 2,6-lutidine in this reaction—it was proposed that the base was used to sequester BF_3 that was generated upon release from the trifluoroborate oxidation. Additionally, the use of an alcoholic solvent was essential for a high yielding reaction, likely for sequestering BF_3 .



Scheme 2.5

A more specific mechanistic picture is illustrated in Scheme 2.6. Photocatalyst $[\text{Ir}(\text{dFCF}_3\text{ppy})_2\text{bpy}]\text{PF}_6$, when irradiated with light $\{E_{1/2}^{\text{red}}[\text{Ir}^{\text{III}}/\text{Ir}^{\text{II}}] = +1.21 \text{ V vs. SCE}\}$ can induce single-electron oxidation of **117** $\{E_{1/2} = +1.11 \text{ V versus SCE}\}$ to form a benzyl radical and the reduced form of the photocatalyst, $\text{Ir}(\text{II})$. Concurrently, a $\text{Ni}(0)$ complex would undergo oxidative addition into an aryl bromide to generate $\text{Ni}(\text{II})$ complex **119**. The benzylic radical could then intercept **119** to generate a $\text{Ni}(\text{III})$ species (**120**) which would undergo rapid reductive elimination to generate the cross-coupled product and a $\text{Ni}(\text{I})$ species (**121**). Another SET event with the reduced state of the photocatalyst would regenerate $\text{Ni}(0)$ and the ground state of the photocatalyst.

The Molander group has proposed an alternative mechanism whereby the Ni(0) complex is intercepted by the benzylic radical to generate a Ni(I) intermediate.¹⁵ This Ni(I) species could then oxidatively add to the aryl halide to generate **120**, which would then follow the same catalytic cycle as previously discussed. Calculations from the Kozlowski group, in collaboration with the Molander group, suggest that once the Ni(0)/(I)/(III) and Ni(0)/(II)/(III) pathways converge on the same intermediate (**120**), and that reductive elimination is slower than the dissociation of the benzylic radical. This study suggests that for asymmetric transformations, reductive elimination may be the selectivity determining step, which would have important implications for reaction/catalyst design.

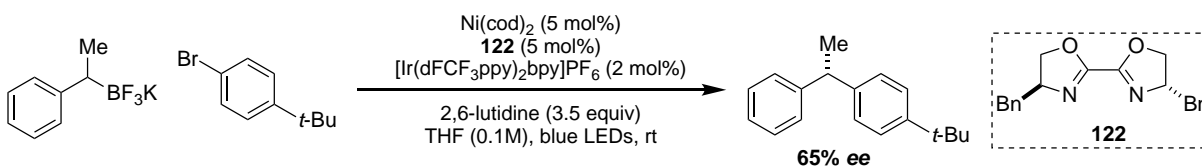


Scheme 2.6

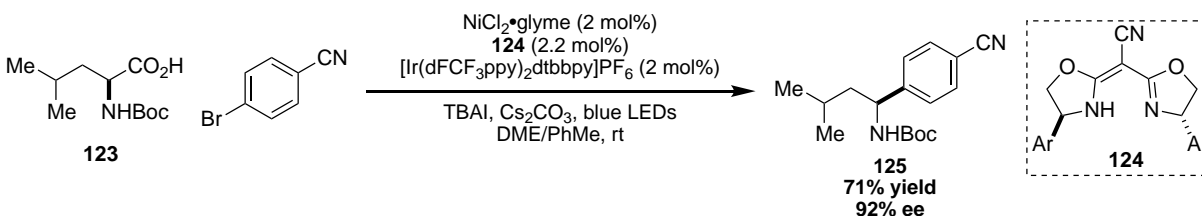
With reductive elimination as the selectivity-determining step, they proposed that the system would be under equilibrium and subject to Curtin-Hammett conditions with two diastereomeric transition states operative. Using their DFT calculations, Molander/Kozlowski tested their hypothesis experimentally, which predicted a steric interaction from the *para* substitution of the

aryl ring would disfavor the minor enantiomer. Experimentally they observed a trend consistent with their hypothesis, with the bulky *t*-butyl group affording the highest levels of enantioselectivity, and less bulky substituents, such as methyl, giving lower selectivity (62% *ee*) (Scheme 2.7). Other reports have capitalized on the combination of nickel and photoredox catalysis for asymmetric catalysis. The MacMillan group, in collaboration with the Fu group disclosed an enantioconvergent synthesis of amino acids and aryl halides to generate enantioenriched benzyl amines (Scheme 2.7).¹⁶ Amino acid **123**, in the presence of blue light and an iridium photocatalyst and base was oxidized to the prochiral α -amino radical. When the resultant radical was interfaced with nickel catalysis, employing semicorrin ligand **124**, they achieved a highly enantioselective formation of **125**. This example represents the first highly enantioselective enantioconvergent photoredox and nickel catalyzed cross-coupling reaction.

Molander/Kozlowski 2015



MacMillan/Fu 2016



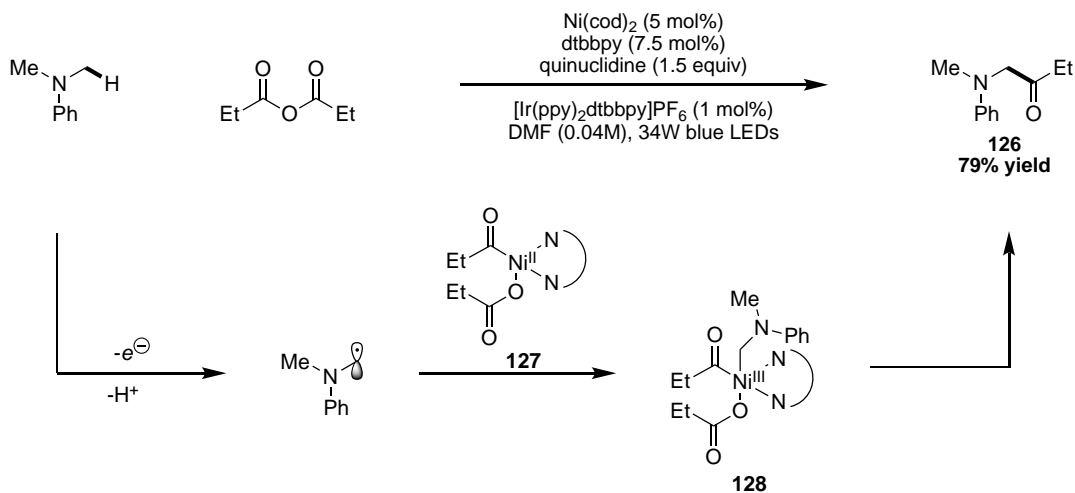
Scheme 2.7

2.2 Reaction design and initial results

After on their initial report C–H cross-coupling of tertiary amines and aryl halides utilizing nickel and photoredox catalysis, the Doyle group extended this reactivity to a more non-classical electrophile–acyl equivalents in place of aryl halides.¹⁷ Dimethyl aniline and propionic anhydride

were coupled in the presence of a nickel catalyst, photoredox catalyst and blue light (Scheme 2.8) to afford α -amino ketone **126**. Mechanistically, they proposed that dimethylaniline after single-electron oxidation and deprotonation by the base, would afford an α -amino radical. After Ni(0) oxidative addition into the anhydride to form **127**, the radical would intercept to form Ni(III) adduct **128**. Reductive elimination would release the product and generate a Ni(I) species which would be reduced by the photocatalyst to Ni(0). This transformation worked for numerous symmetric acyclic anhydrides, as well as other acyl equivalents such as thioesters.

Doyle 2016

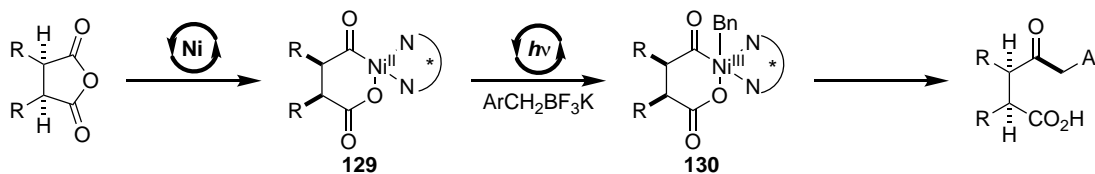


Scheme 2.8

Given the advances of photoredox catalysis, and the combination with transition metal catalysis, we envisioned that we could address the limitations of anhydride chemistry stated in Chapter 1. First, by employing photoredox catalysis, the nucleophile scope could be extended to carboxylic acids, tertiary amines, or alkyl trifluoroborates. Second, as demonstrated by the Molander, MacMillan and Doyle groups, alkyl radicals can be easily interfaced with nickel catalysis to construct new carbon–carbon bonds. Third, the use of an olefin additive may be circumvented by utilizing photoredox catalysis. Although the mechanistic evidence gathered by the Rovis group did not suggest that an olefin additive accelerated reductive elimination in the

anhydride desymmetriation,¹⁸ it was still essential for productive reactivity—its role proposed to be stabilizing catalytic intermediates. Furthermore, the additive had a clear effect on the selectivity of asymmetric transformations. Although in most cases the additive improved the selectivity, it could also limit the selectivity in other cases. We hypothesized that accessing a Ni(III) intermediate may completely obviate the need for olefin additives.^{19,20}

Our preliminary reaction design is demonstrated in Scheme 2.9. Analogous to the advances by the Rovis group, we proposed a stereoselective oxidative addition into a cyclic *meso* anhydride to generate adduct **129** by employing a nickel catalyst and chiral ligand. In the presence of a photoredox catalyst and light, benzylic trifluoroborates will undergo single electron oxidation to form benzylic radicals. The alkyl radical will intercept the oxidative adduct to form a Ni(III) adduct (**130**). Reductive elimination from Ni(III) should occur rapidly to form an enantioenriched keto-acid. Turnover of both catalytic cycles would occur via a second SET event between Ni(I) and the photocatalyst. We hypothesized that this catalytic cycle may obviate the need for an olefin promoter in the reaction by accessing different catalytic intermediates and the formation of a Ni(III) adduct should promote rapid reductive elimination. This may allow for a more successful application of asymmetric catalysis with the large number of chiral ligands that have shown success in nickel catalysis.

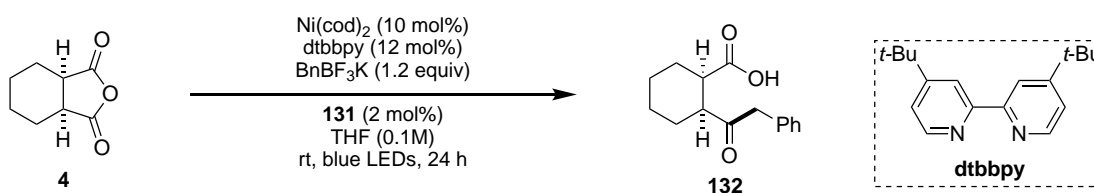


Scheme 2.9

To first demonstrate the feasibility of our reaction design, we chose succinic anhydride and benzyl trifluoroborate as the cross-coupling partners and under similar conditions to the Molander work, observed product formation by ¹H NMR. We chose to study the system under racemic

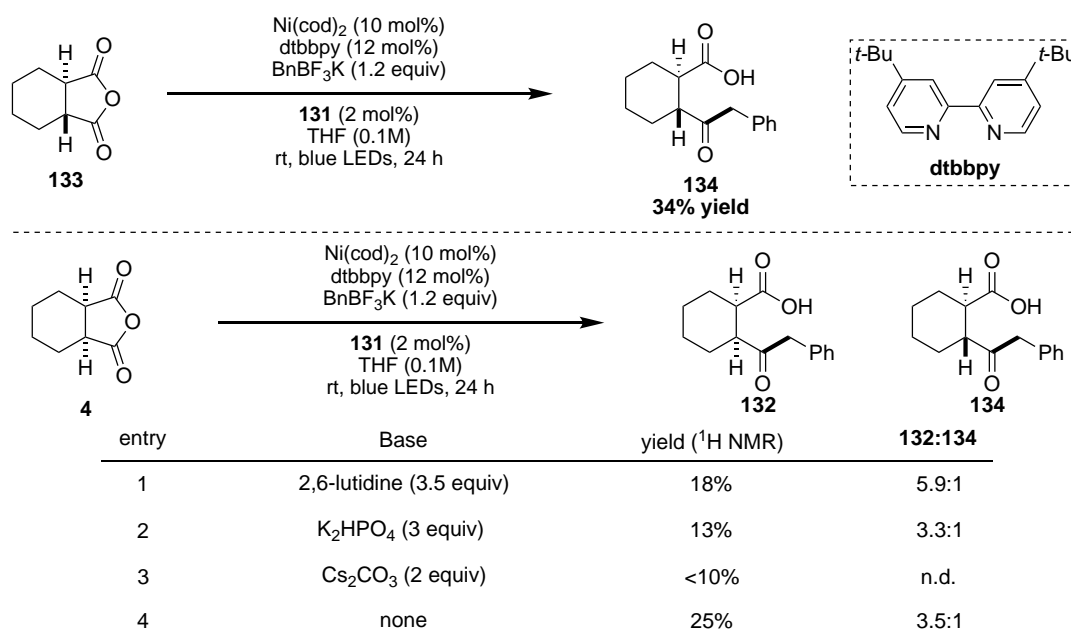
conditions with dtbbpy as the ligand to understand the system before moving to a more complicated asymmetric system. Employing anhydride **4**, in the presence of Ni(cod)₂-dtbbpy, benzyl trifluoroborate (**117**), commercially available iridium photocatalyst [Ir(dFCF₃ppy)₂dtbbpy]PF₆ (**131**) in THF at room temperature under irradiation with blue LEDs, we observed formation of keto-acid product **132** in 44% yield (Table 2.1 entry 1). This reaction lacked the 2,6-lutidine additive necessary in the Molander work, and under our reaction conditions, the addition of 2,6-lutidine does not affect reactivity (entry 2). Interested to see if an olefin additive would impact reactivity, we added a catalytic amount of *p*-CF₃-styrene (**5**), an additive which promoted reactivity with zinc reagents. However, under photoredox conditions, the yield is reduced by the addition of this additive (entry 3). Additives 2,6-lutidine and **5** together give slightly higher yield than **5** alone, but the addition of the olefin additive clearly has a negative effect on reactivity (entry 4). Preliminary control experiments—absence of light and photoredox catalyst, resulted in no product formation.

Table 2.1

		
entry	additive	yield (¹ H NMR)
1	none	44%
2	2,6-lutidine (3 equiv)	45%
3	<i>p</i> -CF ₃ -styrene (5) (20 mol%)	15%
4	2,6-lutidine and 5	24%

During our initial screening, we observed the formation of the *trans* diastereomer of the product. To confirm the identity of this product, we subjected anhydride **133** to the reaction conditions and observed 34% yield of the *trans* product (**134**) (Scheme 2.10). Interestingly, none

of the *cis* isomer (**132**) is observed in this reaction. The formation of *trans* product **134** in the reaction of *cis* anhydride was first observed during a base screen. In the presence of 2,6-lutidine a 5.9:1 ratio of **132**:**134** is observed (Scheme 2.10, entry 1). Using stronger inorganic bases reduces the yield and selectivity to 3.3:1 and 13% yield (entry 2). Decomposition is observed with the use of cesium carbonate as a base (entry 3). It seemed reasonable that the upon the formation of a nickel acyl species, and under photoredox conditions, the α -protons may be acidified and easily deprotonated, resulting in the *trans* product. However, in the absence of a base, formation of product **134** was still observed in a 3.5:1 ratio. A more thorough discussion of the epimerization event will be discussed in section 2.8.

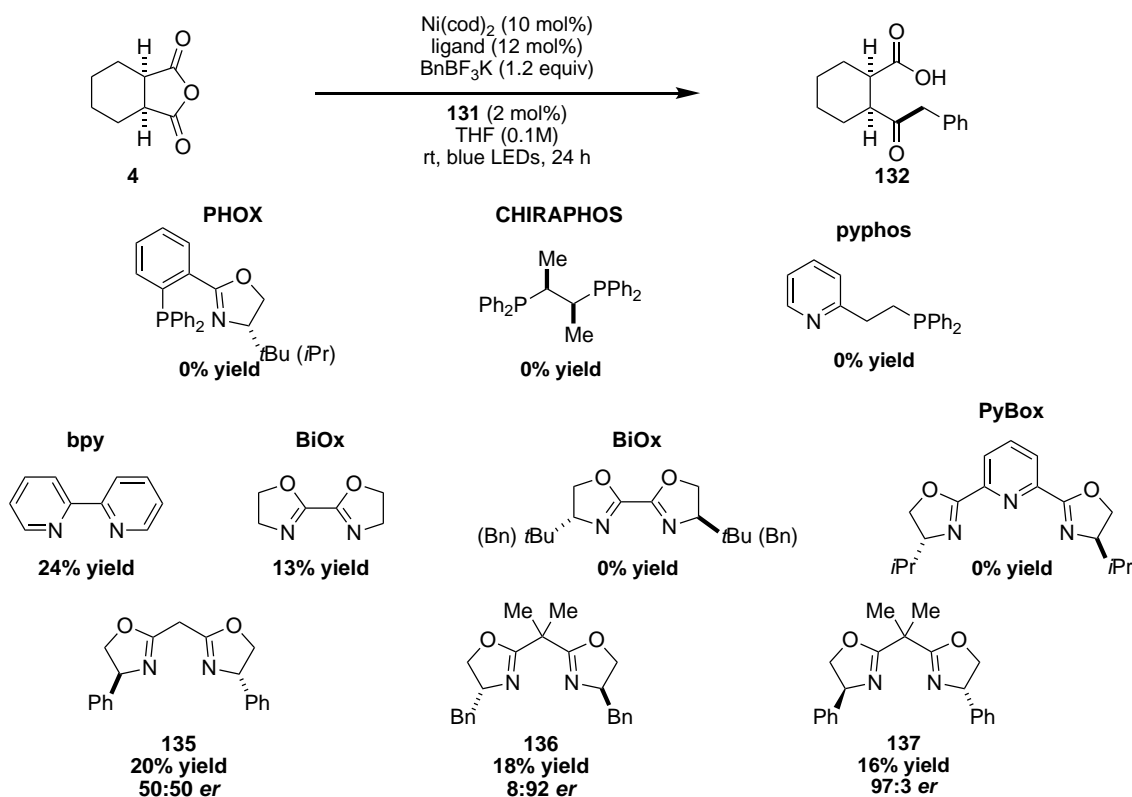


Scheme 2.10

2.3 Chiral ligand screening

We next sought to explore the asymmetric variant of this reaction by employing chiral ligands. We started with ligands that had proven most promising in the original reports of asymmetric desymmetrization under nickel catalysis. However, both PHOX type ligands and CHIRAPHOS

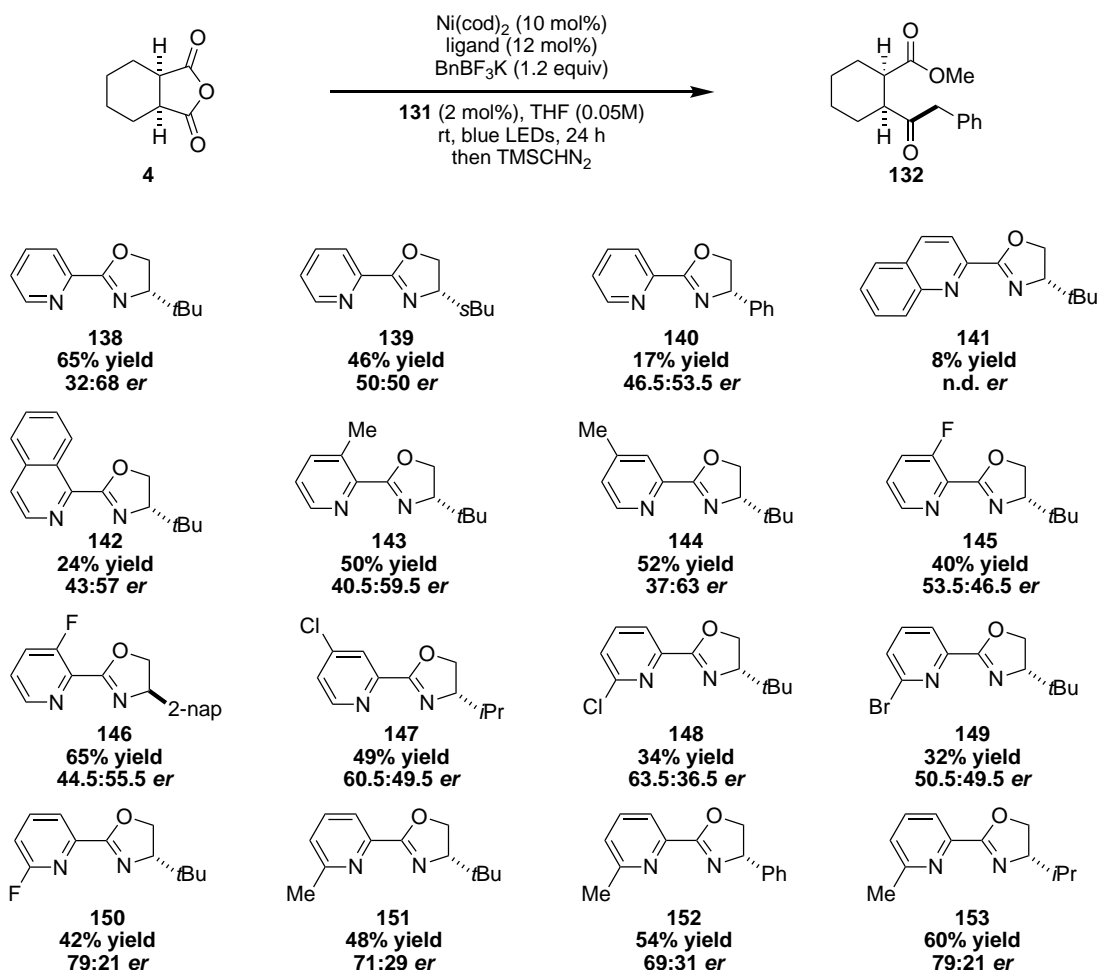
provided no product (Scheme 2.11). Pyphos, although not a chiral ligand, also did not provide any product under our standard reaction conditions. Switching to bpy or unsubstituted BiOx, however, did provide product in 24% and 13% yield, respectively. Any substitution on BiOx inhibited the reaction and substituted PyBox's were also unsuccessful at providing product. Box ligand **135** provided the product in 20% yield, albeit with no enantioinduction. Gratifyingly, however, when benzyl substituted Box **136** was used, the product was formed in 18% yield and 8:92 *er*. By exchanging the benzyl group for phenyl (**137**), the product was formed in 16% yield and 97:3 *er*!



Scheme 2.11

In addition to the success with Box ligands, we found that PyrOx ligands also appeared to be privileged ligand class for this transformation. We screened numerous PyrOx ligands under our standard reaction conditions (Scheme 2.12). Utilizing the parent PyrOx scaffold with *t*-Bu, *s*-Bu or Ph on the oxazoline ring (**138-140**) afforded the product in 17-65% yield, with modest

selectivity (50:50 – 32:68 *er*). Quinoline (**141**) or isoquinoline (**142**) with *t*-Bu substitution on the oxazoline ring gave lower yields and low selectivity (43:57 *er*). Methyl substitution at the 3- or 4-positions (**143-144**) provided the product in 50-52% yield but modest selectivity (40.5:59.5-37:63 *er*). Fluorine substitution at the 3-position (**145-146**) resulted in a flip of selectivity with either *t*-Bu or 2-naphthyl substitution on the oxazoline ring. The product was provided in good yield and low selectivity—40% yield and 53.5:46.5 *er* and 65% yield with 44.5:55.5 *er*. This change in selectivity to the other enantiomer does not appear to be steric-based, but must rely on the electronic substitution of the pyridine ring. Similarly, 4- and 6-chloro and 6-bromo pyridine



Scheme 2.12

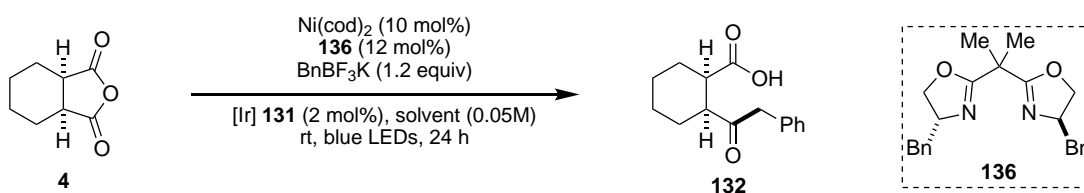
substituted oxazolines (**147-149**) provided the product in modest yield (32-49%) and modest selectivity (50.5:49.5 *er* – 63.5:36.5 *er*) again favoring the opposite enantiomer. Furthermore, switching to 6-substitution, either fluoro or methyl (**150-153**) gave a consistent change in selectivity to the opposite enantiomer, as well as giving the highest levels of selectivity. Despite the improved reactivity with these catalysts, based on the variety already tested and the high selectivity of the Box ligands, we chose to move forward with optimization of the asymmetric reaction with Box ligands.

2.4 Optimization of the asymmetric reaction

2.4.1 Iridium photocatalyst system

A concentration screen revealed 0.05M to be the ideal concentration (37% yield). We then chose to examine optimizing the reaction by conducting a solvent screen. In THF, using **136** as the chiral ligand, product **132** is formed in 35% yield and 10:90 *er* with a ratio of 5.2:1 *cis:trans* (Table 2.2 entry 1). Switching to DMF gives reduced yield and marked reduced selectivity (31:69 *er*)

Table 2.2

				
entry	solvent	yield (¹ H NMR)	132:134	<i>er</i> (<i>cis</i>)
1	THF	35%	5.2:1	10:90
2	DMF	22%	3:1	31:69
3	diethyl ether	13%	1:1	8:92
4	toluene	14%	1.2:1	6.5:93.5
5	PhCF ₃	31%	4:1	33:67
6	THF/PhCF ₃ (19:1)	40%	4:1	9.5:90.5

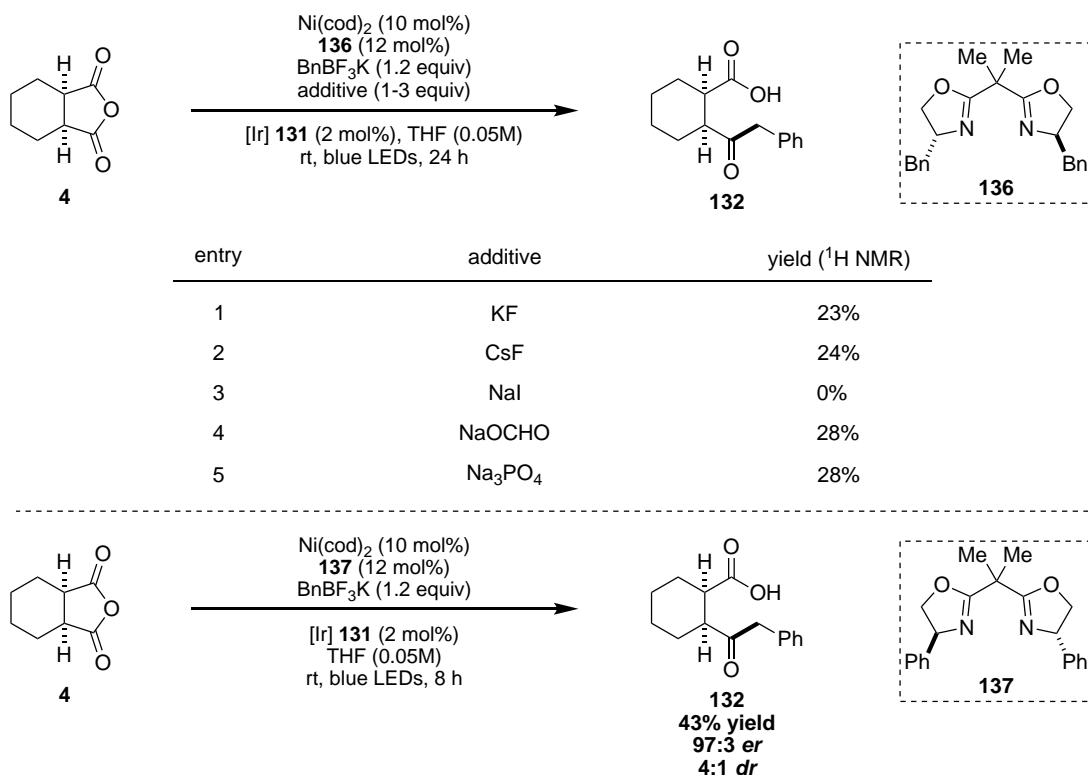
(entry 2). Diethyl ether and toluene both give low yields and low diastereoselectivity (1:1 *cis:trans*), but improved enantioselectivity (entries 3 and 4). While α,α,α -trifluorotoluene (PhCF₃)

gives the product in modest yield and diastereoselectivity, but reduced enantioselectivity (entry 5). PhCF₃ has been used previously as a promoter in nickel catalysis, to accelerate reductive elimination, although it is not as proficient as olefins.^{21,22} However, a mixed solvent system of THF/PhCF₃ gives improved yield and restored selectivity (9.5:90.5 *er*) (entry 6).

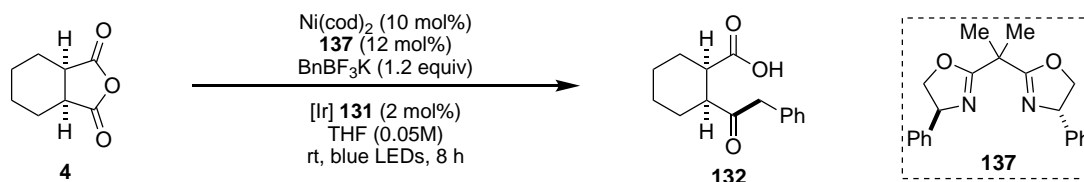
Despite continued optimization efforts, we found that improving the yield was challenging, although selectivity remained constant. We hypothesized that one of the products or byproducts of the reaction may be inhibiting the reaction. When benzoic acid was added to the reaction to probe whether product formation was inhibiting the reaction, we observed reduced yield. However, we were hesitant to treat this result as meaningful, as the product in the reaction is a carboxylate and not a carboxylic acid. We treated tetrahydrophthalic anhydride (**22**) under the standard reaction conditions with 1 equivalent of product **132** and observed product formation. When we added BF₃•OEt₂ to the reaction to mimic the formation of BF₃ from the oxidation of the trifluoroborate we observed no product formation.

In the original report by Molander and coworkers, they employ 2,6-lutidine as a sequestration agent for BF₃ while under our standard reaction conditions, we have no base or additive to serve that role. Therefore, we sought to examine different base additives to sequester BF₃. The addition of fluoride additives afforded the product (**132**) in slightly reduced yield relative to standard conditions (Table 2.3, entries 1-2). Sodium formate and sodium phosphate tribasic gave nearly comparable yields to the standard reaction conditions (entries 4-5). Although we had previously optimized the reaction with ligand **136**, employment of ligand **137** gives improved yield and maintained 97:3 *er*.

Table 2.3

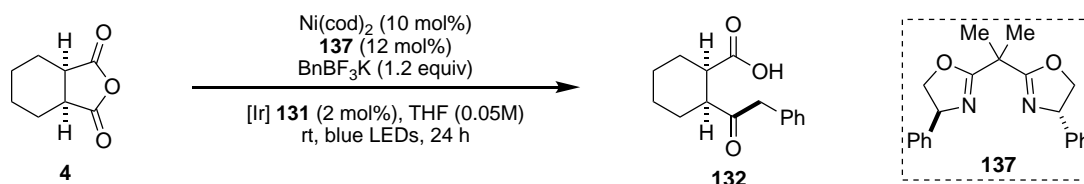


We suspected that in the absence of product or byproduct inhibition, catalyst decomposition may be responsible for the modest yields observed. We ran a series of experiments to test this hypothesis. Under our standard reaction conditions, with all components added at the beginning of the reaction, after 24 h we observed 40% yield of product (**132**) (Table 2.4, entry 1). When 5 mol% of nickel catalyst was added initially and then an additional 5 mol% added at 8 h (10 mol% total), we observed reduced product yield (34%) (entry 2). Interestingly, when we ran the same experiment, but with only 1 mol% $[\text{Ir}]$ at time zero and 1 mol% added after 8 h, we observed restored reactivity (entry 3). The addition of half of the trifluoroborate at time zero and then half at 8 h gave identical results to the standard conditions (entry 4).

Table 2.4

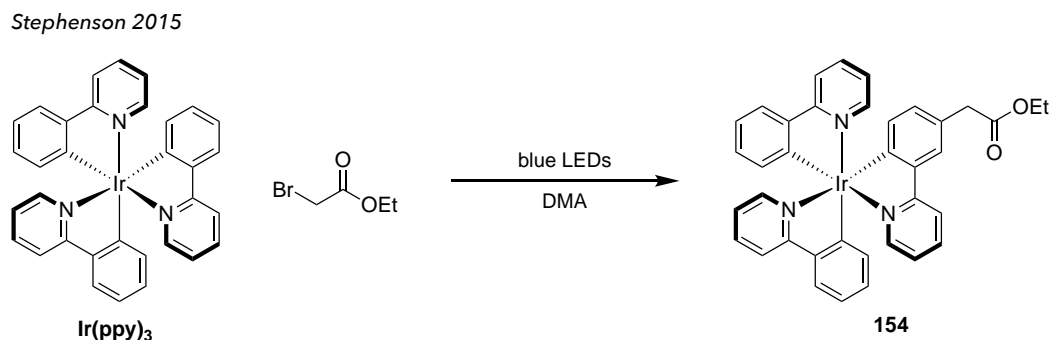
initial loadings				added at 8 h			yield (¹ H NMR)
entry	Ni/ligand	[Ir]	BnBF ₃ K	Ni/ligand	[Ir]	BnBF ₃ K	
1	10 mol%	2 mol%	1.2 equiv	0	0	0	40%
2	5 mol%	2 mol%	1.2 equiv	5 mol%	0	0	34%
3	5 mol%	1 mol%	1.2 equiv	5 mol%	1 mol%	0	40%
4	10 mol%	2 mol%	0.6 equiv	0	0	0.6 equiv	41%

We continued these control experiments in Table 2.5. Under standard reaction conditions we observed 43% yield (Table 2.5, entry 1). Keeping nickel catalyst loading constant and adding 1 mol% [Ir] at time zero and 1 mol% at 8 h gives a comparable yield of **132** to the standard conditions (entry 2). However, if we added 5 mol% nickel catalyst and 1 mol% [Ir] at 8 h, we observed an improved yield to 50% yield. Adding half the [Ir] and the trifluoroborate initially and the remainder at 8 h gives comparable yield to standard reaction conditions.

Table 2.5

initial loadings				added at 8 h			yield (¹ H NMR)
entry	Ni/ligand	[Ir]	BnBF ₃ K	Ni/ligand	[Ir]	BnBF ₃ K	
1	10 mol%	2 mol%	1.2 equiv	0	0	0	43%
2	10 mol%	1 mol%	1.2 equiv	0	1 mol%	0	39%
3	10 mol%	1 mol%	1.2 equiv	5 mol%	1 mol%	0	50%
4	10 mol%	1 mol%	0.6 equiv	0	1 mol%	0.6 equiv	36%

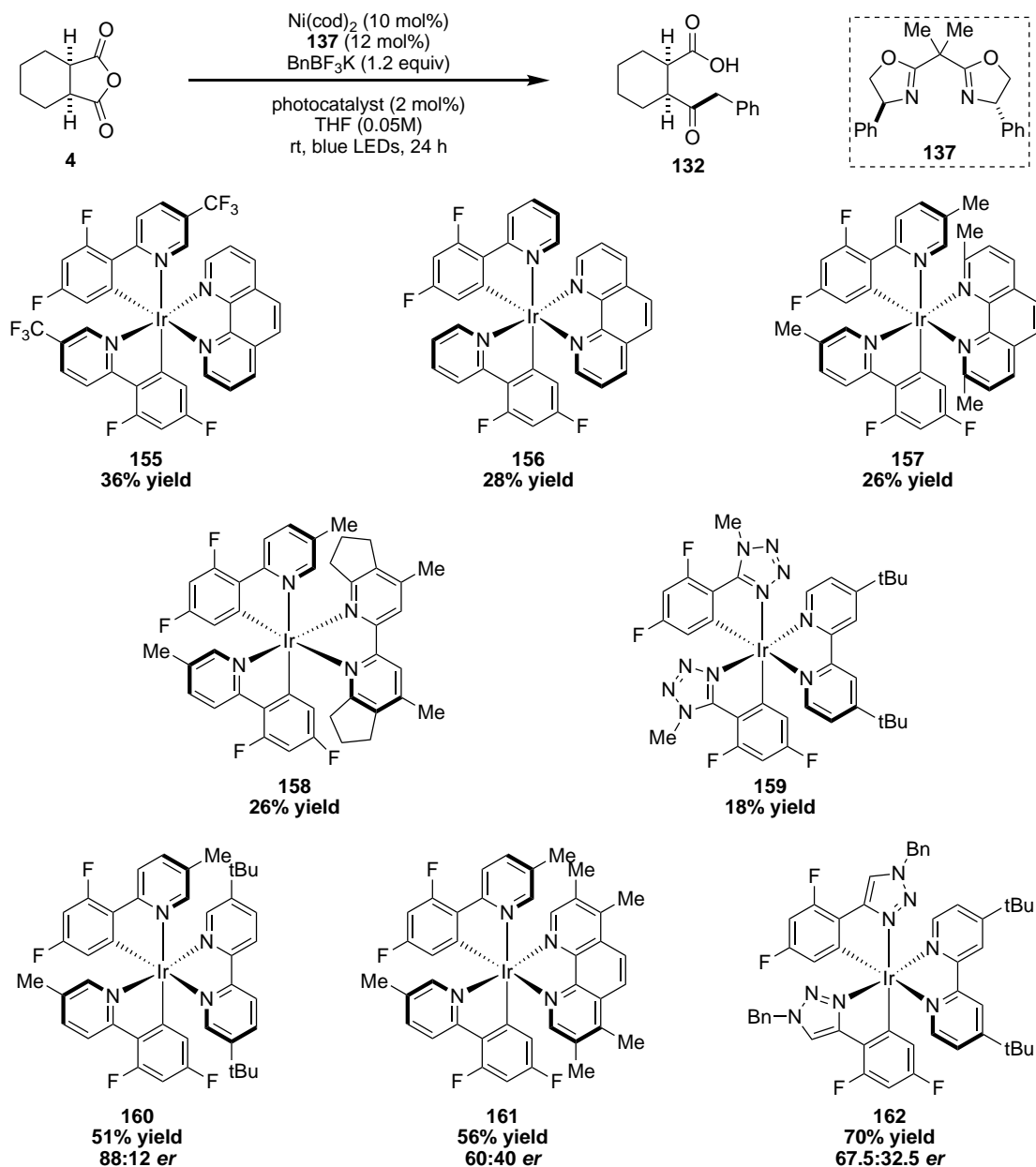
Based on these control experiments, we hypothesized that either the photocatalyst or nickel catalyst, or both, may be decomposing over the course of the reaction. Adding additional nickel catalyst without [Ir] does not improve reaction yields; however, adding additional [Ir] with nickel catalyst results in a boost in yield. The Stephenson group previously reported photocatalyst deactivation via alkylation (Scheme 2.13).²³ In the presence of ethyl bromoacetate and blue LEDs, Ir(ppy)₃ is alkylated via the radical that is generated after single electron reduction to provide **154**. While this complex is competent as a photocatalyst in their test reaction, it quickly decomposes to another product which is not a competent photocatalyst. The repeated radical functionalization of the phenyl pyridine ligands of the photocatalyst will ultimately turn off catalysis. Additionally, the König group has identified alternative deactivation pathways, such as quenching via singlet oxygen.²⁴ The Stephenson group demonstrated that blocking certain position on the phenyl pyridine ring may inhibit catalyst deactivation.



Scheme 2.13

With the hypothesis that the photocatalyst may be decomposing or deactivated during our reaction, we sought to investigate other photocatalysts that may be less predisposed to this radical alkylation pathway (Scheme 2.14). With catalyst **155**, where the dtbbpy ligand is exchanged for phenanthroline, the yield is comparable to our standard reaction conditions. Removal of the CF₃ group from the phenyl pyridine ligand gives reduced yield of product **132** and replacing it with

methyl gives similar results. Use of a phenyl tetrazole ligand on Ir (**159**) which should slow down alkylation, is also ineffective at improving the efficiency of our reaction. Photocatalyst **160**, however, affords the product in improved yield (51%) but reduced enantioselectivity.



Scheme 2.14

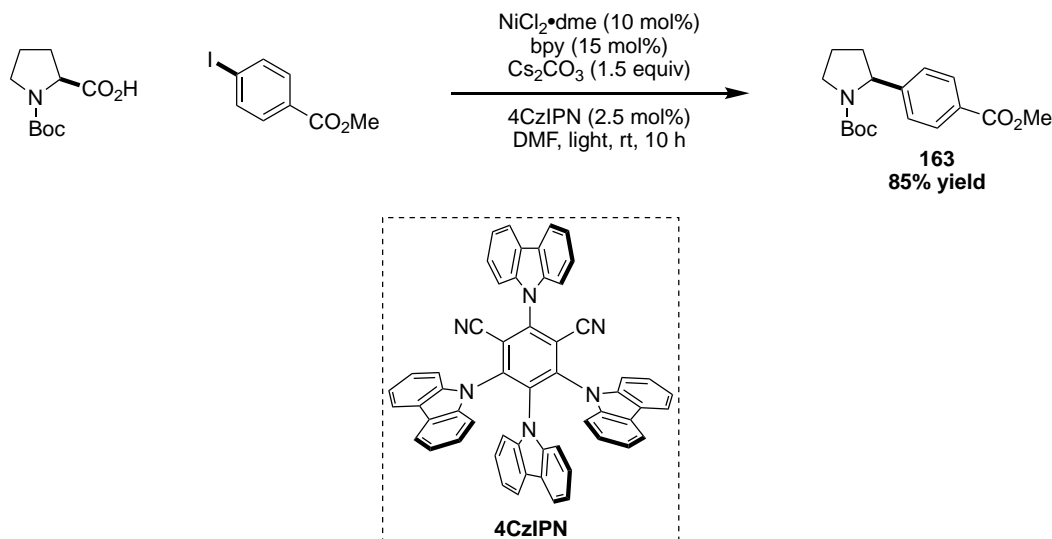
Exchanging the bipyridine ligand to a substituted phenanthroline (**161**) improved the yield further to 56% yield, but even further reduced the selectivity of the transformation. Photocatalyst **162**

improved reaction efficiency to synthetically useful levels, but the enantioselectivity was still eroded relative to [Ir] **131**. The shift in enantioinduction based on photocatalysts is an unusual phenomenon, although the presence of exogenous bipyridine ligand cannot be discounted as an explanation.

2.4.2 4CzIPN and final optimizations

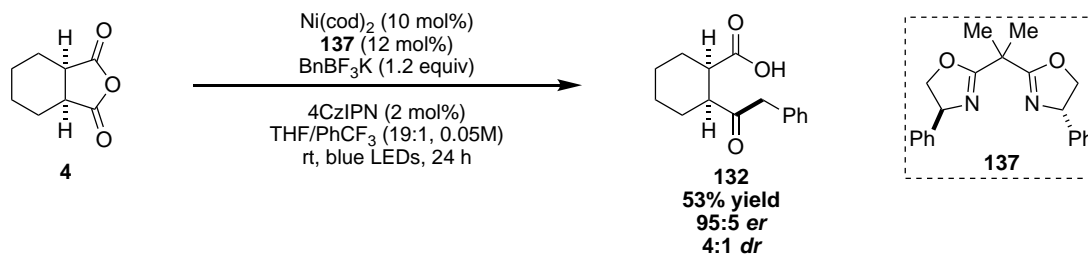
In 2016, the Zhang group reported the use of an organophotoredox catalyst with similar potentials to [Ir] **131**.²⁵ Part of the goal was to single out a photocatalyst that would not be prone to alkylation and decomposition. They demonstrated that 4CzIPN can be used in place of iridium photocatalyst for the nickel catalyzed cross-coupling of carboxylic acids with aryl iodides to form benzyl substituted amines (**163**) (Scheme 2.15). In their study, they found that they could recover the photocatalyst in >50% upon completion of the reaction. Furthermore, they showed that trifluoroborates were functional radical precursors in nickel catalyzed cross-couplings, and with its higher oxidation potential, 4CzIPN could oxidize propyl trifluoroborate to the corresponding radical.

Zhang 2016



Scheme 2.15

We sought to replace the [Ir] **131** based photocatalyst in our standard reaction conditions with 4CzIPN (Scheme 2.16). Under our standard reaction conditions, with PhCF₃ as a co-solvent, we observed increased yield of the desired product with excellent enantioselectivity (95:5 *er*) and identical diastereoselectivity (4:1 *dr*). After this initial result, we examined nickel loading as an optimization parameter (Table 2.6). Under our standard reaction conditions, we observed 48%



Scheme 2.16

Table 2.6

entry	Ni(cod)_2	137	4CzIPN	yield (LCMS)	<i>er</i> (<i>cis</i>)
1	10 mol%	12 mol%	2 mol%	48%	n.d.
2	10 mol%	12 mol%	1 mol%	27%	97:3
3	10 mol%	12 mol%	4 mol%	56%	85.5:14.5
4	15 mol%	18 mol%	2 mol%	40%	97:3
5	5 mol%	6 mol%	2 mol%	53%	86:14
6	2.5 mol%	3 mol%	2 mol%	64%	72:28

yield of desired product **132** (entry 1). Decreasing the photocatalyst loading while keeping nickel catalyst loading constant, we observed a decrease in yield, but a slight increase in enantioselectivity (97:3 *er*) (entry 2). Increasing the photocatalyst loading has the opposite effect, giving improved yields but decreased selectivity (85.5:14.5 *er*) (entry 3). Increasing the nickel loading did not give improved yields as expected, but rather a 10% loss of yield while maintaining

selectivity (entry 4). Decreasing the nickel loading to 5 mol% gave a slight boost in yield, but had a negative impact on enantioselectivity (86:14 *er*) (entry 5). Surprisingly, decreasing nickel loading even further to 2.5 mol% gives a significant increase in yield and the product is observed as a single diastereomer (no **134** was observed by NMR or HPLC) (entry 6).

With improved yields at lower nickel loading, we sought to continue optimization based on these new results. We next conducted a solvent screen, and found that PhCF₃, while an effective co-solvent, gave decreased yields when used alone (Table 2.7 entry 1). Diethyl ether and toluene gave comparable yields and selectivities to our standard reaction conditions (entry 2 and 3). Dioxane gave improved yield, but comparable enantioselectivity (entry 4). DMA, DMF, acetone

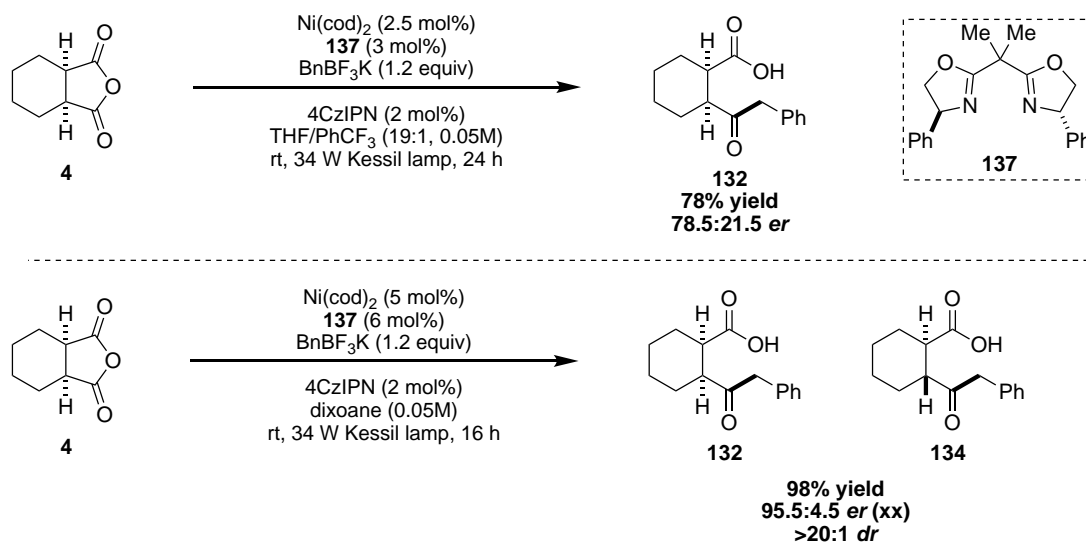
Table 2.7

entry	solvent	yield (LCMS)	<i>er</i> (<i>cis</i>)
1	PhCF ₃	51%	n.d.
2	diethyl ether	67%	70.5:29.5
3	toluene	60%	76:24
4	dioxane	77%	74:26
5	DMA	13%	n.d.
6	DMF	<10%	n.d.
7	acetone	<10%	n.d.
8	MeCN	<10%	n.d.

and MeCN were ineffective as solvents, giving the product in <15% yield (entries 5-8). The decrease in enantioselectivity that we were observing was troubling, as the selectivity had been constant throughout our optimizations with the [Ir] **131** photocatalyst. We ran a “ligand-less” reaction (without **137**) and were surprised to see product **132** formed in about 10% yield. We

hypothesized that this racemic background reaction could be responsible for our loss of enantioselectivity, and at lower nickel loadings, may be more prevalent.

Up until this point, we had been conducting all reactions in the presence of blue LED's (22 W). While these are effective for ascertaining reactivity, we questioned whether a more intense light source may promote our desired reaction, as many nickel catalyzed photoredox reactions have been demonstrated to be photon-limited.²⁶ Gratifyingly, when we switched to a 34 W blue LED (Kessil lamp) we observed a significant increase in yield and a slight increase in diastereoselectivity (Scheme 2.17) When we doubled the nickel catalyst loading, **132** is observed in 69% yield, 94:6 *er*, and 8:1 *dr*. Under those conditions, when we increased our reaction scale to 0.1 mmol (from 0.05 mmol) we observed the product in 81% yield and 89.5:10.5 *er*. Finally, switching from THF to dioxane and the omission of PhCF₃ as a co-solvent affords the product in 98% yield, 95.5:4.5 *er*, and >20:1 *dr*.



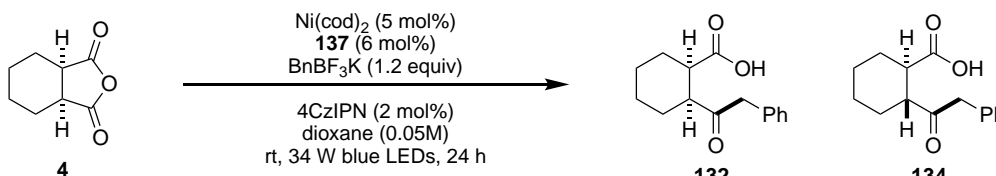
Scheme 2.17

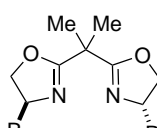
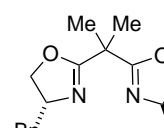
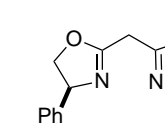
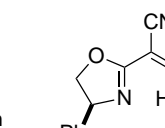
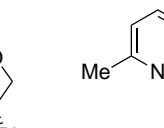
2.4.3 Control reactions and mechanistic hypothesis

Before commencing with scope, we wanted to confirm our mechanistic hypothesis with control reactions. Under our standard reaction conditions at 0.1 mmol scale, we observed the formation of

product **132** in 85% yield and 95:5 *er* (Table 2.8, entry 1). Reactions run in the absence of nickel, light or photocatalyst did not result in any product formation (entries 2-4). In the absence of ligand, we do observe a small racemic background reaction in 7% yield (entry 5). We examined additional Box ligands (**164** and **136**) and found that while they provided product, they did not give high

Table 2.8

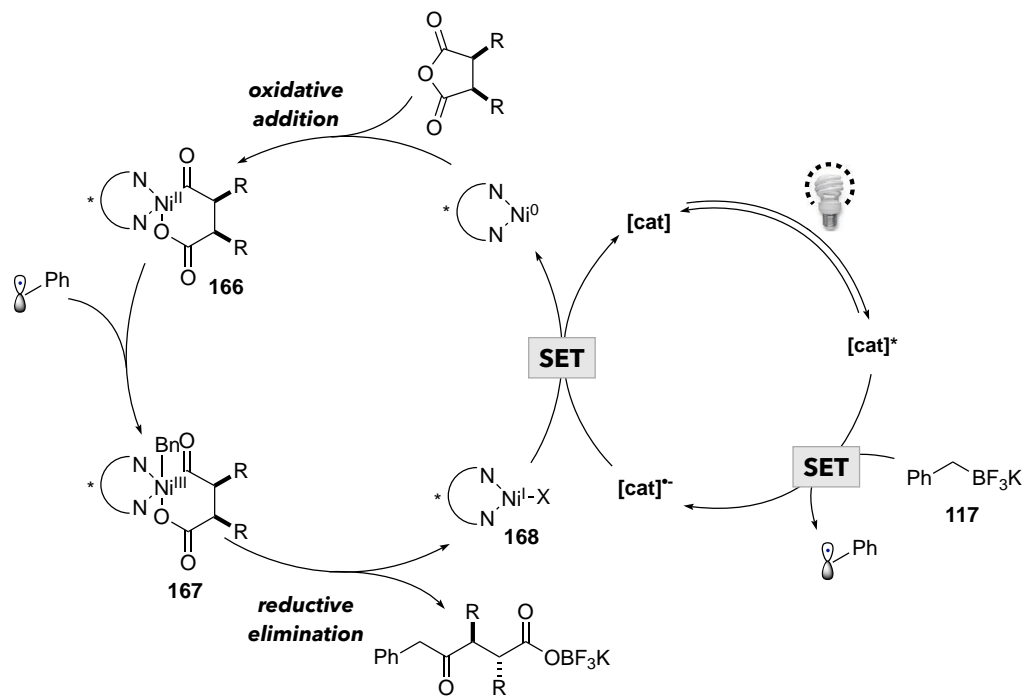
			
entry	deviation from standard conditions	yield (¹ H NMR)	<i>er</i> (<i>cis</i>)
1	none	85%	95:5
2	no nickel	0%	n.d.
3	no light	0%	n.d.
4	no photocatalyst	0	n.d.
5	no ligand	7%	n.d.
6	ligand 164	25%	72.5:27.5
7	ligand 136	71%	28.5:71.5
8	ligand 135	83%	94.5:5.5
9	ligand 165	8%	51:49
10	ligand 151	65%	70:30
11	NiCl ₂ •glyme	64%	66:34
12	[Ir(dFCF ₃ ppy) ₂ dtbbpy]PF ₆ (131)	43%	89:11
13	[Ir] 131 , THF (0.05M)	45%	97:3

				
R = Ph (137) R = <i>t</i> Bu (164)	136	135	165	151

levels of selectivity (entry 6-7). Interestingly, when Box ligand **135** is used in the reaction, the product is formed in high yield and selectivity (entry 8). This is contrary to our original ligand screening when ligand **135** provided the product in 50:50 *er*. This is most likely due to an impurity in the HPLC over the minor enantiomer giving a false negative result. Semicorrin ligand **165** gives

the product in low yield with no selectivity (entry 9). PyrOx ligand **151**, which had previously given the best results of that class gave the product in good yield, but modest selectivity (entry 10). Using air-stable precatalyst $\text{NiCl}_2\cdot\text{glyme}$ affords the product in good yield, but eroded selectivity (entry 11). Use of the [Ir] (**131**) photocatalyst continued to give modest yields and even reduced selectivity in dioxane; in THF, however, the selectivity was restored to 97:3 *er* (entry 12 and 13).

Our proposed mechanism is depicted in Scheme 2.18. The photocatalyst (4CzIPN: [cat]), when irradiated with blue light produces a long-lived triplet excited state and may engage in single-electron oxidation of benzyl trifluoroborate to generate a benzyl radical and the radical anion of the photocatalyst. At the same time, the Ni(0) complex could undergo oxidative addition into the cyclic-*meso* anhydride to generate complex **166** and is likely the stereoselectivity-determining step



Scheme 2.18

(see later sections for a more thorough discussion). The benzyl radical can intercept the Ni(II) adduct to generate Ni(III) complex **167**, which should undergo rapid reductive elimination to generate **168** and the desired keto-carboxylate product. A second SET event between the reduced

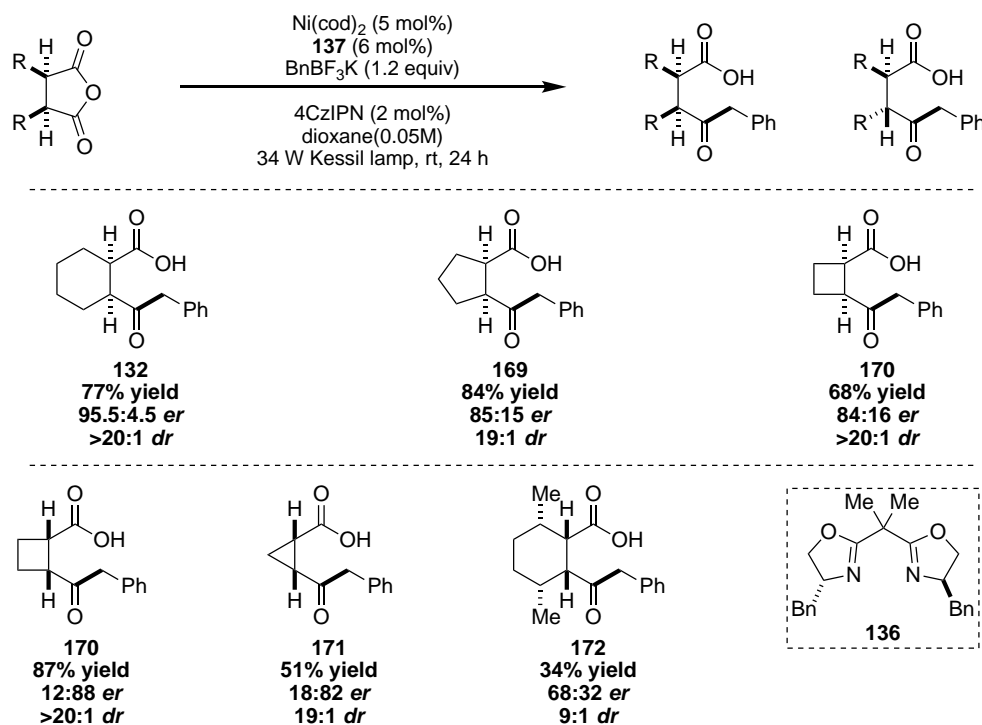
form of the photocatalyst and Ni(I) gives the Ni(0) complex and ground state of the photocatalyst. This mechanistic cycle shares a similarity to the original anhydride chemistry, with oxidative addition at Ni(0) to form a Ni(II) adduct.

We propose that the carboxylate product is responsible for sequestering BF₃. This is important for two reasons: first, no additional base additive is required for reactivity, as was originally observed by Molander. Second, there has been extensive work regarding decarboxylative cross-couplings and other C–C bond formations under similar conditions.^{27,28} However, under our conditions we do not observe any significant formation of the decarboxylated product. We propose that the tight complexation of the BF₃ carboxylate prevents single-electron oxidation of the carboxylate.

2.5 Scope of enantioselective desymmetrization reaction

2.5.1 Anhydride scope

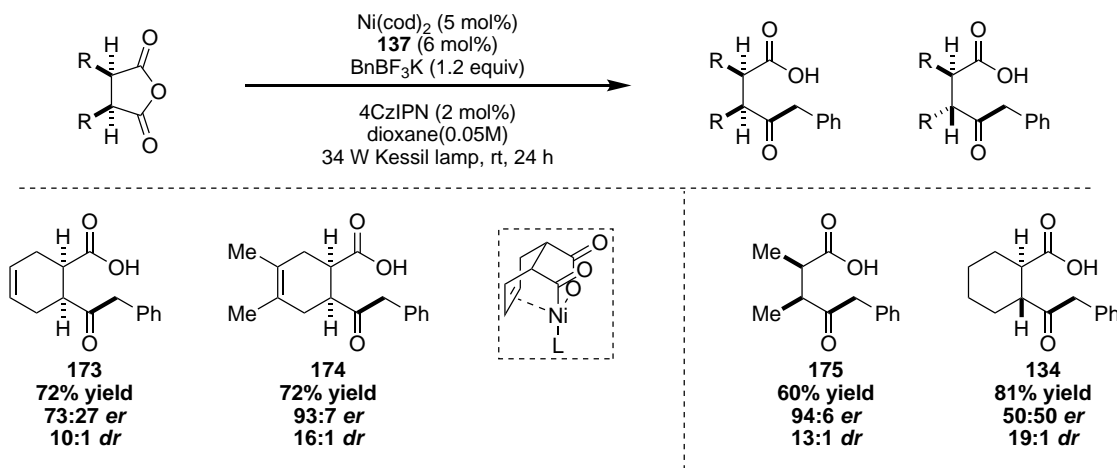
With the optimized conditions in hand, we sought to explore the scope of anhydrides amenable to this reaction using benzyl trifluoroborate as the radical precursor. Under our optimized conditions at 0.25 mmol scale, we isolated **132** in 77% yield 95.5:4.5 *er* and >20:1 *dr* (Scheme 2.19). Smaller ring sizes, such as 5-membered rings also afford the product (**169**) in good yield, albeit reduced stereoselectivity. Cyclobutane substrate **170** is provided in comparable selectivity, but reduced yield under the standard reaction conditions. Through the course of our optimizations, we discovered that ligand **136** worked better with smaller ring sizes. Products **170** and **171** were isolated using this ligand in place of **137** in good yield and selectivity. Similarly, for β -substituted cyclohexane product **172** we observed that use of ligand **136** was superior, giving the product in 34% yield, 68:32 *er* and 9:1 *dr*. We observed that, in general, β -substitution is not well-tolerated under our reaction conditions.



Scheme 2.19

Next, we examined unsaturation in the backbone of the cyclohexane ring (Scheme 2.20). Interestingly, when we subjected anhydride **22** to the reaction conditions we isolated product **173** in good yield, but significantly reduced selectivity (73:27 *er*). We would expect that based on a steric argument, the selectivities should be nearly identical. We hypothesized that the olefin in the backbone may be coordinating to nickel during the oxidative addition step. This had been previously proposed and observed by the Rovis group in their nickel catalyzed zinc coupling with succinic anhydrides.²⁹ They observed that tetrahydrophthalic anhydride **22** reacted at a much faster rate than the fully saturated anhydride, likely due to internal coordination to the nickel complex. We envisioned that employing anhydride **25** in the reaction should afford restored enantioselectivity, as now the methyl groups should inhibit coordination to the nickel complex. Indeed, we isolated **174** in 72% yield, 93:7 *er* and 16:1 *dr*, nearly identical to that of product **132**. Acyclic anhydride **28** is also converted to the enantioenriched keto-acid (**175**) in 60% yield and

94:6 *er*, albeit a longer reaction time (48 h) was required. We had already established that *trans* anhydride **133** was competent under the reaction conditions, and was used to confirm the opposite diastereomer of the desired *cis* product (**132**). When subjected to the optimized conditions, product **134** was isolated in 81% yield, 50:50 *er* and 19:1 *dr*. It is of note that the *cis* isomer is still formed under the reaction conditions. The mechanism of epimerization will be discussed in further detail in section 2.8. Unsuccessful anhydride substrates will be discussed in section 2.5.3.

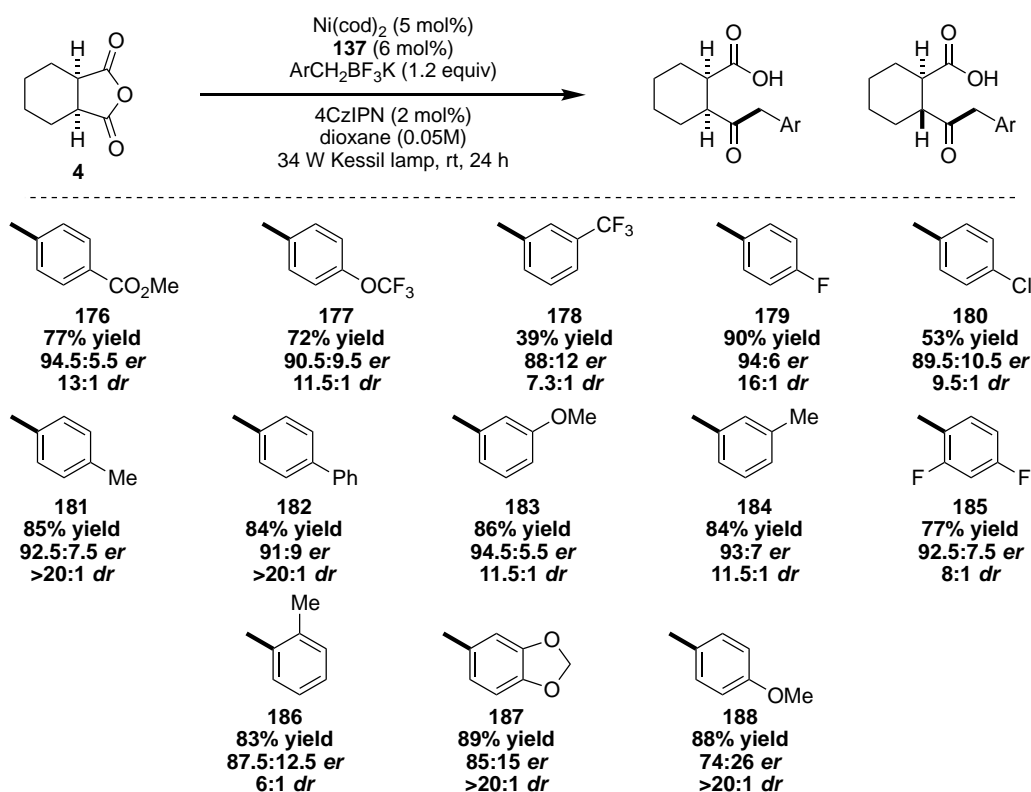


Scheme 2.20

2.5.2 Trifluoroborate scope

After evaluation of anhydrides, we next turned to the trifluoroborate scope employing anhydride **4** (Scheme 2.21). In general, the enantioselectivity was consistent among electron neutral to electron deficient trifluoroborates, giving the products in 92.5:7.5 *er* in most examples. Notable exceptions were **177**, **178**, **182** and **180**—we attribute this lower selectivity to an impurity rather than a mechanistic nuance. Diastereoselectivity was more variable, with electron deficient benzyl radicals giving lower *dr* and electron neutral to electron rich radicals giving much higher selectivity. Product **186** is afforded in 83% yield, 87.5:12.5 *er* and 6:1 *dr*, while very electron rich benzyl radicals afford products **187** and **188** in even lower enantioselectivity (85:15 and 74:26 *er*, respectively), but excellent diastereoselectivity. The lower enantioselectivity in these cases is

attributed to a more prolific racemic background. Under our standard conditions, with benzyl trifluoroborate (**117**) we observe only 7% yield of a racemic background, but observed higher yields with these electron rich trifluoroborates. Given the consistency of selectivities with electronically varied benzyl radicals, we propose that the mechanism goes through a Ni(0)/Ni(II)/Ni(III) cycle (Scheme 2.18), with oxidative addition serving as the selectivity-determining step—dependent of radical nucleophile. The variations in selectivity are likely due to a racemic background reaction (see section 2.6.1) and starting material impurities (see section 2.6.2).

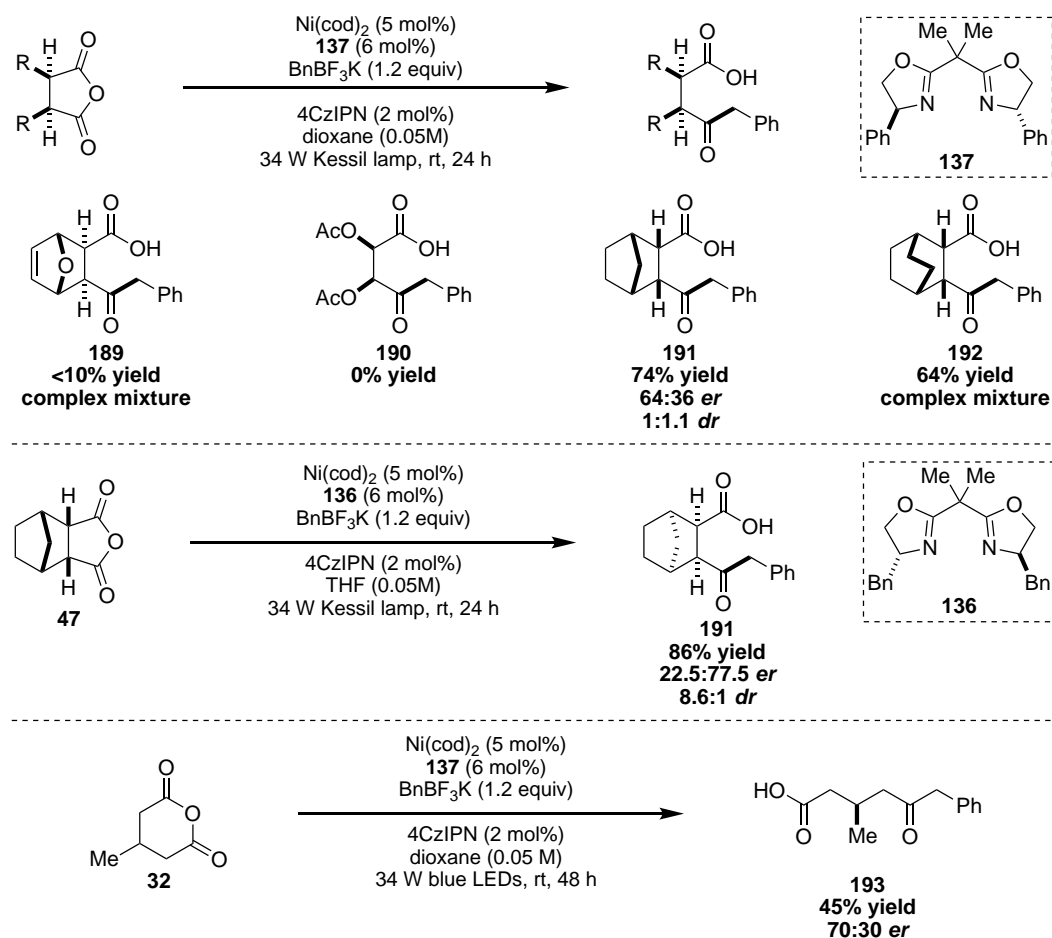


Scheme 2.21

2.5.3 Unsuccessful substrates

We also examined several anhydrides that were not efficiently converted to the corresponding enantioenriched keto-acids (Scheme 2.22). In bicyclic systems, olefins in the backbone were not

tolerated, with product **189** formed in less than 10% yield in a complex mixture. Additionally, acyclic product **190** was not formed in more than trace amounts. We attribute this lack of reactivity to a possible rapid decarbonylation to form a very stable α -oxy radical. Fully saturated bicyclic anhydride **47** is converted to the product in good yield, but low enantioselectivity (*cis*) and low

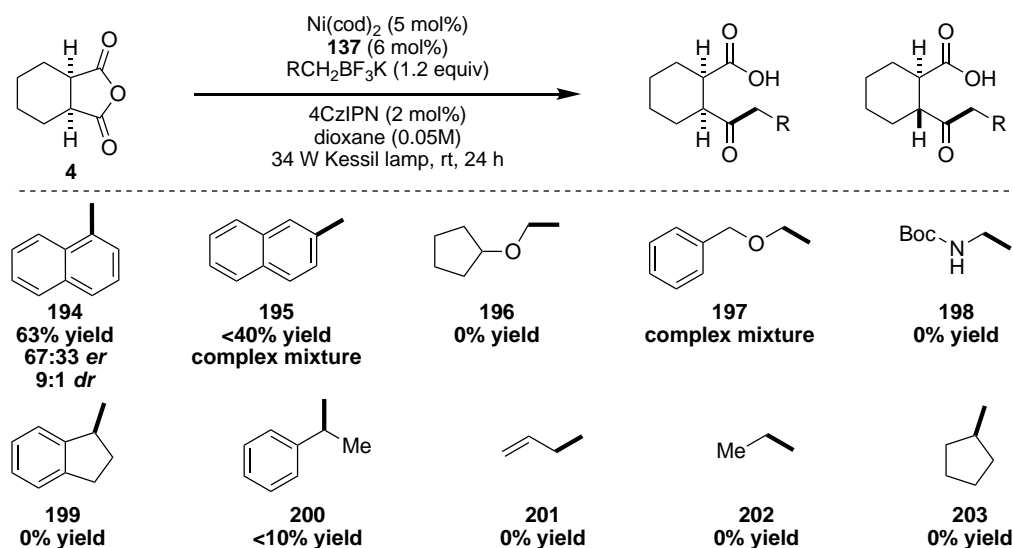


Scheme 2.22

diastereoselectivity where the *trans* diastereomer was formed preferentially. Product **192** was formed in good yield, but was difficult to isolate from a complex mixture. Given the success we had previously with changing ligands from PhBox to BnBox, we subjected anhydride **47** to the reaction conditions with ligand **136** in THF and were gratified to see improved yield and selectivities, now with the *cis* isomer favored in an 8.6:1 ratio. We also investigated glutaric

anhydrides as possible substrates for our desymmetrization chemistry. Unfortunately, our conditions were not amenable for generation of keto-acid **193**, which is formed in modest yield and enantioselectivity after 48 h. We undertook no further efforts to improve this selectivity.

We also examined numerous other trifluoroborates, both other benzylic and non-benzylic BF_3K salts (Scheme 2.23). Product **194** derived from 1-naphthylbenzyl trifluoroborate is formed in good yield and diastereoselectivity, but poor enantioselectivity. Conversely, 2-naphthylbenzyl trifluoroborate is coupled in low yield and delivers a complex mixture. α -Oxy methyltrifluoroborates do not provide product, and instead lead to complex mixtures. α -Aminomethyl trifluoroborate is also not coupled to anhydride **4**. These trifluoroborates have low oxidation potentials and should be



Scheme 2.23

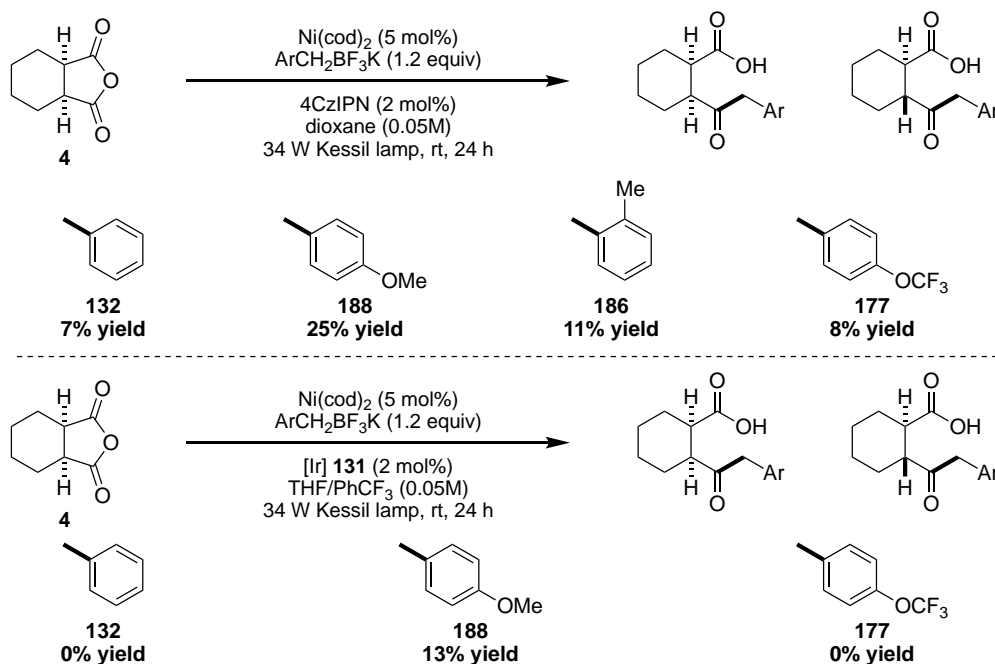
oxidized by the photocatalyst to the corresponding α -heteroatom radical, but resulted in no reaction. Secondary benzylic trifluoroborates, which are more sterically hindered, demonstrated some reactivity, but still only provided product in <10% yield. Unactivated alkyl trifluoroborates have much higher oxidation potentials than benzylic trifluoroborates ($E_{1/2} = +1.50$ V vs. SCE), but

have shown success in nickel catalyzed cross-couplings.³⁰ However, under our reaction conditions, neither ethyl nor cyclopentyl were competent radical precursors to form keto-acids.

2.6 Discussion of trifluoroborate salt and mechanistic implications

2.6.1 Evaluation of racemic background

In section 2.5.2, I reported the scope of the anhydride desymmetrization with regards to benzyl trifluoroborate identity. Although the selectivities were largely consistent with the parent benzyltrifluoroborate, very electron rich trifluoroborates tended to have lower enantioselectivity. In an evaluation of a “ligand-less” reaction, we observed a 7% yield of product **132** in the absence of the Box ligand (Scheme 2.24). When a more electron rich trifluoroborate is used, product **188** is formed in 25% yield. *o*-Methylbenzyl trifluoroborate is coupled to anhydride **4** in 11% yield in the absence of ligand. A more electron deficient trifluoroborate still demonstrates a small



Scheme 2.24

background reaction, where 8% of product **177** is observed. Given the large amount of product **188** that is formed in the absence of ligand, we attribute the lower selectivity in the reaction with

ligand to a competitive racemic background reaction. Additionally, the reaction with *o*-methybenzyl trifluoroborate affords a more considerable racemic background reaction, which is likely responsible for the lower enantioselectivity that is observed with product **186**. Interestingly, when the same “ligand-less” reaction is conducted with the [Ir] (**131**) photocatalyst, none of product **132** is formed. Again, a more electron rich trifluoroborate does give some racemic background reaction (13% yield), but significantly less than that which is observed with 4CzIPN. More electron deficient trifluoroborates, like benzyltrifluoroborate, do not afford any product.

To make this transformation more synthetically useful for all the substituted benzyltrifluoroborates, we questioned whether we could suppress the racemic background reaction. We had observed significant changes in selectivity when the reaction was conducted in different solvents. In diethyl ether, a “ligand-less” reaction provided <5% of product **188** and in toluene, no product is observed. When the reaction is run in the presence of ligand **137** in a toluene/THF mixture, the product is observed in 92% yield and 94.5:5.5 *er* and when the reaction is conducted in diethyl ether/THF, the product is observed in 86% yield and 96.5:3.5 *er* (Table 2.9, entry 2-3). With these new conditions in hand, we isolated product **188** in 90% yield and 97:3 *er* with near perfect diastereoselectivity. When we used a dioxolane substituted trifluoroborate under the new conditions, we isolated the product (**187**) in lower yield and diastereoselectivity, but high enantioselectivity. We attribute the lower yield and *dr* to the insolubility of the trifluoroborate in diethyl ether. This evidence again suggests that the benzyl radical is not involved in the selectivity-determining step.

Table 2.10

entry	solvent	%yield	<i>er</i>	<i>dr</i>
1	dioxane	88%	74:26	>20:1
2	toluene/THF (95:5)	92%	94.5:5.5	24:1
3	Et ₂ O/THF (95:5)	86%	96.5:3.5	24:1
4	15 °C, dioxane	88%	75:25	65:1

		 188	 187	
dioxane		88% yield 74:26 <i>er</i> >20:1 <i>dr</i>	89% yield 85:15 <i>er</i> >20:1 <i>dr</i>	
Et ₂ O/THF		90% yield 97:3 <i>er</i> >20:1 <i>dr</i>	58% yield 97:3 <i>er</i> 4:1 <i>dr</i>	

2.6.2 Discovery of trifluoroborate impurities

The inconsistency among electron neutral and electron deficient trifluoroborates cannot be explained by a racemic background reaction. We initially hypothesized that despite the consistency of selectivity, perhaps the mechanism for the transformation is proceeding via a Ni(0)/Ni(I)/Ni(III) cycle, as proposed by the Molander group. In this mechanism, the benzyl radical would first add to Ni(0) to generate a Ni(I) species, which could undergo oxidative addition into the anhydride. Under this manifold, it may be expected that the identity of the radical nucleophile would play a role in determining selectivity. We hypothesized if this was occurring, a Hammett plot should

show a correlation between selectivity and σ_p values.³¹ As seen in Figure 2.2, there is no correlation between benzyl radical substitution and stereoselectivity.

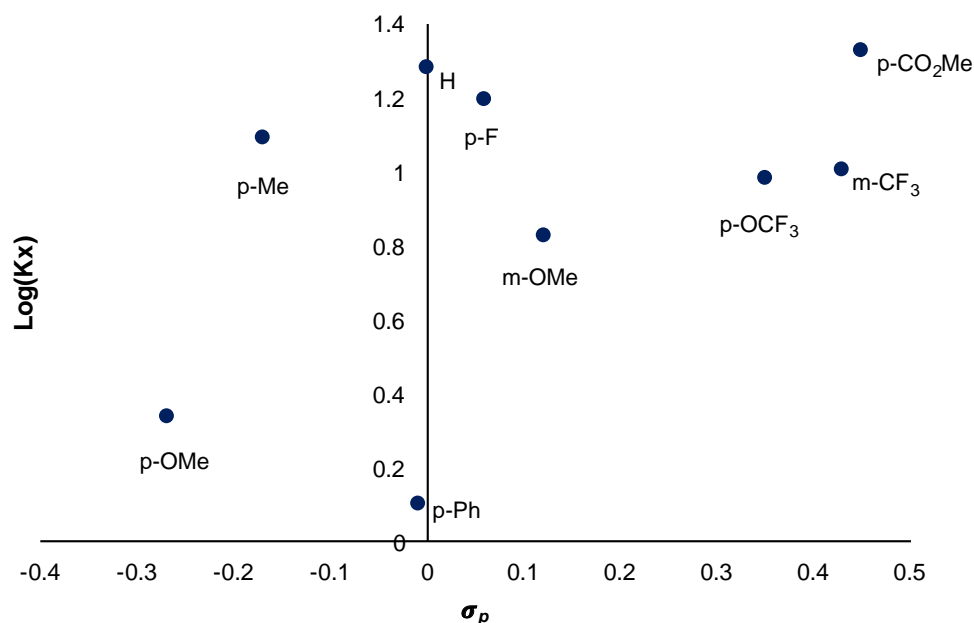
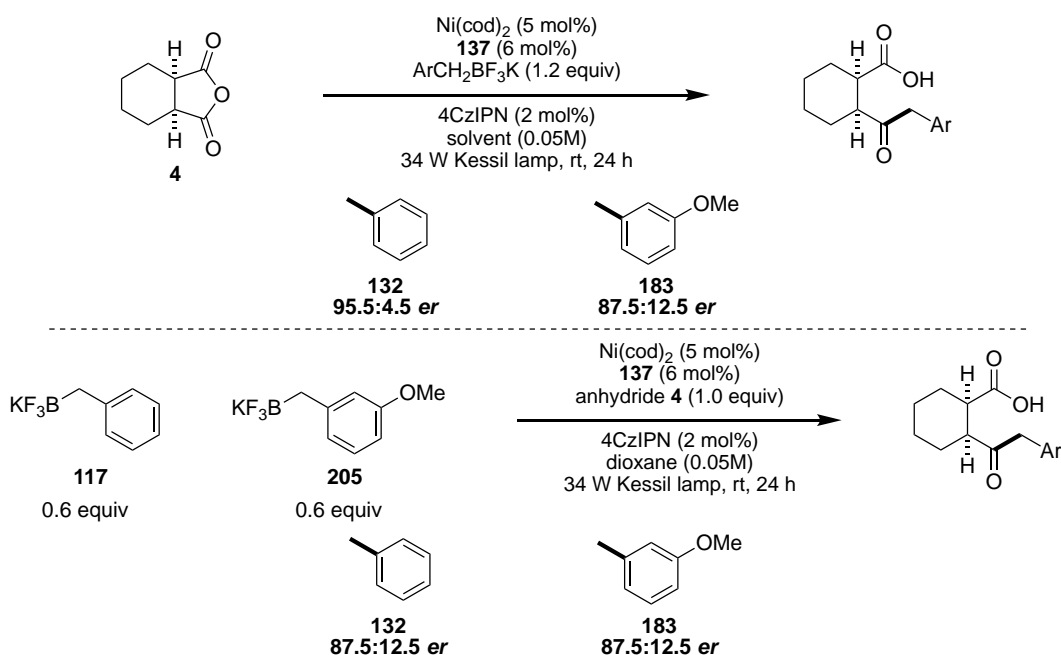


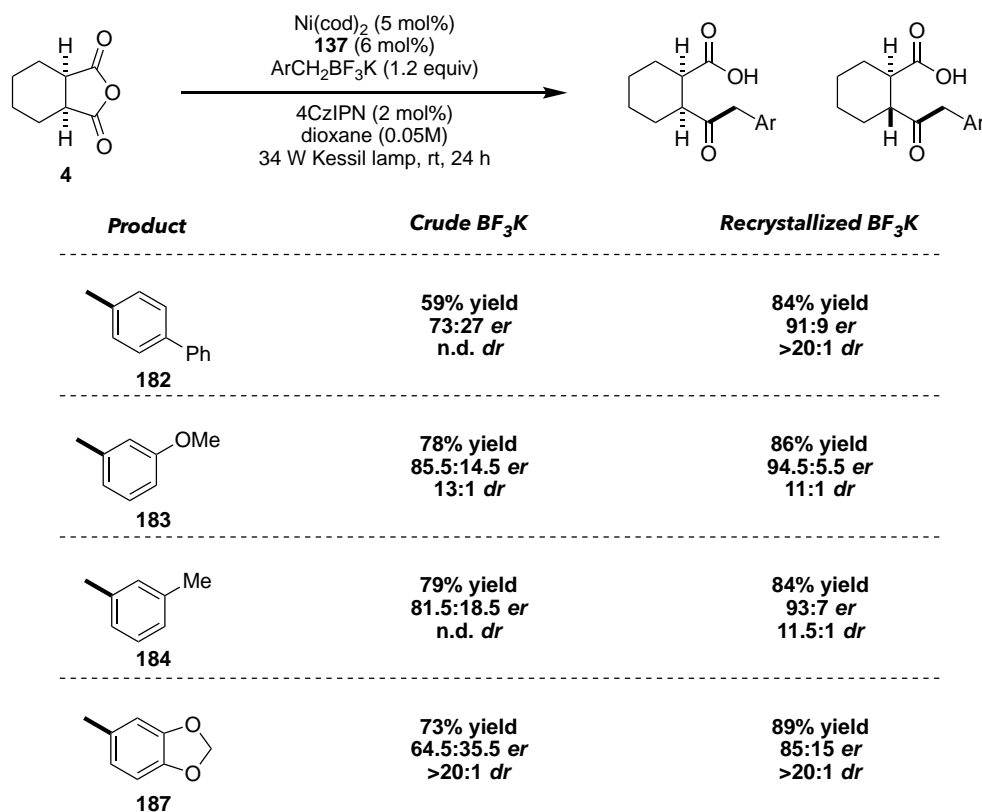
Figure 2.2

It should be noted that all of the trifluoroborates, except for benzyl trifluoroborate, were synthetically prepared, with little to no purification. Although this is traditionally how BF_3K salts are prepared, we questioned whether an impurity may be causing the decrease in enantioselectivity. We hypothesized that by mixing the synthetic trifluoroborate with the commercially available salt, we should be able to determine if an impurity was causing the attenuation of selectivity. Under standard conditions, commercially available benzyl trifluoroborate is cross-coupled with anhydride **4** to form the product in 95.5:4.5 *er*, while trifluoroborate **205** gives product **183** in 87.5:12.5 *er* (Scheme 2.25). When the two trifluoroborate salts are mixed in a 1:1 ratio and coupled to anhydride **4**, both products are isolated in 87.5:12.5 *er*. This result suggests that the low enantioselectivity is due to a trifluoroborate impurity and not a mechanistic nuance.



Scheme 2.25

We sought to test our hypothesis by purifying the trifluoroborate salts and re-examining the selectivity of the products. Product **182** was isolated with crude trifluoroborate in 73:27 *er*, and after several recrystallizations the product is isolated in 91:9 *er* (Scheme 2.26). When crude *m*-methoxybenzyl trifluoroborate was cross-coupled to anhydride **4**, the product is afforded in only 85.5:14.5 *er*. However, after purification, the product (**183**) is afforded in 94.5:5.5 *er*. Similarly, product **184** is provided in 81.5:18.5 *er* and after purification, the product selectivity increased to 93:7 *er*. Furthermore, dioxolane based product **187** is delivered in 64.5:35.5 *er* before purification and 85:15 *er* upon removal of impurities. These results are good evidence for selectivity being attenuated due to an impurity rather than a mechanistic nuance. In some cases, recrystallization of the trifluoroborates was unsuccessful, so we were unable to improve the selectivity in these cases (products **177**, **178**, and **180**). We surmise that if the trifluoroborates used were of similar purity to the commercial substrate, all keto-acid products would be isolated in identical selectivity.

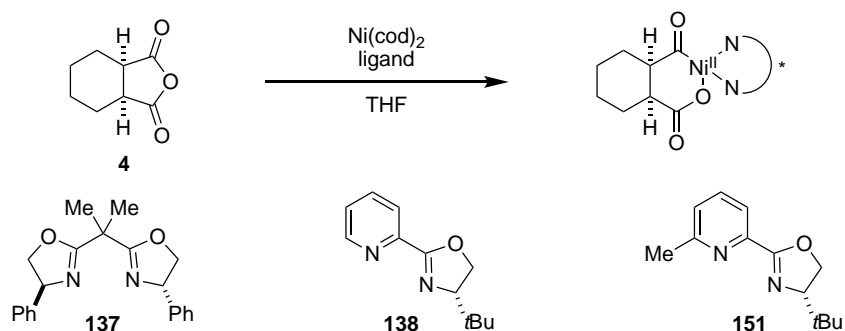


Scheme 2.26

2.7 Oxidative addition experiments

To further gather experimental evidence for our proposed mechanism, we wanted to examine the oxidative addition step and began with UV/vis studies. We combined anhydride **4** with a ligated nickel complex (ligands **137**, **138**, **151**) to determine how quickly oxidative addition occurs (Scheme 2.27). First, a UV/vis spectrum of a mixture of nickel and ligand **137** was taken to ensure that the nickel complex was ligated before adding anhydride. As can be seen in the spectrum, the ligand feature red shifts significantly when mixed with nickel (Figure 2.3). Employing ligand **137**, when anhydride **4** was mixed with the pre-ligated nickel complex we observed very little change in the UV/vis spectrum, even with longer equilibration times. However, when added 20 equivalents of anhydride, mimicking the reagent loadings of the reaction, we begin to see a new

feature develop in the spectrum and a small color change. This data suggests that oxidative addition may be slow under stoichiometric conditions.



Scheme 2.27

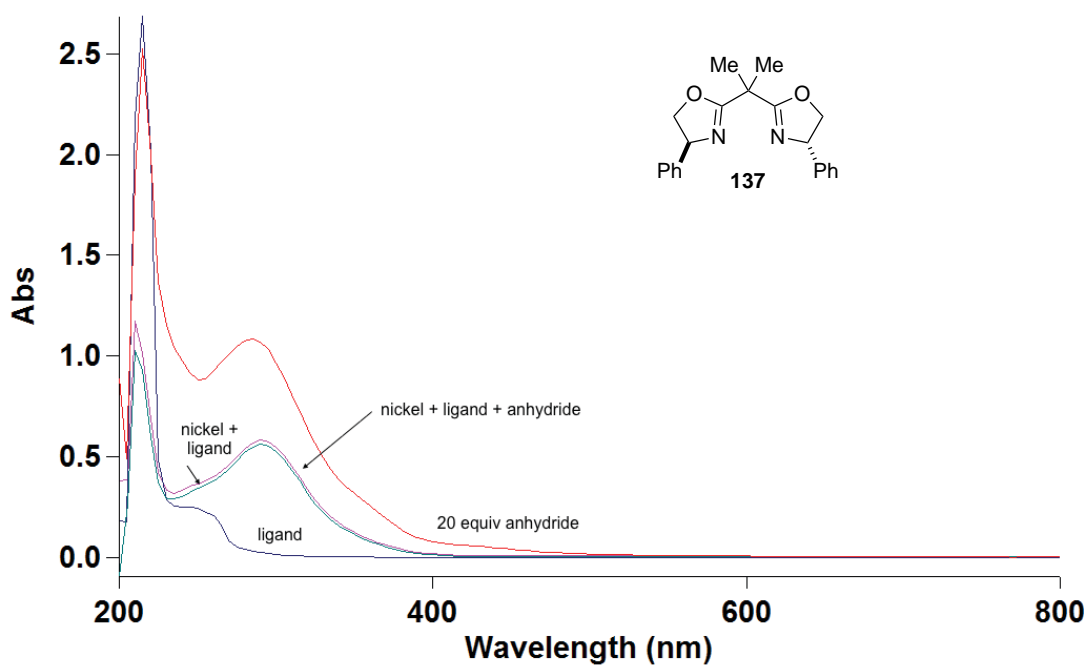


Figure 2.3

In the reports disclosed by the Rovis group, they cite a significant color change upon addition of the anhydride to the ligated nickel-bpy. When anhydride **4** was mixed with ligand **137**, we observed no significant color change, until after the addition of 20 equivalents (Figure 2.4). We also examined PyrOx ligand **138** in a similar experiment. In this case, a dramatic color change, deep purple to red was observed within 1 minute of mixing the anhydride with the ligated nickel

complex. This red shift is clearly observed in the UV/vis spectra shown in Figure 2.4. This data suggests that oxidative addition occurs rapidly with ligand **138**.

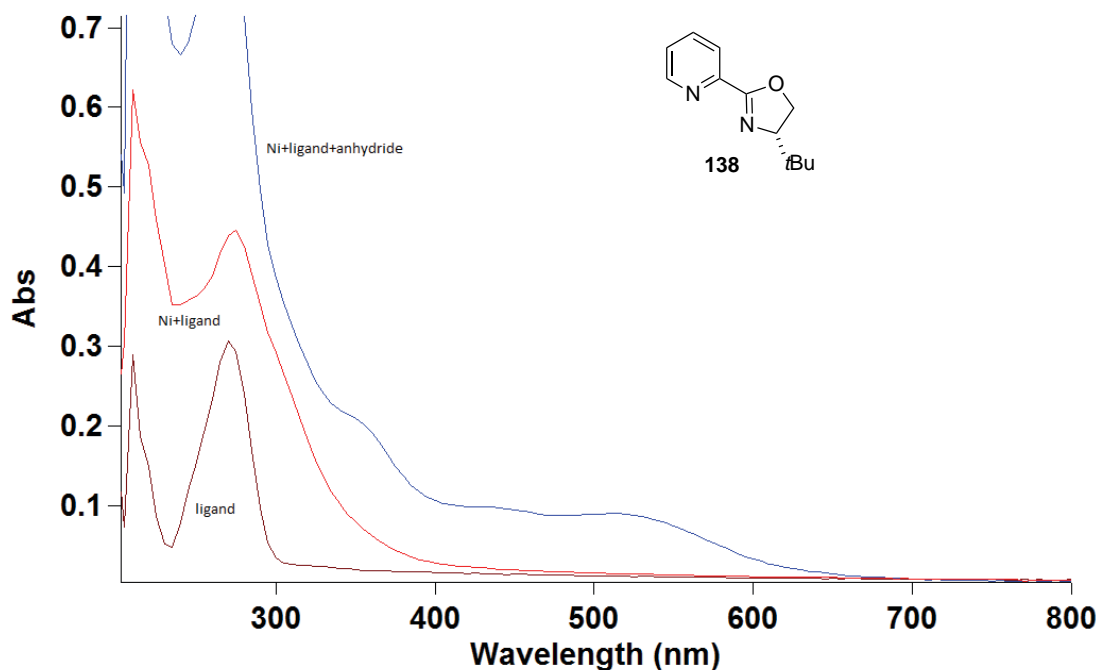


Figure 2.4

Lastly, we sought to conduct the same experiments with ligand **151**, which provided the highest level of selectivity beyond Box ligands. Additionally, this ligand produced a unique effect, relative to other PyrOx ligands, giving the opposite enantiomer from ligand **138**. Like PyrOx ligand **138**, a significant color change was observed upon adding anhydride **4** to the ligated nickel solution, from dark green to red. There is a small change in the UV/vis spectrum (Figure 2.5) to suggest that oxidative addition occurs after a few minutes of equilibration.

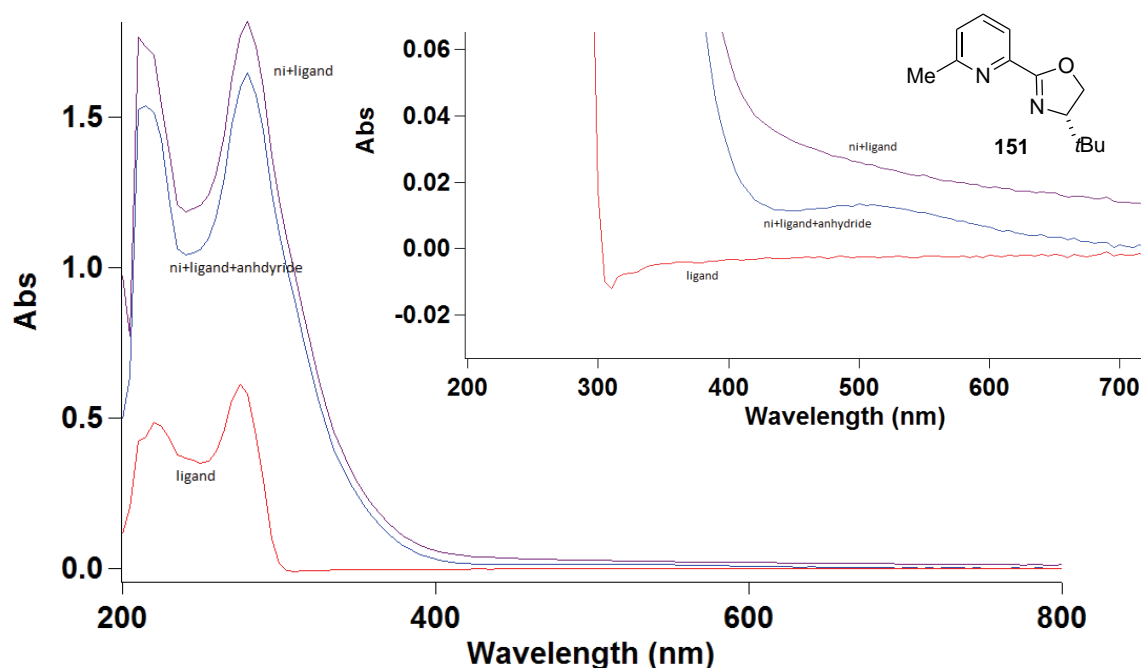


Figure 2.5

To rule out the possibility of a reversible oxidative addition, we conducted anhydride competition experiments like those of the Rovis group in their full mechanistic study (see section 1.3.1, Scheme 1.5).¹⁸ In that case they had observed that under the nickel-bpy conditions, an equilibrium mixture of products is obtained, suggesting a highly reversible oxidative addition event. We subjected anhydride **4** to a stoichiometric mixture of nickel/ligand (**137**) and trifluoroborate (**117**), and allowed the mixture to equilibrate for 10 min (Table 2.10, entry 1). During this time, no dramatic color change was observed signaling oxidative addition, consistent with our UV/vis experiments. After 10 min, anhydride **25** was added and allowed to equilibrate for an additional 10 min, during which time no color change was observed. After 10 min, 4CzIPN was added and the reaction was irradiated with light for 1 h. Analysis of the product mixture showed a 1.9:1 ratio of **132**:**174**. The reverse experiment was then conducted, with anhydride **25**, being mixed with the nickel complex first, and then anhydride **4** added to equilibrate. Analysis of

this product mixture showed a 1.3:1 ratio of **132:174** (entry 2). When anhydride **4** was equilibrated with the nickel complex, then anhydride **25** added and no equilibration was allowed, a nearly identical product ratio was obtained (entry 3). Finally, if both anhydrides were added immediately and allowed to equilibrate for 10 min before irradiation, an identical product ratio was obtained (entry 4). It is interesting to note that when the same set of experiments were conducted using ligand **151**, a similar product distribution was observed.

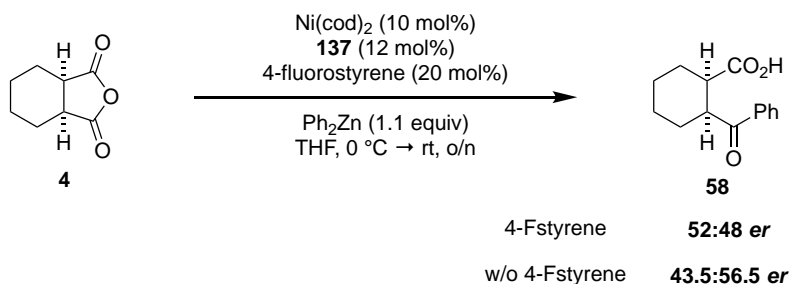
Table 2.10

entry	Procedure	132:174
1	4 , then 23 , then irradiate	1.9:1
2	23 , then 4 , then irradiate	1.3:1
3	4 , then 23 , no stir and irradiate	1.4:1
4	4 and 23 initially	1.3:1

These data demonstrate an equilibrium mixture of products. One conclusion is that oxidative addition may be fast and reversible and would be expected to show an equilibrium mixture of products, as had been observed with the nickel-bpy system. Given the high enantioselectivity obtained, it seems unlikely that oxidative addition is fast and reversible. Alternatively, under the actual reaction conditions, a Ni(0)/Ni(I)/Ni(III) system is operative, and oxidative addition occurs after the benzyl radical has added to nickel. If so, the results of this study would not capture this mechanistic feature. However, the enantioselectivity appears to be independent of radical nucleophile, as the keto-acids are isolated in consistent selectivity. This does not preclude a situation in which the benzyl substituent plays an insignificant role in $\Delta\Delta G^\ddagger$; we have not examined calculations to rule this out. The likely explanation is that oxidative addition is slow under

stoichiometric conditions and therefore an equilibrium mixture of products would be expected. This is consistent with our UV/vis data, where no oxidative addition is observed until 20 equivalents of anhydride are added. If the same experiment is conducted under catalytic conditions (95:5 mix of **4** to [Ni]), oxidative addition is observed within 10 minutes. This conclusion is consistent with all the stoichiometric data collected, as well as the product selectivities. More advanced mechanistic techniques, such as ^{13}C NMR or *in-situ* IR could elucidate the nature of the oxidative addition step.

We also wanted to test the anhydride desymmetrization with aryl zinc reagents with ligand **137**.^{29,32} Presumably, if anhydride oxidative addition is irreversible and therefore selectivity-determining, ligated nickel(0) oxidative addition to anhydride **4** should yield similar selectivities in both systems. Under the standard reaction conditions developed by the Rovis group, the product was obtained in only 52:48 *er* (Scheme 2.28). Interestingly, in the absence of 4-fluorostyrene, the selectivity flipped to favor the opposite enantiomer, in 43.5:56.5 *er*. These data highlight the impact of the olefin on the selectivity of the reaction, in this case having a negative effect. Ultimately, these results do not give insight into the selectivity-determining step of the photochemical reaction.

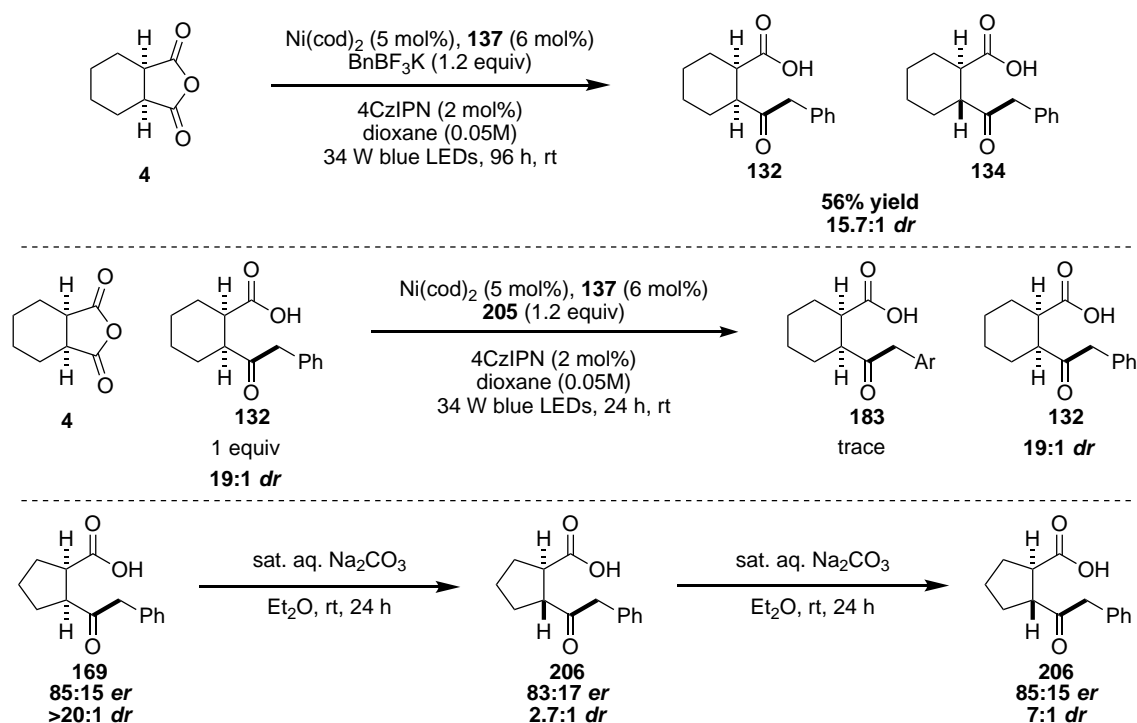


Scheme 2.28

2.8 Evaluation of epimerization event

The formation of the *trans* diastereomer (**134**) had never been reported before by the Rovis group—they observed perfect retention of stereochemical information. Under our reaction conditions however, we had observed as low as a 1:1 ratio of *cis:trans* products, although under our standard reaction conditions, a >20:1 ratio of **132:134** is isolated. We first questioned whether the product itself was being epimerized under the reaction conditions or upon workup. As we used the same workup conditions as previously employed by the Rovis group, we were confident this was not responsible for epimerization. Additionally, extended reaction times did not result in a significant degree of epimerization (Scheme 2.29). Furthermore, subjecting the isolated product to the reaction conditions with a different trifluoroborate did not increase the formation of the *trans* product. Product **183** was only formed in trace amounts, consistent with the carboxylic acid inhibition we had observed during optimization. Some products were prone to epimerization upon workup, however.

It should be noted that product **169**, isolated in >20:1 *dr*, could be epimerized to favor the *trans* diastereomer (**206**) in 2.7:1 ratio when subjected to aqueous basic conditions for 24 h, albeit with retention of enantioselectivity for the *trans* diastereomer (Scheme 2.29). The mixture of diastereomers could be further epimerized to a 7:1 ratio of *trans:cis* isomers by subjecting it to the same basic conditions. This epimerization was not observed with product **132**, and appears to be a unique feature of product **169**. Care was taken with workup conditions to ensure that epimerization was not a function of a base-promoted event.

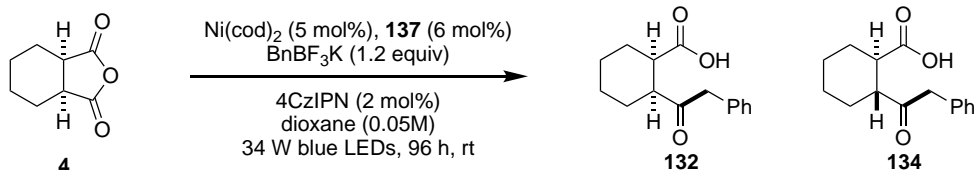


Scheme 2.29

In re-examining our optimization studies, we noticed that the diastereoselectivity appeared to be proportional to nickel loading. At 2.5 mol% nickel loading, product **132** is isolated as a single diastereomer in 89.5:9.5 *er* (Table 2.11, entry 1). We had previously observed that the enantioselectivity is lower with lower nickel catalyst loadings. At 5 mol% loading of nickel we still observe high diastereoselectivity and enantioselectivity (entry 2). Increasing the nickel loading to 10 mol%, however, now gives dramatically reduced diastereoselectivity—3.8:1 **132:134** (entry 3). Interestingly, the enantioselectivity of the *trans* diastereomer is also high—92:8 *er*. Furthermore, increasing the nickel loading even further continues to decrease diastereoselectivity to a 1.4:1 ratio of *cis/trans*, with the *trans* diastereomer formed in high enantioselectivity (entry 4). With this high degree of epimerization, we sought to examine the photocatalyst loading as well. The amount of radical that is generated is directly proportional to the photocatalyst loading, and therefore serves as a measure of radical concentration. Increasing the photocatalyst loading to 4 mol% leads to less

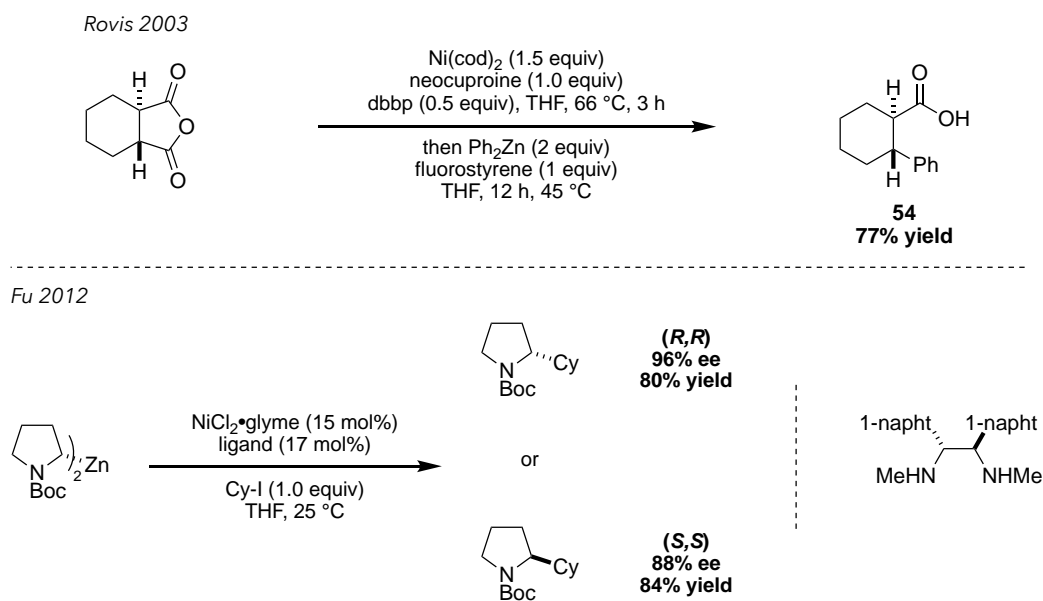
epimerization, now with a 2.1:1 ratio of **132**:**134** (entry 5). In contrast, decreasing 4CzIPN concentration now affords the *trans* diastereomer as the major product in a 1:1.2 ratio of *cis*:*trans*, with retained high enantioselectivity for both isomers. It should be noted that we observed a small percentage of *trans* anhydride in the *cis* starting material, which could account for the slightly lower enantioselectivity observed for the *trans* product.

Table 2.11

						
entry	Nickel	4CzIPN	% yield	dr	<i>er</i> (<i>cis</i>)	<i>er</i> (<i>trans</i>)
1	2.5 mol%	2 mol%	91%	99:1	89.5:9.5	n.d.
2	5 mol%	2 mol%	72%	>20:1	93.5:6.5	n.d.
3	10 mol%	2 mol%	62%	3.8:1	95:5	92:8
4	15 mol%	2 mol%	56%	1.4:1	92.5:7.5	93.5:6.5
5	15 mol%	4 mol%	78%	2.1:1	95:5	92.5:7.5
6	15 mol%	1 mol%	49%	1:1.2	93:7	91:9

With these data, a few observations can be made. First, epimerization increases with increasing nickel loading, which suggests a nickel-mediated epimerization event. Second, increased concentration of radical leads to less epimerization, while less photocatalyst loading leads to the *trans* diastereomer, preferentially. We reasoned that if the *trans* diastereomer is formed in high enantioselectivity, it must be arising from an epimerization of the *meso*-anhydride after stereoselective oxidative addition, therefore occurring on the oxidative addition adduct. This would agree with the dependence on nickel concentration for epimerization. It is unlikely to stem from a radical H-atom abstraction of the α -C–H bond, as epimerization increases with decreasing radical concentration. Instead, we propose a decarbonylation event, followed by nickel–carbon

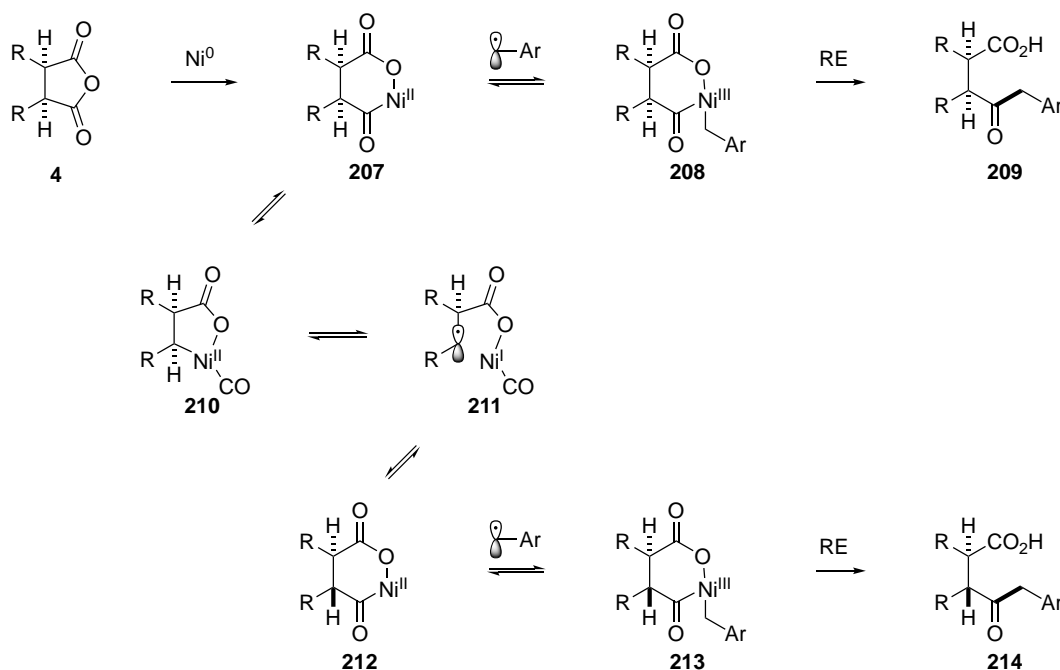
bond homolysis and subsequent recombination and re-carbonylation. Decarbonylation is a well-known pathway for nickel-acyl species, and was demonstrated by the Rovis group in an early report.³³ In this case, they demonstrated a stoichiometric decarbonylative C–C bond cross-coupling reaction using nickel (Scheme 2.30). Nickel–carbon bond homolysis has also been suggested as a mechanism for stereoconvergent cross-couplings. In a report from the Fu group, they observed that stereo-enriched alkyl zinc reagents would undergo stereoconvergent cross-couplings to form both enantiomers of product, depending on the ligand employed. They ruled out consecutive β -hydride eliminations based on deuterium labeling, but propose that a nickel–carbon bond homolysis would generate a planar carbon radical, that would recombine with nickel on either side, depending on the enantiomer of ligand used.³⁴



Scheme 2.30

Our mechanistic proposal for epimerization is shown in Scheme 2.31. After oxidative addition of Ni(0) into anhydride **4** to form adduct **207**, the benzyl radical can add to this adduct to form **208**, and reductive elimination releases the *cis* product (**209**). Alternatively, adduct **207** could undergo decarbonylation (**210**) followed by a nickel–carbon homolytic bond cleavage to form **211**.

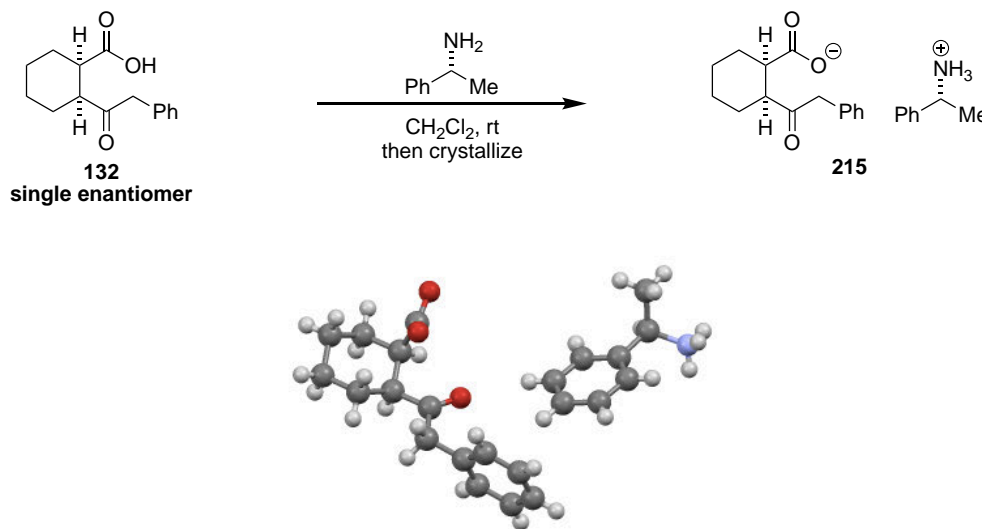
This prochiral radical can either recombine with nickel and undergo re-carbonylation to form *cis* adduct **210** and proceed to *cis* product or combine on the opposite face to form *trans* adduct **212**. Upon radical addition to form adduct **213**, reductive elimination would release *trans* product **214**. Because all intermediates funnel through the enantioenriched *cis* adduct **207**, both *cis* and *trans* products are formed with high selectivity. In reactions with low nickel concentration, thereby higher relative radical concentration, the reaction proceeds without epimerization to *cis* product **209**. More nucleophilic benzyl radicals also add to nickel more readily to proceed to the product with high diastereoselectivity as we saw primarily formation of the *cis* product with electron-rich trifluoroborates, while electron-deficient trifluoroborates afforded lower *dr*. Furthermore, increasing photocatalyst loading, and thereby effective radical concentration, increases the diastereoselectivity, as the oxidative addition adduct is trapped more readily. This proposed mechanism of epimerization also precludes a Ni(0)/Ni(I)/Ni(III) mechanism, wherein decarbonylation would need to occur on a fully saturated Ni(III) intermediate.



Scheme 2.31

2.9 Structure determination and derivatization of enantioenriched keto-acids

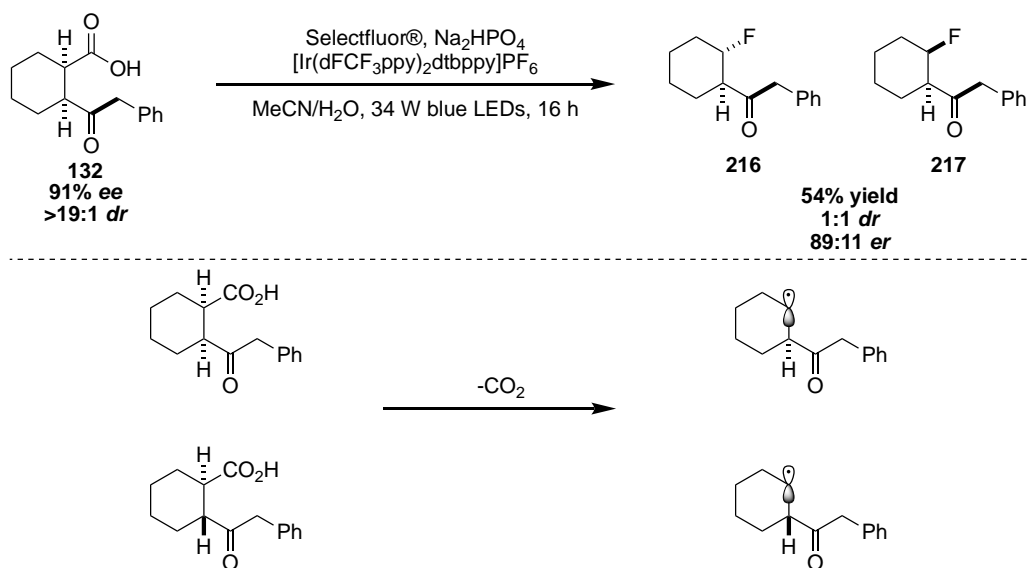
To determine the absolute configuration of the keto-acid product, we first purified **132** to isolate a single enantiomer, and then mixed with (*R*)-methylbenzylamine to form an acid base pair (Scheme 2.32). The salt was crystallized and afforded an X-ray diffraction quality crystal, which assigned the absolute stereochemistry as shown.



Scheme 2.32

We also wanted to demonstrate the utility of these enantioenriched keto-acid compounds, particularly in the context of photoredox chemistry. Based on the work of other groups, carboxylic acids are easily oxidized to the corresponding alkyl radical under photoredox catalysis. The MacMillan group reported a decarboxylative fluorination of alkyl carboxylic acids, which we imagine would be a useful derivatization for our keto-acid compounds.³⁵ This reaction employs Selectfluoro® as an electrophilic fluoride source which can intercept the nucleophilic alkyl radical. When we subjected keto-acid **132** to the reaction conditions, we were gratified to find the fluorinated product in 54% yield and a 1:1 ratio of *cis/trans* diastereomers (Scheme 2.33). The enantioselectivity, however, was significantly eroded from the parent keto-acid compound. We reasoned that by using the mixture of diastereomers, once decarboxylation occurred, a mixture of

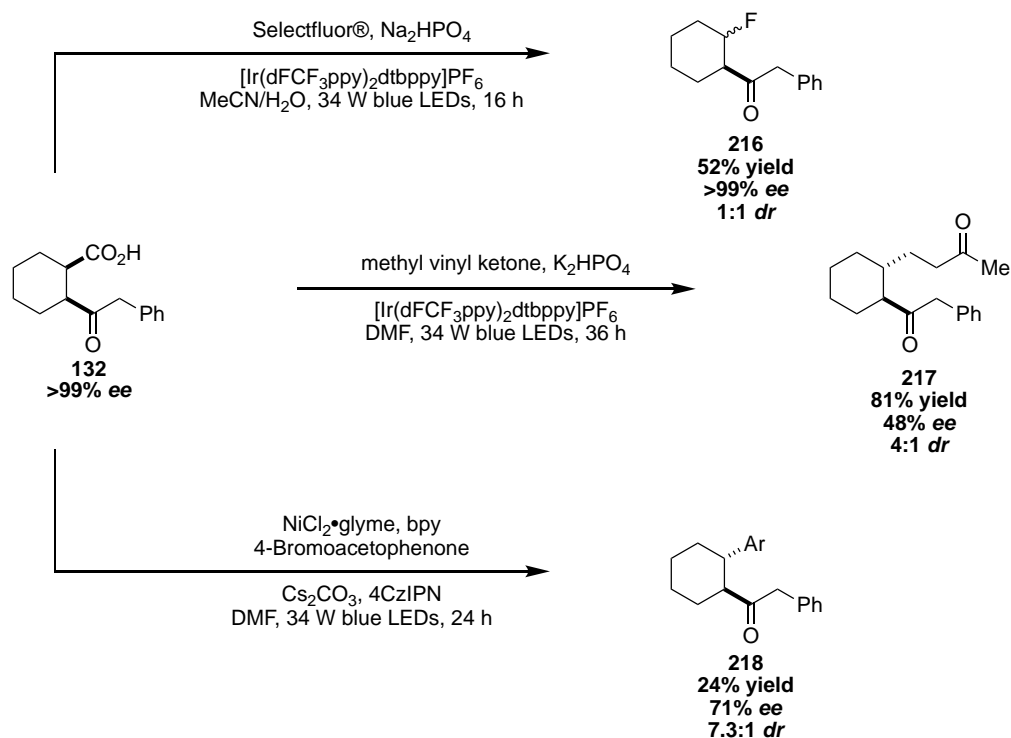
enantiomers would be formed, thus eroding the ultimate enantioselectivity. Additionally, this result confirms the epimerization of the ketone stereocenter, as we had previously proposed.



Scheme 2.33

After purification of keto-acid **132** to a single diastereomer and enantiomer, we again subjected it to the fluorination conditions, and obtained the fluorinated product (**216**) in a 1:1 ratio of diastereomers, with >99% *ee* and no loss of stereochemical information (Scheme 2.34). Additionally, we demonstrated a C–C bond forming reaction employing a carbon radical acceptor. In the presence of a photoredox catalyst, base and methyl vinyl ketone, radical conjugate addition to the Michael acceptor to form an α -acyl radical, which is subsequently reduced by the photocatalyst to form the enolate.²⁷ Product **217** is isolated in excellent yield and 4:1 *dr*, but only 48% *ee*. This reduced enantioselectivity is attributed to the increased acidity of the α -proton of the intermediate radical which could be easily epimerized under basic conditions. An alternative mechanism may involve reversible addition of the radical into the carbonyl compound, which would afford a *meso* compound, erasing all stereochemical information. Furthermore, we subjected keto-acid **132** to nickel and a photoredox catalyst in an effort to effect a decarboxylative

arylation reaction.²⁵ The reaction proceeded in modest yield, but good diastereoselectivity and enantioselectivity, affording **218**. Overall, a two-step sequence starting from a *meso*-cyclic anhydride can afford these rather diverse products, with non-traditional bond disconnections, which may be of interest for industrial applications.³⁶

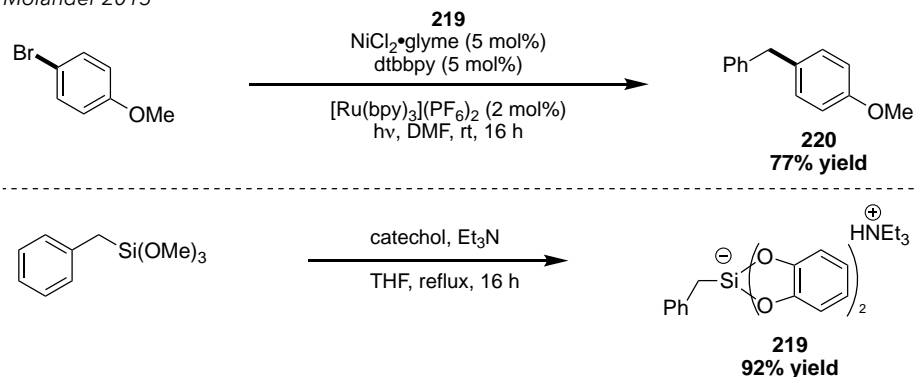


Scheme 2.34

2.10 Additional radical coupling partners

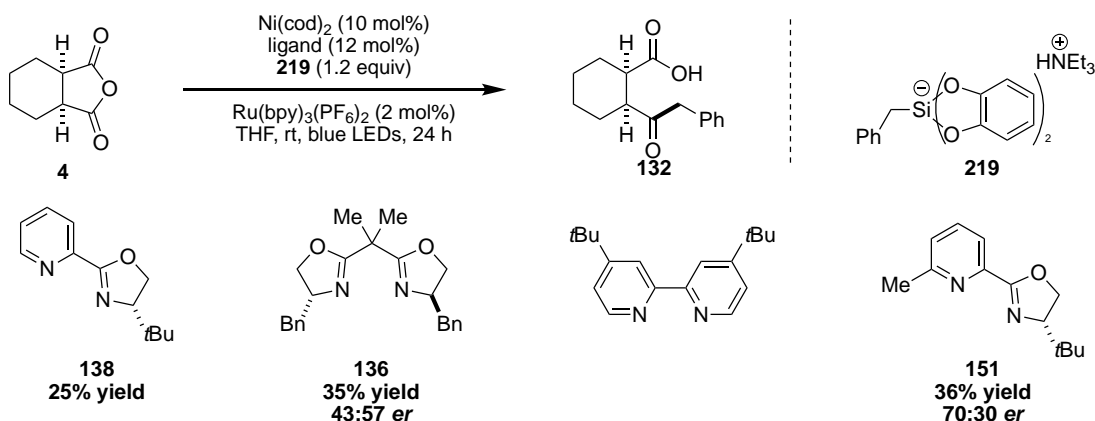
One of the most exciting features of this chemistry is the possibility of structural diversity that may stem from a vast number of radical precursors. While we chose to begin our studies with trifluoroborates, we have also observed that organosilicates are competent coupling partners. In 2015, the Molander group reported a dual nickel- and photoredox catalyzed coupling of organosilicates and aryl halides (Scheme 2.35).³⁷ Organosilicates are versatile radical precursors that have very low oxidation potentials ($E_{1/2} = +0.75$ V vs. SCE for 1° alkyl), and can be readily synthesized using commercially available materials.

Molander 2015



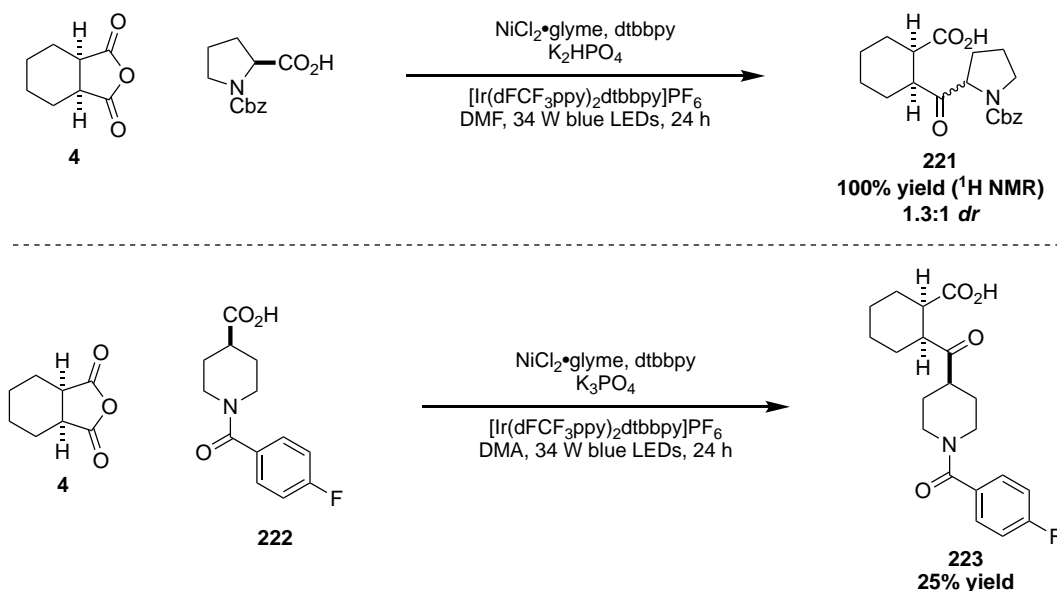
Scheme 2.35

We tested silicate **219** using several ligands, standard catalyst loadings and $\text{Ru(bpy)}_3(\text{PF}_6)_2$ as a photocatalyst (Scheme 2.36). Due to the lower oxidation potentials of silicates, using a ruthenium based photocatalyst rather than iridium was feasible. Using PyrOx ligand **138** afforded the product in reduced yield, while Box ligand **136** gave improved yield, but much lower enantioselectivity relative to the trifluoroborates. Dtbbpy, as a racemic ligand check, gave the product in only 25% yield, while 6-methyl substituted PyrOx ligand **151**, gave the product in modest yield and comparable selectivity to the trifluoroborate radical precursor (71:29 *er* using BnBF_3K). Despite these initially promising results, we did not pursue silicates any further in the asymmetric reaction.



Scheme 2.36

Alkyl carboxylic acids are one of the most ubiquitous functional groups in organic molecules and are inexpensive and readily available. As such, they serve as excellent radical precursors and can be easily oxidized by commonly used inorganic and organic photoredox catalysts. We questioned whether we might be able to employ alkyl carboxylic acids as radical coupling partners in our cross-coupling reaction to access a diverse array of keto-acid products. Gratifyingly, we found that amino acids can be coupled to anhydride **4** in quantitative yield after some optimization to yield **221** (Scheme 2.37). Oxidation potentials for amino acids are significantly lower than unactivated alkyl carboxylic acids, so we rationalized that the amino acids would be preferentially oxidized by the photocatalyst to generate the α -amino radical. We have demonstrated some success with alkyl, unactivated carboxylic acids, coupling **222** to anhydride **4** under nickel catalysis in 25% yield. Presumably, with the stoichiometric loading, carboxylic acid **222** outcompetes product decarboxylation during the early course of the reaction. More reaction engineering will be necessary to use unactivated primary and secondary carboxylic as radical coupling partners in this chemistry.



Scheme 2.37

2.11 Conclusion

In summary, we have developed a highly enantioselective desymmetrization of *meso*-cyclic anhydrides using a dual catalytic approach.³⁸ The utilization of photoredox catalysis opens a wealth of radical precursors that can be coupled to access a diverse array of stereodefined keto-acid products. Additionally, it permits the use of a nickel-catalyzed desymmetrization of anhydrides in high enantioselectivity, as it precludes the use of olefin additives to promote reactivity. Isolation of the enantioenriched *trans* keto-acid products also appears to be a unique feature of our approach, as this epimerization event had not been observed previously. Simply by modifying the catalyst loadings, the *trans* product can be formed preferentially and in high enantioselectivity from the *cis meso* anhydride. Furthermore, coupling partners can be extended beyond benzyltrifluoroborates, as alkyl silicates, amino acids and unactivated alkyl carboxylic acids have also shown promising results in the cross-coupling reaction. Lastly, by utilizing previous reports of photoredox catalyzed transformations, we have derivatized the keto-acid products into more complex structures in just two steps from the *meso* anhydride. Overall, this chemistry represents an important advance in enantioselective photoredox transformations, and addresses longstanding challenges associated with anhydride desymmetrizations.

References

- (1) Shaw, M. H.; Twilton, J.; MacMillan, D. W. C. *J. Org. Chem.* **2016**, *81* (16), 6898.
- (2) Twilton, J.; Le, C. C.; Zhang, P.; Shaw, M. H.; Evans, R. W.; MacMillan, D. W. C. *Nature Reviews Chemistry* **2017**, *1* (7), 0052.
- (3) Welin, E. R.; Le, C.; Arias-Rotondo, D. M.; McCusker, J. K.; MacMillan, D. W. C. *Science* **2017**, *355* (6323), 380.
- (4) Romero, N. A.; Nicewicz, D. A. *Chem. Rev.* **2016**, *116* (17), 10075.
- (5) Prier, C. K.; Rankic, D. A.; MacMillan, D. *Chem. Rev.* **2013**, *113* (7), 5322.
- (6) Narayanam, J. M. R.; Tucker, J. W.; Stephenson, C. R. J. *J. Am. Chem. Soc.* **2009**, *131* (25), 8756.
- (7) Ischay, M. A.; Anzovino, M. E.; Du, J.; Yoon, T. P. *J. Am. Chem. Soc.* **2008**, *130* (39), 12886.
- (8) Nicewicz, D. A.; MacMillan, D. W. C. *Science* **2008**, *322* (5898), 77.
- (9) McNally, A.; Prier, C. K.; MacMillan, D. W. C. *Science* **2011**, *334* (6059), 1114.
- (10) Zuo, Z.; MacMillan, D. W. C. *J. Am. Chem. Soc.* **2014**, *136* (14), 5257.
- (11) Weix, D. J. *Acc. Chem. Res.* **2015**, *48* (6), 1767.
- (12) Biswas, S.; Weix, D. J. *J. Am. Chem. Soc.* **2013**, *135* (43), 16192.
- (13) Zuo, Z.; Ahneman, D. T.; Chu, L.; Terrett, J. A.; Doyle, A. G.; MacMillan, D. W. C. *Science* **2014**, *345* (6195), 437.
- (14) Tellis, J. C.; Primer, D. N.; Molander, G. A. *Science* **2014**, *345* (6195), 433.
- (15) Gutierrez, O.; Tellis, J. C.; Primer, D. N.; Molander, G. A.; Kozlowski, M. C. *J. Am. Chem. Soc.* **2015**, *137* (15), 4896.

- (16) Zuo, Z.; Cong, H.; Li, W.; Choi, J.; Fu, G. C.; MacMillan, D. W. C. *J. Am. Chem. Soc.* **2016**, *138* (6), 1832.
- (17) Joe, C. L.; Doyle, A. G. *Angew. Chem. Int. Ed. Engl.* **2016**, *55* (12), 4040.
- (18) Johnson, J. B.; Bercot, E. A.; Rowley, J. M.; Coates, G. W.; Rovis, T. *J. Am. Chem. Soc.* **2007**, *129* (9), 2718.
- (19) Huang, C.-Y. D.; Doyle, A. G. *J. Am. Chem. Soc.* **2015**, *137* (17), 5638.
- (20) Huang, C.-Y.; Doyle, A. G. *J. Am. Chem. Soc.* **2012**, *134* (23), 9541.
- (21) Giovannini, R.; Stüdemann, T.; Dussin, G.; Knochel, P. *Angew. Chem. Int. Ed. Engl.* **1998**, *37* (17), 2387.
- (22) Giovannini, R.; Stüdemann, T.; Devasagayaraj, A.; Dussin, G.; Knochel, P. *J. Org. Chem.* **1999**, *64*, 3544.
- (23) Devery Iii, J. J.; Douglas, J. J.; Nguyen, J. D.; Cole, K. P.; Flowers Ii, R. A.; Stephenson, C. R. J. *Chem. Sci.* **2015**, *6* (1), 537.
- (24) Schmidbauer, S.; Hohenleutner, A.; König, B. *Beilstein J. Org. Chem.* **2013**, *9*, 2088.
- (25) Luo, J.; Zhang, J. *ACS Catal* **2016**, *6* (2), 873.
- (26) Le, C. C.; Wismer, M. K.; Shi, Z.-C.; Zhang, R.; Conway, D. V.; Li, G.; Vachal, P.; Davies, I. W.; MacMillan, D. W. C. *ACS Cent Sci* **2017**, *3* (6), 647.
- (27) Chu, L.; Ohta, C.; Zhiwei, Z.; MacMillan, D. W. C. *J. Am. Chem. Soc.* **2014**, *136* (31), 10886.
- (28) Noble, A.; McCarver, S. J.; MacMillan, D. W. C. *J. Am. Chem. Soc.* **2015**, *137* (2), 624.
- (29) Bercot, E. A.; Rovis, T. *J. Am. Chem. Soc.* **2005**, *127* (1), 247.
- (30) Primer, D. N.; Karakaya, I.; Tellis, J. C.; Molander, G. A. *J. Am. Chem. Soc.* **2015**, *137* (6), 2195.

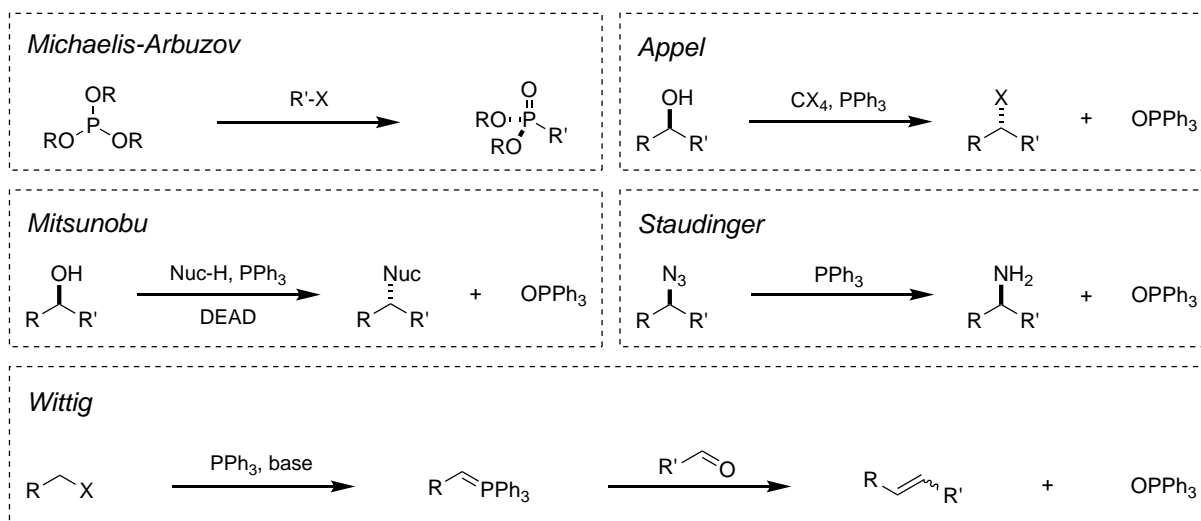
- (31) Hansch, C.; Leo, A.; Taft, R. W. *Chem. Rev.* **1991**, *91*, 165.
- (32) Bercot, E. A.; Rovis, T. *J. Am. Chem. Soc.* **2002**, *124* (2), 174.
- (33) O'Brien, E. M.; Bercot, E. A.; Rovis, T. *J. Am. Chem. Soc.* **2003**, *125* (35), 10498.
- (34) Cordier, C. J.; Lundgren, R. J.; Fu, G. C. *J. Am. Chem. Soc.* **2013**, *135* (30), 10946.
- (35) Ventre, S.; Petronijevic, F. R.; MacMillan, D. W. C. *J. Am. Chem. Soc.* **2015**, *137*, 5654.
- (36) Zhao, W.; Zhao, D.; Guizzetti, S.; Schwindeman, J. A.; Daniels, D. S. B.; Guerrero, C.; Knight, J. *Org. Process Res. Dev.* **2017**, *21*, 1187.
- (37) Jouffroy, M.; Primer, D. N.; Molander, G. A. *J. Am. Chem. Soc.* **2015**, *138* (2), 475.
- (38) Stache, E. E.; Rovis, T.; Doyle, A. G. *Angew. Chem. Int. Ed. Engl.* **2017**, *56* (13), 3679.

Chapter 3

Single-electron chemistry of phosphines: phosphine radical cations and phosphoranyl radicals—their generation and synthetic applications

3.1 Introduction

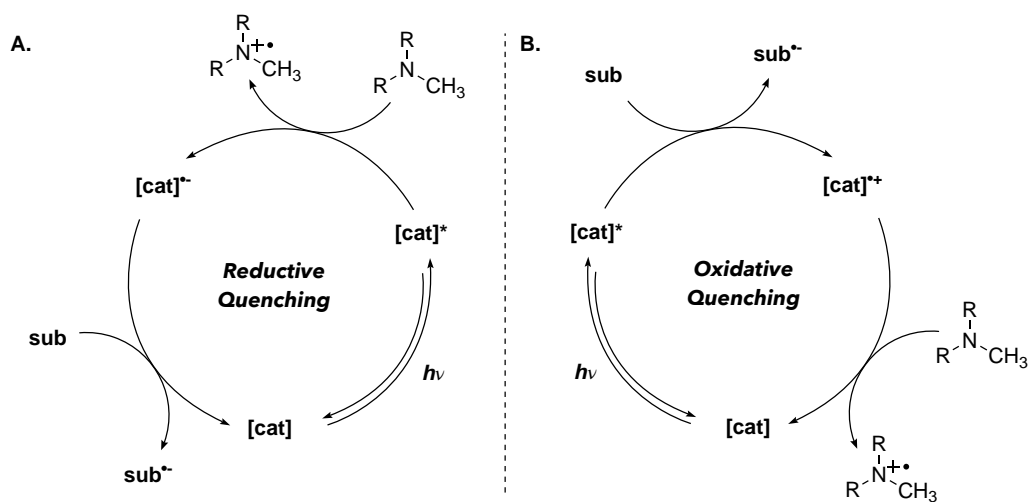
In the whole of synthetic organic chemistry, countless transformations and reagents have been developed to both understand organic compounds, as well as construct complex molecules. One of the most intriguing things about modern organic chemistry is the development of new synthetic methods employing conventional reagents with burgeoning synthetic tools. Phosphines represent one such example—typical reactions include the Appel, Michaelis-Arbuzov, Mitsunobu, Staudinger and of course the Wittig reaction and its variations (Scheme 3.1).¹ While these reactions are powerful, traditional synthetic organic methods and incredibly useful for building molecules, they only comprise the two-electron chemistry of phosphines.



Scheme 3.1

Nitrogen containing compounds, such as tertiary amines, have recently gained new synthetic utility when used in concert with photoredox catalysis,² as their oxidation potentials are

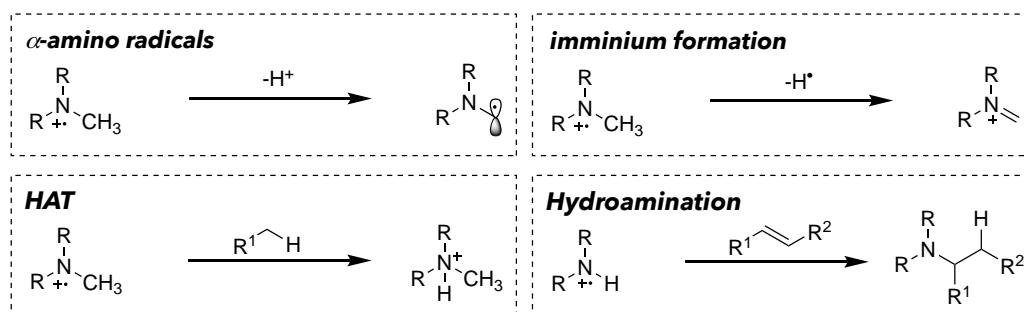
accessible to many photoredox catalysts.^{3,4} For example, an amine is used to quench the photocatalyst to generate a highly reducing species ($[\text{cat}]^{\bullet-}$) that is then capable of reducing an organic substrate of interest (Scheme 3.2).^{5,6} The resultant amine radical cation can act as an H-atom source or undergo some other decomposition pathway. Alternatively, a tertiary amine can be used to close the photocatalytic cycle, after the excited state photocatalyst has reduced a substrate, to form an amine radical cation. When thinking about single-electron organophosphorus chemistry, it is helpful to consider this single-electron chemistry of nitrogen, one row above in the periodic table.



Scheme 3.2

Amine radical cations are utilized in a variety of synthetic applications (Scheme 3.3). They can undergo a polar deprotonation at the α -carbon to form an α -amino radical or H-atom abstraction to form an imminium ion.⁷ Alternatively, amine radical cations have shown incredible utility in hydrogen atom transfer (HAT) reactions, affording a new alkyl radical species and an ammonium salt.⁸ Additionally, hydroamination is a particularly attractive application, achieved by adding an amine radical cation across an olefin acceptor.⁹ In this chapter, I will discuss the one-electron chemistry of phosphines, particularly as it relates to phosphine radical cations and

phosphoranyl radicals. While there has been a great deal of studies dedicated to these intermediates, they have not been frequently employed in modern synthetic chemistry and could be further utilized in the development of new synthetic methods, particularly when applied in concert with photoredox catalysis.



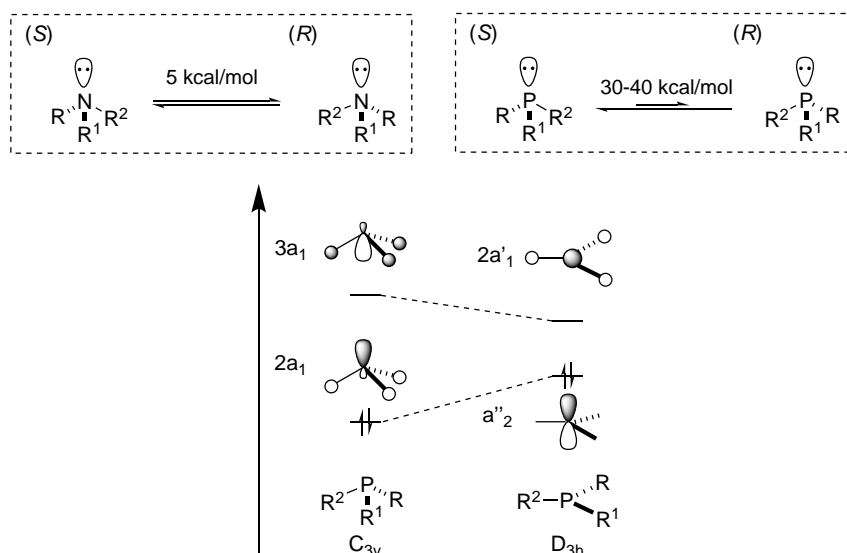
Scheme 3.3

3.2 Generation of phosphine radical cations

3.2.1 Stereochemical inversion

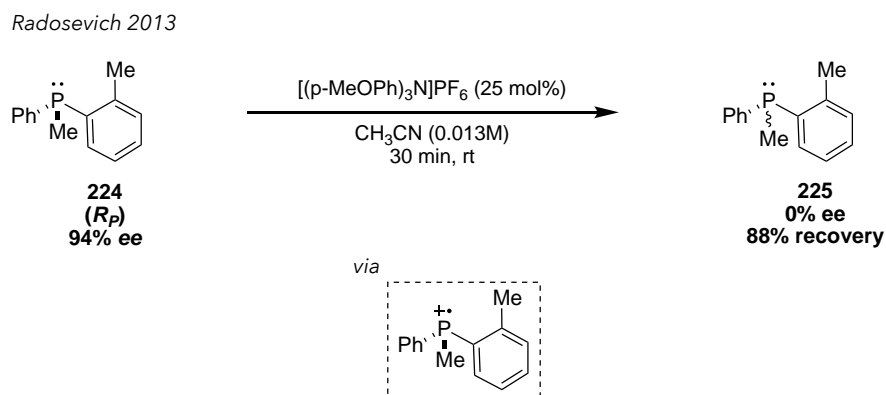
In 2013, the Radosevich group published a catalytic racemization of enantioenriched phosphines.¹⁰ Highlighting a difference between nitrogen and phosphorus-containing compounds, amines undergo rapid pyramidal inversion at room temperature (Scheme 3.4). Conversely, phosphines have a much higher barrier to inversion, and will not convert at room temperature, allowing the synthesis and isolation of enantioenriched phosphines. This barrier to inversion can be rationalized by examining the frontier orbitals of a trivalent phosphine compound. The pyramidal configuration contains significant HOMO-LUMO orbital mixing, thus lowering the HOMO energy. To invert, the phosphine must go through a planar configuration, which after a loss of HOMO-LUMO orbital mixing (more significant in phosphines compared to amines), raises the energy of the HOMO significantly, providing the high barrier to inversion. By removing one electron from the phosphine, it adopts a much more planar structure as the repulsion of the substituents now overcomes the repulsion from the radical cation left in the p-

orbital. From a more planar configuration, there is less of an energetic penalty to fully planarize, and thus the inversion barrier can be lowered to ~5 kcal/mol.



Scheme 3.4

Experimentally, Radosevich and coworkers demonstrated this hypothesis by subjecting enantioenriched phosphines to a single-electron oxidant. At room temperature, they observed near complete erosion of enantioselectivity for a variety of diaryl alkyl phosphines (**225**), as well as a dialkyl aryl phosphine (Scheme 3.5). Interestingly, more bulky phosphines did not undergo

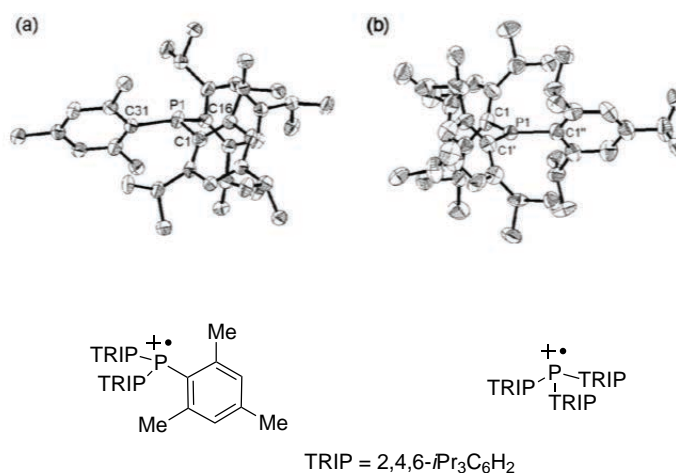


Scheme 3.5

complete inversion; this feature is attributed to a more difficult electron transfer. Additionally, while they observed high mass recovery of the racemic phosphines, they did observe up to 10%

yield of a phosphine oxide product. They attribute the formation of the phosphine oxide to adventitious water that is present in acetonitrile.

The degree of planarity of a phosphine radical cation largely depends on the substituents on the phosphine and calculations have suggested a slightly distorted pyramidal configuration, although the actual structure of a phosphine radical cation had not been observed experimentally. The Wang group, however, was able to obtain X-ray quality crystals after subjecting two tri-aryl phosphine species to single-electron oxidation with silver(I) salts (Scheme 3.6).¹¹ With two TRIP substituents and mesityl group, the phosphine radical cation is far less pyramidalized than its neutral phosphine precursor. With three very bulky TRIP substituents, the phosphine radical is fully trigonal planar; calculations agree with the crystal structure, with the radical existing in a pure p-character orbital.



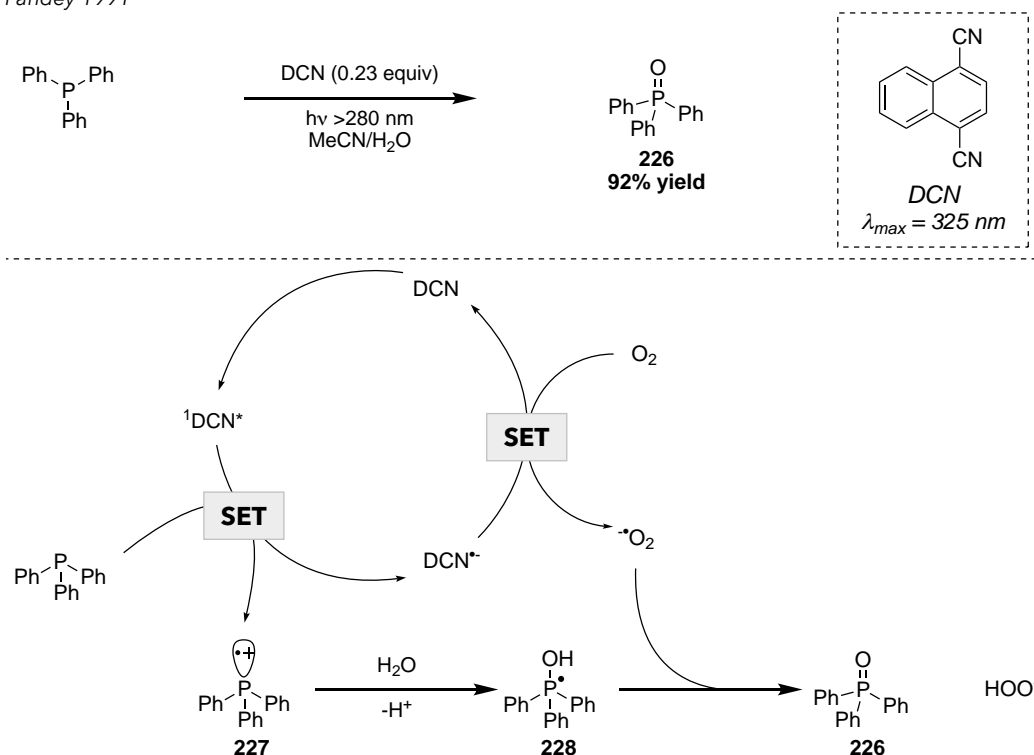
Scheme 3.6

3.2.2 Phosphine radical cations via photocatalysis

The formation of the phosphine oxide in the Radosevich work speaks to the reactivity of the phosphine radical cation, beyond reversible SET to regenerate the phosphine. Formation of phosphine oxide resulting from reaction of water and phosphine radical cation had been

previously reported. Pandey and coworkers observed a photocatalyzed oxidation of triphenylphosphine to triphenylphosphine oxide (Scheme 3.7).¹² Using dicyanonaphthalene (DCN) as a photocatalyst in the presence of UV light and aqueous MeCN, they observed high conversion to triphenylphosphine oxide (**226**). As a control reaction, in the absence of water, they did not observe the oxide product. Mechanistically, they envision after photoexcitation of DCN to the singlet excited state ($^1\text{DCN}^*$) [$E_{red}^{SI} = +2.30$ V vs. SCE], single-electron oxidation

Pandey 1991



Scheme 3.7

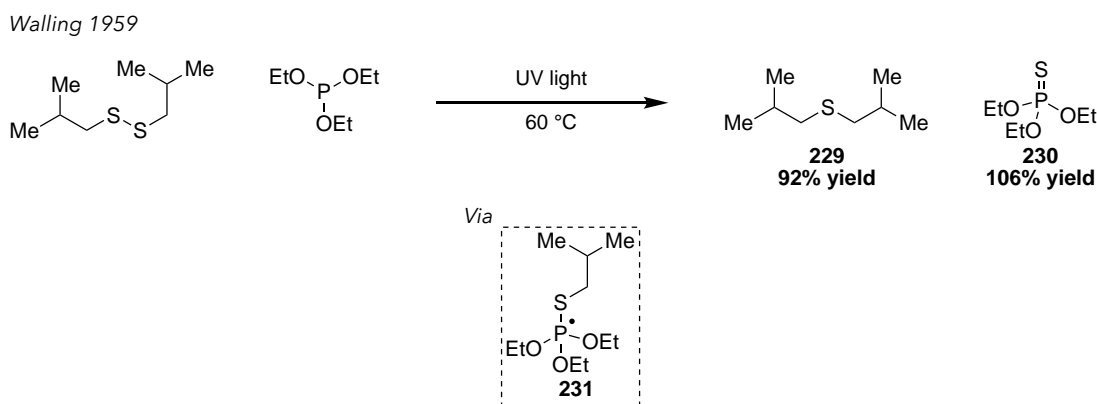
of triphenylphosphine [$E_{1/2} = +0.98$ V vs. SCE] gives phosphine radical cation **227**. Water could then add into the phosphine radical cation in a two-electron pathway to give a phosphoranyl radical (**228**). After a SET event between the reduced form of the photocatalyst and advantageous oxygen, superoxide ($\text{O}_2^{\bullet-}$) may undergo SET with **228**, followed by proton transfer

to give the product. Alternatively, H-atom abstraction from the phosphoranyl radical could give the product directly and peroxide anion as the byproduct.

3.3 Synthesis of phosphoranyl radicals

3.3.1 Identification and structure

Phosphoranyl radicals and their unique reactivity were proposed in 1959 by Walling,¹³ although their reactivity was disclosed by Hoffmann in 1956.¹⁴ Both Walling and Hoffmann disclosed desulfurization reactions in the presence of triethylphosphite and either light or heat. Walling, believing the reaction to proceed via radicals, demonstrated that disulfides were also competent reagents in this reaction (Scheme 3.8). Upon homolysis of the disulfide bond when exposed to UV light, the resultant thiyl radical will add to triethylphosphite to make phosphoranyl radical **231**. β -Scission of **231** would give the alkyl radical which could combine with the other equivalent of thiyl radical to give the sulfide product (**229**), and the thiophosphate **230** as the byproduct. Alternatively, oxidation of the phosphoranyl radical by the other equivalent of thiyl radical would give the phosphonium and S_N2 displacement would afford the same products.



Scheme 3.8

Since then, phosphoranyl radicals have been well documented and studied within the literature. They are a tetravalent phosphorus compound with an unpaired electron. The Coote group summarized the possible structures of phosphoranyl radicals based on the attached ligands (Scheme 3.9).¹⁵ Frequently they adopt a trigonal bipyramidal structure where the unpaired electron is found either in the equatorial plane. In rare examples, it has been suggested that the radical may occupy the apical position, although this has been disputed by Roberts.^{16,17} Alternatively, the species may adopt a tetrahedral geometry, where the radical sits in the σ^* orbital of the basal bond. Most phosphoranyl radicals adopt structures somewhere between trigonal bipyramidal and tetrahedral. A ligand π complex can also arise, usually occurring when one or more of the substituents are an aryl ring that can accommodate the radical, leaving a positive charge on phosphorus.



Scheme 3.9

Reactions to form phosphoranyl radicals have typically arisen from radical addition to a trivalent phosphine.¹⁸ Bentrude has classified these radical additions under three possible conditions. First, radicals may add to trivalent phosphine rapidly and irreversibly, with high exothermicity on the order of 10-20 kcal/mol, depending on the respective identities of radical and phosphine. Typical radical species and phosphines that fall under this regime are shown in Table 3.1. It is interesting to note that a phosphine radical cation can add to another equivalent of a trivalent phosphine to make a phosphorus–phosphorus bond. Second, the radical may add reversibly to a trivalent phosphine. In this case, a subsequent α - or β -scission fragmentation is

needed to push the reaction forward. Radicals of intermediate stability, such as primary alkyl or aminyl radicals fall under this type of reactivity where the intermediate phosphoranyl radical may only be observed spectroscopically. Third, reactions of stable alkyl radicals with trivalent phosphines generally are not observed spectroscopically, although this is highly dependent on the phosphine used. If diphenyl phosphinites or triphenylphosphine is employed, these radicals would fall under a case 2 regime, where radical addition is highly reversible. Benstrude suggests that in structures with 2 or more phenyl rings, a more stable ligand- π structure is likely obtained.

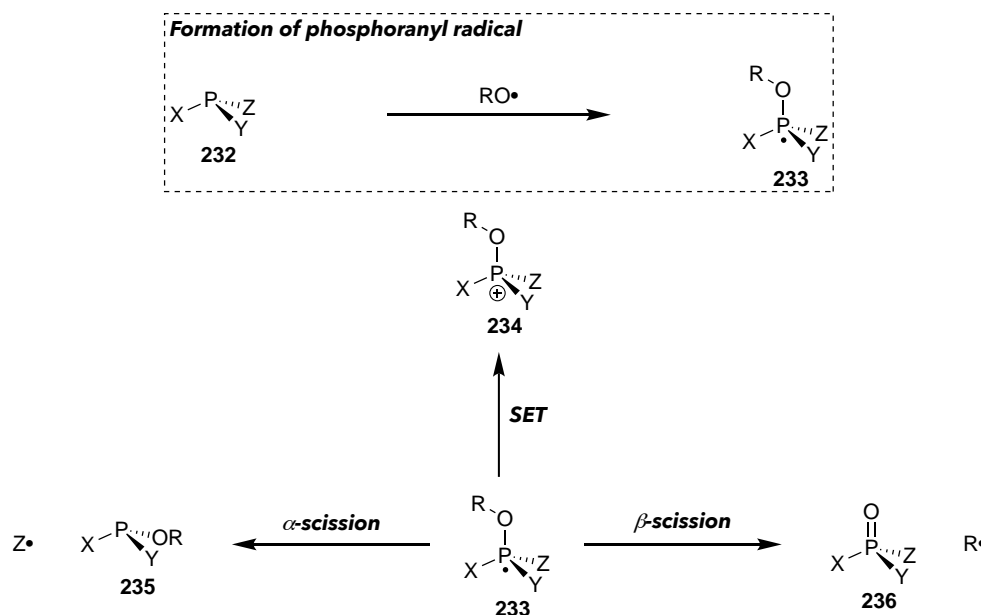
Table 3.1

	R•		PX ₃	
Case 1: fast and irreversible addition	RO•	TMSO•	PPh ₃	P(OEt) ₃
	Ph•	X ₃ P ⁺⁺	PEt ₃	PhP(OMe) ₂
	BzO•	RS•		
Case 2: fast and reversible addition	Et•	Me•	PPh ₃	P(OEt) ₃
	Me ₂ N•	CF ₃ •	PEt ₃	PhP(OMe) ₂
	C ₂ F ₅ •		P(O <i>i</i> Pr) ₃	
Case 3: no addition	PhCH ₂ •	<i>t</i> Bu•	P(OEt) ₃	PhP(OEt) ₂
	<i>i</i> Pr•			

3.3.2 Possible reaction pathways

Phosphoranyl radicals have been very well studied spectroscopically, and are known to undergo fragmentation pathways as well as radical additions or direct oxidations.¹⁸⁻²¹ As depicted in Scheme 3.10, the phosphoranyl radical is generally formed via radical addition to a trivalent phosphine. Radical **233** can undergo SET with an oxidant to form a phosphonium ion (**234**), which may further undergo Arbuzov type reactivity to form a phosphine oxide, depending on the substituents. Alternatively, radical **233** can undergo α -scission to form a new trivalent phosphine species (**235**) and radical, resulting in a net substitution reaction on phosphorus. This process is proposed to occur from the apical position on the phosphine. Finally, β -scission of

radical **233** can occur to form a phosphine oxide (**236**) and a new radical species. Whether β -scission occurs from the apical position or the equatorial position is not fully agreed upon, although it likely depends on the structure of the phosphoranyl radical.



Scheme 3.10

3.3.3 α - versus β -scission

The relative rates of α - and β -scission are largely dictated by relative radical stabilities of the phosphoranyl radical and possible leaving groups, as well as respective bond strengths.^{18,19,22} Table 3.2 summarizes the competition between α - and β -scission, when all substituents on phosphorus are the same, after radical addition to the trivalent phosphine. It also lists the P–X bond strength for PX_3 . In entry 1, when *t*-butoxy radical is added to triethylphosphite at 130 °C, β -scission is exclusively observed, forming *t*-butyl radical and the phosphate. When the same radical is added to triphenylphosphine, exclusive oxidation is observed to triphenylphosphine oxide with *t*-butyl radical formation (entry 2). Addition to triethylphosphine at -80 °C, however, results in formation of the substitution product and ethyl radical (entry 3). In contrast, when

tributylphosphine is employed at 130 °C, a mixture of substitution and oxidation products are observed (entry 4). The formation of an oxidation product is clearly the thermodynamic product, while the substitution product is a kinetic product. The difference in reactivity of these two similar phosphines may be explained by the difference in temperature. Triphenylphosphite undergoes substitution with *t*-butoxy radical to form phenoxy radical and the substitution product (entry 5). Thiyl radicals also give oxidation products when added to triethylphosphite and triphenylphosphine (entry 6 and 7), but when added to triphenylphosphite, the phenoxy radical and α -scission still predominates.

Table 3.2

entry	RO• or RS•	X = Y = Z	temp (°C)	α -scission	β -scission	radical	PX ₃ *
1	<i>t</i> BuO	OEt	130	–	+	<i>t</i> Bu	84
2	<i>t</i> BuO	Ph	130	–	+	<i>t</i> Bu	77
3	<i>t</i> BuO	Et	-80	+	–	Et	62
4	<i>t</i> BuO	<i>n</i> Bu	130	+	+	<i>n</i> Bu, <i>t</i> Bu	62
5	<i>t</i> BuO	OPh	130	+	–	OPh	69-74
6	<i>t</i> BuS	OEt	60-120	–	+	<i>t</i> Bu	84
7	<i>n</i> BuS	Ph	70	–	+	<i>n</i> Bu	77
8	<i>n</i> BuS	OPh	70	+	–	OPh	69-74

* P–X bond strength from PX₃; (+) refers to >10% yield of observed product

Based on the data in Table 3.2, the competition between α - and β -scission is not determined by radical stability alone, as *t*-butyl radical would be the most stable radical formed in all cases. Bentrude surmises that the relative C–O (or C–S) and P–X bond strengths also contribute to the observed product distribution.¹⁹ In cases where substitution is favored, the P–X bond strength is estimated at less than 75 kcal/mol. The exception is the comparison of entry 3 and 4, where

oxidation becomes competitive with substitution, despite the weak P–C bond strength. This result could be attributed to a temperature effect, where the thermodynamic product becomes competitive.

Bentrude also examined the product distribution in cases of alkoxy radical addition to diethylphosphonites (Table 3.3).¹⁹ In cases where X = ethyl, *t*Bu, benzyl or NR₂, he observed almost exclusive substitution to form a new phosphinite and the corresponding alkyl or aminyl radical (entry 1-4). These observations highlight that relative bond strength seems to dominate over radical stability. As the corresponding P–X bond becomes stronger, –Cl or –OAc, β-scission becomes competitive or becomes the exclusive fragmentation pathway (entry 5 and 6). In entries

Table 3.3

entry	RO•	X	α-scission	β-scission	radical	PX ₃ *
1	<i>t</i> BuO	Et	86%	0%	Et	62
2	<i>t</i> BuO	<i>t</i> Bu	82%	0%	<i>t</i> Bu	n/a
3	<i>t</i> BuO	PhCH ₂	81%	0%	PhCH ₂	48
4	<i>t</i> BuO	nBu ₂ N	84%	4%	Bu ₂ N	59-69
5	<i>t</i> BuO	Cl	36%	41%	Cl or <i>t</i> Bu	77
6	<i>t</i> BuO	OAc	0%	84%	<i>t</i> Bu	<84
7	PhCH ₂ O	Me	20%	57%	PhCH ₂	67
8	PhCH ₂ O	Et	56%	11%	Et	62
9	PhCH ₂ O	<i>t</i> Bu	58%	3%	<i>t</i> Bu	n/a
10	PhCH ₂ O	PhCH ₂	67%	3%	PhCH ₂	48

* P–X bond strength from PX₃; temperature 60-65 °C

7-10, decreasing P–X bond strength leads to increasing α-scission across a range of alkyl substituents. It is interesting to note that the same reactions with thiyl radical addition tend to favor exclusively β-scission products (i.e. entry 1 gives 87% β-scission when *t*BuS• is used).

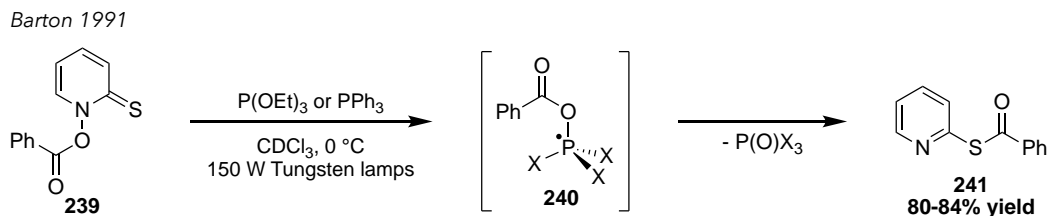
Bentrude concludes that these data together point to relative C–S and P–X bond strengths as being the dominant factor in deciding substitution versus oxidation, rather than radical stability, although other factors cannot be ignored, such as temperature and entropic effects. He also notes that phenyl substitution tends to favor β -scission, perhaps because of lowering the activation barrier by the intermediacy of a ligand- π complex.

3.4 Synthetic applications of phosphoranyl radicals

Phosphoranyl radical intermediates have ample synthetic applications. In addition to the α - and β -scission pathways to generate new radical species, they have been used en route to diverse phosphorus containing compounds. This section will highlight some important applications of phosphoranyl radicals to synthesis, including recent examples of photocatalysis.

3.4.1 By β -Scission pathways

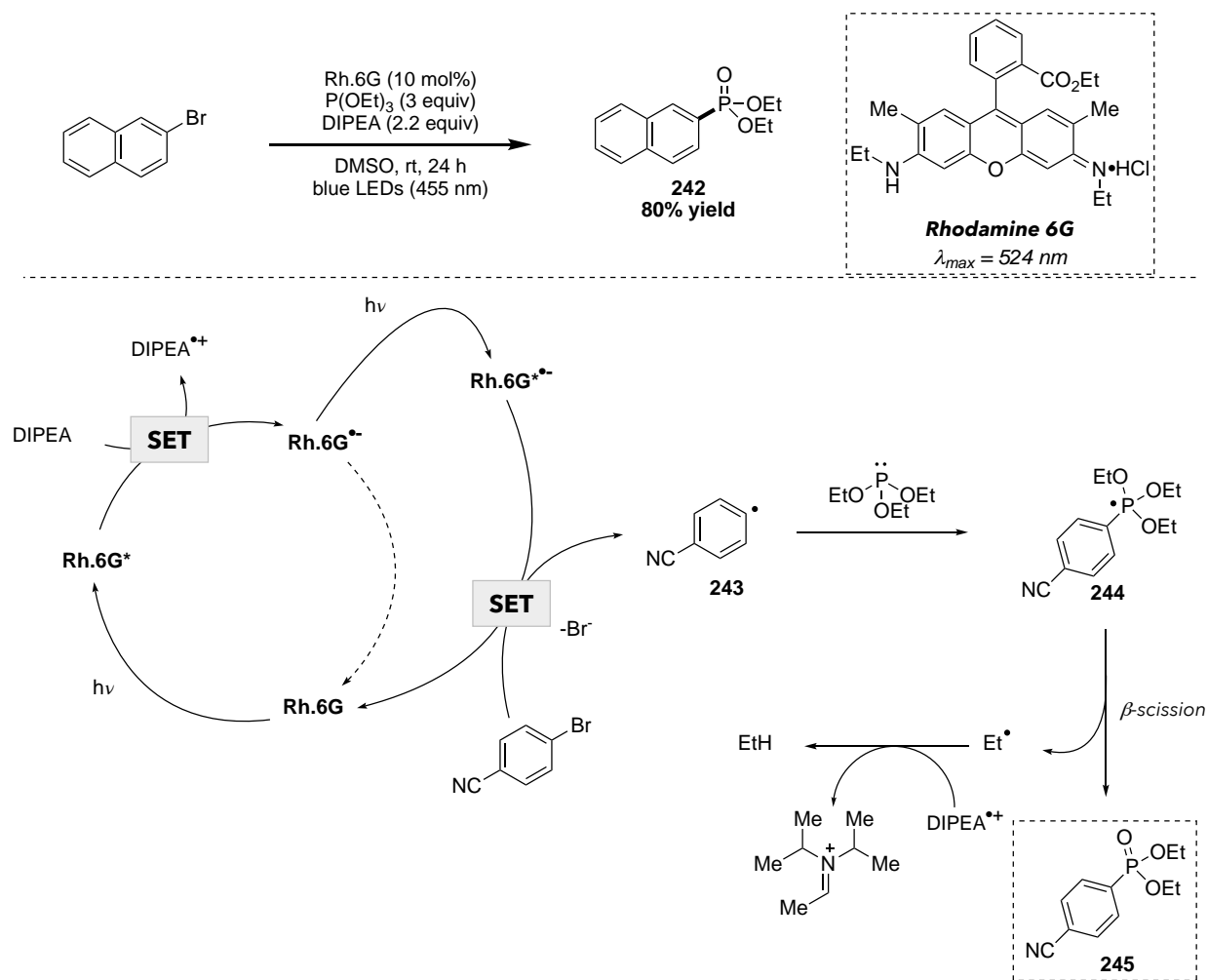
In 1991, Barton disclosed an activation of acyl equivalents to form acyl radicals (Scheme 3.11).²³ Photolysis of *N*-hydroxy-2-thiopyridone **239** can generate a carboxy radical, which upon addition to a phosphine equivalent (either triphenylphosphine or triethylphosphite) would give phosphoranyl radical **240**. Upon β -scission, an acyl radical would be generated along with a phosphine oxide byproduct. The acyl radical could combine with another equivalent of **239** to form product **241**, as well as propagate the chain to form a new carboxy radical equivalent. They also demonstrated addition of electrophilic carboxy radicals to ethyl vinyl ether in the absence of a phosphine equivalent.



Scheme 3.11

In 2016, König and coworkers reported the synthesis of aryl phosphonates using phosphites and aryl halides under photocatalysis (Scheme 3.12).²⁴ They employed Rhodamine 6G as the photocatalyst, which has the unique property of consecutive photoinduced electron transfer (conPET).²⁵ This rather unique mechanism arises when an excited state photocatalyst [Rh.6G*] undergoes single-electron transfer with a substrate to generate a radical anion [Rh.6G^{•-}], which

König 2016



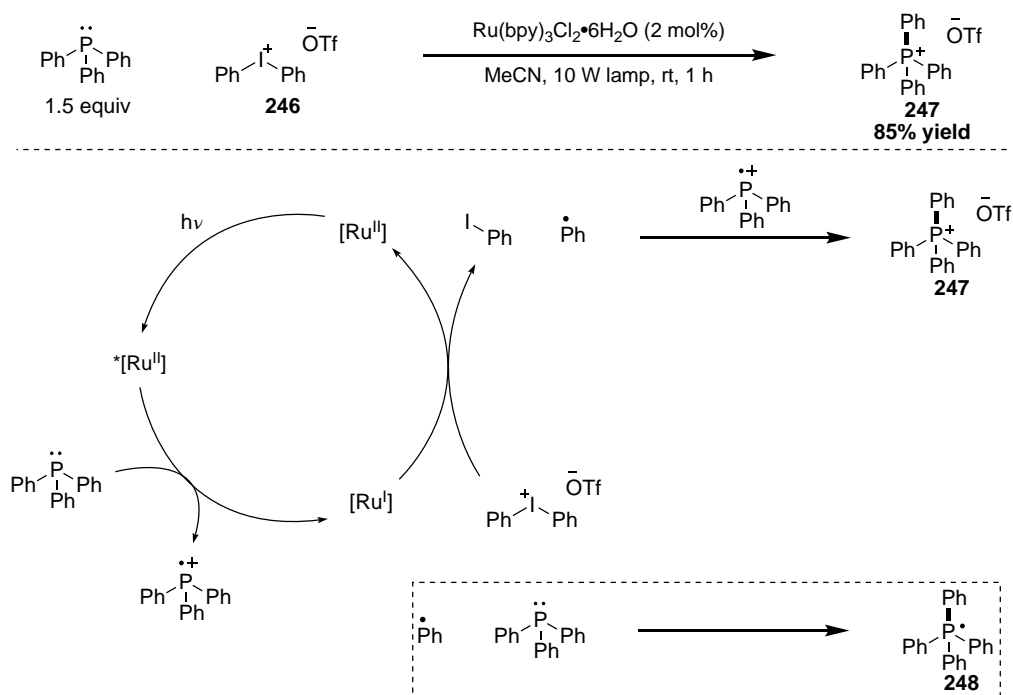
Scheme 3.12

can then absorb an additional photon of light to move into an excited state radical anion [Rh.6G^{•-}*]. This second excited state has a very high reducing potential { $E_{ox}^* = -2.4$ V vs. SCE}, compared to the ground state radical anion { $E_{ox} = -1.0$ V vs. SCE}. In this example, after

irradiation with visible light, Rh.6G can undergo single-electron oxidation with Hünig's base to afford $[\text{Rh.6G}^{\bullet-}]$ which is then photoexcited to $[\text{Rh.6G}^{\bullet-*}]$. This highly reducing species could engage in single-electron transfer with 4-bromobenzonitrile to form aryl radical **243**. The aryl radical would add to triethylphosphite to generate phosphoranyl radical **244**, where upon β -scission, the product (**245**) would be afforded and resultant ethyl radical would abstract an H-atom to generate ethane.

In 2016, Denton and coworkers disclosed a synthesis of quaternary aryl phosphoniums (**247**) utilizing photocatalysis (Scheme 3.13).²⁶ Mechanistically, they proposed single-electron oxidation of triphenylphosphine to the phosphine radical cation via an excited state $\text{Ru}(\text{bpy})_3^{*2+}$.

Denton 2016

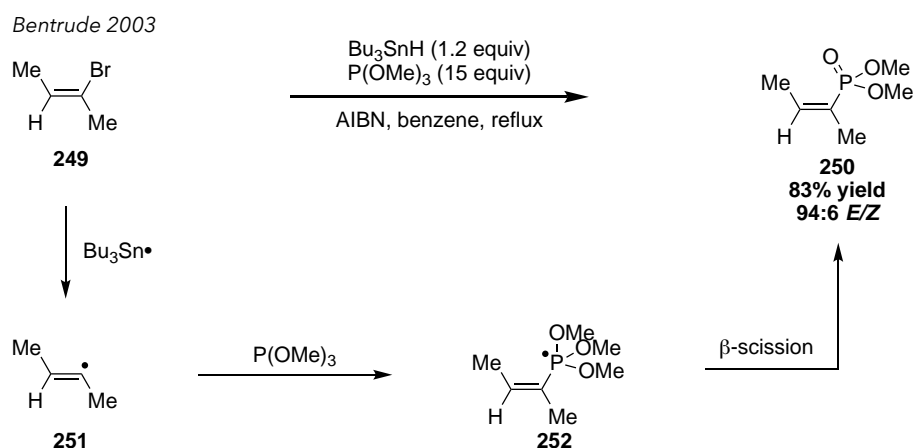


Scheme 3.13

Reduction of the iodonium salt (**246**) by the reduced form of the photocatalyst would give iodobenzene and phenyl radical. They then propose that the phenyl radical and phosphine radical cation combine to form the desired product. Alternatively, a radical chain process may be

occurring, where the phenyl radical adds irreversible to triphenylphosphine, followed by oxidation of phosphoranyl radical **248** to the product.

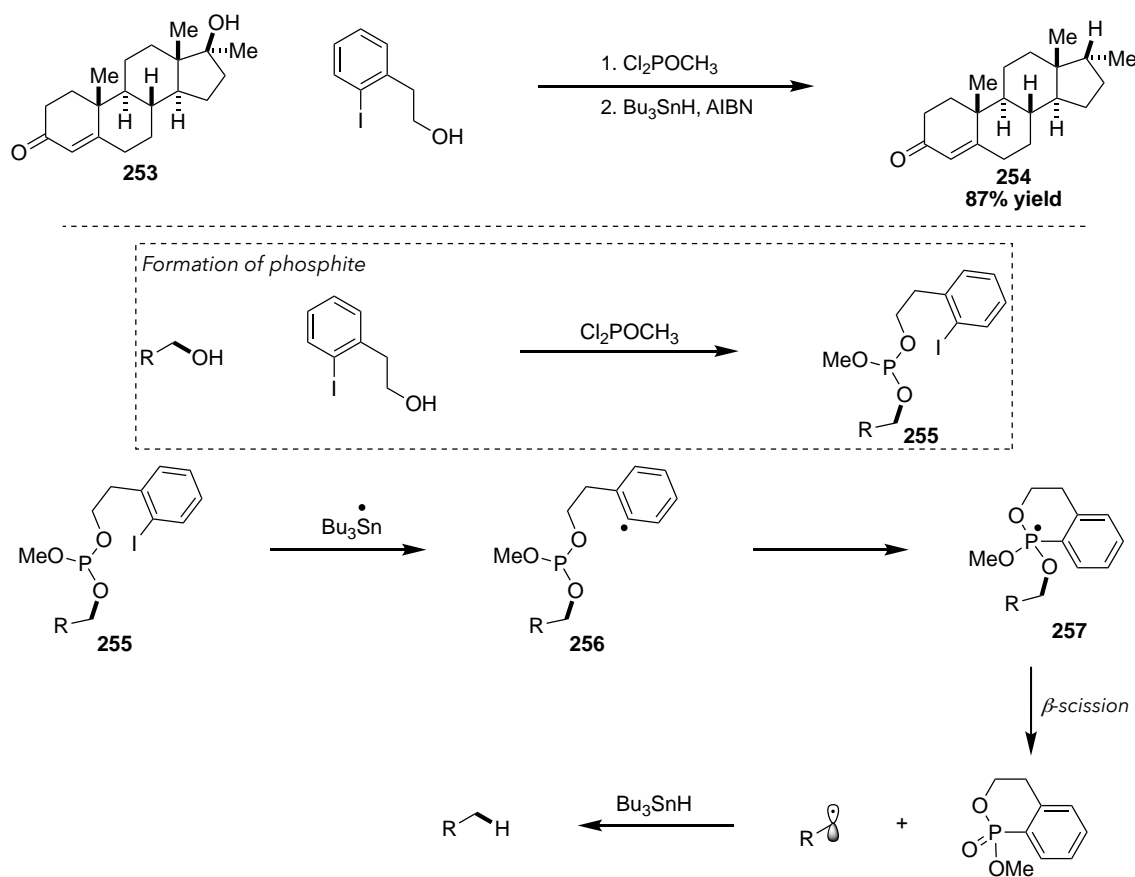
In 2003, Bentrude disclosed a synthesis of vinyl phosphonates via phosphoranyl radicals (Scheme 3.14).²⁷ Vinyl halides (**249**), in the presence of radical initiator AIBN and tributyltin hydride, could lead to generation of vinyl radical **251**. Addition into trimethylphosphite would afford phosphoranyl radical **252** and subsequent β -scission could give methyl radical and vinyl phosphonate product **250** in 94:6 *E/Z*. Methyl radical could abstract an H-atom from another equivalent of tributyltin hydride to propagate the radical chain. Use of *cis* or *trans* vinyl halides resulted in formation of the *trans* product selectively, likely through a radical mediated isomerization.



Scheme 3.14

In 2004, Koreeda reported the deoxygenation of primary, secondary and tertiary alkyl alcohols employing phosphoranyl radicals (Scheme 3.15).²⁸ In a two-step procedure, an alcohol is first mixed with a methyl dichlorophosphite to generate phosphite **255**. Then, in the presence of AIBN, tributyltin radical may be formed, which could abstract iodide from the aryl iodide to generate an aryl radical (**256**). Intramolecular cyclization of the radical onto the phosphite would generate a phosphoranyl radical (**257**). Preferred β -scission could occur to afford the desired

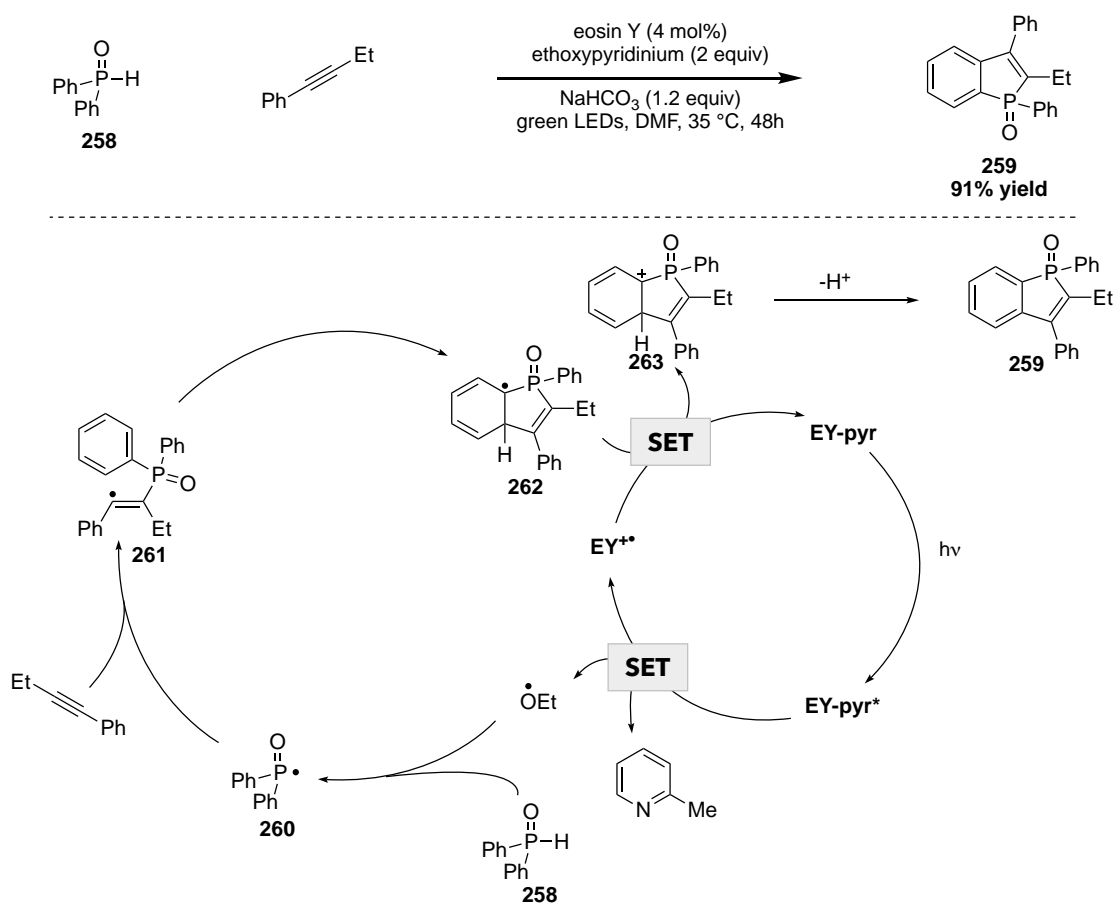
alkyl radical and phosphonate byproduct. H-atom transfer from another equivalent of tributyl tin hydride would provide the desired product (**254**), and propagate the radical chain process. Interestingly, in cases of primary alcohols, they observed a small amount of β -scission of the $-\text{OCH}_3$ to form methyl radical. With secondary alcohols, this side reaction was observed less, and not observed at all in the case of tertiary alcohols. The authors attribute this selectivity to the bulkiness of groups around the alcohol, and the preference for a ligand- π phosphoranyl radical structure. However, this could also be attributed to the relative radical stability, where methyl radical is significantly less stable than secondary or tertiary alkyl radicals.



Scheme 3.15

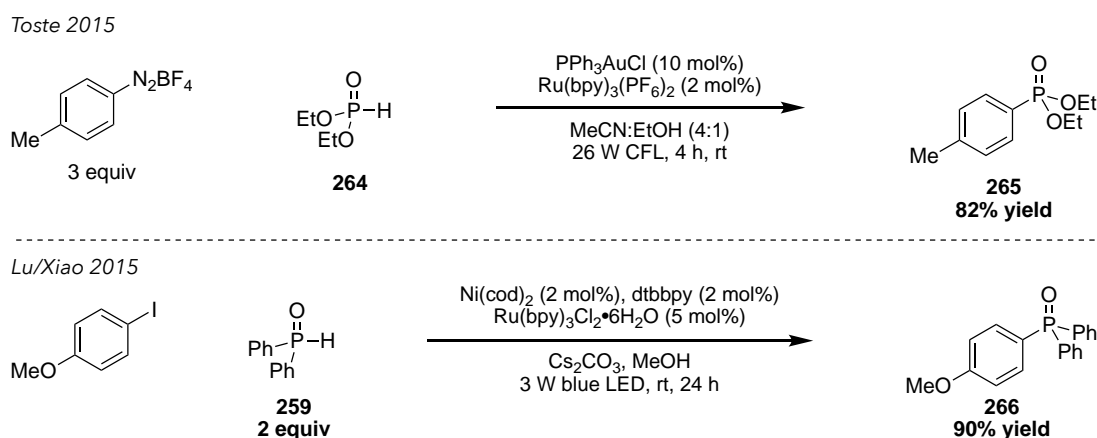
3.4.2 Phosphinoyl radicals

In 2016, the Lakhdar group reported a synthesis of benzo[*b*]phosphole oxides employing photocatalysis to generate phosphinoyl radicals, a variant of phosphoranyl radicals (Scheme 3.16).²⁹ Mechanistically, they proposed that *N*-ethoxy-2-methylpyridinium forms a ground state donor-acceptor complex with eosin Y based on extensive spectroscopic studies. Upon excitation with light, SET from the photocatalyst to the pyridinium would afford [EY^{•+}] and ethoxy radical, which could then abstract an H-atom from phosphine oxide **258** to afford phosphinoyl radical **260**. Addition into an alkyne would provide vinyl radical **261**, which could then cyclize onto the aromatic ring to generate radical **262**. Oxidation of the α -phosphino radical to **263** and subsequent deprotonation would give the product (**259**) and close the photocatalytic cycle.



Scheme 3.16

Phosphinoyl radicals have also been interfaced with transition metal catalysis. In 2015, the Toste group employed gold catalysis in concert with photocatalysis to couple *H*-phosphonates (**264**) with aryl diazoniums to generate aryl phosphonates (**265**) (Scheme 3.17).³⁰ Also in 2015, Lu/Xiao disclosed a cross-coupling of diarylphosphine oxides with aryl halides to generate mixed-aryl phosphine oxides.³¹ Under their photocatalytic conditions, they propose that the phosphinous acid (tautomer of **259**) undergoes single-electron oxidation with the excited state photocatalyst to generate a radical cation, which upon oxidation, forms a phosphorus-centered radical. The phosphinoyl radical interfaces with a Ni(II) oxidative adduct and reductive elimination from Ni(III) would afford the product (**266**).



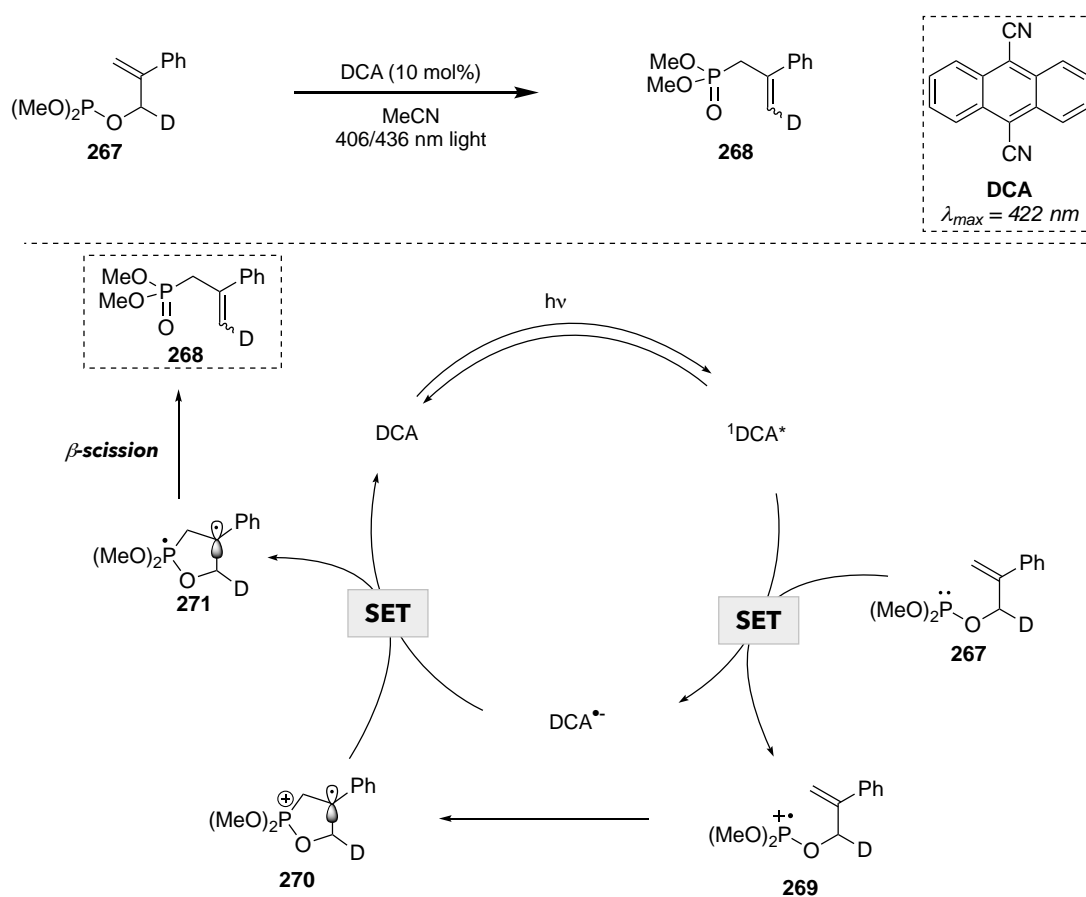
Scheme 3.17

3.5 Synthetic applications of phosphine radical cations

3.5.1 Radical additions

Phosphine radical cations have been used in numerous synthetic applications. In 1993, Bentrude and coworkers disclosed a photoinduced rearrangement of phenylallyl phosphites (Scheme 3.18).³² In the presence of dicyanoanthracene and visible light, the singlet excited state [¹DCA*] may undergo reductive quenching with **267** to form radical cation **269**. The phosphine radical cation can then cyclize onto the intramolecular styrene moiety to form radical cation **270**.

Single-electron reduction of **270** to turn over the photocatalyst and subsequent β -scission of **271** would afford the rearranged phosphonate product. Alternatively, ring opening of **270** may occur first to form an alkyl radical cation, which upon single-electron reduction by the photocatalyst would also afford the product. Alternatively, triplet sensitization of the styrene and subsequent cyclization onto the phosphine would afford the common phosphoranyl radical intermediate (**271**) to proceed to product. Under these conditions, the triplet energies of DCA and styrene are dissimilar, but this mechanistic pathway has been implicated in other publications.³³

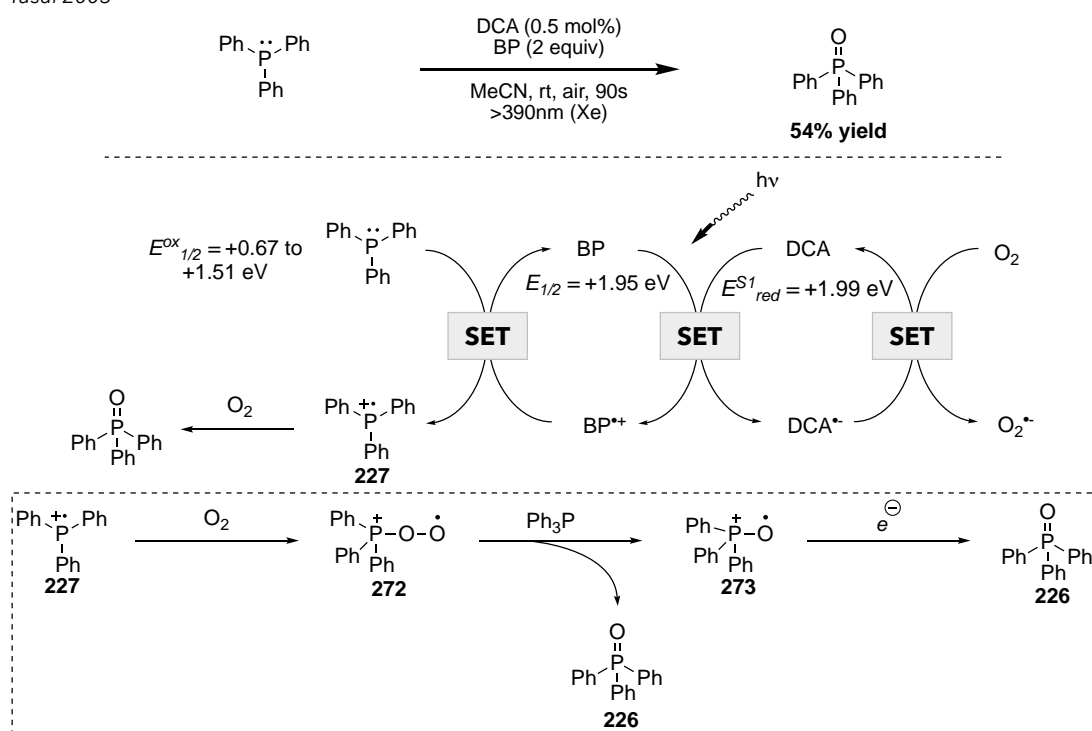


Scheme 3.18

In 2005, Yasui and coworkers conducted preparative and spectroscopic studies on the photocatalyzed reactions of triarylphosphines with oxygen (Scheme 3.19).^{34,35} After irradiation with light, [$^1\text{DCA}^*$] undergoes reductive quenching with biphenyl (BP). They propose that BP is

acting as an electron shuttle, which, upon formation of the radical cation, oxidizes triphenylphosphine to the radical cation (**227**). They then suggest that in an oxygen-rich environment, the phosphine radical cation reacts with molecular oxygen to ultimately afford the phosphine oxide. They propose that reaction with oxygen affords peroxide **272** which then reacts with another equivalent of phosphine. Upon β -scission, this gives phosphine oxide **226**, and phosphonium radical **273**. Reduction of this species, likely via oxidation of another equivalent of

Yasui 2005



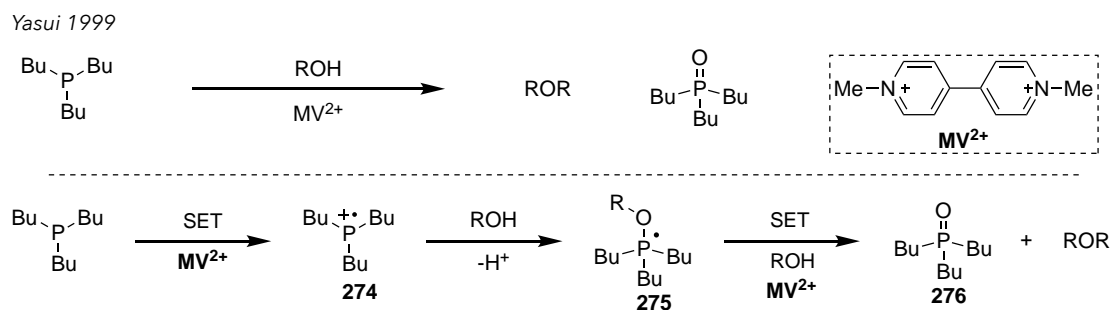
Scheme 3.19

triphenylphosphine to **273**, gives another equivalent of phosphine oxide. Alternatively, the authors have suggested that biphenyl may donate an electron to generate triphenylphosphine oxide and BP^{++} . They discounted formation of $^1\text{O}_2$ via $^1\text{DCA}^*$ on the basis that BP quenches the excited state of the photocatalyst much faster than the formation of singlet oxygen. However, they do observe that the reaction proceeds in the absence of BP, albeit at a significantly lower rate. The reaction also takes place under an ambient air environment, but again at a much slower

rate. They conducted a time-course reaction of consumption of different triarylphosphines under the reaction conditions with more electron-rich triarylphosphines are consumed more quickly. Interestingly, *ortho* substitution results in a retardation of rate of consumption. They propose that the flattening of the phosphine radical cation may result in electron delocalization into the aryl rings, and therefore a slower reaction with oxygen may occur.

3.5.2 Cationic trapping

Numerous reports of a phosphine radical cation acting as a cation, rather than a nucleophile have also been reported.^{10,12} In the examples by Radosevich and Pandey, they observed water trapping of a phosphine radical cation, likely followed by oxidation, to the phosphine oxide. Yasui and coworkers disclosed an alcohol trapping of phosphine radical cations, to ultimately synthesize the corresponding phosphine oxides, as well as ethers (Scheme 3.20).³⁶ In the presence of methyl viologen (MV^{2+}), tributylphosphine is oxidized to the corresponding radical cation (**274**). In an alcohol solvent, cationic trapping of **274** followed by proton transfer would afford phosphoranyl radical **275**. In the presence of stoichiometric MV^{2+} , **275** is quickly oxidized to the phosphonium and Arbuzov-type reactivity could give the phosphine oxide (**276**) as well as the alkyl ether.



Scheme 3.20

Yasui conducted a kinetic study on the reaction of alcohols with phosphine radical cations (Table 3.4). Using ethanol as the simplest primary alcohol and the starting point, they assigned a

k_{rel} value of 1 (entry 1). Water and methanol were slightly less reactive, with a k_{rel} of 0.61 and 0.55, respectively (entry 2 and 3). They attribute this slower reactivity to a less nucleophilic species. In contrast, *n*-butanol displayed a k_{rel} of 1.7, almost twice that of ethanol (entry 4). Again, they attribute this faster reactivity to a more electron rich oxygen species, and thus more nucleophilic for trapping the phosphine radical cation. A tertiary alcohol, *t*-butanol was significantly slower to react, likely to do with the more sterically hindered environment around the alcohol (entry 5). *n*-Butanethiol was three times slower to react than the corresponding alcohol, as thiols are less nucleophilic than the corresponding alcohols (entry 6). Interestingly,

Table 3.4

entry	alcohol	k_{rel}
1	EtOH	1
2	H ₂ O	0.61
3	MeOH	0.50
4	<i>n</i> BuOH	1.7
5	<i>t</i> BuOH	0.077
6	<i>n</i> BuSH	0.56
7	HO(CH ₂) ₃ OH	6.3
8	HO(CH ₂) ₄ OH	1.0

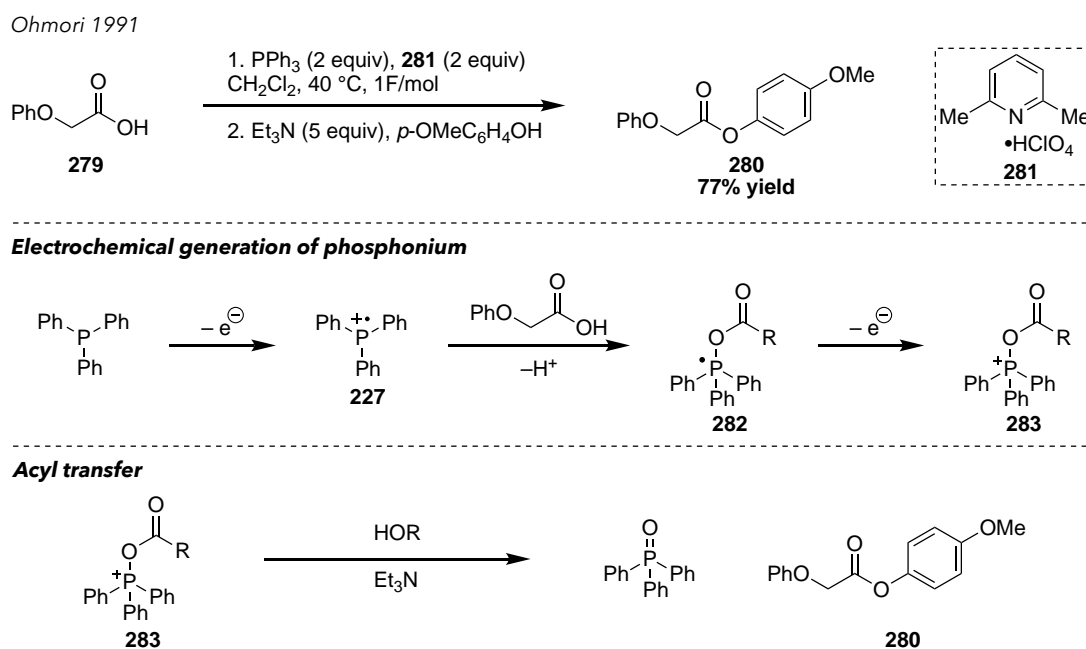
277

278

when they employed 1,3-propanediol, they observed a large rate enhancement (entry 7), but when 1,4-butanediol was used, the rate matched that of ethanol (entry 8). They hypothesized that in the alcohol addition step, a buildup of positive charge arises on oxygen (**277**). They attribute this rate difference to a chelating effect, where a 6-membered transition state (**278**) can alleviate

the buildup of positive charge onto two oxygen atoms. Yasui and coworkers have also conducted kinetic studies on the reaction of pyridines with phosphine radical cations under similar conditions.³⁷

The most synthetically relevant examples of nucleophilic quenching of phosphine radical cations has been explored by Ohmori and coworkers, using electrochemical methods. In 1991, they disclosed a mild esterification of carboxylic acids, using triphenylphosphine and **281** as an electrolyte under constant-current electrolysis (Scheme 3.21).³⁸ They proposed that single-electron oxidation of triphenylphosphine to the radical cation (**227**) would be followed by nucleophilic trapping of the cation by a carboxylic acid to form phosphoranyl radical **282**. Under

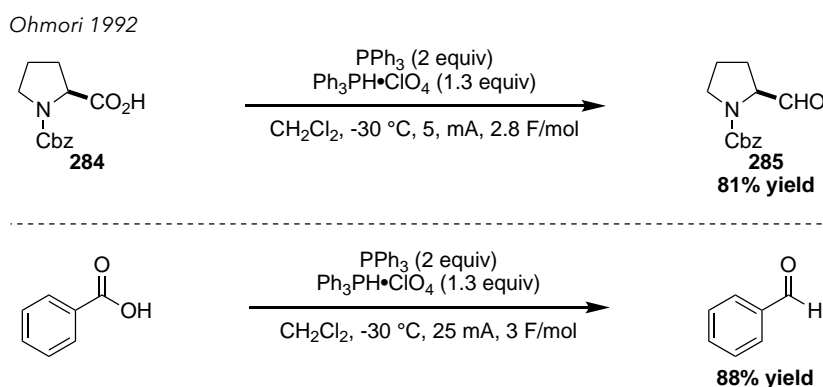


Scheme 3.21

the oxidizing electrochemical conditions, this species would be quickly oxidized to the corresponding phosphonium (**283**). Upon completion of this step, triethylamine and the corresponding nucleophile were added, rapid acyl transfer occurred to give ester **280** in 77%

yield. This procedure was also amenable to other acyl transfer reactions, such as the formation of amides and lactams.

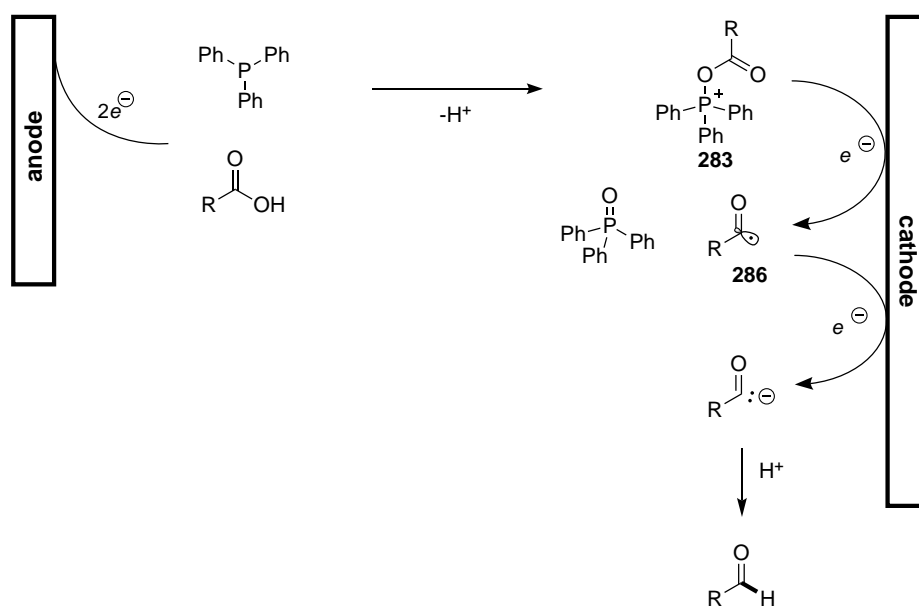
In 1992, Ohmori and coworkers demonstrated an electrochemical reduction of carboxylic acids to the corresponding aldehydes using constant current electrolysis (Scheme 3.22).³⁹ Using triphenylphosphine and $\text{Ph}_3\text{P}\cdot\text{HClO}_4$ as the electrolyte, they observed reduction of amino acid **284** to the corresponding amino aldehyde (**285**) in excellent yield. Importantly, they observed no loss of stereochemical information. Additionally, they demonstrated the reduction of benzoic acid to benzaldehyde under similar conditions. Interestingly, at higher temperatures, they observed formation of the acid anhydride, presumably via acyl transfer from the phosphonium.



Scheme 3.22

The proposed mechanistic hypothesis is shown in Scheme 3.23. At the anode, single-electron oxidation of triphenylphosphine to the phosphine radical cation, followed by nucleophilic quenching and subsequent oxidation of the phosphoranyl radical affords phosphonium **283**. At the cathode, single-electron reduction of the phosphonium yields triphenylphosphine oxide and acyl radical **286**. They do not propose the intermediate phosphoranyl radical followed by β -scission, although it likely follows the former mechanism proposed above. They suggest that the acyl radical is reduced to the acyl anion, followed by proton transfer to afford the desired aldehyde. It is interesting to note the high yields observed in the reduction of amino acids.

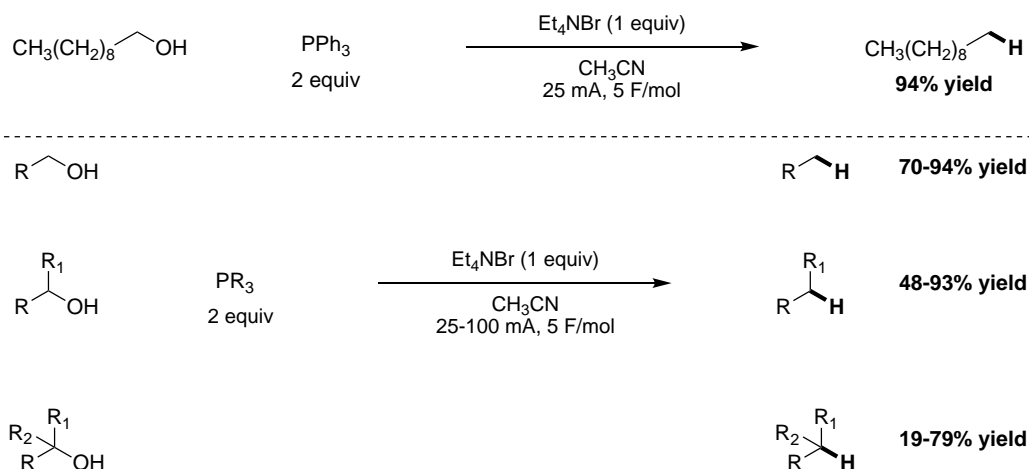
Despite their proposed intermediacy of an acyl radical, they do not observe decarbonylation, which is expected to be very rapid to form an α -amino radical. This suggests that the reaction does not proceed through an intermediate acyl radical, or that it is immediately reduced to the corresponding acyl anion, thereby avoiding rapid decarbonylation.



Scheme 3.23

Ohmori further explored this electrochemical approach in the context of aliphatic alcohol reduction (Scheme 3.24).⁴⁰ Like the acid reduction, in the presence of triphenylphosphine, tetraethylammonium bromide as the supporting electrolyte in acetonitrile, they observed the reduction of decanol to decane in excellent yield. They extended this methodology to the reduction of a series of primary, secondary and even tertiary alcohols to the corresponding alkanes in good to excellent yield. Interestingly, with tertiary alcohols, the phosphine dependence was significant, as they observed the formation of elimination products, and needed to increase the current to achieve the desired reduction to alkane. Mechanistically, they propose a similar process as that shown in Scheme 3.23, although they do not explicitly define an alkyl anion intermediate.

Ohmori 1994



Scheme 3.24

3.6 Conclusion

A wealth of spectroscopic studies on the radical chemistry of phosphines have been conducted. Numerous synthetic examples have showcased the power of phosphine radical chemistry in new bond-forming reactions. Despite these promising advances, synthetic opportunities exploiting this reactivity, particularly in the context of photoredox catalysis, have not been thoroughly explored. The electrochemical advances by Ohmori represent the most promising synthetic applications, but they have not been developed further. In the next chapter, I will discuss our progress toward realizing this goal through C–O bond activation via photocatalysis and phosphines and the synthetic opportunities that remain to be explored.

References

- (1) *Strategic Applications of Named Reactions in Organic Synthesis*. Kürti, L.; Czakó, B. Elsevier: Burlington, MA, **2005**.
- (2) Beeson, T. D.; Mastracchio, A.; Hong, J.-B.; Ashton, K.; MacMillan, D. W. C. *Science* **2007**, *316* (5824), 582.
- (3) Romero, N. A.; Nicewicz, D. A. *Chem. Rev.* **2016**, *116* (17), 10075.
- (4) Roth, H. G.; Romero, N. A.; Nicewicz, D. A. *Synlett* **2015**, 27 (05), 714.
- (5) Ischay, M. A.; Anzovino, M. E.; Du, J.; Yoon, T. P. *J. Am. Chem. Soc.* **2008**, *130* (39), 12886.
- (6) Narayanam, J. M. R.; Tucker, J. W.; Stephenson, C. R. J. *J. Am. Chem. Soc.* **2009**, *131* (25), 8756.
- (7) McNally, A.; Prier, C. K.; MacMillan, D. W. C. *Science* **2011**, *334* (6059), 1114.
- (8) Jeffrey, J. L.; Terrett, J. A.; MacMillan, D. W. C. *Science* **2015**, *349* (6255), 1532.
- (9) Musacchio, A. J.; Lainhart, B. C.; Zhang, X.; Naguib, S. G.; Sherwood, T. C.; Knowles, R. R. *Science* **2017**, *355* (6326), 727.
- (10) Reichl, K. D.; Ess, D. H.; Radosevich, A. T. *J. Am. Chem. Soc.* **2013**, *135* (25), 9354.
- (11) Pan, X.; Chen, X.; Li, T.; Li, Y.; Wang, X. *J. Am. Chem. Soc.* **2013**, *135* (9), 3414.
- (12) Pandey, G.; Pooranchand, D.; Bhalerao, U. T. *Tetrahedron* **1991**, *47*, 1745.
- (13) Walling, C.; Rabinowitz, R. *J. Am. Chem. Soc.* **1959**, *79*, 1243.
- (14) Hoffmann, F. W.; Ess, R. J.; Simmons, T. C.; Hanzel, R. S. *J. Am. Chem. Soc.* **1956**, *75*, 6414.
- (15) Hodgson, J. L.; Coote, M. L. *J. Phys. Chem. A* **2005**, *109* (44), 10013.

- (16) Giles, J. R. M.; Roberts, B. P. *J. Chem. Soc., Perkin Trans. 2* **1981**, 1211.
- (17) Roberts, B. P.; Singh, K. *J. Chem. Soc. Perkin Trans. 2* **1980**, 1549.
- (18) Bentrude, W. G. *Acc. Chem. Res.* **1982**, *15*, 117.
- (19) Bentrude, W. G.; Hansen, E. R.; Khan, W. A.; Min, T. B.; Rogers, P. E. *J. Am. Chem. Soc.* **1973**, *95*, 2286.
- (20) Yasui, S.; Shioji, K.; Yoshihara, M.; Maeshima, T.; Ohno, A. *Tetrahedron Lett.* **1992**, *33* (47), 7189.
- (21) Yasui, S.; Shioji, K.; Ohno, A. *Heteroatom Chem.* **1994**, *5* (1), 85.
- (22) Bentrude, W. G.; Hansen, E. R.; K. W. A.; Rogers, P. E. *J. Am. Chem. Soc.* **1972**, *94*, 2867.
- (23) Barton, D. H. R.; Jaszberenyi, J. C.; Morrell, A. I. *Tetrahedron Lett.* **1991**, *32* (3), 311.
- (24) Shaikh, R. S.; Düsel, S.; König, B. *ACS Catal.* **2016**, *6* (12), 8410.
- (25) Ghosh, I.; Ghosh, T.; Bardagi, J. I.; König, B. *Science* **2014**, *346* (6210), 725.
- (26) Fearnley, A. F.; An, J.; Jackson, M.; Lindovska, P.; Denton, R. M. *Chem. Commun.* **2016**, *52* (28), 4987.
- (27) Jiao, X.-Y.; Bentrude, W. G. *J. Org. Chem.* **2003**, *68* (8), 3303.
- (28) Zhang, L.; Koreeda, M. *J. Am. Chem. Soc.* **2004**, *126* (41), 13190.
- (29) Quint, V.; Morlet-Savary, F.; Lohier, J.-F.; Lalevée, J.; Gaumont, A.-C.; Lakhdar, S. *J. Am. Chem. Soc.* **2016**, *138* (23), 7436.
- (30) He, Y.; Wu, H.; Toste, F. D. *Chem. Sci.* **2015**, *6* (2), 1194.
- (31) Xuan, J.; Zeng, T. T.; Chen, J. R.; Lu, L. Q.; Xiao, W. J. *Chem. Eur. J.* **2015**, *21* (13), 4962.
- (32) Ganapathy, S.; Dockery, K. P.; Sopchik, A. E.; Bentrude, W. G. *J. Am. Chem. Soc.*

1993, *115*, 8863.

- (33) Bentrude, W. G.; Dockery, K. P.; Ganapathy, S.; Lee, S.-G.; Tabet, M.; Wu, Y.-W.; Cambron, R. T.; Harris, J. M. *J. Am. Chem. Soc.* **1996**, *118*, 6192.
- (34) Yasui, S.; Tojo, S.; Majima, T. *J. Org. Chem.* **2005**, *70* (4), 1276.
- (35) Tojo, S.; Yasui, S.; Fujitsuka, M.; Majima, T. *J. Org. Chem.* **2006**, *71* (21), 8227.
- (36) Yasui, S.; Shioji, K.; Tsujimoto, M.; Ohno, A. *J. Chem. Soc. Perkin Trans. 2* **1999**, 855.
- (37) Yasui, S.; Shioji, K.; Tsujimoto, M.; Ohno, A. *Heteroatom Chem.* **1999**, *11*, 152.
- (38) Ohmori, H.; Maeda, H.; Kikuoka, M.; Maki, T.; Masui, M. *Tetrahedron* **1991**, *47* (45), 767.
- (39) Maeda, H.; Maki, T.; Ohmori, H. *Tetrahedron Lett.* **1992**, *33* (10), 1347.
- (40) Maeda, H.; Maki, T.; Eguchi, K.; Koide, T.; Ohmori, H. *Tetrahedron Lett.* **1994**, *35* (24), 4129.

Chapter 4

Phosphine mediated C–O bond activation via photoredox catalysis

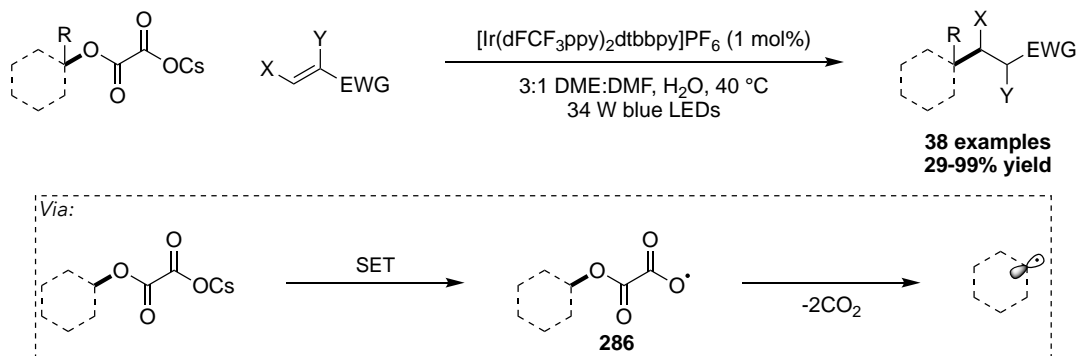
4.1 Introduction

Photoredox catalysis has been widely used over the last decade to enable new bond disconnections not accessible by other two-electron methods.^{1,2} This tool has been used in concert with transition metal catalysis as well as organocatalysis to broadly expand its impact on synthetic methods.^{3,4} However, photoredox catalysis has only seen limited application to single-electron chemistry of phosphines, despite some of the promising advances discussed in Chapter 3.⁵⁻⁸ We envisioned that by accessing single-electron phosphine chemistry via photoredox catalysis, we might broadly extend this chemistry to new bond disconnection and novel synthetic methods.

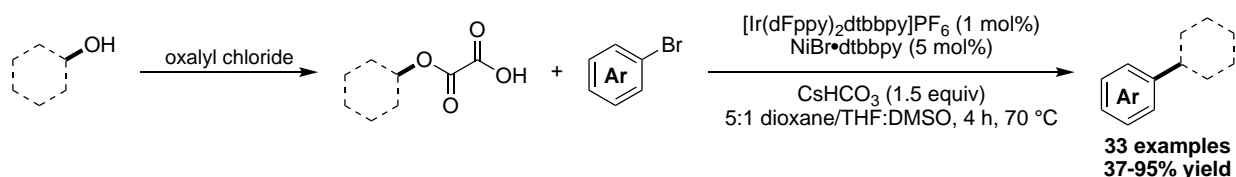
One of the most promising applications of single-electron phosphine chemistry is C–O bond activation. Despite the prevalence of alcohols, methods to activate C–O bonds in a single step remain elusive. The MacMillan and Overman groups recently disclosed a method for the activation of alcohols via photoredox catalysis employing oxalates (Scheme 4.1).^{9,10} In 2015, they observed that cesium oxalate salts could undergo reductive quenching with an [Ir*] photocatalyst to form a carboxy radical (**286**). After two successive decarboxylations, an alkyl radical could be generated, which would undergo subsequent addition into a Michael acceptor to forge a new (*Csp*³)–(*Csp*³) bond. In a later report, MacMillan and coworkers disclosed the merger of this chemistry with a nickel catalyzed cross-coupling. Alkyl oxalates were generated in one step using oxalyl chloride from the corresponding alcohol and used without purification. Upon the addition of a photoredox catalyst, the oxalate could undergo single-electron oxidation and subsequent decarboxylations to

afford the alkyl radical which could intercept a Ni(II) oxidative addition adduct to generate a new $(Csp^3)-(Csp^2)$ bond.

Overman/MacMillan 2015



MacMillan 2016

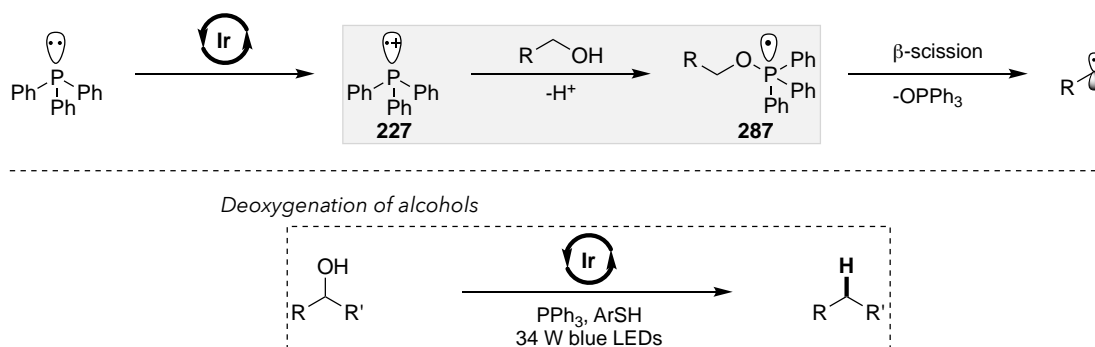


Scheme 4.1

4.2 Reaction design and initial results

These reports represent the state of the art for C–O bond activation via photoredox catalysis. However, these reports still require pre-functionalization of an alcohol substrate to activate it for single-electron transfer (SET) from a photoredox catalyst and access the desired alkyl radical. Given the reports by Ohmori and the recent advances of photoredox catalysis, we envisioned exploiting the single-electron chemistry of phosphines for a new activation platform of C–O bonds that might circumvent pre-functionalization. Additionally, substrate activation via SET is dependent on voltage-gated electron transfer via an excited state photocatalyst and substrate.^{11,12} This mechanism limits the type of substrates that are accessible by any one photocatalyst and prevents some substrates from SET due to their inaccessible redox potentials and strong bond dissociation free energies (BDFEs).¹³

To address these limitations, we proposed an SET/polar crossover mechanism, where substrate activation occurs via a two-electron pathway to ultimately generate a highly reactive radical species. Our proposed reactivity is depicted in Scheme 4.2. Triphenylphosphine, when exposed to an excited state photoredox catalyst, could undergo single-electron oxidation to generate phosphine radical cation **227**.¹⁴ In a polar/SET crossover, an alcohol could then add into the cation to afford phosphoranyl radical **287**. Upon β -scission, an alkyl radical would be generated, along with triphenylphosphine oxide (**226**) as a byproduct. The resulting alkyl radical can undergo H-atom transfer to afford a deoxygenated product or can add to a radical acceptor to forge a new C–X bond.



Scheme 4.2

We sought to test our hypothesis in the C–O bond activation of alcohols with terminal H-atom transfer to ultimately effect a deoxygenation. We began our studies with triphenylphosphine as the phosphine source, as phosphoranyl radicals based on triphenylphosphine are known to undergo β -scission exclusively. We first tested Ir photocatalyst **131** in the presence of 2,6-dMePhSH as the H-atom source and found only trace reduction of alcohol **288** to toluene **289** in acetonitrile (MeCN) (Table 4.1, entry 1). Use of the organophotocatalyst 4CzIPN or Ru(bpy)₃(PF₆)₂ were ineffective at promoting the deoxygenation reaction (entry 2 and 3). Use of photocatalyst **290**, however, affords the product in 25% yield by GC analysis with triphenylphosphine oxide as the expected byproduct.

Initial control reactions showed that light, photocatalyst, and triphenylphosphine were all essential for reactivity. Interestingly, we did observe some product in the absence of H-atom source.

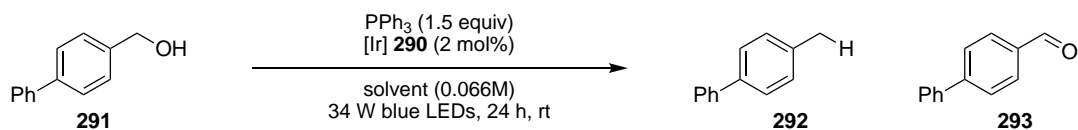
Table 4.1

entry	photocatalyst	result
1	[Ir(dFCF ₃ ppy) ₂ dtbbpy]PF ₆ (131)	trace
2	4CzIPN	none
3	Ru(bpy) ₃ (PF ₆) ₂	none
4	[Ir(dFMeppy) ₂ dtbbpy]PF ₆ (290)	detected by NMR GC ~25% yield

4.3 Alcohol deoxygenation reaction

4.3.1 Mechanistic studies

Before moving forward with optimization, we exchanged alcohol **288** for alcohol **291**. When the reaction was conducted without H-atom source in acetonitrile, the product (**292**) was obtained in 47% yield (Table 4.2, entry 1). A solvent screen revealed that acetonitrile was a uniquely effective solvent, acting as the H-atom source, with product formation in only 1% to 8% yield (entry 2-5). In DMF, the product was obtained in only 11% yield in the absence of H-atom source (entry 6). Interestingly, we did observe some formation of the aldehyde product (**293**). We attribute this formation to a possible H-atom abstraction of the α -C–H bond of the alcohol and subsequent single-electron oxidation to generate the aldehyde. Alternatively, advantageous oxygen may form superoxide ($O_2^{\bullet-}$) which could abstract an H-atom. Regardless, upon scale-up to 0.2 mmol, we observed 80% yield of product **292** after 43 h.

Table 4.2

entry	solvent	%conversion	%yield	%aldehyde	%PPh ₃ O
1	MeCN	55	47	5	53
2	DMA	18	6	6	43
3	acetone	10	8	4	22
4	PhMe	10	1	4	14
5	THF	6	1	3	14
6	DMF	23	11	3	28

With our highly effective deoxygenation reaction, we sought to gain some mechanistic evidence for our proposal. We conducted Stern-Volmer quenching studies on all of the reaction components (Figure 4.1).¹⁵ When photocatalyst emission spectra were taken at various concentrations of alcohol, no change in emission was observed, signifying that the alcohol does not quench the excited state of the photocatalyst. When the same experiment is conducted with triphenylphosphine as the quencher, as the concentration increases, the emission of the photocatalyst decreases, indicating that PPh₃ does quench the excited state of the photocatalyst. This result is consistent with an SET event to oxidize triphenylphosphine to the phosphine radical cation (**227**). When both components are present, mimicking the reaction conditions, the rate of quenching is nearly identical to that of triphenylphosphine alone, again suggesting that PPh₃ is responsible for quenching the excited state of the photocatalyst.

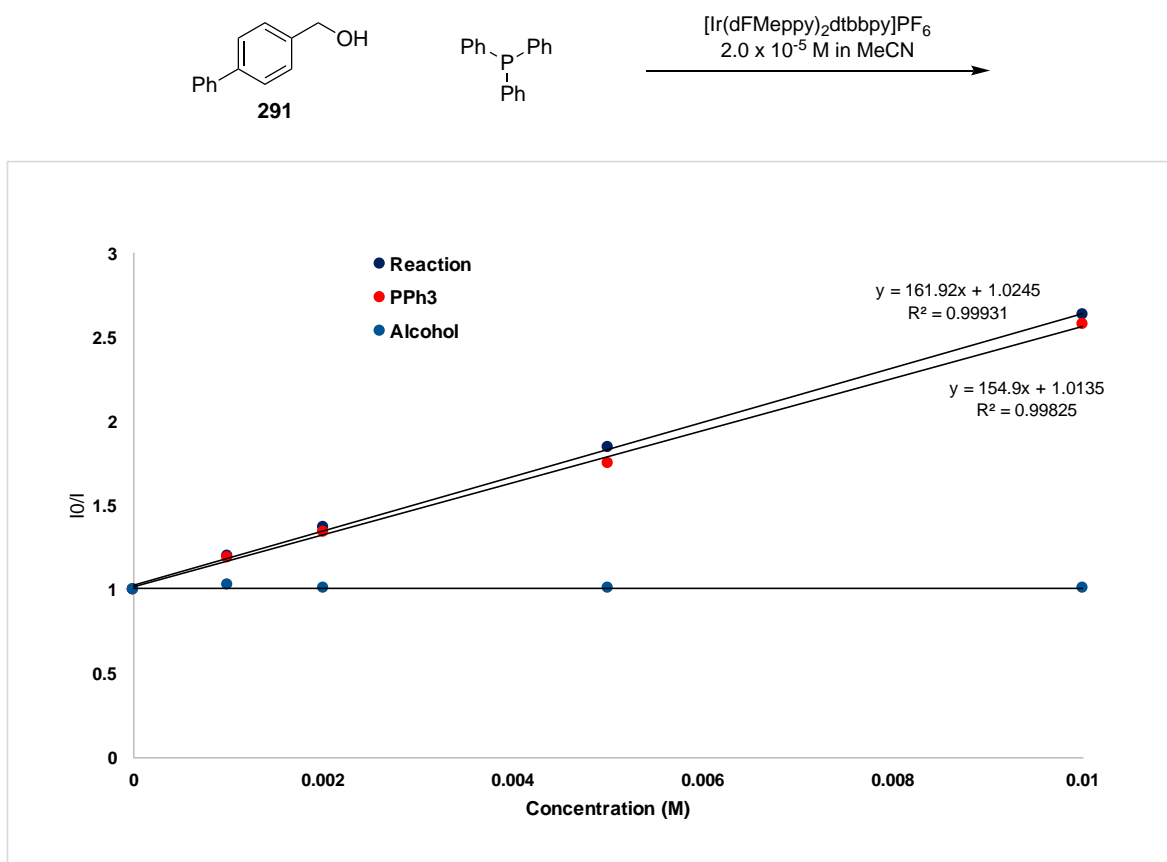
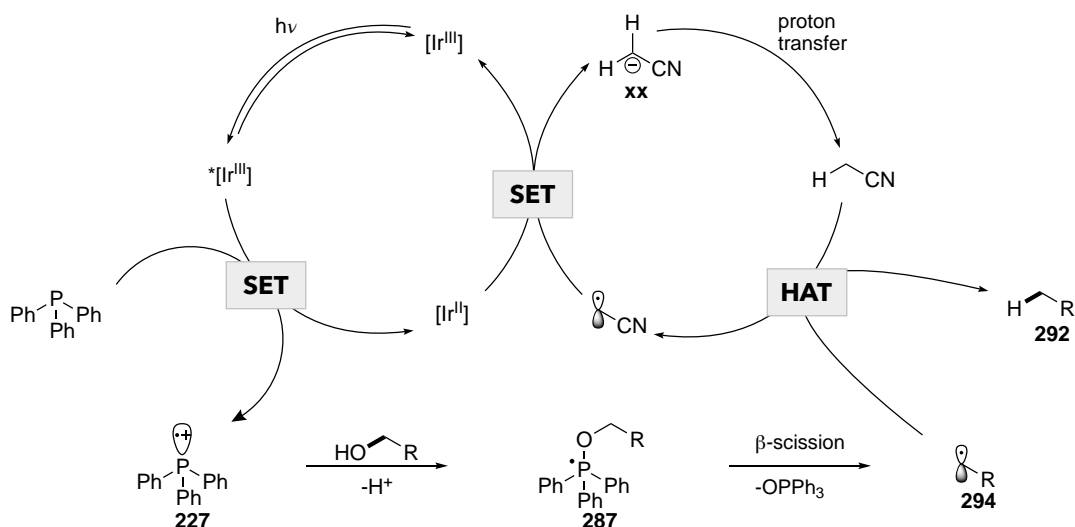


Figure 4.1

Our mechanistic hypothesis is depicted in Scheme 4.3. After an initial excitation of the photocatalyst to $[\text{Ir(III)}]^*$, a single-electron oxidation of triphenylphosphine would give phosphine radical cation **227**. Addition of an alcohol to the phosphine radical cation would provide phosphoranyl radical **287** after proton transfer. A β -scission event would afford alkyl radical **294** and triphenylphosphine oxide as the byproduct. We propose that H-atom transfer from acetonitrile solvent could give the desired alkane (**292**) and an acetonitrile radical. After a second single-electron transfer from $[\text{Ir(II)}]$ to the acetonitrile radical to form the corresponding anion, which after proton transfer would regenerate the solvent and close the photocatalytic cycle.¹⁶ The initial oxidation to form **227** is supported by Stern-Volmer quenching studies. We also conducted

deuterium labeling studies where we employed CD₃CN as the solvent, and observed the product with >50% deuterium incorporation.



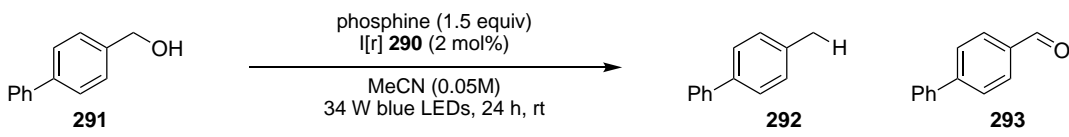
Scheme 4.3

4.3.2 Alcohol deoxygenation and further optimizations

To gain further insights into this new reaction platform, we sought to examine additional phosphines which may be amenable to formation of phosphine radical cations and subsequent β-scission steps. Employment of more electron rich triaryl phosphines resulted in low product yields and low conversion (Table 4.3, entry 1-3). As these phosphines are more electron rich, their oxidation potentials are lower than triphenylphosphine, suggesting that initial formation of a phosphine radical cation is not problematic. However, formation of the phosphoranyl radical would make a very electron rich species which may be oxidized prior to β-scission, resulting in low conversion and decreased product formation. Using alkyl diaryl phosphine 1,2-bis(diphenylphosphino)ethane (dppe) did not improve reaction efficiency (entry 4). Conversely, use of a more electron deficient phosphonite also did not improve product formation, although this is likely due to a higher oxidation potential for this species that is significantly uphill relative to the excited state of the photocatalyst (entry 5). Methyl diphenylphosphinite, however, which has

a similar oxidation potential to PPh_3 , afforded the product in 88% yield (entry 6). Interestingly, PyPhos was incredibly effective for the deoxygenation reaction, affording the product in quantitative yield (entry 7). Use of 2,6-lutidine as an exogenous base only affords the product in 69% yield under similar conditions with triphenylphosphine. The intramolecular nature of the pyridine moiety may enhance the rate of phosphine radical cation trapping. We also sought to examine the reaction with respect to photocatalyst and observed that only **290** was competent in the reaction, with all other photocatalysts affording the product in <20% yield (Table 4.4). This was surprising to us, as the excited state oxidation potentials of many of these photocatalysts matched or exceeded that of **290**.

Table 4.3

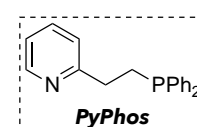


entry	phosphine (PAr_3)	%conversion	%yield	%aldehyde
1	2-furyl	22	7	3
2	o-tolyl	8	1	5
3	o-OMePh	10	0	6
<hr style="border-top: 1px dashed black;"/>				
phosphine				
4	dppe	20	16	2
5	$\text{PhP}(\text{OMe})_2$	54	7	1
6	Ph_2POMe	90	88	1
7	PyPhos	100	100	0

PPh_3 $E^{\text{ox}}_{1/2} = +0.98 \text{ V}$

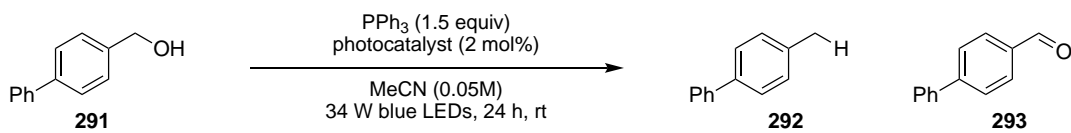
Ph_2POMe $E^{\text{ox}}_{1/2} = +1.0 \text{ V}$

$\text{PhP}(\text{OMe})_2$ $E^{\text{ox}}_{1/2} = +1.28 \text{ V}$



PyPhos

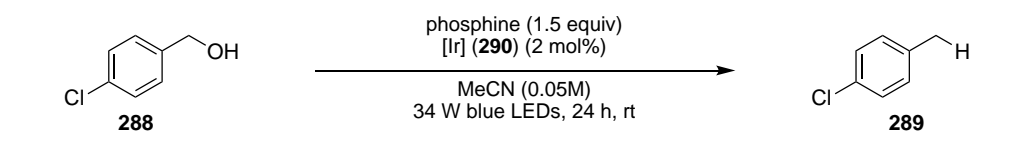
Table 4.4



entry	photocatalyst	%conversion	%yield	%aldehyde
1	[Ir(dFCF ₃ ppy) ₂ dtbbpy]PF ₆	48	9	33
2	4CzIPN	14	0	2
3	[Ir(dFCF ₃ ppy) ₂ bpy]PF ₆	10	2	10
4	[Ir(dFMeppy) ₂ dOMebpy]PF ₆	23	10	3
5	[Ir(dFCF ₃ ppy) ₂ phenan]PF ₆	5	0	5
6	[Ir(dFphtl) ₂ dtbbpy]PF ₆	19	14	4
7	[Ir(dFphtl) ₂ dCF ₃ ppy]PF ₆	14	1	6
8	[Ir(dFppy) ₂ phenan]PF ₆	10	0	8

We were concerned that by using alcohol **291**, which would provide a very stabilized benzylic radical, we may be optimizing for a very specialized class of benzylic alcohols, and ultimately may not be tolerant of diverse substitution patterns. Therefore, we sought to re-examine alcohol **288** which is neither as highly stabilized, nor as nucleophilic as **291**. Under the optimized conditions,

Table 4.5



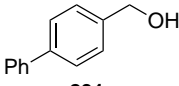
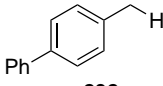
entry	phosphine	%conversion	%yield
1	PPh ₃	n/a	21
2	PhP(OMe) ₂	30	6
3	Ph ₂ POMe	86	74
4	(<i>p</i> -FPh) ₃ P	30	17
5	(<i>p</i> -CF ₃ Ph) ₃ P	14	3
6	(3,5-dCF ₃ Ph) ₃ P	21	1

we found that toluene **289** is formed in only 21% yield (Table 4.5, entry 1). Switching to a more electron deficient phosphonite affords reduced product yield (entry 2). However, use of a

phosphinite provides the product in high yield (74% yield), like that of benzylic alcohol **291** (entry 3). More electron-deficient triaryl phosphines are less competent in the reaction, likely due to their higher oxidation potentials (entry 4-6).

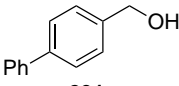
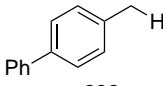
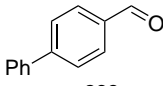
During this time, we found that with a new batch of photocatalyst **290**, our reaction efficiencies dropped significantly, now forming only a small amount of deoxygenated product. Upon examination of both batches of photocatalyst, we found that there was an impurity that was promoting the reaction. We tried numerous different additives to try to mimic the effect of the unidentified impurity (Table 4.6). In the absence of any additive after just 7 h, the product is observed in only 3% yield (entry 1). Addition of NH_4PF_6 or TBACl appear to improve the yield of product formation to 5% and 10% yield, respectively (entry 2 and 3). Although TBACl appeared to improve reaction efficiency, examining numerous other chloride additives did not have a similar effect on the reaction outcome. Other additives that may have been the photocatalyst impurity failed to have any appreciable effect on the reaction (entry 4-7). However, adding a small amount of air at the beginning of the reaction appeared to promote the deoxygenation reaction (entry 8). The addition of oxygen as a reaction promoter is somewhat counterintuitive, as Yasui and coworkers have previously reported that a phosphine radical cation can react with O_2 to form phosphine oxide (Scheme 3.19).^{17,18} However, the initial phosphine radical cation adduct with O_2 (**272**) itself can act as a single-electron oxidant, thereby generating another equivalent of phosphine radical cation. Alternatively, oxygen may be responsible for quenching the excited state of the photocatalyst, which would generate a highly oxidizing [Ir(IV)] species $\{E_{1/2}^{\text{ox}}[\text{Ir}^{\text{IV}}/\text{Ir}^{\text{III}}] = +1.51 \text{ V vs. SCE}\}$ to generate phosphine radical cation **227**.¹⁹ When we placed a needle in the reaction vessel to equilibrate the reaction contents with ambient air, we observed 56% yield of the deoxygenated product after 24 hours.

Table 4.6

$ \begin{array}{ccc} \text{PPh}_3 \text{ (1.5 equiv)} \\ [\text{Ir}] \text{ (290) (2 mol\%)} \\ \text{additive (2 mol\%)} \\ \hline \text{MeCN (0.05M)} \\ 34 \text{ W blue LEDs, 7 h, rt} \end{array} $			
 291	→	 292	
entry	additive	%conversion	%yield
1	none	3	3
2	NH ₄ PF ₆	39	5
3	TBACl	5	10
4	Bu ₄ NPF ₆	0	2
5	IrCl ₃ •XH ₂ O	17	7
6	NaBF ₄	22	2
7	NaPF ₆	3	2
8	50 μ L air	33	9

With the observation that air seemed to promote the reaction, we questioned whether the problematic step was formation of the phosphine radical cation and lifetime, relative to the alcohol addition required to generate the phosphoranyl radical. We hypothesized that increasing the rate

Table 4.7

$ \begin{array}{ccc} \text{PPh}_3 \text{ (1.5 equiv)} \\ [\text{Ir}] \text{ (290) (2 mol\%)} \\ 2,6\text{-lutidine (x equiv)} \\ \hline \text{MeCN (0.05M)} \\ 34 \text{ W blue LEDs, 24 h, rt} \end{array} $					
 291	→	 292	 293		
entry	lutidine	%conversion	%yield	%CHO	%PPh ₃ O
1	none	13	3	6	13
2	0.5 equiv	59	46	3	57
3	1.0 equiv	88	71	10	10
4	1.5 equiv	88	67	3	81
5	2.0 equiv	82	74	2	86
6	1.0 equiv + air needle	97	77	6	150

of alcohol addition to the phosphine radical cation might also promote the reaction, which could be achieved by the addition of a base. As Yasui and coworkers noted in their kinetic study on alcoholic trapping of phosphine radical cations, buildup of positive charge on the oxygen atom can

slow down the rate of alcohol addition.²⁰ By adding 2,6-lutidine to the reaction as a base, we found we could restore the deoxygenation reactivity (Table 4.7, entry 1 vs. 2). Increasing the base loading up to 2.0 equivalents improved the reaction efficiency to 74% yield (entry 3-5). Combination of an air needle and 2,6-lutidine led to similar reaction yields, although it does lead to full conversion of triphenylphosphine to triphenylphosphine oxide (entry 6).

4.3.3 Final optimizations and additional mechanistic studies

With the new protocol in hand, we sought to briefly re-investigate photocatalyst identity, as the new conditions may be more amenable to more rapid trapping of the phosphine radical cation. Photocatalyst **131** now gives product in almost 20% yield, while [Ir(dMeppy)₂dOMebpy]PF₆ also

Table 4.8

entry	photocatalyst	%conversion	%yield	%CHO	%PPh ₃ O
1	[Ir(dFCF ₃ ppy) ₂ dtbbpy]PF ₆	51	18	10	148
2	[Ir(dMeppy) ₂ dOMebpy]PF ₆	25	16	0	39
3	[Ir(dFMeppy) ₂ Me ₄ Phen]PF ₆	90	85	0	98
4	[Ir(dFBnphtl) ₂ dtbbpy]PF ₆ (162)	100	96	0	112

entry	photocatalyst	%conversion	%yield	%CHO	%PPh ₃ O
1	[Ir(dFCF ₃ ppy) ₂ dtbbpy]PF ₆	51	18	10	148
2	[Ir(dMeppy) ₂ dOMebpy]PF ₆	25	16	0	39
3	[Ir(dFMeppy) ₂ Me ₄ Phen]PF ₆	90	85	0	98
4	[Ir(dFBnphtl) ₂ dtbbpy]PF ₆ (162)	100	96	0	112

gives product in 16% yield (Table 4.8, entry 1 and 2). Gratifyingly, [Ir(dFMeppy)₂Me₄Phen]PF₆ and photocatalyst **162** give the product in >85% yield at nearly complete conversion (entry 3 and

4).¹⁹ After further optimization of concentration, phosphine loading, and 2,6-lutidine loading, toluene **292** was isolated in 91% yield on 0.5 mmol scale (Table 4.8).

The oxidation potential of **162** $\{E^{red}_{1/2} = +1.0 \text{ V v SCE}\}$ is only 30 mV higher than that of **290**, yet it yields a much more efficient reaction. We sought to conduct further mechanistic studies of the system with photocatalyst **162**. We began with Stern-Volmer studies, carried out identically to those in Figure 4.1. As can be seen in Figure 4.2, 2,6-lutidine and the alcohol do not demonstrate any quenching of the excited state of the photocatalyst. It should be noted that at 0.002M, a reduction in photocatalyst emission is observed, but this is likely due to oxygen contamination,

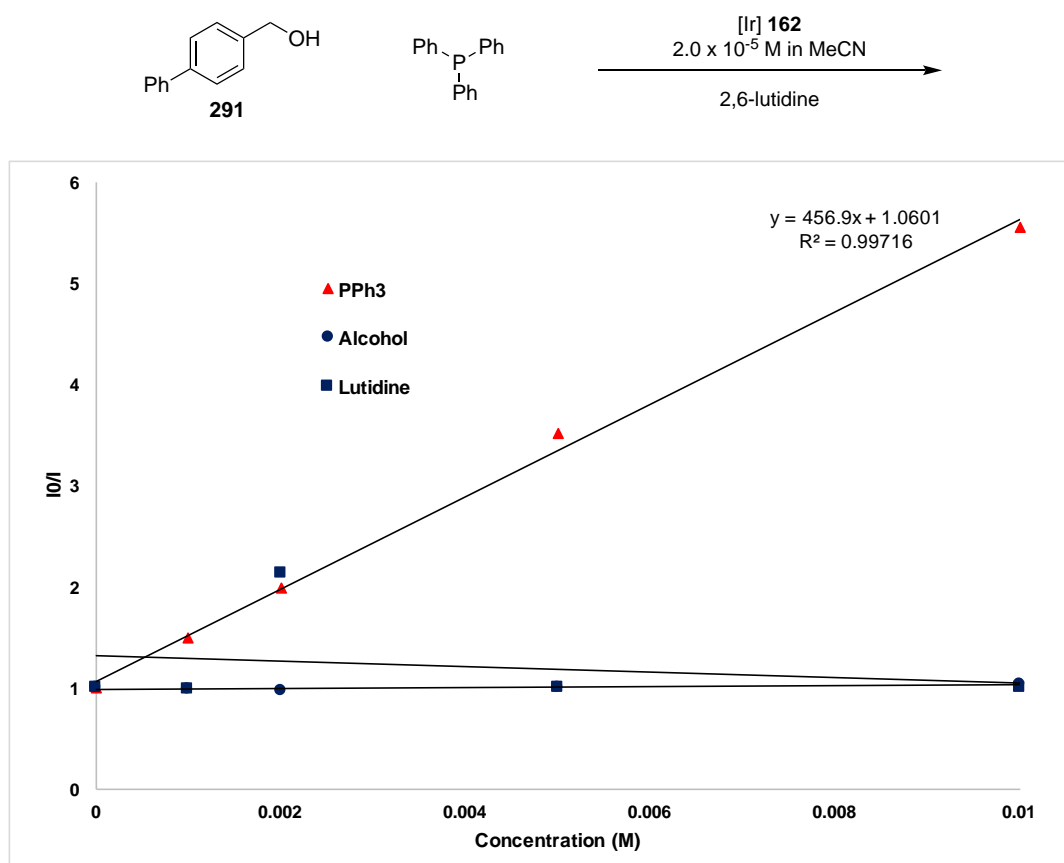


Figure 4.2

and not reagent quenching of the photocatalyst. Triphenylphosphine again exhibits clear quenching of the excited state of the photocatalyst, consistent with a SET event with the excited

state of the photocatalyst. Interestingly, when we compared the quenching rates of the two photocatalysts (**290** and **162**), we observed that **162** quenches the excited state of the photocatalyst much faster than **290**, despite their similar redox potentials (Figure 4.3). This is also consistent with the higher reaction efficiencies observed with photocatalyst **162**. More sophisticated spectroscopic techniques are needed to fully understand the difference between these photocatalysts. One possible explanation involves a pre-complexation of triphenylphosphine and the photocatalyst prior to photoexcitation—an example of static quenching. Alternatively, back-electron transfer (BET) may be rapid in these systems, which would explain the privileged nature of photocatalysts used in this system. This, however, would not explain the initial rates of quenching between these two photocatalysts.

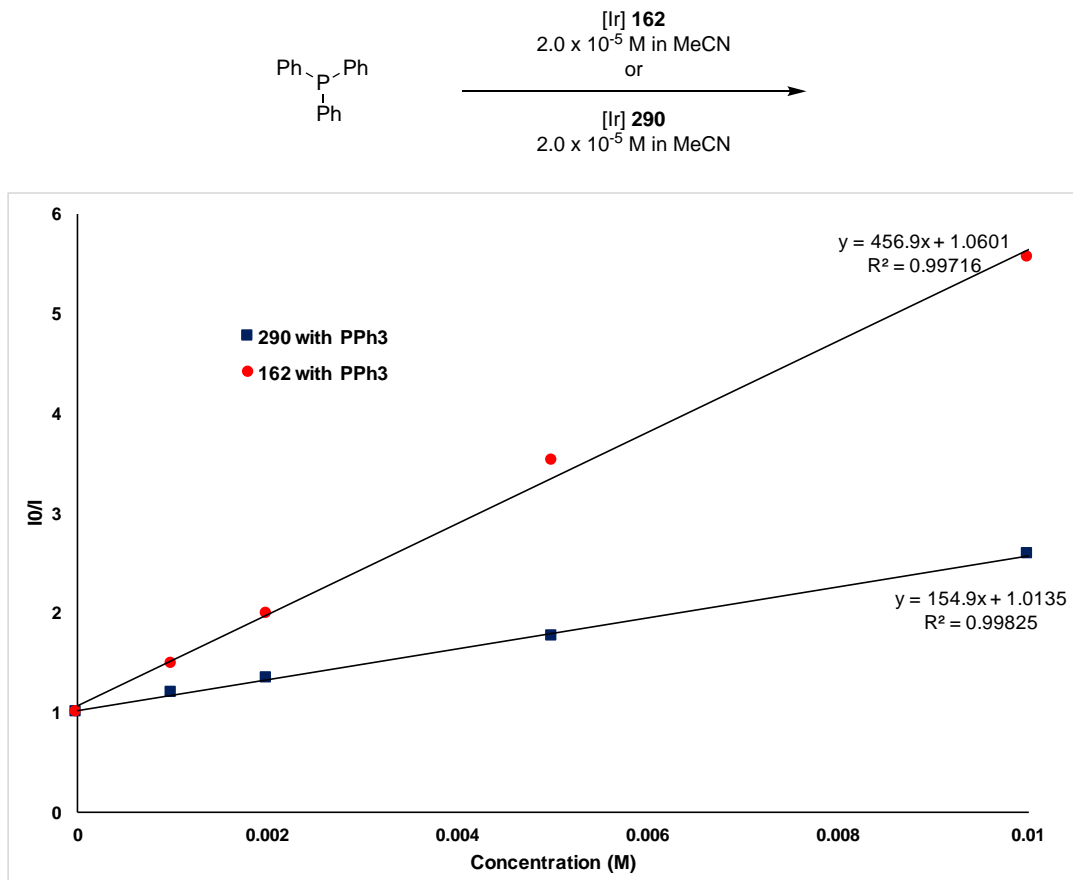
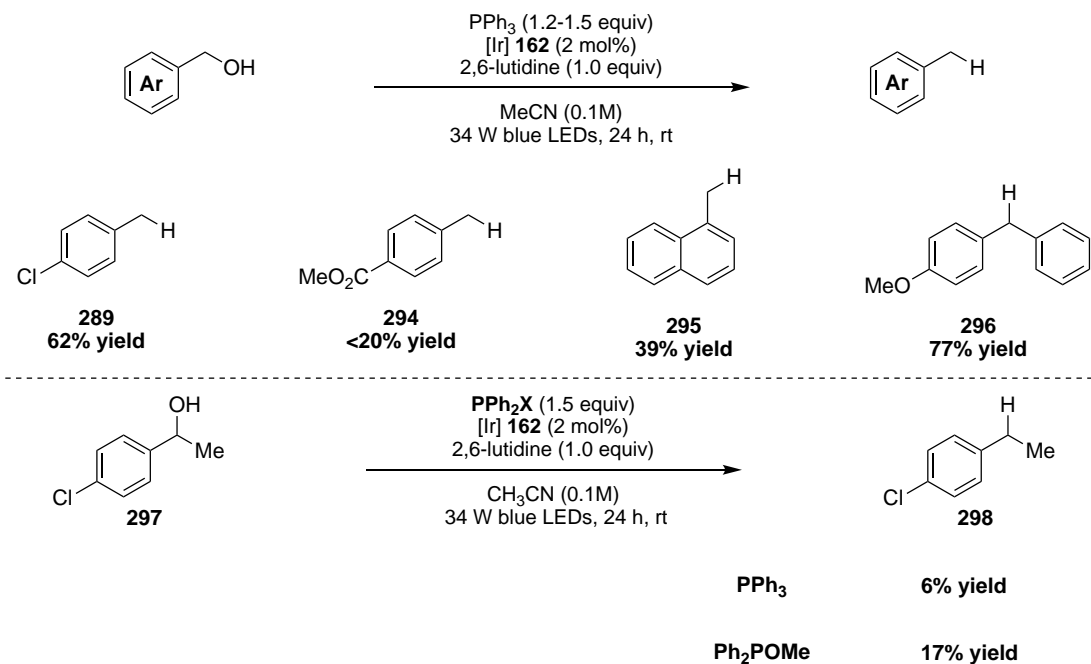


Figure 4.3

4.3.4 Substrate scope of other alcohols

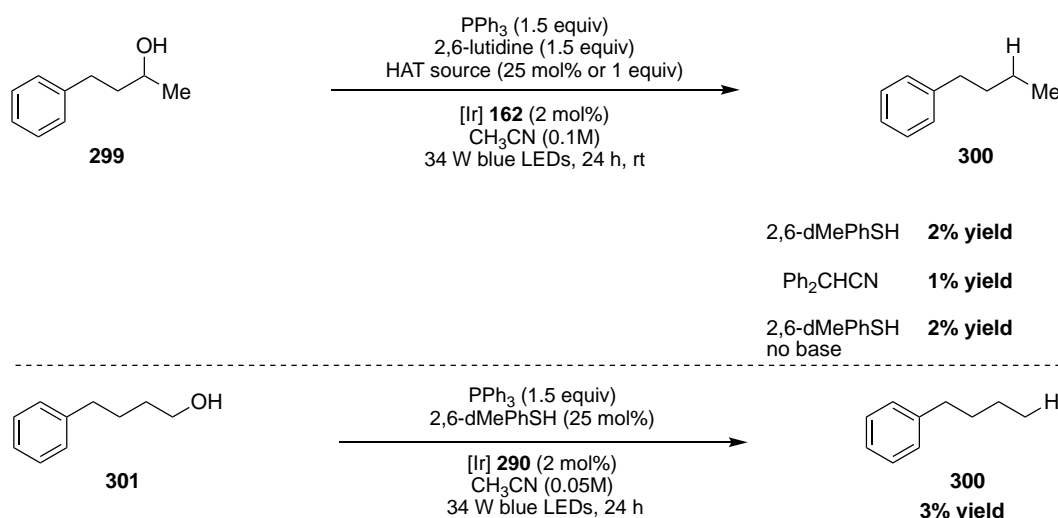
We sought to evaluate the initial scope of the deoxygenation reaction for benzyl alcohols with our optimized protocol (Scheme 4.4). A more electron deficient *p*-chlorosubstituted alcohol, when subjected to the reaction conditions, affords toluene **289** in 61% yield. Even more electron deficient *p*-methyl benzoate benzyl alcohol is converted to the product (**294**) in less than 20% yield. We attributed this lower reaction efficiency to a less nucleophilic benzylic alcohol. More sterically hindered 1-naphthyl benzyl alcohol is reduced to 1-methylnaphthlene (**295**) in 39% yield. Use of a secondary, albeit highly activated, benzhydrol undergoes deoxygenation to benzyl product **296** in 52% yield. When we turned to less activated secondary alcohol **297**, we observed that product **298** is formed in only 6% yield. Use of more electron deficient methyl diphenylphosphinite, however, affords the product in an improved 17% yield.



Scheme 4.4

We wanted to effect deoxygenations of unactivated primary and secondary alcohols, as these are often more challenging. Under our standard reaction conditions, we observed 0% yield of the

desired deoxygenation of 4-phenylbutan-2-ol (**299**) to phenylbutane (**300**) (Scheme 4.5). With the addition of an H-atom source, we observed some yield of the desired deoxygenated product, albeit never greater than 5% yield. Conversions for these reactions appeared to be significantly higher than the yields indicated, sometimes in greater than 50%, and triphenylphosphine oxide was also observed in larger amounts than deoxygenated product. Primary alcohol **301** was also not efficiently reduced under our reaction conditions, again providing less than 5% yield of the desired alkane product and similar conversions and yields of triphenylphosphine oxide were observed. Removing the cooling fan from these reactions to raise the internal temperature also had no positive effect on the yield of deoxygenation. The literature precedents for β -scission of primary



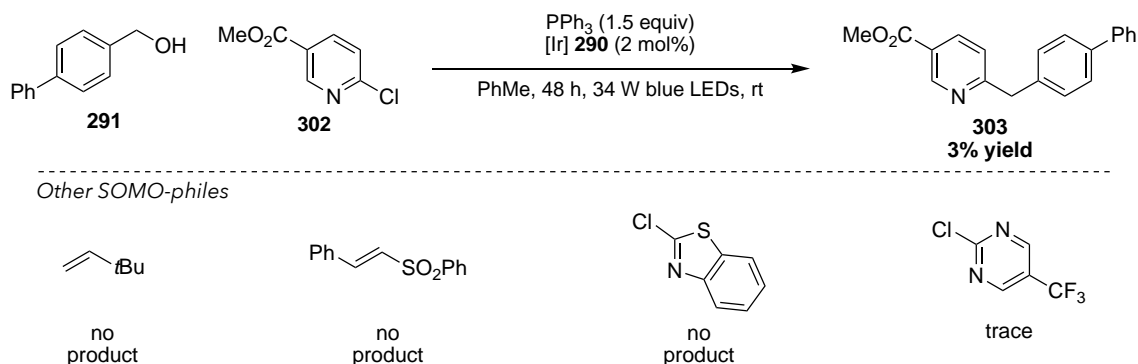
Scheme 4.5

and secondary alkyl radicals is sufficient to suggest that fragmentation should occur under these reaction conditions.^{21,22} Additionally, primary unactivated alcohols should be comparable to benzylic alcohols in terms of nucleophilic addition to the phosphine radical cation and is unlikely to be the problematic step. Given the large quantities of phosphine oxide formed, and results that will be discussed in a later section, we hypothesized that oxidation of the intermediate phosphoranyl radical may be outcompeting β -scission, therefore inhibiting desired product

formation. A more thorough investigation of phosphines and photocatalysts may ultimately increase the efficiency of this transformation.

4.3.5 Radical additions beyond terminal HAT

Ultimately, to fully realize the utility of this activation platform, we would like to extend this reactivity to C–C and C–X bond forming reactions. We first examined addition into an activated heteroaryl chloride species (**302**), which affords the desired product (**303**) in 3% yield by ^1H NMR (Scheme 4.6).²³ We also examined other SOMO-philes such as acrylates,²⁴ activated styrenyl sulfones,²⁵ 2-chlorobenzothiazole and pyrimidines, only observing product formation in the case of pyrimidines, detected by mass spectrometry. While little effort has been put into these coupling reactions thus far, it is likely that competitive phosphine or phosphine radical cation addition to these SOMO-philes is occurring. In most cases these processes should be reversible, but more reaction engineering may be required to achieve these C–C bond forming reactions.



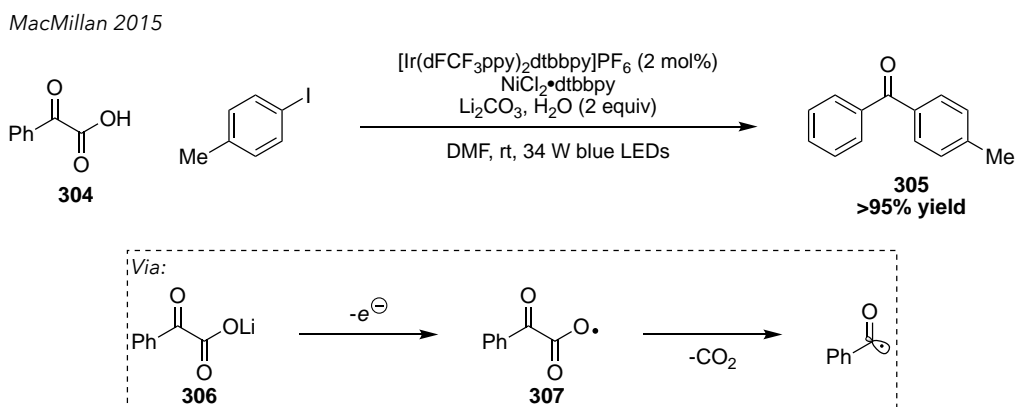
Scheme 4.6

4.4 Carboxylic acid C–O bond activation

4.4.1 Introduction

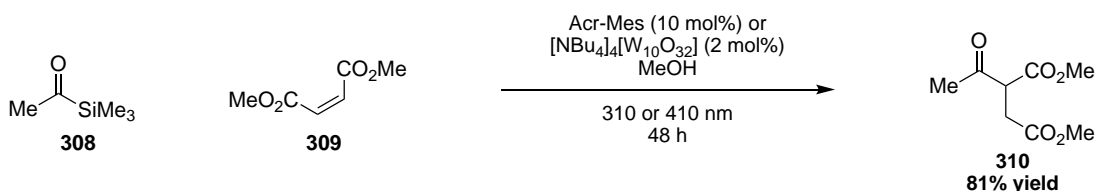
Carboxylic acids represent one of the most ubiquitous functional groups in organic molecules. Many recent methods have exploited carboxylic acids as precursors for alkyl radicals, formed upon single-electron oxidation and subsequent decarboxylation.^{24,26} Alternatively, attention has been

focused on generating acyl radicals, which have incredible potential for numerous C–C and C–X bond forming reactions.²⁷ In 2015, MacMillan and coworkers disclosed a report documenting acyl radical formation via radical decarboxylation from α -oxo acids and combination with nickel catalysis to generate ketones. (Scheme 4.7).²⁸ Upon formation of lithium carboxylate **306**, single-electron oxidation by the excited state [Ir] photocatalyst would afford carboxy radical **307**, which undergoes decarboxylation to form an acyl radical. The acyl radical can then intercept a Ni(II) oxidative adduct to forge a new C–C bond after reductive elimination.

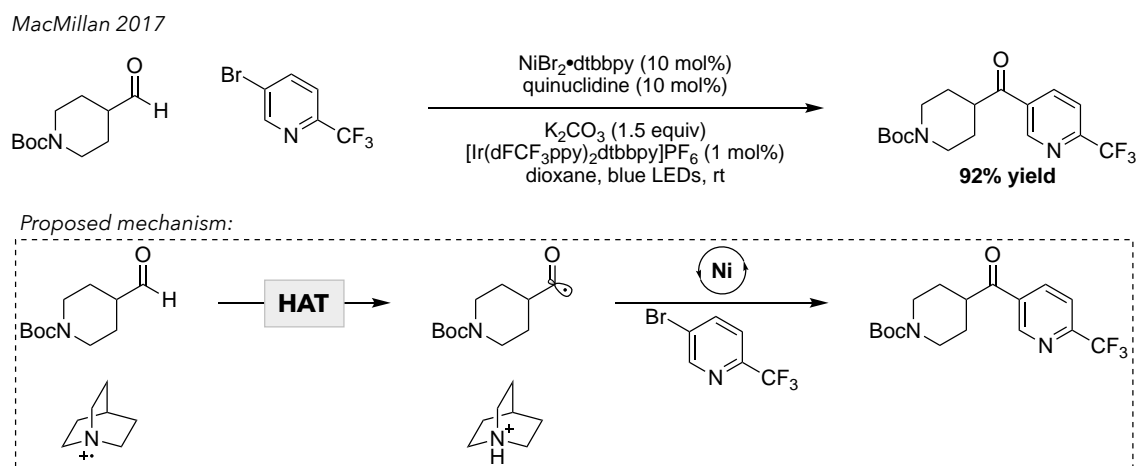


Scheme 4.7

Earlier this year, Fagnoni and coworkers reported an oxidative formation of acyl radicals from acyl silanes (Scheme 4.8).²⁹ After synthesis of **308** in a two-step procedure from the corresponding aldehyde, single-electron oxidation by the highly oxidizing Acr-Mes photocatalyst may afford an acyl radical and silane cation. Acyl radical addition into SOMO-phile **309** and subsequent reduction of the resulting α -radical would afford product **310** in 81% yield. Acyl chlorides have also been employed to generate acyl radicals via photocatalytic oxidative quenching methods.³⁰

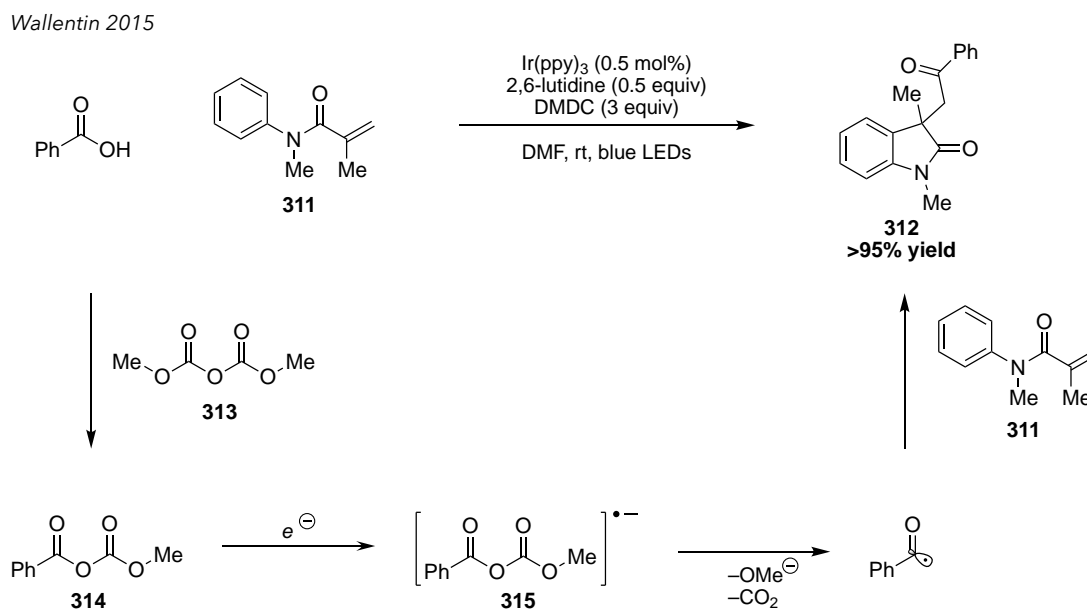
**Scheme 4.8**

MacMillan and coworkers also recently reported a nickel catalyzed cross-coupling of acyl radicals generated from aldehydes using HAT (Scheme 4.9).³¹ Upon oxidation of quinuclidine to the amine radical cation, H-atom abstraction from an alkyl aldehyde can afford the corresponding acyl radical. This intermediate can be intercepted with nickel catalysis to forge the new C–C bond. It is interesting to note that 2.0 equivalents of alkyl aldehyde are needed to achieve high yields in this reaction. Additionally, 5.0 equivalents of aromatic aldehydes are necessary to generate the α -acyl aromatic radical. While aldehydes certainly represent an alternative to carboxylic acids to generate acyl radicals, they typically are much more difficult to handle and will quickly oxidize to the corresponding acid.

**Scheme 4.9**

It should be noted that all the above examples require prefunctionalization of carboxylic acid derivatives. Ideally, acyl radicals could be generated directly from carboxylic acids without any

prefunctionalization. Wallentin and coworkers reported an *in situ* activation of carboxylic acids employing reagents such as dimethyldicarbonate (DMDC (**313**)) or Boc-anhydride to generate mixed anhydrides (Scheme 4.10).³² They propose that in the presence of **313**, benzoic acid may be converted to mixed anhydride **314**. Then, upon single-electron reduction by the highly reducing [Ir(ppy)₃]* photocatalyst, radical anion **315** may be formed, which subsequently fragments to the acyl radical. Addition into acrylamide **311** followed by cyclization would afford oxindole product **312**. This is one of the only examples of *in situ* carboxylic acid activation to form acyl radicals. It should be noted that this method still proceeds via a voltage-gated substrate single-electron reduction, and is not amenable to alkyl carboxylic acids. Recently, Zhu and coworkers have demonstrated a photocatalyzed reduction of carboxylic acids to aldehydes using DMDC and superstoichiometric *tris*(trimethylsilyl)silane as an H-atom source.³³

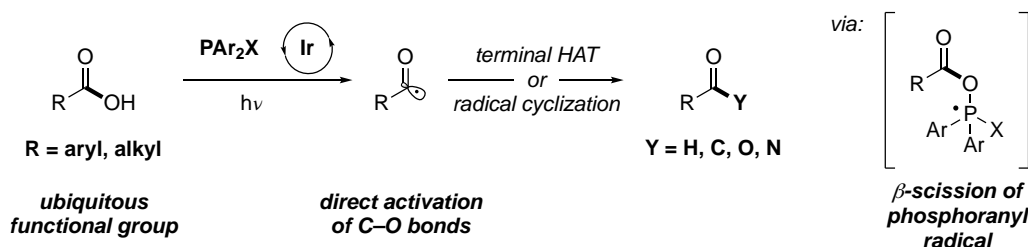


Scheme 4.10

4.4.2 Initial results

We envisioned employing our phosphine activation chemistry to address these substrate specific redox activation limitations (Scheme 4.11). With terminal H-atom transfer, this method

would provide an incredibly mild protocol for the reduction of both aromatic and aliphatic carboxylic acids to aldehydes, a challenging transformation that commonly suffers from over-reduction. Furthermore, given the wealth of transformations accessible to acyl radicals,²⁷ we envisioned forging new C–C and C–X bonds directly from carboxylic acids.



Scheme 4.11

For our initial screening, we employed our standard protocol for alcohol deoxygenation and gratifyingly observed the aldehyde product in 34% yield (Table 4.9). All initial control reactions demonstrated that phosphine, photocatalyst and light were necessary for reduction. A quick solvent screen in the absence of exogenous H-atom source revealed that DMF was half as efficient as

Table 4.9

entry	solvent	%CHO	% toluene	% PPh ₃ O
1	MeCN	22	0	142
2	DMF	11	0	120
3	PhCF ₃ + 25 mol% 2,6-dMePhSH	47	22	139

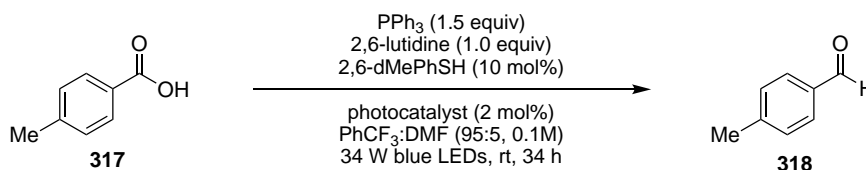
acetonitrile (entry 1 vs. 2). When PhCF₃ was used in concert with 2,6-dMePhSH as an H-atom source, the product was observed in 47% yield (entry 3). Interestingly, we also observed formation

of over-reduction to toluene **292**. This result and additional optimizations will be discussed in Section 4.7. Ultimately, with more optimization, we found that 10 mol% thiol loading was optimal for reduction to the aldehyde without over-reduction to the toluene.

4.4.3 Aromatic acid reduction optimization

We elected to change our substrate to a less activated carboxylic acid—*p*-toluic acid (**317**) and in a photocatalyst screen, found that [Ir] photocatalyst **290** was competent, providing desired aldehyde **318** in 78% yield (Table 4.10, entry 1). Reducing photocatalyst loading to 1 mol% improved reaction efficiency to yield the product in 81% yield (entry 2). Photocatalyst **162**, most successful in alcohol deoxygenation, also provides the product in comparable yield (entry 3). Interestingly, photocatalyst **131**, which was largely ineffective in the alcohol deoxygenation reaction, now affords reduction product **318** in 78% yield (entry 4).

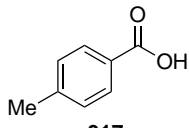
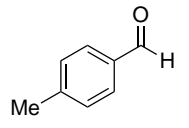
Table 4.10

			
entry	photocatalyst	%yield	% PPh ₃ O
1	[Ir(dFMeppy) ₂ dtbbpy]PF ₆ (290)	78	131
2	290 (1 mol%)	81	128
3	[Ir(dFBnphtl) ₂ dtbbpy]PF ₆ (162)	79	138
4	[Ir(dFCF ₃ ppy) ₂ dtbbpy]PF ₆ (131)	78	142

We next conducted a solvent screen and were gratified to find that numerous solvents are amenable to this reaction (Table 4.11) We employed a mixed solvent system containing 5% DMF to improve solubility of the acid starting materials. When toluene is used as the solvent, the product is afforded in 72% yield (entry 1). Dioxane and benzene (PhH) are also competent solvents, providing the product in 78% and 76%, respectively (entry 2 and 3). More polar solvents such as DMA and NMP can also be used, which is particularly useful for very insoluble carboxylic acids,

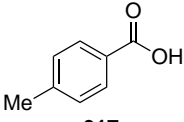
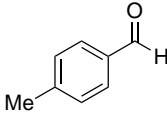
providing aldehyde in 72% and 74% yield respectively (entry 4 and 5). Interestingly, 2,6-lutidine is unnecessary in this protocol, with product being formed in 81% yield (entry 6).

Table 4.11

<div style="display: flex; align-items: center; justify-content: space-around;"> <div style="text-align: center;">  <p>317</p> </div> <div style="text-align: center;"> <p>PPh₃ (1.5 equiv) 2,6-lutidine (1.0 equiv) 2,6-dMePhSH (10 mol%)</p> <hr style="width: 100%;"/> <p>[Ir] 290 (2 mol%) solvent: DMF (95:5, 0.1M) 34 W blue LEDs, rt, 34 h</p> </div> <div style="text-align: center;">  <p>318</p> </div> </div>			
entry	solvent	%yield	% PPh ₃ O
1	PhMe	72	109
2	dioxane	78	99
3	PhH	76	111
4	DMA	72	107
5	NMP	74	113
6	PhMe, no lutidine	81	96

Examination of H-atom sources also demonstrated that numerous thiols could be employed in the reduction of acid to aldehyde (Table 4.12). Electron rich and deficient *o*-substituted thiophenols provided the product in 68-72% yield (entry 1-3). An alkyl thiol also acted as an H-atom source, albeit in reduced yield (20%, entry 4). Disulfides were also amenable to the reaction as H-atom sources, with Ph₂S₂ affording the product in 74% yield (entry 6). The 2-pyridiyl derivative, however, did not afford any product (entry 7). Both (*p*-MeC₆H₄)₂S₂ and (*p*-OMeC₆H₄)₂S₂ also provided the product in good yield (entry 8 and 9), as did very sterically hindered TRIP₂S₂ (entry 10).

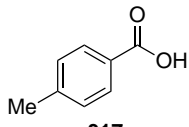
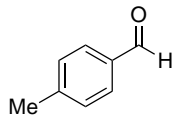
Table 4.12

<div style="display: flex; align-items: center; justify-content: center;"> <div style="text-align: center;">  <p>317</p> </div> <div style="margin: 0 20px; text-align: center;"> $\xrightarrow[\text{[Ir] 290 (2 mol\%), dioxane:DMF (95:5, 0.1M), 34 W blue LEDs, rt, 34 h}]{\text{PPh}_3 (1.5 \text{ equiv}), 2,6\text{-lutidine (1.0 equiv), HAT source (10 mol\%)}}$ </div> <div style="text-align: center;">  <p>318</p> </div> </div>			
entry	HAT source	%yield	% PPh ₃ O
1	<i>o</i> -tBuPhSH	68	125
2	<i>o</i> -MePhSH	72	124
3	<i>o</i> -CF ₃ PhSH	69	113
4	CO ₂ Et(CH)MeSH	20	100
5	2,6-dMePhSH	78	99
6	Ph ₂ S ₂	74	110
7	2-pyr ₂ S ₂	0	110
8	<i>p</i> -tol ₂ S ₂	70	91
9	<i>p</i> -OMePh ₂ S ₂	79	108
10	TRIP ₂ S ₂	74	100

After further studies of concentration, photocatalyst loading and phosphine loading, the optimized protocol yields product **318** in 87% yield after 24 h (Table 4.13, entry 1). However, a time-course study of the reaction revealed that conversion is nearly complete after 12 h; reaction times were set to 24 h to accommodate carboxylic acids that react more slowly. Control reactions revealed that triphenylphosphine, light and photocatalyst are all necessary for reactivity; however, the reaction does proceed to 2% yield in the absence of thiol (entry 2-5). The solvent is likely acting as the H-atom source in the absence of thiol. Addition of 2,6-lutidine or omission of DMF had little effect on the outcome of the reaction, providing the product in 80% and 83% yield, respectively (entry 6 and 7). Numerous thiols or disulfides also afford the product in 82 – 87% yield (entry 8-10). Methyl diphenylphosphinite in place of triphenylphosphine affords aldehyde **318** in 64% yield (entry 11). When NMP was used as the solvent, the reaction still proceeded in high efficiency to 76% yield (entry 12). Photocatalysts **131** and **162** also provided the product in

excellent yield, highlighting the versatility of conditions amenable for the reduction of a carboxylic acid to aldehyde (entry 13 and 14).

Table 4.13

<div style="display: flex; align-items: center; justify-content: center;"> <div style="text-align: center;">  <p>317</p> </div> <div style="margin: 0 20px; text-align: center;"> $\xrightarrow[\text{PhMe:DMF (95:5, 0.2M)}]{\begin{array}{l} \text{PPh}_3 \text{ (1.2 equiv)} \\ \text{TRIP-SH (10 mol\%)} \\ [\text{Ir}] \textbf{290} \text{ (1 mol\%)} \end{array}}$ <p>34 W blue LEDs, rt, 24 h</p> </div> <div style="text-align: center;">  <p>318</p> </div> </div>		
entry	deviation from std. conditions	%yield
1	none	87%
2	no PPh ₃	0%
3	no thiol	2%
4	no light	0%
5	no photocatalyst	0%
6	2,6-lutidine	80%
7	no DMF	83%
8	2,6-dMeC ₆ H ₃ SH	82%
9	Ph ₂ S ₂	84%
10	(<i>p</i> -OMeC ₆ H ₄) ₂ S ₂	87%
11	Ph ₂ POMe (1.5 equiv)	64%
12	NMP (0.2M)	76%
13	[Ir(dFCF ₃ ppy) ₂ dtbbpy]PF ₆ (131) (1 mol%)	90%
14	[Ir(dFBnphl) ₂ dtbbpy]PF ₆ (162) (1 mol%)	87%

4.4.4 Stern-Volmer quenching studies

We sought to conduct further mechanistic studies of the system with Stern-Volmer quenching experiments. As can be seen in Figure 4.4, 2,6-lutidine and the carboxylic acid do not demonstrate any quenching of the photocatalyst excited state. Importantly, this suggests that the carboxylic acid is not undergoing single-electron oxidation followed by carboxy radical addition to triphenylphosphine to form a phosphoranyl radical. Additionally, TRIP-SH demonstrates only a small degree of quenching, albeit under stoichiometric conditions. Triphenylphosphine demonstrates clear quenching of the excited state of the photocatalyst, consistent with reductive

quenching of the excited state of the photocatalyst by triphenylphosphine and our mechanistic hypothesis.

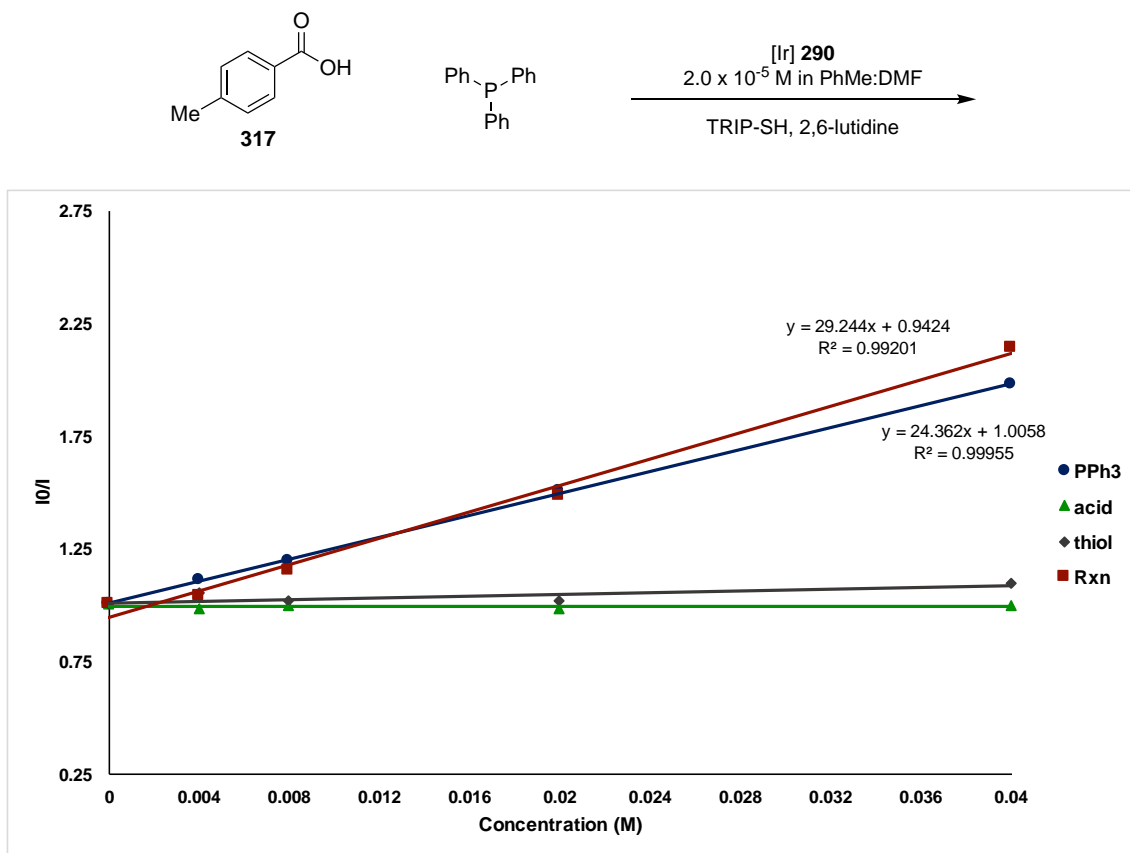
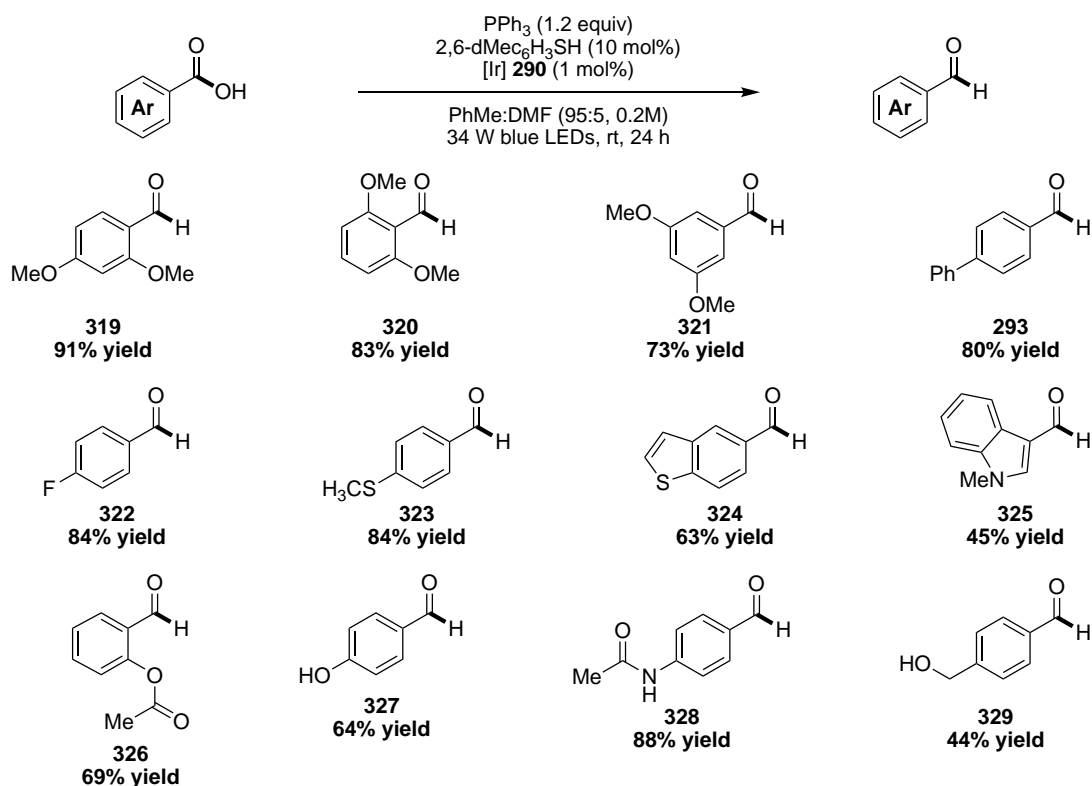


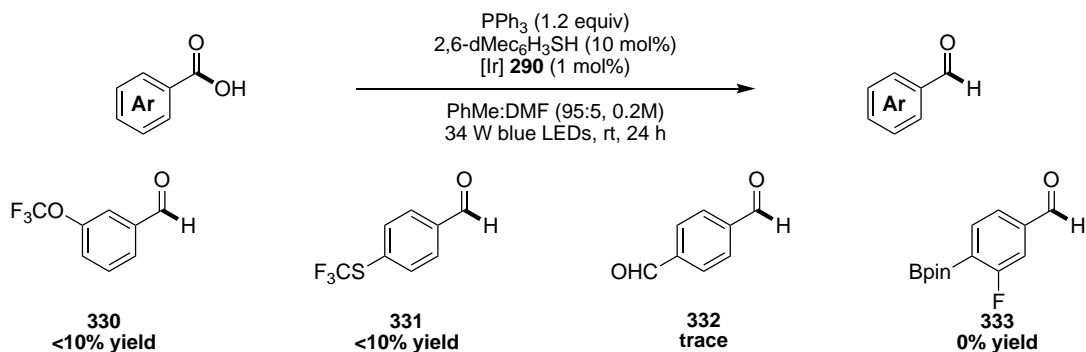
Figure 4.4

Our proposed mechanism is depicted in Scheme 4.12. Upon irradiation with light, photocatalyst **290** transitions into a long-lived triplet excited state, which could undergo single-electron reduction with triphenylphosphine, to form a phosphine radical cation (**227**). Two-electron addition of the carboxylic acid into the phosphine radical cation would afford phosphoranyl radical **318**. A β -scission event would then give triphenylphosphine oxide and the desired acyl radical. With terminal H-atom transfer, the desired aldehyde product could be afforded and the thiyl radical would undergo single-electron reduction from the reduced form of the photocatalyst to afford a thiolate and regenerate the iridium photocatalyst.



Scheme 4.13

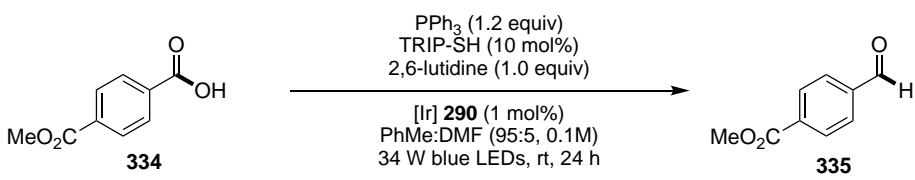
All the carboxylic acids in Scheme 4.13 are electron-rich or electron-neutral. When we examined electron-deficient carboxylic acids, we began to observe very low yields and in some cases, over-reduction to the alcohol or toluene. Either *m*-OCF₃ or *p*-SCF₃ substituted benzoic acids afforded the corresponding aldehydes (**330-331**) in <10% yield (Scheme 4.14). Aldehydes **332** and **333** were only observed in trace amounts and 0% yield, respectively.



Scheme 4.14

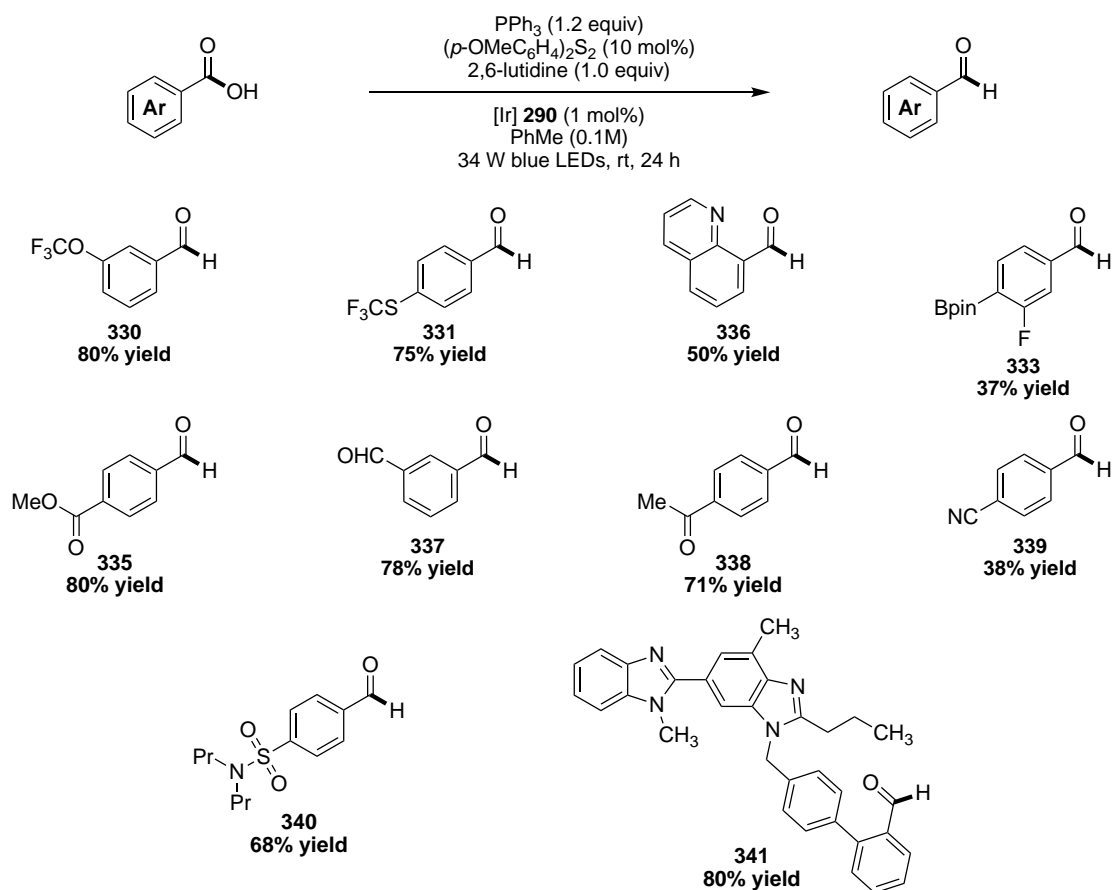
We sought to re-optimize the reaction conditions for electron-deficient aromatic carboxylic acids using acid **334**. Under the standard conditions, aldehyde **335** was observed in <5% yield (Table 4.14, entry 1). When 2,6-lutidine was added, the yield improved to 15% yield (entry 2). Use of TRIP₂S₂ in place of TRIP-SH improved the yield an additional 5% (entry 3). Removal of DMF from the reaction conditions affords the product in 43% yield (entry 4). Use of (*p*-OMePh)₂S₂ in place of TRIP-SH improved the yield to 57%, and omission of DMF with this disulfide afforded the product in 82% yield (entry 5 and 6). Furthermore, removal of 2,6-lutidine, under the otherwise optimal conditions (entry 6) gave reduced yield to 62% (entry 7).

Table 4.14

		
entry	deviation from std. conditions	%yield
1	no 2,6-lutidine	<5%
2	none	15%
3	TRIP ₂ S ₂	20%
4	no DMF	43%
5	(<i>p</i> -OMeC ₆ H ₄) ₂ S ₂ (10 mo%)	57%
6	(<i>p</i> -OMeC ₆ H ₄) ₂ S ₂ (10 mo%), no DMF	82%
7	(<i>p</i> -OMeC ₆ H ₄) ₂ S ₂ (10 mo%), no DMF, lutidine	62%

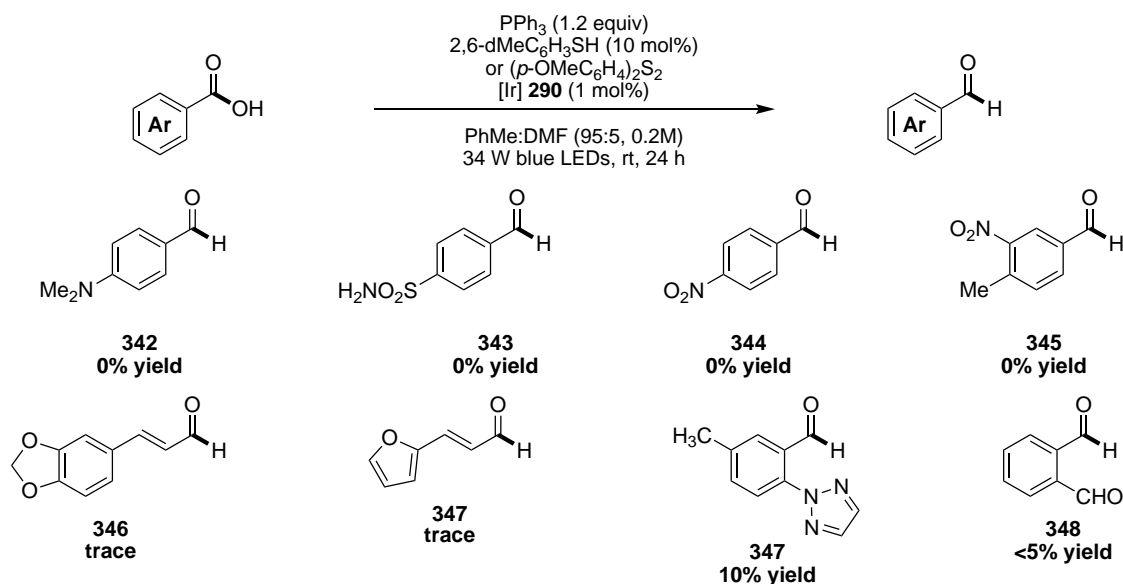
With the new protocol for electron-deficient acids in hand, we sought to examine the scope of reduction (Scheme 4.15). Aldehydes **330** and **331**, which were isolated in <10% yield under the previous conditions, are now isolated in 80% and 75% yield, respectively. Aldehyde **336** is also afforded under the new reaction conditions in 50% yield. Aldehyde **333**, which previously gave no product, is now isolated in 37% yield, although benzylic alcohol is also observed in up to 10% yield. The exceptional functional group orthogonality is highlighted by aldehydes **335**, **337-339**,

now provided in good to excellent yield. Pharmaceuticals Probenecid and Telmisartan are also efficiently reduced under the conditions in 68% and 80% yield, respectively (**340**, **341**).



Scheme 4.15

Numerous aromatic aldehydes were ineffective for reduction under the reaction conditions. Aldehyde **342** was not observed, likely due to preferential single-electron oxidation of dimethylaniline moiety (Scheme 4.16). Unprotected sulfonamides and nitro-containing aromatics also do not provide any aldehyde under the reaction conditions. Cinnamic acids are also not reduced under the standard protocols; a likely explanation is that a phosphine radical cation may competitively add into the Michael acceptor. Very deficient aldehyde **347** is provided in about 10% yield. Furthermore, *o*-carboxy aldehyde **348** is not isolated from the reaction conditions, likely because the starting acid exists as an acetal rather than the aldehyde acid.

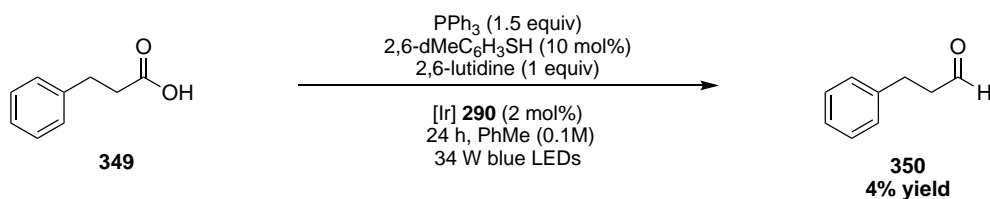


Scheme 4.16

4.5. Extension to aliphatic carboxylic acids

4.5.1 Optimization

Many existing photocatalytic strategies exist for activating aromatic acids to generate acyl radicals, but few are amenable to aliphatic acids and no general protocol exists for the activation of both aromatic and aliphatic acids. We wanted to develop a general procedure of C–O bond activation that could address these limitations. When we subjected hydrocinnamic acid to our optimized aromatic reduction conditions, however, we observed aldehyde in only 4% yield (Scheme 4.17).

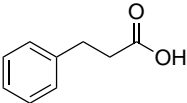
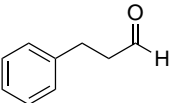


Scheme 4.17

We sought to optimize the reaction by examining the different reaction components. We began by examining the role of base on reaction efficiency, using Ph_2S_2 as the H-atom source (Table

4.15). In the absence of base, trace product was observed (entry 1). With 2,6-lutidine under these conditions, the product was observed in 15% yield (entry 2). Inorganic bases such as K_3PO_4 , Cs_2CO_3 or Na_2HPO_4 were ineffective at promoting the reaction (entry 3-5). It should be noted however, that these are commonly used bases to effect single-electron oxidation of carboxylates. Their ineffectiveness at promoting the reaction provides additional support that carboxy radical addition is not responsible for formation of the phosphoranyl radical. Furthermore, in the presence of Cs_2CO_3 , the decarboxylated product is observed in 15% yield. Pyridine is only moderately effective as a base under these conditions (entry 6).

Table 4.15

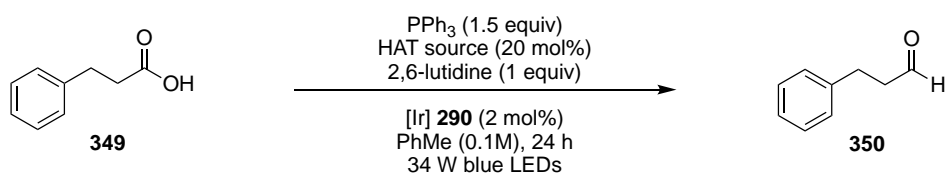
<div style="display: flex; align-items: center; justify-content: center;"> <div style="text-align: center;">  <p>349</p> </div> <div style="margin: 0 20px; text-align: center;"> $\xrightarrow[\text{[Ir] 290 (2 mol\%), PhMe (0.1M), 24 h, 34 W blue LEDs}]{\text{PPh}_3 (1.5 \text{ equiv}), \text{Ph}_2\text{S}_2 (20 \text{ mol\%}), \text{base (1 equiv)}}$ </div> <div style="text-align: center;">  <p>350</p> </div> </div>			
entry	base	% yield	%ethylbenzene
1	none	1%	0%
2	2,6-lutidine	15%	0%
3	K_3PO_4	1%	0%
4	Cs_2CO_3	2%	15%
5	Na_2HPO_4	2%	0%
6	pyridine	7%	0%

We questioned whether a phosphine other than triphenylphosphine might be more effective for acid reduction (Table 4.16). Exchanging PPh_3 for a more electron deficient phosphinite such as Ph_2POMe , improved the yield from 16% to 30% (entry 1 and 2). Use of an even more deficient phosphonite gave a less efficient reaction, with hydrocinnamaldehyde observed in only 10% yield (entry 3). However, the corresponding methyl ester is observed in 26% yield. This product may result from S_N2 displacement of a methyl group of the phosphine radical cation. Fluoro-substituted triphenylphosphine provided product **350** in only 11% yield (entry 4).

Table 4.16

entry	phosphine	% yield	% 351
1	PPh_3	16%	0%
2	Ph_2POMe	30%	3%
3	PhP(OMe)_2	10%	26%
4	$(p\text{-FC}_6\text{H}_4)_3\text{P}$	11%	0%

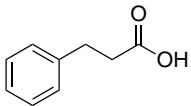
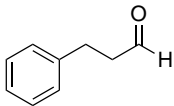
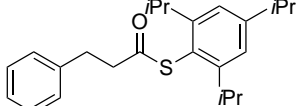
We surmised that H-atom source would have a significant impact on the efficiency of the reduction reaction (Table 4.17). Use of $(p\text{-OMeC}_6\text{H}_4)_2\text{S}_2$, which was very effective in the reduction of aromatic acids, gave little aliphatic aldehyde (entry 1). TRIP_2S_2 , however, gave improved yield with PPh_3 , providing hydrocinnamaldehyde in 25% yield (entry 2). A number of substituted aryl thiols were also employed in the reaction, but did not give significantly better results (entry 3-5). Use of Ph_2CHCN as an H-atom source was completely ineffective at providing the reduced product (entry 6).

Table 4.17

entry	HAT source	% yield
1	$(p\text{-OMeC}_6\text{H}_4)_2\text{S}_2$	3%
2	TRIP_2S_2	25%
3	$\alpha\text{-CF}_3\text{C}_6\text{H}_4\text{SH}$	2%
4	$\alpha\text{-MeC}_6\text{H}_4\text{SH}$	7%
5	$\alpha\text{-}t\text{-BuC}_6\text{H}_4\text{SH}$	13%
6	Ph_2CHCN	0%

We next sought to examine the solvent tolerance for this reaction with Ph₂POMe using TRIP₂S₂ as an H-atom source (Table 4.18). In PhCF₃, we observed reduced yield of product **350** and 6% yield of the methyl ester (**351**). Interestingly, with use of TRIP₂S₂ as the H-atom source, we observed the formation of thioester **352** in significant yield (entry 1). Product **352** likely arises from formation of a phosphonium intermediate which is capable of rapid acyl transfer. In DMF, this reaction is even more prevalent, forming 34% yield of the thioester product (entry 2). Similarly, amide solvents NMP and DMA give trace reduction product, but significant amounts of **352** (entry 3 and 4). Dioxane and PhH were more effective for the transformation, giving product in nearly comparable yields to PhMe (entry 5 and 6). ACN and THF were also tolerated as solvents in the reaction, but gave lower yields and variable amounts of thioester product (entry 7 and 8).

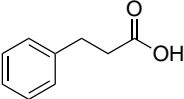
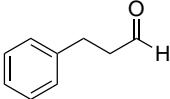
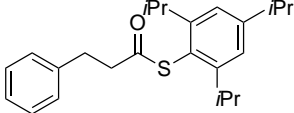
Table 4.18

<div style="display: flex; align-items: center; justify-content: center;"> <div style="text-align: center;">  <p>349</p> </div> <div style="margin: 0 20px; text-align: center;"> $\xrightarrow[\text{[Ir] 290 (2 mol\%), solvent (0.1M), 24 h, 34 W blue LEDs}]{\text{Ph}_2\text{POMe (1.5 equiv), TRIP}_2\text{S}_2 \text{ (20 mol\%), 2,6-lutidine (1 equiv)}}$ </div> <div style="display: flex; gap: 20px;"> <div style="text-align: center;">  <p>350</p> </div> <div style="text-align: center;">  <p>352</p> </div> </div> </div>				
entry	solvent	% yield 350	% yield 352	% yield 351
1	PhCF ₃	10%	11%	6%
2	DMF	11%	34%	0%
3	NMP	2%	16%	0%
4	DMA	5%	20%	10%
5	dioxane	23%	17%	0%
6	PhH	25%	8%	12%
7	ACN	18%	18%	0%
8	THF	18%	33%	5%

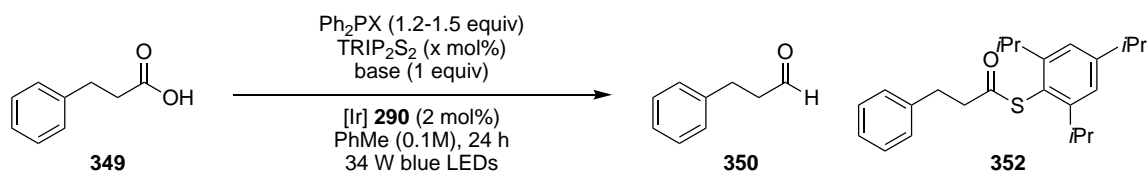
Another base screen examining pyridine bases revealed that 2,4,6-collidine appeared to be privileged, giving the product in 47% yield with TRIP₂S₂ as the H-atom source (Table 4.19, entry 1). Other substituted pyridines gave comparable or slightly improved yield to 2,6-lutidine, although they gave significantly increased amounts of methyl ester byproduct (**351**) (entry 2-4).

Photocatalyst screens revealed **290** to be the best photocatalyst, with all others giving reduced or no yield.

Table 4.19

$ \begin{array}{c} \text{Ph}_2\text{POMe (1.5 equiv)} \\ \text{TRIP}_2\text{S}_2 \text{ (20 mol\%)} \\ \text{base (1 equiv)} \\ \hline \text{[Ir] } \mathbf{290} \text{ (2 mol\%)} \\ \text{PhMe (0.1M), 24 h} \\ \text{34 W blue LEDs} \end{array} $				
 349	→	 350	 352	
entry	base	% yield 350	% yield 352	% yield 351
1	2,4,6-collidine	47%	13%	7%
2	(2,6-dOMe)C ₅ H ₃ N	33%	3%	20%
3	(2,6-di <i>t</i> Bu)C ₅ H ₃ N	38%	3%	23%
4	(4-OMe)C ₅ H ₄ N	41%	13%	20%

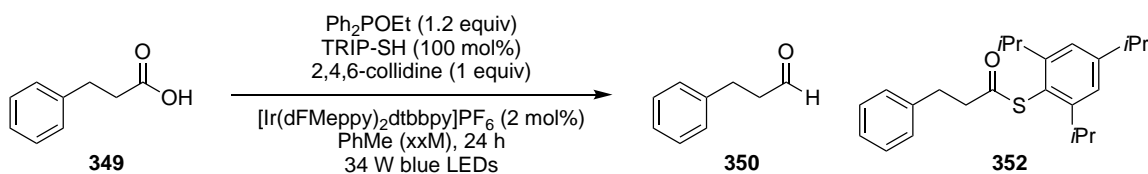
Examining disulfide loading versus phosphine identity gave us additional insights into the reaction (Table 4.20). At 10 mol% TRIP₂S₂ loading with 1.5 equivalents of PPh₃, we observed small amounts of products **350** and **352** (entry 1). Increasing the loading to 20 mol% gave improved product yield, but also considerably more thioester (entry 2). Finally, increasing disulfide loading to 50 mol% gave reduced product yield, and 57% of the thioester product (entry 3). The same trend was observed for Ph₂POEt, with increasing disulfide loading giving more thioester product (entry 4-7). We suspected that single-electron oxidation of the intermediate phosphoranyl radical was giving rise to a phosphonium species that could participate in rapid acyl transfer with a nucleophile, such as TRIP-SH. Increasing the loading of TRIP₂S₂ would give more thiyl radical– a species capable of single-electron oxidation of the phosphoranyl radical.

Table 4.20

entry	TRIP ₂ S ₂ loading w/ PPh ₃	% yield 350	% yield 352	% yield 351
1	10 mol%	1%	2%	n/a
2	20 mol%	24%	15%	n/a
3	50 mol%	18%	57%	n/a

TRIP ₂ S ₂ loading w/ Ph ₂ POEt				
4	10 mol%	52%	7%	6%
5	20 mol%	56%	16%	6%
6	30 mol%	51%	26%	5%
7	50 mol%	36%	43%	5%

We hypothesized that by decreasing the concentration of the reaction, we might increase the rate of unimolecular β -scission relative to unproductive bimolecular electron transfer. We had previously observed that while TRIP₂S₂ generally gave improved yields to TRIP-SH, the yield was not affected by concentration changes. We determined that 50-100 mol% TRIP-SH was optimal,

Table 4.21

entry	concentration	% yield 350	% yield 351	% yield 352
1	0.1M	46%	4%	12%
2	0.05M	56%	4%	10%
3	0.02M	63%	2%	4%
4	0.0133M	70%	5%	2%
5	0.01M	71%	3%	2%

giving nearly identical yield, while minimizing the amount of thioester (**352**) formed. We then examined this new protocol as a function of concentration (Table 4.21). At 0.1M, we observed

46% yield of the product, with 12% of the ethyl ester byproduct (entry 1). Diluting the reaction to 0.05M gave improved yield to 56% (entry 2). Diluting the reaction even farther ultimately gave the desired product in 70% yield at 0.0133M, with minimal byproducts (entry 3-5). We re-evaluated TRIP₂S₂ with the new conditions, but observed no comparable boost in yield at low concentration.

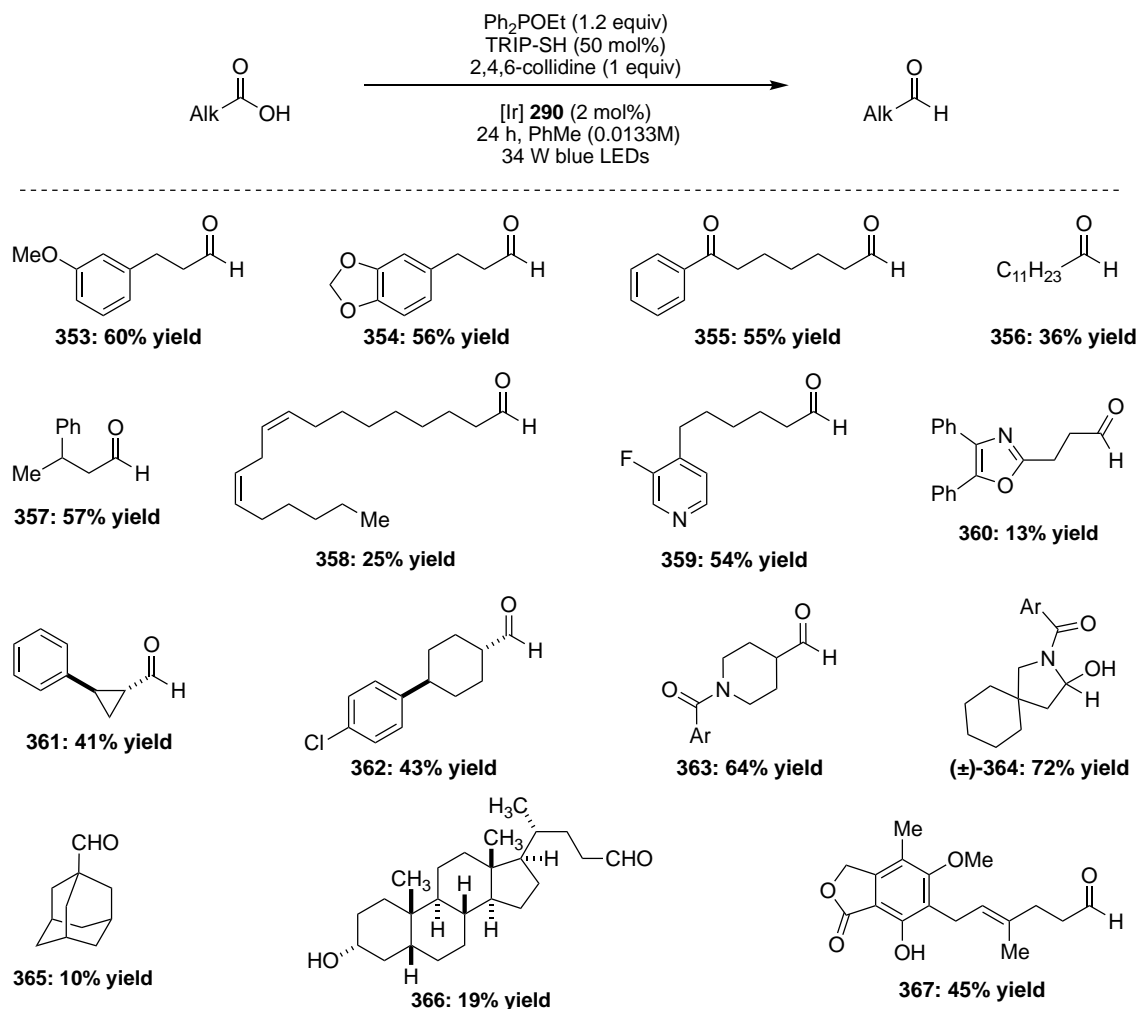
4.5.2 Aliphatic acid reduction scope

With our optimized conditions in hand, we sought to evaluate the control reactions for this transformation and evaluate scope of aliphatic acids (Table 4.22). Variations in concentration or H-atom source did not improve the yield of the reaction (entry 1-4) compared to the optimized conditions, which, on scale, afforded hydrocinnamaldehyde in 68% yield (entry 5). With triphenylphosphine, the reaction proceeded to only 8% yield under dilute conditions (entry 6). In the absence of light, photocatalyst, phosphine or TRIP-SH, no product was observed (entry 7-10).

Table 4.22

entry	deviation from conditions	% yield 350	% yield 352	% yield 351
1	TRIP-SH (10 mol%), 0.1M	42%	1%	0%
2	TRIP ₂ S ₂ (10 mol%), 0.1M	50%	6%	0%
3	0.1M	43%	7%	3%
4	0.02M	60%	1%	0%
5	none	68%	1%	0%
6	PPh ₃ (1.2 equiv)	8%	1%	0%
7	0.02M, no light	0%	0%	0%
8	0.02M, no [Ir]	0%	0%	0%
9	0.02M, no Ph ₂ POEt	0%	0%	0%
10	0.02M, no TRIP-SH	0%	0%	0%

The full substrate scope is depicted in Scheme 4.18. Hydrocinnamaldehyde derivatives **353** and **354** were isolated in good yield under the standard reaction conditions. Aldehyde **355**, derived from a keto-acid is also isolated in good yield, highlighting the functional group orthogonality of our reduction method. Long chain saturated and unsaturated aliphatic acids are also tolerated in the reaction, albeit give lower yields of the corresponding aldehydes (**356**, **358**). Heterocyclic

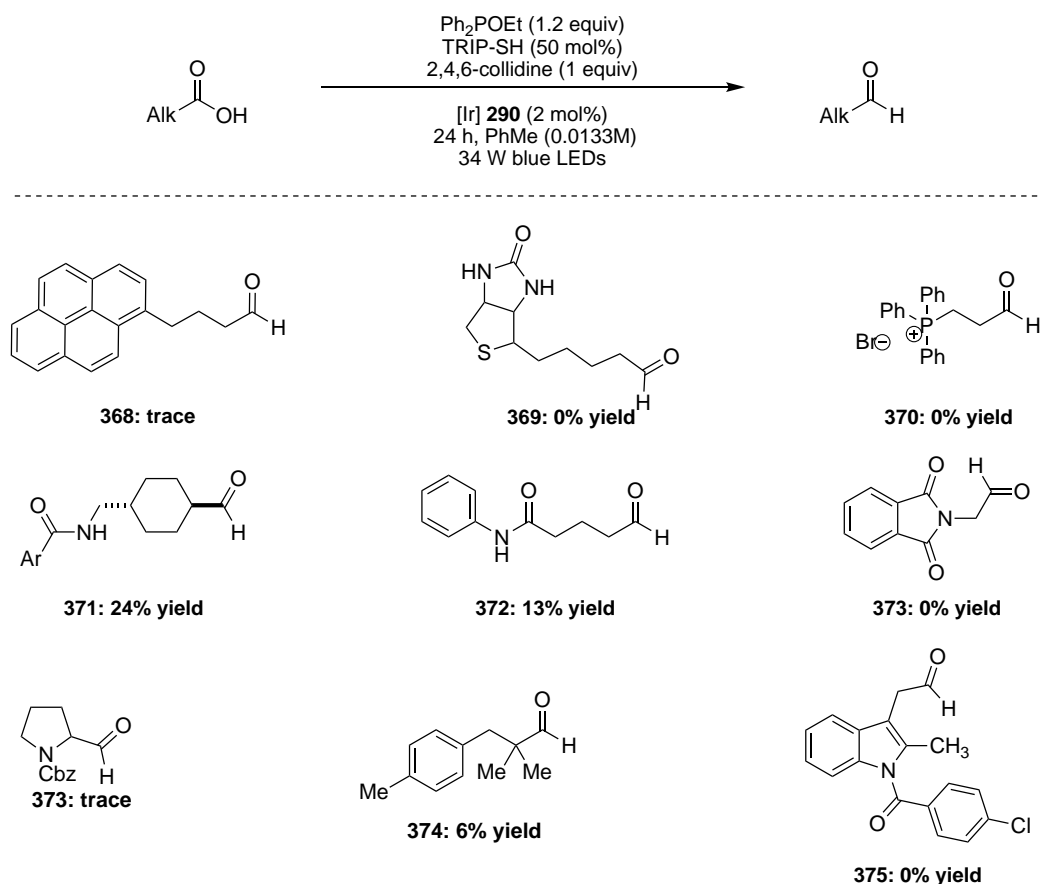


Scheme 4.18

containing acids can also be efficiently reduced to the aldehydes, with pyridine **359** isolated in 54% yield. Oxaprozin was also reduced to the corresponding aldehyde (**360**), albeit in reduced yield (30% by ^1H NMR). α -Branched acids are also tolerated in the reaction, with stereodefined

aldehydes **361** and **362** isolated in good yields without loss of stereochemical information. It should be noted that ring-opened products from *trans*-phenylcyclopropanecarboxylic acid are observed in <5% yield, consistent with a radical intermediate. Tertiary benzamides are also well tolerated under the reaction conditions, with aldehyde **363** (Ar = 4-FC₆H₄) isolated in 64% yield. Under these conditions, we do observe some of the decarbonylated product in α -branched acids. A neopentyl acid derived from Gabapentin is also efficiently reduced to the corresponding aldehyde, although it is isolated as the *N,O*-acetal (**364**) (Ar = 4-FC₆H₄). 1-Adamantyl carboxylic acid is also reduced to the corresponding aldehyde (**365**), albeit in low yield. Presumably, the intermediate acyl radical undergoes rapid decarbonylation to form the alkane product. We were also able to extend our methodology to complex aliphatic acids, with lithocholic acid reduced to the aldehyde (**366**) in 19% yield and Mycophenolic acid reduced product (**367**) successfully isolated in 45% yield.

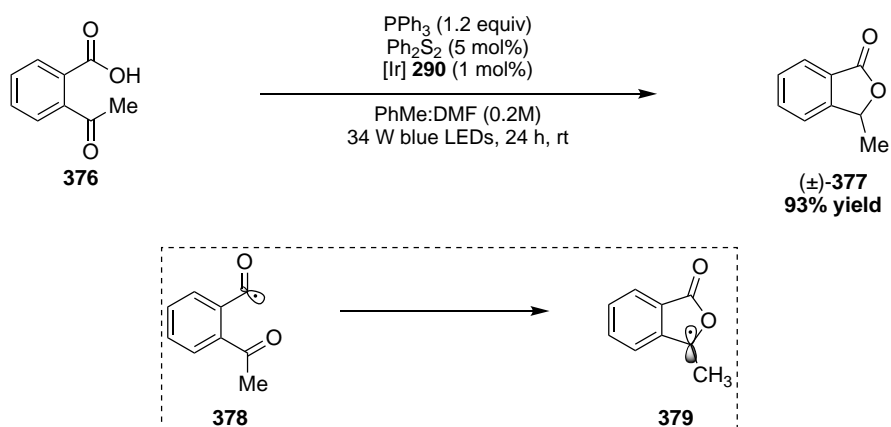
A number of aliphatic acids are not amenable to our optimized reduction conditions (Scheme 4.19). Carboxylic acids with low solubility in PhMe were not reduced to the corresponding aldehydes (**368-370**). We did not attempt to try other solvents for these particular substrates, although that may address the solubility limitation. Secondary benzamides are competent under the reaction conditions, but suffered from poor solubility (**371**). Aldehyde **372** was observed as a mixture of linear aldehyde and mixed acetal. Any α -amino acids were not able to be converted to the corresponding aldehydes. Presumably the acyl radical rapidly decarbonylates to form a very stabilized α -amino radical. Similarly, aldehyde **375** was not formed from Indomethacin, as the decarbonylation event would lead to a stabilized benzylic radical. Tertiary aldehyde **374** was only observed in 6% yield, like 1-adamantyl carboxaldehyde.



Scheme 4.19

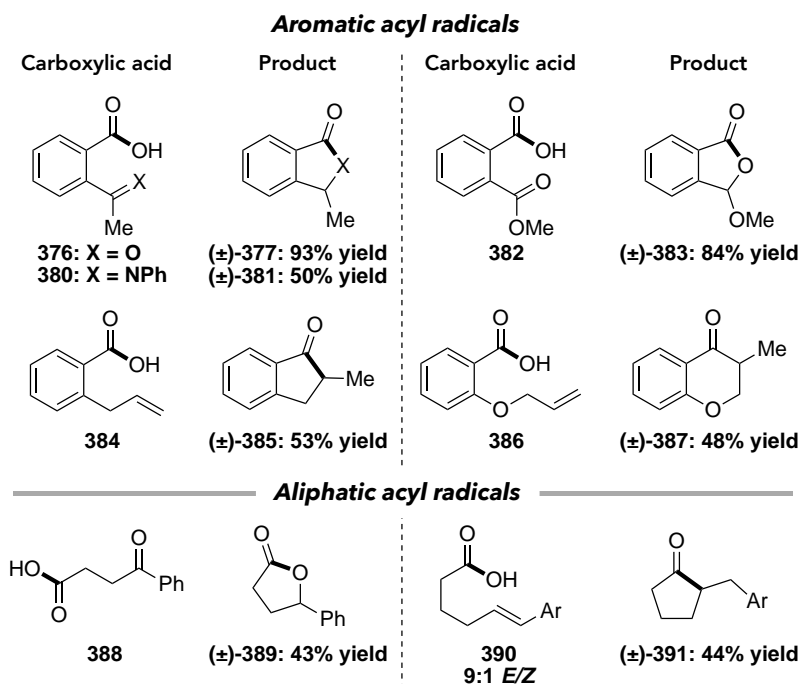
4.6 Cyclization reactions

During the course of aromatic carboxylic acid reduction studies, we observed that acid **376** was not reduced to the aldehyde, but rather formed lactone **377** in excellent yield (Scheme 4.20). This reaction likely proceeds through intermediate acyl radical **378**, which rapidly cyclizes onto the ketone to form α -oxy radical **379**, where upon H-atom transfer gives the lactone product. These types of radical cyclizations have been well documented in the literature, and are known to proceed rapidly ($2.0 \times 10^8 \text{ s}^{-1}$).²⁷



Scheme 4.20

We envisioned that we could utilize this rapid radical cyclization to generate numerous different ketones, lactones and amide products (Scheme 4.21). With no additional optimization studies, imine **380** was efficiently cyclized to the corresponding lactam (**381**) in 50% yield. We

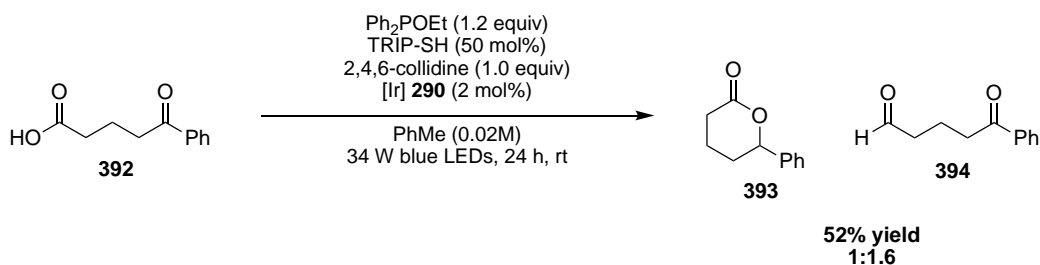


Scheme 4.21

also demonstrated that cyclization onto an ester moiety (**382**) affords acetal product **383** in excellent yield. Additionally, aromatic acyl radical cyclization onto pendant alkenes affords

product **385** and **387** with complete regioselectivity for the *exo* adducts in good yield. Furthermore, we extended this methodology to aliphatic acyl radical cyclizations, with lactone **389** and ketone **391** (Ar = 4-FC₆H₄) afforded in good yield. Presumably with additional optimization, the yield of these transformations may be improved to yield numerous cyclized products in good yield. Additionally, as all of these cyclizations form new stereocenters, use of a chiral H-atom source may lend highly enantioselective transformations.

Interestingly, when aliphatic acid **392** was subjected to the reaction conditions we saw a competition between cyclization to form lactone **393** and H-atom transfer to form aldehyde **394** (Scheme 4.22). The mixture of products was observed in 52% yield, with a 1:1.6 ratio of lactone to aldehyde. A longer chain linker in acid **355**, ultimately led to formation of the aldehyde exclusively (Scheme 4.18)



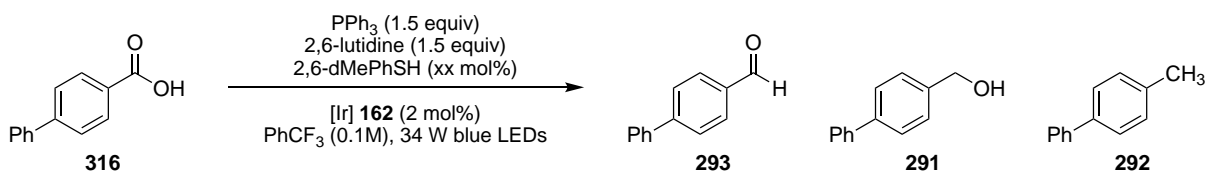
Scheme 4.22

4.7 Over-reduction of carboxylic acids

As noted in Table 4.9, we observed over-reduction of the carboxylic acid to the corresponding toluene. When we examined thiol loading, we found an interesting trend (Table 4.23). With only 12.5 mol% thiol, we observe the aldehyde in 60% yield and 13% toluene (entry 1). When thiol loading is increased to 50 mol%, aldehyde yield is significantly reduced, and toluene **292** is observed in 30% yield (entry 2). With a full equivalent of thiol, now alcohol **291** is observed in

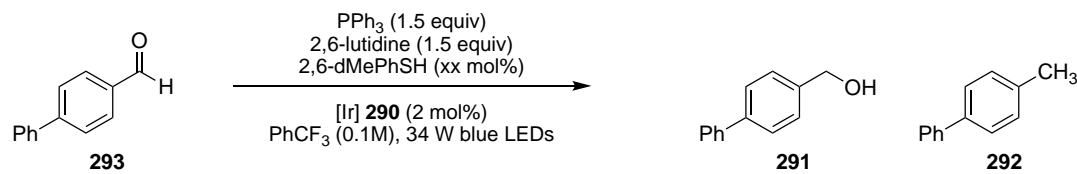
21% yield, and toluene in 32% yield (entry 3). Two equivalents of thiol provide even more alcohol (33% yield) and toluene (31% yield) and only trace yield of the desired product.

Table 4.23

					
entry	2,6-dMePhSH	%yield 293	%yield 291	%yield 292	%PPh ₃ O
1	12.5 mol%	60	0	13	125
2	50 mol%	20	0	30	145
3	1.0 equiv	7	21	32	126
4	2.0 equiv	4	33	31	121

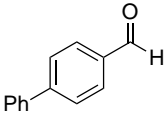
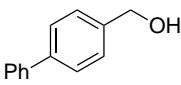
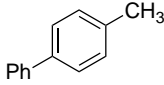
To establish the intermediacy of the aldehyde in this over-reduction, we subjected aldehyde **293** to similar reaction conditions as a function of thiol loading (Table 4.24). With only 25 mol% thiol, we observed incomplete conversion to toluene **292** as the only product – no alcohol intermediate was observed (entry 1). Doubling the thiol loading doubles conversion and yield to 40% (entry 2). Increasing to 75 mol%, the product is obtained in 61% yield with 61% conversion. With a full equivalent of thiol, we observed nearly complete conversion with a 73% yield of toluene product **292**. The alcohol intermediate product was not observed in any of these cases.

Table 4.24

					
entry	2,6-dMePhSH	%conversion	%yield 291	%yield 292	% PPh ₃ O
1	25 mol%	36	0	17	41
2	50 mol%	63	0	40	58
3	75 mol%	61	0	61	71
4	1.0 equiv	97	0	73	93

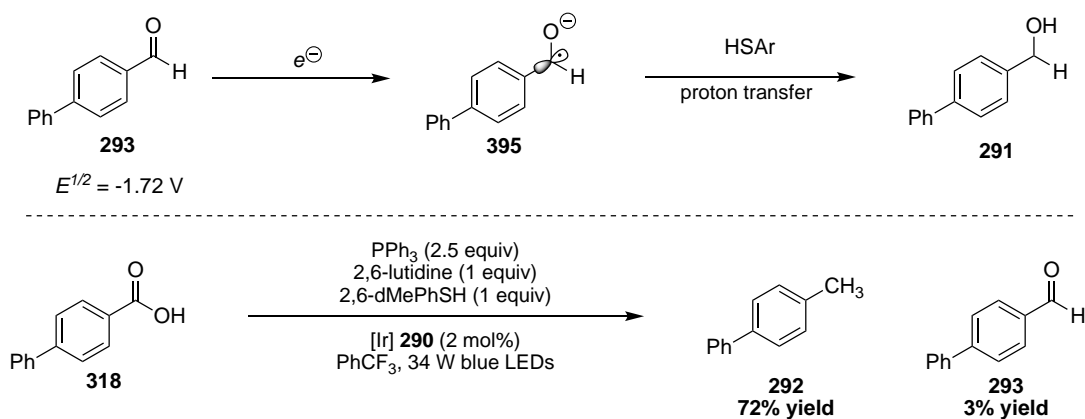
We next sought to examine the control reactions for this transformation. Under standard conditions, we observed 70% yield of the toluene product with no alcohol formation (Table 4.25, entry 1). Interestingly, in the absence of phosphine, we do not observe any toluene product, but we do observe 38% yield of alcohol **291** (entry 2). In the absence of iridium or light there is no reaction (entry 3 and 4). Additionally, there is no reduction in the absence of thiol, although we do observe 29% conversion (entry 5). In the absence of base, the reaction is less efficient, affording toluene **292** in only 52% yield, and alcohol in 7% yield (entry 6).

Table 4.25

<div style="display: flex; align-items: center; justify-content: center;"> <div style="text-align: center;">  <p>293</p> </div> <div style="margin: 0 20px; text-align: center;"> <math>\xrightarrow[\text{PhCF}_3 (0.1\text{M}), 34 \text{ W blue LEDs}]{\begin{array}{l} \text{PPh}_3 (1.5 \text{ equiv}) \\ 2,6\text{-lutidine} (1.5 \text{ equiv}) \\ 2,6\text{-dMePhSH} (100 \text{ mol}\%) \\ [\text{Ir}] \text{ 290 (2 mol}\%) \end{array}}</math> </div> <div style="display: flex; gap: 20px;"> <div style="text-align: center;">  <p>291</p> </div> <div style="text-align: center;">  <p>292</p> </div> </div> </div>					
entry	deviation	%conversion	%alcohol	% toluene	% PPh ₃ O
1	none	100	0	70	90
2	no PPh ₃	86	38	0	n/a
3	no [Ir]	8	0	0	15
4	no light	6	0	0	33
5	no thiol	29	0	0	36
6	no base	94	7	52	126

Given these experimental results, we concluded that the aldehyde is first reduced to the alcohol and subsequent deoxygenation via our previously proposed pathway affords toluene **292**. The first reduction occurs in the absence of triphenylphosphine, but thiol is necessary, in stoichiometric amounts, suggesting that the thiol is serving as the stoichiometric reductant. This reaction occurs in minimal amounts with aldehyde **318**, suggesting that the aldehyde reduction may be voltage-gated. A possible mechanism is depicted in Scheme 4.23. Single-electron reduction of the aldehyde would provide ketyl radical **395**, which upon H-atom transfer would afford alcohol **291**. Our previously established alcohol deoxygenation protocol would afford the final reduction product

(**292**). We surmised that if acid **318** were subjected to acid reduction conditions with 2.5 equivalents of PPh₃ and stoichiometric thiol, we might realize a full reduction of acid to toluene in one pot. Indeed, toluene **292** was observed in 72% yield under these conditions (Scheme 4.23).



Scheme 4.23

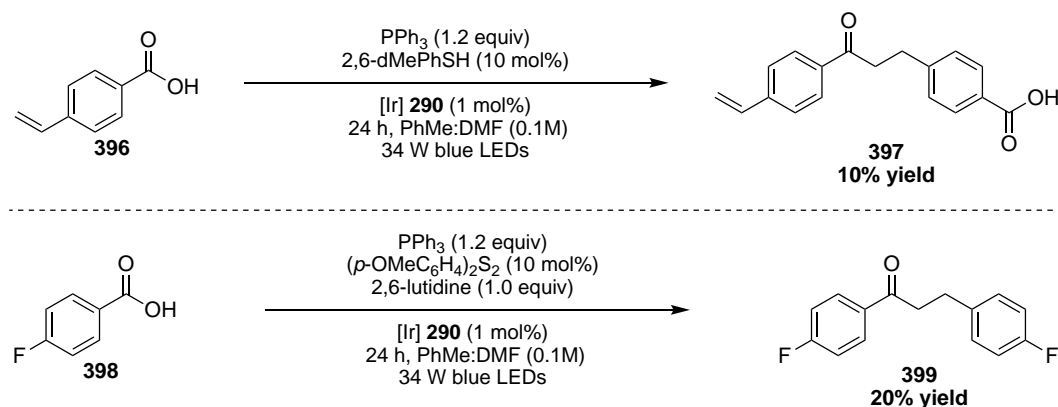
4.8 Conclusion and outlook

We have demonstrated C–O bond activation using photoredox catalysis to access unique phosphoranyl radical intermediates. Aliphatic alcohols can be reduced to the corresponding toluene products in excellent yield under exceptionally mild conditions in a one-step procedure. The scope of this transformation has been broadly expanded by graduate student Alyssa Ertel to include electron-rich and electron-poor benzylic alcohols. Unactivated primary and secondary aliphatic alcohols can also be reduced, although these transformations require further optimization. We have also shown that these radicals can be parlayed into C–C bond forming events with heteroaromatic chlorides. These transformations have not been extensively studied, and with further optimization, would represent a very powerful technique for coupling C–O bonds of alcohols with radical acceptors. Furthermore, although we have no preliminary results, it is feasible that this method could be combined with transition metal catalysis to construct more complex molecules.

The reduction of carboxylic acids to aldehydes in a single step under mild conditions is a long-standing challenge in organic synthesis. Many photocatalyzed methods have been developed to try to access acyl radicals with subsequent H-atom transfer to realize a more general protocol. However, they all suffer from voltage-gated redox events, which precludes any one generalized procedure for all carboxylic acids (i.e. aromatic and aliphatic acids require completely different approaches, reductive vs. oxidative). Our photocatalyzed procedure with phosphines has overcome this challenge, with efficient reduction of aromatic and aliphatic acids under similar conditions. We have demonstrated that use of different phosphines can address substrate limitations, rather than having to develop a new approach. Furthermore, this access to acyl radicals has been utilized to form new C–C, C–O and C–N bonds through intramolecular cyclization reactions.

4.8.1 Intermolecular C–C bond formation

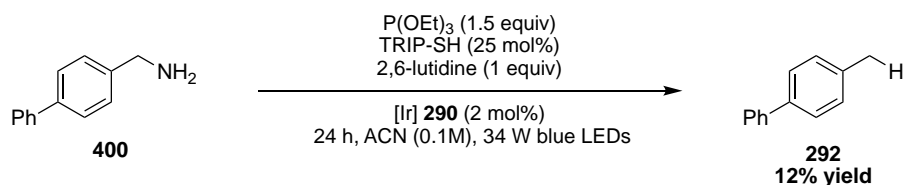
These demonstrations represent an exciting new approach to substrate activation, and are not limited to terminal H-atom transfer, nor C–O bond activation. In the course of aromatic acid reduction evaluation, we observed that 4-vinyl benzoic acid (**396**) afforded a mixture of products, identified as aldehyde and acyl radical addition to styrene in ~10% yield (Scheme 4.24). This intermolecular radical addition has been improved to 20% yield with benzoic acid **398** and *p*-fluorostyrene by graduate student Alyssa Ertel. It is conceivable that this will be further extended to unactivated alkenes, which has been previously demonstrated in the literature, along with numerous other examples of intermolecular acyl radical additions.²⁷



Scheme 4.24

4.8.2 C–N bond activation

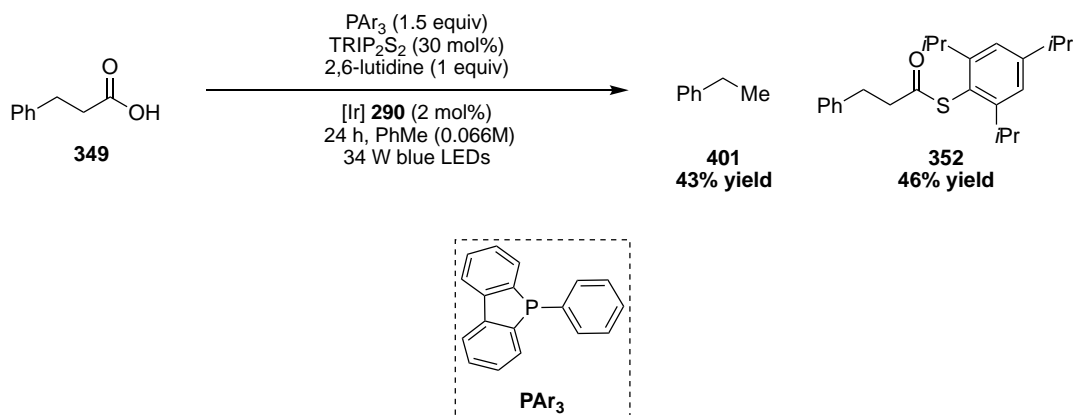
We also proposed that we might be able to use this methodology for the activation of other types of C–X bonds, such as amines. Graduate student Alyssa Ertel has taken up this project and in an initial evaluation, observed that benzyl amine **400** could be de-aminated to afford toluene **292**, in 12% yield (Scheme 4.25). In an important advance, we have observed that use of $\text{P}(\text{OEt})_3$ under these conditions leads to significantly improved results. This is a critical development. We had previously explored phosphinites and phosphonites as phosphine radical cation precursors, but had not extended this to phosphites, given the higher redox potentials. However, the material advantage of using a phosphite is clearly outlined in Chapter 3. β -Scission is thought to occur from the equatorial position of trigonal bipyramidal phosphoranyl radicals, and oxy-substituents prefer to be axial. Furthermore, use of phenyl substituted phosphines can lead to a π -ligand complex which may have different rates of β -scission and rotation, whereas $\text{P}(\text{OEt})_3$ derived phosphoranyl radicals are certainly existing as a trigonal bipyramidal complex. Use of a phosphite will increase the likelihood of any nucleophile to be in the equatorial plane, primed for rapid β -scission (Scheme 3.9).



Scheme 4.25

4.8.3 α -Scission for radical formation

Lastly, we have thus far explored β -scission as a means to generate alkyl radicals from phosphine radical cations using photocatalysis. However, α -scission is also an incredibly well-studied fragmentation pathway of phosphoranyl radicals, and could rise to formation of X^\bullet radicals from X^- . During optimization of aliphatic carboxylic acid reduction, we observed that use of phosphine **PAr₃**, did not lead to any desired product (Scheme 4.26). Instead, we observed complete conversion to thioester **352** and decarboxylated (or decarbonylated) product **401**. Even under conditions primed to do decarboxylation of hydrocinnamic acid, we only observed formation of ethylbenzene (**401**) in 15% yield. It is possible that use of this phosphine leads to a very activated



Scheme 4.26

carboxylate salt that can undergo single-electron oxidation and subsequent decarboxylation. However, an alternative, and very exciting hypothesis is that the carboxylate undergoes α -scission from the phosphoranyl radical to form a carboxy radical, which undergoes rapid decarbonylation.

Use of this phosphine could significantly limit the rate of β -scission, and actually increase the rate of α -scission. Carboxy radicals will not rapidly undergo α -scission, but other nucleophiles, such as amines, could be employed to form aminyl radicals, which are very important synthetic intermediates.³⁴ Lastly, other types of nucleophiles, such as a fluoride anion, may be able to add to a phosphine radical cation. The resultant phosphoranyl radical species could serve as an electrophilic source of fluorine. If successful, this method would represent an *in situ* conversion of nucleophilic fluoride to electrophilic fluorine without expensive, sensitive reagents, and could prove broadly useful.

References

- (1) Shaw, M. H.; Twilton, J.; MacMillan, D. W. C. *J. Org. Chem.* **2016**, *81* (16), 6898.
- (2) Prier, C. K.; Rankic, D. A.; MacMillan, D. *Chem. Rev.* **2013**, *113* (7), 5322.
- (3) Twilton, J.; Le, C. C.; Zhang, P.; Shaw, M. H.; Evans, R. W.; MacMillan, D. W. C. *Nat. Rev. Chem.* **2017**, *1* (7), 0052.
- (4) Nicewicz, D. A.; MacMillan, D. W. C. *Science* **2008**, *322* (5898), 77.
- (5) Ohmori, H.; Maeda, H.; Kikuoka, M.; Maki, T.; Masui, M. *Tetrahedron* **1991**, *47* (4-5), 767.
- (6) Maeda, H.; Maki, T.; Eguchi, K.; Koide, T.; Ohmori, H. *Tetrahedron Lett.* **1994**, *35* (24), 4129.
- (7) Maeda, H.; Maki, T.; Ohmori, H. *Tetrahedron Lett.* **1992**, *33* (10), 1347.
- (8) Jiao, X.-Y.; Bentrude, W. G. *J. Org. Chem.* **2003**, *68* (8), 3303.
- (9) Nawrat, C. C.; Jamison, C. R.; Slutskyy, Y.; MacMillan, D. W. C.; Overman, L. E. *J. Am. Chem. Soc.* **2015**, *137* (35), 11270.
- (10) Zhang, X.; MacMillan, D. W. C. *J. Am. Chem. Soc.* **2016**, *138* (42), 13862.
- (11) Romero, N. A.; Nicewicz, D. A. *Chem. Rev.* **2016**, *116* (17), 10075.
- (12) Roth, H. G.; Romero, N. A.; Nicewicz, D. A. *Synlett* **2015**, *27* (05), 714.
- (13) Mayer, J. M. *Acc. Chem. Res.* **2011**, *44* (1), 36.
- (14) Yasui, S.; Tsujimoto, M. *J. Phys. Org. Chem.* **2013**, *26*, 1090.
- (15) Arias-Rotondo, D. M.; McCusker, J. K. *Chem. Soc. Rev.* **2016**, *45* (21), 5803.
- (16) Bortolamei, N.; Isse, A. A.; Gennaro, A. *Electrochimica Acta* **2010**, *55* (27), 8312.
- (17) Yasui, S.; Tojo, S.; Majima, T. *J. Org. Chem.* **2005**, *70* (4), 1276.

- (18) Tojo, S.; Yasui, S.; Fujitsuka, M.; Majima, T. *J. Org. Chem.* **2006**, *71* (21), 8227.
- (19) Ladouceur, S.; Fortin, D.; Zysman-Colman, E. *Inorg. Chem.* **2011**, *50* (22), 11514.
- (20) Yasui, S.; Shioji, K.; Tsujimoto, M.; Ohno, A. *J. Chem. Soc., Perkin Trans. 2* **1999**, *0* (4), 855.
- (21) Bentrude, W. G. *Acc. Chem. Res.* **1982**, *15*, 117.
- (22) Bentrude, W. G.; Hansen, E. R.; Khan, W. A.; Min, T. B.; Rogers, P. E. *J. Am. Chem. Soc.* **1973**, *95*, 2286.
- (23) Prier, C. K.; MacMillan, D. W. C. *Chem. Sci.* **2014**, *5* (11), 4173.
- (24) Chu, L.; Ohta, C.; Zhiwei, Z.; MacMillan, D. W. C. *J. Am. Chem. Soc.* **2014**, *136* (31), 10886.
- (26) Zuo, Z.; MacMillan, D. W. C. *J. Am. Chem. Soc.* **2014**, *136* (14), 5257.
- (27) Chatgililoglu, C.; Crich, D.; Komatsu, M.; Ryu, I. *Chem. Rev.* **1999**, *99*, 1991.
- (28) Chu, L.; Lipshultz, J. M.; MacMillan, D. W. C. *Angew. Chem. Int. Ed. Engl.* **2015**, *54* (27), 7929.
- (29) Capaldo, L.; Riccardi, R.; Ravelli, D.; Fagnoni, M. *ACS Catal.* **2018**, *8* (1), 304.
- (30) Li, C.-G.; Xu, G.-Q.; Xu, P.-F. *Org. Lett.* **2017**, *19* (3), 512.
- (31) Zhang, X.; MacMillan, D. W. C. *J. Am. Chem. Soc.* **2017**, *139* (33), 11353.
- (32) Bergonzini, G.; Cassani, C.; Wallentin, C. J. *Angew. Chem. Int. Ed. Engl.* **2015**, *54* (47), 14066.
- (33) Zhang, M.; Li, N.; Tao, X.; Ruzi, R.; Yu, S.; Zhu, C. *Chem. Commun.* **2017**, *53* (73), 10228.
- (34) Musacchio, A. J.; Lainhart, B. C.; Zhang, X.; Naguib, S. G.; Sherwood, T. C.; Knowles, R. R. *Science* **2017**, *355* (6326), 727.

Appendix I

Nickel- and photoredox-catalyzed desymmetrization of cyclic *meso*-anhydrides¹

General methods. Unless otherwise noted, reactions were performed under a nitrogen atmosphere with the exclusion of moisture. N₂-flushed stainless steel needles and plastic syringes were used to transfer air- and moisture-sensitive reagents. Reactions were monitored by thin-layer chromatography (TLC) on EMD Silica Gel 60 F254 plates, visualizing with UV light (254 nm) or KMnO₄ stain. Solvent was freshly distilled/degassed prior to use unless otherwise noted. Organic solutions were concentrated under reduced pressure using a rotary evaporator (25 °C, <50 torr). Automated column chromatography was performed using pre-packed silica gel cartridges on a Biotage SP4 (40-53 µm, 60 Å).

Materials. Commercial reagents were purchased from Sigma-Aldrich, Alfa Aesar, Acros, Strem, TCI, Boron Molecular, Frontier Scientific or Oakwood and used as received with the following exceptions. Diethyl ether (Et₂O), tetrahydrofuran (THF), dichloromethane (CH₂Cl₂), toluene (PhCH₃) and 1,4-dioxane were dried by passing through activated alumina columns and stored over molecular sieves in a N₂-filled glovebox; *N,N*-dimethylformamide (DMF) was dried by passing through a column of activated molecular sieves. Ni(cod)₂ was purchased from Strem and (-)-2,2'-Isopropylidenebis-(4*S*)-4-phenyl-2-oxazoline (**137**) was purchased from Sigma-Aldrich and both stored at -40 °C in a N₂-filled glovebox. Nickel (II) chloride dimethoxymethane (Strem) was stored at room temperature in a N₂-filled glovebox. Anhydride **4** was used without further purification. Anhydrides were treated with trifluoroacetic acid in CH₂Cl₂ to ensure purity of the anhydride.² Anhydride **25** was synthesized according to literature procedures.² Benzyl

trifluoroborate was purchased from Boron Molecular and used without further purification. All other trifluoroborates were synthesized according to literature procedures.

Instrumentation: Proton nuclear magnetic resonance (^1H NMR) spectra were recorded on a Bruker 500 MHz or NB 300 MHz AVANCE spectrometer. Proton chemical shifts are reported in parts per million downfield from tetramethylsilane and are referenced to residual protium in the NMR solvent ($\text{CHCl}_3 = \delta$ 7.26 ppm or $(\text{CD}_3)_2\text{CO} = 2.05$). Carbon nuclear magnetic resonance (^{13}C NMR) were recorded on a Bruker 500 AVANCE spectrometer (125 MHz). Chemical shifts for carbon are reported in parts per million downfield from tetramethylsilane and are referenced to the carbon resonances of the solvent residual peak ($\text{CDCl}_3 = \delta$ 77.16 ppm or $((\text{CD}_3)_2\text{CO} = 206.26$ ppm and 29.840 ppm). Fluorine nuclear magnetic resonance (^{19}F NMR) were reported on a Bruker NB 300 AVANCE (282 MHz) spectrometer. Boron nuclear magnetic resonance (^{11}B NMR) were reported on a Bruker NB 300 AVANCE (96 MHz) spectrometer. NMR data are represented as follows: chemical shift (δ ppm), multiplicity (s = singlet, d = doublet, t = triplet, q = quartet, m = multiplet), coupling constant in Hertz (Hz), integration. High-resolution mass spectrometry was performed on an Agilent 6220 LC/MS using electrospray ionization time-of-flight (ESI-TOF). FT-IR spectra were recorded on a Perkin- Elmer Paragon 500 and are reported in terms of frequency of absorption (cm^{-1}). Reversed-phase liquid chromatography/mass spectrometry (LC/MS) was performed on an Agilent 1260 Infinity analytical LC and Agilent 6120 Quadrupole LC/MS system using electrospray ionization/atmospheric-pressure chemical ionization (ESI/APCI) and UV detection at 254 nm and 280 nm. Ultraviolet-visible absorption spectra were collected on an Agilent Cary 60 Spectrophotometer using 10 mm quartz cuvettes. High-performance liquid chromatography (HPLC) was performed on an Agilent 1200 series instrument with a binary pump and a diode array detector, using Chiralcel OD-H (25 cm x 0.46 cm), Chiralcel OJ-H (25 cm x

0.46 cm), Chiralpak AS-H (25 cm x 0.46 cm), Chiralpak AD-H (25 cm x 0.46 cm), Chiralpak IC (25 cm x 0.46 cm) and Chiralpak ID (25 cm x 0.46 cm). Optical rotations were taken with a Jasco P-1010 polarimeter Na/Hal lamp with a 0.5 dm/1 mL cell in spectral grade CHCl_3 or acetone.

Light Sources. Screening scale reactions (0.025-0.1 mmol) were carried out using 12-inch Sapphire Flex LED Strips (5050, High Density, 12V DC Power Leads, Waterproof, Black backing) purchased from Creative Lightings. The strips were wrapped on the inside of a Pyrex crystallizing dish. Scale up reactions (0.25 mmol) were carried out using Blue Kessil H150 LED Grow Lights. Larger scale up reactions (0.5 mmol) were carried out using the Merck Photoreactor (450 nm light).

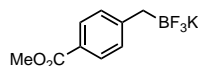
General procedure A for trifluoroborate preparation:³ An oven-dried 3-neck round bottom flask fitted with a reflux condenser was charged with magnesium, and the magnesium was activated by stirring under N_2 overnight. Benzyl bromide (3.00 mmol) in diethyl ether (6.5 mL) was added to the magnesium at a rate maintaining a gentle reflux. The suspension was refluxed for a further 3 h, then cooled to room temp. To a separate flame-dried flask was added trimethyl borate (0.502 mL, 4.50 mmol) and THF (6.0 mL) under N_2 . The flask was cooled to $-78\text{ }^\circ\text{C}$, at which point the Grignard reagent was added dropwise at $-78\text{ }^\circ\text{C}$. The reaction was stirred for 1 h at $-78\text{ }^\circ\text{C}$, then slowly warmed to room temperature over 1 h. The reaction was then cooled to $0\text{ }^\circ\text{C}$, and MeOH (4.0 mL) was added over 5 min. The flask was opened to air, and a solution of KHF_2 (1.41 g, 18.0 mmol) was added in H_2O (4.0 mL) at $0\text{ }^\circ\text{C}$ over 15 min. The reaction was stirred an additional 30 min at $0\text{ }^\circ\text{C}$, then warmed to room temperature and stirred for an additional hour. The solvent was removed, and then the remaining water was removed by azeotrope with toluene. The residue was dried under high vacuum overnight. (*Note: Important to have the residue completely dry, any remaining water made precipitation difficult and could affect purity.) The solid was pulverized with a spatula, then washed in hot acetone and filtered through celite (3 x 30

mL). The filtrate was concentrated, then taken up in a minimal amount of diethyl ether (~10 mL) and CH₂Cl₂ (~5 mL). Hexanes (~200 mL) was added and the product flocculated out of solution. The solid was collected by vacuum filtration, then washed with hexanes (~20 mL) and CH₂Cl₂ (~10 mL) and dried to afford a white powder. Refer to each individual entry for further purification.

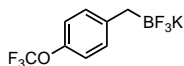
General procedure B for trifluoroborate preparation:⁴ A 20 mL reaction vial was charged with benzyl bromide (5.00 mmol), copper iodide (95.2 mg, 0.500 mmol), PPh₃ (170 mg, 0.650 mmol), lithium methoxide (380 mg, 10.0 mmol), and B₂Pin₂ (1.93g, 7.60 mmol) and a stir bar. The reaction vial was fitted with a septa cap and evacuated and backfilled with N₂ five times. DMF (10.0 mL) was added, and the reaction was sealed with electrical tape. The mixture was stirred vigorously at room temperature for 20 h. The reaction vial was uncapped, then filtered through a plug of silica with EtOAc. The solvent was removed, then EtOAc (~20 mL) and MeOH (~30 mL) were added, and the reaction was cooled to 0 °C under air. KHF₂ (2.42 g, 30.0 mmol) in H₂O (6.67 mL) was added over 15 min at 0 °C. The reaction was stirred an additional 30 min at 0 °C, then warmed to room temp and stirred for 1h. The solvent was removed, then pinacol and water were azeotroped with toluene several times. The residue was placed under high vacuum overnight. (*Note: Important to have the residue completely dry, any remaining DMF or water made precipitation difficult and could affect purity.) The solid was pulverized with a spatula, then washed in hot acetone (3 x 35 mL) and filtered through celite. The filtrate was concentrated to ~10 mL acetone, then precipitated with hexanes or pentane (~200 mL). The solid was filtered and dried to afford a white powder. Refer to each individual entry for further purification.

General procedure C for trifluoroborate preparation:² An oven dried flask was charged with benzyl bromide (5.00 mmol), Pd(dba)₂ (86.3 mg, 0.150 mmol), P(*p*-tol)₃ (91.3 mg, 0.300 mmol), KOAc (736 mg, 7.50 mmol), and B₂Pin₂ (1.40 g, 5.50 mmol). The flask was evacuated and

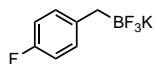
backfiled with N₂ (3x). Toluene (31.3 mL) was added, and the suspension was heated to 50 °C for 24h. Upon cooling, the reaction was filtered through a silica plug with EtOAc, then the solvent removed. Then EtOAc (~20 mL) and MeOH (~30 mL) were added, and the reaction was cooled to 0 °C under air. KHF₂ (2.42 g, 30.0 mmol) in H₂O (6.67 mL) was added over 15 min at 0 °C. The reaction was stirred an additional 30 min at 0 °C, then warmed to room temp and stirred for 1h. The solvent was removed, then pinacol and water were azeotroped with toluene several times. The residue was placed under high vacuum overnight. (*Note: Important to have the residue completely dry, any remaining water made precipitation difficult and could affect purity.) The solid was pulverized with a spatula, then washed in hot acetone (3 x 35 mL) and filtered through celite. The filtrate was concentrated to ~10 mL acetone, then precipitated with hexanes or pentane (~200 mL). The solid was filtered and dried to afford a white powder. Refer to each individual entry for further purification.



According to general procedure C. 825 mg, 64% yield. No further purification necessary. Characterization data matched literature values.²

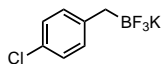


According to general procedure A. 700 mg, 50% yield. No recrystallization performed. Characterization data matched literature values.²

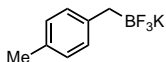


According to general procedure A. 317 mg, 49% yield. No further purification necessary. **¹H NMR (501 MHz, Acetone-d₆):** δ 7.08 (t, *J* = 6.9 Hz, 2H), 6.79 (t, *J* = 8.8 Hz, 2H), 1.61 (bs, 2H). **¹³C NMR (126 MHz, Acetone-d₆):** δ 161.29, 159.51, 143.26, 130.63 (d, *J* = 8.2 Hz), 114.13 (d, *J* =

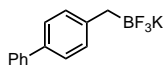
20.6 Hz). **¹¹B NMR (96 MHz, Acetone-d₆):** δ 4.34 (q, J = 58.6 Hz) **HRMS:** (ESI-TOF) calculated for ([C₇H₆BF₄]⁻): 177.0499, found 177.0505. **IR (ATR, cm⁻¹):** 3041, 2915, 1600, 1503, 1244, 1217, 1086, 1066, 965, 932, 836, 779, 730, 692.



According to general procedure B. 942 mg, 81% yield. Recrystallized from isopropanol (1x) to afford a white powder. **¹H NMR (501 MHz, Acetone-d₆):** δ 7.07 (d, J = 8.2 Hz, 2H), 7.02 (d, J = 8.5 Hz, 2H), 1.60 (bs, 2H). **¹³C NMR (126 MHz, Acetone-d₆):** δ 147.14, 131.31, 128.03, 127.64 **¹⁹F NMR (282 MHz, Acetone-d₆):** δ -139.16 (q, J = 59.2 Hz) **¹¹B NMR (96 MHz, Acetone-d₆):** δ 4.46 (q, J = 58.6 Hz). **HRMS:** (ESI-TOF) calculated for ([C₇H₆BClF₃]⁻): 193.0203, found 193.0201. **IR (ATR, cm⁻¹):** 2895, 1488, 1240, 1092, 1064, 967, 834, 775, 726, 656.

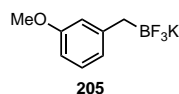


According to general procedure A. 517 mg, 49% yield. No further purification necessary. **¹H NMR (501 MHz, Acetone-d₆):** δ 6.98 (d, J = 7.6 Hz, 2H), 6.85 (d, J = 7.5 Hz, 2H), 2.19 (s, 3H), 1.58 (bs, 2H). **¹³C NMR (126 MHz, Acetone-d₆):** δ 144.74, 131.53, 129.67, 128.57, 21.03. **¹⁹F NMR (282 MHz, Acetone-d₆):** δ -140.78 (q, J = 64.9 Hz) **¹¹B NMR (96 MHz, Acetone-d₆):** δ 4.85 (q, J = 59.5 Hz). **HRMS:** (ESI-TOF) calculated for ([C₈H₉BF₃]⁻): 173.0749, found 173.0750. **IR (ATR, cm⁻¹):** 3020, 2901, 1609, 1509, 1364, 1244, 1099, 1065, 949, 774, 731.

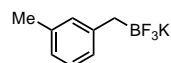


According to general procedure B. 703 mg, 51% yield. Recrystallized from EtOH (3x) to afford a white solid with a cotton-like consistency (very small needles). **¹H NMR (501 MHz, Acetone-d₆):** δ 7.58 (d, J = 7.7 Hz, 2H), 7.44 – 7.32 (m, 4H), 7.25 (t, J = 7.4 Hz, 1H), 7.19 (d, J = 7.7 Hz, 2H), 1.68 (s, 2H). **¹³C NMR (126 MHz, Acetone-d₆):** δ 147.84, 142.89, 135.68, 130.24, 129.48,

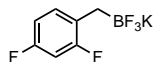
127.26, 127.05, 126.43. **^{19}F NMR (282 MHz, Acetone- d_6):** δ -140.57 (q, J = 64.9 Hz) **^{11}B NMR (96 MHz, Acetone- d_6):** δ 4.76 (q, J = 56.6 Hz). **HRMS:** (ESI-TOF) calculated for ($[\text{C}_{13}\text{H}_{11}\text{BF}_4]^-$): 235.0906, found 235.0909. **IR (ATR, cm^{-1}):** 2970, 1612, 1484, 1368, 1231, 1217, 1097, 958, 940, 762, 739, 698.



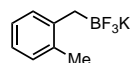
According to general procedure B. 875 mg, 77% yield. Recrystallized from EtOH (slightly hazy solution filtered through standard filter paper before crystallizing) (1x) as needles. **^1H NMR (501 MHz, Acetone- d_6):** δ 6.93 (t, J = 7.8 Hz, 1H), 6.70 – 6.60 (m, 2H), 6.45 (dd, J = 8.0, 2.6 Hz, 1H), 3.69 (s, 3H), 1.61 (s, 2H). **^{13}C NMR (126 MHz, Acetone- d_6):** δ 160.01, 149.71, 128.48, 122.41, 115.34, 108.47, 54.99. **^{19}F NMR (282 MHz, Acetone- d_6):** δ -140.53 (q, J = 67.7 Hz) **^{11}B NMR (96 MHz, Acetone- d_6):** δ 4.39 (q, J = 56.6 Hz) **HRMS:** (ESI-TOF) calculated for ($[\text{C}_8\text{H}_9\text{BF}_3\text{O}]^-$): 189.0699, found 189.0701. **IR (ATR, cm^{-1}):** 2961, 1607, 1577, 1486, 1242, 1155, 1070, 1049, 974, 958, 773, 720.



According to general procedure B. 721 mg, 68% yield. Recrystallized from EtOH (slightly hazy solution filtered through standard filter paper before crystallizing) (1x) to afford a white solid with a cotton-like consistency. **^1H NMR (501 MHz, Acetone- d_6):** δ 7.00 – 6.81 (m, 3H), 6.69 (d, J = 7.2 Hz, 1H), 2.20 (s, 3H), 1.60 (s, 2H). **^{13}C NMR (126 MHz, Acetone- d_6):** δ 147.83, 136.64, 130.60, 127.79, 126.87, 123.73, 21.65. **^{19}F NMR (282 MHz, Acetone- d_6):** δ -140.61 (q, J = 62.0 Hz) **^{11}B NMR (96 MHz, Acetone- d_6):** δ 4.50 (q, J = 58.6 Hz) **HRMS:** (ESI-TOF) calculated for ($[\text{C}_8\text{H}_9\text{BF}_3]^-$): 173.0749, found 173.0759. **IR (ATR, cm^{-1}):** 3015, 2921, 1602, 1364, 1259, 1225, 1064, 950, 776, 716.

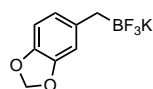


According to general procedure B. 884 mg, 76% yield. Recrystallized from EtOH (slightly hazy solution filtered through standard filter paper before crystallizing) (1x). Characterization data matched literature values.³

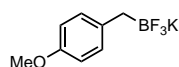


According to general procedure A. 340 mg, 32% yield. No further purification necessary.

Characterization data matched literature values.³

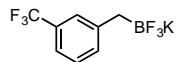


According to general procedure C. 864 mg, 71% yield. Recrystallized from MeOH (slightly hazy solution filtered through standard filter paper before crystallizing) (1x) as needles. Characterization data matched literature values.³ Best if used immediately after purification to avoid decomposition.



According to general procedure B. 482 mg, 42% yield. Recrystallized from EtOH (1x) as plates.

Characterization data matched literature values.³



¹H NMR (501 MHz, Acetone-d6): δ 7.42 (s, 1H), 7.35 (d, J = 7.6 Hz, 1H), 7.23 (dd, J = 19.1, 7.7 Hz, 2H), 1.73 (s, 2H). **¹³C NMR (126 MHz, Acetone-d6):** δ 149.91, 133.50, 128.37, 125.94, 119.56. **¹⁹F NMR (282 MHz, Acetone-d6):** δ -62.69, -140.11 (q, J = 56.4 Hz). **¹¹B NMR (96 MHz, Acetone-d6):** δ 4.11 (q, J = 59.5 Hz)

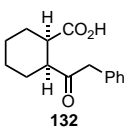
General procedure for screening: Cyclohexanecarboxylic anhydride **4** (0.025 mmol-0.1 mmol) and benzyl trifluoroborate **117** (1.2 equiv) were weighed into a 1-dram vial or 13 x 100 mm reaction tube and equipped with a stir bar. The reaction tube was then brought into an N₂-filled glovebox. Then a pre-stirred dissolved solution in THF of Ni(cod)₂ and ligand were added. The mixture was allowed to stir for ~5 minutes at room temperature, at which point the reaction mixture became homogenous. A solution of photocatalyst in solvent was added, and the reaction tube sealed with a septa cap. The vial was wrapped with electrical tape, and then removed from the glovebox, where it was immediately irradiated with blue LED's. A fan was used to keep the reaction cool. After the reaction was complete, the reaction tube was removed from the light source where benzoic acid (1 equiv) was added as an external standard. The solvent was then removed. The residue was dissolved in equal volumes 1 M HCl and diethyl ether. A small aliquot was removed, dried over Na₂SO₄ and concentrated to determine yield by ¹H NMR. The remaining organic layer was then extracted with sat. aq. Na₂CO₃ (2 x 1 mL). The combined aqueous layers were acidified with conc. HCl until ~pH 2. The aqueous layer was extracted with diethyl ether (2 x 5 mL). The combined organic layers were then dried over Na₂SO₄, filtered and concentrated. The crude acid was analyzed by HPLC analysis on a chiral stationary phase. The product was converted to the methyl ester (when necessary) by dissolving the product in a 1:1 mixture of CH₂Cl₂/MeOH (~0.04 M). The reaction was cooled to 0 °C, at which point TMSCHN₂ (2.0 M in hexanes) was added dropwise until a light yellow color persisted. The reaction was stirred for 1 h at 0 °C. The reaction was quenched by adding an excess of acetic acid, until the yellow color disappeared. The solvent was removed, and the residue was taken up in diethyl ether and 1 M HCl. The organic layer was subsequently washed with sat. aq. Na₂CO₃, then dried over Na₂SO₄, filtered and concentrated. The methyl ester was then analyzed by HPLC on a chiral stationary phase. In

cases where diastereoselectivity was determined by ^1H NMR, the methyl ester protons or benzylic protons were used as the diagnostic peaks.

General procedure A for anhydride opening: Cyclohexanecarboxylic anhydride **4** (38.5 mg, 0.25 mmol) and benzyl trifluoroborate (59.4 mg, 0.30 mmol) were weighed into a 16 x 100 mm threaded reaction tube, equipped with a teflon coated stirbar. The reaction tube was then brought into an N_2 -filled glovebox and 1.0 mL dioxane was added. Then a pre-stirred dissolved solution of $\text{Ni}(\text{cod})_2$ (3.4 mg, 0.0125 mmol) and (-)-2,2'-Isopropylidenebis-(4*S*)-4-phenyl-2-oxazoline (**137**) (5.0 mg, 0.0150 mmol) in 3.0 mL of dioxane was added. The mixture was allowed to stir for ~5 minutes at room temperature, at which point the reaction mixture became homogenous. A solution of 4CzIPN (3.9 mg, 0.005 mmol) in 1.0 mL dioxane was added, and the reaction tube sealed with a septa cap. The vial was wrapped with electrical tape, and then removed from the glovebox, where it was immediately irradiated with a 34 W blue LED lamp, ~3 cm from the light source. A fan was used to keep the reaction cool. After 24 h, the reaction tube was removed from the light source, and the solvent was removed. The residue was dissolved in 1 M HCl (20 mL) and diethyl ether (25 mL). The aqueous layer was extracted once with additional diethyl ether (10 mL). The combined ether layers were then extracted with sat. aq. Na_2CO_3 (4 x 15 mL). The combined aqueous layers were acidified with conc. HCl until ~pH 2. The aqueous layer was extracted with diethyl ether (3 x 20 mL). The combined organic layers were washed with brine (30 mL) and then dried over Na_2SO_4 , filtered and concentrated. The crude product was purified over silica gel using $\text{CH}_2\text{Cl}_2 \rightarrow 5\%$ MeOH in CH_2Cl_2 . The product was converted to the methyl ester (when necessary) by dissolving the product in a 1:1 mixture of $\text{CH}_2\text{Cl}_2/\text{MeOH}$ (~0.04 M). The reaction was cooled to 0 °C, at which point TMSCHN_2 (2.0 M in hexanes) was added dropwise until a light yellow color persisted. The reaction was stirred for 1 h at 0 °C. The reaction was quenched by adding an

excess of acetic acid, until the yellow color disappeared. The solvent was removed, and the residue was taken up in diethyl ether and 1 M HCl. The organic layer was subsequently washed with sat. aq. Na₂CO₃ and brine, then dried over Na₂SO₄, filtered and concentrated. The crude product may be run through a silica plug if additional purification was necessary.

General procedure B for anhydride opening: Cyclohexanecarboxylic anhydride **4** (38.5 mg, 0.25 mmol) and benzyl trifluoroborate (59.4 mg, 0.30 mmol) were weighed into a 16 x 100 mm threaded reaction tube, equipped with a teflon coated stirbar. The reaction tube was then brought into an N₂-filled glovebox and 1.0 mL Et₂O was added. Then a pre-stirred dissolved solution of Ni(cod)₂ (3.4 mg, 0.0125 mmol) and (-)-2,2'-Isopropylidenebis-(4*S*)-4-phenyl-2-oxazoline (**137**) (5.0 mg, 0.0150 mmol) in 0.5 mL of THF was added. The mixture was allowed to stir for ~5 minutes at room temperature, at which point the reaction mixture became homogenous. 4CzIPN (3.9 mg, 0.005 mmol) was added in 4.0 mL Et₂O and the reaction tube sealed with a septa cap. The vial was wrapped with electrical tape, and then removed from the glovebox, where it was immediately irradiated with a 34 W blue LED lamp, ~3 cm from the light source. A fan was used to keep the reaction cool. After 24 h, the reaction tube was removed from the light source. The reaction was partitioned in 1 M HCl (20 mL) and diethyl ether (25 mL). The aqueous layer was extracted with additional diethyl ether (1 x 10 mL). The combined ether layers were then extracted with sat. aq. Na₂CO₃ (4 x 15 mL). The combined aqueous layers were acidified with conc. HCl until ~pH 2. The aqueous layer was extracted with diethyl ether (3 x 20 mL). The combined organic layers were washed with brine (30 mL) and then dried over Na₂SO₄, filtered and concentrated. The crude product was purified over silica gel using CH₂Cl₂ -> 5% MeOH in CH₂Cl₂.

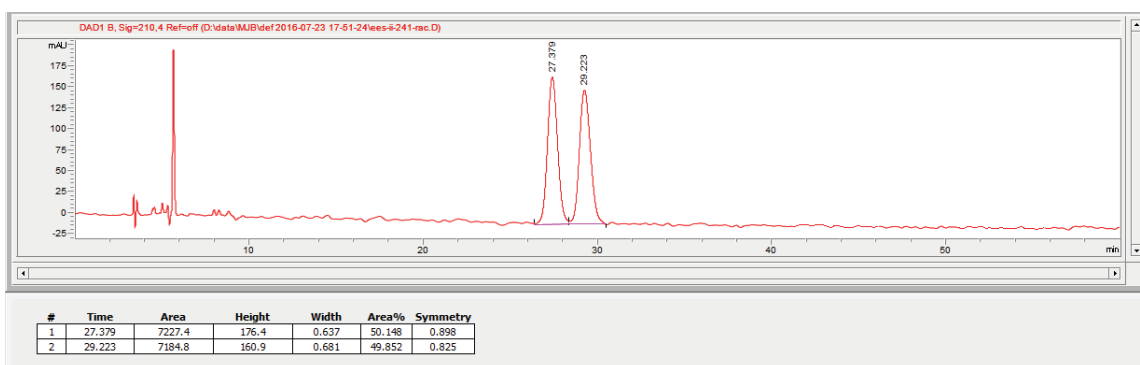


According to general procedure A, **4** (38.5 mg, 0.25 mmol) and benzyl trifluoroborate (59.4 mg, 0.3 mmol) afforded the product as a pale yellow oil (47.3 mg, 77% yield,

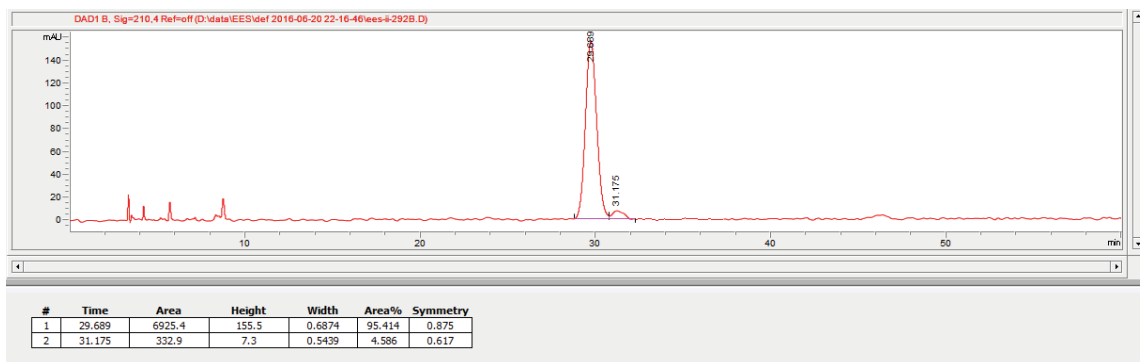
91% ee, 24:1 dr). Run 2 afforded 77% yield, 90% ee, 19:1 dr. NMR data based on methyl ester.

¹H NMR (501 MHz, CDCl₃): δ 7.32 (t, *J* = 7.4 Hz, 2H), 7.24 (d, *J* = 6.1 Hz, 1H), 7.19 (d, *J* = 6.8 Hz, 2H), 3.80 (s, 2H), 3.60 (s, 3H), 2.92-2.91 (m, 1H), 2.79 (dt, *J* = 8.9, 4.5 Hz, 1H), 2.15 – 1.94 (m, 1H), 1.83 (ddt, *J* = 13.2, 8.6, 4.4 Hz, 1H), 1.76 (ddt, *J* = 12.7, 8.0, 4.1 Hz, 1H), 1.64 – 1.52 (m, 1H), 1.49 – 1.33 (m, 4H). **¹³C NMR (126 MHz, CDCl₃):** δ 209.39, 174.51, 134.58, 129.67, 128.65, 126.92, 51.74, 48.92, 47.55, 42.83, 26.26, 26.07, 24.00, 23.64. **HRMS:** (ESI-TOF) calculated for ([C₁₅H₁₈O₃ + Na]⁺): 269.1148, found: 269.1144. **IR (ATR, cm⁻¹):** 3029, 2932, 1699, 1453, 1259, 1217, 733, 699. **Optical Rotation:** [α]_D²⁶ -57.4 (*c* 0.72, CHCl₃). **HPLC:** ChiralPak[®] IC, 5% IPA (1% TFA) in Hexanes, 60 min run, 1 mL/min. **HPLC (methyl ester):** Chiralcel[®] OJ-H, 5% IPA in Hexanes, 3 min run, 1 mL/min. Optimization screening was performed using this method.

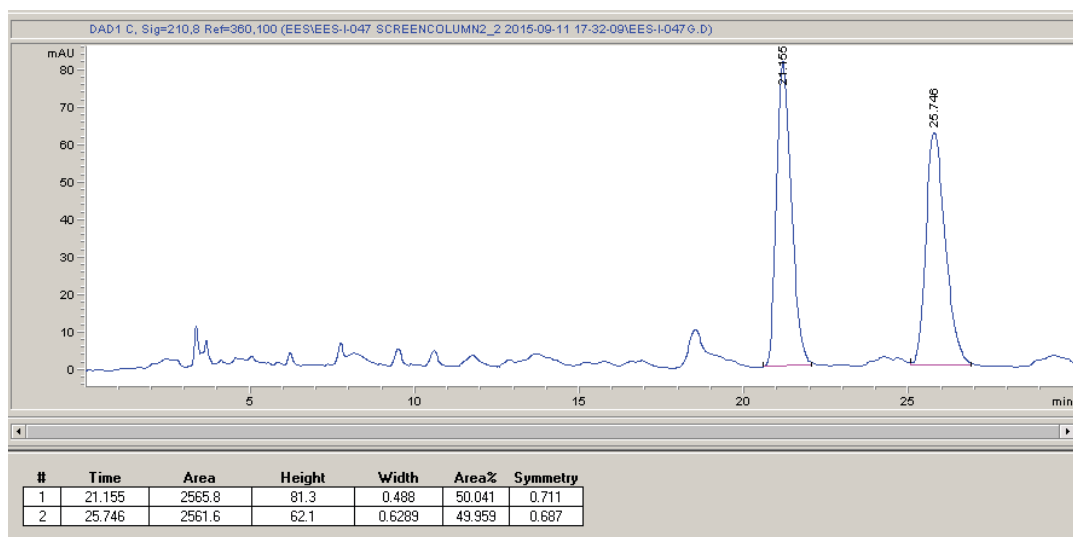
Racemic std:



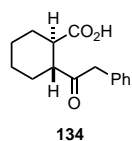
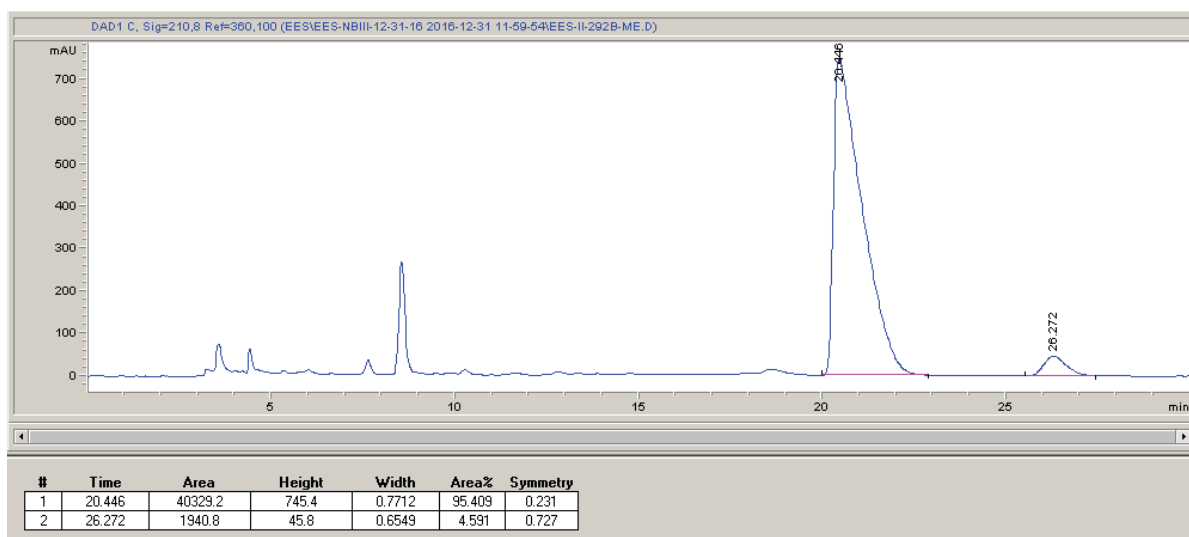
Enantioenriched:



Racemic std (methyl ester):



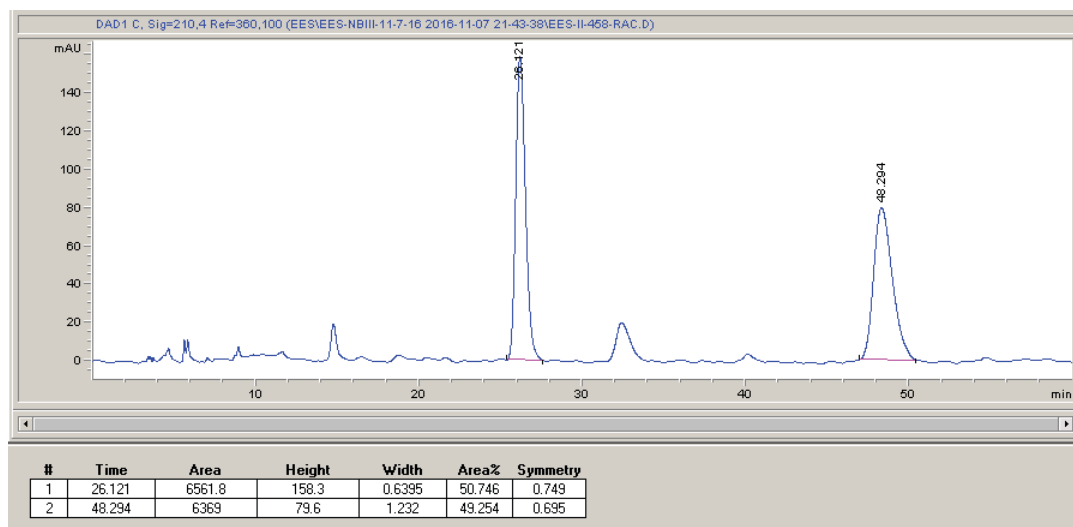
Enantioenriched (methyl ester):



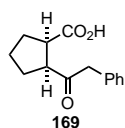
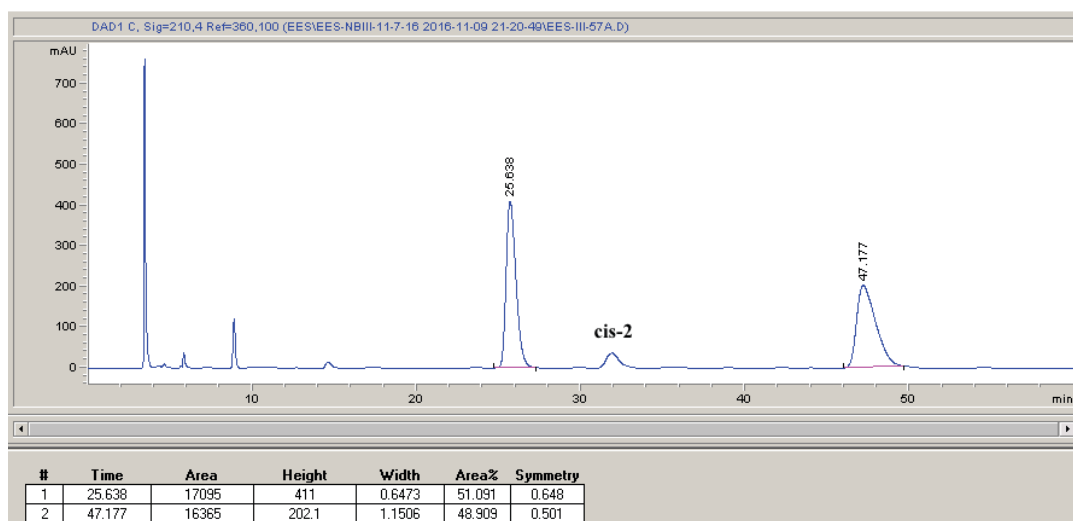
According to general procedure **A**, anhydride **133** (38.5 mg, 0.25 mmol) and benzyl trifluoroborate (59.4 mg, 0.3 mmol) afforded the product as a pale yellow oil (51.3 mg, 83% yield, -2% ee, 19:1 dr). Run 2 afforded 79% yield, -2% ee, 15.7:1 dr. All characterization performed on the acid. **¹H NMR (501 MHz, CDCl₃):** δ 7.35 – 7.28 (m, 2H), 7.27 – 7.22 (m, 1H), 7.22 – 7.12 (m, 2H), 3.82 (ABq, J = 15.0 Hz, $\Delta\nu$ = 26.5 Hz, 2H), 2.80 (td, J = 11.1, 3.5 Hz, 1H), 2.73 (td, J = 11.2, 3.7 Hz, 1H), 2.23 – 2.08 (m, 1H), 2.02 – 1.89 (m, 1H), 1.87 – 1.72 (m, 2H), 1.42

– 1.04 (m, 4H). **¹³C NMR (126 MHz, CDCl₃):** δ 210.58, 180.92, 134.17, 129.83, 128.64, 127.01, 50.85, 48.75, 44.25, 28.92, 28.75, 25.54, 25.45. **HRMS:** (ESI-TOF) calculated for ([C₁₅H₁₉O₃ + Na]⁺): 269.1148, found: 269.1146. **IR (ATR, cm⁻¹):** 3029, 2936, 2859, 1734, 1702, 1495, 1451, 1367, 1264, 1216, 732, 701. **HPLC:** ChiralPak[®] IC, 5% IPA in Hexanes, 60 min run, 1 mL/min.

Racemic std:



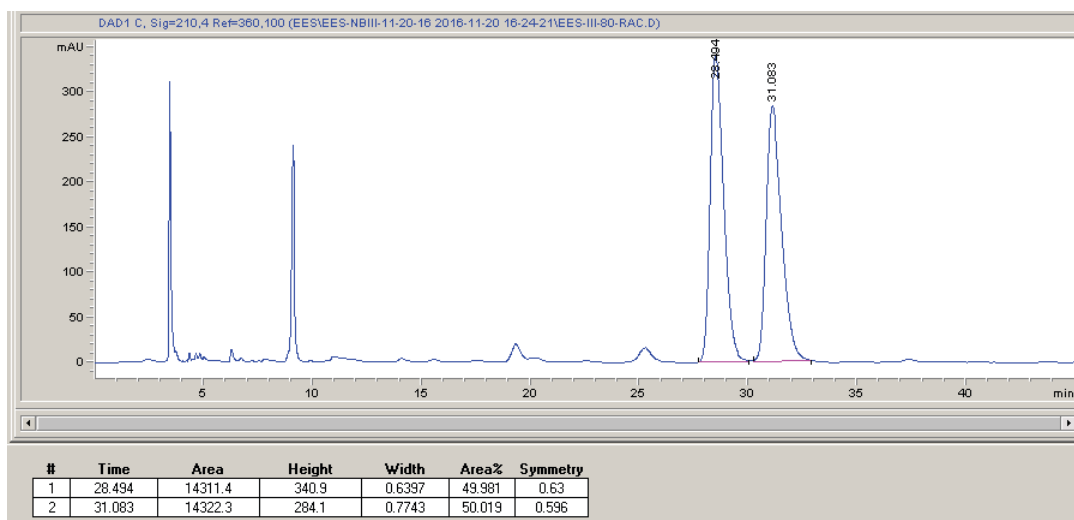
Product of reaction:



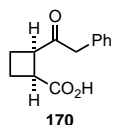
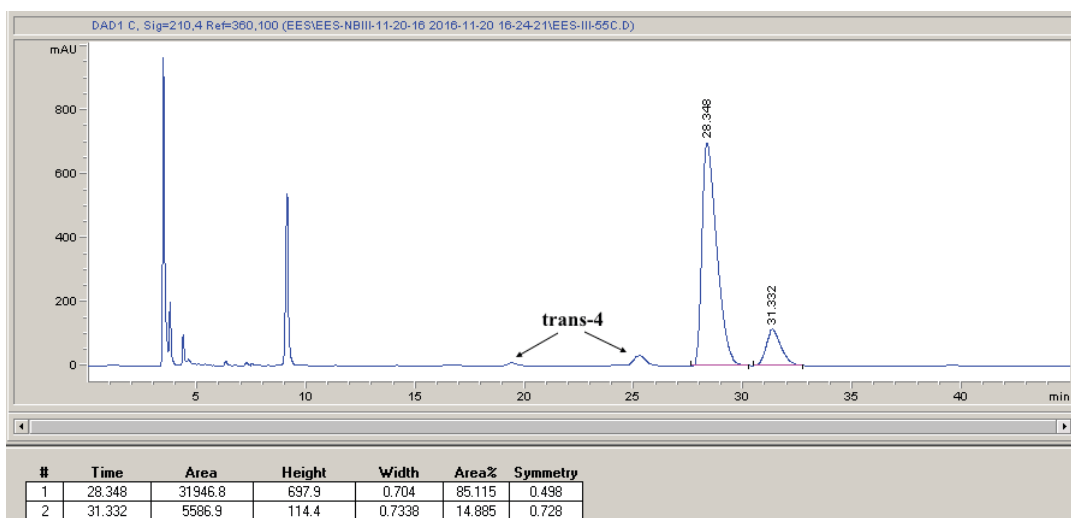
According to general procedure A, anhydride (35.0 mg, 0.25 mmol) and benzyl trifluoroborate (59.4 mg, 0.3 mmol) afforded the product as a pale yellow oil (47.8 mg,

82% yield, 70% ee, 24:1 dr). Run 2 afforded 85% yield, 69% ee, 19:1 dr. NMR data based on methyl ester. **¹H NMR (501 MHz, CDCl₃)**: δ 7.33 (t, *J* = 7.4 Hz, 2H), 7.30 – 7.23 (m, 1H), 7.20 (d, *J* = 7.5 Hz, 2H), 3.77 (m, 2H), 3.59 (s, 3H), 3.27 (q, *J* = 7.7 Hz, 1H), 2.98 (q, *J* = 7.9 Hz, 1H), 2.16 – 2.00 (m, 1H), 2.00 – 1.87 (m, 3H), 1.83 (dt, *J* = 13.8, 6.9 Hz, 1H), 1.61 (dt, *J* = 12.2, 7.8 Hz, 1H). **¹³C NMR (126 MHz, CDCl₃)**: δ 208.96, 174.64, 134.24, 129.70, 128.71, 127.05, 52.90, 51.77, 49.57, 47.26, 28.74, 28.49, 23.99. **HRMS**: (ESI-TOF) calculated for ([C₁₄H₁₆O₃ + Na]⁺): 255.0992, found 255.0987. **IR (ATR, cm⁻¹)**: 3030, 2958, 1702, 1496, 1453, 1413, 1180, 948, 802, 733, 699. **Optical Rotation**: [α]_D²⁶ -19.3 (*c* 0.71, CHCl₃). **HPLC**: ChiralPak[®] IC, 5% IPA in Hexanes, 45 min run, 1 mL/min.

Racemic Std:

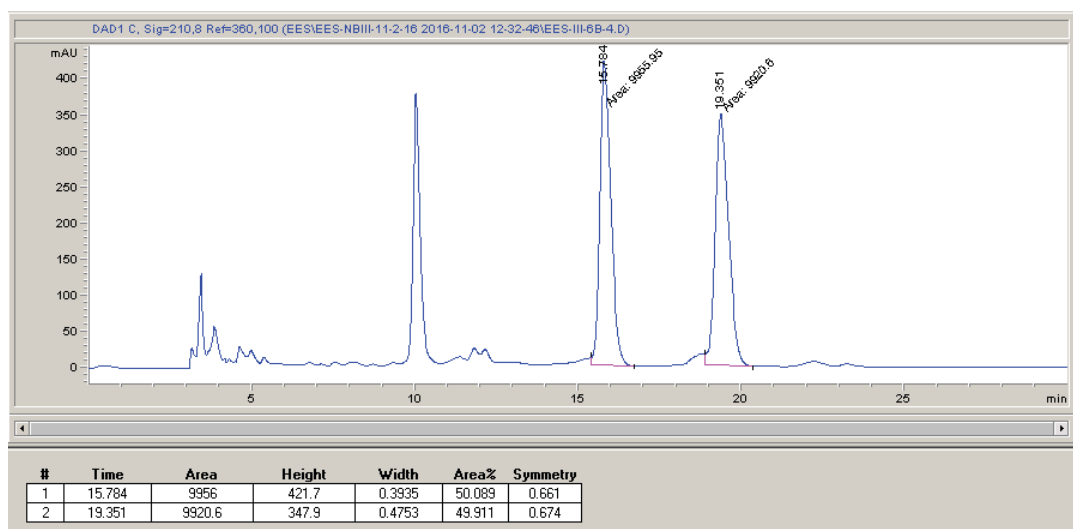


Enantioenriched:

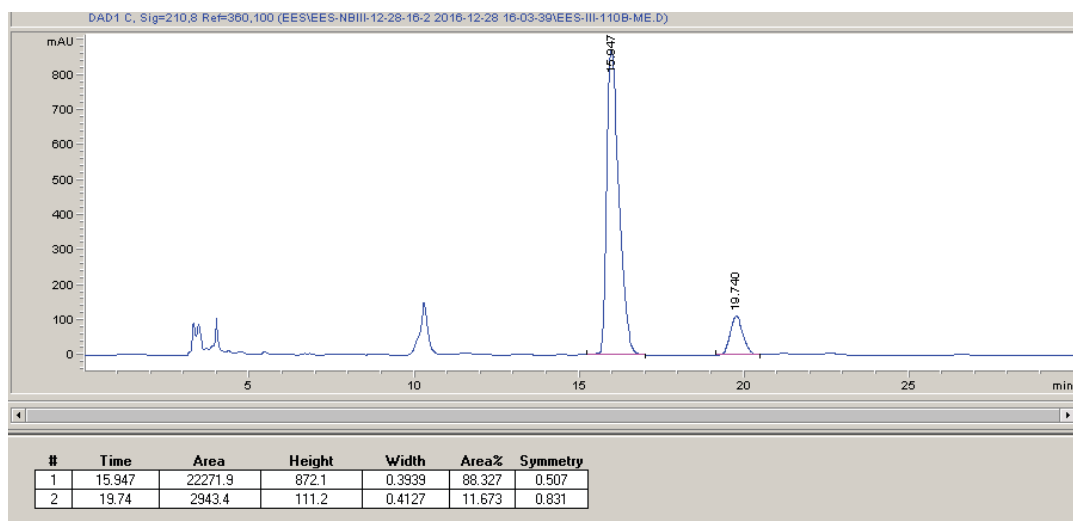


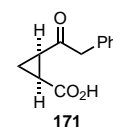
(+)-2,2'-Isopropylidenebis-(4*R*)-4-benzyl-2-oxazoline (**136**) was used as the ligand (5.4 mg, 0.0150 mmol). According to general procedure **A**, anhydride (31.5 mg, 0.25 mmol) and benzyl trifluoroborate (59.4 mg, 0.3 mmol) afforded the product as a pale yellow oil (40.5 mg, 74% yield, 77% ee, >20:1 dr). Run 2 afforded 66% yield, 74% ee, >20:1 dr. Enantioselectivity was determined using the methyl ester. NMR data based on methyl ester. **¹H NMR (501 MHz, CDCl₃):** δ 7.35 – 7.29 (m, 2H), 7.28 – 7.23 (m, 1H), 7.19 (dd, *J* = 7.0, 1.6 Hz, 2H), 3.75 – 3.63 (m, 5H), 3.62 – 3.54 (m, 1H), 3.37 – 3.29 (m, 1H), 2.38 – 2.24 (m, 2H), 2.22 – 2.11 (m, 1H), 2.11 – 2.03 (m, 1H). **¹³C NMR (126 MHz, CDCl₃):** δ 207.49, 174.15, 134.09, 129.68, 128.77, 127.10, 51.93, 48.56, 46.60, 41.05, 22.19, 21.81. **HRMS (acid):** (ESI-TOF) calculated for ([C₁₃H₁₄O₃ + Na]⁺): 241.0835, found: 241.0835. **IR (acid, ATR, cm⁻¹):** 2951, 1704, 1495, 1454, 1360, 1228, 1030, 923, 700. **Optical Rotation(acid):** [α]_D²⁶ +0.3 (*c* 0.62, CHCl₃). **HPLC (methyl ester):** ChiralPak[®] AS-H, 5% IPA in Hexanes, 30 min run, 1 mL/min.

Racemic Std:



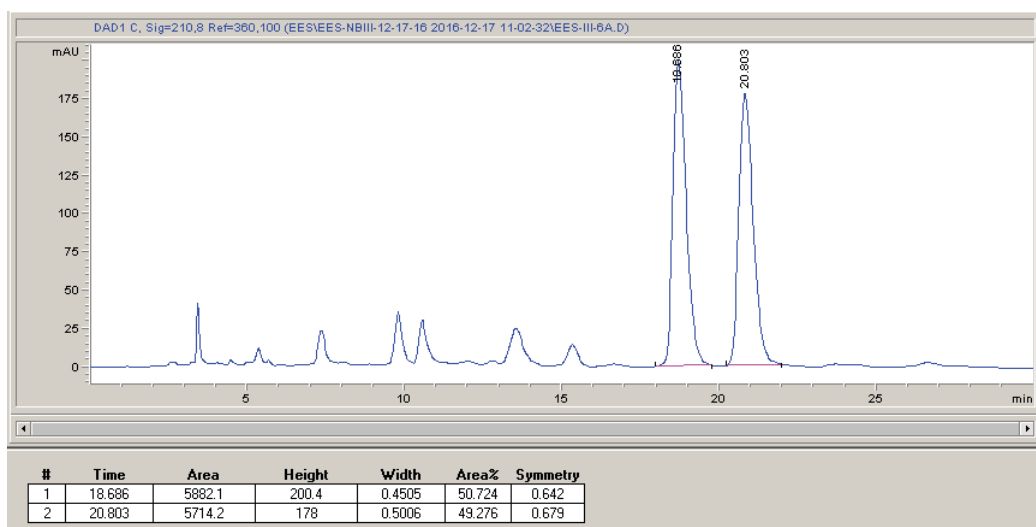
Enantioenriched:



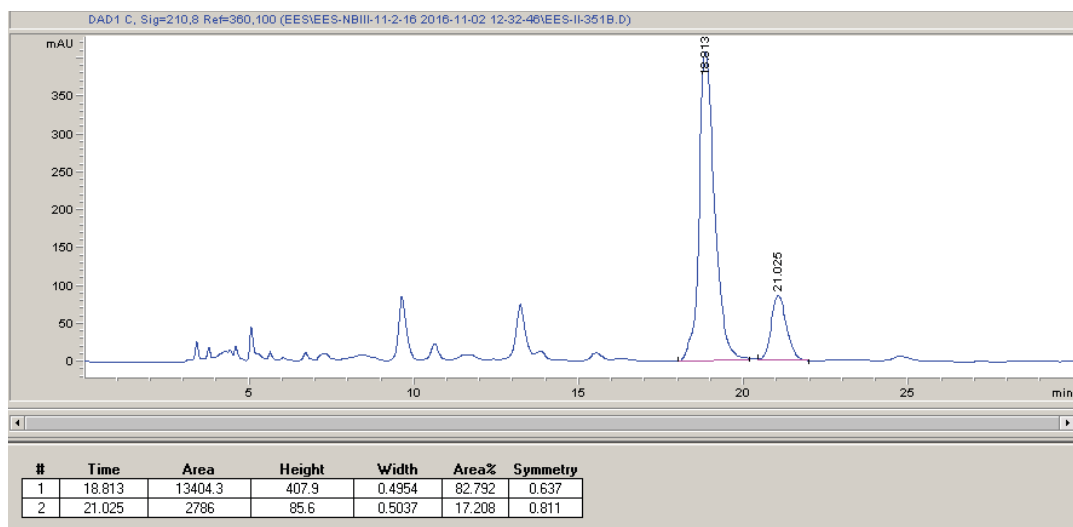

 (+)-2,2'-Isopropylidenebis-(4*R*)-4-benzyl-2-oxazoline (**136**) was used as the ligand (5.4 mg, 0.0150 mmol). According to general procedure **A**, anhydride (28.0 mg, 0.25 mmol) and benzyl trifluoroborate (59.4 mg, 0.3 mmol) afforded the product as a pale yellow oil (30.9 mg, 61% yield, 65% ee, 24:1 dr). Run 2 afforded 41% yield, 63% ee, 17:1 dr. Enantioselectivity was determined using the methyl ester. **¹H NMR (501 MHz, CDCl₃):** δ 7.33 (t, *J* = 7.3 Hz, 2H), 7.28-7.26 (m, 1H), 7.22 (d, *J* = 7.0 Hz, 2H),

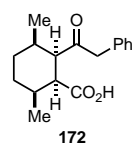
3.83 (s, 2H), 3.64 (s, 3H), 2.26 (ddd, $J = 9.3, 8.2, 6.7$ Hz, 1H), 2.06 (td, $J = 8.8, 6.8$ Hz, 1H), 1.73 (td, $J = 6.7, 4.8$ Hz, 1H), 1.19 (td, $J = 8.3, 4.8$ Hz, 1H). **^{13}C NMR (126 MHz, CDCl_3)**: δ 203.41, 170.40, 133.97, 129.75, 128.85, 127.21, 52.28, 50.87, 27.67, 23.82, 12.76. **HRMS (acid)**: (ESI-TOF) calculated for $([\text{C}_{12}\text{H}_{13}\text{O}_3 + \text{H}]^+)$: 205.0859, found: 205.0858. **IR (acid, ATR, cm^{-1})**: 3450, 3026, 2970, 1725, 1496, 1454, 1370, 1228, 1217, 1074, 905, 700. **Optical Rotation (acid)**: $[\alpha]_{\text{D}}^{26} +11.3$ (c 0.47, CHCl_3). **HPLC (methyl ester)**: Chiralcel[®] OD-H, 5% IPA in Hexanes, 30 min run, 1 mL/min.

Racemic Std:

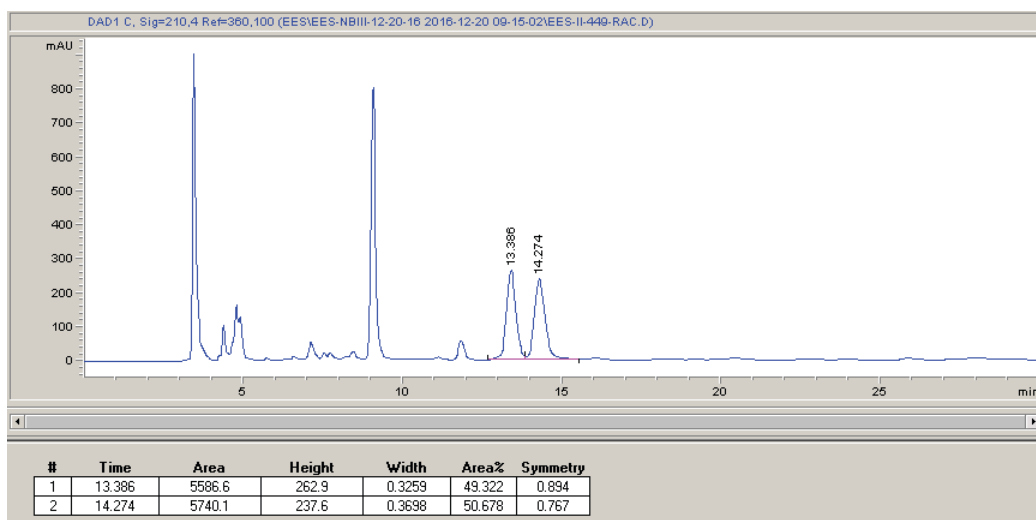


Enantioenriched:

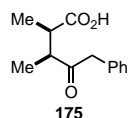
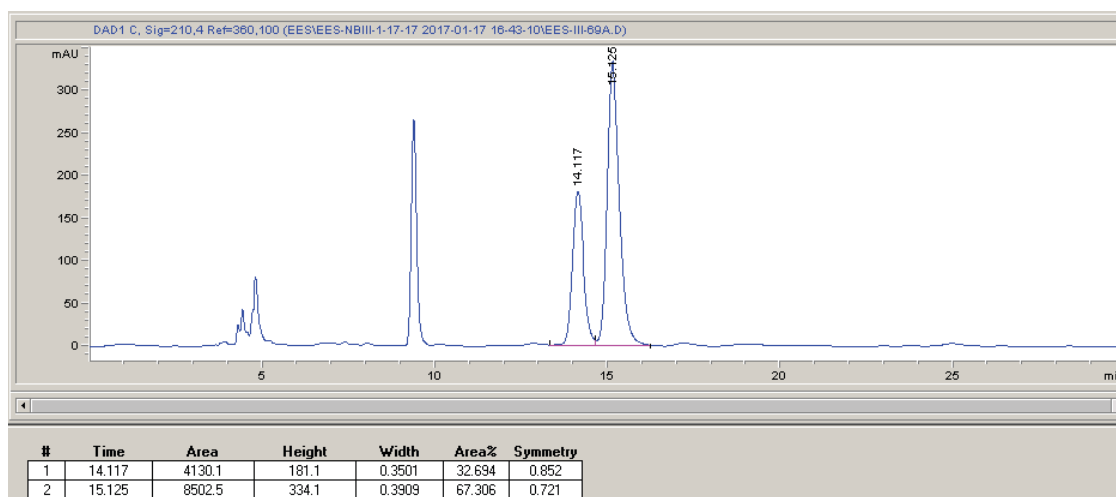



 (+)-2,2'-Isopropylidenebis-(4R)-4-benzyl-2-oxazoline (**136**) was used as the ligand (5.4 mg, 0.0150 mmol). According to general procedure **A**, anhydride (45.6 mg, 0.25 mmol) and benzyl trifluoroborate (59.4 mg, 0.3 mmol) afforded the product as a pale yellow oil (19.0 mg, 28% yield, 37% ee, 8.3:1 dr). Run 2 afforded 40% yield, 35% ee, 9.5:1 dr. NMR data based on methyl ester. **¹H NMR (501 MHz, CDCl₃):** δ 7.34 – 7.28 (m, 2H), 7.27 – 7.22 (m, 1H), 7.21 – 7.16 (m, 2H), 3.93, 3.90, 3.78, 3.75 (m, 2H), 3.65 (s, 3H), 2.95 (t, *J* = 5.2 Hz, 1H), 2.86 (t, *J* = 5.3 Hz, 1H), 2.30 – 2.18 (m, 1H), 1.90 – 1.79 (m, 1H), 1.77 – 1.64 (m, 2H), 1.53 – 1.44 (m, 1H), 1.37 (ddt, *J* = 10.0, 6.3, 2.9 Hz, 1H), 1.07 (d, *J* = 7.2 Hz, 3H), 1.01 (d, *J* = 7.0 Hz, 3H). **¹³C NMR (126 MHz, CDCl₃):** δ 208.76, 174.24, 134.71, 129.78, 128.67, 126.97, 53.85, 51.35, 49.11, 46.49, 33.20, 30.60, 30.49, 26.78, 18.66, 16.98. **HRMS:** (ESI-TOF) calculated for ([C₁₇H₂₂O₃ + Na]⁺): 297.1461, found 297.1455. **IR (ATR, cm⁻¹):** 3029, 2925, 1701, 1496, 1453, 1298, 1228, 1057, 925, 803, 742, 699. **Optical Rotation:** [α]_D²⁶ +12.8 (*c* 0.69, CHCl₃). **HPLC:** ChiralPak[®] IC, 5% IPA in Hexanes, 60 min run, 1 mL/min.

Racemic Std:



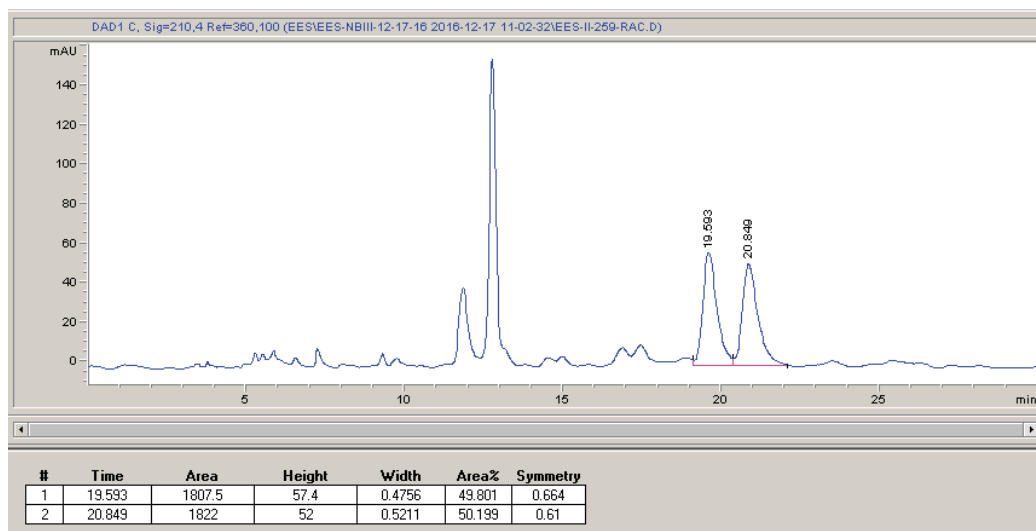
Enantioenriched:



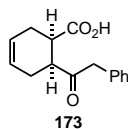
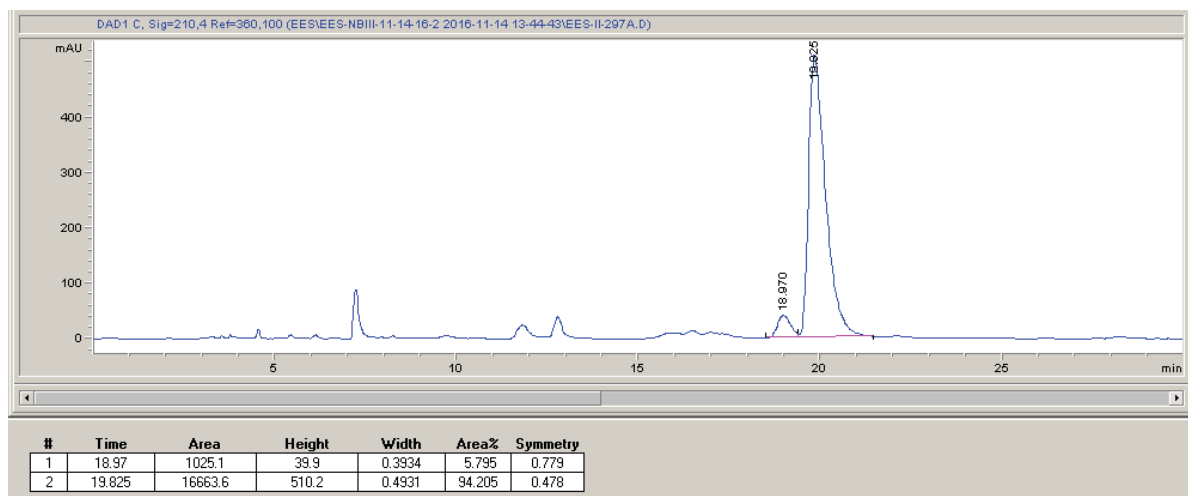
Reaction run for 48 h. According to general procedure **A**, anhydride **28** (32.0 mg, 0.25 mmol) and benzyl trifluoroborate (59.4 mg, 0.3 mmol) afforded the product as a pale yellow oil (38.8 mg, 70% yield, 88% ee, 12.3:1 dr). Run 2 afforded 69% yield, 88% ee, 13.4:1 dr. NMR data based on methyl ester. **^1H NMR (501 MHz, CDCl_3)**: δ 7.38 – 7.29 (m, 2H), 7.29 – 7.23 (m, 1H), 7.23 – 7.12 (m, 2H), 3.76 (s, 2H), 3.66 (s, 3H), 2.96 – 2.87 (m, 1H), 2.80 (qd, J = 8.6, 6.9 Hz, 1H), 1.09 (d, J = 6.9 Hz, 3H), 1.03 (d, J = 7.0 Hz, 3H). **^{13}C NMR (126 MHz, CDCl_3)**: δ 209.75, 175.73, 133.68, 129.72, 128.83, 127.23, 51.83, 49.59, 48.10, 42.07, 15.57, 15.30. **HRMS**: (ESI-TOF) calculated for $([\text{C}_{13}\text{H}_{16}\text{O}_3 + \text{Na}]^+)$: 243.0992, found 243.0990. **IR (ATR, cm^{-1})**

^1J : 3063, 2932, 1699, 1496, 1453, 1381, 1283, 1071, 948, 801, 712, 700. **Optical Rotation:** $[\alpha]_{\text{D}}^{26}$ -42.3 (c 0.65, CHCl_3). **HPLC:** ChiralPak[®] IC, 3% IPA in Hexanes, 60 min run, 1 mL/min.

Racemic Std:



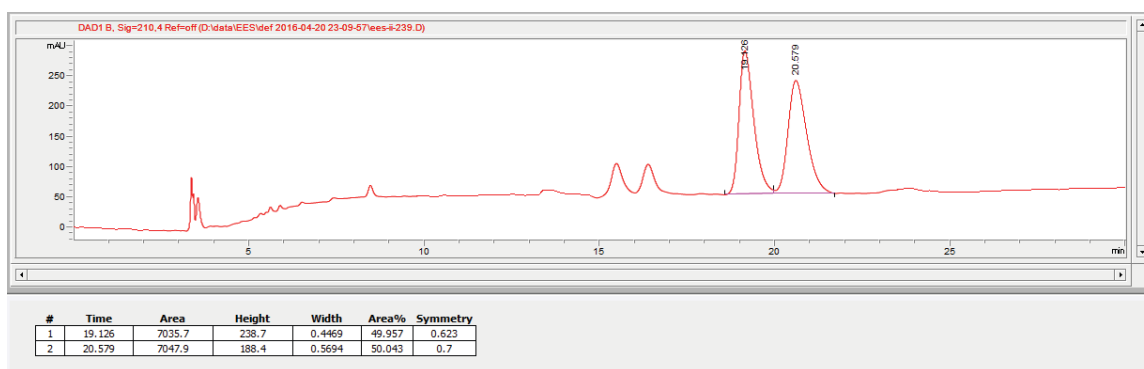
Enantioenriched:



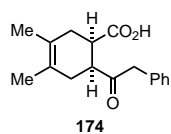
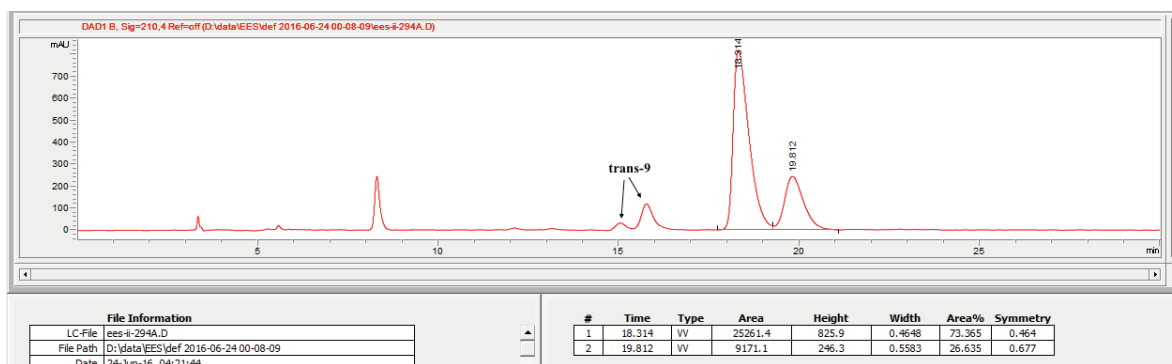
According to general procedure **A**, anhydride **22** (38.0 mg, 0.25 mmol) and benzyl trifluoroborate (59.4 mg, 0.3 mmol) afforded the product as a pale yellow oil (40.4 mg, 66% yield, 47% ee, 9.5:1 dr). Run 2 afforded 75% yield, 45% ee, 11.5:1 dr. NMR data based on methyl ester. **^1H NMR (501 MHz, CDCl_3):** δ 7.36 – 7.28 (m, 2H), 7.28 – 7.23 (m, 1H), 7.23 –

7.11 (m, 2H), 5.76 – 5.61 (m, 2H), 3.83 (s, 2H), 3.63 (s, 3H), 3.07 (td, $J = 6.2, 3.5$ Hz, 1H), 3.03 (td, $J = 6.8, 3.6$ Hz, 1H), 2.67 – 2.48 (m, 2H), 2.44 – 2.31 (m, 2H). **^{13}C NMR (126 MHz, CDCl_3):** δ 208.36, 174.00, 134.40, 129.66, 128.72, 127.02, 125.88, 124.53, 51.19, 47.36, 45.95, 39.65, 26.38, 25.33. **HRMS:** (ESI-TOF) calculated for $([\text{C}_{15}\text{H}_{16}\text{O}_3 + \text{Na}]^+)$: 267.0992, found: 267.0984. **IR (ATR, cm^{-1}):** 3028, 2923, 1736, 1706, 1496, 1436, 1366, 1229, 1216, 699. **Optical Rotation:** $[\alpha]_{\text{D}}^{26}$ -9.1 (c 0.76, CHCl_3). **HPLC:** ChiralPak[®] ID, 5% IPA (1% TFA) in Hexanes, 30 min run, 1 mL/min.

Racemic Std:



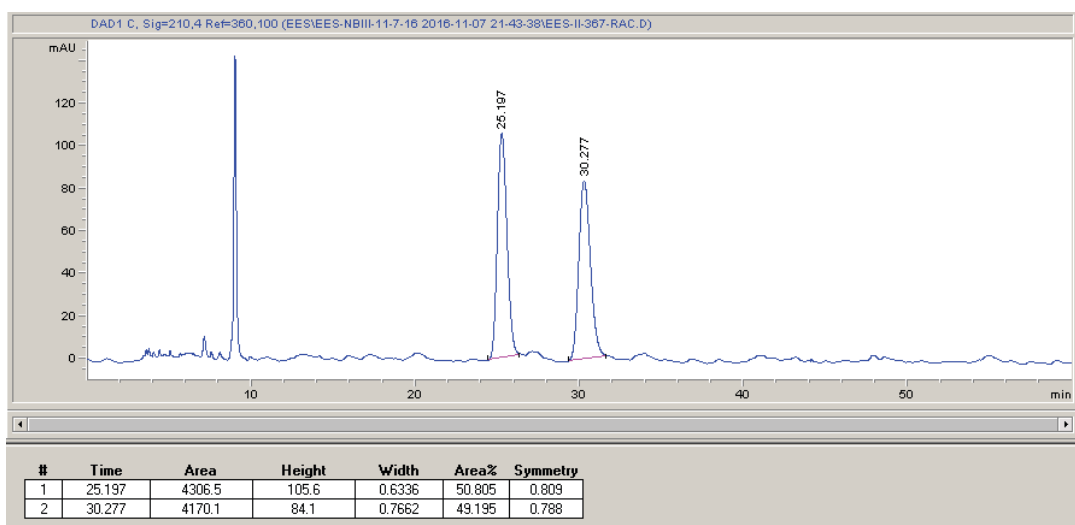
Enantioenriched:



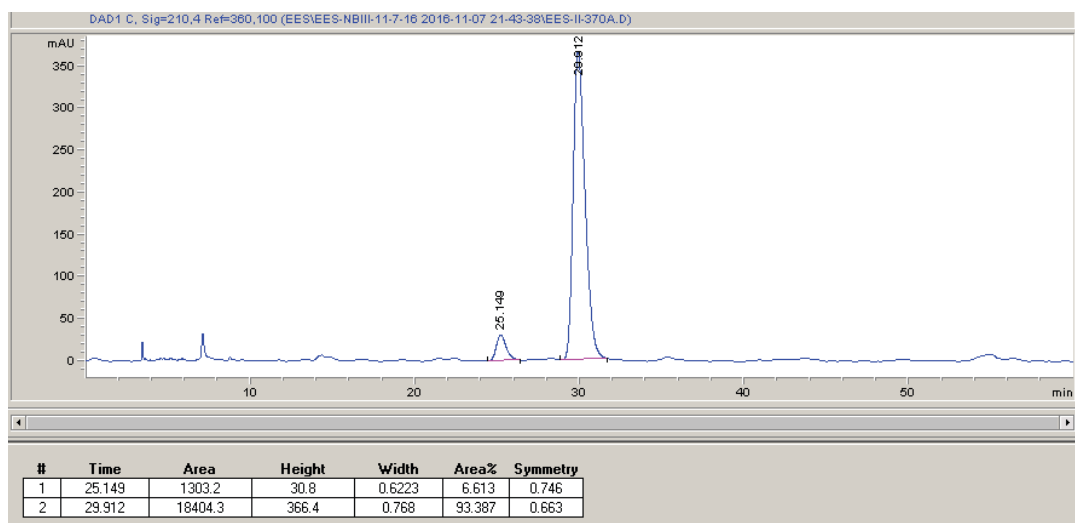
According to general procedure **A**, anhydride **23** (45.1 mg, 0.25 mmol) and benzyl trifluoroborate (59.4 mg, 0.3 mmol) afforded the product as a pale yellow oil (52.4 mg, 77% yield, 87% ee, 18:1 dr). Run 2 afforded 67% yield, 85% ee, 14:1 dr. NMR data based on methyl ester. **^1H NMR (501 MHz, CDCl_3):** δ 7.31 (t, $J = 7.4$ Hz, 2H), 7.25 (d, $J = 8.1$ Hz, 1H),

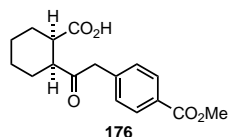
7.18 (d, $J = 7.5$ Hz, 2H), 3.80 (s, 2H), 3.63 (s, 3H), 3.10 – 2.84 (m, 2H), 2.51-2.41 (m, 2H), 2.36 – 2.20 (m, 2H), 1.60 (s, 6H). **^{13}C NMR (126 MHz, CDCl_3):** δ 208.50, 174.16, 134.49, 129.61, 128.69, 126.97, 124.74, 123.33, 51.88, 47.37, 46.85, 40.44, 32.31, 31.59, 19.16, 18.98 **HRMS:** (ESI-TOF) calculated for $[\text{C}_{17}\text{H}_{20}\text{O}_3 - \text{H}]^-$: 271.1340, found: 271.1340. **IR (ATR, cm^{-1}):** 3186, 3029, 2920, 1706, 1497, 1454, 1258, 1190, 1085, 798, 701. **Optical Rotation:** $[\alpha]_{\text{D}}^{26} -10.5$ (c 0.81, CHCl_3). **HPLC:** ChiralPak[®] IC, 5% IPA in Hexanes, 60 min run, 1 mL/min.

Racemic Std:



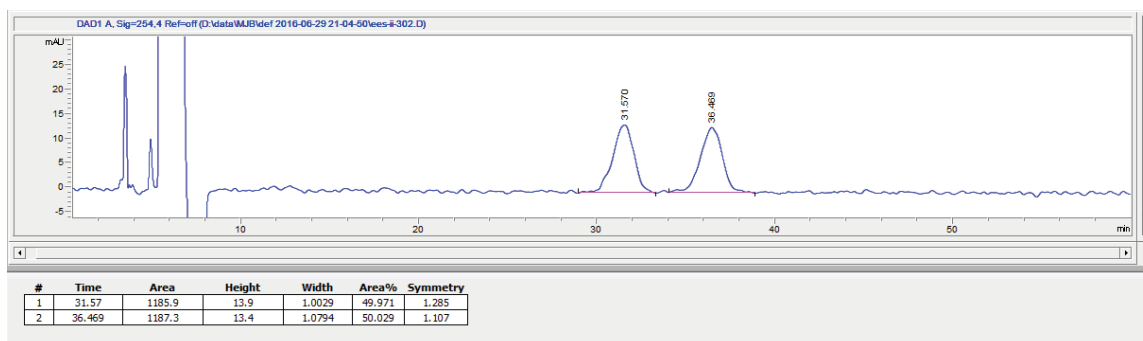
Enantioenriched:



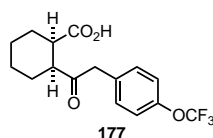
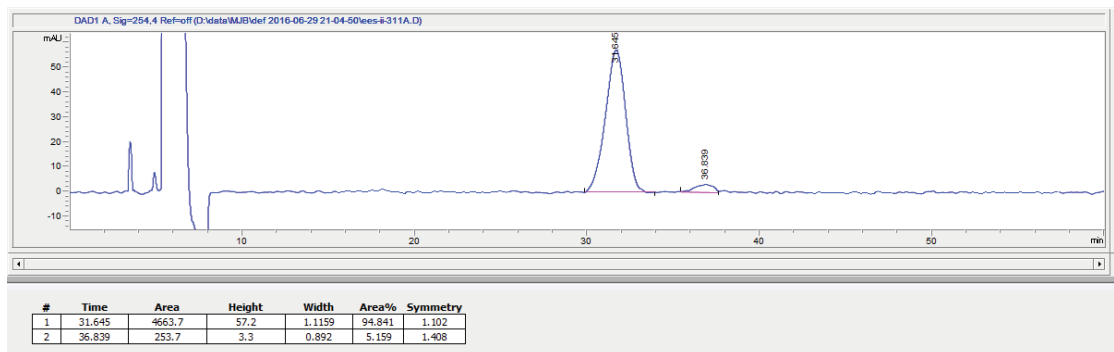


According to general procedure A, anhydride **4** (38.5 mg, 0.25 mmol) and *p*-methylbenzoatebenzyl trifluoroborate (76.8 mg, 0.3 mmol) afforded the product as a pale yellow oil (56.3 mg, 74% yield, 90% ee, 13.3:1 dr). Run 2 afforded 79% yield, 88% ee, 12.7:1 dr. NMR data based on methyl ester. Diastereoselectivity based on ^1H NMR in acetone- d_6 . **^1H NMR (501 MHz, CDCl_3):** δ 7.99 (d, J = 5.0 Hz, 2H), 7.26 (d, J = 10 Hz, 2H), 3.90 (s, 3H), 3.86 (s, 2H), 3.61 (s, 3H), 2.89 (m, 1H), 2.82 (m, 1H), 2.08 (m, 1H), 2.01 (m, 1H), 1.84 (m, 1H), 1.76 (m, 1H), 1.55 (m, 1H), 1.44 (m, 1H), 1.39 (m, 2H). **^{13}C NMR (126 MHz, CDCl_3):** δ 208.55, 174.42, 167.10, 139.87, 129.88, 129.81, 128.81, 52.21, 51.80, 49.19, 47.39, 42.96, 26.29, 25.99, 23.95, 23.61. **HRMS:** (ESI-TOF) calculated for $[\text{C}_{17}\text{H}_{21}\text{O}_5 + \text{H}]^+$: 305.1384, found 305.1382. **IR (ATR, cm^{-1}):** 3006, 2943, 1737, 1722, 1611, 1436, 1368, 1280, 1217 1109, 1021, 757. **Optical Rotation:** $[\alpha]_D^{26}$ -39.1 (c 0.66, CHCl_3). **HPLC:** ChiralPak[®] IC, 15% IPA (1% TFA) in Hexanes, 60 min run, 1 mL/min (sample prep in HPLC grade acetone).

Racemic Std:

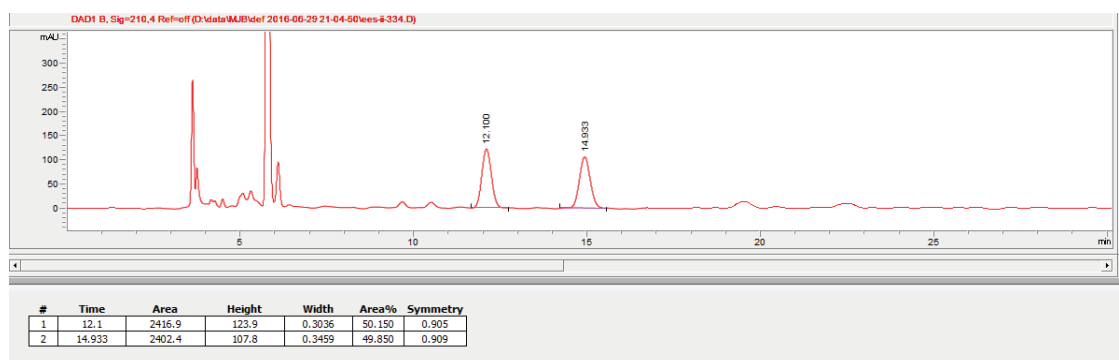


Enantioenriched:

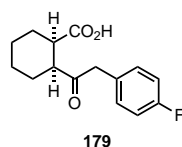
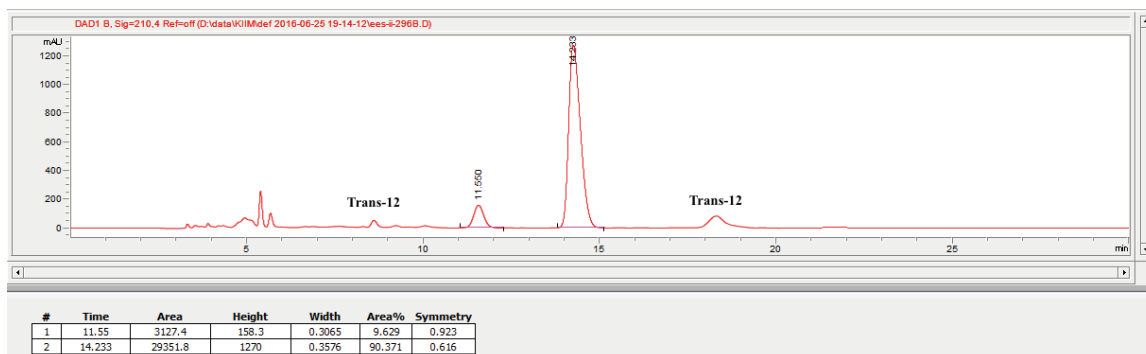


Reaction run for 46 h. According to general procedure **A**, anhydride **4** (38.5 mg, 0.25 mmol) and *p*-trifluoromethoxybenzyl trifluoroborate (84.6 mg, 0.3 mmol) afforded the product as a pale yellow oil (61.0 mg, 74% yield, 81% ee, 12.3:1 dr). Run 2 afforded 70% yield, 81% ee, 11.5:1 dr. NMR data based on methyl ester. **¹H NMR (501 MHz, CDCl₃):** δ 7.21 (d, *J* = 8.7 Hz, 2H), 7.18 – 7.14 (m, 2H), 3.87 – 3.77 (m, 2H), 3.61 (s, 3H), 2.94 – 2.78 (m, 2H), 2.16 – 1.97 (m, 2H), 1.92 – 1.71 (m, 2H), 1.63 – 1.35 (m, 4H). **¹³C NMR (126 MHz, CDCl₃):** δ 208.92, 174.48, 148.22, 133.27, 131.12, 121.12, 115.41, 51.81, 49.12, 46.56, 43.02, 26.33, 26.02, 23.98, 23.63. **¹⁹F NMR (282 MHz, CDCl₃):** δ -57.87 **HRMS:** (ESI-TOF) calculated for ([C₁₆H₁₈F₃O₄ + H]⁺): 331.1152, found 331.1155. **IR (ATR, cm⁻¹):** 2936, 2860, 1736, 1704, 1509 1366, 1254, 1218, 1159, 1019, 811, 736. **Optical Rotation:** [α]_D²⁶ -31.6 (*c* 0.75, CHCl₃). **HPLC:** ChiralPak[®] IC, 5% IPA (1% TFA) in Hexanes, 30 min run, 1 mL/min.

Racemic Std:



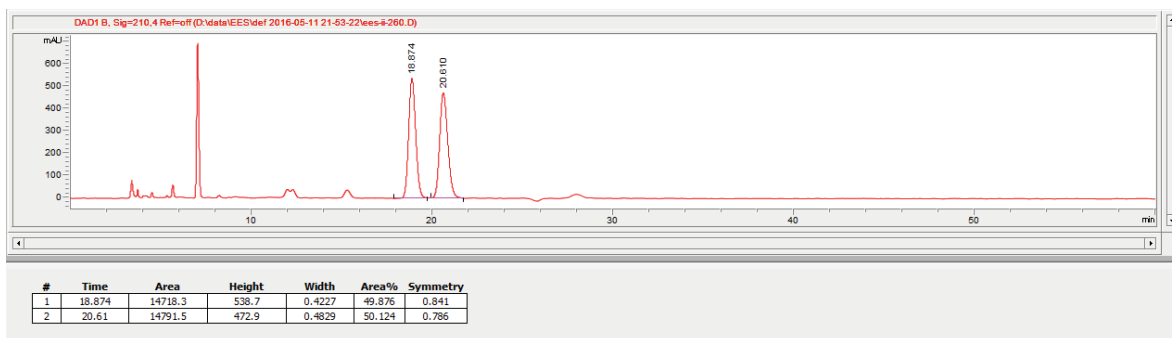
Enantioenriched:



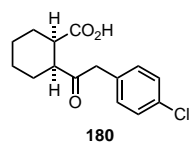
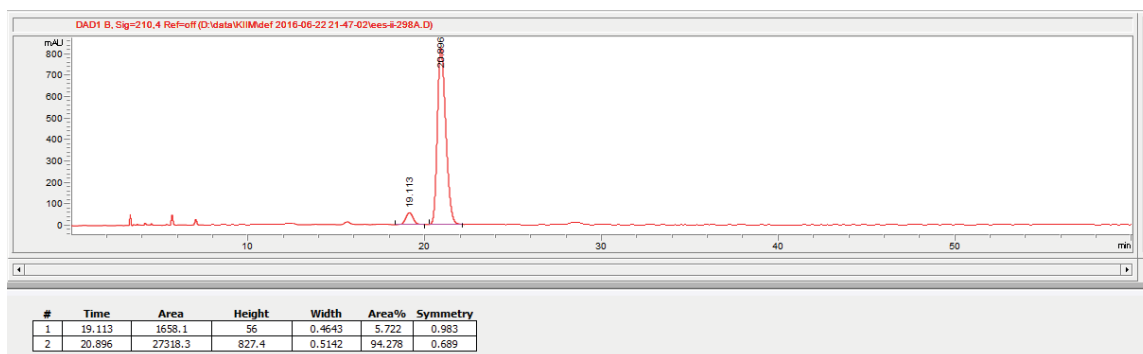
1.5 equiv of trifluoroborate was used. According to general procedure **A**, anhydride **4** (38.5 mg, 0.25 mmol) and 4-fluorobenzyl trifluoroborate (79.3 mg, 0.37 mmol) afforded the product as a pale yellow oil (59.4 mg, 90% yield, 88%

ee, 15.7:1 dr). Run 2 afforded 89% yield, 88% ee, 15.7:1 dr. NMR data based on methyl ester. **¹H NMR (501 MHz, CDCl₃)**: δ 7.14 (dd, *J* = 8.4, 5.5 Hz, 2H), 7.00 (t, *J* = 8.7 Hz, 2H), 3.78 (ABq, *J* = 15.0 Hz, Δ*v* = 13.2 Hz, 2H), 3.61 (s, 3H), 2.95 – 2.85 (m, 1H), 2.85 – 2.75 (m, 1H), 2.08 (tq, *J* = 12.4, 4.5 Hz, 1H), 2.01 (ddt, *J* = 14.3, 7.3, 3.7 Hz, 1H), 1.84 (ddt, *J* = 13.0, 8.4, 4.4 Hz, 1H), 1.76 (ddt, *J* = 12.5, 7.7, 4.0 Hz, 1H), 1.56 (dq, *J* = 7.7, 3.6 Hz, 1H), 1.50 – 1.32 (m, 3H). **¹³C NMR (126 MHz, CDCl₃)**: δ 209.26, 174.50, 162.94, 131.22 (d, *J* = 7.5 Hz), 130.23 (d, *J* = 2.5 Hz), 115.46 (d, *J* = 21.3 Hz), 51.79, 48.99, 46.53, 42.94, 26.29, 26.03, 23.99, 23.63. **¹⁹F NMR (282 MHz, CDCl₃)**: δ -118.57 **HRMS**: (ESI-TOF) calculated for ([C₁₅H₁₈FO₃ + H]⁺): 265.1234, 265.1237. **IR (ATR, cm⁻¹)**: 2935, 2857, 1703, 1508, 1450, 1366, 1219, 1158, 1016, 823, 792. **Optical Rotation**: [α]_D²⁶ -42.6 (*c* 0.86, CHCl₃). **HPLC**: ChiralPak[®] IC, 5% IPA (1% TFA) in Hexanes, 60 min run, 1 mL/min.

Racemic std:

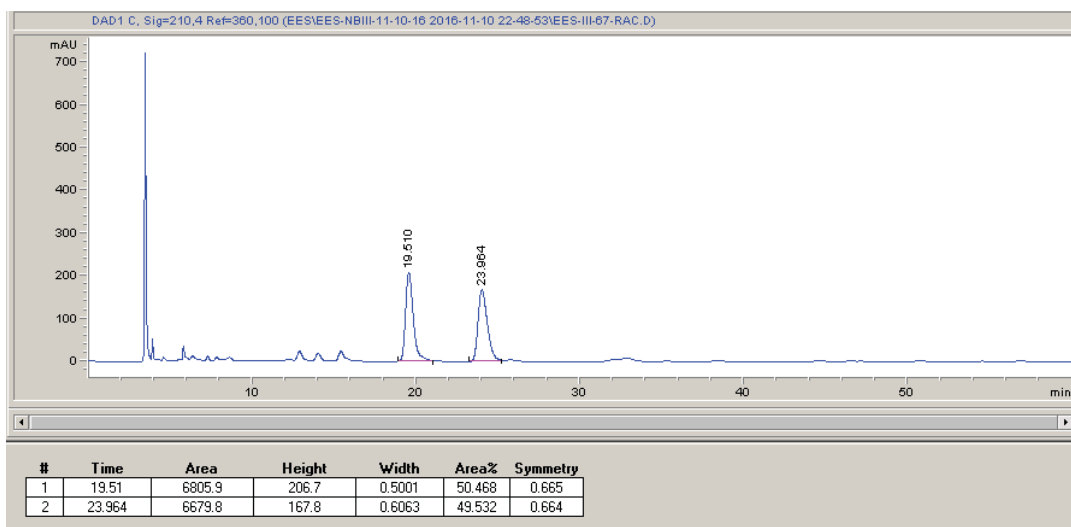


Enantioenriched:

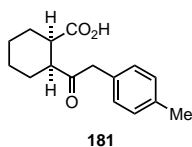
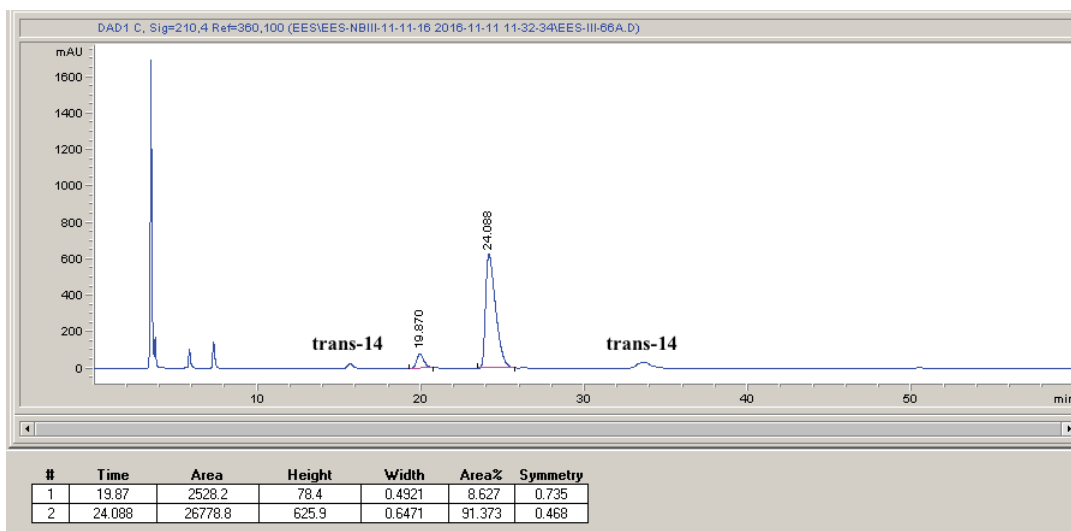


According to general procedure **A**, anhydride **4** (38.5 mg, 0.25 mmol) and *p*-chlorobenzyl trifluoroborate (69.7 mg, 0.3 mmol) afforded the product as a pale yellow oil (45.0 mg, 64% yield, 83% ee, 11.5:1 dr). Run 2 afforded 39% yield, 76% ee, 8.5:1 dr. A third run afforded 56% yield, 78% ee and 9.5:1 dr. NMR data based on methyl ester. **¹H NMR (501 MHz, CDCl₃):** δ 7.28 (d, *J* = 8.2 Hz, 2H), 7.12 (d, *J* = 8.2 Hz, 2H), 3.82 – 3.72 (m, 2H), 3.62 (s, 3H), 2.91 – 2.76 (m, 2H), 2.11-1.99 (m, 2H), 1.86-1.74 (m, 2H), 1.61 – 1.34 (m, 4H). **¹³C NMR (126 MHz, CDCl₃):** δ 208.92, 174.47, 133.01, 132.85, 131.09, 128.75, 51.81, 49.06, 46.71, 42.97, 26.31, 26.02, 23.98, 23.64. **HRMS:** 2932, 2857, 1701, 1492, 1449, 1409, 1364, 1219, 1089, 1014, 799, 739. **IR (ATR, cm⁻¹):** (ESI-TOF) calculated for ([C₁₅H₁₈ClO₃ + H]⁺): 281.0939, found 281.0933. **Optical Rotation:** [α]_D²⁶ -36.7 (*c* 0.64, CHCl₃). **HPLC:** ChiralPak[®] IC, 5% IPA in Hexanes, 60 min run, 1 mL/min.

Racemic Std:



Enantioenriched:



According to general procedure **A**, anhydride **4** (38.5 mg, 0.25 mmol) and *p*-methylbenzyl trifluoroborate (63.6 mg, 0.3 mmol) afforded the product as a pale yellow oil (55.3 mg, 85% yield, 85% ee, >20:1 dr). Run 2 afforded 85% yield, 85% ee, >20:1 dr. NMR data based on methyl ester. **¹H NMR (501 MHz, CDCl₃)**: δ 7.12 (d, *J* = 7.5 Hz, 2H), 7.07 (d, *J* = 8.1 Hz, 2H), 3.75 (s, 2H), 3.61 (s, 3H), 2.90 (t, *J* = 3.8 Hz, 1H), 2.82 – 2.74 (m, 1H), 2.32 (s, 3H), 2.12 – 1.98 (m, 2H), 1.85–1.73 (m, 2H), 1.56 (dt, *J* = 12.3, 3.4 Hz, 1H), 1.41 (dddd, *J* = 17.7, 15.4, 8.4, 4.3 Hz, 3H). **¹³C NMR (126 MHz, CDCl₃)**: δ 209.59, 174.51,

136.50, 131.49, 129.51, 129.37, 51.72, 48.83, 47.16, 42.79, 26.26, 26.08, 23.99, 23.67, 21.23.

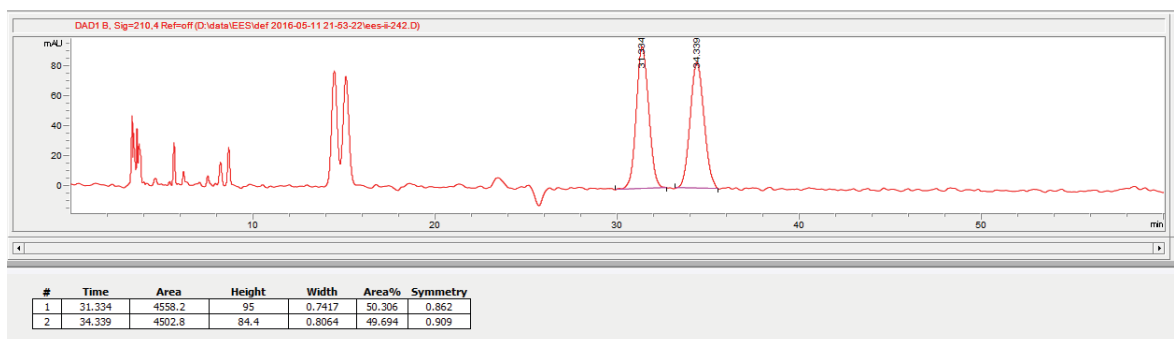
HRMS: (ESI-TOF) calculated for $[(C_{16}H_{20}O_3 + Na)^+]$: 283.1305, found 283.1301. **IR (ATR, cm^{-1})**:

2934, 2958, 1737, 1701, 1515, 1450, 1418, 1367, 1264, 1217, 1020, 732, 702. **Optical**

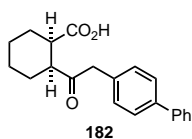
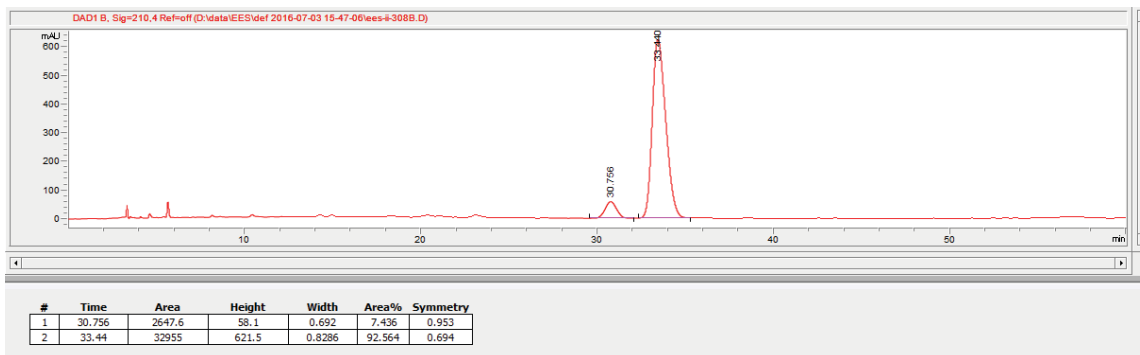
Rotation: $[\alpha]_D^{26}$ -51.7 (c 0.83, $CHCl_3$). **HPLC:** ChiralPak[®] IC, 5% IPA (1% TFA) in Hexanes,

60 min run, 1 mL/min.

Racemic Std:



Enantioenriched:



According to general procedure **A**, anhydride **4** (38.5 mg, 0.25 mmol) and *p*-phenylbenzyl trifluoroborate (82.2 mg, 0.3 mmol) afforded the product as a pale

yellow oil (69.4 mg, 86% yield, 84% ee, >20:1 dr). Run 2 afforded 81% yield, 81% ee, >20:1 dr.

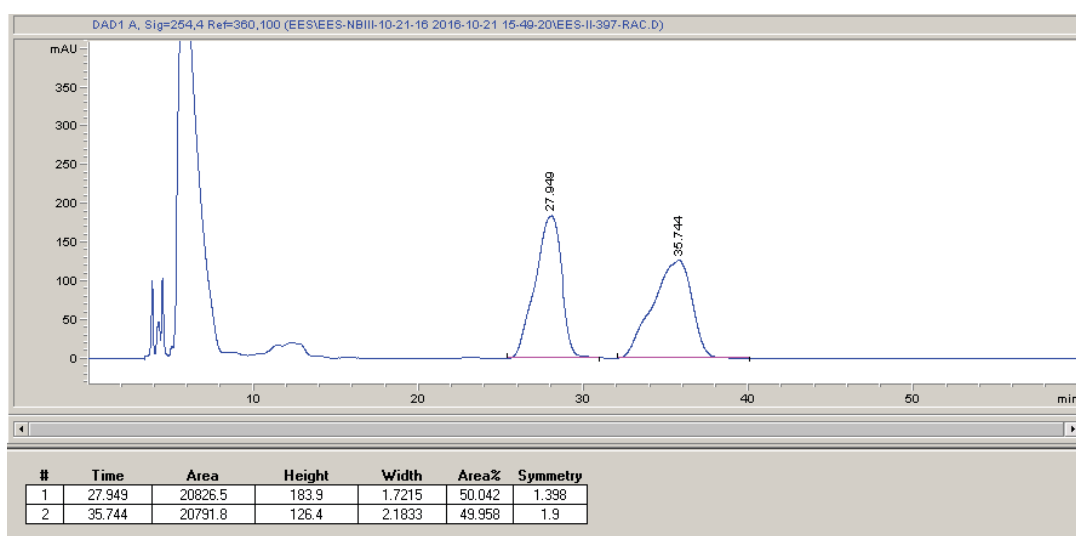
NMR data based on methyl ester. **1H NMR (501 MHz, $CDCl_3$):** δ 7.60 – 7.53 (m, 4H), 7.43 (dd,

J = 8.4, 7.0 Hz, 2H), 7.36 – 7.31 (m, 1H), 7.29 – 7.24 (m, 2H), 3.85 (s, 2H), 3.62 (s, 3H), 2.94 (d,

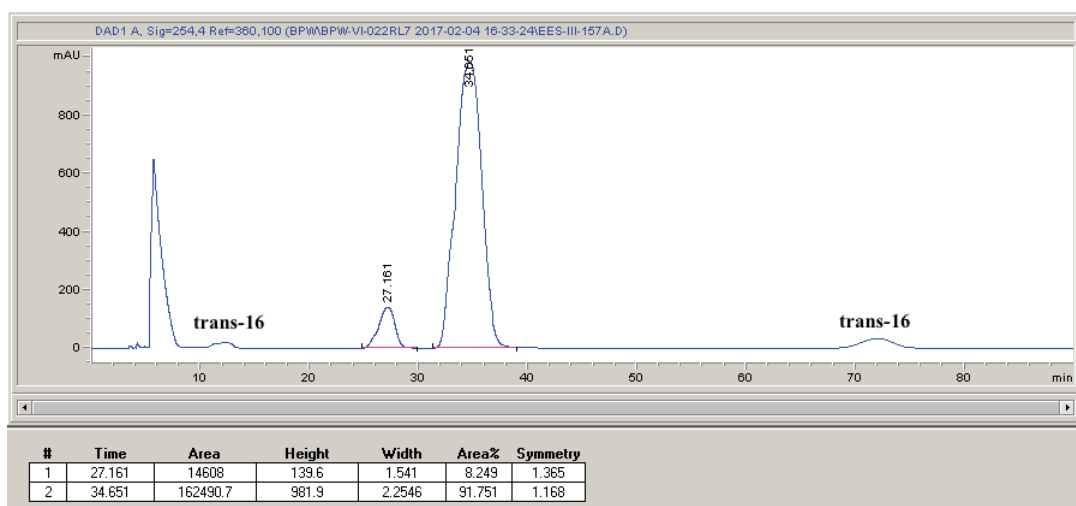
J = 6.8 Hz, 1H), 2.87 – 2.79 (m, 1H), 2.09 (tdd, J = 13.8, 6.1, 3.6 Hz, 2H), 1.89-1.76 (m, 2H), 1.65

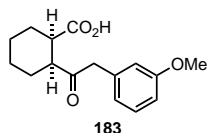
– 1.45 (m, 2H), 1.46 – 1.36 (m, 2H). **¹³C NMR (126 MHz, CDCl₃):** δ 209.39, 174.52, 141.02, 139.87, 133.64, 130.12, 128.87, 127.41, 127.33, 127.20, 51.78, 49.02, 47.16, 42.90, 26.30, 26.10, 24.01, 23.67. **HRMS:** (ESI-TOF) calculated for ([C₂₁H₂₃O₃ + H]⁺): 323.1642, found 323.1640. **IR (ATR, cm⁻¹):** 3229, 2933, 2857, 1701, 1487, 1449, 1207, 1007, 843, 759, 697. **Optical Rotation:** [α]_D²⁶ -36.1 (c 0.68, CHCl₃). **HPLC:** ChiralPak[®] IC, 10% IPA in Hexanes, 60 min run, 1 mL/min (sample prep in HPLC grade acetone).

Racemic Std:



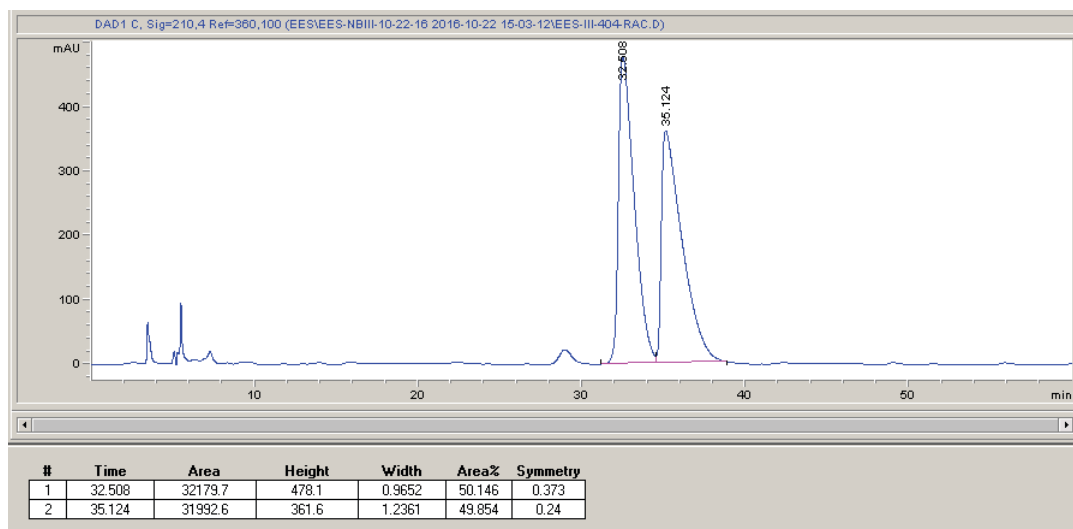
Enantioenriched:



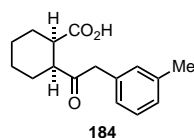
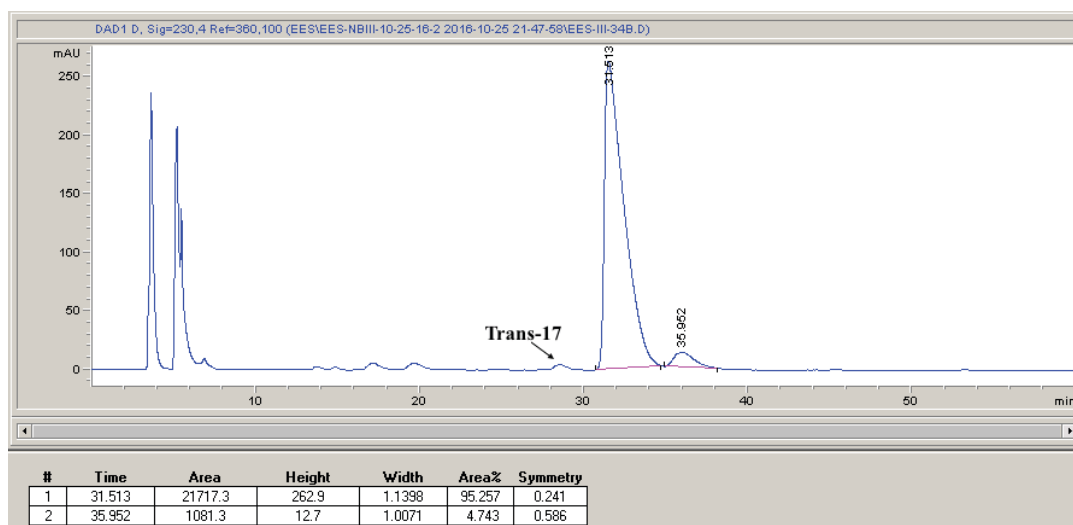


According to general procedure **A**, anhydride **4** (38.5 mg, 0.25 mmol) and benzyl trifluoroborate **205** (68.4 mg, 0.3 mmol) afforded the product as a pale yellow oil (60.8 mg, 88% yield, 90% ee, 12:1 dr). Run 2 afforded 83% yield, 88% ee, 10.5:1 dr. NMR data based on methyl ester. Diastereoselectivity based on ^1H NMR in acetone- d_6 . **^1H NMR (501 MHz, CDCl_3):** δ 7.23 (t, $J = 7.9$ Hz, 1H), 6.81 – 6.76 (m, 2H), 6.74 (t, $J = 2.1$ Hz, 1H), 3.79 (s, 3H), 3.76 (s, 2H), 3.61 (s, 3H), 2.96 – 2.86 (m, 1H), 2.82 – 2.75 (m, 1H), 2.14 – 1.96 (m, 2H), 1.84–1.73(m, 2H), 1.62 – 1.51 (m, 1H), 1.51 – 1.33 (m, 3H). **^{13}C NMR (126 MHz, CDCl_3):** δ 209.29, 174.49, 159.79, 136.04, 129.61, 122.02, 115.29, 112.41, 55.31, 51.72, 48.88, 47.59, 42.80, 26.25, 26.06, 23.96, 23.65. **HRMS:** (ESI-TOF) calculated for $([\text{C}_{16}\text{H}_{20}\text{O}_4 - \text{H}])$: 275.1289, found: 275.1295. **IR (ATR, cm^{-1}):** 3306, 2936, 2857, 1707, 1600, 1490, 1453, 1367, 1257, 1217, 1043, 775, 691. **Optical Rotation:** $[\alpha]_D^{26}$ -60.7 (c 0.78, acetone). **HPLC:** ChiralPak[®] ID, 5% IPA in Hexanes, 60 min run, 1 mL/min (sample prep in HPLC grade acetone).

Racemic Std:



Enantioenriched:

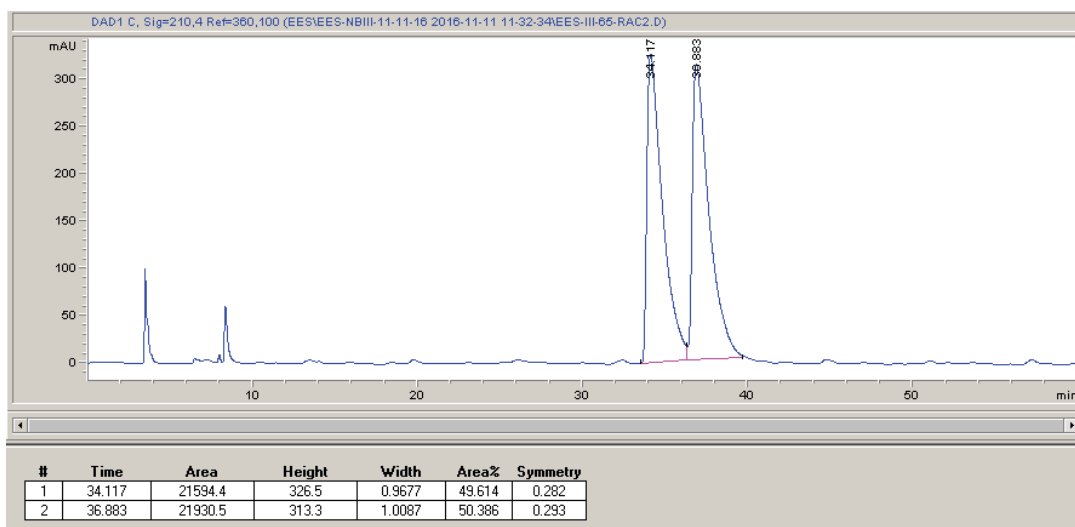


According to general procedure **A**, anhydride **4** (38.5 mg, 0.25 mmol) and *m*-methylbenzyl trifluoroborate (63.6 mg, 0.3 mmol) afforded the product as a pale yellow oil (60.6 mg, 93% yield, 87% ee, 10.3:1 dr). Run 2 afforded 75% yield, 84% ee, 12.6:1 dr.

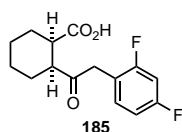
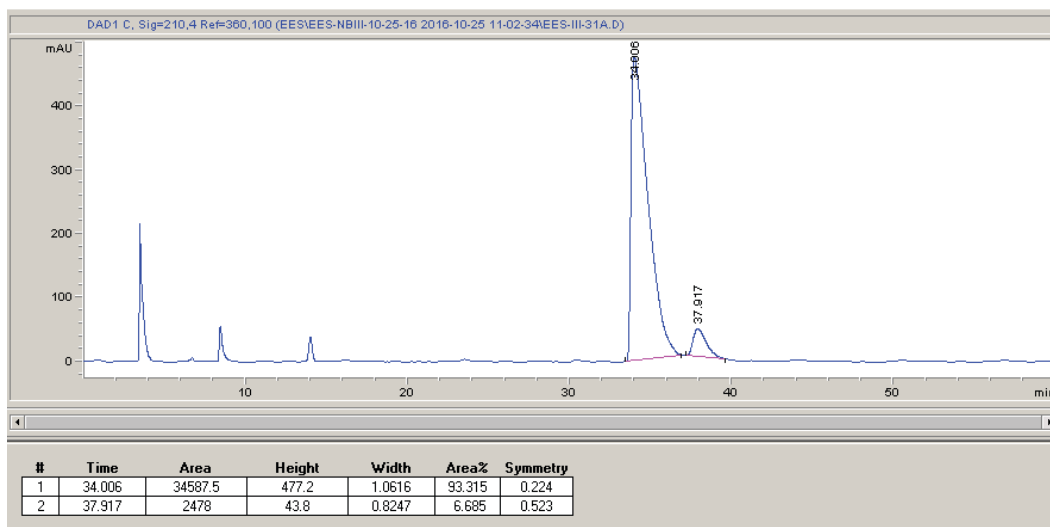
NMR data based on methyl ester. **¹H NMR (501 MHz, CDCl₃):** δ 7.20 (t, *J* = 7.5 Hz, 1H), 7.06 (d, *J* = 7.6 Hz, 1H), 7.03 – 6.96 (m, 2H), 3.76 (s, 2H), 3.61 (s, 3H), 2.90 (t, *J* = 5.9 Hz, 1H), 2.83 – 2.74 (m, 1H), 2.33 (s, 3H), 2.13 – 1.99 (m, 2H), 1.85–1.73 (m, 2H), 1.57 (ddd, *J* = 16.3, 7.9, 3.8 Hz, 1H), 1.50 – 1.34 (m, 3H). **¹³C NMR (126 MHz, CDCl₃):** δ 209.52, 174.51, 138.24, 134.44, 130.42, 128.53, 127.69, 126.66, 51.72, 48.90, 47.48, 42.79, 26.27, 26.07, 23.98, 23.66, 21.53.

HRMS: (ESI-TOF) calculated for ([C₁₆H₂₀O₃ + Na]⁺): 283.1305, found 283.1303. **IR (ATR, cm⁻¹):** 3022, 2930, 2856, 1698, 1608, 1489, 1449, 1257, 1219, 914, 771, 703. **Optical Rotation:** [α]_D²⁶ -42.6 (*c* 0.60, CHCl₃). **HPLC:** ChiralPak[®] ID, 2% IPA in Hexanes, 60 min run, 1 mL/min.

Racemic Std:



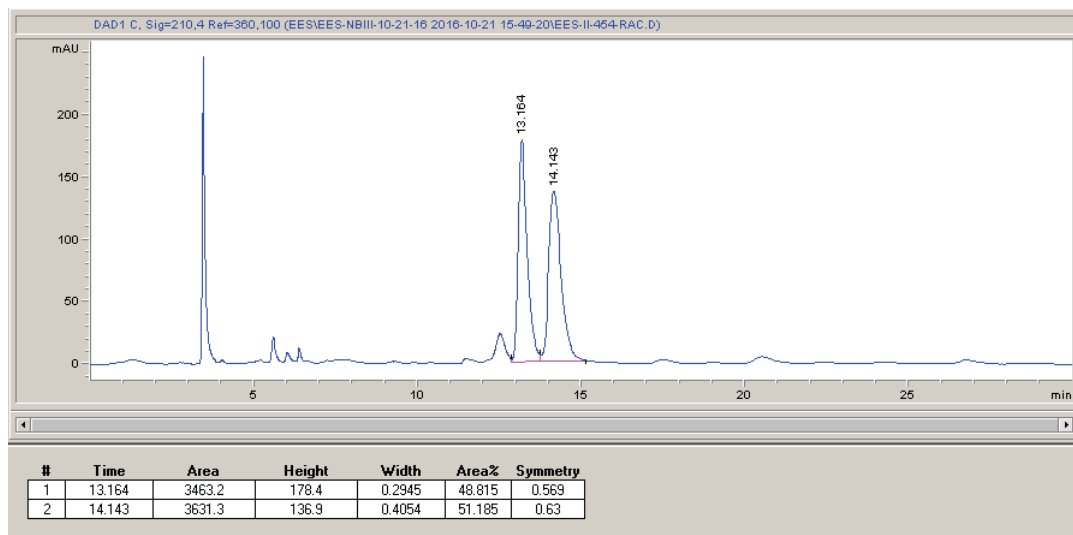
Enantioenriched:



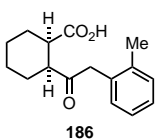
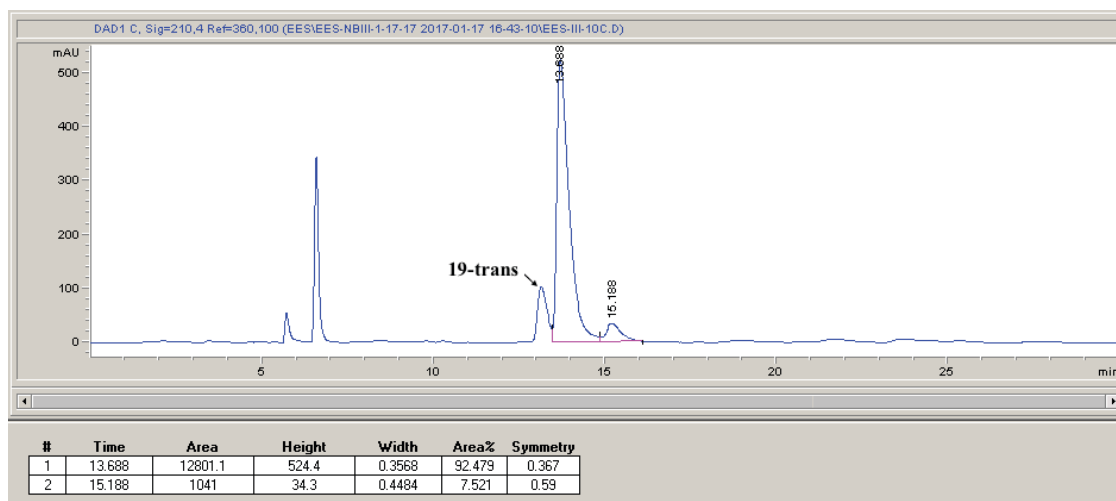
According to general procedure **A**, anhydride **4** (38.5 mg, 0.25 mmol) and 2,4-difluorobenzyl trifluoroborate (70.2 mg, 0.3 mmol) afforded the product as a pale yellow oil (52.8 mg, 75% yield, 86% ee, 6:1 dr). Run 2 afforded 79% yield, 84% ee, 11.8:1 dr. NMR data based on methyl ester. **¹H NMR (501 MHz, CDCl₃):** δ 7.14 (td, *J* = 8.4, 6.4 Hz, 1H), 6.87 – 6.77 (m, 2H), 3.88 – 3.74 (m, 2H), 3.63 (s, 3H), 2.98 – 2.88 (m, 1H), 2.84 (dd, *J* = 7.7, 4.3 Hz, 1H), 2.07 (dddd, *J* = 21.3, 14.6, 8.0, 3.7 Hz, 2H), 1.88 (td, *J* = 8.7, 4.2 Hz, 1H), 1.78 (td, *J* = 8.4, 3.9 Hz, 1H), 1.62 – 1.37 (m, 4H). **¹³C NMR (126 MHz, CDCl₃):** Inseparable mixture of

diastereomers. See spectrum for details. **^{19}F NMR (282 MHz, CDCl_3):** δ -111.95, -113.27. **HRMS:** (ESI-TOF) calculated for $([\text{C}_{15}\text{H}_{16}\text{F}_2\text{O}_3 + \text{Na}]^+)$: 305.0960, found 305.0955. **IR (ATR, cm^{-1}):** 3019, 2970, 1740, 1438, 1368, 1228, 1217, 1091, 901. **Optical Rotation:** $[\alpha]_{\text{D}}^{26}$ -15.5 (c 0.79, acetone). **HPLC:** ChiralPak[®] ID, 5% IPA in Hexanes, 30 min run, 1 mL/min.

Racemic Std:



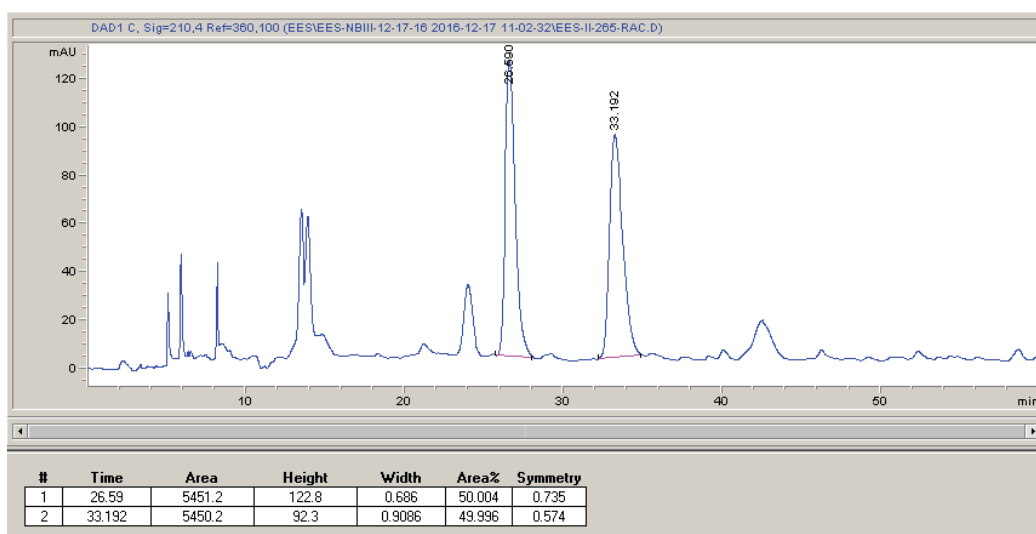
Enantioenriched:



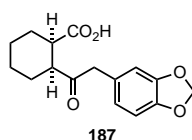
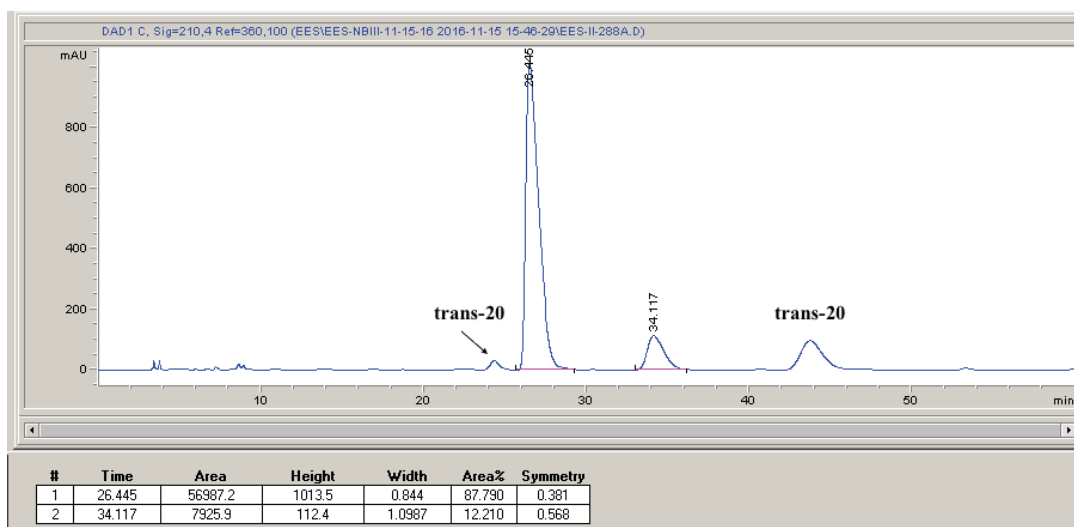
According to general procedure **A**, anhydride **4** (38.5 mg, 0.25 mmol) and *o*-methylbenzyl trifluoroborate (63.6 mg, 0.3 mmol) afforded the product as a pale

yellow oil (51.0 mg, 78% yield, 76% ee, 6.4:1 dr). Run 2 afforded 87% yield, 74% ee, 5.7:1 dr. NMR data based on methyl ester. **¹H NMR (501 MHz, CDCl₃)**: δ 7.21 – 7.12 (m, 3H), 7.11 – 7.06 (m, 1H), 3.82 (s, 2H), 3.62 (s, 3H), 3.01 – 2.90 (m, 1H), 2.80 – 2.73 (m, 1H), 2.22 (s, 3H), 2.17 – 2.00 (m, 2H), 1.89 – 1.72 (m, 2H), 1.67 – 1.54 (m, 1H), 1.53 – 1.42 (m, 2H), 1.36-1.42 (m, 1H). **¹³C NMR (126 MHz, CDCl₃)**: Inseparable mixture of diastereomers. See spectrum for details. **HRMS**: (ESI-TOF) calculated for ([C₁₆H₂₁O₃ + Na]⁺): 261.1485, found 261.1483. **IR** (ATR, cm⁻¹): 3017, 2933, 2858, 1706, 1495, 1449, 1417, 1361, 1219, 1078, 897, 743, 689. **Optical Rotation**: [α]_D²⁶ -40.0 (c 0.74, CHCl₃). **HPLC**: ChiralPak[®] IC, 5% IPA in Hexanes, 60 min run, 1 mL/min.

Racemic std:

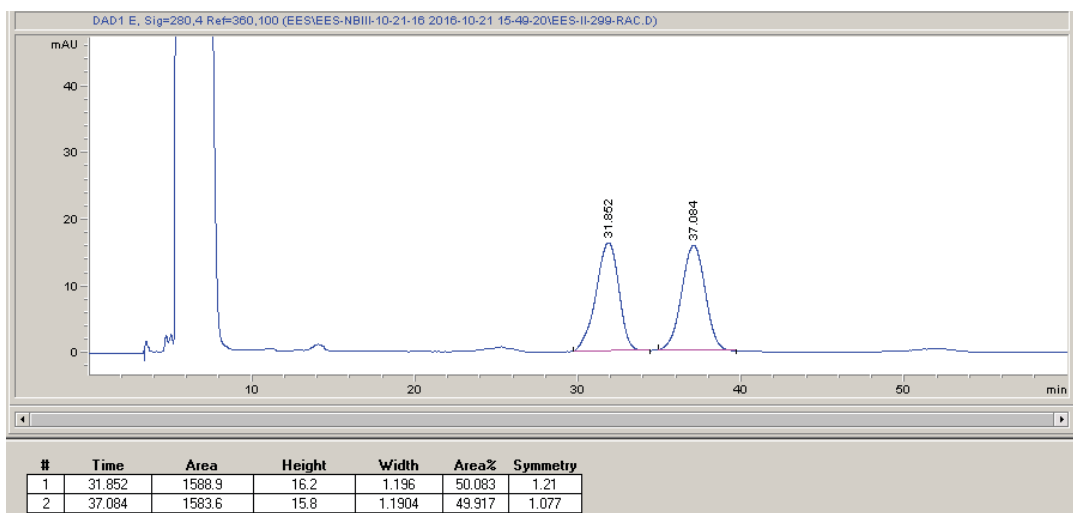


Enantioenriched:

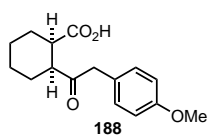
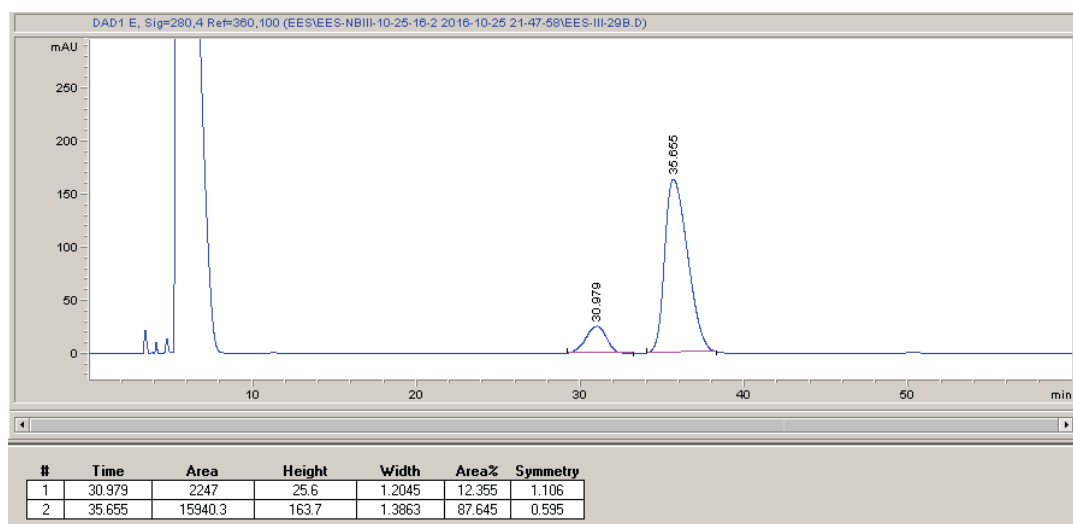


According to general procedure A, anhydride **4** (38.5 mg, 0.25 mmol) and benzyl trifluoroborate (72.6 mg, 0.3 mmol) afforded the product as a pale yellow oil (64.3 mg, 89% yield, 75% ee, >20:1 dr). Run 2 afforded 89% yield, 65% ee, >20:1 dr. NMR data based on methyl ester. **¹H NMR (501 MHz, CDCl₃):** δ 6.75 (d, *J* = 7.9 Hz, 1H), 6.68 (d, *J* = 1.7 Hz, 1H), 6.62 (dd, *J* = 7.9, 1.7 Hz, 1H), 5.93 (s, 2H), 3.71 (ABq, *J* = 15.0 Hz, Δ*v* = 13.2 Hz, 2H), 3.62 (s, 3H), 2.89 (q, *J* = 5.5 Hz, 1H), 2.79 (dt, *J* = 8.6, 4.6 Hz, 1H), 2.08 (dtd, *J* = 13.4, 7.9, 3.6 Hz, 1H), 2.01 (ddt, *J* = 14.4, 7.4, 3.8 Hz, 1H), 1.82 (ddt, *J* = 13.3, 8.6, 4.5 Hz, 1H), 1.75 (ddt, *J* = 12.6, 7.9, 4.2 Hz, 1H), 1.61 – 1.50 (m, 1H), 1.52 – 1.33 (m, 3H). **¹³C NMR (126 MHz, CDCl₃):** δ 209.56, 174.51, 147.83, 146.58, 128.17, 122.73, 110.12, 108.42, 101.08, 51.77, 48.81, 47.12, 42.88, 26.28, 26.07, 23.98, 23.66. **HRMS:** (ESI-TOF) calculated for ([C₁₆H₁₈O₅ + Na]⁺): 313.1046, found 313.1044. **IR (ATR, cm⁻¹):** 2933, 2858, 1736, 1699, 1503, 1489, 1443, 1364, 1245, 1037, 928, 811, 735. **Optical Rotation:** [α]_D²⁶ -31.3 (*c* 0.65, CHCl₃). **HPLC:** ChiralPak[®] IC, 10% IPA in Hexanes, 60 min run, 1 mL/min (sample prep in HPLC grade acetone).

Racemic std:



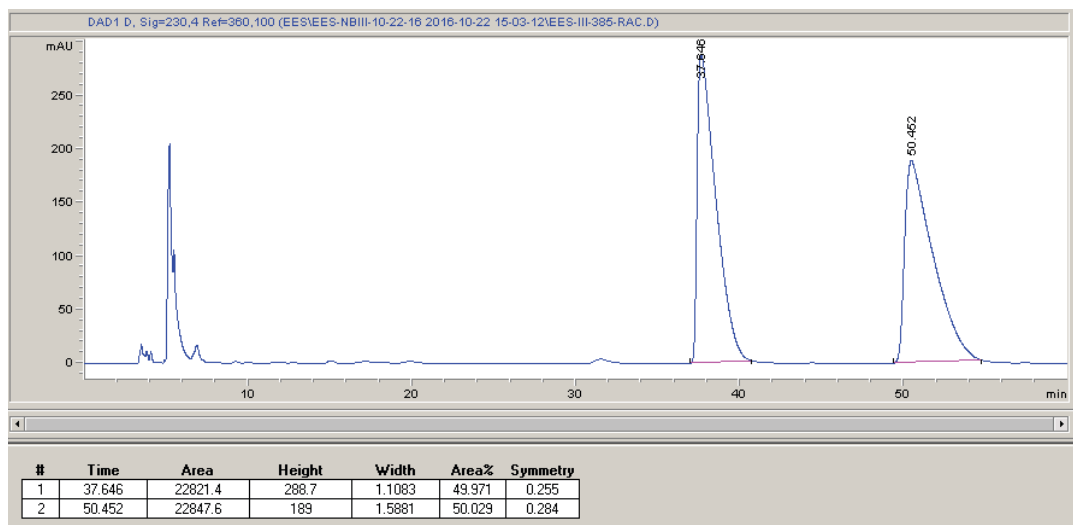
Enantioenriched:



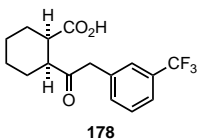
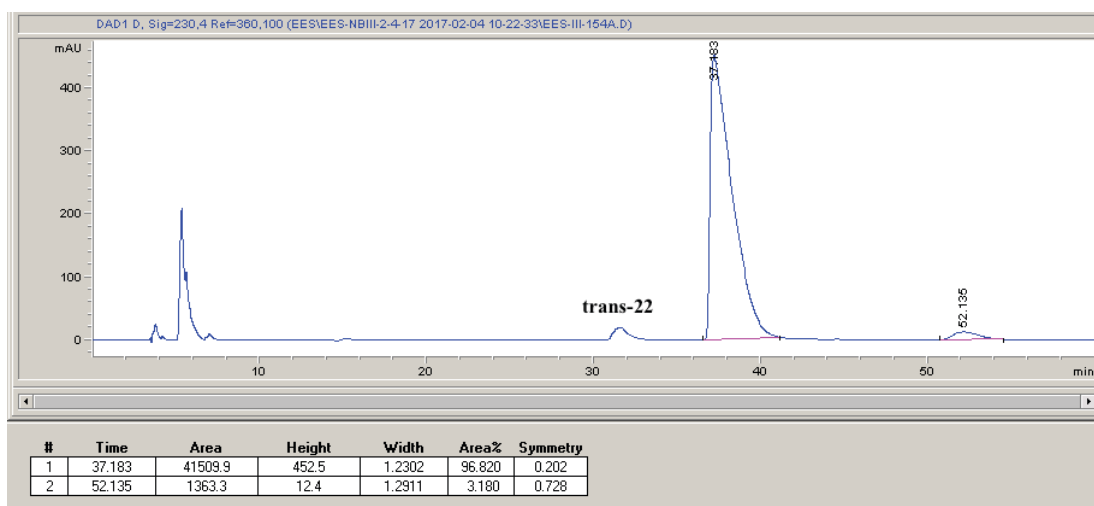
According to general procedure **B**, anhydride **4** (38.5 mg, 0.25 mmol) and *p*-methoxybenzyl trifluoroborate (68.4 mg, 0.3 mmol) afforded the product as a pale yellow oil (58.7 mg, 85% yield, 94% ee, >20:1 dr). Run 2 afforded 95% yield, 94% ee, >20:1 dr. NMR data based on methyl ester. **¹H NMR (501 MHz, CDCl₃):** δ 7.03 (d, *J* = 8.1 Hz, 2H), 6.83 – 6.76 (m, 2H), 3.72 (s, 3H), 3.66 (s, 2H), 3.54 (s, 3H), 2.89 – 2.78 (m, 1H), 2.75 – 2.67 (m, 1H), 2.07 – 1.85 (m, 2H), 1.85 – 1.60 (m, 2H), 1.58 – 1.44 (m, 1H), 1.44 – 1.24 (m, 3H). **¹³C NMR (126 MHz, CDCl₃):** δ 209.78, 174.54, 158.59, 130.65, 126.63, 114.11, 55.39, 51.74, 48.79, 46.65,

42.82, 26.27, 26.08, 24.00, 23.66. **HRMS:** (ESI-TOF) calculated for $([C_{16}H_{20}O_4 - H]^-)$: 275.1289, found: 275.1287. **IR (ATR, cm^{-1}):** 2934, 2855, 1736, 1612, 1513, 1450, 1368, 1229, 1217, 1033, 800. **Optical Rotation:** $[\alpha]_D^{26}$ -27.5 (c 0.63, $CHCl_3$). **HPLC:** ChiralPak[®] ID, 5% IPA in Hexanes, 60 min run, 1 mL/min (sample prep in HPLC grade acetone).

Racemic Std:



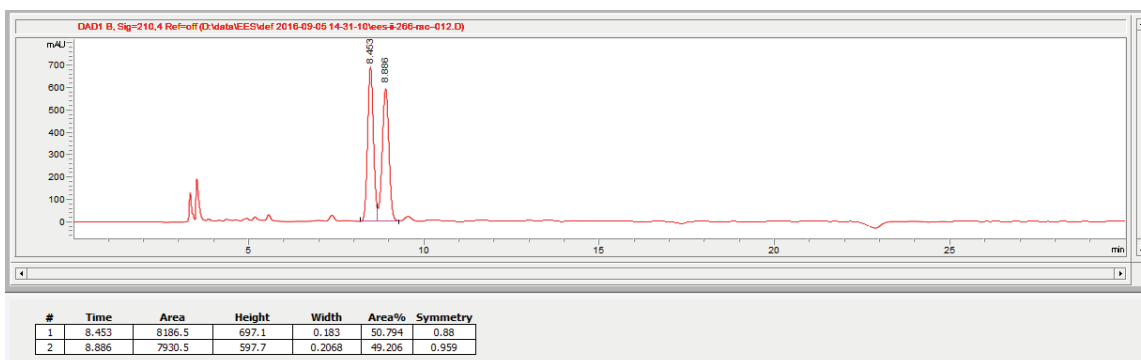
Enantioenriched:



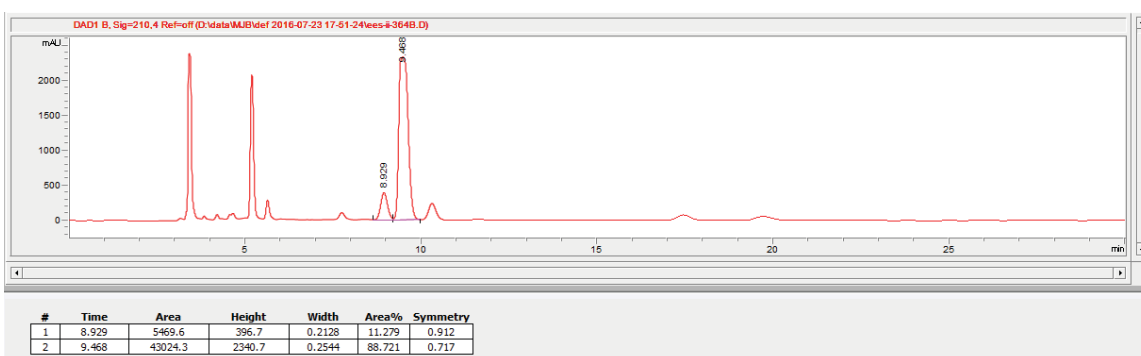
According to general procedure A, anhydride **4** (38.5 mg, 0.25 mmol) and *m*-trifluoromethylbenzyl trifluoroborate (79.8 mg, 0.3 mmol) afforded the product

as a pale yellow oil (31.6 mg, 40% yield, 75% ee, 7.3:1 dr). Run 2 afforded 37% yield, 77% ee, 7.3:1 dr. **HPLC:** ChiralPak[®] IC, 5% IPA in Hexanes, 60 min run, 1 mL/min.

Racemic Std:



Enantioenriched:



General Procedure for stoichiometric UV/Vis studies of oxidative addition: All materials were prepared in an N₂-filled glovebox. Analyte solutions were dispensed into the cuvette, and the cuvette sealed with a Teflon septum and cap, then further sealed with electrical tape. All spectra were taken immediately following removal of the sample from the glovebox. The Ni(cod)₂ (6.68 x 10⁻⁵ M in THF) spectrum was taken from earlier work.⁵

Ligand solution (LS): A ligand stock solution was prepared as follows: ligand (0.018 mmol) was weighed into a 2-dram vial equipped with a Teflon coated stir bar, then 1.0 mL of THF was added. The stock solution was further diluted with THF to a final concentration of 3.6 x 10⁻⁴ M.

Nickel + ligand solution (CS): A catalyst stock solution was prepared as follows: Ni(cod)₂ (5.0 mg, 0.018 mmol) and ligand (1 equiv, 0.018 mmol) were weighed into a 2-dram vial equipped with a Teflon coated stir bar, then 1.0 mL of THF was added. The stock solution was stirred for ~10 min to ensure ligation, at which point any color change was noted. Then the stock solution was further diluted with THF to a final concentration of 3.6×10^{-4} M.

Anhydride solution (AS): A stock solution was prepared as follows: Anhydride **4** (5.6 mg, 0.036 mmol) was weighed into a 2-dram vial equipped with a Teflon coated stir bar, then dissolved in 1 mL THF. The stock solution was further diluted with THF to a final concentration of 3.6×10^{-4} M.

Nickel + Ligand + Anhydride solution: CS (0.2 mL) and AS (0.1 mL) were added to a 2-dram vial equipped with a Teflon coated stir bar and diluted to 0.5 mL with THF for a concentration of 7.3×10^{-3} M. The solution was allowed to stir for 10 min, at which point any color change was noted. The solution was then further diluted with THF to a final concentration of 3.6×10^{-4} M.

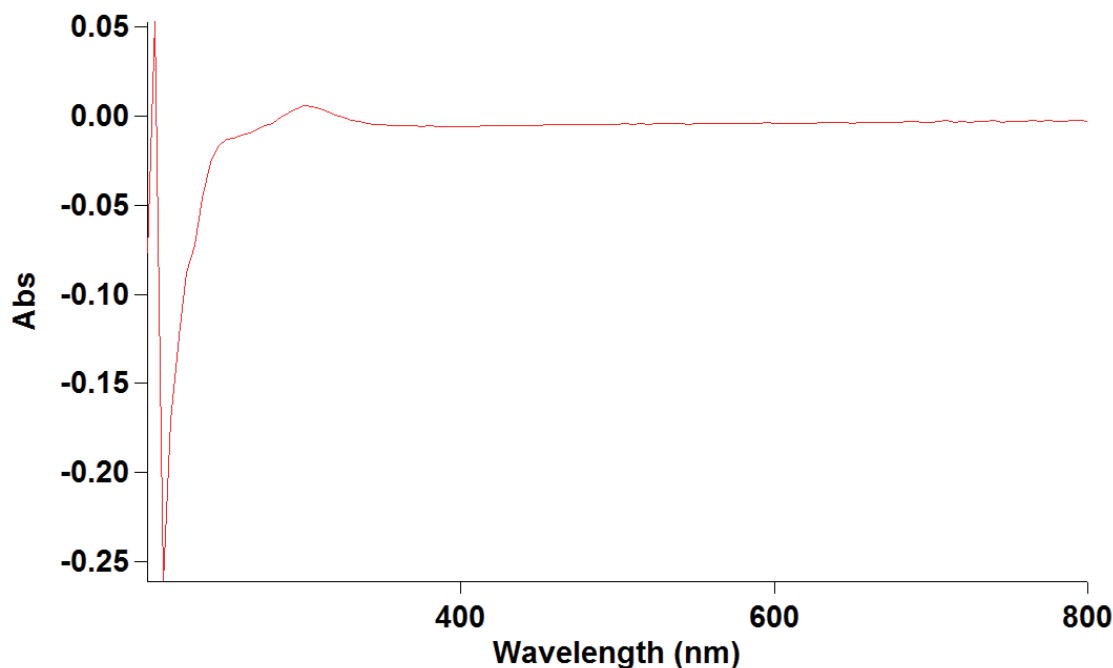


Figure A1.1. UV/Vis spectrum anhydride **4**

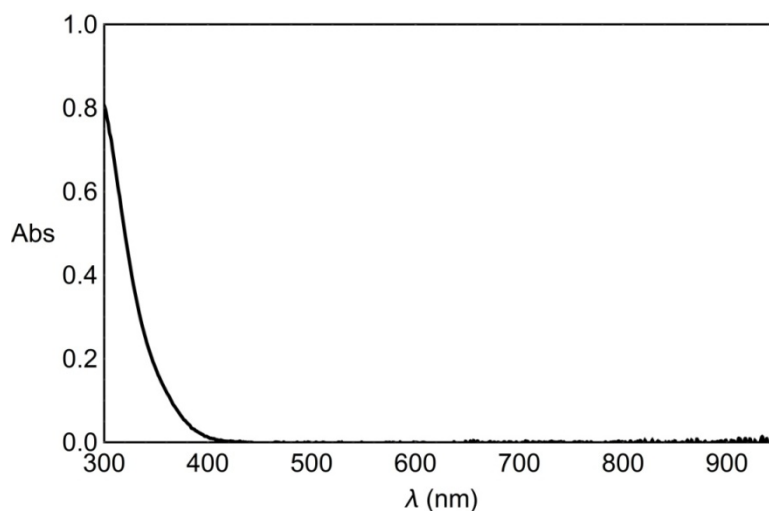


Figure A1.2. UV/Vis spectrum $\text{Ni}(\text{cod})_2$

(*S,S*)-PhBox (137):

The catalyst solution (**CS**) had no observable color change after mixing for 10 min. The mixed solution of **CS** and **AS** also had no observable color change after mixing for 10 min. To mimic the actual reaction conditions, an additional 19 equivalents of anhydride was added to the previously stirring stock solution of **CS** and **AS** and stirred an additional 10 min (total stir time in excess of 30 min). A slight color change to orange was noted at the end of 10 min.

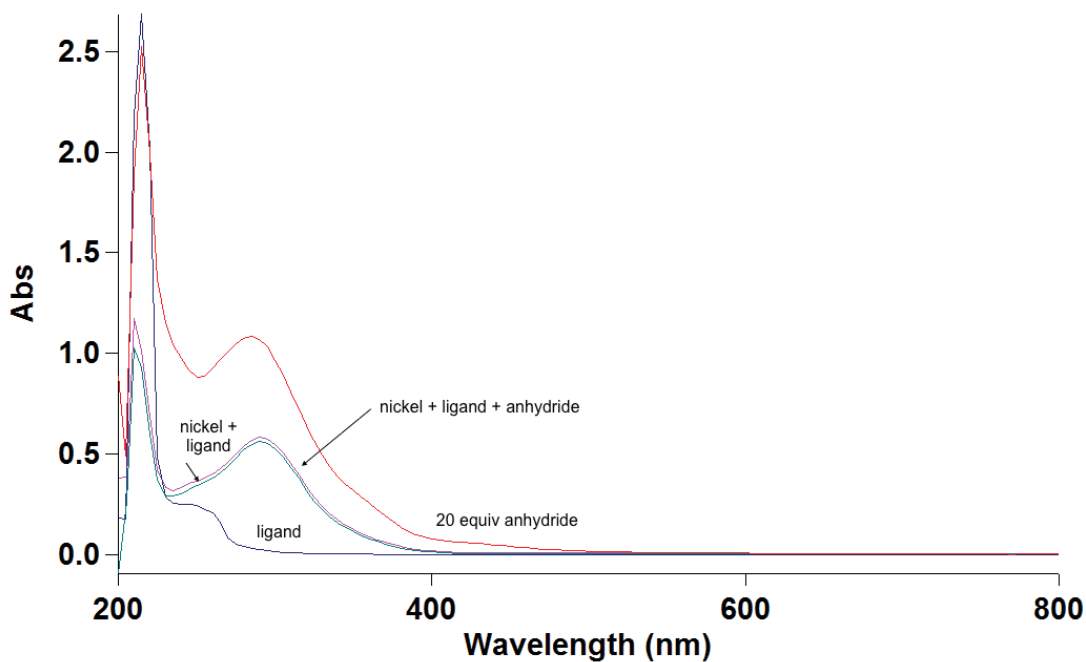


Figure A1.3. Anhydride and $\text{Ni}(\text{cod})_2$ spectra were omitted for clarity. The initial mixture of **CS** and **AS** shows no indication of oxidative addition, by color change or the development of changes in the visible region. However, after the addition of more anhydride and longer stir time, a slight change in color and change in spectrum were observed. These data suggest that oxidative addition, under stoichiometric conditions, is slow.

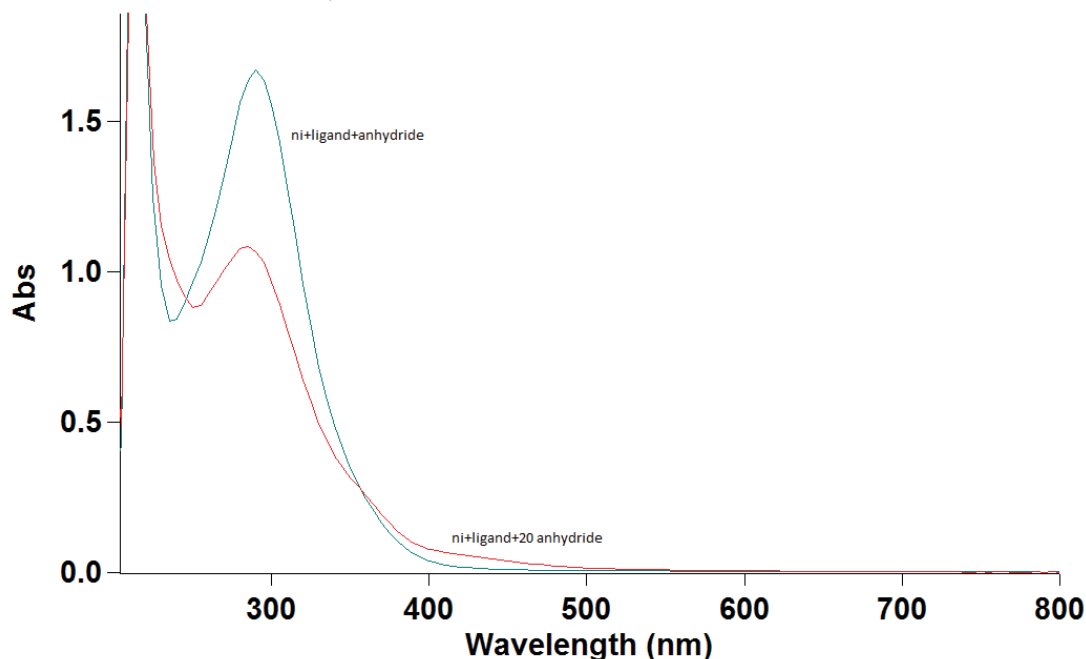


Figure A1.4. Anhydride, ligand, nickel + ligand and $\text{Ni}(\text{cod})_2$ spectra were omitted for clarity. Anhydride **4** was used stoichiometrically and in excess (20 equiv). A stir time of 10 minutes was used for mixing **CS** and **AS** according to the general procedure. With an excess of anhydride, mimicking reaction conditions, oxidative addition is observed after only 10 min.

(S)-*t*BuPyrOx (138):

The catalyst solution (**CS**) formed a deep violet color after 10 min. The mixed solution of **CS** and **AS** formed a red color (within 1 min of mixing) and maintained the color after 10 min.

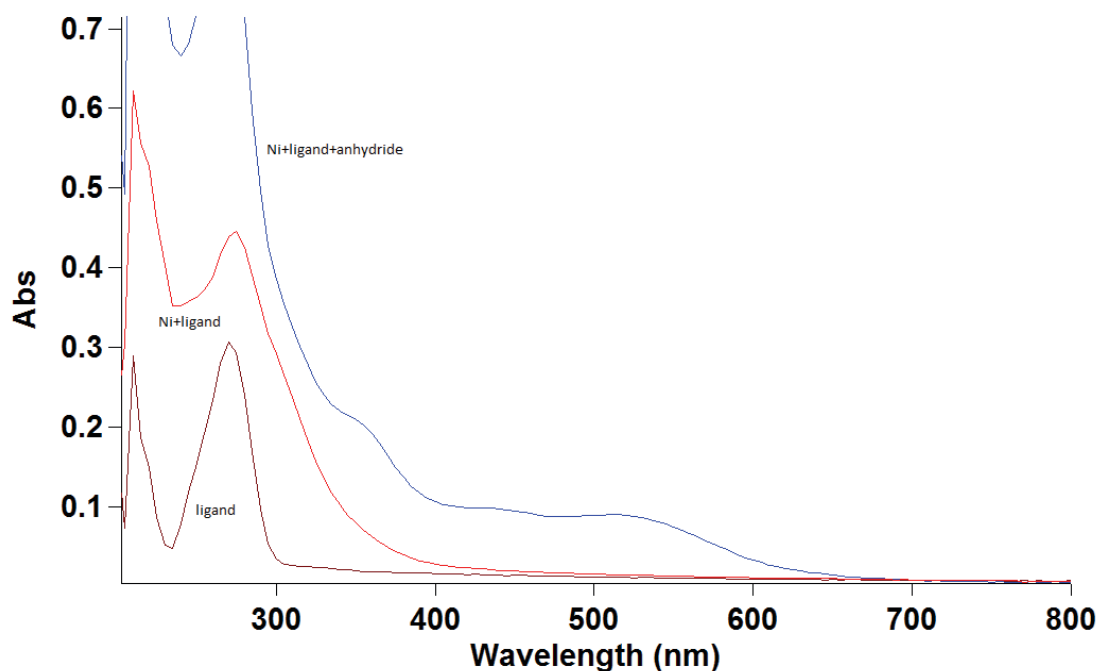


Figure A1.5. Anhydride and $\text{Ni}(\text{cod})_2$ spectra were omitted for clarity. A significant change, consistent with the color change and probable oxidative addition, is observed in the spectrum, developing features in the 350-500 nm range. These data suggest that oxidative addition is occurring (within 10 min) under these catalyst conditions.

(*S*)-6-Me-*t*BuPyrOx (151):

The catalyst solution (**CS**) formed a dark green color after 10 min. The mixed solution of **CS** and **AS** formed a red color (within 2 min of mixing) and maintained the color after 10 min.

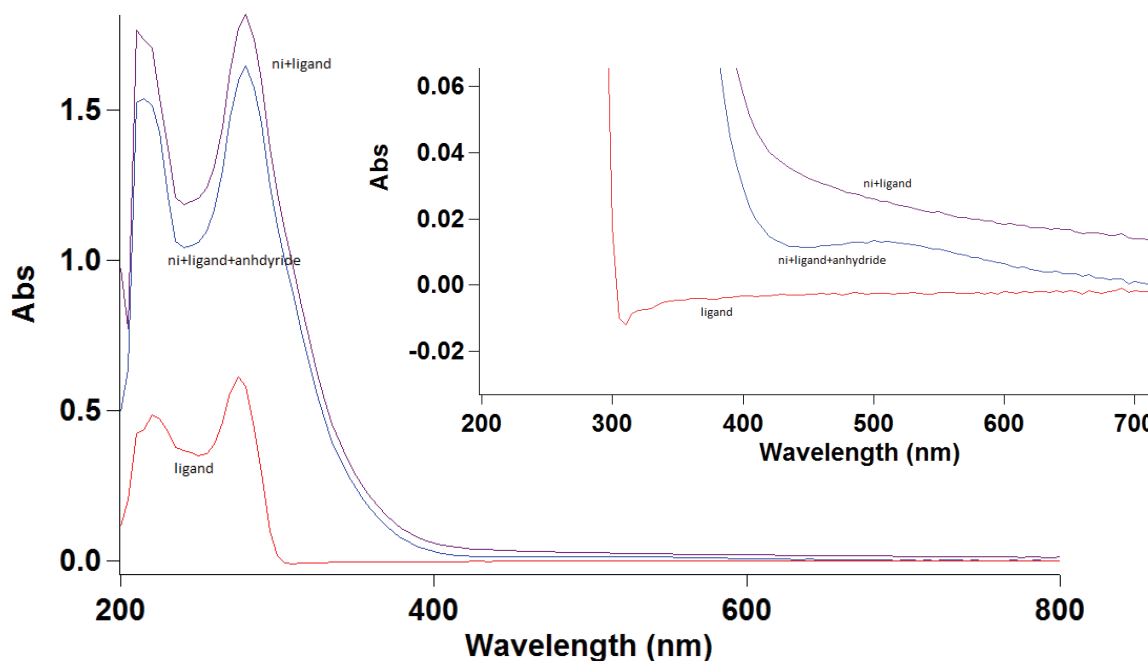


Figure A1.6. Anhydride and Ni(cod)₂ spectra were omitted for clarity. A small but significant change, consistent with the color change and probable oxidative addition, is observed in the spectrum, developing a feature at 500 nm. These data suggest that oxidative addition is occurring (within 10 min) under these catalyst conditions.

Stoichiometric competition studies to probe oxidative addition:⁶

Procedure A: Cyclohexanecarboxylic anhydride **4** (1.9 mg, 0.013 mmol, 1 equiv) and benzyl trifluoroborate (2.0 mg, 0.01 mmol, 0.8 equiv) were weighed into a 1-dram vial equipped with a Teflon coated stirbar. The reaction tube was then brought into an N₂-filled glovebox. Then a pre-stirred dissolved solution of Ni(cod)₂ (3.4 mg, 0.013 mmol, 1 equiv) and (-)-2,2'-Isopropylidenebis-(4*S*)-4-phenyl-2-oxazoline (**137**) (3.1 mg, 0.015 mmol, 1.2 equiv) in 0.9 mL of THF was added. The reaction was stirred for 10 min. After 10 min a solution of anhydride **23** (2.3 mg, 0.013 mmol, 1 equiv) in 0.1 mL of THF was added, and the reaction stirred for an additional 10 min. 4CzIPN (7.9 mg, 0.01 mmol, 0.8 equiv) was added and the reaction vial sealed with a septa cap. The vial was wrapped with electrical tape, and then removed from the glovebox, where it was immediately irradiated with a 34 W blue LED lamp, ~3 cm from the light source for 1 h. A

fan was used to keep the reaction cool. After 1 h, the reaction was diluted with equal volumes Et₂O and 1 M HCl. The organic layer was dried over Na₂SO₄, filtered and concentrated and analyzed by ¹H NMR to determine the product ratio.

Procedure **B**: Following procedure **A**, addition of anhydride **23** and anhydride **4** was reversed.

Procedure **C**: Following procedure **A**, upon addition of **23** no 10 min stir was performed.

Procedure **D**: Following procedure **A**, anhydrides **4** and **23** were both added initially and stirred for 10 min with nickel and ligand.

Scale up procedure: Scale-up reaction, 0.5 mmol. Procedure: Cyclohexanecarboxylic anhydride **4** (77.1 mg, 0.50 mmol) and benzyl trifluoroborate (119 mg, 0.60 mmol) were weighed into a 20 mL scintillation vial, equipped with a teflon coated stirbar. The reaction vessel was then brought into an N₂-filled glovebox. Ni(cod)₂ (6.9 mg, 0.025 mmol) and (-)-2,2'-Isopropylidenebis-(4*S*)-4-phenyl-2-oxazoline (**137**) (10.0 mg, 0.030 mmol) were added to the vial, along with 10 mL dioxane. The mixture was allowed to stir for ~10 minutes at room temperature, at which point the reaction mixture became homogenous. 4CzIPN (7.9 mg, 0.010 mmol) was added and the reaction vessel sealed with a septa cap. The vial was removed from the glovebox, where it was immediately irradiated with the Merck photoreactor (450 nm light). A fan was used to keep the reaction cool. After 24 h, the reaction tube was removed from the light source, and the solvent was removed. The residue was dissolved in 1 M HCl (30 mL) and diethyl ether (30 mL). The aqueous layer was extracted once with additional diethyl ether (15 mL). The combined ether layers were then extracted with sat. aq. Na₂CO₃ (4 x 25 mL). The combined aqueous layers were acidified with conc. HCl until ~ pH 2. The aqueous layer was extracted with diethyl ether (3 x 30 mL). The combined organic layers were washed with brine (30 mL) and then dried over Na₂SO₄, filtered

and concentrated. The crude product was purified over silica gel using CH₂Cl₂ -> 5% MeOH in CH₂Cl₂ to afford **132** (92.1 mg, 75% yield, 89% ee, 19:1 dr).

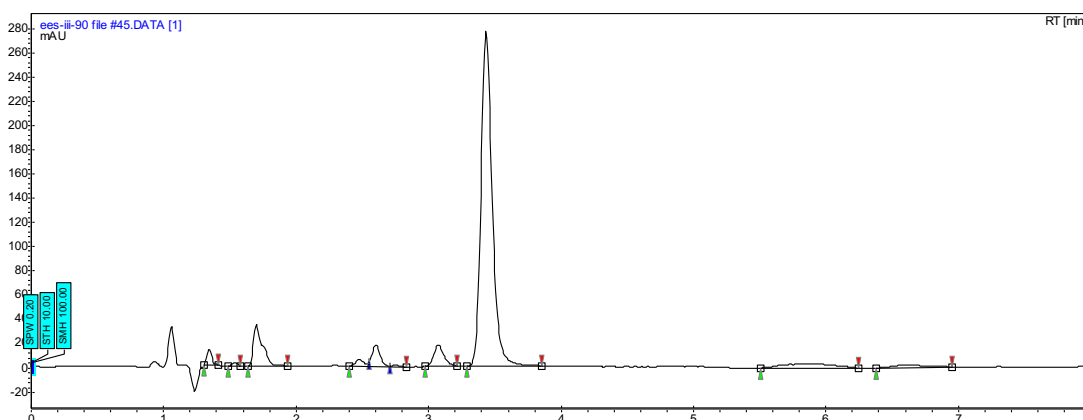


Figure A1.7. Diastereomers and enantiomers were separated using preparative HPLC analysis on a chiral stationary phase (AD-H 2 x 25 cm, 15% EtOH/CO₂, 100 bar, 70 mL/min, 220 nm). In the process, the minor enantiomer was also removed, leaving the product in excess of 99% ee.

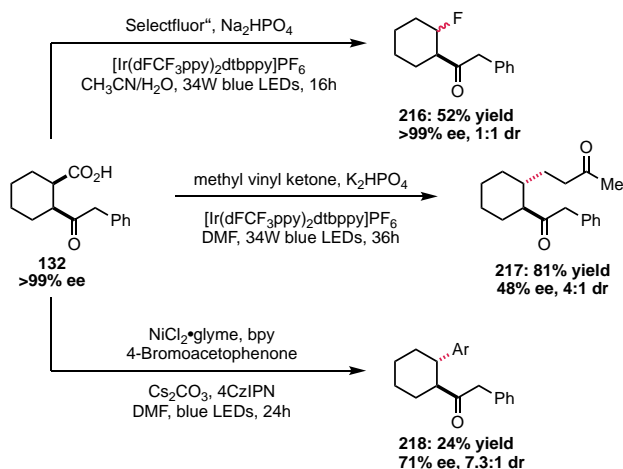
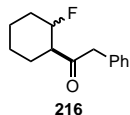


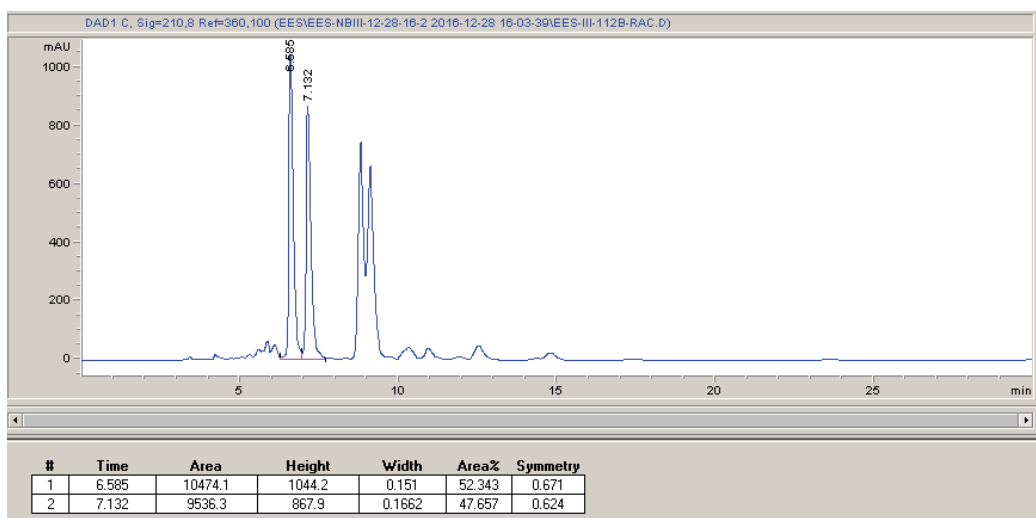
Figure A1.8 Derivatization reactions. The use of acyl electrophiles such as anhydrides in cross coupling has been investigated by a number of research groups, but in the case of acyclic electrophiles, the acyl leaving group is lost as stoichiometric waste. In the case of meso cyclic anhydrides, the resultant product is a carboxylic acid, which can act as a traceless functional group for manipulation into further molecular complexity. For example, conversion of the carboxylic acid into the corresponding fluoride using Selectfluor[®] provides the fluorinated product in good yield with no erosion of enantioselectivity.⁷ Carbon–carbon bond formation via decarboxylative Michael addition is also possible in excellent yield, good diastereoselectivity.⁸ Interestingly, racemization of the ketone stereocenter was observed, eroding the enantioselectivity. Further, Ni/photoredox-catalyzed arylation of the keto-acid generates **218** in good diastereoselectivity albeit in low yield.⁹ Again, racemization of the ketone stereocenter was observed, eroding the enantioselectivity. These examples highlight the power of photoredox catalysis combined with

cross coupling catalysis to access complex products in modest to high enantioselectivity from simple symmetric starting materials in two steps.

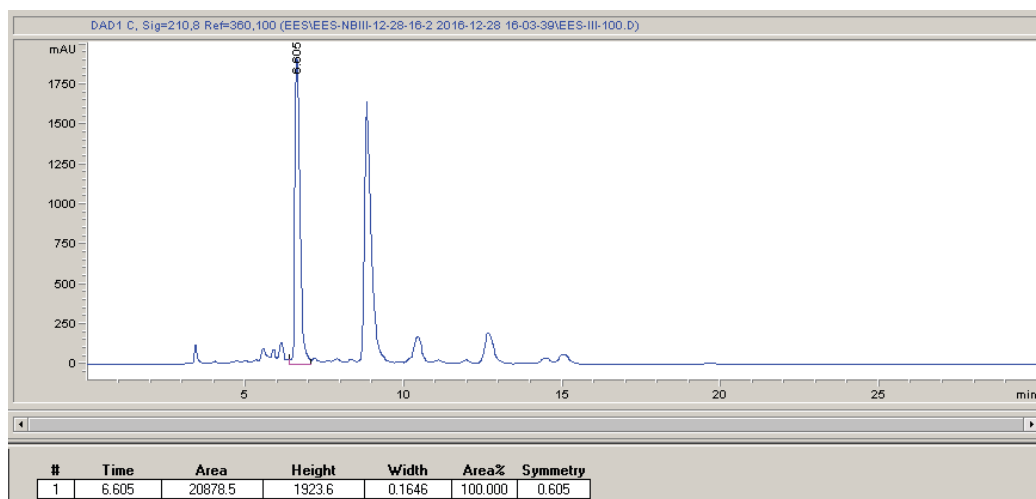


Procedure for decarboxylative fluorination: Enantiopure keto acid **132** (80 mg, 0.325 mmol), Selectfluor® (345 mg, 0.974 mmol), Na₂HPO₄ (92 mg, 0.650 mmol), [Ir(dFCF₃ppy)₂dtbbpy]PF₆ (3.6 mg, 0.00325 mmol) were weighed into a 2-dram vial. MeCN/H₂O (1:1, 3.3 mL) was added, a stirbar added and the vial sealed with a teflon septum. The contents were degassed for 10 minutes with stirring with N₂ by sparging. The vial was then irradiated with two 34 W blue LED lamps ~4cm from the vial, with a fan used for cooling for 17 h. Upon completion of the reaction, the reaction was extracted with diethyl ether (3 x 10 mL). The combined organic layers were dried over Na₂SO₄, filtered and concentrated. The crude oil was purified over silica gel using hexanes → 15% EtOAc in hexanes to afford a yellow oil (37.2 mg, 52% yield, >99% ee, 1:1 dr). **¹H NMR (501 MHz, CDCl₃):** Isolated as 1:1 mixture of diastereomers. See NMR spectra for details. **¹³C NMR (126 MHz, CDCl₃):** δ Isolated as 1:1 mixture of diastereomers. See NMR spectra for details. **¹⁹F NMR (282 MHz, CDCl₃):** δ -171.04 and -171.22. **HRMS:** (ESI-TOF) calculated for ([C₁₄H₁₇FO + Na]⁺): 243.1156, found 243.1160. **IR (ATR, cm⁻¹):** 2939, 2865, 1711, 1497, 1452, 1327, 1119, 1030, 953, 806, 752, 703. **HPLC:** **Isomer 1:** Chiralcel® OD-H, 5% IPA in Hexanes, 30 min run, 1 mL/min. **HPLC: Isomer 2:** ChiralPak® AS-H, 5% IPA in Hexanes, 30 min run, 1 mL/min.

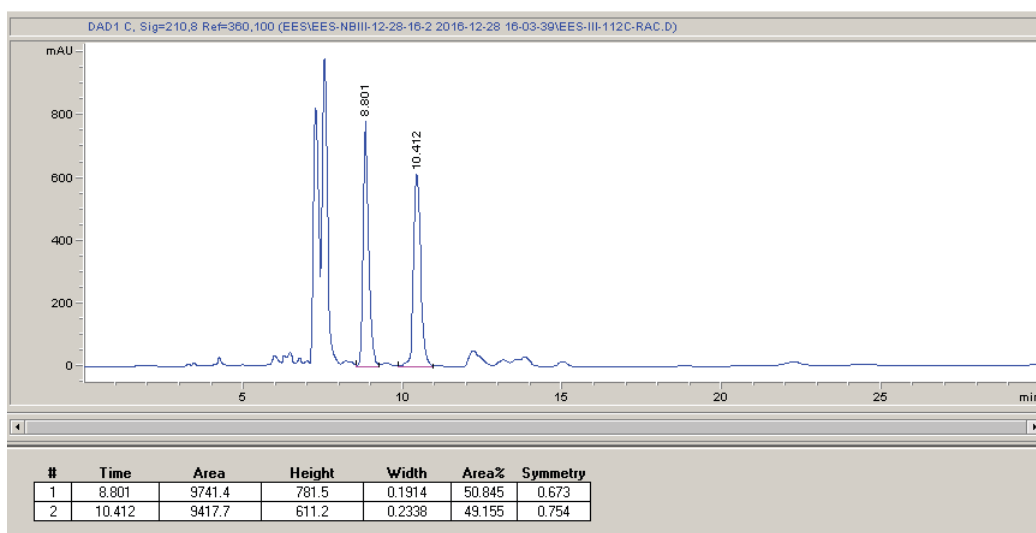
Racemic Std 1:



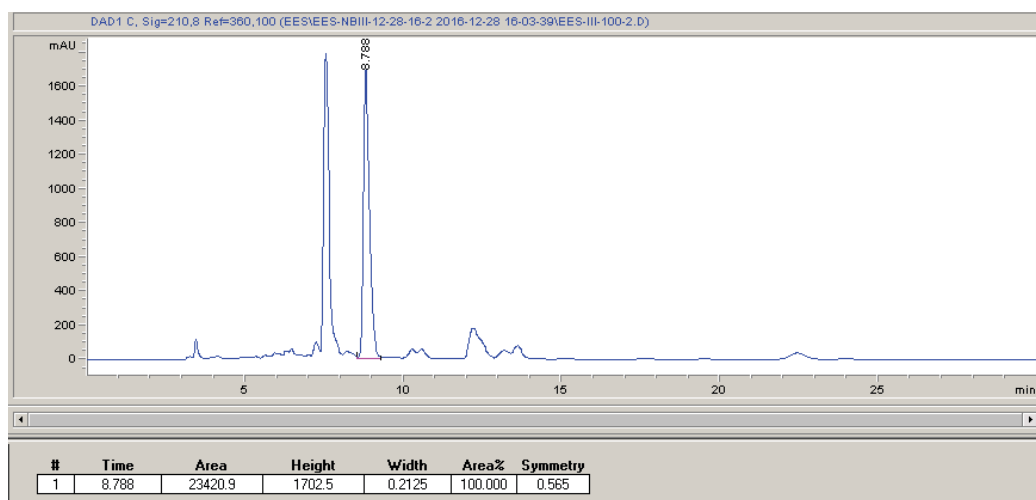
Enantioenriched 1:



Racemic Std 2:



Enantioenriched 2:



Confirmation of epimerization on ketone stereocenter:

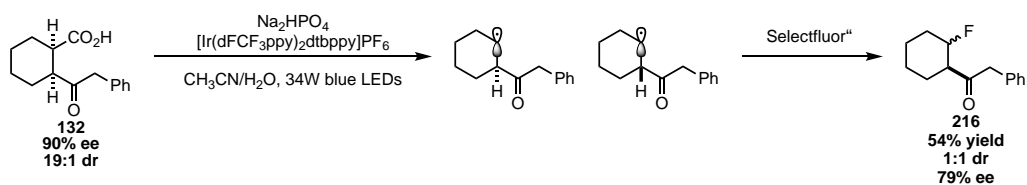
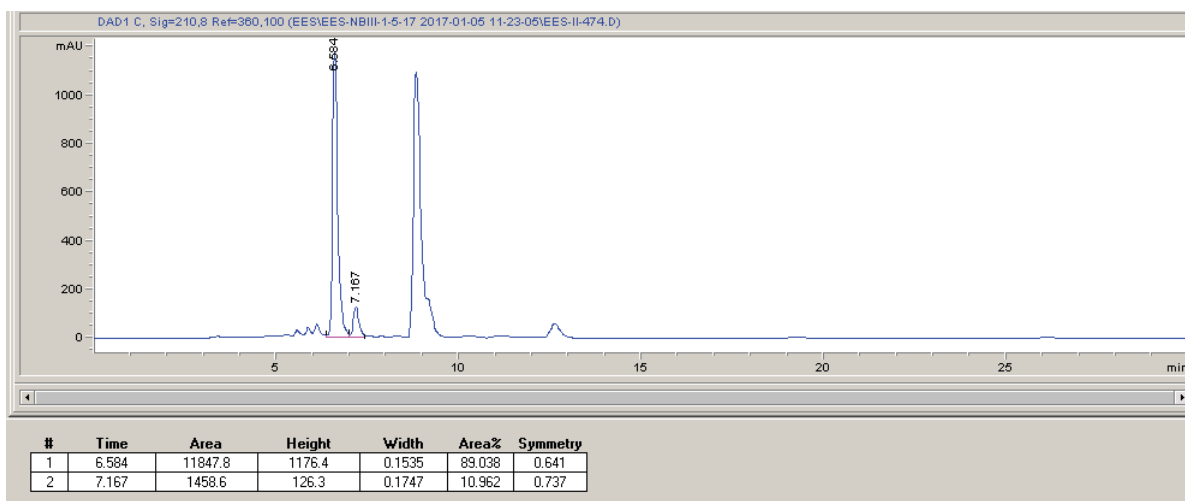
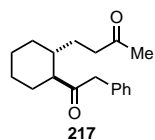
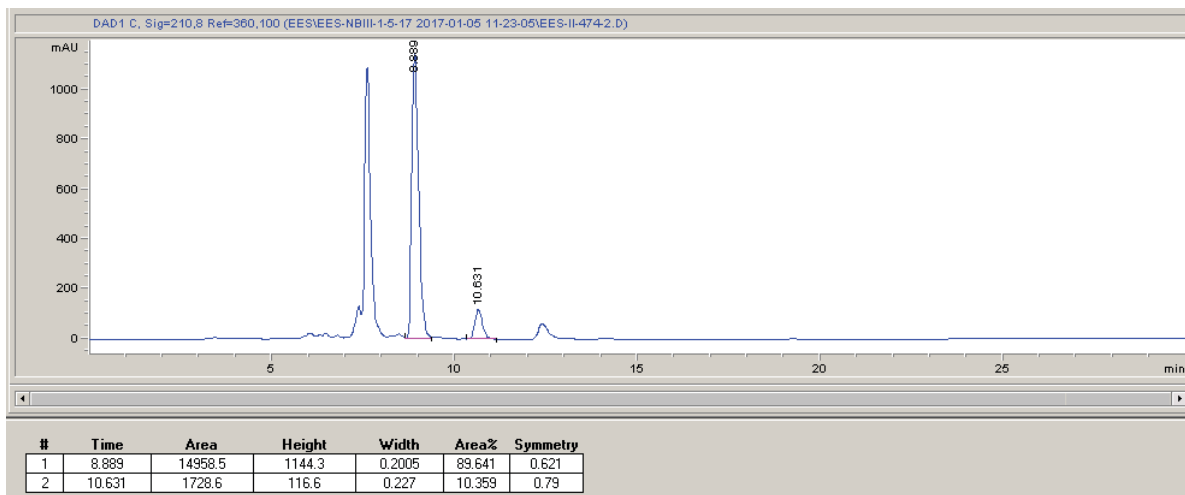


Figure A1.9. When a mixture of diastereomers **132** and **134** was employed in the fluorination reaction, an erosion of enantioselectivity was observed. This is attributed to the formation of enantiomers upon decarboxylation.

Eroded enantioenriched 1:



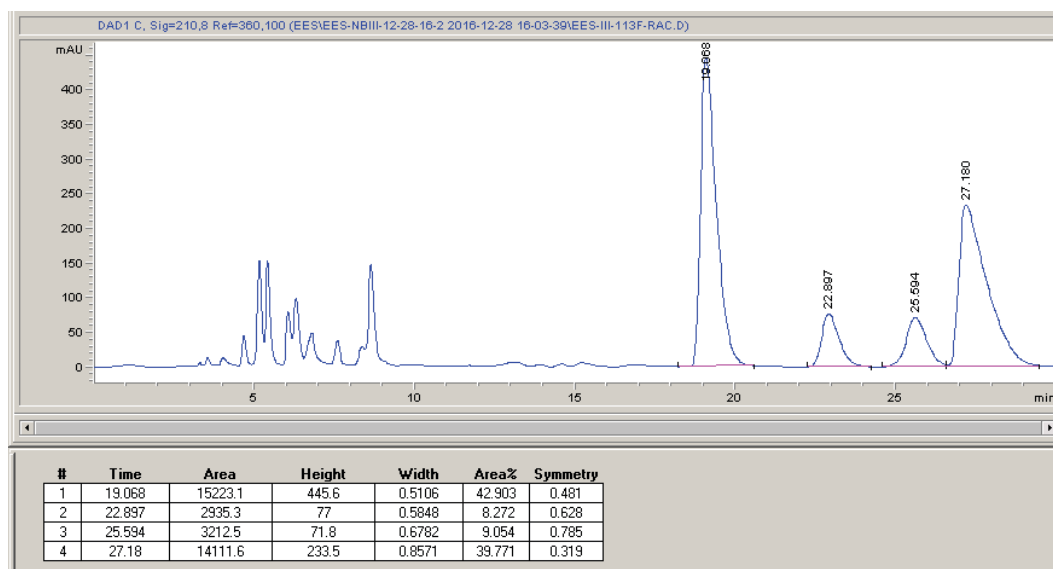
Eroded enantioenriched 2:



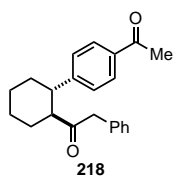
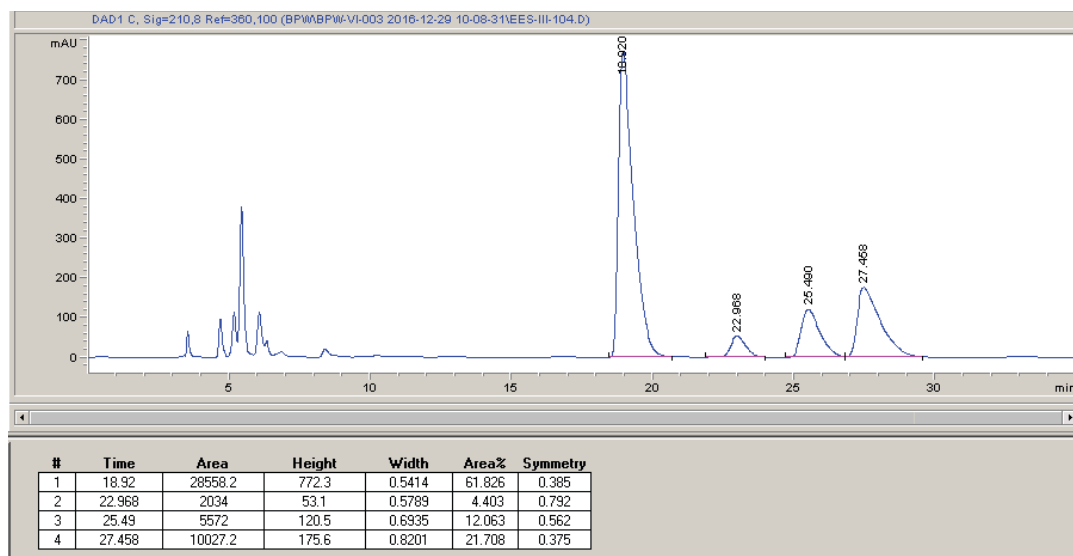
Procedure for decarboxylative alkylation: An 8 mL vial equipped with a stir bar was charged with enantiopure keto-acid **132** (63.9 mg, 0.259 mmol, 1.0 equiv), [Ir(dFCF₃ppy)₂dtbbpy]PF₆ (2.9 mg, 0.0026 mmol, 1.0 mol%), K₂HPO₄ (54 mg, 0.311 mmol, 1.2 equiv) and DMF (0.65 mL, 0.4M). The mixture was sealed with a Teflon septum and the contents were degassed for 10 minutes with stirring with N₂ by sparging. At the same time, methyl vinyl ketone (used without purification) was sparged by N₂. Under N₂, methyl vinyl ketone (21.0 μ L, 0.259 mmol, 1.0 equiv) was added to the reaction. The vial was sealed with electrical tape, then irradiated with a 34 W blue LED lamp for 36 h, using a fan for cooling. Upon completion, the

reaction was diluted with sat. aq. NaHCO₃ and extracted with Et₂O (3x20mL). The combined organic layers were washed with water and brine, dried over Na₂SO₄ and concentrated. The crude oil **xx** was purified over silica gel using hexanes → 10% EtOAc in hexanes to afford a yellow oil (56.8 mg, 81% yield, 48% ee, 4:1 dr). **¹H NMR (501 MHz, CDCl₃):** δ 7.32 (dd, *J* = 8.3, 6.6 Hz, 2H), 7.28 – 7.24 (m, 1H), 7.23 – 7.18 (m, 2H), 3.79 – 3.66 (m, 2H), 2.37 – 2.25 (m, 3H), 2.05 (m, 3H), 1.83 – 1.66 (m, 4H), 1.49 – 1.39 (m, 1H), 1.31 – 1.11 (m, 4H). **¹³C NMR (126 MHz, CDCl₃):** δ 211.64, 209.06, 133.97, 129.76, 128.75, 127.09, 55.90, 49.74, 41.01, 37.54, 30.62, 30.24, 29.84, 28.54, 25.89, 25.67. **HRMS:** (ESI-TOF) calculated for ([C₁₈H₂₄O₂ + Na]⁺): 295.1669, found 295.1669. **IR (ATR, cm⁻¹):** 2926, 2855, 1737, 1709, 1496, 1448, 1359, 1219, 1164, 1031, 704. **HPLC:** Chiralcel[®] OJ-H, 5% IPA in Hexanes, 35 min run, 1 mL/min.

Racemic std:



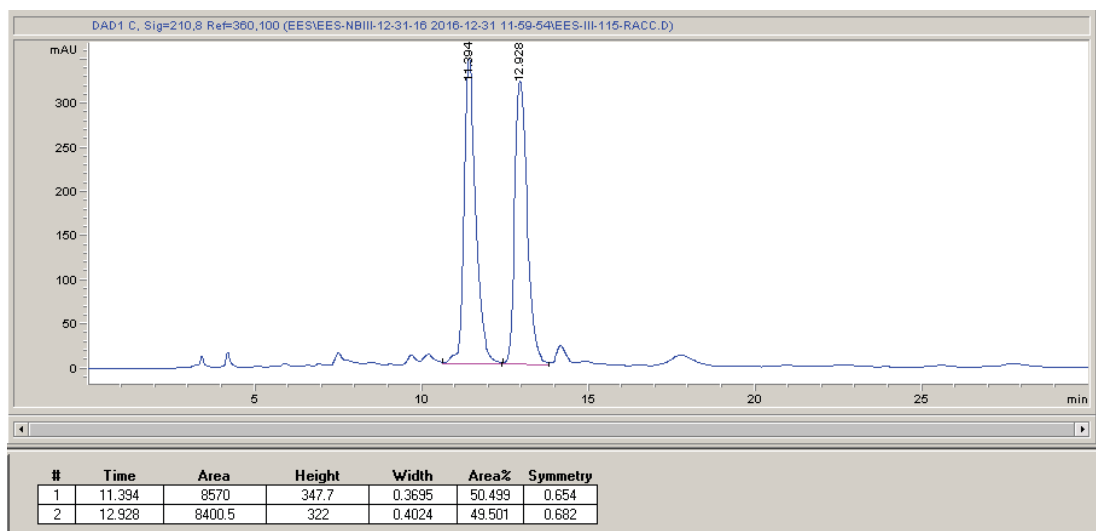
Enantioenriched:



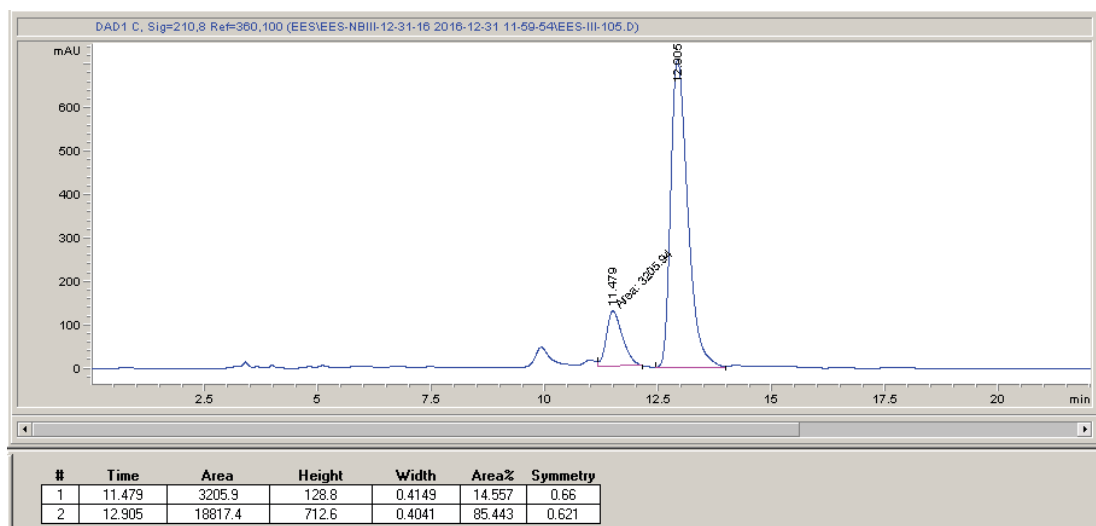
Procedure: A 20 mL vial equipped with a stir bar was charged with enantiopure keto-acid **132** (104 mg, 0.422 mmol, 3.0 equiv), $\text{NiCl}_2 \cdot \text{glyme}$ (3.1mg, 0.0141 mmol, 10 mol%), 2,2'-bipyridine (3.3 mg, 0.0212 mmol, 15 mol%), 4CzIPN (2.8 mg, 0.0034 mmol, 2.5 mol%), Cs_2CO_3 (137 mg, 0.422 mmol, 3.0 equiv), 4-bromoacetophenone (28 mg, 0.141mmol, 1.0 equiv) and DMF (7.1 mL, 0.02M). The mixture was sealed with a Teflon septum and the contents were degassed for 10 minutes with stirring with N_2 by sparging. The vial was sealed with electrical tape, then irradiated in the Merck photobox at 450 nm for 24 h, using a fan for cooling. Upon completion, the reaction was poured into 40 mL water and extracted with EtOAc (3 x 20 mL). The combined organic layers were washed with brine, dried over Na_2SO_4 and concentrated. The crude oil was purified over silica gel using hexanes \rightarrow 15% EtOAc in hexanes to afford a yellow oil (10.9 mg, 24% yield, 71% ee, 7.3:1 dr). **^1H NMR (501 MHz, CDCl_3):** δ 7.78 (d, $J = 7.9$ Hz, 2H), 7.23 – 7.09 (m, 5H), 6.83 (dd, $J = 6.8, 2.5$ Hz, 2H), 3.40 – 3.29 (m, 2H), 2.94 – 2.81 (m, 2H), 2.57 (s, 3H), 1.97 – 1.76 (m, 4H), 1.53 – 1.11 (m, 4H). **^{13}C NMR (126 MHz, CDCl_3):** δ 210.14, 197.80, 150.46, 135.31, 133.28, 129.41, 128.57, 128.53, 127.63, 126.82, 55.16, 50.22, 46.00, 33.60, 29.91, 26.61, 25.94, 25.56. **HRMS:** (ESI-TOF) calculated for $[\text{C}_{22}\text{H}_{25}\text{O}_2 +$

H]⁺): 321.1849, found 321.1850. **IR (ATR, cm⁻¹):** 3019, 2926, 2855, 1735, 1708, 1681, 1495, 1447, 1267, 1216, 750, 703. **Optical Rotation:** [α]_D²⁶ +7.3 (c 0.19, CHCl₃). **HPLC:** Chiralcel[®] OD-H, 5% IPA in Hexanes, 30 min run, 1 mL/min.

Racemic std:



Enantioenriched:



Confirmation of absolute stereochemistry:

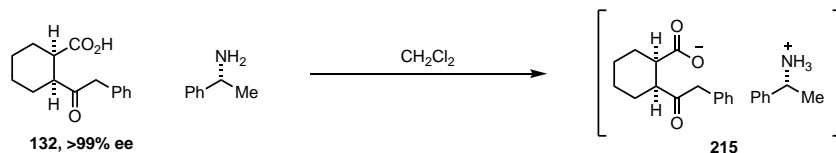


Figure A1.10. Enantiopure **132** was mixed in a 1:1 ratio with (*R*)-(+)- α -methylbenzylamine in CH_2Cl_2 at room temperature. After a few minutes of stirring, a precipitate began to form and afforded the ammonium salt (**215**). The salt was recrystallized by slow evaporation from Et_2O to afford an X-ray quality crystal, confirming the absolute stereochemistry.

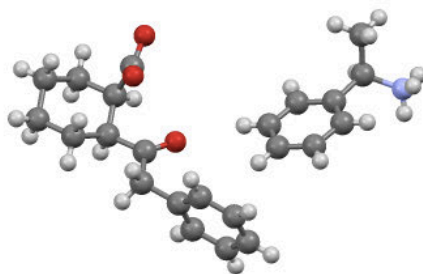


Figure A1.11. X-Ray structure of **215**. A thin rod-like specimen of $\text{C}_{23}\text{H}_{29}\text{NO}_3$, approximate dimensions 0.043 mm x 0.069 mm x 0.282 mm, was used for the X-ray crystallographic analysis. The X-ray intensity data were measured.

A total of 5790 frames were collected. The total exposure time was 40.19 hours. The frames were integrated with the Bruker SAINT software package using a narrow-frame algorithm. The integration of the data using a monoclinic unit cell yielded a total of 15314 reflections to a maximum θ angle of 68.24° (0.83 \AA resolution), of which 3613 were independent (average redundancy 4.239, completeness = 99.8%, $R_{\text{int}} = 2.65\%$, $R_{\text{sig}} = 2.18\%$) and 3500 (96.87%) were greater than $2\sigma(F^2)$. The final cell constants of $a = 10.8239(7) \text{ \AA}$, $b = 6.0156(4) \text{ \AA}$, $c = 15.9544(10) \text{ \AA}$, $\beta = 104.142(2)^\circ$, volume = $1007.34(11) \text{ \AA}^3$, are based upon the refinement of the XYZ-centroids of 9869 reflections above $20 \sigma(I)$ with $5.712^\circ < 2\theta < 140.2^\circ$. Data were corrected for absorption effects using the multi-scan method (SADABS). The ratio of minimum to maximum apparent transmission was 0.927. The calculated minimum and maximum transmission coefficients (based on crystal size)

are 0.8420 and 0.9730.

The structure was solved and refined using the Bruker SHELXTL Software Package, using the space group P 1 21 1, with $Z = 2$ for the formula unit, $C_{23}H_{29}NO_3$. The final anisotropic full-matrix least-squares refinement on F^2 with 255 variables converged at $R1 = 2.52\%$, for the observed data and $wR2 = 5.98\%$ for all data. The goodness-of-fit was 1.042. The largest peak in the final difference electron density synthesis was $0.171 \text{ e}^-/\text{\AA}^3$ and the largest hole was $-0.133 \text{ e}^-/\text{\AA}^3$ with an RMS deviation of $0.027 \text{ e}^-/\text{\AA}^3$. On the basis of the final model, the calculated density was 1.212 g/cm^3 and $F(000)$, 396 e^- .

Table A1.1.

	dx/m m	2 θ /°	ω /°	ϕ /°	χ /°	Width h /°	Fram es	Tim e/s	Wave - length /Å	Volt age/ kV	Curre nt/m A	Te mp/ K
Omeg a	33.9 08	- 52.5 4	- 216.7 9	- 105.0 0	54.7 4	0.50	297	30.0 0	1.541 84	50	1.0	100
Omeg a	33.9 08	- 52.5 4	- 216.7 9	0.00	54.7 4	0.50	297	30.0 0	1.541 84	50	1.0	100
Omeg a	33.9 08	88.8 9	- 77.11	270.0 0	54.7 4	0.50	304	30.0 0	1.541 84	50	1.0	100
Omeg a	33.9 08	88.8 9	- 77.11	180.0 0	54.7 4	0.50	304	30.0 0	1.541 84	50	1.0	100
Phi	33.9 08	74.1 9	- 92.00	0.00	54.7 4	0.50	720	30.0 0	1.541 84	50	1.0	100
Omeg a	33.9 08	103. 89	- 61.12	45.00	54.7 4	0.50	300	30.0 0	1.541 84	50	1.0	100
Omeg a	33.9 08	-4.10	- 169.1 0	0.00	54.7 4	0.50	300	15.0 0	1.541 84	50	1.0	100
Omeg a	33.9 08	103. 89	- 61.12	- 45.00	54.7 4	0.50	300	30.0 0	1.541 84	50	1.0	100
Phi	33.9 08	104. 19	- 62.00	0.00	54.7 4	0.50	720	25.0 0	1.541 84	50	1.0	100
Omeg a	33.9 08	- 43.8 8	- 209.8 8	0.00	54.7 4	0.50	304	15.0 0	1.541 84	50	1.0	100

Omeg a	33.9 08	103. 89	- 61.12	0.00	54.7 4	0.50	300	25.0 0	1.541 84	50	1.0	100
Omeg a	33.9 08	- 58.8 8	- 224.8 8	0.00	54.7 4	0.50	304	15.0 0	1.541 84	50	1.0	100
Omeg a	33.9 08	103. 89	- 61.12	90.00	54.7 4	0.50	300	25.0 0	1.541 84	50	1.0	100
Phi	33.9 08	- 59.1 9	- 73.00	0.00	54.7 4	0.50	720	20.0 0	1.541 84	50	1.0	100
Phi	33.9 08	89.1 9	- 77.00	0.00	54.7 4	0.50	320	25.0 0	1.541 84	50	1.0	100

Table A1.2. Sample and crystal data for **215**.

Identification code	xx	
Chemical formula	$\text{C}_{23}\text{H}_{29}\text{NO}_3$	
Formula weight	367.47 g/mol	
Temperature	100(2) K	
Wavelength	1.54178 Å	
Crystal size	0.043 x 0.069 x 0.282 mm	
Crystal system	monoclinic	
Space group	P 1 21 1	
Unit cell dimensions	a = 10.8239(7) Å	$\alpha = 90^\circ$
	b = 6.0156(4) Å	$\beta = 104.142(2)^\circ$
	c = 15.9544(10) Å	$\gamma = 90^\circ$
Volume	1007.34(11) Å ³	
Z	2	
Density (calculated)	1.212 g/cm ³	
Absorption coefficient	0.630 mm ⁻¹	
F(000)	396	

Table A1.3. Data collection and structure refinement for **215**.

Theta range for data collection	2.86 to 68.24°
Index ranges	-13<=h<=12, -7<=k<=6, -19<=l<=19
Reflections collected	15314
Independent reflections	3613 [R(int) = 0.0265]
Coverage of independent reflections	99.8%
Absorption correction	multi-scan

Max. and min. transmission	0.9730 and 0.8420	
Structure solution technique	direct methods	
Structure solution program	SHELXT (Sheldrick, 2016)	
Refinement method	Full-matrix least-squares on F^2	
Refinement program	SHELXL-2014/7 (Sheldrick, 2014)	
Function minimized	$\sum w(F_o^2 - F_c^2)^2$	
Data / restraints / parameters	3613 / 4 / 255	
Goodness-of-fit on F^2	1.042	
Final R indices	3500 data; $I > 2\sigma(I)$	R1 = 0.0252, wR2 = 0.0591
	all data	R1 = 0.0266, wR2 = 0.0598
Weighting scheme	$w = 1/[\sigma^2(F_o^2) + (0.0227P)^2 + 0.2180P]$ where $P = (F_o^2 + 2F_c^2)/3$	
Absolute structure parameter	-0.01(6)	
Largest diff. peak and hole	0.171 and -0.133 $e\text{\AA}^{-3}$	
R.M.S. deviation from mean	0.027 $e\text{\AA}^{-3}$	

Table A1.4. Atomic coordinates and equivalent isotropic atomic displacement parameters (\AA^2).

$U(\text{eq})$ is defined as one third of the trace of the orthogonalized U_{ij} tensor.

	x/a	y/b	z/c	$U(\text{eq})$
O1	0.91501(11)	0.1636(2)	0.41199(7)	0.0212(3)
N1	0.12993(13)	0.2258(2)	0.54822(9)	0.0174(3)
C1	0.88831(14)	0.2476(3)	0.33658(10)	0.0170(3)
O2	0.88524(11)	0.4513(2)	0.32107(8)	0.0220(3)
C2	0.85891(16)	0.0831(3)	0.26061(10)	0.0174(3)
O3	0.61851(11)	0.2709(2)	0.22461(8)	0.0255(3)
C3	0.97763(17)	0.9453(3)	0.25809(12)	0.0223(4)
C4	0.07671(17)	0.0833(3)	0.22785(11)	0.0235(4)
C5	0.01981(17)	0.1833(3)	0.13924(11)	0.0242(4)
C6	0.90437(16)	0.3287(3)	0.14030(11)	0.0209(4)
C7	0.80412(15)	0.1975(3)	0.17355(10)	0.0180(3)
C8	0.68318(16)	0.3245(3)	0.17599(10)	0.0184(4)
C9	0.64234(17)	0.5125(3)	0.11135(12)	0.0241(4)
C10	0.50849(16)	0.5927(3)	0.10493(11)	0.0207(4)
C11	0.48410(18)	0.7951(3)	0.13970(11)	0.0241(4)

C12	0.35990(19)	0.8644(3)	0.13339(12)	0.0289(4)
C13	0.25863(18)	0.7323(4)	0.09260(11)	0.0302(4)
C14	0.28191(18)	0.5300(3)	0.05744(12)	0.0283(4)
C15	0.40562(17)	0.4613(3)	0.06356(11)	0.0237(4)
C16	0.35619(16)	0.2514(4)	0.62033(11)	0.0263(4)
C17	0.26076(16)	0.1717(3)	0.53907(11)	0.0199(4)
C18	0.28794(15)	0.2688(3)	0.45802(10)	0.0192(4)
C19	0.37227(16)	0.1558(3)	0.41939(11)	0.0234(4)
C20	0.40537(17)	0.2427(3)	0.34743(11)	0.0266(4)
C21	0.35454(17)	0.4424(4)	0.31253(12)	0.0255(4)
C22	0.27145(17)	0.5564(3)	0.35056(12)	0.0256(4)
C23	0.23863(17)	0.4705(3)	0.42336(11)	0.0232(4)

Table A1.5. Bond lengths (Å) for **215**.

O1-C1	1.271(2)	N1-C17	1.494(2)
N1-H1A	0.907(19)	N1-H1B	0.889(19)
N1-H1C	0.92(2)	C1-O2	1.249(2)
C1-C2	1.537(2)	C2-C7	1.534(2)
C2-C3	1.538(2)	C2-H2	1.0
O3-C8	1.209(2)	C3-C4	1.525(2)
C3-H3A	0.99	C3-H3B	0.99
C4-C5	1.521(3)	C4-H4A	0.99
C4-H4B	0.99	C5-C6	1.529(2)
C5-H5A	0.99	C5-H5B	0.99
C6-C7	1.537(2)	C6-H6A	0.99
C6-H6B	0.99	C7-C8	1.525(2)
C7-H7	1.0	C8-C9	1.521(2)
C9-C10	1.507(2)	C9-H9A	0.99
C9-H9B	0.99	C10-C11	1.390(3)
C10-C15	1.393(3)	C11-C12	1.388(3)
C11-H11	0.95	C12-C13	1.382(3)
C12-H12	0.95	C13-C14	1.388(3)
C13-H13	0.95	C14-C15	1.382(3)
C14-H14	0.95	C15-H15	0.95
C16-C17	1.524(2)	C16-H16A	0.98
C16-H16B	0.98	C16-H16C	0.98
C17-C18	1.512(2)	C17-H17	1.0
C18-C23	1.385(3)	C18-C19	1.396(2)
C19-C20	1.386(3)	C19-H19	0.95
C20-C21	1.381(3)	C20-H20	0.95
C21-C22	1.383(3)	C21-H21	0.95

C22-C23	1.394(2)	C22-H22	0.95
C23-H23	0.95		

Table A1.6. Bond angles (°) for **215**.

C17-N1-H1A	109.8(13)	C17-N1-H1B	110.8(13)
H1A-N1-H1B	107.8(19)	C17-N1-H1C	112.9(13)
H1A-N1-H1C	105.5(19)	H1B-N1-H1C	109.8(19)
O2-C1-O1	124.49(15)	O2-C1-C2	119.03(14)
O1-C1-C2	116.48(15)	C7-C2-C1	112.66(14)
C7-C2-C3	111.02(13)	C1-C2-C3	110.76(14)
C7-C2-H2	107.4	C1-C2-H2	107.4
C3-C2-H2	107.4	C4-C3-C2	111.82(15)
C4-C3-H3A	109.3	C2-C3-H3A	109.3
C4-C3-H3B	109.3	C2-C3-H3B	109.3
H3A-C3-H3B	107.9	C5-C4-C3	110.67(14)
C5-C4-H4A	109.5	C3-C4-H4A	109.5
C5-C4-H4B	109.5	C3-C4-H4B	109.5
H4A-C4-H4B	108.1	C4-C5-C6	111.25(14)
C4-C5-H5A	109.4	C6-C5-H5A	109.4
C4-C5-H5B	109.4	C6-C5-H5B	109.4
H5A-C5-H5B	108.0	C5-C6-C7	110.97(15)
C5-C6-H6A	109.4	C7-C6-H6A	109.4
C5-C6-H6B	109.4	C7-C6-H6B	109.4
H6A-C6-H6B	108.0	C8-C7-C2	110.26(13)
C8-C7-C6	115.75(15)	C2-C7-C6	113.17(14)
C8-C7-H7	105.6	C2-C7-H7	105.6
C6-C7-H7	105.6	O3-C8-C9	121.03(15)
O3-C8-C7	121.20(15)	C9-C8-C7	117.67(14)
C10-C9-C8	113.54(14)	C10-C9-H9A	108.9
C8-C9-H9A	108.9	C10-C9-H9B	108.9
C8-C9-H9B	108.9	H9A-C9-H9B	107.7
C11-C10-C15	118.58(16)	C11-C10-C9	121.78(17)

C15-C10-C9	119.64(16)	C12-C11-C10	120.63(18)
C12-C11-H11	119.7	C10-C11-H11	119.7
C13-C12-C11	120.29(19)	C13-C12-H12	119.9
C11-C12-H12	119.9	C12-C13-C14	119.55(17)
C12-C13-H13	120.2	C14-C13-H13	120.2
C15-C14-C13	120.13(18)	C15-C14-H14	119.9
C13-C14-H14	119.9	C14-C15-C10	120.82(18)
C14-C15-H15	119.6	C10-C15-H15	119.6
C17-C16-H16A	109.5	C17-C16-H16B	109.5
H16A-C16-H16B	109.5	C17-C16-H16C	109.5
H16A-C16-H16C	109.5	H16B-C16-H16C	109.5
N1-C17-C18	112.73(14)	N1-C17-C16	108.04(13)
C18-C17-C16	111.89(14)	N1-C17-H17	108.0
C18-C17-H17	108.0	C16-C17-H17	108.0
C23-C18-C19	118.68(16)	C23-C18-C17	122.92(15)
C19-C18-C17	118.30(16)	C20-C19-C18	120.76(17)
C20-C19-H19	119.6	C18-C19-H19	119.6
C21-C20-C19	120.26(17)	C21-C20-H20	119.9
C19-C20-H20	119.9	C20-C21-C22	119.47(17)
C20-C21-H21	120.3	C22-C21-H21	120.3
C21-C22-C23	120.48(17)	C21-C22-H22	119.8
C23-C22-H22	119.8	C18-C23-C22	120.35(17)
C18-C23-H23	119.8	C22-C23-H23	119.8

Table A1.7. Anisotropic atomic displacement parameters (\AA^2) for **215**.

	U ₁₁	U ₂₂	U ₃₃	U ₂₃	U ₁₃	U ₁₂
O1	0.0224(6)	0.0234(7)	0.0161(6)	0.0024(5)	0.0016(5)	- 0.0029(5)
N1	0.0185(7)	0.0184(8)	0.0152(7)	0.0000(6)	0.0041(6)	- 0.0015(6)
C1	0.0125(8)	0.0203(9)	0.0189(8)	- 0.0002(7)	0.0052(6)	- 0.0014(6)
O2	0.0298(7)	0.0176(7)	0.0200(6)	- 0.0022(5)	0.0087(5)	- 0.0003(5)
C2	0.0189(8)	0.0164(8)	0.0173(8)	0.0004(7)	0.0054(6)	- 0.0007(7)
O3	0.0227(6)	0.0320(7)	0.0237(6)	0.0064(5)	0.0094(5)	0.0026(5)
C3	0.0255(9)	0.0185(9)	0.0239(9)	- 0.0010(7)	0.0080(7)	0.0024(7)
C4	0.0200(9)	0.0264(10)	0.0259(9)	- 0.0015(8)	0.0089(7)	0.0031(7)
C5	0.0237(9)	0.0275(10)	0.0239(9)	- 0.0007(8)	0.0105(7)	- 0.0008(8)
C6	0.0226(9)	0.0226(10)	0.0188(8)	0.0007(7)	0.0075(7)	- 0.0005(7)
C7	0.0201(8)	0.0185(9)	0.0159(8)	- 0.0038(6)	0.0049(6)	- 0.0021(7)
C8	0.0187(8)	0.0206(9)	0.0151(8)	- 0.0027(7)	0.0027(7)	- 0.0025(7)
C9	0.0232(9)	0.0258(10)	0.0250(10)	0.0049(7)	0.0091(7)	0.0024(7)
C10	0.0238(9)	0.0232(9)	0.0163(8)	0.0056(7)	0.0073(7)	0.0021(7)
C11	0.0297(10)	0.0239(10)	0.0191(9)	0.0033(7)	0.0067(7)	- 0.0012(7)
C12	0.0406(12)	0.0254(10)	0.0236(10)	0.0056(8)	0.0134(9)	0.0126(8)
C13	0.0251(9)	0.0442(13)	0.0234(9)	0.0113(9)	0.0098(7)	0.0133(9)
C14	0.0241(10)	0.0418(12)	0.0184(9)	0.0037(8)	0.0043(7)	- 0.0032(8)
C15	0.0296(10)	0.0240(10)	0.0186(9)	- 0.0007(7)	0.0077(7)	0.0012(8)
C16	0.0190(9)	0.0369(11)	0.0224(9)	0.0054(8)	0.0040(7)	0.0026(8)
C17	0.0208(9)	0.0185(9)	0.0220(9)	0.0014(7)	0.0080(7)	0.0034(7)
C18	0.0171(8)	0.0207(9)	0.0192(8)	- 0.0008(7)	0.0032(6)	- 0.0025(7)
C19	0.0232(9)	0.0221(9)	0.0254(9)	0.0024(7)	0.0070(7)	0.0034(7)
C20	0.0221(9)	0.0348(11)	0.0251(9)	- 0.0015(8)	0.0101(7)	0.0023(8)
C21	0.0235(9)	0.0336(10)	0.0195(9)	0.0027(8)	0.0056(7)	- 0.0084(8)

C22	0.0264(10)	0.0227(10)	0.0267(10)	0.0081(7)	0.0044(7)	- 0.0013(7)
C23	0.0226(9)	0.0224(10)	0.0259(10)	0.0004(8)	0.0081(7)	0.0016(7)

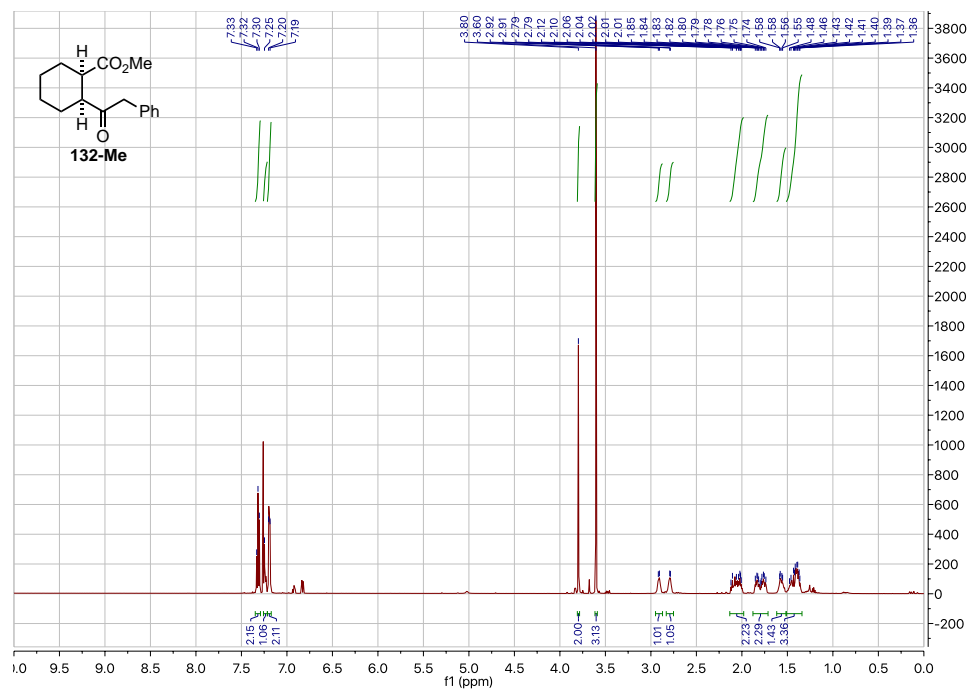
Table A1.8. Hydrogen atomic coordinates and isotropic atomic displacement parameters (\AA^2) for **215**.

	x/a	y/b	z/c	U(eq)
H1A	0.1111(19)	0.140(4)	0.5903(12)	0.026
H1B	0.0721(18)	0.198(4)	0.4993(12)	0.026
H1C	0.1223(19)	0.370(3)	0.5650(13)	0.026
H2	0.7927	-0.0224	0.2708	0.021
H3A	1.0159	-0.1141	0.3165	0.027
H3B	0.9520	-0.1825	0.2185	0.027
H4A	1.1079	0.2039	0.2699	0.028
H4B	1.1502	-0.0120	0.2250	0.028
H5A	0.9937	0.0623	0.0965	0.029
H5B	1.0852	0.2740	0.1212	0.029
H6A	0.8660	0.3833	0.0811	0.025
H6B	0.9321	0.4592	0.1780	0.025
H7	0.7761	0.0744	0.1310	0.022
H9A	0.7018	0.6388	0.1283	0.029
H9B	0.6489	0.4611	0.0537	0.029
H11	0.5531	0.8869	0.1680	0.029
H12	0.3444	1.0034	0.1572	0.035
H13	0.1736	0.7795	0.0886	0.036
H14	0.2127	0.4386	0.0291	0.034
H15	0.4207	0.3228	0.0392	0.028
H16A	0.3394	0.1767	0.6710	0.039
H16B	0.3477	0.4125	0.6263	0.039
H16C	0.4428	0.2164	0.6160	0.039
H17	0.2680	0.0063	0.5360	0.024
H19	0.4074	0.0179	0.4427	0.028
H20	0.4632	0.1644	0.3220	0.032
H21	0.3765	0.5011	0.2628	0.031
H22	0.2365	0.6941	0.3269	0.031
H23	0.1822	0.5508	0.4493	0.028

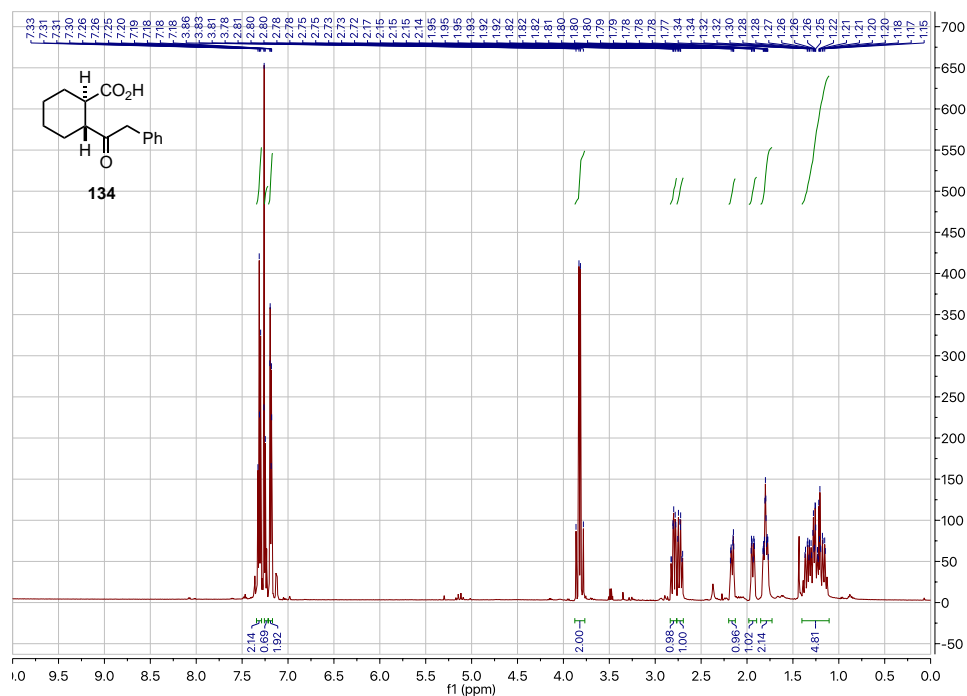
Table A1.9. Hydrogen bond distances (\AA) and angles ($^\circ$) for **215**.

	Donor-H	Acceptor-H	Donor-Acceptor	Angle
N1-H1A \cdots O2	0.907(19)	1.81(2)	2.6961(19)	165.7(19)
N1-H1B \cdots O1	0.889(19)	1.928(19)	2.7937(18)	164.2(18)
N1-H1C \cdots O1	0.92(2)	1.87(2)	2.7800(19)	172.1(19)

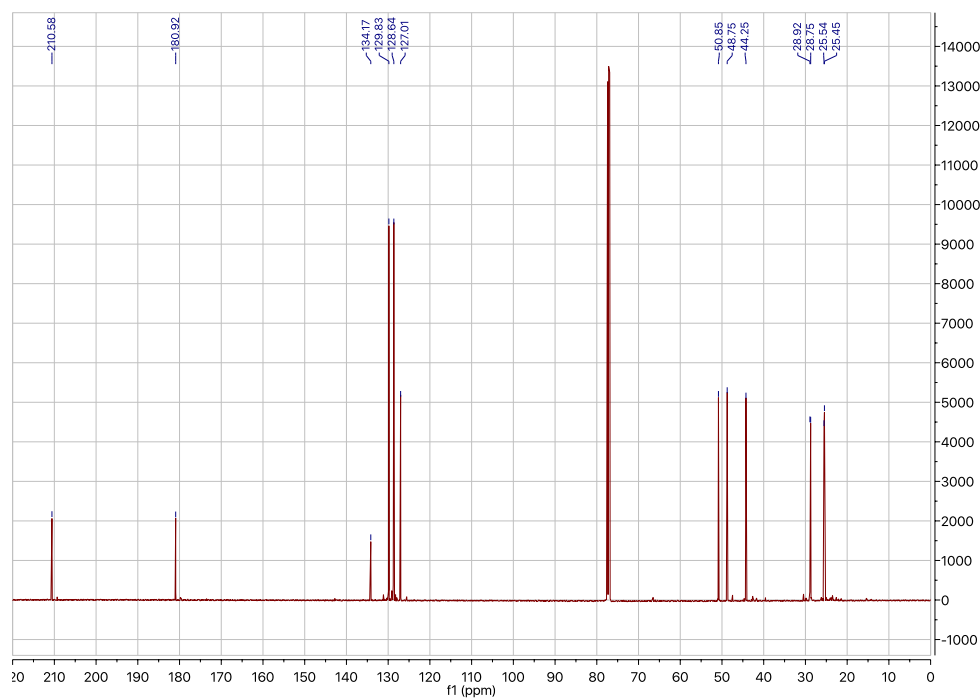
^1H NMR (501 MHz, CDCl_3): methyl (1*R*,2*S*)-2-(2-phenylacetyl)cyclohexane-1-carboxylate
(132-Me)



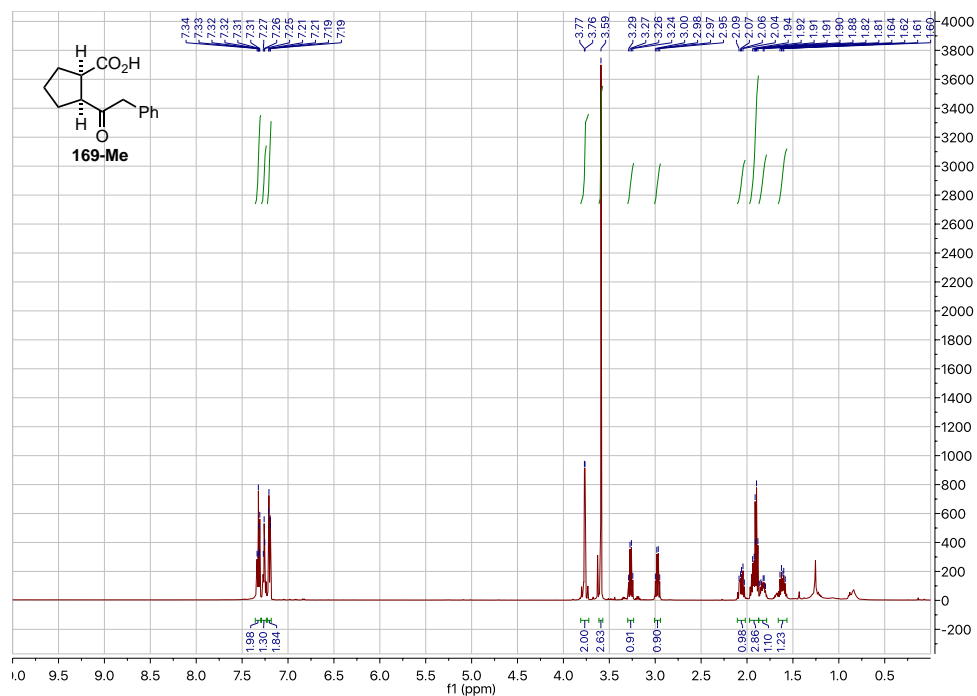
^1H NMR (501 MHz, CDCl_3): 2-(2-phenylacetyl)cyclohexane-1-carboxylic acid (134)



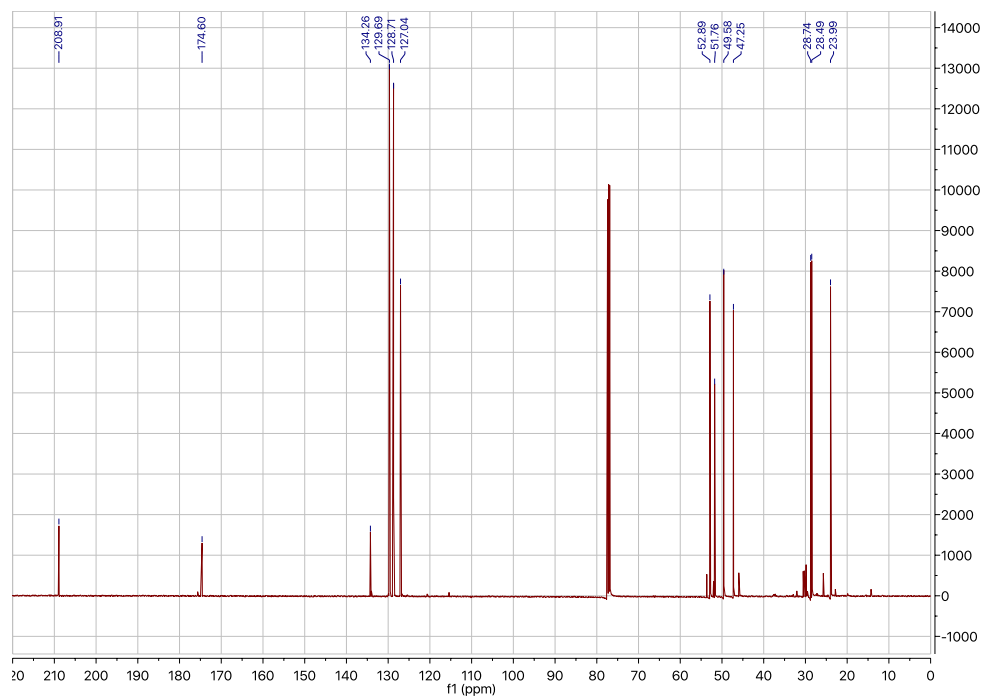
^{13}C NMR (126 MHz, CDCl_3): 2-(2-phenylacetyl)cyclohexane-1-carboxylic acid



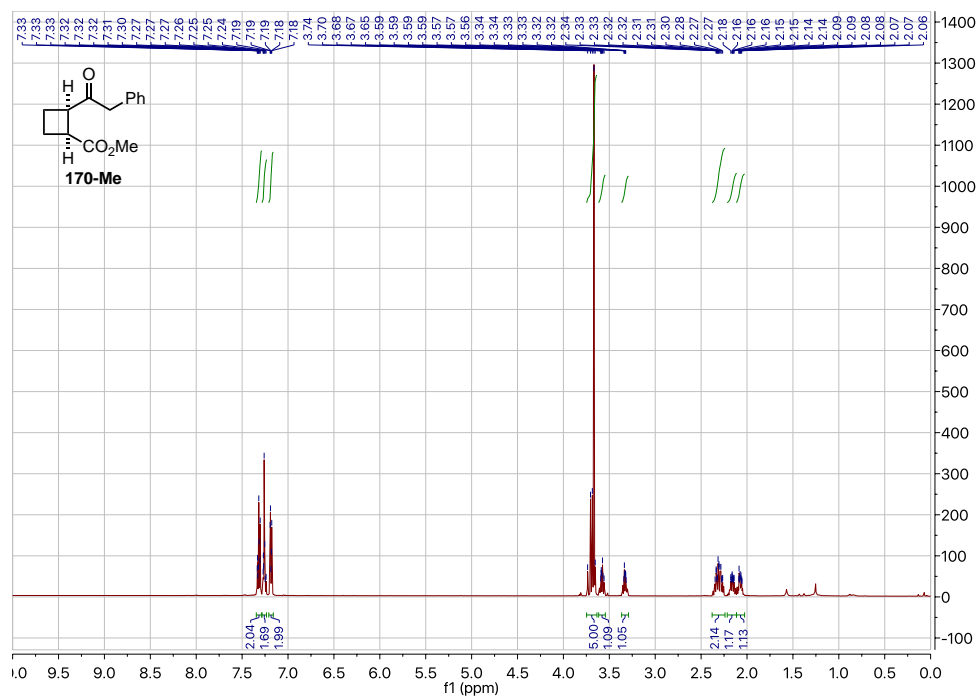
^1H NMR (501 MHz, CDCl_3): methyl (1*R*,2*S*)-2-(2-phenylacetyl)cyclopentane-1-carboxylate
(169-Me)



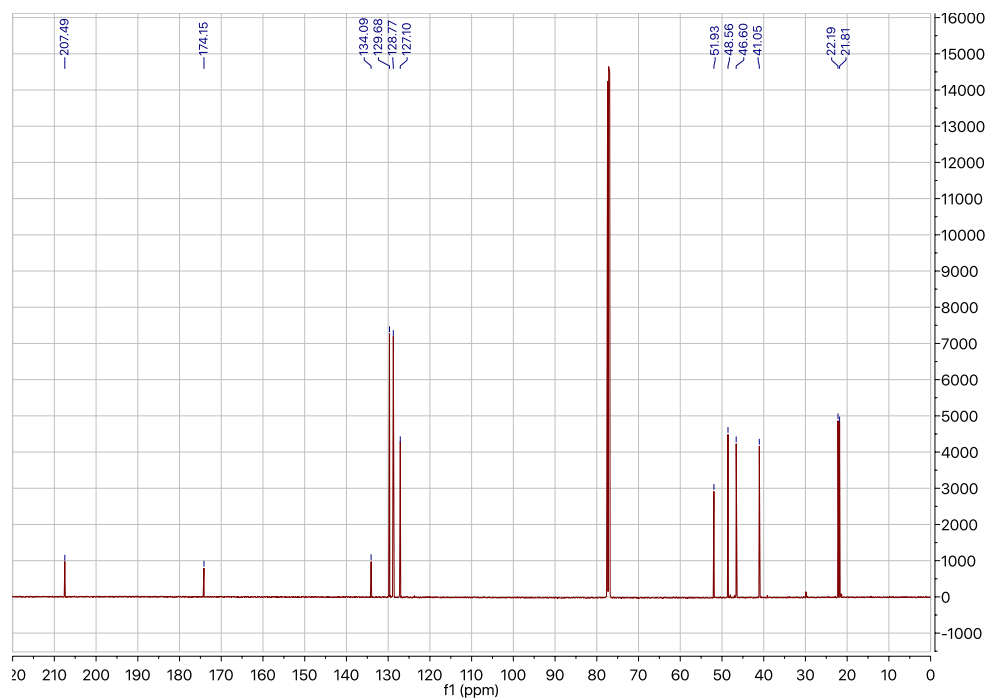
^{13}C NMR (126 MHz, CDCl_3): methyl (1*R*,2*S*)-2-(2-phenylacetyl)cyclopentane-1-carboxylate



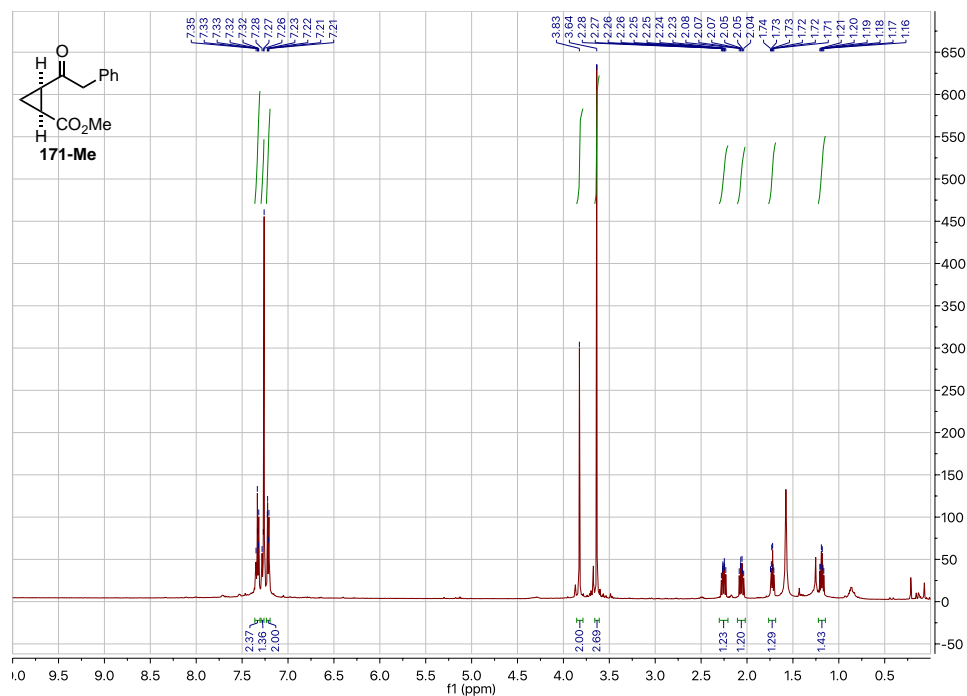
^1H NMR (501 MHz, CDCl_3): methyl (1*S*,2*R*)-2-(2-phenylacetyl)cyclobutane-1-carboxylate
(170-Me)



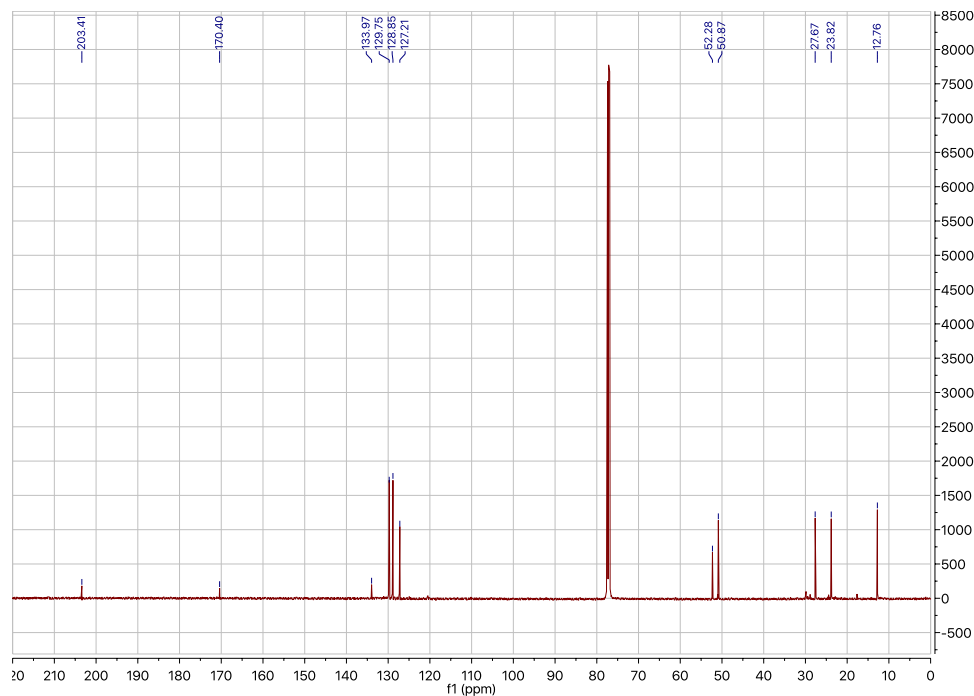
^{13}C NMR (126 MHz, CDCl_3): methyl (1*S*,2*R*)-2-(2-phenylacetyl)cyclobutane-1-carboxylate



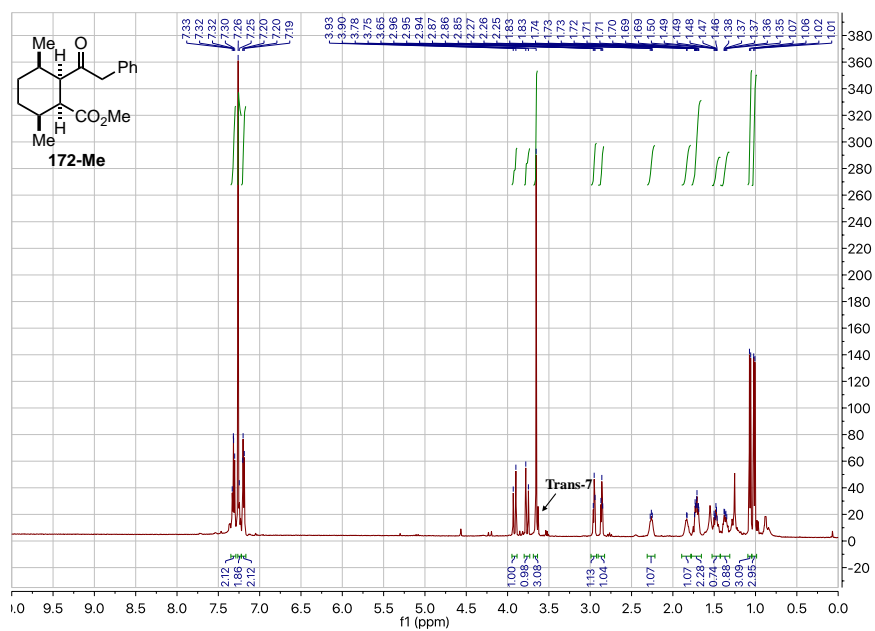
^1H NMR (501 MHz, CDCl_3): methyl (1*S*,2*R*)-2-(2-phenylacetyl)cyclopropane-1-carboxylate (171-Me)



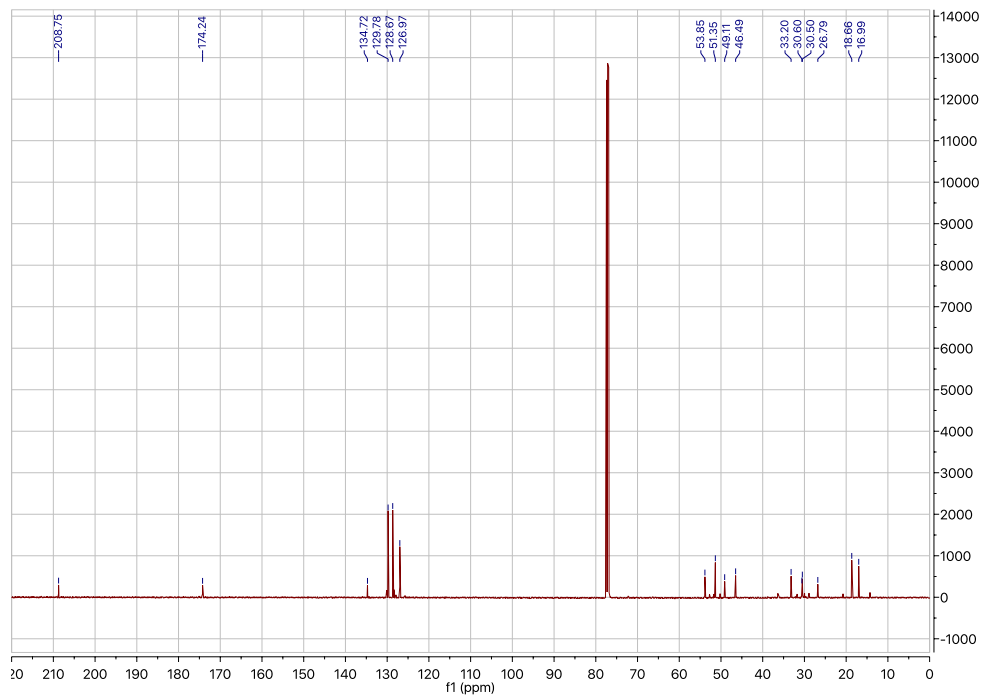
^{13}C NMR (126 MHz, CDCl_3): methyl (1*S*,2*R*)-2-(2-phenylacetyl)cyclopropane-1-carboxylate



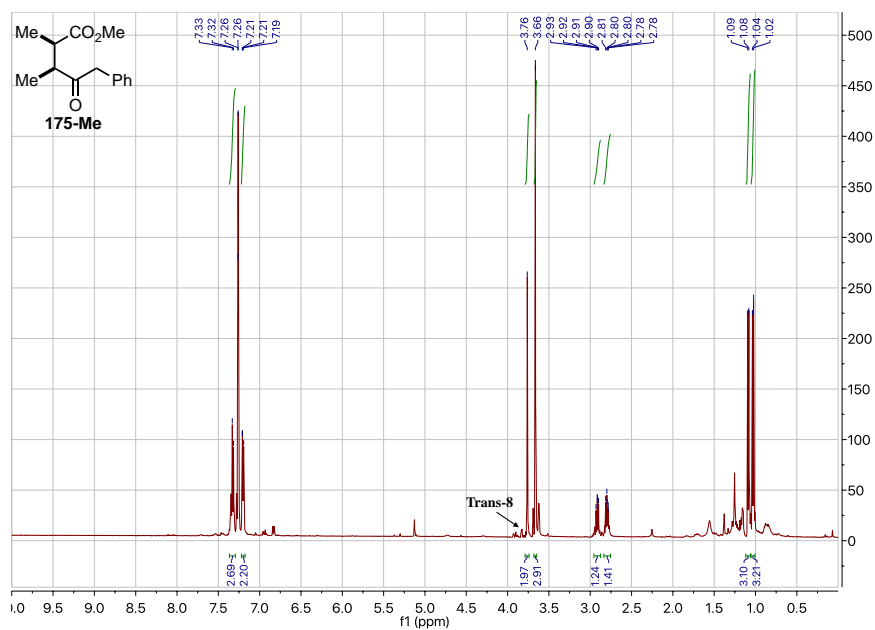
^1H NMR (501 MHz, CDCl_3): methyl (1*S*,2*R*,3*R*,6*S*)-3,6-dimethyl-2-(2-phenylacetyl) cyclohexane-1-carboxylate (172-Me)



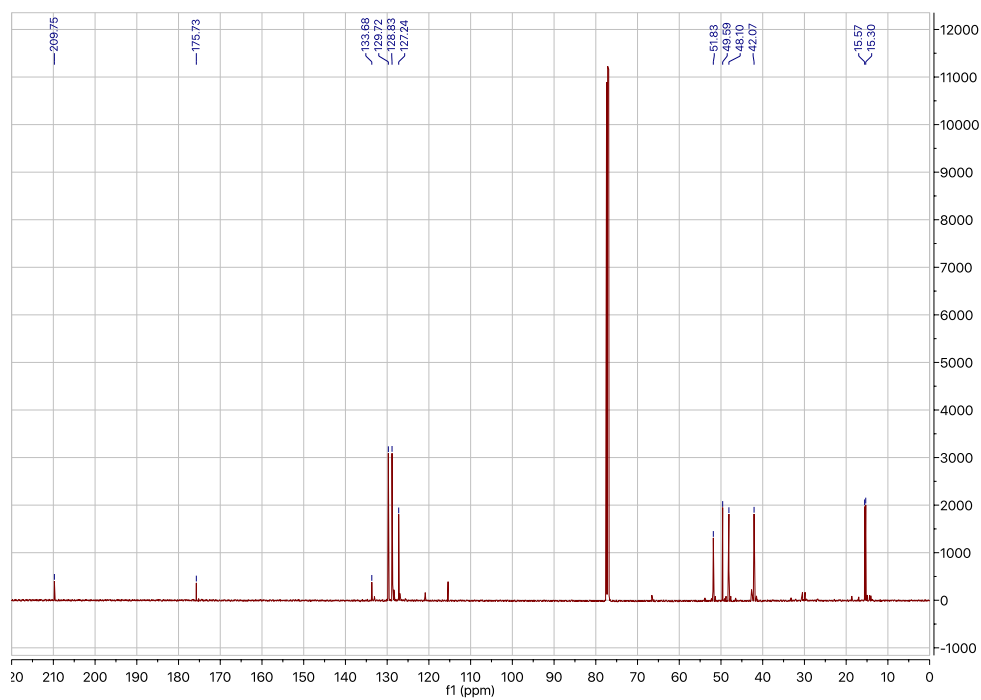
^{13}C NMR (126 MHz, CDCl_3): methyl (1*S*,2*R*,3*R*,6*S*)-3,6-dimethyl-2-(2-phenylacetyl) cyclohexane-1-carboxylate



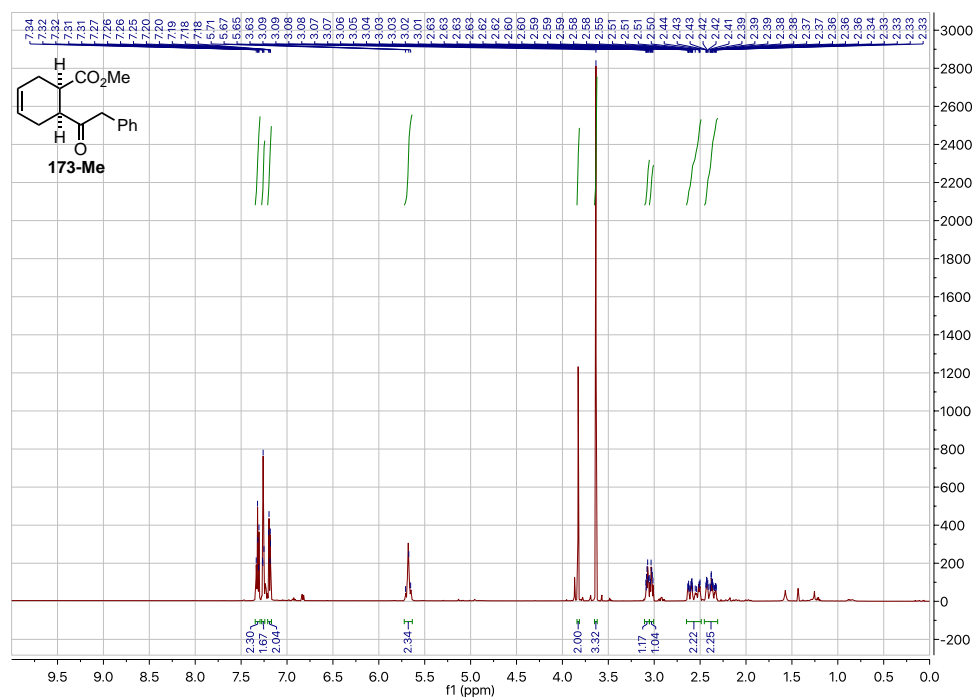
^1H NMR (501 MHz, CDCl_3): methyl (2*R*,3*S*)-2,3-dimethyl-4-oxo-5-phenylpentanoate (175-Me)



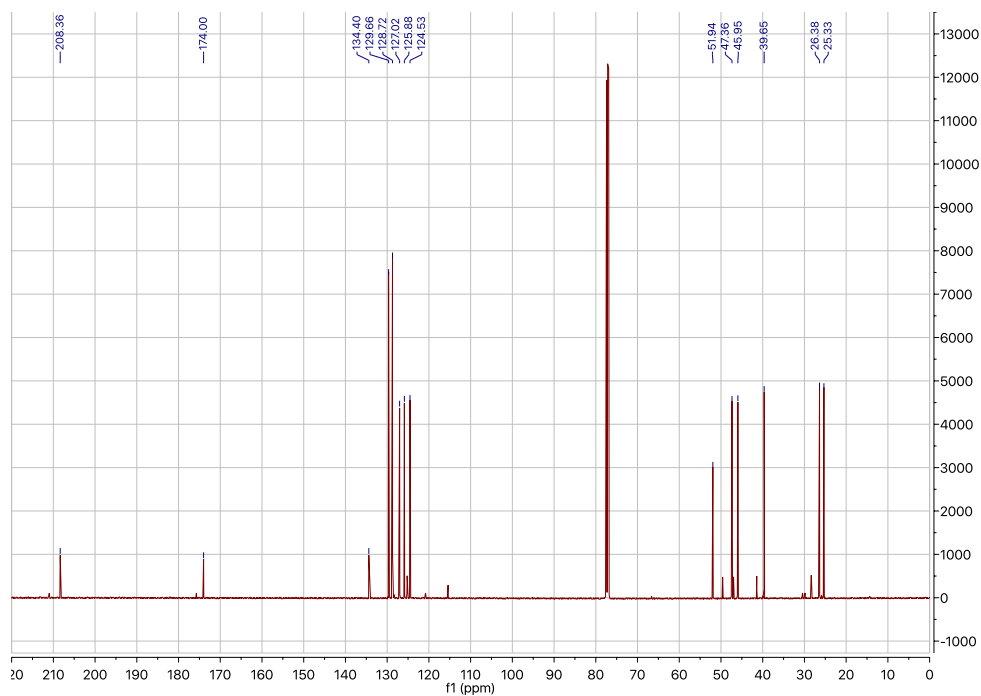
^{13}C NMR (126 MHz, CDCl_3): methyl (2*R*,3*S*)-2,3-dimethyl-4-oxo-5-phenylpentanoate



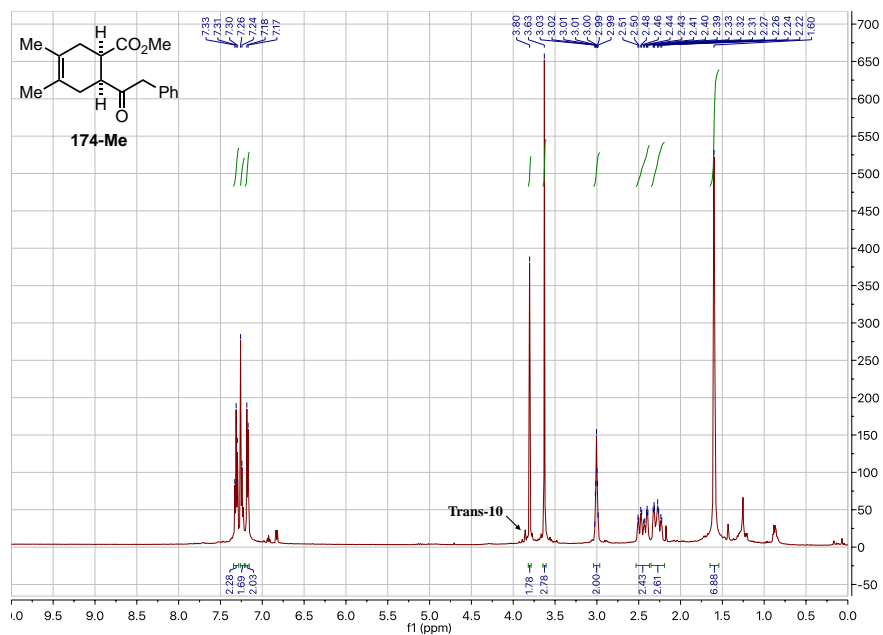
^1H NMR (501 MHz, CDCl_3): methyl (1*R*,6*S*)-6-(2-phenylacetyl)cyclohex-3-ene-1-carboxylate
(173-Me)



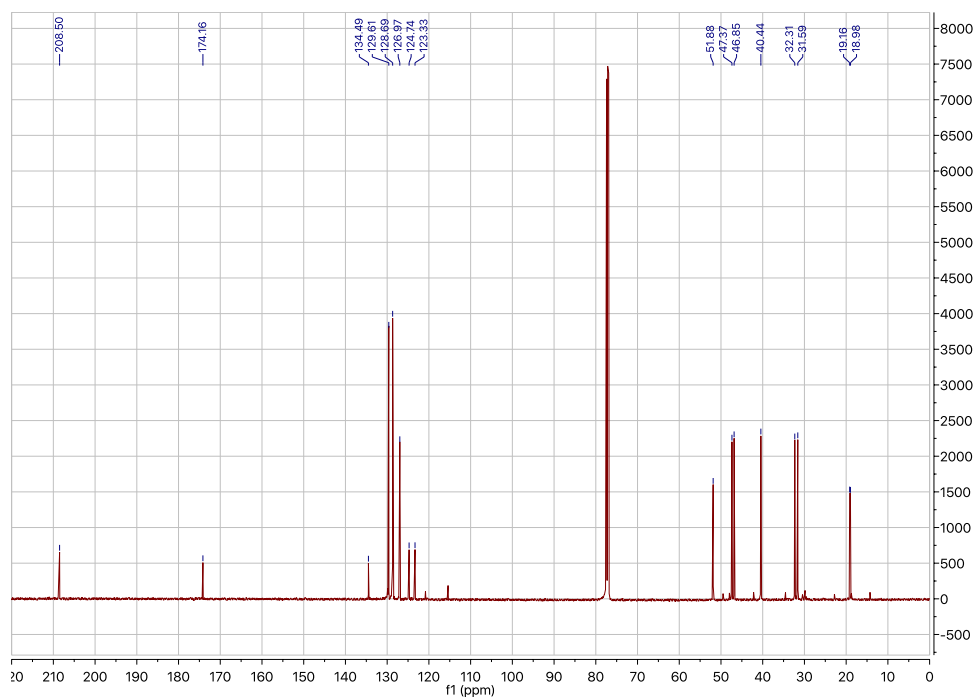
^{13}C NMR (126 MHz, CDCl_3): methyl (1*R*,6*S*)-6-(2-phenylacetyl)cyclohex-3-ene-1-carboxylate



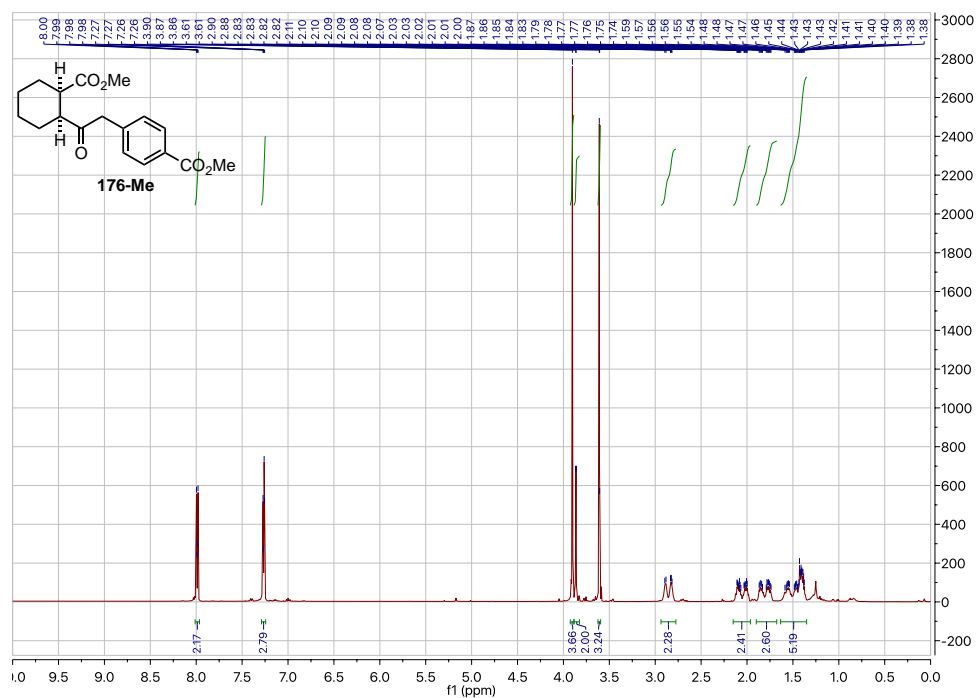
¹H NMR (501 MHz, CDCl₃): methyl (1*R*,6*S*)-3,4-dimethyl-6-(2-phenylacetyl)cyclohex-3-ene-1-carboxylate (174-Me)



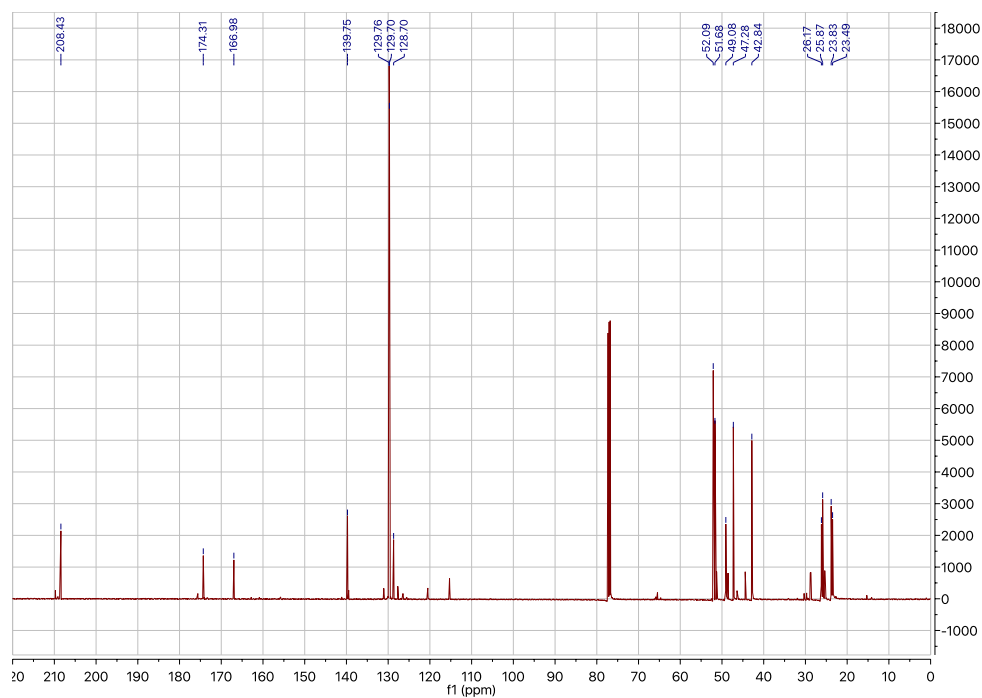
¹³C NMR (126 MHz, CDCl₃): methyl (1*R*,6*S*)-3,4-dimethyl-6-(2-phenylacetyl)cyclohex-3-ene-1-carboxylate



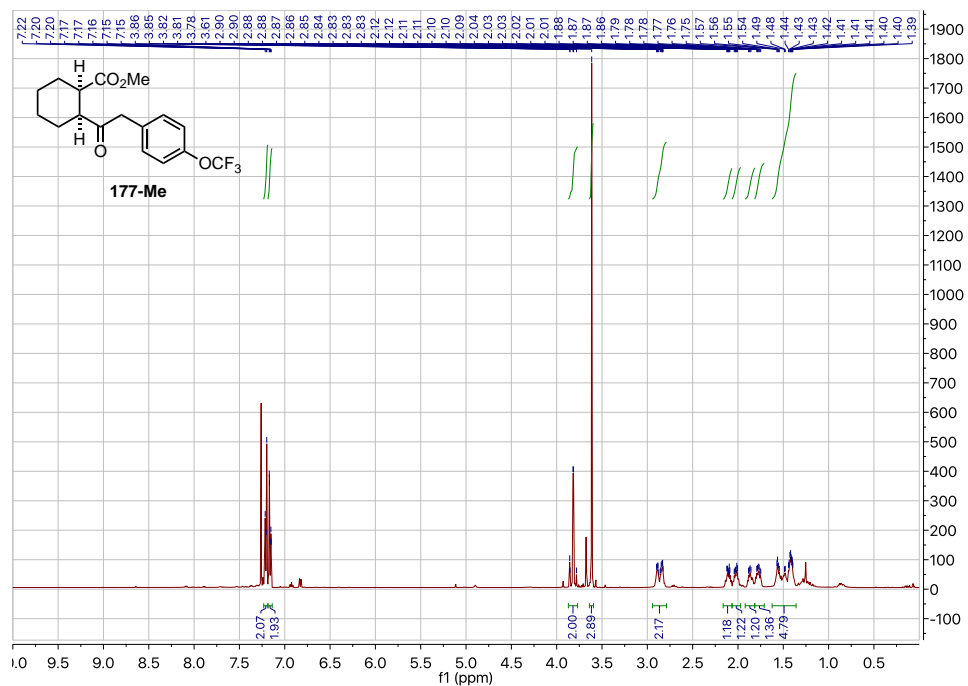
^1H NMR (501 MHz, CDCl_3): methyl 4-(2-((1*S*,2*R*)-2-(methoxycarbonyl)cyclohexyl)-2-oxoethyl)benzoate (176-Me)



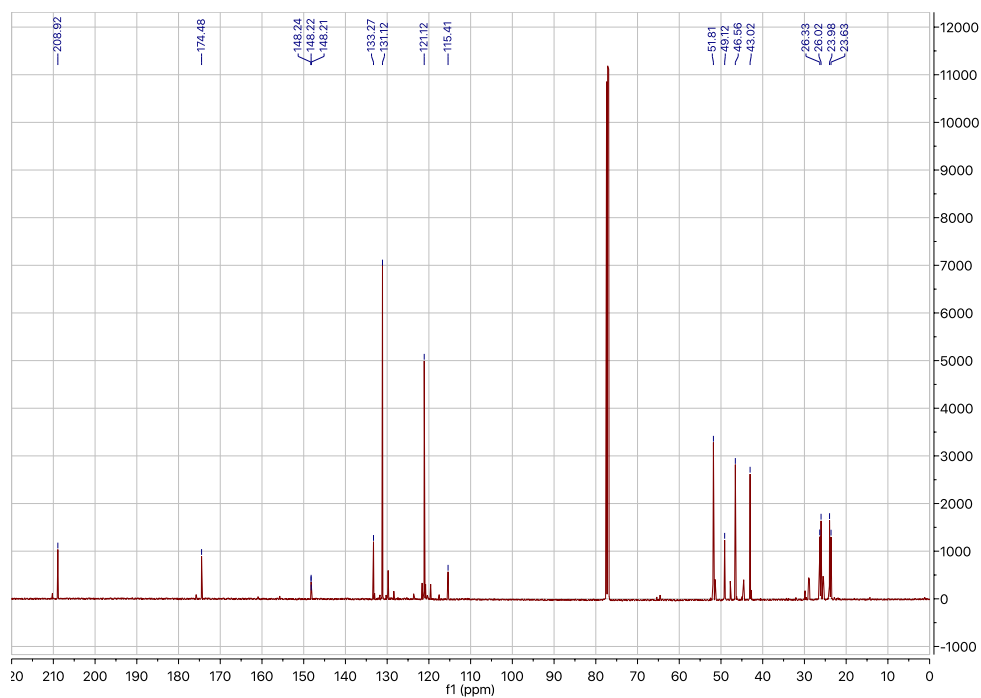
^{13}C NMR (126 MHz, CDCl_3): methyl 4-(2-((1*S*,2*R*)-2-(methoxycarbonyl)cyclohexyl)-2-oxoethyl)benzoate



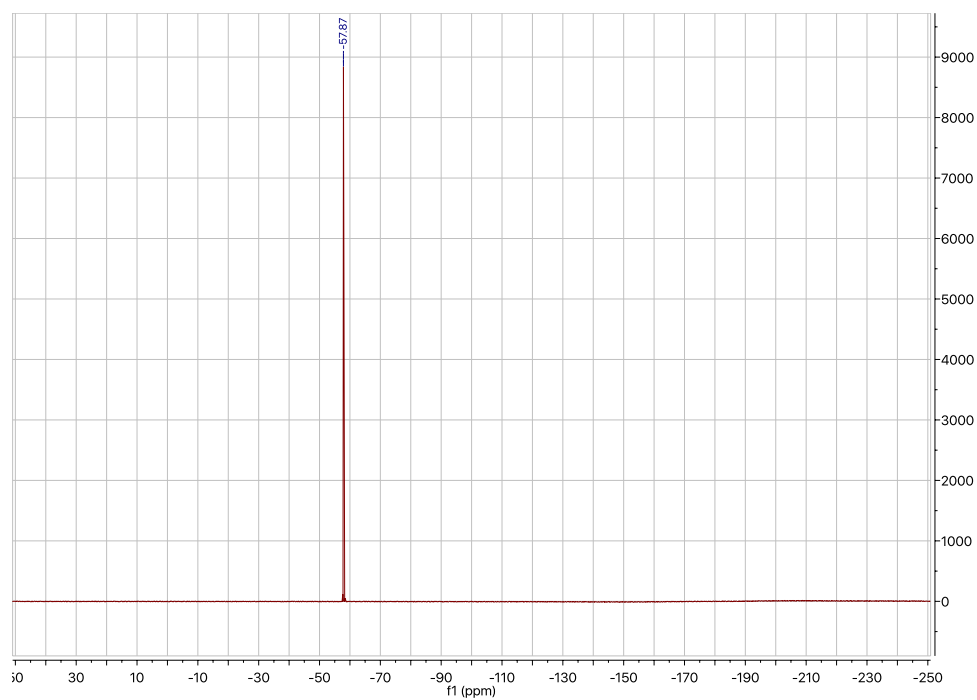
^1H NMR (501 MHz, CDCl_3): methyl (1*R*,2*S*)-2-(2-(4-(trifluoromethoxy)phenyl)acetyl) cyclohexane-1-carboxylate (177-Me)



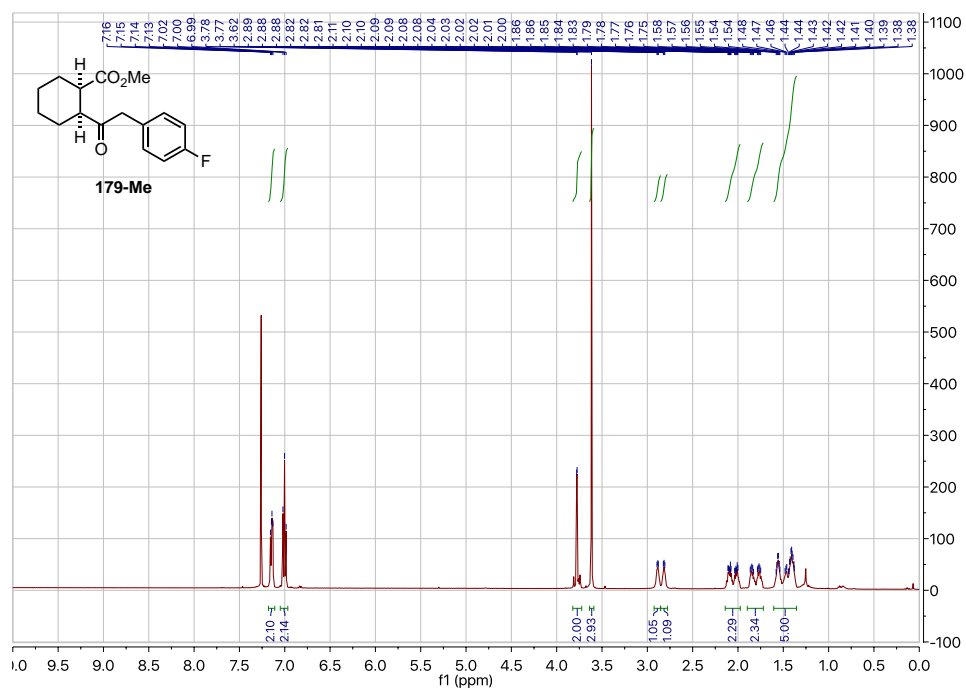
^{13}C NMR (126 MHz, CDCl_3): methyl (1*R*,2*S*)-2-(2-(4-(trifluoromethoxy)phenyl)acetyl) cyclohexane-1-carboxylate



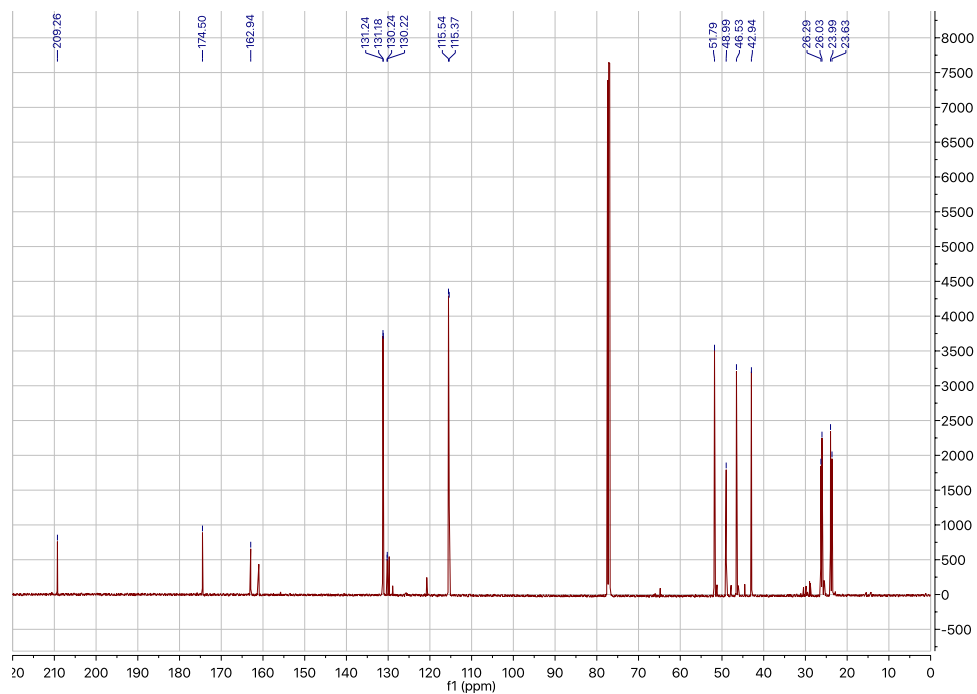
^{19}F NMR (282 MHz, CDCl_3): methyl (1R,2S)-2-(2-(4-(trifluoromethoxy)phenyl)acetyl)cyclohexane-1-carboxylate (177-Me)



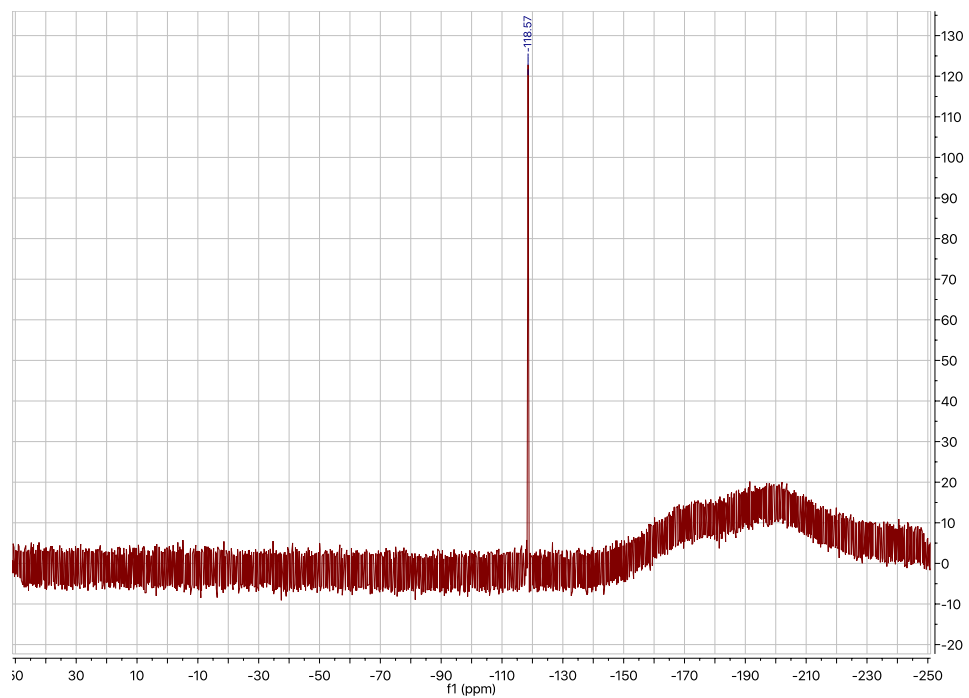
^1H NMR (501 MHz, CDCl_3): methyl (1*R*,2*S*)-2-(2-(4-fluorophenyl)acetyl)cyclohexane-1-carboxylate (179-Me)



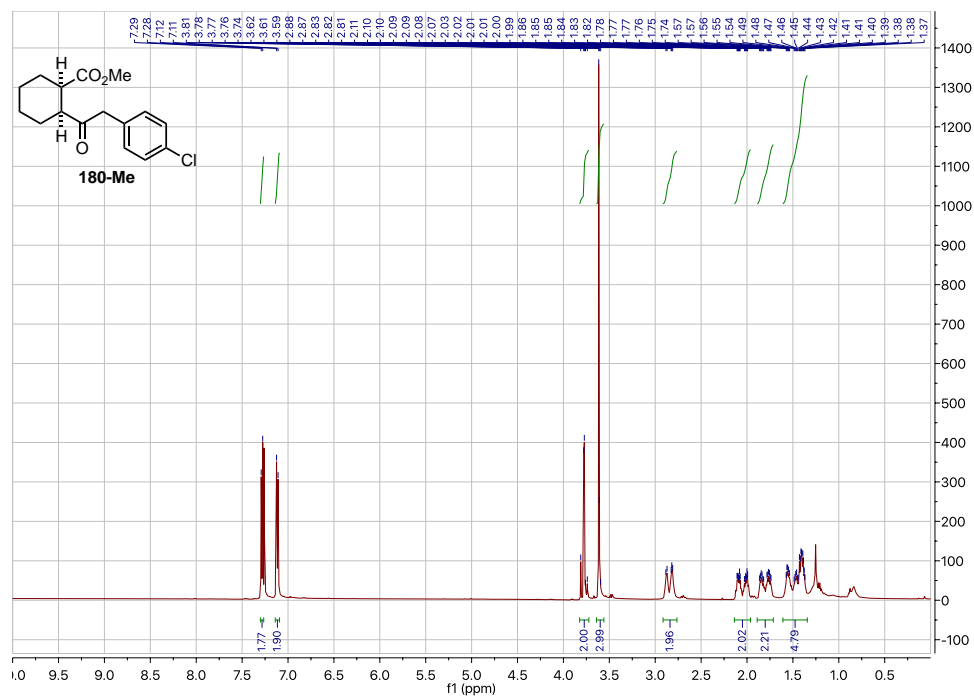
^{13}C NMR (126 MHz, CDCl_3): methyl (1*R*,2*S*)-2-(2-(4-fluorophenyl)acetyl)cyclohexane-1-carboxylate



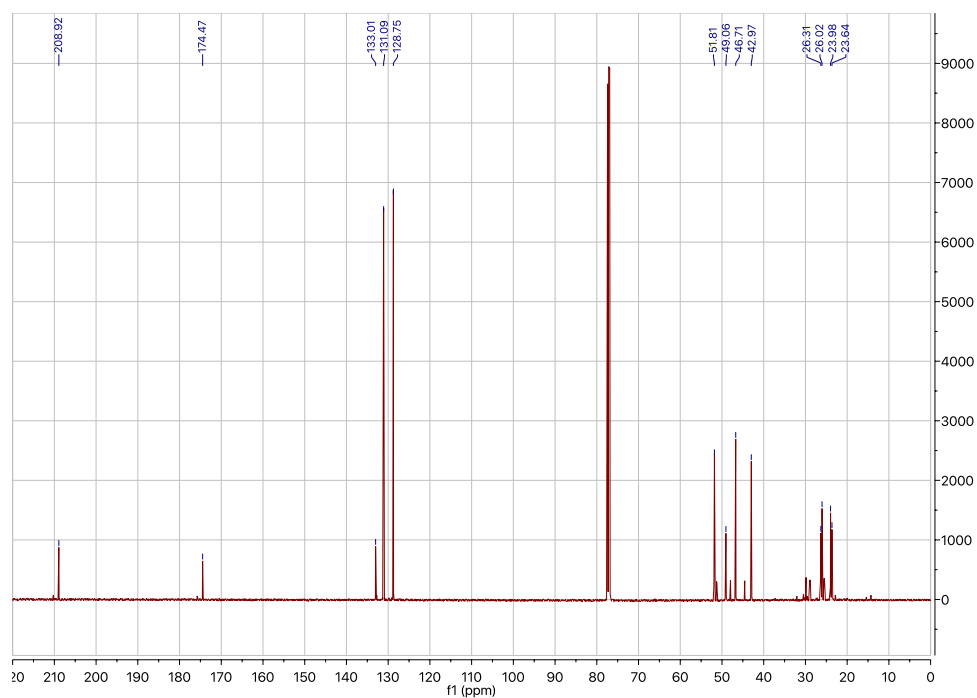
^{19}F NMR (282 MHz, CDCl_3): methyl (1*R*,2*S*)-2-(2-(4-fluorophenyl)acetyl)cyclohexane-1-carboxylate (179-Me)



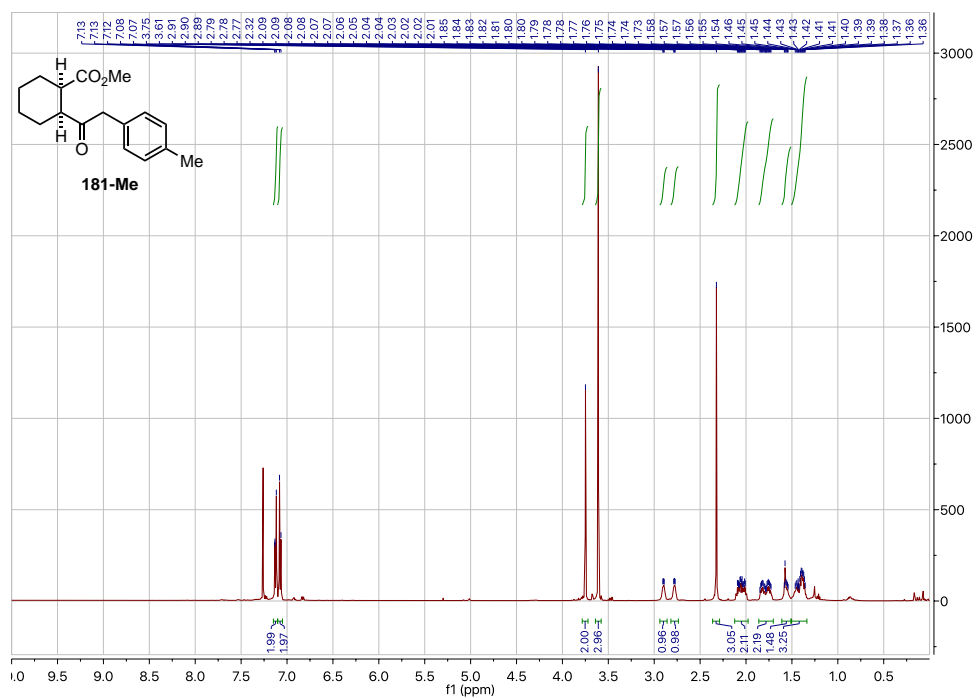
^1H NMR (501 MHz, CDCl_3): methyl (1*R*,2*S*)-2-(2-(4-chlorophenyl)acetyl)cyclohexane-1-carboxylate (180-Me)



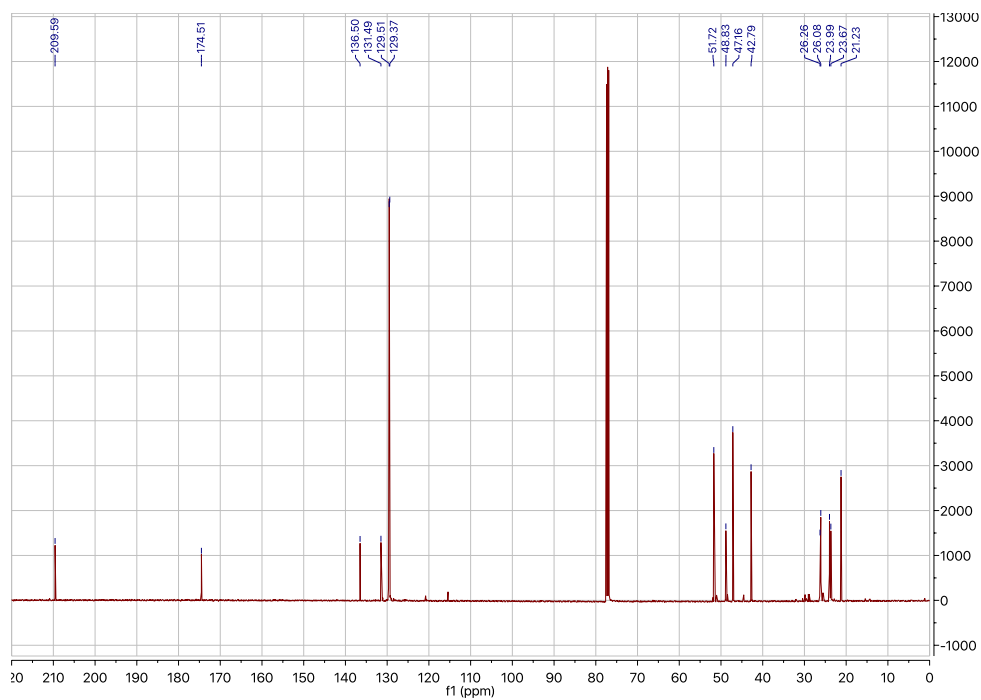
^{13}C NMR (126 MHz, CDCl_3): methyl (1*R*,2*S*)-2-(2-(4-chlorophenyl)acetyl)cyclohexane-1-carboxylate



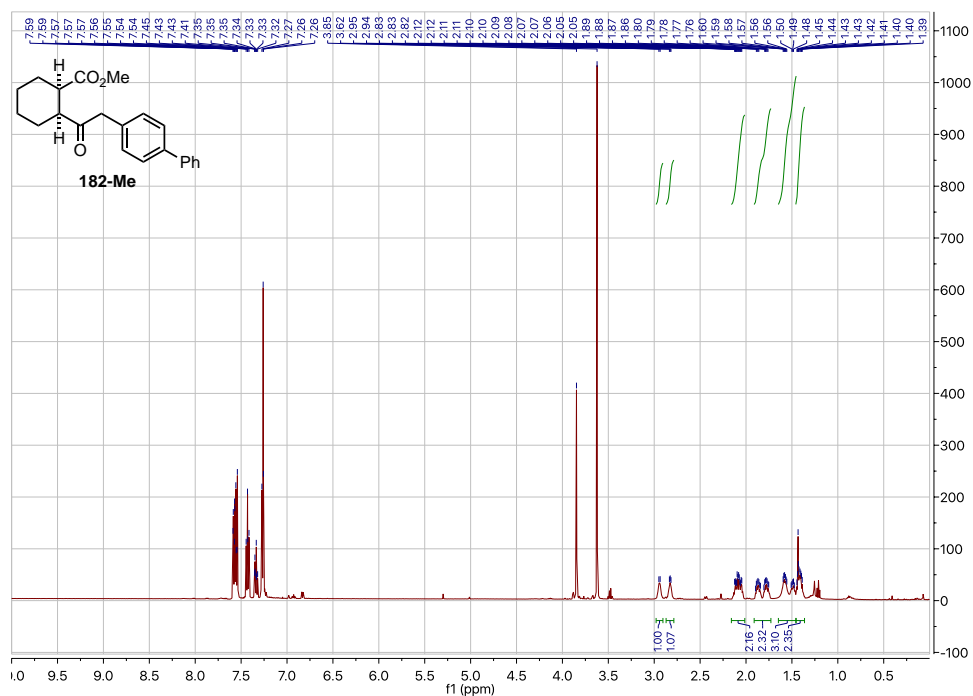
^1H NMR (501 MHz, CDCl_3): methyl (1*R*,2*S*)-2-(2-(*p*-tolyl)acetyl)cyclohexane-1-carboxylate
(181-Me)



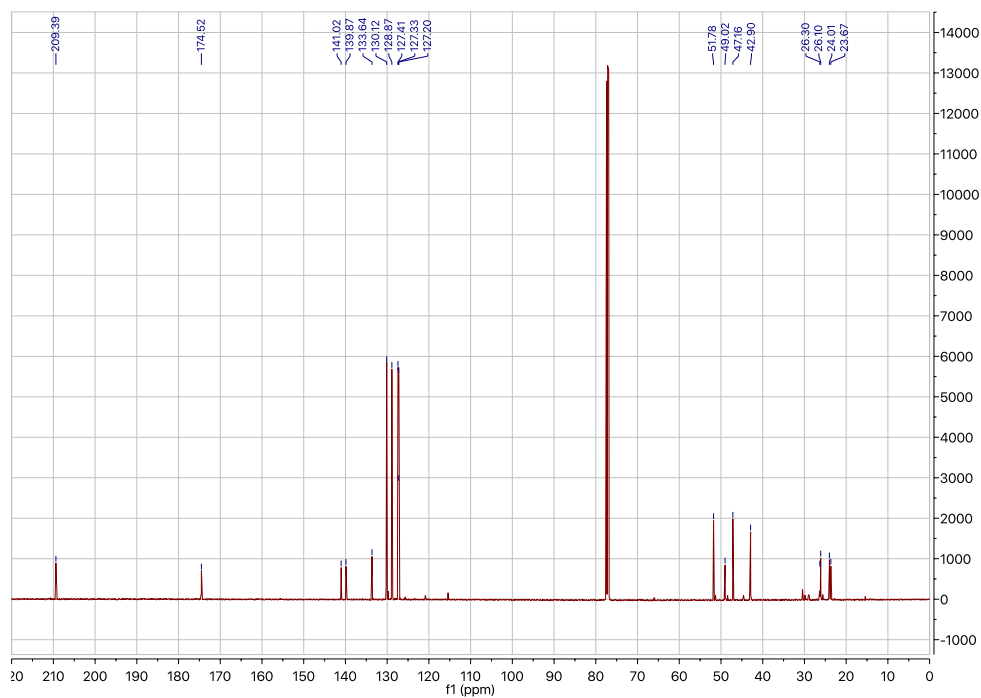
^{13}C NMR (126 MHz, CDCl_3): methyl (1*R*,2*S*)-2-(2-(*p*-tolyl)acetyl)cyclohexane-1-carboxylate



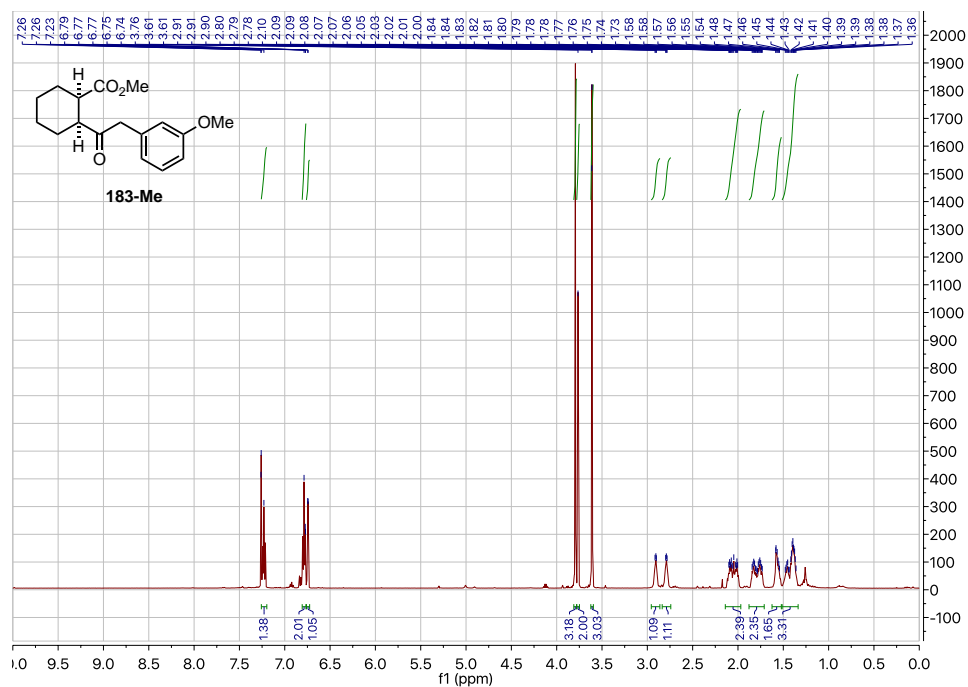
^1H NMR (501 MHz, CDCl_3): methyl (1*R*,2*S*)-2-(2-([1,1'-biphenyl]-4-yl)acetyl)cyclohexane-1-carboxylate (182-Me)



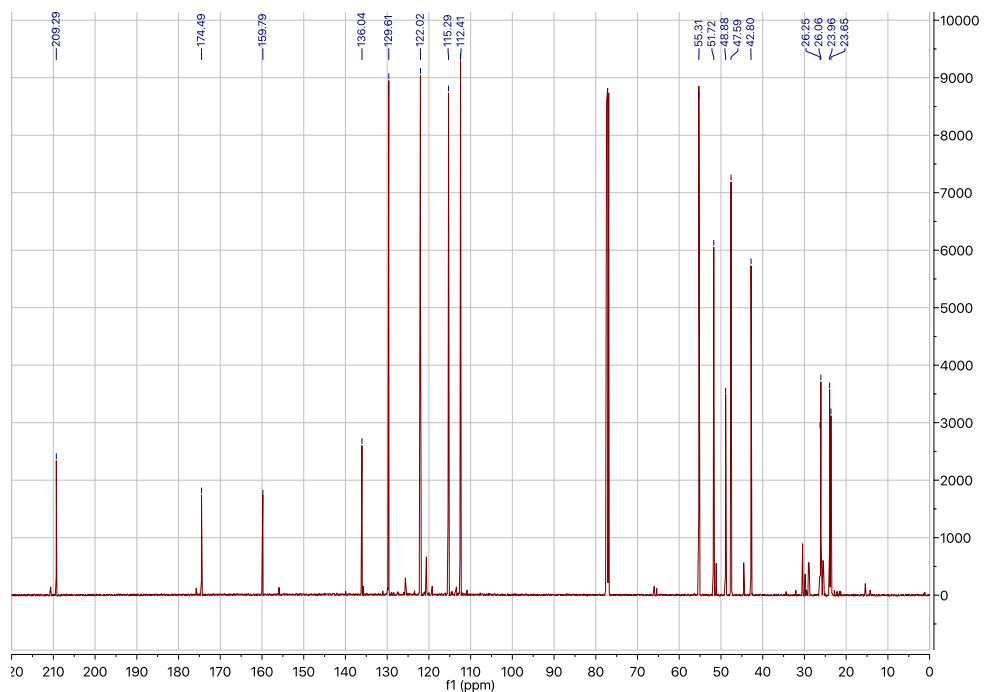
^{13}C NMR (126 MHz, CDCl_3): methyl (1*R*,2*S*)-2-(2-([1,1'-biphenyl]-4-yl)acetyl)cyclohexane-1-carboxylate



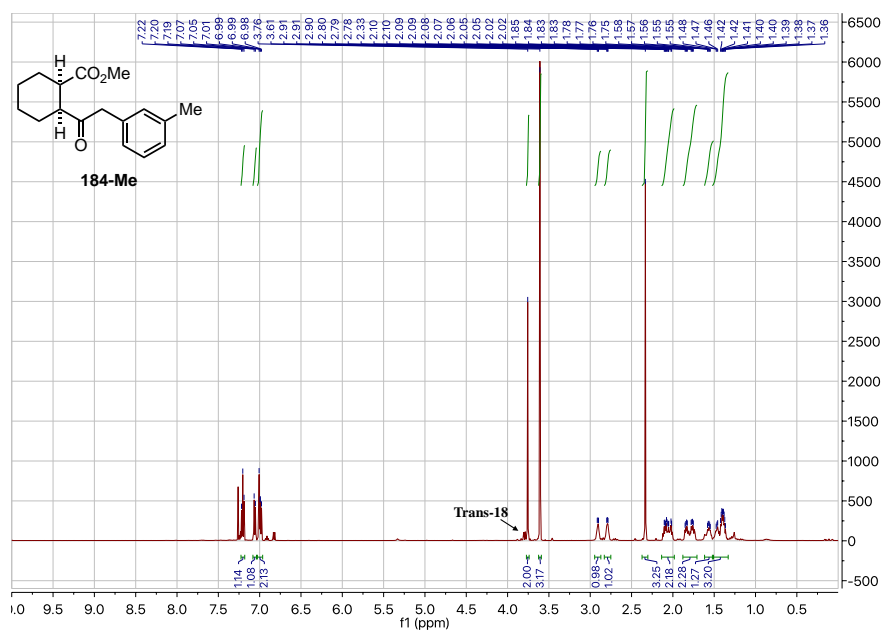
^1H NMR (501 MHz, CDCl_3): methyl (1*R*,2*S*)-2-(2-(3-methoxyphenyl)acetyl)cyclohexane-1-carboxylate (183-Me)



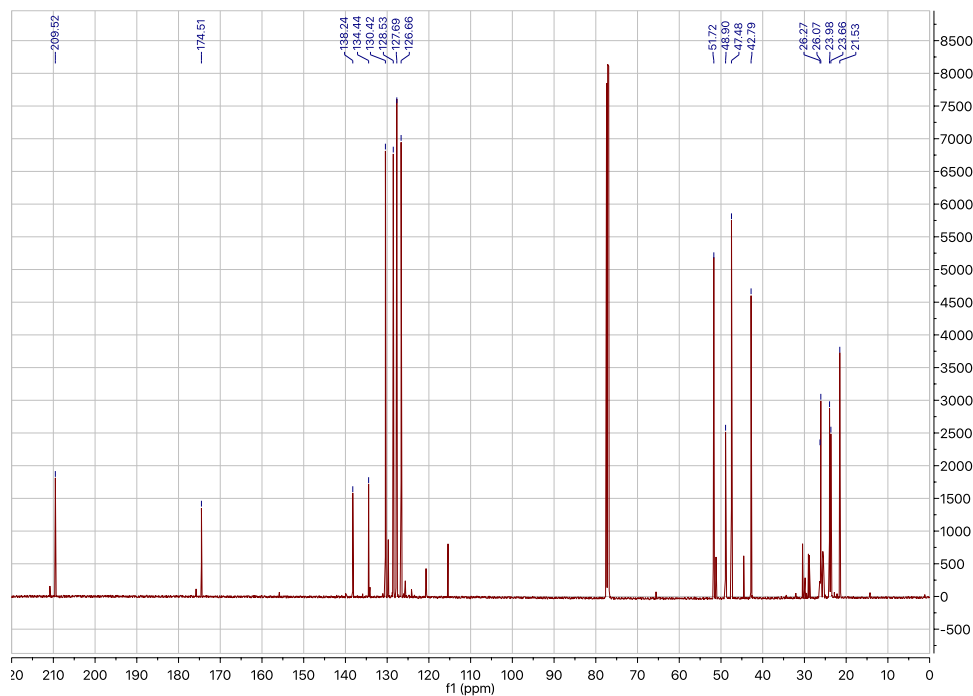
^{13}C NMR (126 MHz, CDCl_3): methyl (1*R*,2*S*)-2-(2-(3-methoxyphenyl)acetyl)cyclohexane-1-carboxylate



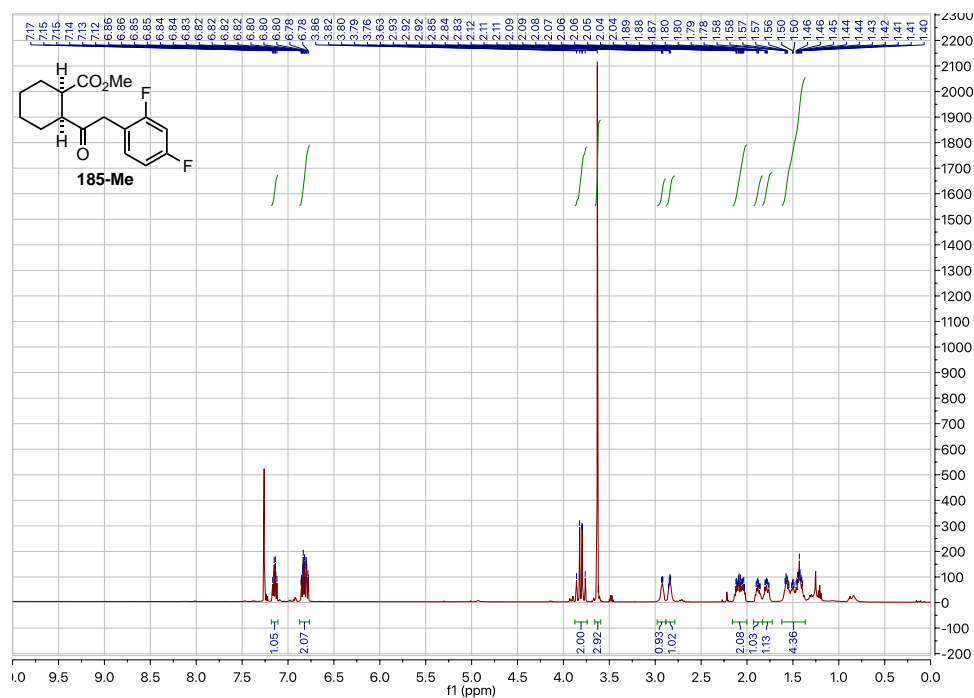
^1H NMR (501 MHz, CDCl_3): methyl (1*R*,2*S*)-2-(2-(*m*-tolyl)acetyl)cyclohexane-1-carboxylate
(184-Me)



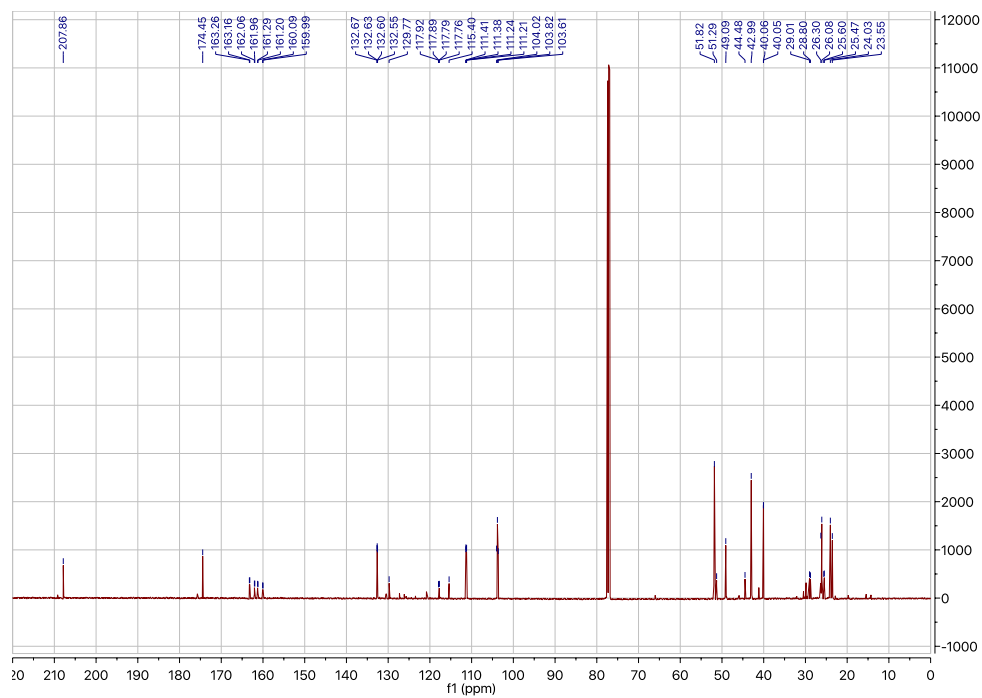
^{13}C NMR (126 MHz, CDCl_3): methyl (1*R*,2*S*)-2-(2-(*m*-tolyl)acetyl)cyclohexane-1-carboxylate



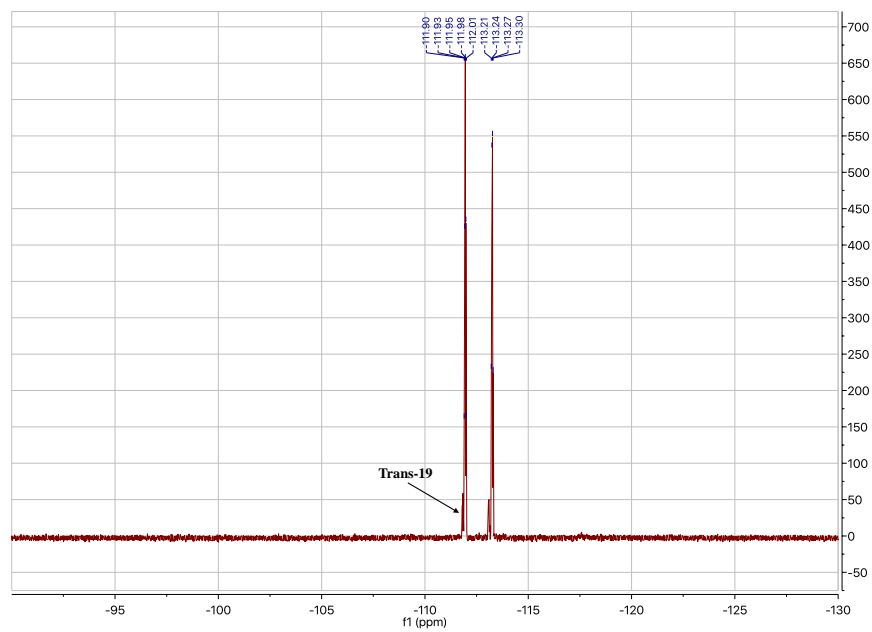
^1H NMR (501 MHz, CDCl_3): methyl (1*R*,2*S*)-2-(2-(2,4-difluorophenyl)acetyl)cyclohexane-1-carboxylate (185-Me)



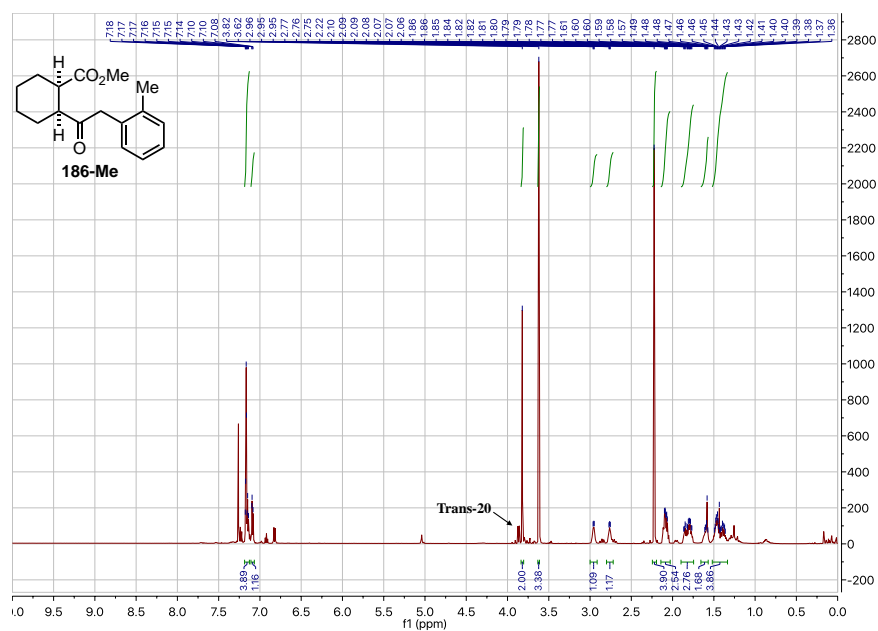
^{13}C NMR (126 MHz, CDCl_3): methyl (1*R*,2*S*)-2-(2-(2,4-difluorophenyl)acetyl)cyclohexane-1-carboxylate



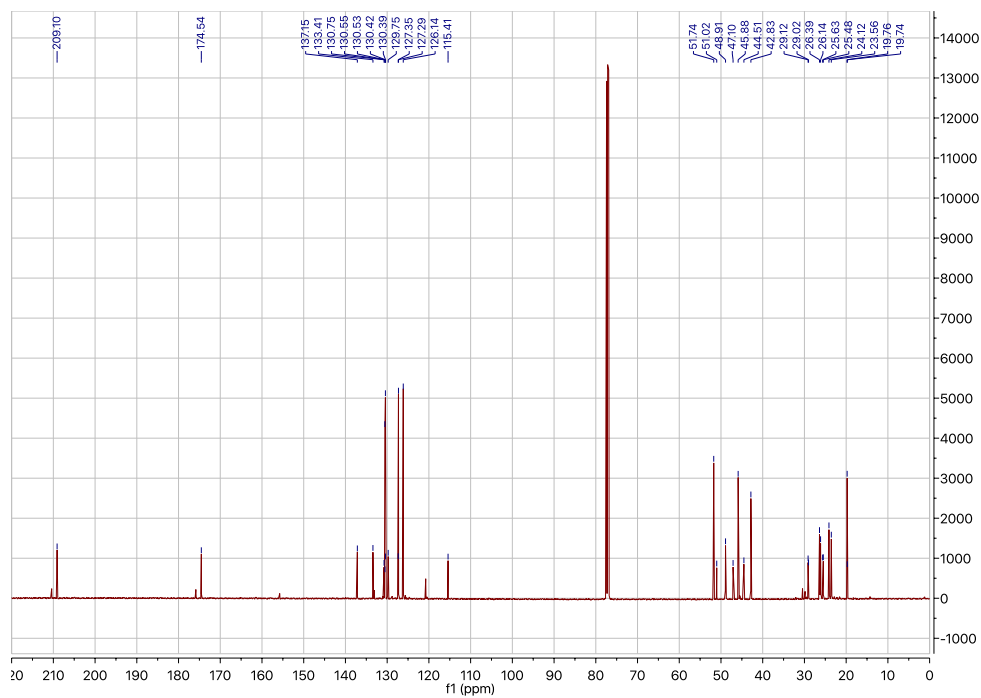
^{19}F NMR (282MHz, CDCl_3): methyl (1*R*,2*S*)-2-(2-(2,4-difluorophenyl)acetyl)cyclohexane-1-carboxylate (185-Me)



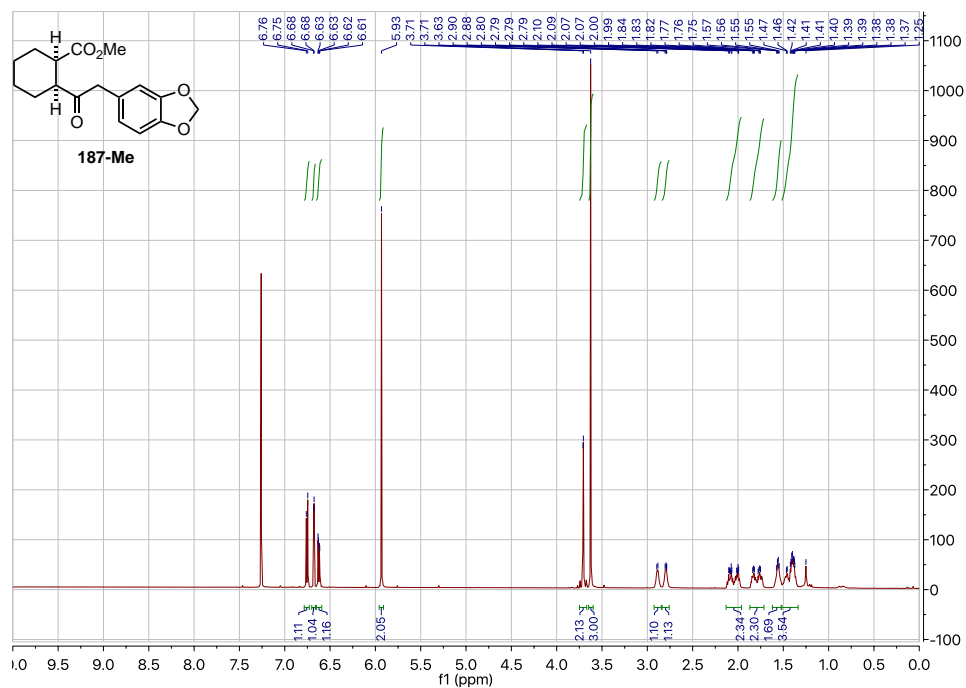
^1H NMR (501 MHz, CDCl_3): methyl (1*R*,2*S*)-2-(2-(*o*-tolyl)acetyl)cyclohexane-1-carboxylate
(186-Me)



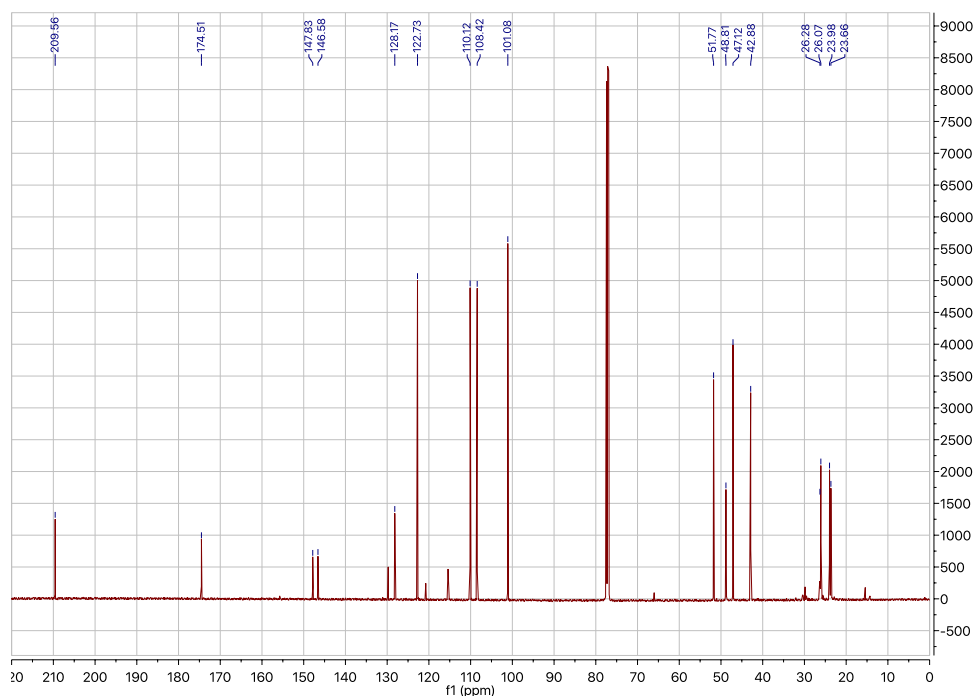
^{13}C NMR (126 MHz, CDCl_3): methyl (1*R*,2*S*)-2-(2-(*o*-tolyl)acetyl)cyclohexane-1-carboxylate



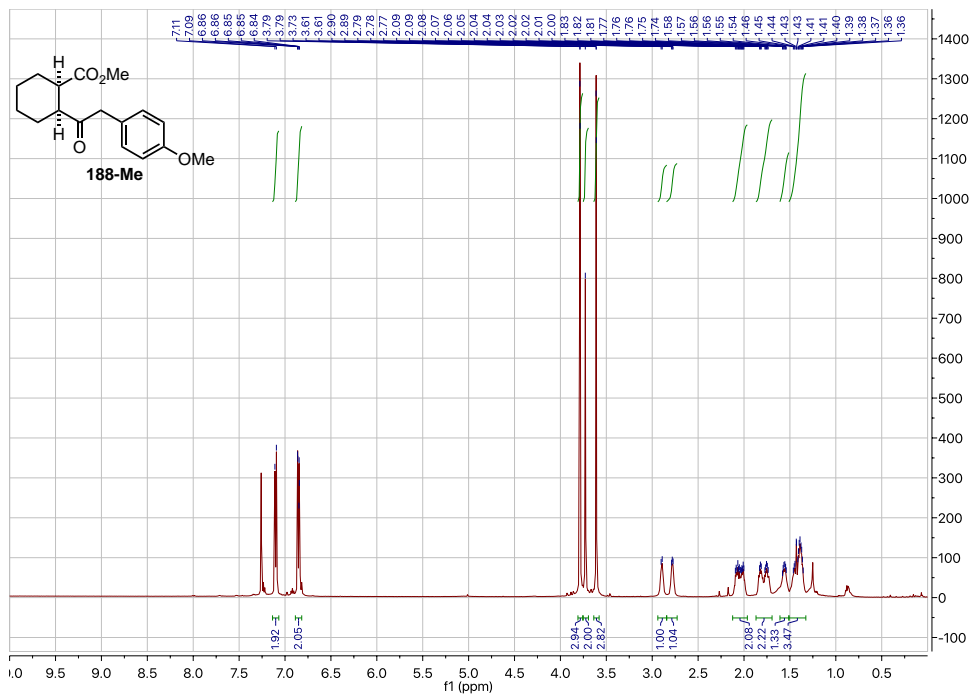
^1H NMR (501 MHz, CDCl_3): methyl (1*R*,2*S*)-2-(2-(benzo[*d*][1,3]dioxol-5-yl)acetyl)cyclohexane-1-carboxylate (187-Me)



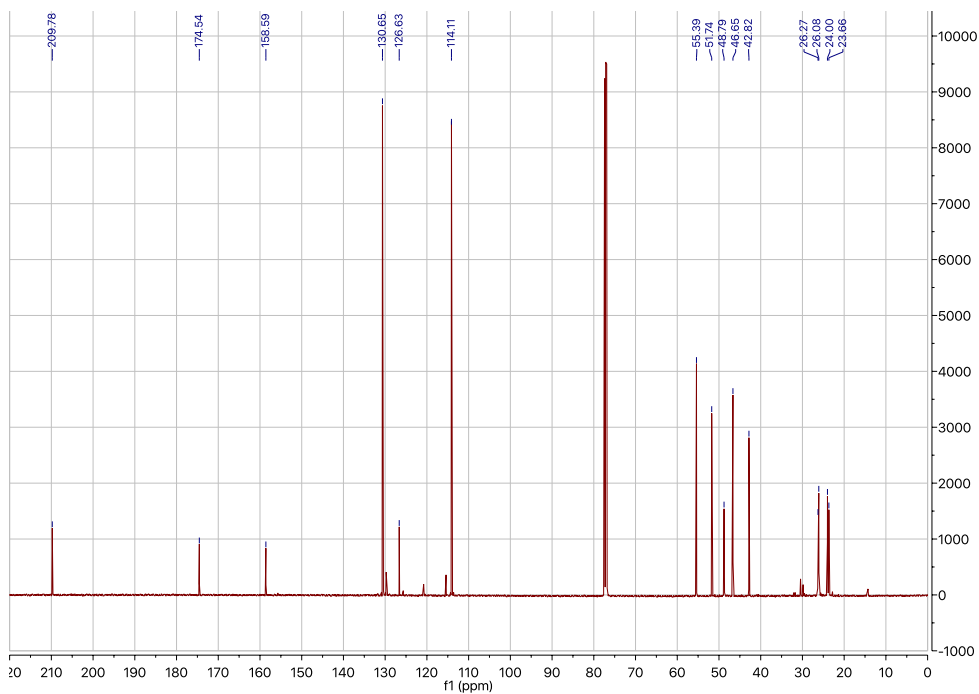
^{13}C NMR (126 MHz, CDCl_3): methyl (1*R*,2*S*)-2-(2-(benzo[*d*][1,3]dioxol-5-yl)acetyl)cyclohexane-1-carboxylate



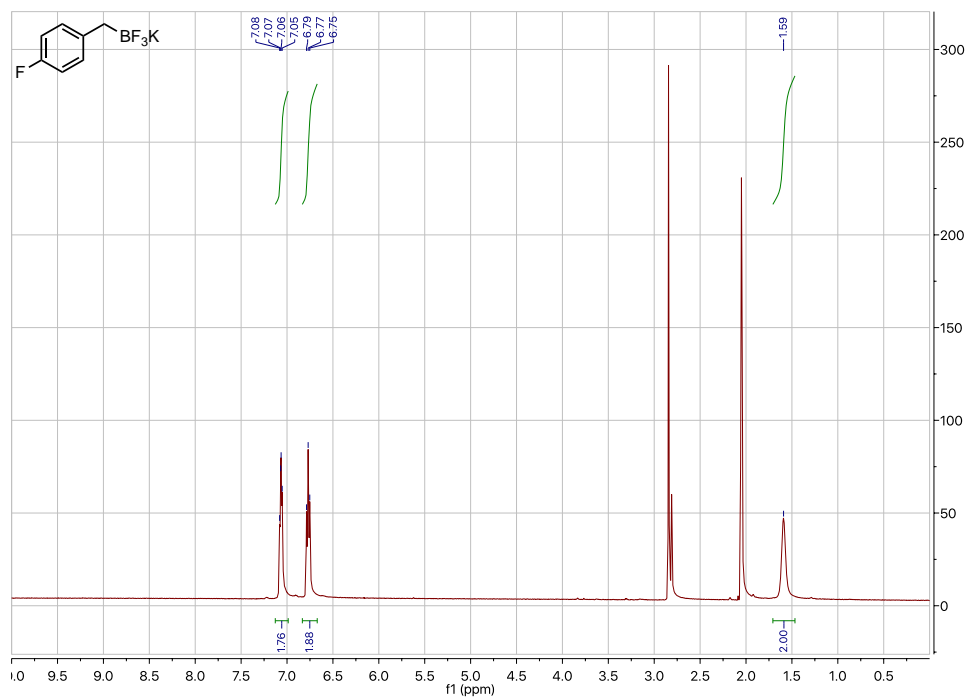
¹H NMR (501 MHz, CDCl₃): methyl (1*R*,2*S*)-2-(2-(4-methoxyphenyl)acetyl)cyclohexane-1-carboxylate (188-Me)



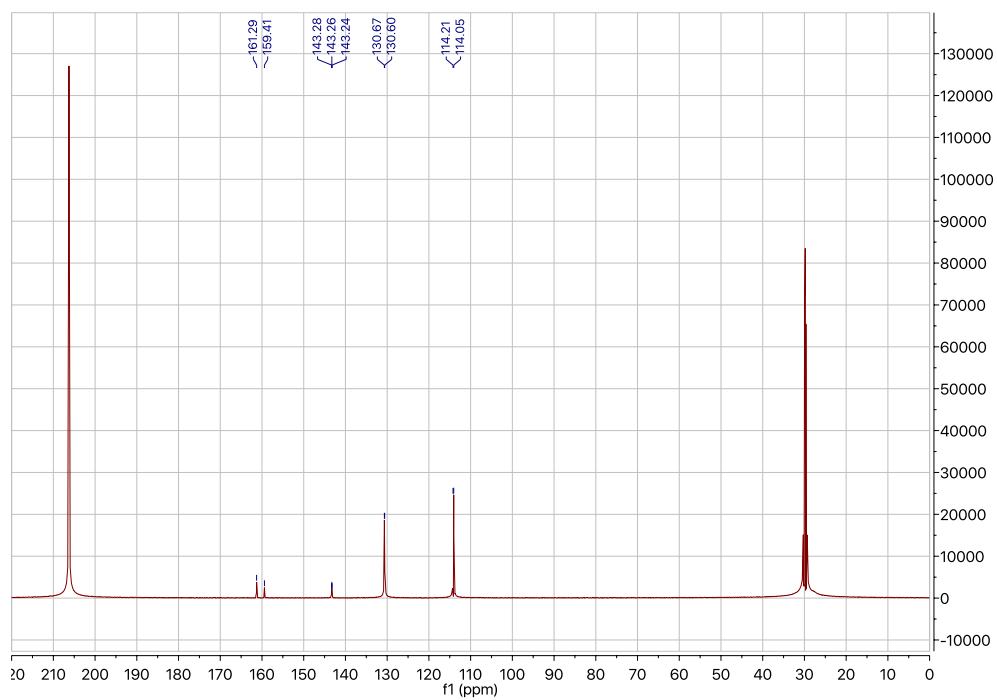
¹³C NMR (126 MHz, CDCl₃): methyl (1*R*,2*S*)-2-(2-(4-methoxyphenyl)acetyl)cyclohexane-1-carboxylate



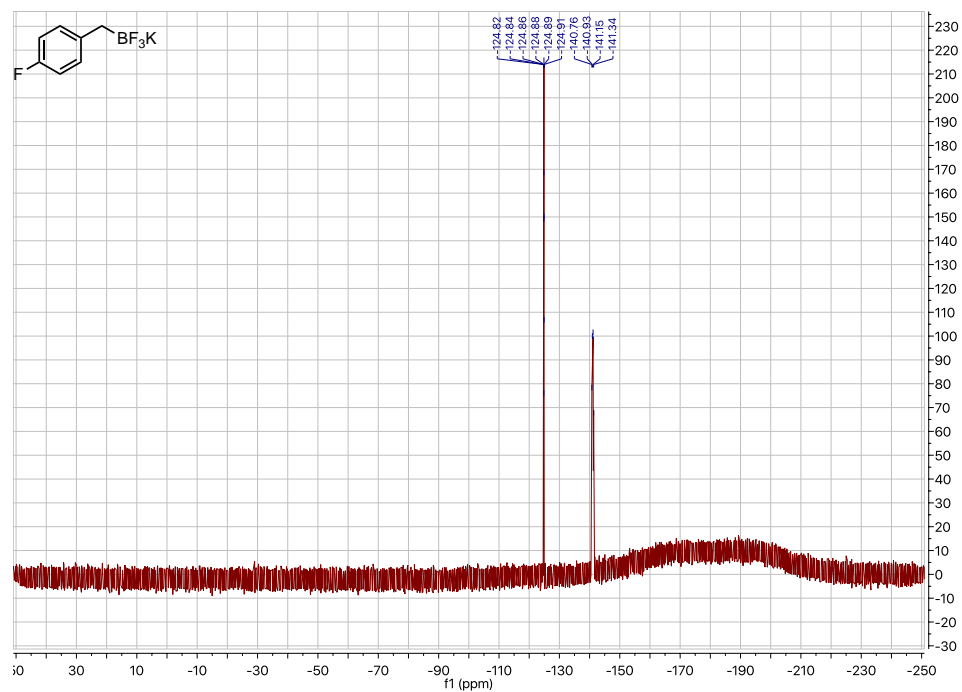
^1H NMR (501 MHz, acetone- d_6): trifluoro(4-fluorobenzyl)- λ^4 -borane, potassium salt



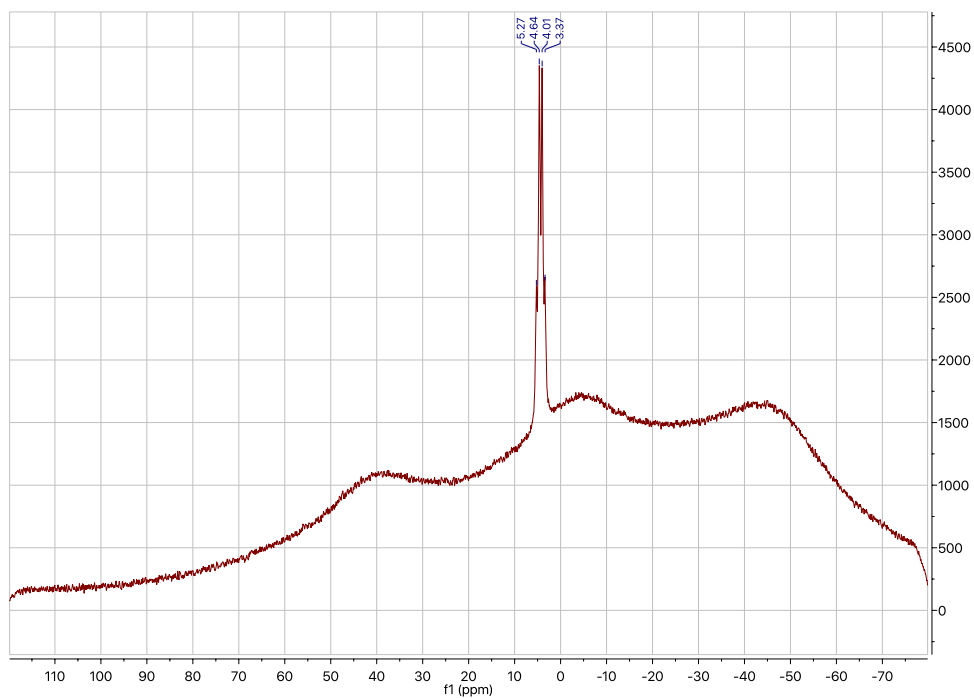
^{13}C NMR (126 MHz, acetone- d_6): trifluoro(4-fluorobenzyl)- λ^4 -borane, potassium salt



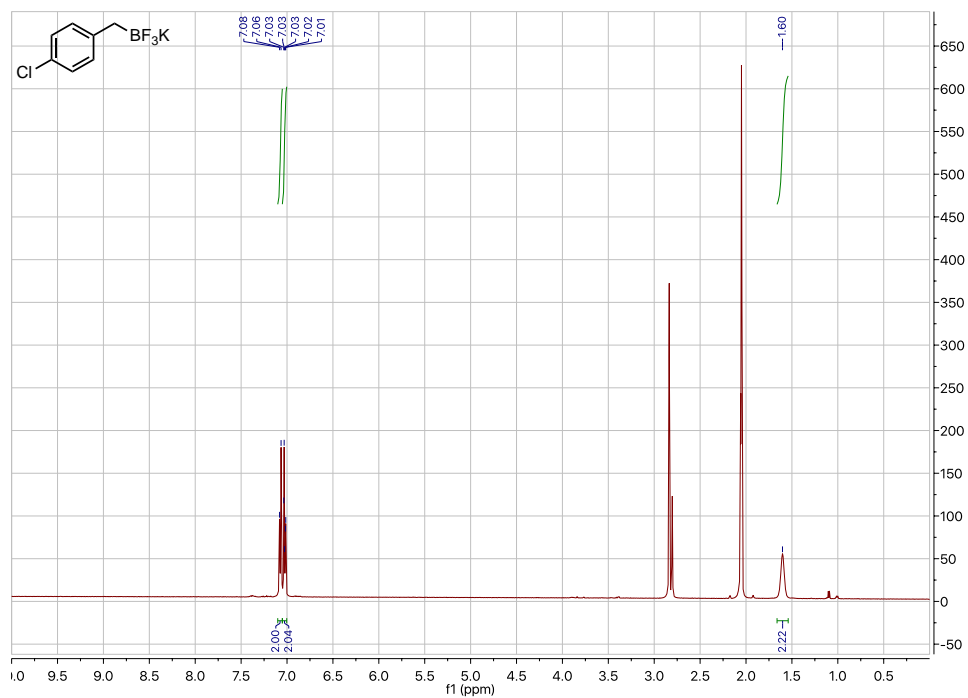
^{19}F NMR (282 MHz, acetone- d_6): trifluoro(4-fluorobenzyl)- λ^4 -borane, potassium salt



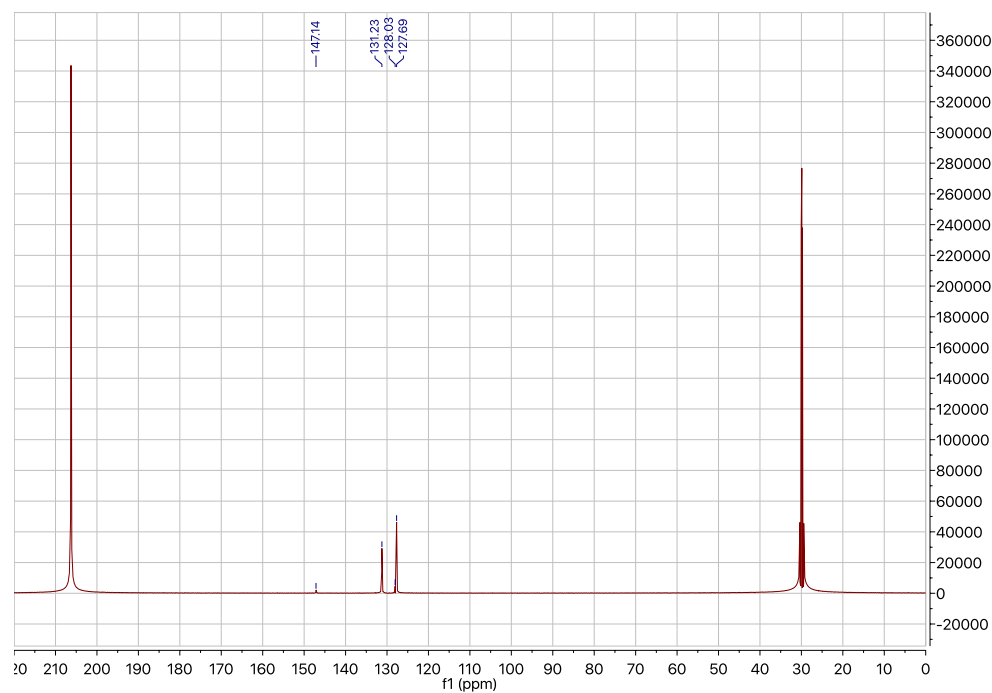
^{11}B NMR (96 MHz, acetone- d_6): trifluoro(4-fluorobenzyl)- λ^4 -borane, potassium salt



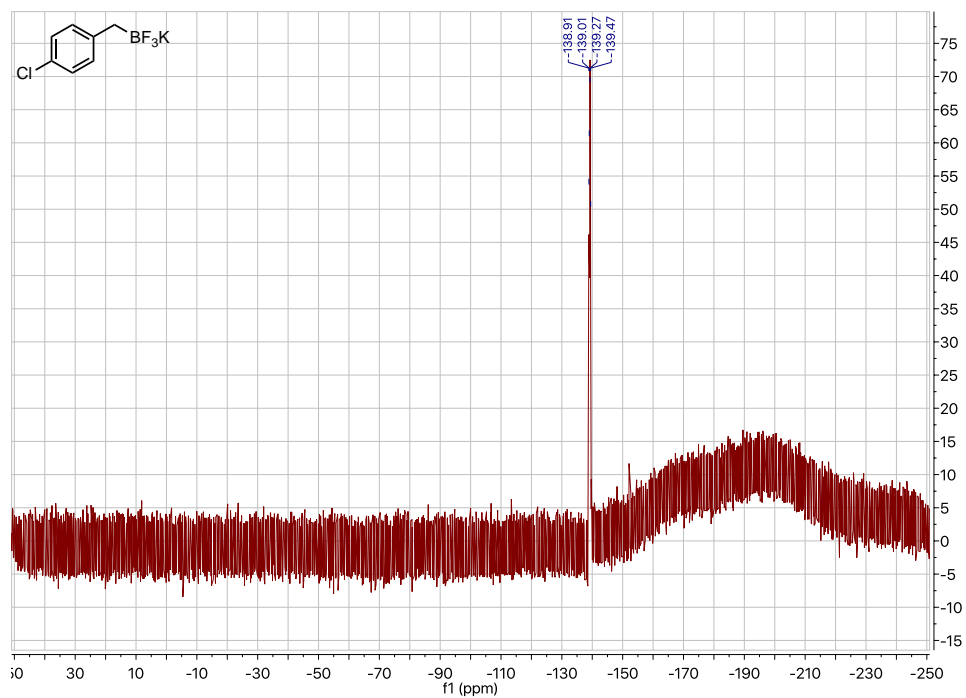
^1H NMR (501 MHz, acetone- d_6): (4-chlorobenzyl)trifluoro- λ^4 -borane, potassium salt



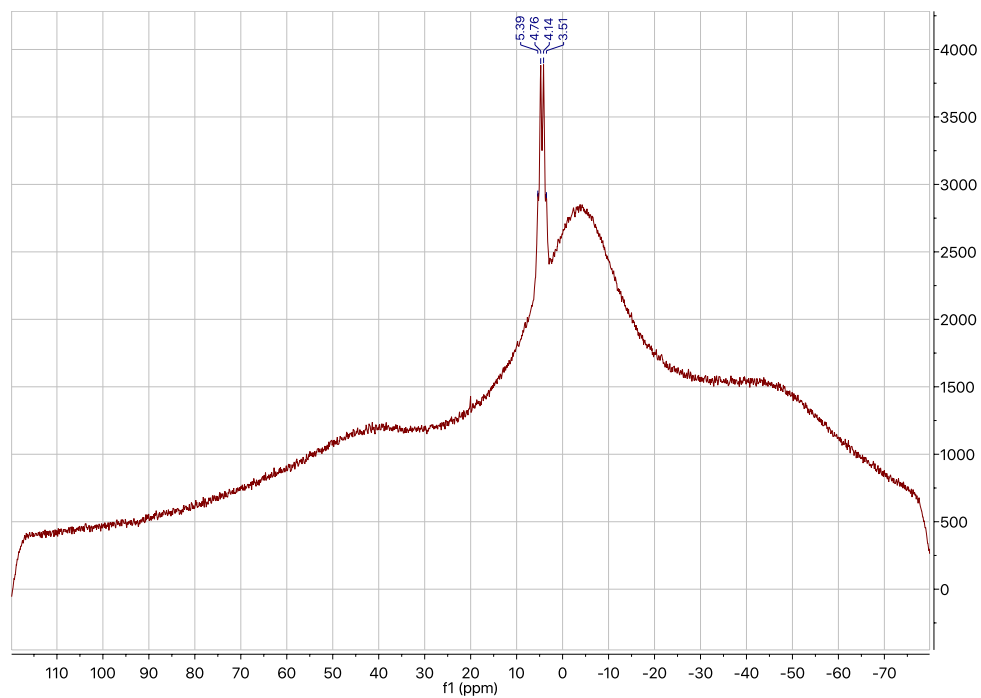
^{13}C NMR (126 MHz, acetone- d_6): (4-chlorobenzyl)trifluoro- λ^4 -borane, potassium salt



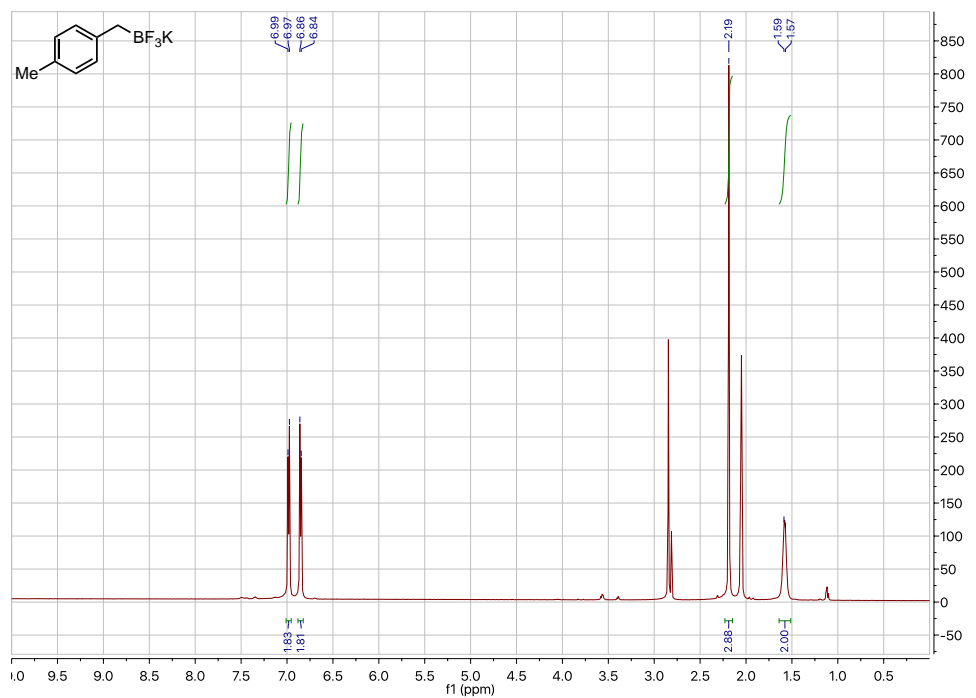
^{19}F NMR (282 MHz, acetone- d_6): (4-chlorobenzyl)trifluoro- λ^4 -borane, potassium salt



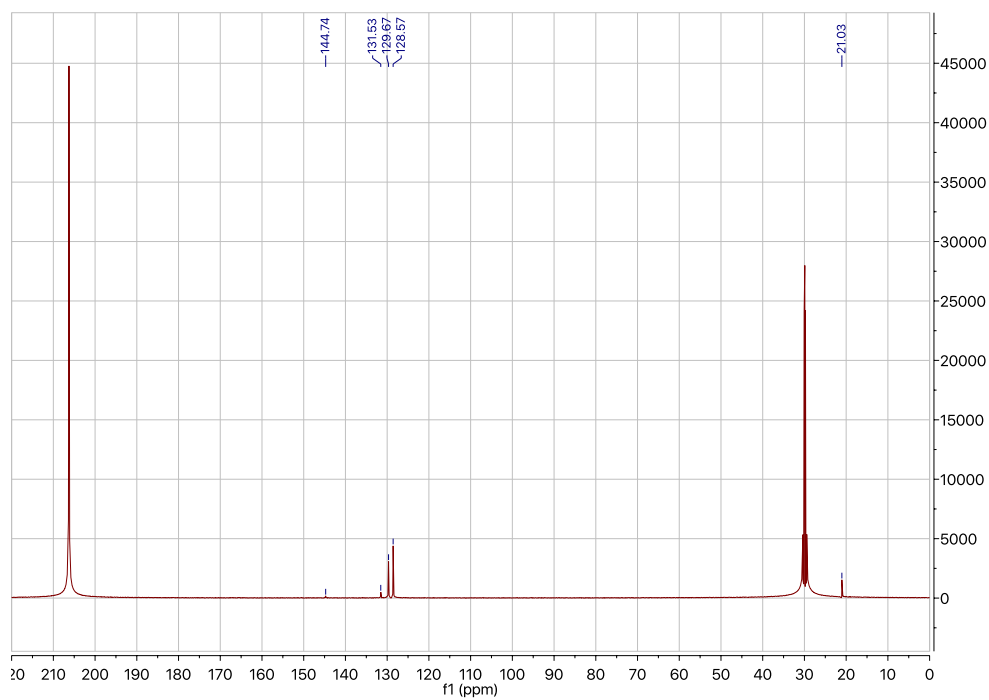
^{11}B NMR (96 MHz, acetone- d_6): (4-chlorobenzyl)trifluoro- λ^4 -borane, potassium salt



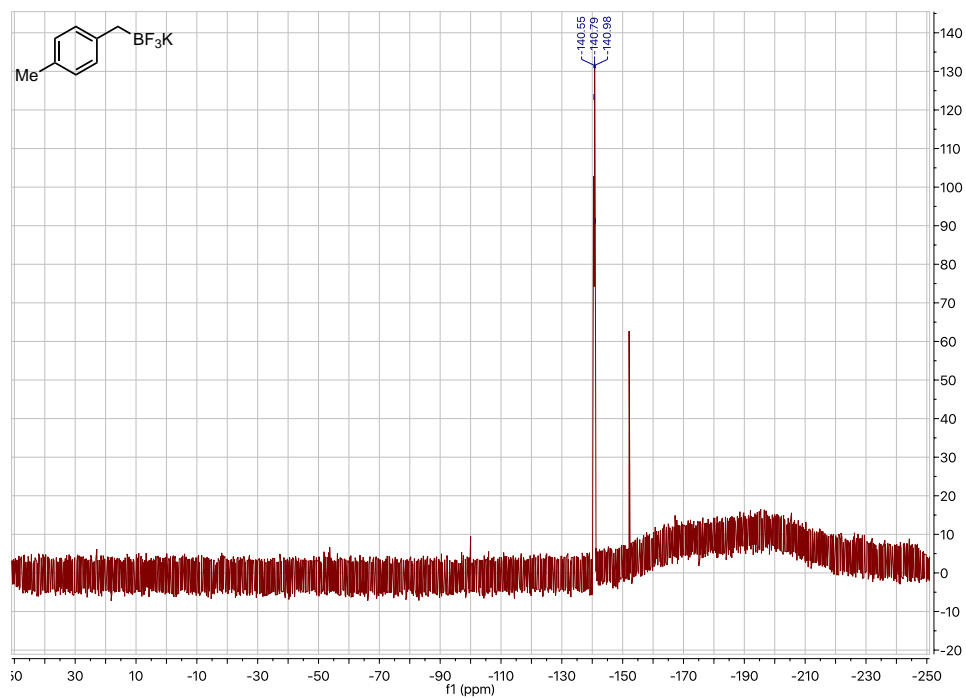
^1H NMR (501 MHz, acetone- d_6): trifluoro(4-methylbenzyl)- λ^4 -borane, potassium salt



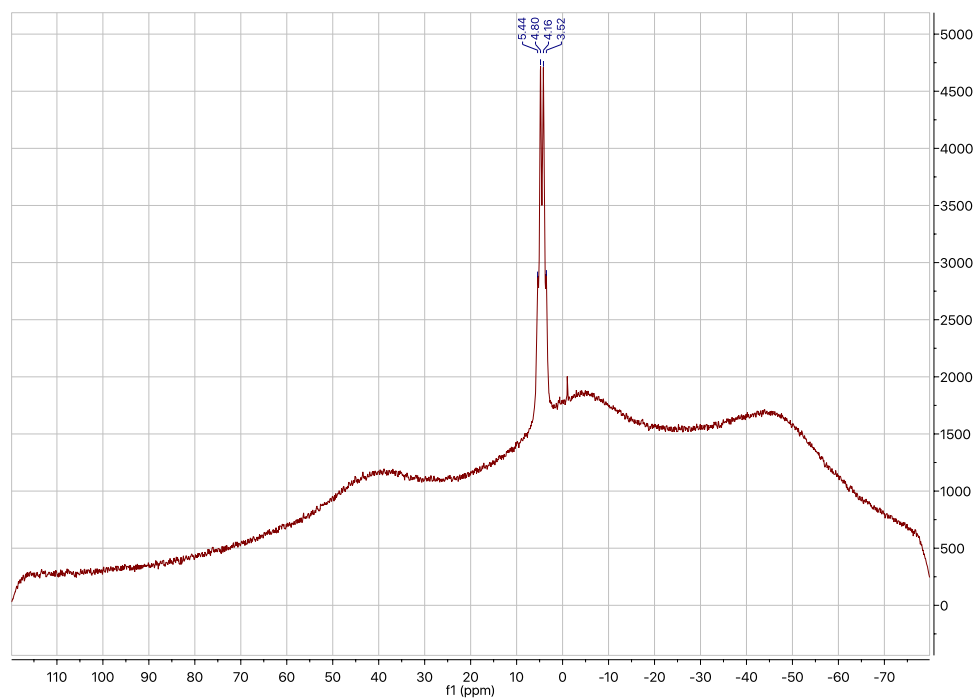
^{13}C NMR (126 MHz, acetone- d_6): trifluoro(4-methylbenzyl)- λ^4 -borane, potassium salt



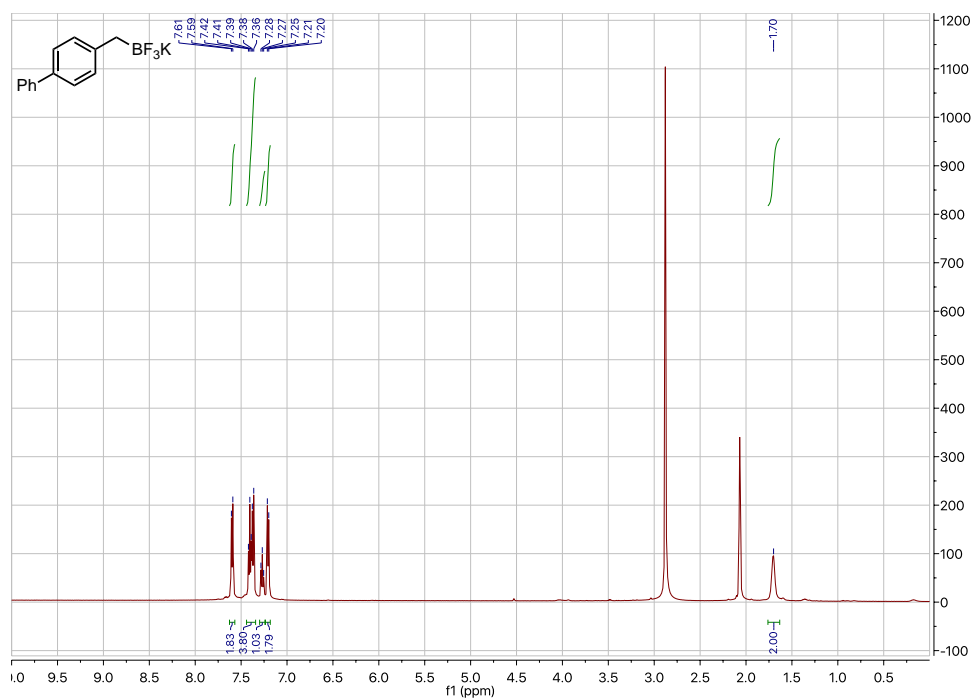
^{19}F NMR (282 MHz, acetone- d_6): trifluoro(4-methylbenzyl)- λ^4 -borane, potassium salt



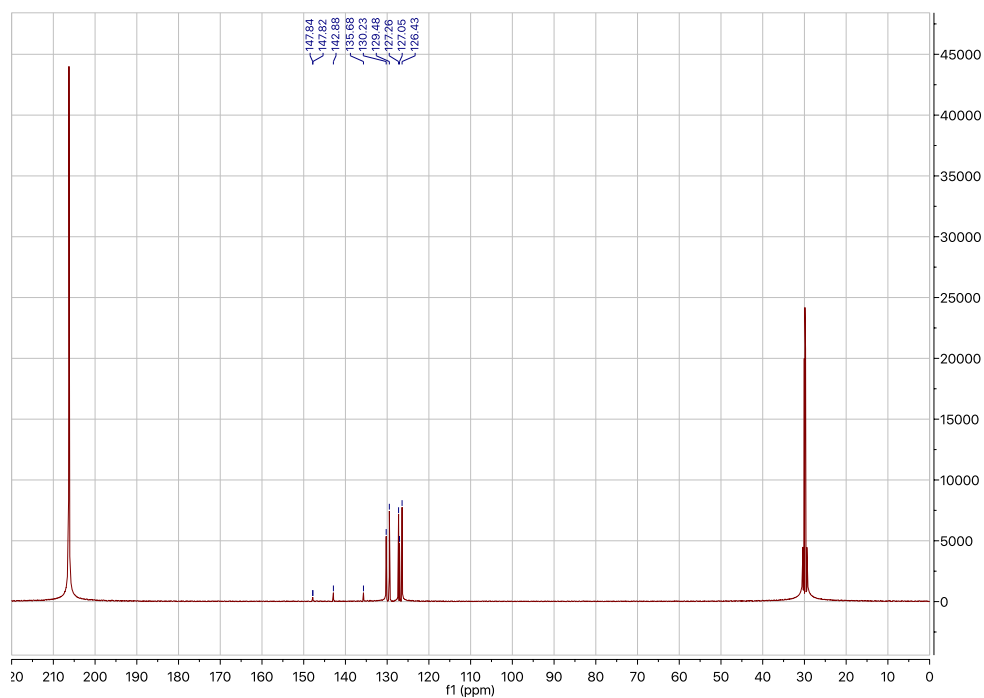
^{11}B NMR (96 MHz, acetone- d_6): trifluoro(4-methylbenzyl)- λ^4 -borane, potassium salt



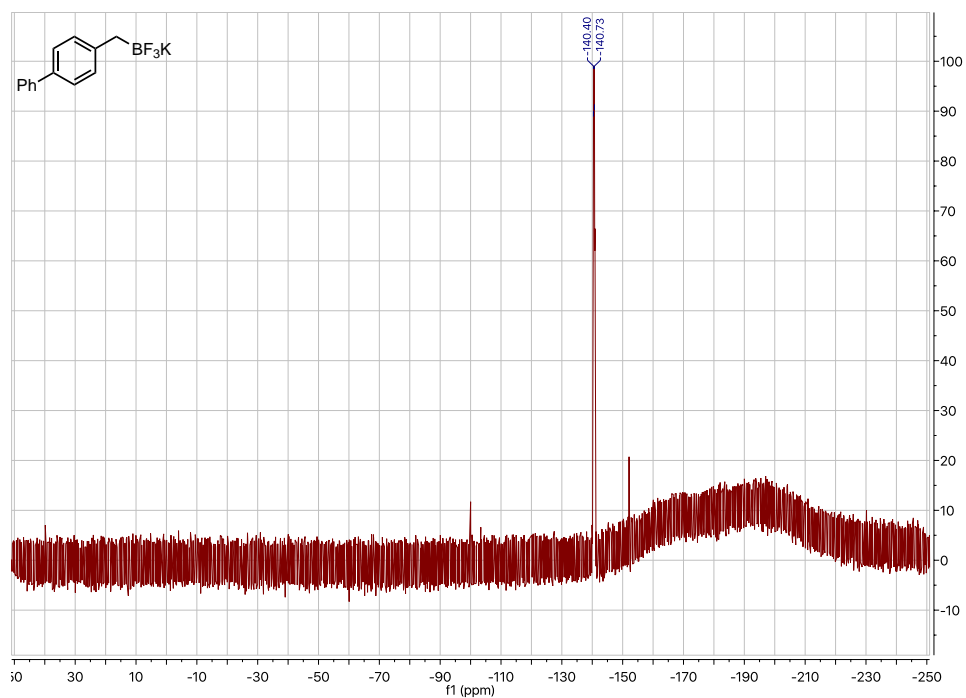
^1H NMR (501 MHz, acetone- d_6): ([1,1'-biphenyl]-4-ylmethyl)trifluoro- λ^4 -borane, potassium salt



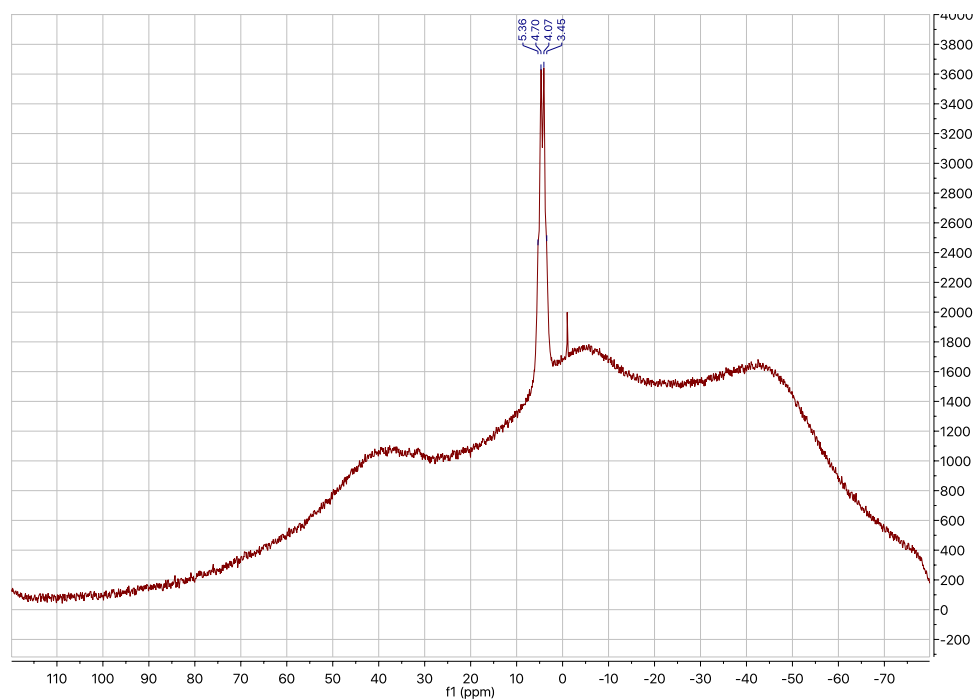
^{13}C NMR (126 MHz, acetone- d_6): ([1,1'-biphenyl]-4-ylmethyl)trifluoro- λ^4 -borane, potassium salt



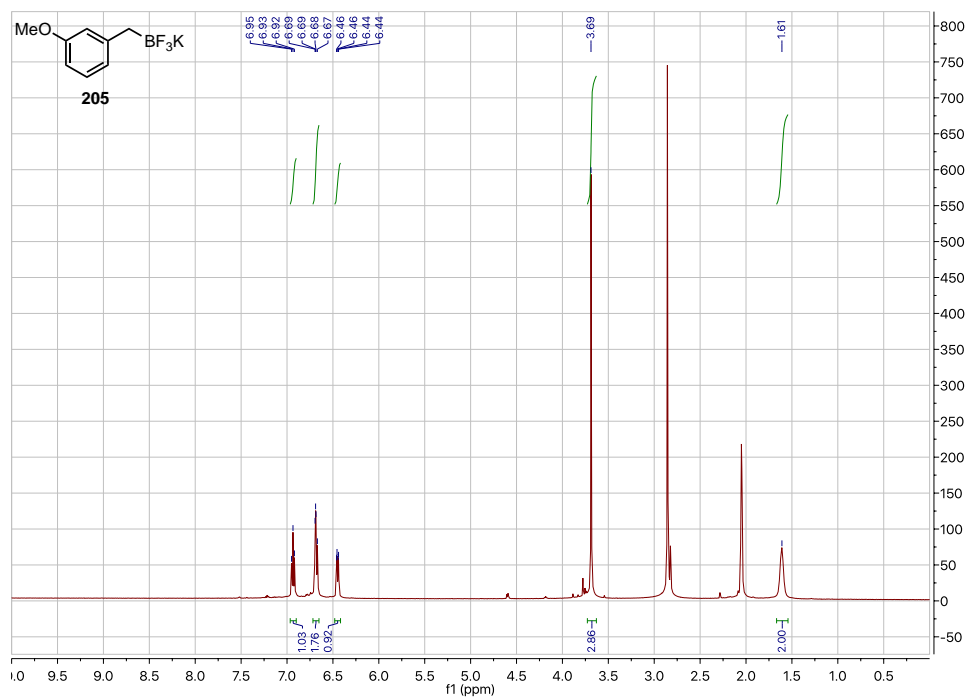
^{19}F NMR (282 MHz, acetone- d_6): ([1,1'-biphenyl]-4-ylmethyl)trifluoro- λ^4 -borane, potassium salt



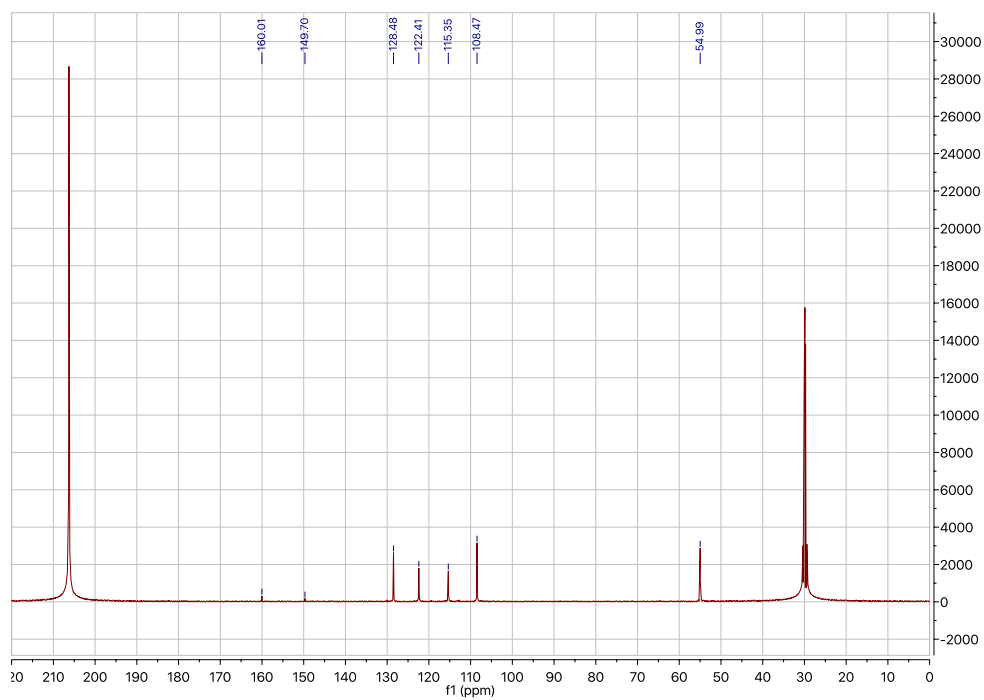
^{11}B NMR (96 MHz, acetone- d_6): ([1,1'-biphenyl]-4-ylmethyl)trifluoro- λ^4 -borane, potassium salt



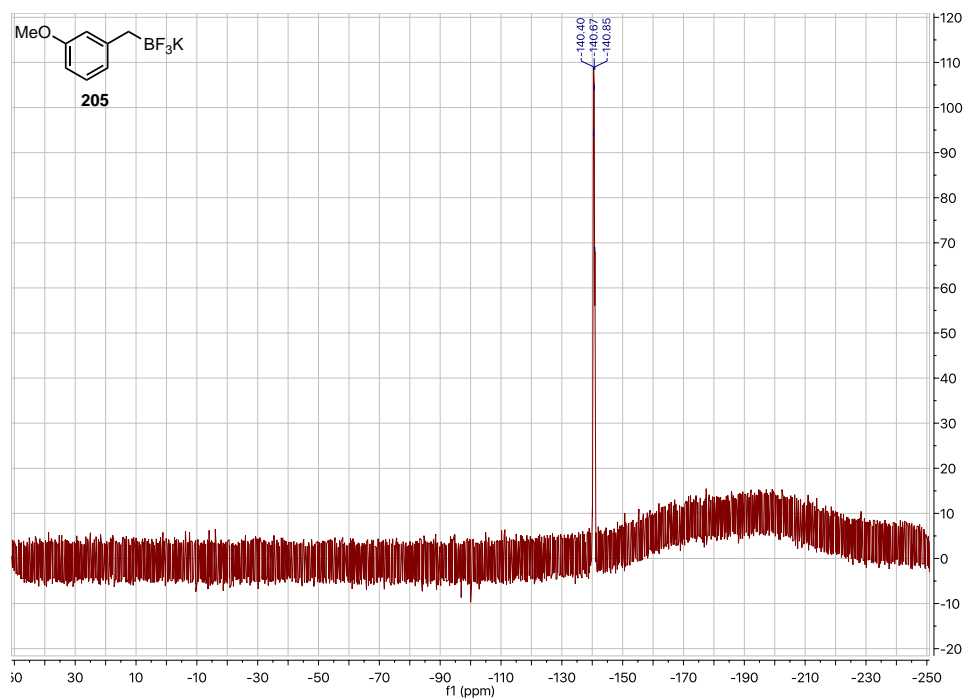
^1H NMR (501 MHz, acetone- d_6): trifluoro(3-methoxybenzyl)- λ^4 -borane, potassium salt (205)



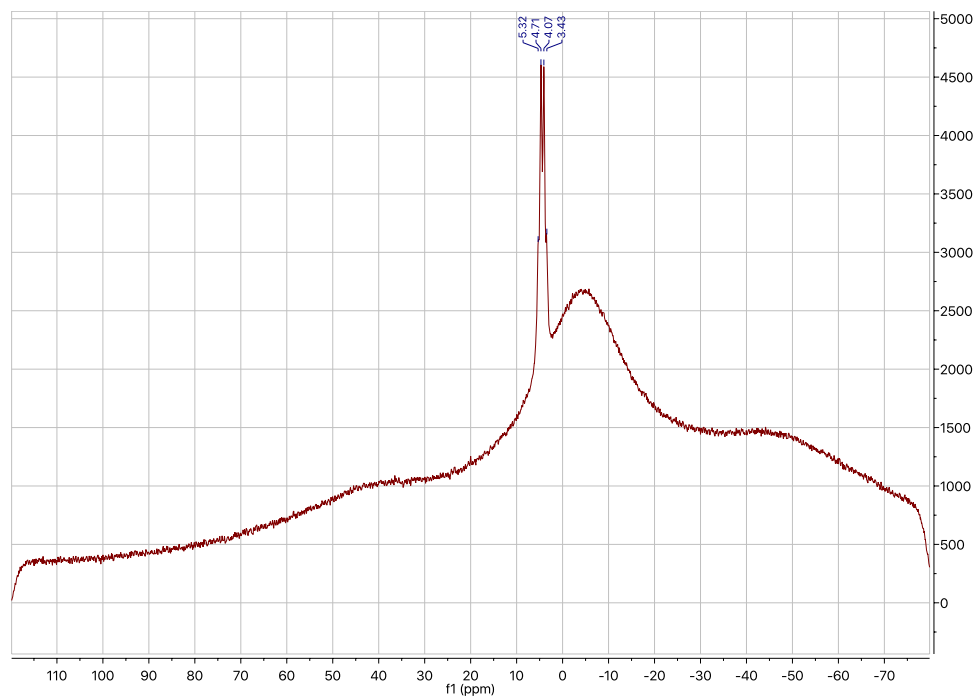
^{13}C NMR (126 MHz, acetone- d_6): trifluoro(3-methoxybenzyl)- λ^4 -borane, potassium salt



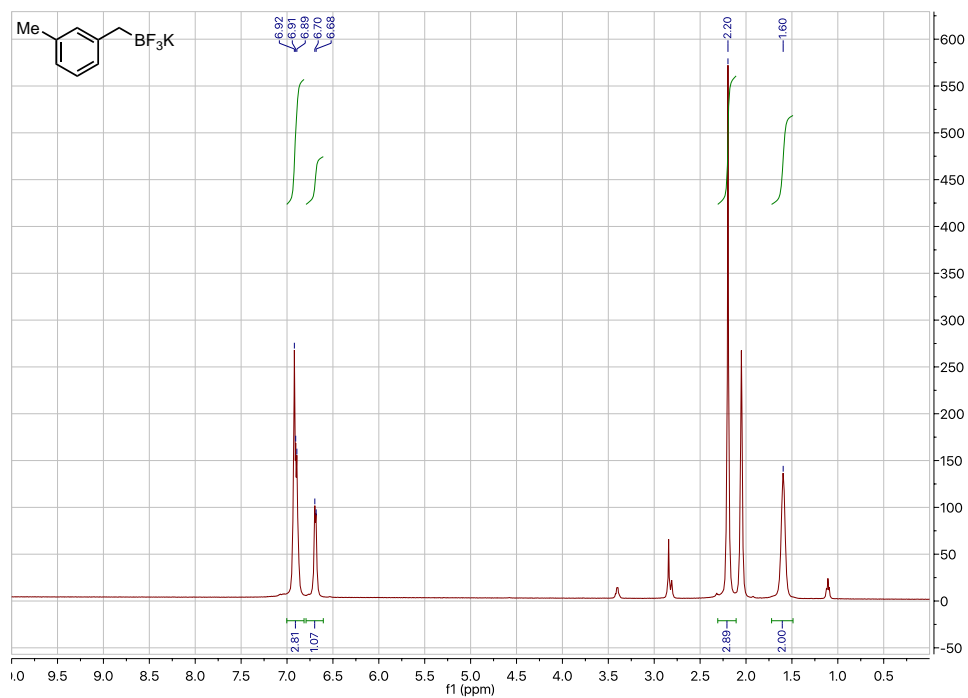
^{19}F NMR (282 MHz, acetone- d_6): trifluoro(3-methoxybenzyl)- λ^4 -borane, potassium salt
(205)



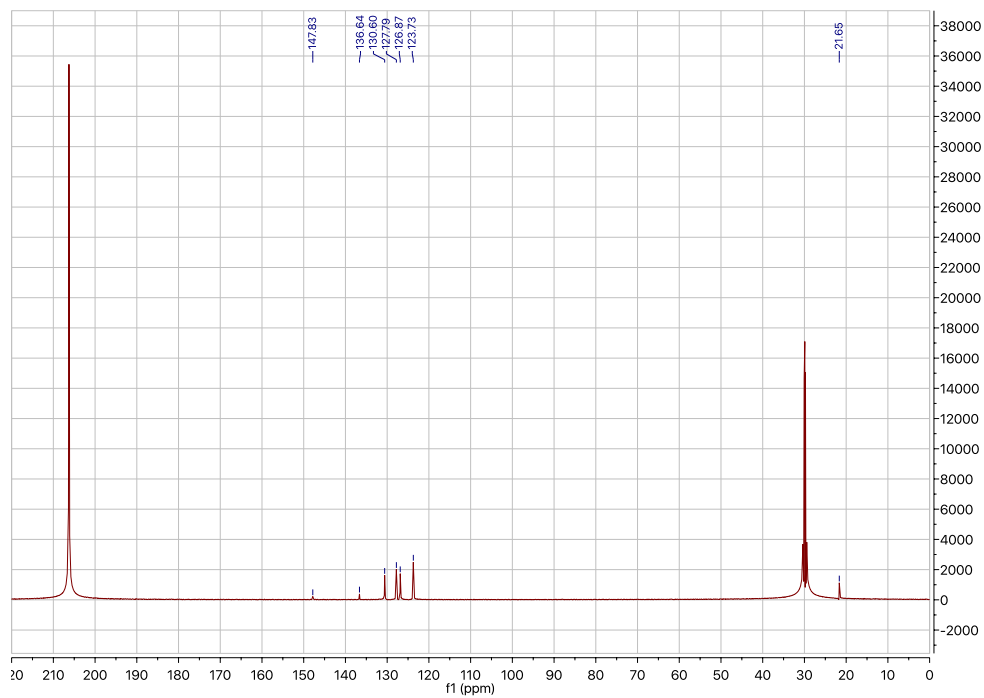
^{11}B NMR (96 MHz, acetone- d_6): trifluoro(3-methoxybenzyl)- λ^4 -borane, potassium salt



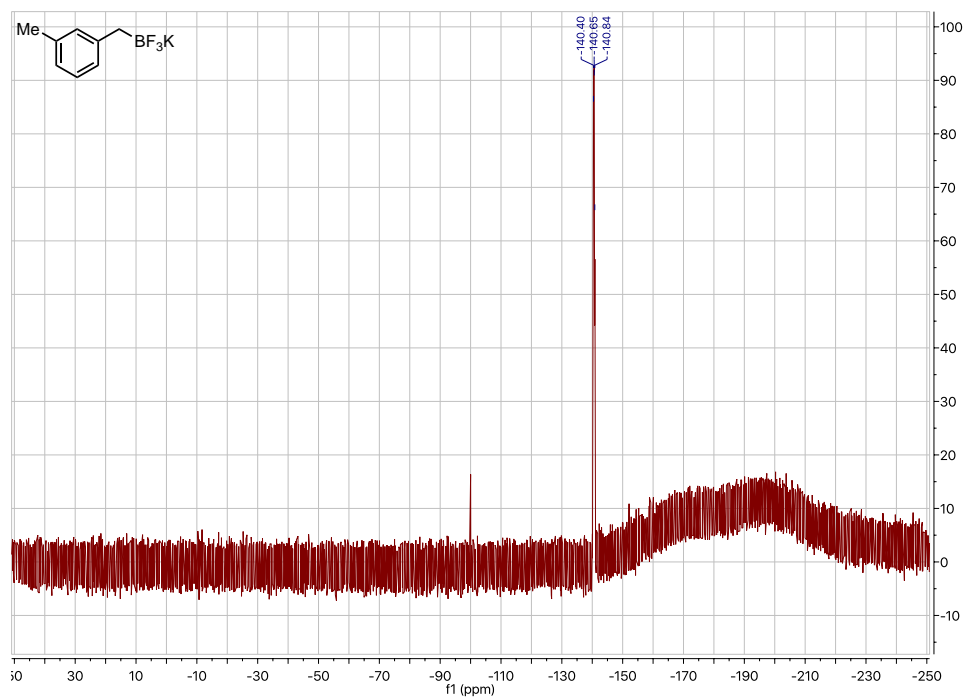
^1H NMR (501 MHz, acetone- d_6): trifluoro(3-methylbenzyl)- λ^4 -borane, potassium salt



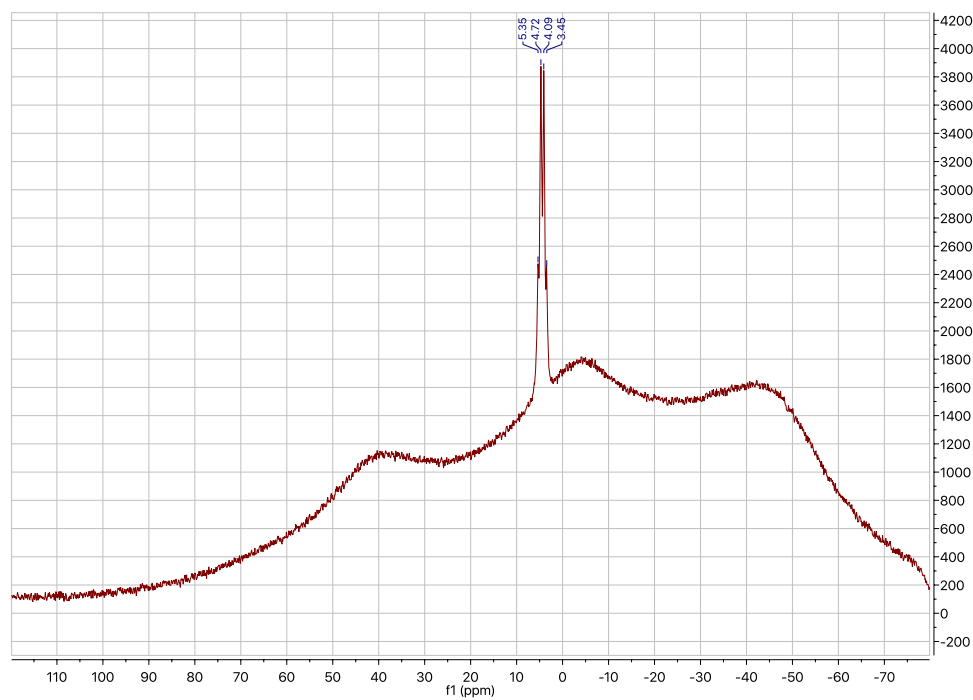
^{13}C NMR (126 MHz, acetone- d_6): trifluoro(3-methylbenzyl)- λ^4 -borane, potassium salt



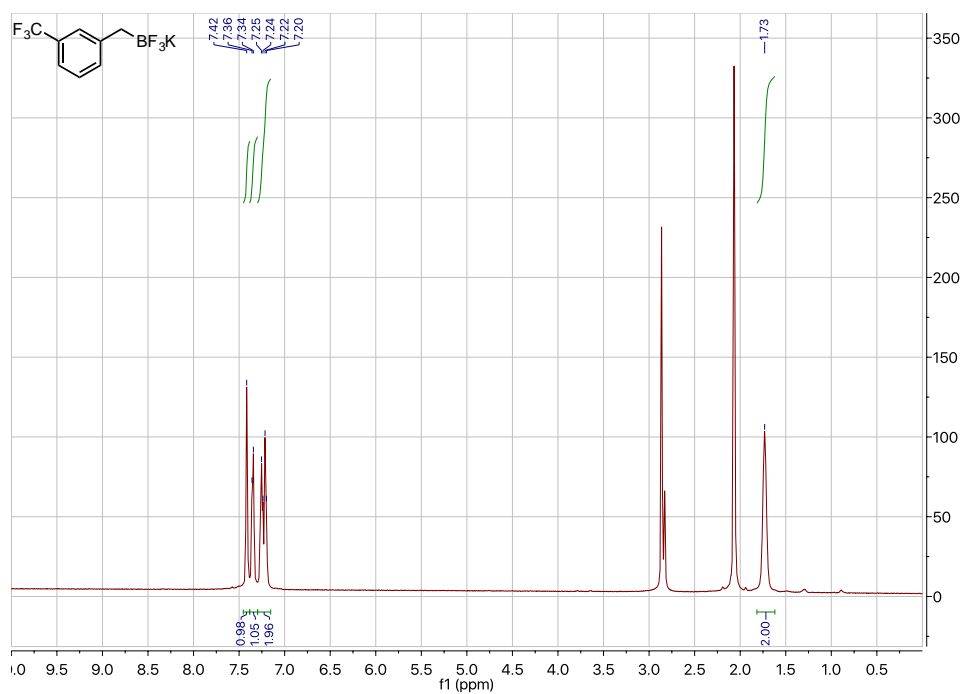
^{19}F NMR (282 MHz, acetone- d_6): trifluoro(3-methylbenzyl)- λ^4 -borane, potassium salt



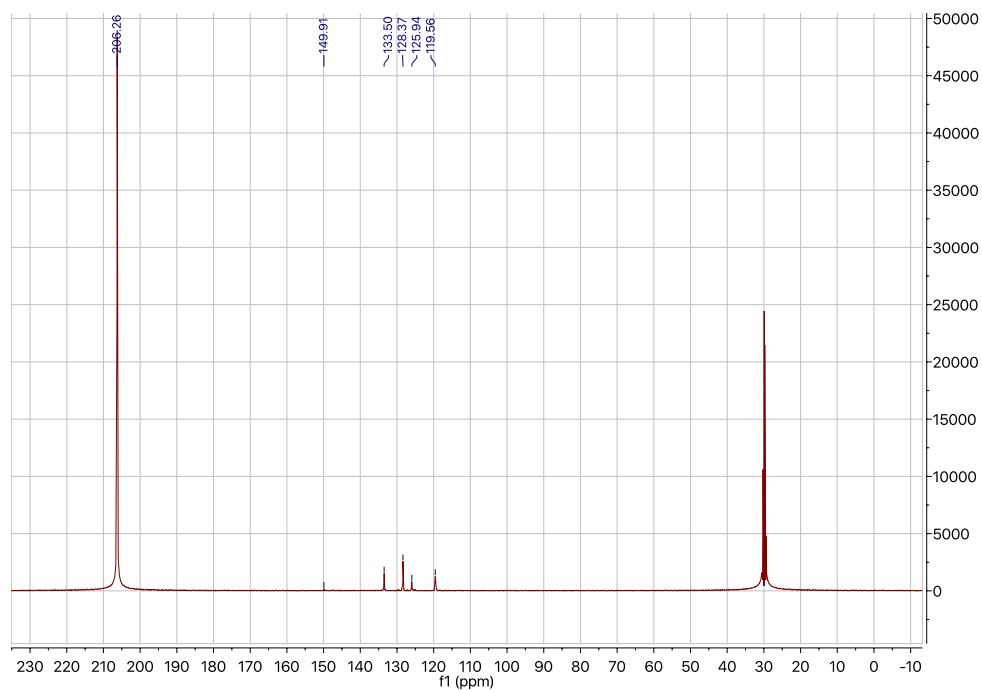
^{11}B NMR (96 MHz, acetone- d_6): trifluoro(3-methylbenzyl)- λ^4 -borane, potassium salt



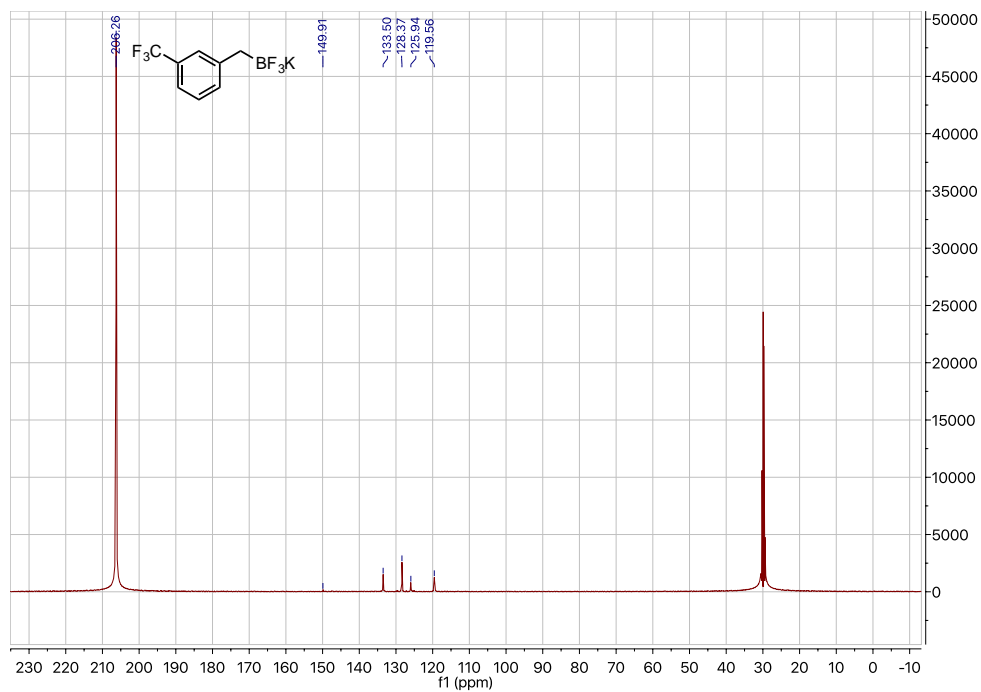
^1H NMR (501 MHz, acetone- d_6): trifluoro(3-(trifluoromethyl)benzyl)- λ^4 -borane, potassium salt



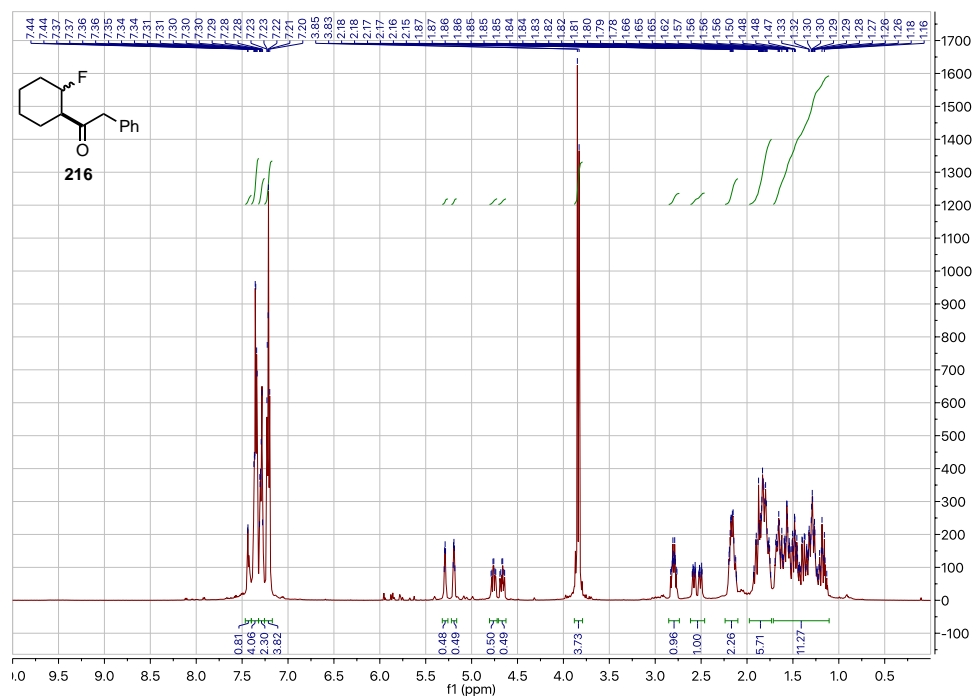
^{13}C NMR (126 MHz, acetone- d_6): trifluoro(3-(trifluoromethyl)benzyl)- λ^4 -borane, potassium salt



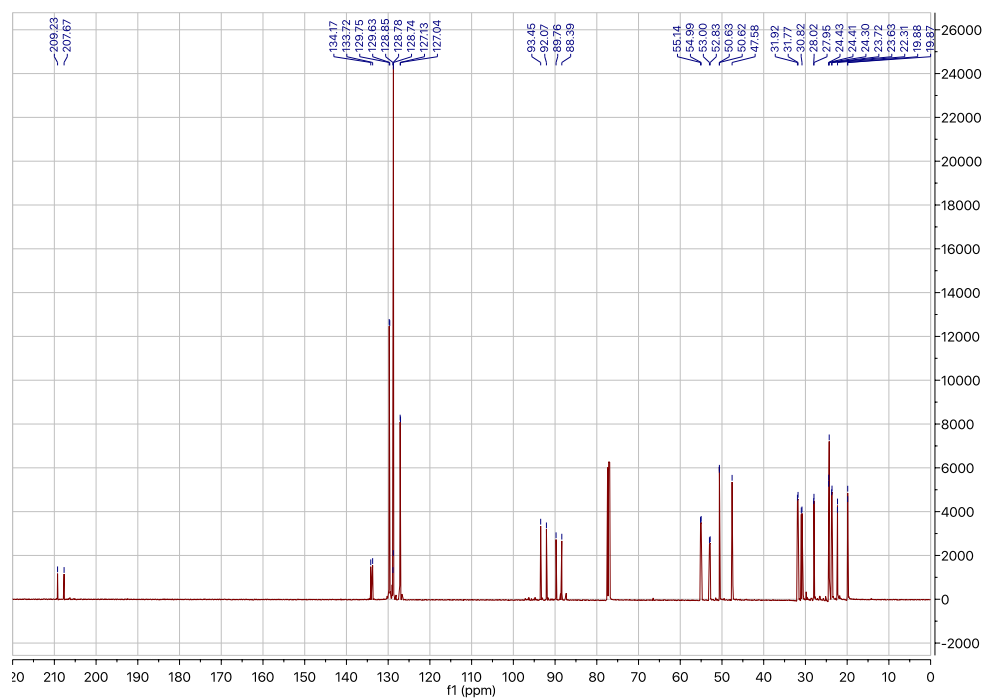
^{19}F NMR (282 MHz, acetone- d_6): trifluoro(3-(trifluoromethyl)benzyl)- λ^4 -borane, potassium salt



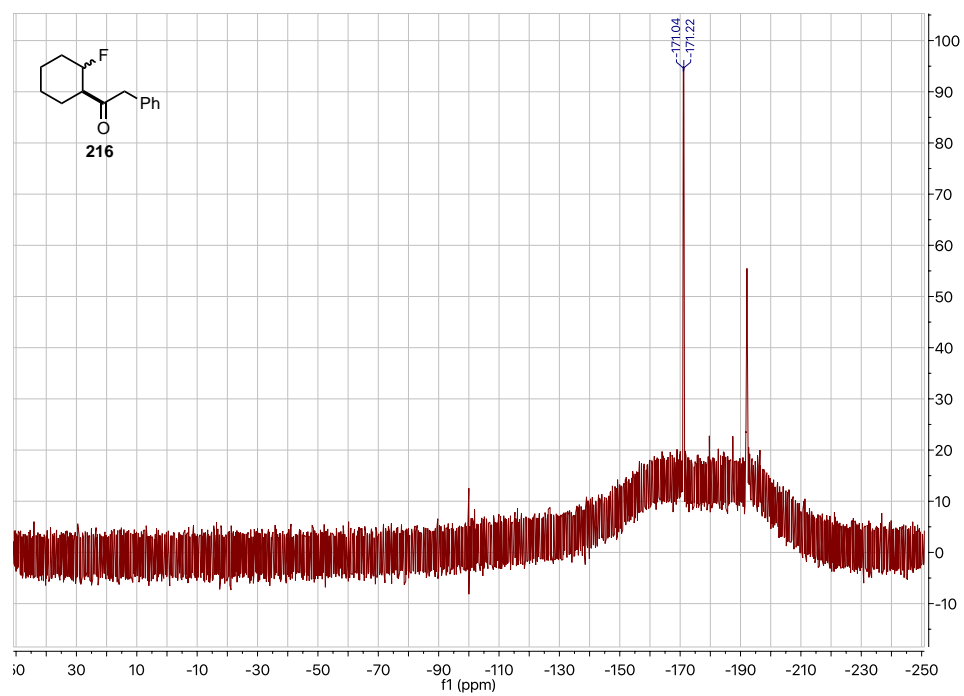
¹H NMR (501 MHz, CDCl₃): 1-((1*R*)-2-fluorocyclohexyl)-2-phenylethan-1-one (216)



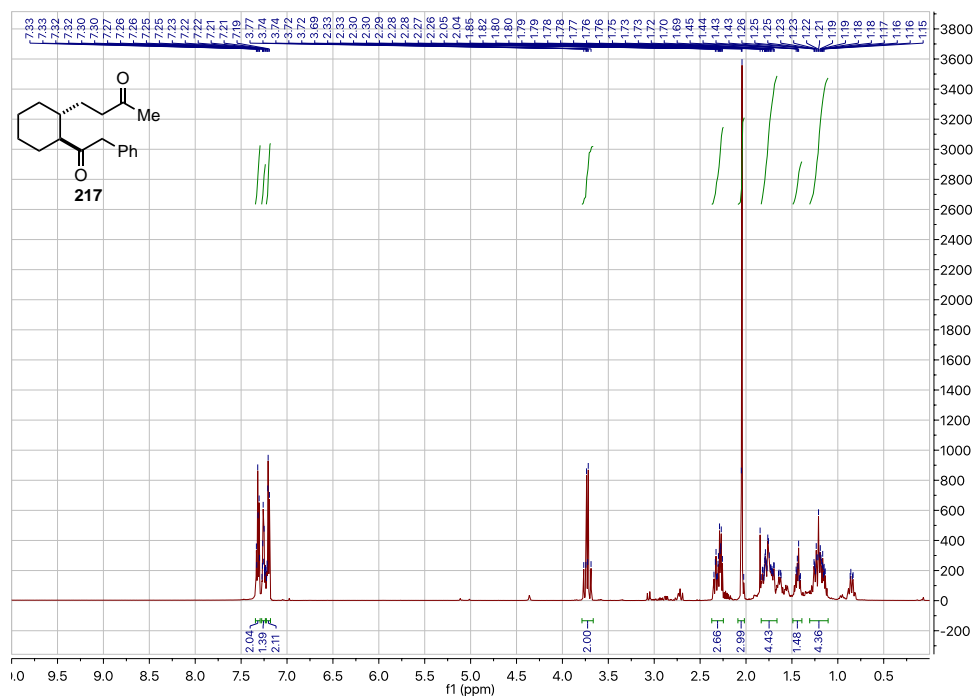
¹³C NMR (126 MHz, CDCl₃): 1-((1*R*)-2-fluorocyclohexyl)-2-phenylethan-1-one



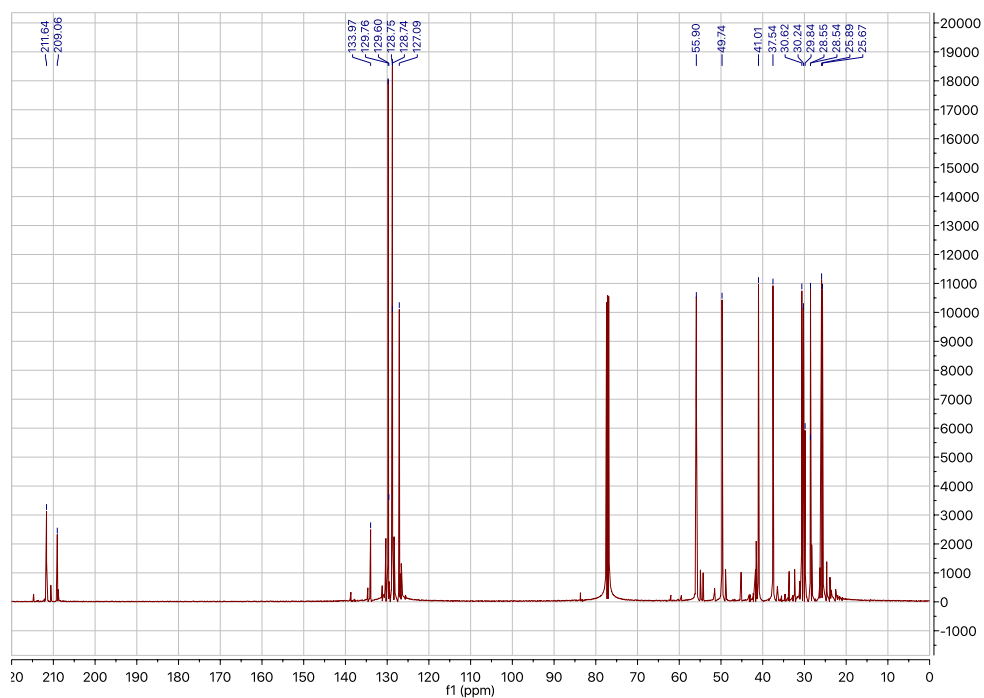
^{19}F NMR (282 MHz, CDCl_3): 1-((1*R*)-2-fluorocyclohexyl)-2-phenylethan-1-one (216)



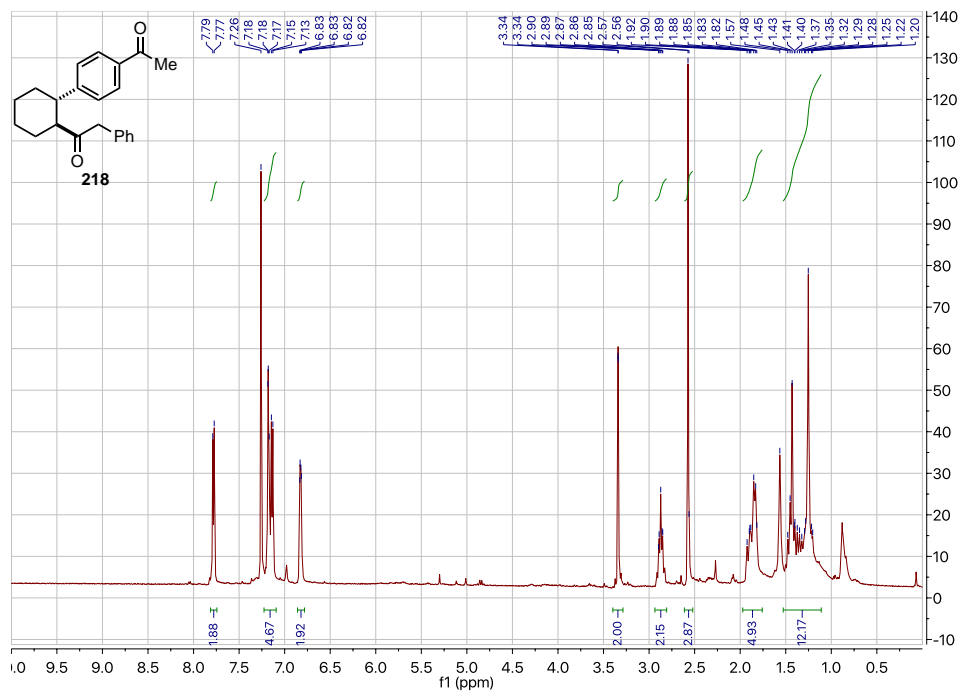
^1H NMR (501 MHz, CDCl_3): 4-((1*R*,2*S*)-2-(2-phenylacetyl)cyclohexyl)butan-2-one (217)



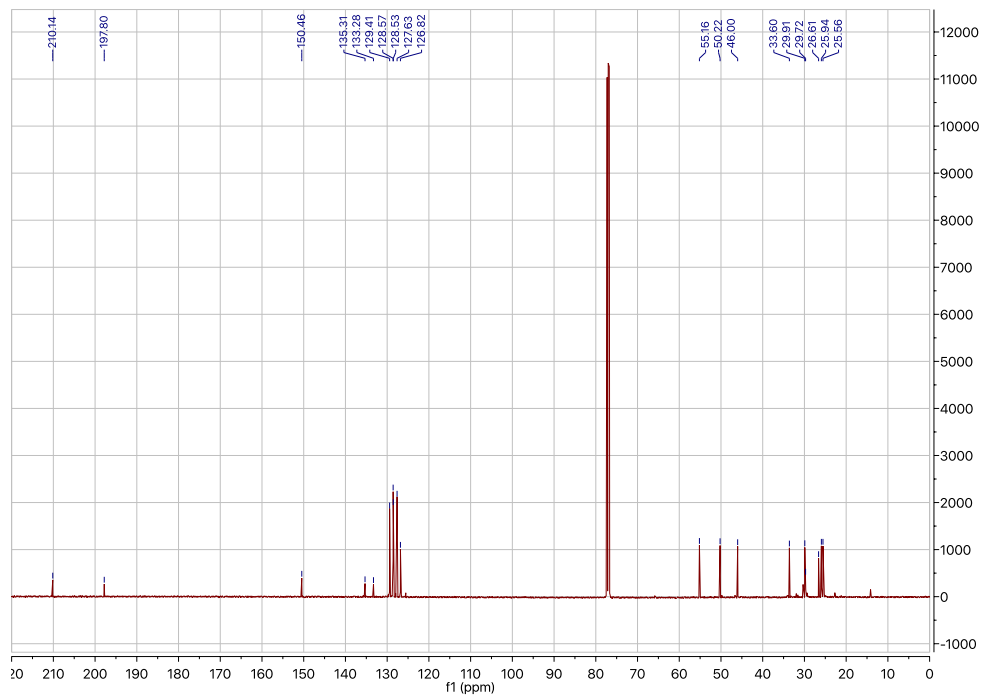
^{13}C NMR (126 MHz, CDCl_3): 4-((1*R*,2*S*)-2-(2-phenylacetyl)cyclohexyl)butan-2-one



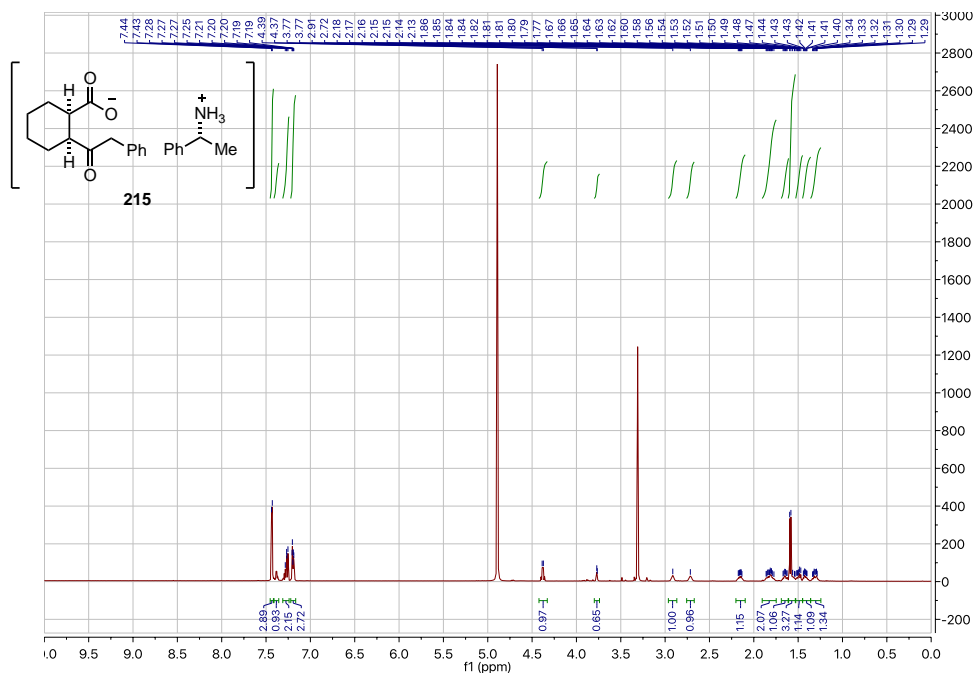
^1H NMR (501 MHz, CDCl_3): 1-((1*S*,2*S*)-2-(4-acetylphenyl)cyclohexyl)-2-phenylethan-1-one
(218)



^{13}C NMR (126 MHz, CDCl_3): 1-((1*S*,2*S*)-2-(4-acetylphenyl)cyclohexyl)-2-phenylethan-1-one



^1H NMR (501 MHz, CD_3OD): (*R*)-1-phenylethan-1-aminium (1*R*,2*S*)-2-(2-phenylacetyl)cyclohexane-1-carboxylate (215)



References

- (1) Stache, E. E.; Rovis, T.; Doyle, A. G. *Angew. Chem. Int. Ed. Engl.* **2017**, *56* (13), 3679.
- (2) Bercot, E. A.; Kindrachuk, D. E.; Rovis, T. *Org. Lett.* **2005**, *7* (1), 107.
- (3) Jain, P.; Yi, S.; Flaherty, P. T. *J. Heterocyclic Chem.* **2013**, *50*, E166-E173
- (4) Tellis, J. C.; Primer, D. N.; Molander, G. A. *Science* **2014**, *345* (6195), 433.
- (5) Shields, B. J.; Doyle, A. G. *J. Am. Chem. Soc.* **2016**, *138* (39), 12719.
- (6) Johnson, J. B.; Bercot, E. A.; Rowley, J. M.; Coates, G. W.; Rovis, T. *J. Am. Chem. Soc.* **2007**, *129* (9), 2718.
- (7) Ventre, S.; Petronijevic, F. R.; MacMillan, D. W. C. *J. Am. Chem. Soc.* **2015**, *137*, 5654.
- (8) Chu, L.; Ohta, C.; Zhiwei, Z.; MacMillan, D. W. C. *J. Am. Chem. Soc.* **2014**, *136* (31), 10886.
- (9) Luo, J.; Zhang, J. *ACS Catal* **2016**, *6* (2), 873.

Appendix II

Phosphine mediated C–O bond activation via photoredox catalysis

General Procedures. Unless otherwise noted, reactions were performed under a nitrogen atmosphere with the exclusion of moisture. N₂-flushed stainless steel needles and plastic syringes were used to transfer air- and moisture-sensitive reagents. Reactions were monitored by thin-layer chromatography (TLC) on EMD Silica Gel 60 F254 plates, visualizing with UV light (254 nm) or KMnO₄ stain. Solvent was freshly distilled/degassed prior to use unless otherwise noted. Organic solutions were concentrated under reduced pressure using a rotary evaporator (25 °C, <50 torr). Automated column chromatography was performed using pre-packed silica gel cartridges on a Biotage SP4 (40-53 µm, 60 Å).

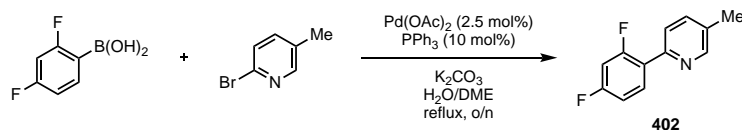
Materials. Commercial reagents were purchased from Sigma-Aldrich, Alfa Aesar, Acros, Strem, TCI, Boron Molecular, Frontier Scientific or Oakwood and used as received with the following exceptions. *p*-Toluic acid and hydrocinnamic acid were recrystallized from toluene and CHCl₃, respectively. Diethyl ether (Et₂O), tetrahydrofuran (THF), toluene (PhMe) and 1,4-dioxane were dried by passing through activated alumina columns and stored over molecular sieves in a N₂-filled glovebox; *N,N*-dimethylformamide (DMF) was dried by passing through a column of activated molecular sieves. NMP (*N*-methyl pyrrolidinone), trifluorotoluene (PhCF₃), and acetonitrile (ACN or MeCN) were obtained in anhydrous form from Sigma-Aldrich, taken into an N₂-filled glovebox and used as received.

Instrumentation. Proton nuclear magnetic resonance (¹H NMR) spectra were recorded on a Bruker 500 MHz or NB 300 MHz AVANCE spectrometer. Proton chemical shifts are reported in parts per million downfield from tetramethylsilane and are referenced to residual protium in the

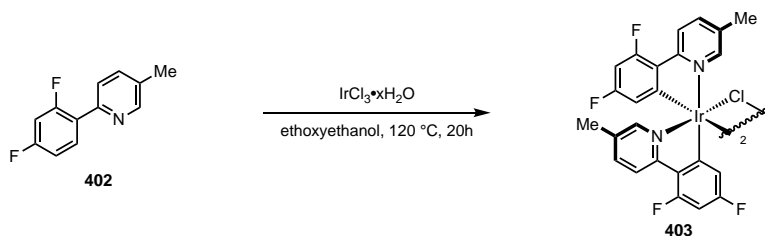
NMR solvent ($\text{CHCl}_3 = \delta$ 7.26 ppm or $(\text{CD}_3)_2\text{CO} = 2.05$). Carbon nuclear magnetic resonance (^{13}C NMR) were recorded on a Bruker 500 AVANCE spectrometer (126 MHz). Chemical shifts for carbon are reported in parts per million downfield from tetramethylsilane and are referenced to the carbon resonances of the solvent residual peak ($\text{CDCl}_3 = \delta$ 77.16 ppm or $((\text{CD}_3)_2\text{CO} = 206.26$ ppm and 29.840 ppm). Fluorine nuclear magnetic resonance (^{19}F NMR) were reported on a Bruker NB 300 AVANCE (282 MHz) spectrometer. Boron nuclear magnetic resonance (^{11}B NMR) were reported on a Bruker NB 300 AVANCE (96 MHz) spectrometer. NMR data are represented as follows: chemical shift (δ ppm), multiplicity (s = singlet, d = doublet, t = triplet, q = quartet, m = multiplet), coupling constant in Hertz (Hz), integration. Gas chromatography (GC) was performed on an Agilent 7890A series instrument equipped with a split-mode capillary injection S4 system and flame ionization detectors. High-resolution mass spectrometry was performed on an Agilent 6220 LC/MS using electrospray ionization time-of-flight (ESI-TOF) or an Agilent 7200 GC/MS spectrometer using electron impact time-of-flight (EI-TOF). FT-IR spectra were recorded on a Perkin-Elmer Paragon 500 and are reported in terms of frequency of absorption (cm^{-1}). Reversed-phase liquid chromatography/mass spectrometry (LC/MS) was performed on an Agilent 1260 Infinity analytical LC and Agilent 6120 Quadrupole LC/MS system using electrospray ionization/atmospheric-pressure chemical ionization (ESI/APCI) and UV detection at 254 nm and 280 nm.

Light Sources. All reaction scales (0.05-0.5 mmol) were carried out using Blue Kessil H150 LED Grow Lights.

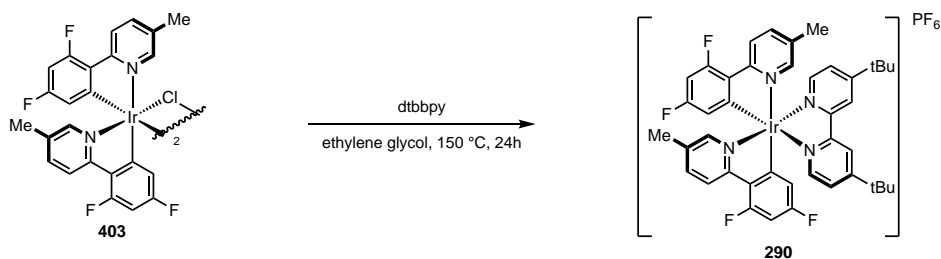
Preparation of starting materials:



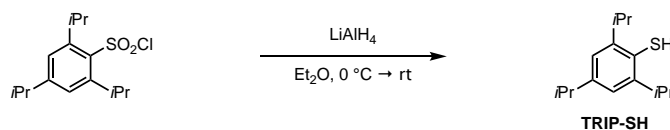
2-(2,4-difluorophenyl)-5-methylpyridine (402):¹ A 3-neck round bottom flask was charged with 2-bromo-5-methyl pyridine (1.03 g, 6.0 mmol, 1.0 equiv), (2,4-difluorophenyl)boronic acid (1.14 g, 7.2 mmol, 1.2 equiv), triphenylphosphine (157 mg, 0.6 mmol, 0.1 equiv), and potassium carbonate (2.24 g, 16.2 mmol, 2.7 equiv). Dimethoxyethane (10.9 mL, 0.55M) and water (8.1 mL, 0.73M) were added, and the reaction was sparged with N₂ for 15 min at room temperature. Then palladium acetate (34 mg, 0.15 mmol, 2.5 mol%) was added, and the reaction was sparged with N₂ for an additional 15 min at room temperature. The reaction was heated to reflux for 20 h. Upon completion, the reaction was cooled to room temperature and diluted with CH₂Cl₂ and water. The organic layer was washed with H₂O (3x) and brine (1x). The organic layer was dried over Na₂SO₄, filtered and concentrated to afford dark brown crystals. The crude residue was purified over silica with 5% → 20% EtOAc in hexanes to afford a light beige crystalline solid (1.01 g, 82% yield). Characterization matched literature data.



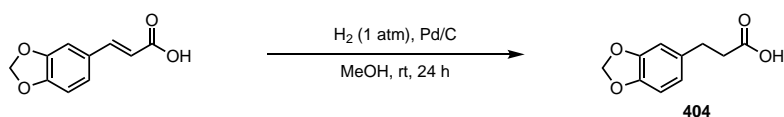
[Ir(dFMeppy)₂Cl]₂:² A 3-neck round bottom flask was charged with **402** (1.03 g, 5.0 mmol, 2.2 equiv) and IrCl₃•xH₂O (679 mg, 2.27 mmol, 1.0 equiv), then evacuated and backfilled with N₂ (5x). Ethoxyethanol/H₂O (3:1, 36.4 mL, 0.137M; previously degassed for 2 h by sparging with N₂) was added under N₂ and the reaction was heated to 120 °C for 20 h. The yellow mixture was filtered and the filter cake washed with copious amounts of water and hexanes. The fine yellow powder was dried under high vacuum overnight to afford **403** (1.13 g, 78% yield). No further characterization.



[Ir(dFMeppy)₂dtbbpy]PF₆ (290):² A round bottom flask was charged with dimer **403** (636 mg, 0.5 mmol, 1.0 equiv) and 4,4'-di-*tert*-butyl-2,2'-bipyridine (323 mg, 1.21 mmol, 2.41 equiv), then evacuated and backfilled with N₂ (5x). Ethylene glycol (33.3 mL, 0.015M, previously degassed for 2 h by sparging with N₂) was added under N₂. The suspension was then heated to 150 °C for 24 h, at which time the reaction became homogenous. The reaction was then cooled to room temperature and transferred to a separatory funnel with water. The aqueous was washed with hexanes (3x). The aqueous layer was then heated to 85 °C with stirring for 10 min to remove any residual hexanes. The mixture was then cooled to room temperature and an aqueous solution of ammonium hexafluorophosphate (2.5 g in 25 mL) was added. A precipitate formed immediately, and the suspension was stirred for 3 h at room temperature. The solid was collected by filtration and the filter cake was washed with copious amounts of hexanes and water to afford **290** as a fine yellow powder (828 mg, 82% yield). The powder was further purified by vapor diffusion recrystallization from acetone/hexanes. Characterization matches the literature values. **¹H NMR (300 MHz, (CD₃)₂CO):** δ 8.89 (d, *J* = 1.7 Hz, 2H), 8.27 (dd, *J* = 8.5, 1.5 Hz, 2H), 8.08 (d, *J* = 5.9 Hz, 2H), 7.89 (d, *J* = 8.7 Hz, 2H), 7.75 (dd, *J* = 5.9, 1.9 Hz, 2H), 7.56 (s, 2H), 6.73 (ddd, *J* = 12.5, 9.4, 2.3 Hz, 2H), 5.77 (dd, *J* = 8.6, 2.3 Hz, 2H), 2.13 (s, 6H), 1.43 (s, 18H).

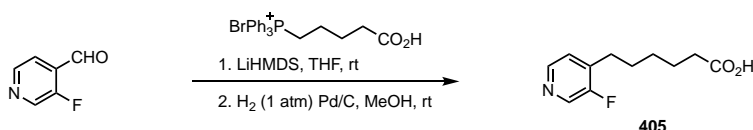


TRIP-SH.³ A flame dried round bottom flask was charged with lithium aluminum hydride (2.66 g, 70.0 mmol, 2.0 equiv). Diethyl ether (22.8 mL) was added under N₂, and the suspension was cooled to 0 °C. Then 2,4,6-triisopropylbenzenesulfonylchloride (10.6 g, 35.0 mmol, 1.0 equiv) in diethyl ether (35.0 mL) was added slowly to the suspension at 0 °C under N₂. After the vigorous reaction had ceased, lithium aluminum hydride (1.33 g, 35.0 mmol, 1.0 equiv) was added. The reaction was warmed to room temperature and stirred overnight under N₂. Upon completion, the reaction was cooled to 0 °C and diethyl ether (70 mL) was added. The reaction was quenched at 0 °C with water (3.99 mL), then 15% NaOH (aq) (3.99 mL) and finally water (11.97 mL). The suspension was stirred for 10 min at 0 °C, then MgSO₄ was added. The suspension was stirred for a further 30 min, then filtered and concentrated. The crude oil was distilled under reduced pressure to afford **TRIP-SH** as a colorless oil (6.37 g, 77% yield). Characterization data matched literature values. **¹H NMR (500 MHz, CDCl₃):** δ 7.02 (s, 2H), 3.52 (hept, *J* = 6.8 Hz, 2H), 3.09 (s, 1H), 2.88 (hept, *J* = 7.0 Hz, 1H), 1.38 – 1.18 (m, 18H).



3-(benzo[*d*][1,3]dioxol-5-yl)propanoic acid (404): A flask was charged with Pd/C (40 mg, 2 wt%) and purged with N₂. 3-(1,3-benzodioxol-5-yl)-2-propenoic acid (1.922 g, 10 mmol, 1 equiv) was added, and the flask was again purged with N₂. MeOH (50 mL, 0.2M) was added, and the mixture was sparged with N₂ for 15 min. Then the flask was fitted with an H₂ balloon, and the mixture was sparged with H₂ for 30 min, then stirred at room temp, under H₂ overnight. The reaction mixture was sparged with N₂ for 30 min to remove H₂, then the reaction filtered through

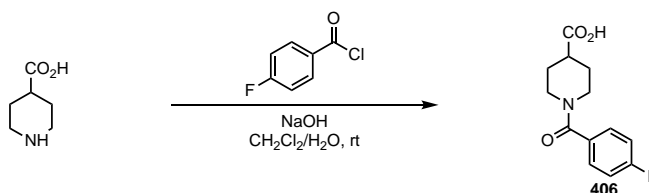
celite with EtOAc. The filtrate was concentrated to afford **404** as a white powder (1.82 mg, 94% yield) with no further purification necessary. **¹H NMR (500 MHz, CDCl₃):** δ 6.78 – 6.59 (m, 3H), 5.93 (s, 2H), 2.87 (t, *J* = 7.7 Hz, 2H), 2.64 (t, *J* = 7.7 Hz, 2H). **¹³C NMR (126 MHz, CDCl₃):** δ 178.32, 147.81, 146.16, 134.09, 121.25, 108.92, 108.45, 101.02, 36.01, 30.52.



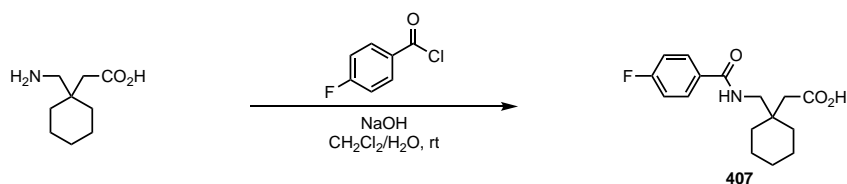
(*E*)-6-(4-fluorophenyl)hex-5-enoic acid:⁴ A flame dried round bottom flask was charged with 4-(carboxybutyl)triphenylphosphonium bromide (2.217 g, 5.00 mmol, 1.0 equiv) and THF (6.7 mL, 0.75M). To this slurry was added LiHMDS (1.0M in THF) (10.5 mL, 10.5 mmol, 2.1 equiv) at room temperature under N₂. The reaction became homogenous and orange-red in color, and stirred for 15 min at room temperature. Then, 3-fluoro-4-pyridinecarboxyaldehyde (498 μ L, 5.00 mmol, 1.0 equiv) in THF (2.22 mL, 2.25M) was added at room temperature under N₂. The reaction was stirred an additional 15 min at room temp. Then diethyl ether (20 mL) and water (20 mL) were added. The aqueous layer was separated. The organic layer was washed with water (10 mL). The combine aqueous layers were acidified to pH ~2 with conc. HCl, then extracted with ethyl acetate (2 x 20 mL). The combine organics were dried over MgSO₄, filtered and concentrated to afford a brown solid. The solid was further recrystallized from EtOH/water to afford the product as a beige solid (586 mg, 56% yield, 4:1 *E/Z*). Characterization data is from a 1.3:1 sample of *E/Z* isomers. **¹H NMR (500 MHz, CDCl₃):** δ 8.41 (d, *J* = 1.9 Hz, 1H, *cis*), 8.38 (d, *J* = 2.5 Hz, 1H, *trans*), 8.33 (d, *J* = 5.0 Hz, 1H, *cis*), 8.27 (d, *J* = 5.1 Hz, 1H, *trans*), 7.34 – 7.27 (m, 2H, *cis* and *trans*), 6.60 – 6.49 (m, 2H, *trans*), 6.44 (d, *J* = 11.7 Hz, 1H, *cis*), 5.98 (dt, *J* = 11.7, 7.6 Hz, 1H, *cis*), 2.45 – 2.34 (m, 6H, *cis* and *trans*), 2.35 – 2.27 (m, 2H, *cis*), 1.88 (p, *J* = 7.3 Hz, 2H, *trans*), 1.82 (p, *J* = 7.2 Hz, 2H, *cis*). **¹³C NMR (126 MHz, CDCl₃):** δ 177.88, 177.47, 157.11 (d, *J* = 252 Hz), 156.75 (d,

$J = 257$ Hz), 144.86 (d, $J = 5.0$ Hz), 144.53 (d, $J = 5.0$ Hz), 138.45 (d, $J = 4.8$ Hz), 138.05, 137.93, 137.84, 137.65, 137.44, 133.53 (d, $J = 12.6$ Hz), 133.21 (d, $J = 10.1$ Hz), 124.97, 121.12, 121.10, 120.20 (d, $J = 2.5$ Hz), 33.49, 33.29, 33.08, 28.30, 24.38, 23.86. **^{19}F NMR (282 MHz, CDCl_3):** δ -129.19 (d, $J = 6.3$ Hz, *cis*), -132.39 – -133.27 (m, *trans*). **HRMS:** (ESI-TOF) calculated for $([\text{C}_{11}\text{H}_{13}\text{FNO}_2 + \text{H}]^+)$: 210.0925, found 210.0920. **IR (ATR, cm^{-1}):** 2954, 2498, 1711, 1610, 1418, 1337, 1226, 1194, 1071, 856

6-(3-fluoropyridin-4-yl)hexanoic acid (405): A flask was charged with Pd/C (18 mg, 5 wt%) and purged with N_2 . Then (*E*)-6-(3-fluoropyridin-4-yl)hex-5-enoic acid (360 mg, 1.72 mmol, 1 equiv) was added, and the flask was again purged with N_2 . MeOH (8.6 mL, 0.2M) was added, and the mixture was sparged with N_2 for 15 min. Then the flask was fitted with an H_2 balloon, and the mixture was sparged with H_2 for 30 min, then stirred at room temp, under H_2 overnight. The reaction mixture was sparged with N_2 for 30 min to remove H_2 , then the reaction filtered through celite with EtOAc. The filtrate was concentrated to afford **405** as a white powder (268 mg, 74% yield) with no further purification necessary. **^1H NMR (500 MHz, CDCl_3):** δ 8.37 (s, 1H), 8.30 (d, $J = 4.4$ Hz, 1H), 7.16 (t, $J = 5.4$ Hz, 1H), 2.68 (t, $J = 7.7$ Hz, 2H), 2.35 (t, $J = 7.4$ Hz, 2H), 1.66 (p, $J = 7.9$ Hz, 4H), 1.47 – 1.31 (m, 2H). **^{13}C NMR (126 MHz, CDCl_3):** δ 178.36, 158.66 (d, $J = 254.5$ Hz), 145.18, 138.63 (d, $J = 13.7$ Hz), 137.41 (d, $J = 25.5$ Hz), 125.37, 34.08, 28.90, 28.68, 28.23, 24.58. **^{19}F NMR (282 MHz, Chloroform-*d*):** δ -132.79 (d, $J = 6.2$ Hz). **HRMS:** (ESI-TOF) calculated for $([\text{C}_{11}\text{H}_{14}\text{FNO}_2 + \text{H}]^+)$: 212.1081, found 212.1083. **IR (ATR, cm^{-1}):** 2934, 2862, 2512, 1712, 1615, 1415, 1244, 1198, 1052, 848

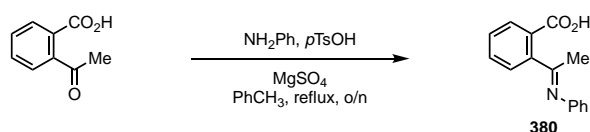


1-(4-fluorobenzoyl)piperidine-4-carboxylic acid (406): To 4-piperidine carboxylic acid (261 mg, 2.02 mmol, 1.01 equiv) and sodium hydroxide (138 mg, 3.46 mmol, 1.73 equiv) in water (1.75 mL, 1.16M) was added *p*-fluorobenzoyl chloride (236 μ L, 2.00 mmol, 1.0 equiv) in CH₂Cl₂ (1.75 mL, 1.16M) at room temperature, under air. The suspension was stirred vigorously overnight at room temperature. The layers were separated. The aqueous layer was acidified to pH ~2 with conc. HCl. The aqueous layer was extracted with EtOAc (3 x 20 mL). The combined organics were washed with brine, dried over MgSO₄, filtered and concentrated. The crude product was recrystallized from a water/ethanol mixture to afford a white powder. **¹H NMR (500 MHz, CDCl₃):** δ 7.41 (dd, *J* = 8.5, 5.4 Hz, 2H), 7.10 (t, *J* = 8.6 Hz, 2H), 4.62 – 4.30 (m, 1H), 3.87 – 3.60 (m, 1H), 3.09 (bs, 2H), 2.64 (t, *J* = 10.6 Hz, 1H), 2.18 – 1.58 (m, 4H). **¹³C NMR (126 MHz, CDCl₃):** δ 179.18, 169.86, 163.57 (d, *J* = 250.7 Hz), 131.82 (d, *J* = 3.8 Hz), 129.37, 129.33 (d, *J* = 8.5 Hz), 115.78 (d, *J* = 21.8 Hz), 47.01, 41.80, 40.72, 27.34. **¹⁹F NMR (282 MHz, Chloroform-*d*):** δ -110.13 (ddd, *J* = 14.1, 8.6, 5.3 Hz). **HRMS:** (ESI-TOF) calculated for ([C₁₃H₁₄FNO₃ + H]⁺): 252.1031, found 252.1025. **IR (ATR, cm⁻¹):** 2955, 2866, 1722, 1601, 1580, 1447, 1294, 1221, 1010, 846, 761

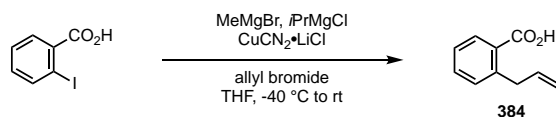


2-(1-((4-fluorobenzamido)methyl)cyclohexyl)acetic acid (407): To Gabapentin (432.4 mg, 2.525 mmol, 1.01 equiv) and sodium hydroxide (173 mg, 4.33 mmol, 1.73 equiv) in water (2.2 mL, 1.16M) was added *p*-fluorobenzoyl chloride (295 μ L, 2.50 mmol, 1.0 equiv) in CH₂Cl₂ (2.2 mL, 1.16M) at room temperature under air. The suspension was stirred vigorously overnight at room temperature. The layers were separated. The aqueous layer was acidified to pH ~2 with conc.

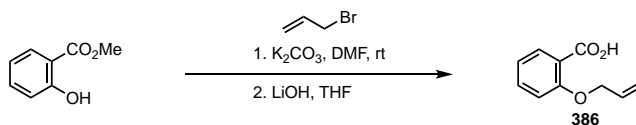
HCl. The aqueous layer was extracted with EtOAc (3 x 20 mL). The combined organics were washed with brine, dried over MgSO₄, filtered and concentrated. The crude product was recrystallized from a water/ethanol mixture to afford a white powder (574 mg, 78% yield). **¹H NMR (500 MHz, CDCl₃):** δ 7.83 (dd, *J* = 8.6, 5.3 Hz, 2H), 7.13 (t, *J* = 8.5 Hz, 2H), 6.96 (s, 1H), 3.50 (d, *J* = 6.5 Hz, 2H), 2.41 (s, 2H), 1.74 – 1.35 (m, 10H). **¹³C NMR (126 MHz, CDCl₃):** δ 175.07, 167.86, 165.14 (d, *J* = 253.3 Hz), 129.91, 129.56 (d, *J* = 9.0 Hz), 115.95 (d, *J* = 22.0 Hz), 47.72, 41.83, 38.00, 34.53, 25.95, 21.50. **¹⁹F NMR (282 MHz, CDCl₃):** δ -107.28. **HRMS:** (ESI-TOF) calculated for ([C₁₆H₂₀FNO₃ + H]⁺): 294.1500, found 294.1492. **IR (ATR, cm⁻¹):** 3303, 2929, 2568, 1712, 1603, 1561, 1503, 1367, 1231, 1160, 850, 673



2-(1-(phenylimino)ethyl)benzoic acid (380): 2-acetylbenzoic acid (1.64 g, 10.0 mmol, 1.0 equiv), aniline (1.0 mL, 11.0 mmol, 1.1 equiv), *p*-toluenesulfonic acid monohydrate (38.0 mg, 0.200 mmol, 0.02 equiv), MgSO₄ (2.4 g, 20 mmol, 2.0 equiv) and PhMe (33.3 mL, 0.3M) were combined and heated to reflux overnight. Upon cooling to room temp, the reaction was poured into 1 M HCl (aq) (~50 mL). The aqueous layer was extracted with EtOAc (1 x 25 mL). The combined organic layers were washed with brine, dried over MgSO₄, filtered and concentrated. The crude oil was purified over silica 15% → 25% EtOAc in hexanes to afford a mauve solid (904 mg, 38% yield). **¹H NMR (500 MHz, CDCl₃):** δ 7.90 (d, *J* = 7.6 Hz, 1H), 7.69 (t, *J* = 7.5 Hz, 1H), 7.60 – 7.53 (m, 2H), 7.09 – 7.02 (m, 2H), 6.86 (t, *J* = 7.4 Hz, 1H), 6.55 (d, *J* = 7.9 Hz, 2H), 4.66 (s, 1H), 1.96 (s, 3H). **¹³C NMR (126 MHz, CDCl₃):** δ 168.75, 150.26, 142.00, 134.55, 130.32, 129.09, 127.80, 125.94, 122.43, 122.17, 119.85, 97.39, 28.76.

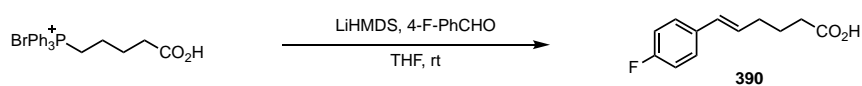


2-allylbenzoic acid (384):⁵ To 2-iodobenzoic acid (2.48 g, 10.0 mmol, 1.0 equiv) in THF (30.3 mL, 0.33M) at -30 °C under N₂ was slowly added methyl magnesium bromide (3.0M in THF, 3.33 mL, 10.0 mmol, 1.0 equiv) and stirred for 5 min at -30 °C. Then isopropyl magnesium chloride (2.0M in THF, 6.0 mL, 12.0 mmol, 1.2 equiv) was added slowly and then stirred for 1 hour at -30 °C. Reaction cooled to -40 °C then CuCN₂•LiCl (3.3M in THF, 152 μ L, 0.5 mmol, 0.05 equiv) was added dropwise and stirred for 10 minutes while warming to -30 °C. Allyl bromide (2.60 mL, 30.0 mmol, 3.0 equiv) was added all at once and the reaction was warmed to room temperature and stirred overnight. The reaction was diluted with EtOAc and acidified to pH ~3 with 1 M HCl. The aqueous was extracted with EtOAc (4 x 10 mL). The combined organics were washed with brine, dried over MgSO₄, filtered and concentrated. The purple-white solid was dissolved in ethyl acetate, then extracted with sat. aq. Na₂CO₃ (3 x 10 mL). The combined aqueous layers were acidified to pH ~2 with conc. HCl. The resulting white precipitate was filtered, washed with distilled water and dried to afford the desired 2-allylbenzoic acid (1.38 g, 85% yield), with no further purification. **¹H NMR (500 MHz, CDCl₃):** δ 8.06 (dd, J = 8.1, 1.5 Hz, 1H), 7.51 (td, J = 7.5, 1.5 Hz, 1H), 7.37 – 7.28 (m, 2H), 6.05 (ddt, J = 16.9, 10.4, 6.5 Hz, 1H), 5.10 – 5.00 (m, 2H), 3.85 (d, J = 6.5 Hz, 2H). **¹³C NMR (126 MHz, CDCl₃):** δ 173.05, 142.93, 137.44, 133.25, 131.79, 131.31, 128.30, 126.48, 115.91, 38.72.



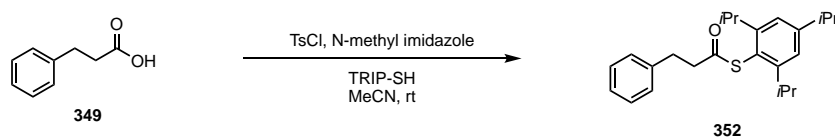
2-(allyloxy)benzoic acid (386): To methyl-2-hydroxybenzoate (1.95 mL, 15.0 mmol, 1.0 equiv) and potassium carbonate (4.21 g, 30.45 mmol, 2.03 equiv) in DMF (15.0 mL, 1.0M) was added

allyl bromide (1.69 mL, 19.5 mmol, 1.30 equiv) at room temperature under ambient atmosphere. The reaction was stirred overnight at room temperature. Water was added. The mixture was extracted with EtOAc (1 x 30 mL). The organic layer was washed with sat. aq. NaHCO₃, 5% aq. LiCl and brine. The organic layer was dried over MgSO₄, filtered through a short plug of silica and concentrated. The crude oil was taken onto the next step without any purification or characterization. To the crude oil was added lithium hydroxide (359 mg, 15.0 mmol, 1.0 equiv) in THF/H₂O (45 mL, 2:1, 0.33M) under ambient conditions. The reaction was stirred overnight. The solvent was removed. The aqueous layer was extracted with EtOAc. The organic layer was extracted with Na₂CO₃ (1 x 10 mL). The combined aqueous layers were acidified with conc. HCl to pH ~2. The aqueous layer was extracted with EtOAc (2 x 40 mL). The combined organic layers were washed with brine, dried over MgSO₄, filtered and concentrated to afford **386** as a white solid (1.89 g, 71% yield) with no further purification. **¹H NMR (500 MHz, CDCl₃):** δ 10.90 (s, 1H), 8.20 (dd, *J* = 7.8, 1.8 Hz, 1H), 7.55 (ddd, *J* = 8.9, 7.7, 1.8 Hz, 1H), 7.15 (t, *J* = 7.6 Hz, 1H), 7.05 (d, *J* = 8.4 Hz, 1H), 6.10 (ddt, *J* = 16.5, 10.9, 5.7 Hz, 1H), 5.55 – 5.38 (m, 2H), 4.80 (d, *J* = 5.7 Hz, 2H). **¹³C NMR (126 MHz, CDCl₃):** δ 165.43, 157.28, 135.11, 134.02, 130.98, 122.57, 120.80, 118.07, 113.10, 70.94.



(*E*)-6-(4-fluorophenyl)hex-5-enoic acid (390):⁴ A flame dried round bottom flask was charged with 4-(carboxybutyl)triphenylphosphonium bromide (2.217 g, 5.00 mmol, 1.0 equiv) and THF (6.7 mL, 0.75M). To this slurry was added LiHMDS (1.0M in THF) (10.5 mL, 10.5 mmol, 2.1 equiv) at room temperature under N₂. The reaction became homogenous and orange-red in color, and stirred for 15 min at room temperature. Then, 4-fluorobenzaldehyde (536 μL, 5.00 mmol, 1.0 equiv) in THF (2.22 mL, 2.25M) was added at room temperature under N₂. The reaction was stirred

an additional 15 min at room temp. Then diethyl ether (20 mL) and water (20 mL) were added. The aqueous layer was separated. The organic layer was washed with water (10 mL). The combine aqueous layers were acidified to pH ~2 with conc. HCl, then extracted with ethyl acetate (2 x 20 mL). The combine organics were dried over MgSO₄, filtered and concentrated. The crude product was obtained as an 8.8:1 *E/Z* mixture of isomers. The crude product was purified over silica with 15% → 25% EtOAc in hexanes as eluent to afford **390** as a colorless oil (579.6 mg, 56% yield, 9:1 *E/Z*) and a mixture with PPh₃O (254 mg, 25% yield). **¹H NMR (500 MHz, CDCl₃):** δ (*E* isomer) 11.31 (bs, 1H), 7.29 (dd, *J* = 8.7, 5.5 Hz, 2H), 6.98 (t, *J* = 8.7 Hz, 2H), 6.37 (d, *J* = 15.8 Hz, 1H), 6.15 – 6.03 (m, 1H), 2.41 (t, *J* = 7.4 Hz, 2H), 2.27 (q, *J* = 7.6 Hz, 2H), 1.82 (p, *J* = 7.4 Hz, 2H). **¹³C NMR (126 MHz, CDCl₃):** δ 179.61, 162.12 (d, *J* = 247.0 Hz), 133.75, 129.92, 129.15, 127.55 (d, *J* = 7.9 Hz), 115.49 (d, *J* = 21.5 Hz), 33.39, 32.31, 24.33. **¹⁹F NMR (282 MHz, CDCl₃):** δ -115.47 (ddd, *J* = 14.1, 8.9, 5.5 Hz). **HRMS:** (ESI-TOF) calculated for ([C₁₂H₁₃FO₂ + Na]⁺): 231.0792, found 231.0790. **IR (ATR, cm⁻¹):** 2933, 1703, 1601, 1507, 1412, 1225, 1157, 965, 840



***S*-(2,4,6-triisopropylphenyl) 3-phenylpropanethioate (352):**⁶ To **349** (150.2 mg, 1.00 mmol, 1.0 equiv) and N-methyl imidazole (239 μ L, 3.00 mmol, 3.0 equiv) in MeCN (1.0 mL) at 0 °C was added *p*-toluenesulfonyl chloride (229 mg, 1.20 mmol, 1.2 equiv) in MeCN (1.0 mL) under N₂. The reaction was stirred at 0 °C for 30 min. Then TRIP-SH (236 mg, 1.00 mmol, 1.0 equiv) in MeCN (1.0 mL) and a few drops of CH₂Cl₂ for solubility was added at 0 °C, under N₂. The reaction immediately turned cloudy. The reaction was stirred a further 2 h at 0 °C. Water was added to the mixture and the aqueous extracted with diethyl ether (1x). The organics were washed with water

(1x) and brine (1x) dried over MgSO_4 , filtered and concentrated. The crude was purified over silica with 0% \rightarrow 25% EtOAc in hexanes as eluent to afford **352** as a colorless oil. **^1H NMR (500 MHz, CDCl_3):** δ 7.31 (t, $J = 7.4$ Hz, 2H), 7.23 (dd, $J = 10.6, 7.6$ Hz, 3H), 7.07 (s, 2H), 3.27 (hept, $J = 6.8$ Hz, 2H), 3.07 – 2.98 (m, $J = 4.2$ Hz, 4H), 2.90 (p, $J = 6.9$ Hz, 1H), 1.26 (d, $J = 6.9$ Hz, 6H), 1.14 (d, $J = 6.8$ Hz, 12H). **^{13}C NMR (126 MHz, CDCl_3):** δ 197.51, 152.44, 151.16, 140.13, 128.62, 128.59, 126.46, 122.12, 121.74, 44.94, 34.48, 31.97, 31.73, 24.00. **HRMS:** (ESI-TOF) calculated for $([\text{C}_{24}\text{H}_{32}\text{OS} + \text{H}]^+)$: 369.2247, found 369.2233. **IR (ATR, cm^{-1}):** 2960, 2868, 1699, 1598, 1425, 1362, 1030, 966, 876, 736, 697

Optimization procedures for screening:

In a typical reaction, to an oven-dried 0.5, 1 or 2-dram reaction vessel was added acid (0.05-0.1 mmol, 1.0 equiv), disulfide (when used) and [Ir]. The vessel was equipped with stir bar and Teflon tape on the threads, then taken into an N_2 -filled glovebox. To the vial was added phosphine (1.0-1.5 equiv), base, and **TRIP-SH** (when used). Solvent was added. The reaction vial was then capped with a septum cap and sealed with electrical tape. The vial was removed from the glovebox, where 2,6- Me_2PhSH (when used) was added via Hamilton syringe from a degassed vial of reagent. The vial was again sealed with electrical tape. The vial was irradiated for specified time with a 34 W blue LED Kessil lamp at ~ 3 cm and a cooling fan to keep reactions at room temperature. Upon reaction completion, external standard (dodecane, 1 equiv) in EtOAc and brine (1 mL) was added. The organic layer was dried over Na_2SO_4 , then the product analyzed by GC or ^1H NMR.

General procedure A: To an oven-dried 1- or 2-dram reaction vessel was added **290** (5.1 mg, 0.01 equiv), acid (0.5 mmol, 1.0 equiv) and (*p*- OMeC_6H_4) $_2\text{S}_2$ (5-10 mol%). The vessel was equipped with stir bar and Teflon tape on the threads, then taken into an N_2 -filled glovebox. To the vial was added PPh_3 (157.4 mg, 0.6 mmol, 1.2 equiv), 2,6-lutidine (57.9 μL , 0.5 mmol, 1.0

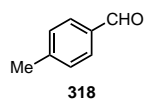
equiv) (when indicated) and solvent (5.0 mL, 0.1M) was added. The reaction vial was then capped with a septum cap and sealed with electrical tape. The vial was removed from the glovebox. The vial was irradiated for 24 h with Kessil lamp at ~ 3 cm and a cooling fan to keep reactions around room temperature. Upon reaction completion, the mixture was poured into sat. aq. sodium bicarbonate (~25 mL) and ethyl acetate (~20 mL). The aqueous layer was washed with ethyl acetate (1 x 25 mL). The combined organic layers were washed with brine (~40 mL), dried over MgSO₄, filtered and concentrated. The crude product was purified over silica under the specified conditions.

General procedure B: To an oven-dried 20 mL or 40 mL reaction vessel was added **290** (10.1 mg, 0.02 equiv) and acid (0.5 mmol, 1.0 equiv) (5-10 mol%). The vessel was equipped with stir bar and Teflon tape on the threads, then taken into an N₂-filled glovebox. To the vial was added Ph₂POEt (129.6 μ L, 0.6 mmol, 1.2 equiv), **TRIP-SH** (59.1 μ L, 0.25 mmol, 0.5 equiv), 2,4,6-collidine (66.1 μ L, 0.5 mmol, 1.0 equiv) and PhMe (0.02-0.0133M). The reaction vial was then capped with a septum cap and sealed with electrical tape. The vial was removed from the glovebox. The vial was irradiated for 24 h with Kessil lamp at ~ 3 cm and a cooling fan to keep reactions around room temperature. Upon reaction completion, the mixture was poured into 1M HCl (aqueous) (~25 mL) and ethyl acetate (~20 mL). The aqueous layer was washed with ethyl acetate (1 x 25 mL). The combined organic layers were washed with brine (~40 mL), dried over MgSO₄, filtered and concentrated. The crude product was purified over silica under the specified conditions.

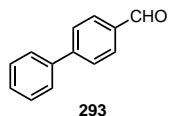
General procedure C: To an oven-dried 1- or 2-dram reaction vessel was added **290** (5.1 mg, 0.01 equiv), acid (0.5 mmol, 1.0 equiv) and disulfide (5-10 mol%). The vessel was equipped with stir bar and Teflon tape on the threads, then taken into an N₂-filled glovebox. To the vial was added

PPh₃ (1.1-1.2 equiv), and PhMe:DMF (95:5) (2.5 mL, 0.2M) was added. ****NOTE**** When **TRIP-SH** (11.8 μ L, 0.05 mmol, 0.1 equiv) was used as H-atom source, it was added in the glovebox. The reaction vial was then capped with a septum cap and sealed with electrical tape. The vial was removed from the glovebox. ****NOTE**** When 2,6-Me₂PhSH (6.7 μ L, 0.05 mmol, 0.1 equiv) (degassed and stored under N₂ on powdered 4 Å molecular sieves) was used, it was added via a Hamilton syringe and the vial was sealed with additional electrical tape. The vial was irradiated for 24 h with Kessil lamp at ~ 3 cm and a cooling fan to keep reactions around room temperature. Upon reaction completion, the mixture was poured into sat. aq. sodium bicarbonate (~25 mL) and ethyl acetate (~20 mL). The aqueous layer was washed with ethyl acetate (1 x 25 mL). The combined organic layers were washed with brine (~40 mL), dried over MgSO₄, filtered and concentrated. The crude product was purified over silica under the specified conditions. ****NOTE**** H-atom sources can be used interchangeably for this procedure.

Characterization of compounds:

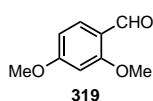


According to general procedure **C**, **317** (68.1 mg, 0.5 mmol), **290** (5.1 mg, 0.005 mmol, 0.01 equiv), PPh₃ (144.3 mg, 0.55 mmol, 1.1 equiv), 2,6-Me₂PhSH (6.7 μ L, 0.05 mmol, 0.1 equiv) PhMe:DMF (95:5, 2.5 mL, 0.2M). GC yield vs. dodecane as an external standard (90% yield). Run 2 afforded 88% yield.

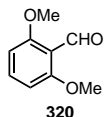


According to general procedure **A**, 4-phenylbenzoic acid (99.1 mg, 0.5 mmol), **290** (5.1 mg, 0.005 mmol, 0.01 equiv), PPh₃ (157.4 mg, 0.6 mmol, 1.2 equiv), (*p*-OMeC₆H₄)₂S₂ (7.0 mg, 0.025 mmol, 0.05 equiv), PhMe (5.0 mL, 0.1M). Purified over silica using 0 → 20% EtOAc in hexanes to afford **293** as a white solid (79.1 mg, 87% yield). Run 2 afforded 80.5 mg, 88% yield. **¹H NMR (500 MHz, CDCl₃):** δ 10.06 (s, 1H), 7.97 (d, *J* = 1.8 Hz, 2H), 7.76 (d, *J* = 8.2 Hz, 2H), 7.64 (d, *J* = 7.2 Hz, 2H), 7.49 (t, *J* = 7.5 Hz, 2H), 7.42 (t, *J* = 7.3 Hz, 1H). **¹³C**

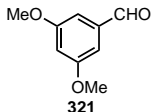
NMR (126 MHz, CDCl₃): δ 192.10, 147.35, 139.86, 135.32, 130.43, 129.16, 128.62, 127.84, 127.52.



According to general procedure A, PPh₃ (157.4 mg, 0.6 mmol, 1.2 equiv) was weighed into a 2-dram vial in the glovebox (for storage purposes only). The vial was removed from the glovebox and opened to air where 2,4-dimethoxybenzoic acid (91.1 mg, 0.5 mmol), (*p*-OMeC₆H₄)₂S₂ (7.0 mg, 0.025 mmol, 0.05 equiv) and **290** (5.1 mg, 0.005 mmol, 0.01 equiv) were added. PhMe (5.0 mL, 0.1M) was added, then the vial was capped and sparged with N₂ for 15 minutes. The vial was sealed with electrical tape and irradiated. Purified over silica using 0 \rightarrow 10% EtOAc in hexanes to afford **319** as a beige solid (67.8 mg, 82% yield). Run 2 afforded 65.3 mg, 79% yield. **¹H NMR (500 MHz, CDCl₃):** δ 10.28 (s, 1H), 7.80 (d, *J* = 8.7 Hz, 1H), 6.54 (dd, *J* = 8.7, 2.2 Hz, 1H), 6.44 (d, *J* = 2.2 Hz, 1H), 3.90 (s, 3H), 3.87 (s, 3H). **¹³C NMR (126 MHz, CDCl₃):** δ 188.54, 166.31, 163.74, 130.94, 119.18, 105.84, 98.09, 55.79, 55.76.

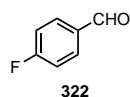


According to general procedure A, 2,6-dimethoxybenzoic acid (91.1 mg, 0.5 mmol), **290** (5.1 mg, 0.005 mmol, 0.01 equiv), PPh₃ (157.4 mg, 0.6 mmol, 1.2 equiv), (*p*-OMeC₆H₄)₂S₂ (7.0 mg, 0.025 mmol, 0.05 equiv), PhMe (5.0 mL, 0.1M). Purified over silica using 0 \rightarrow 10% EtOAc in hexanes to afford **320** as a beige solid (71.8 mg, 86% yield). Run 2 afforded 71.6 mg, 86% yield. **¹H NMR (500 MHz, CDCl₃):** δ 10.51 (s, 1H), 7.45 (t, *J* = 8.5 Hz, 1H), 6.58 (d, *J* = 8.5 Hz, 2H), 3.90 (s, 6H). **¹³C NMR (126 MHz, CDCl₃):** δ 189.61, 162.34, 136.06, 114.44, 103.97, 56.22.

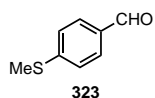


According to general procedure C, 3,5-dimethoxybenzoic acid (91.1 mg, 0.5 mmol), **290** 5.1 mg, 0.005 mmol, 0.01 equiv), PPh₃ (144.3 mg, 0.55 mmol, 1.1 equiv), 2,6-Me₂PhSH (6.7 μ L, 0.05 mmol, 0.1 equiv), PhMe:DMF (95:5, 2.5 mL, 0.2M). Purified over silica using 0 \rightarrow 10% EtOAc in hexanes to afford **321** as a white solid (60.9 mg, 73% yield). Run 2

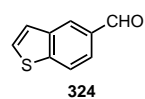
afforded 61.0 mg, 73% yield. **^1H NMR (500 MHz, CDCl_3)**: δ 9.91 (s, 1H), 7.02 (d, J = 2.4 Hz, 2H), 6.71 (t, J = 2.3 Hz, 1H), 3.85 (s, 6H). **^{13}C NMR (126 MHz, CDCl_3)**: δ 192.12, 161.38, 138.52, 107.33, 107.27, 55.80.



According to general procedure A, 4-fluorobenzoic acid (70.1 mg, 0.5 mmol), **290** (5.1 mg, 0.005 mmol, 0.01 equiv), PPh_3 (157.4 mg, 0.60 mmol, 1.2 equiv), 2,6- Me_2PhSH (6.7 μL , 0.05 mmol, 0.1 equiv), $\text{PhMe}:\text{DMF}$ (95:5, 2.5 mL, 0.2M). ^{19}F NMR yield v. 1-fluoronaphthalene as an external standard (82% yield). Run 2 afforded 85% yield. **^{19}F NMR (282 MHz, CDCl_3)**: δ -102.35.

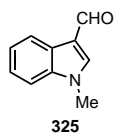


According to general procedure A, 4-thiomethylbenzoic acid (84.1 mg, 0.5 mmol), **290** (5.1 mg, 0.005 mmol, 0.01 equiv), PPh_3 (157.4 mg, 0.6 mmol, 1.2 equiv), ($p\text{-OMeC}_6\text{H}_4$) $_2\text{S}_2$ (7.0 mg, 0.025 mmol, 0.05 equiv), PhMe (5.0 mL, 0.1M). Purified over silica using 0 \rightarrow 10% EtOAc in hexanes to afford **323** as a pale-yellow oil (71.6 mg, 94% yield). Run 2 afforded 71.0 mg, 93% yield. **^1H NMR (500 MHz, CDCl_3)**: δ 9.92 (s, 1H), 7.77 (d, J = 8.5 Hz, 2H), 7.33 (d, J = 8.4 Hz, 2H), 2.54 (s, 3H). **^{13}C NMR (126 MHz, CDCl_3)**: δ 191.38, 148.03, 133.05, 130.13, 125.29, 14.82.



According to general procedure A, benzo[*b*]thiophene-5-carboxylic acid (89.1 mg, 0.5 mmol), **290** (5.1 mg, 0.005 mmol, 0.01 equiv), PPh_3 (157.4 mg, 0.6 mmol, 1.2 equiv), ($p\text{-OMeC}_6\text{H}_4$) $_2\text{S}_2$ (7.0 mg, 0.025 mmol, 0.05 equiv), PhMe (5.0 mL, 0.1M). Purified over silica using 0 \rightarrow 15% EtOAc in hexanes to afford **324** as a light yellow solid (72.1 mg, 89% yield). Run 2 afforded 69.8 mg, 86% yield. **^1H NMR (500 MHz, CDCl_3)**: δ 10.11 (s, 1H), 8.32 (d, J = 1.2 Hz, 1H), 8.01 (d, J = 8.4 Hz, 1H), 7.87 (dd, J = 8.4, 1.5 Hz, 1H), 7.57 (d, J = 5.5 Hz, 1H), 7.49

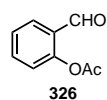
(d, $J = 5.9$ Hz, 1H). **^{13}C NMR (126 MHz, CDCl_3):** δ 192.29, 145.80, 139.67, 133.42, 128.45, 127.21, 124.66, 123.59, 123.29.



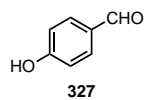
According to general procedure **A**, 1-methyl-1*H*-indole-3-carboxylic acid (87.6 mg, 0.5 mmol), **290** (5.1 mg, 0.005 mmol, 0.01 equiv), PPh_3 (157.4 mg, 0.6 mmol, 1.2 equiv), $(p\text{-OMeC}_6\text{H}_4)_2\text{S}_2$ (7.0 mg, 0.025 mmol, 0.05 equiv), NMP (5.0 mL, 0.1M). ****Note**:** NMP (5.0 mL, 0.1M) was used in place of PhMe. Purified over silica using 10 \rightarrow 40% EtOAc in hexanes to afford **325** as a beige solid (26.4 mg, 33% yield). Run 2 afforded 25.9 mg, 33% yield.

Alternative prep:

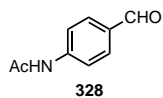
According to general procedure **A**, 1-methyl-1*H*-indole-3-carboxylic acid (99.1 mg, 0.5 mmol), **290** (5.1 mg, 0.005 mmol, 0.01 equiv), PPh_3 (144.3 mg, 0.55 mmol, 1.1 equiv), 2,6- Me_2PhSH (6.7 μL , 0.05 mmol, 0.1 equiv) NMP (2.5 mL, 0.2M). Purified over silica using 10 \rightarrow 40% EtOAc in hexanes to afford **325** as a beige solid (36.3 mg, 46% yield). Run 2 afforded 34.7 mg, 44% yield. **^1H NMR (500 MHz, CDCl_3):** δ 9.99 (s, 1H), 8.33 – 8.27 (m, 1H), 7.67 (s, 1H), 7.39 – 7.29 (m, 3H), 3.87 (s, 3H). **^{13}C NMR (126 MHz, CDCl_3):** δ 184.55, 139.33, 137.99, 125.40, 124.16, 123.08, 122.19, 118.20, 109.97, 33.85.



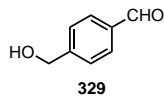
According to general procedure **A**, aspirin (90.1 mg, 0.5 mmol), **290** (5.1 mg, 0.005 mmol, 0.01 equiv), PPh_3 (157.4 mg, 0.6 mmol, 1.2 equiv), $(p\text{-OMeC}_6\text{H}_4)_2\text{S}_2$ (7.0 mg, 0.025 mmol, 0.05 equiv), PhMe (5.0 mL, 0.1M). Purified over silica using 0 \rightarrow 12% EtOAc in hexanes to afford **326** as a colorless oil (67.7 mg, 82% yield). Run 2 afforded 66.2 mg, 81% yield. **^1H NMR (500 MHz, CDCl_3):** δ 10.11 (s, 1H), 7.88 (dd, $J = 7.7, 1.7$ Hz, 1H), 7.63 (td, $J = 7.8, 1.7$ Hz, 1H), 7.40 (t, $J = 7.3$ Hz, 1H), 7.18 (d, $J = 8.1$ Hz, 1H), 2.39 (s, 3H). **^{13}C NMR (126 MHz, CDCl_3):** δ 188.88, 169.38, 151.56, 135.44, 131.45, 128.12, 126.57, 123.60, 21.00.



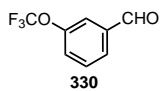
According to general procedure **A**, 4-hydroxybenzoic acid (69.1 mg, 0.5 mmol), **290** (5.1 mg, 0.005 mmol, 0.01 equiv), PPh₃ (157.4 mg, 0.6 mmol, 1.2 equiv), (*p*-OMeC₆H₄)₂S₂ (7.0 mg, 0.025 mmol, 0.05 equiv). ****Note****: NMP (5.0 mL, 0.1M) was used in place of PhMe. Purified over silica using 10 → 35% EtOAc in hexanes to afford **327** as a white solid (35.2 mg, 58% yield). Run 2 afforded 36.6 mg, 60% yield. **¹H NMR (500 MHz, CDCl₃)**: δ 9.87 (s, 1H), 7.82 (d, *J* = 8.6 Hz, 2H), 6.97 (d, *J* = 8.6 Hz, 2H), 5.79 (s, 1H). **¹³C NMR (126 MHz, CDCl₃)**: δ 191.14, 161.35, 132.59, 130.20, 116.09.



According to general procedure **A**, 4-acetimidobenzoic acid (89.5 mg, 0.5 mmol), **290** (5.1 mg, 0.005 mmol, 0.01 equiv), PPh₃ (157.4 mg, 0.6 mmol, 1.2 equiv), (*p*-OMeC₆H₄)₂S₂ (7.0 mg, 0.025 mmol, 0.05 equiv), PhMe (5.0 mL, 0.1M). Purified over silica using 20 → 40% EtOAc in hexanes to afford **328** as a beige solid (76.6 mg, 94% yield). Run 2 afforded 76.8 mg, 94% yield. **¹H NMR (500 MHz, CDCl₃)**: δ 9.92 (s, 1H), 7.91 – 7.78 (m, 2H), 7.70 (d, *J* = 8.1 Hz, 2H), 7.51 (s, 1H), 2.24 (d, *J* = 2.0 Hz, 3H). **¹³C NMR (126 MHz, CDCl₃)**: δ 191.15, 168.68, 143.52, 132.43, 131.33, 119.30, 25.03.

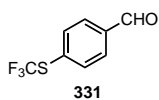


According to general procedure **C**, 4-(hydroxymethyl)-benzoic acid (76.1 mg, 0.5 mmol), **290** (5.1mg, 0.005 mmol, 0.01 equiv), PPh₃ (157.4 mg, 0.6 mmol, 1.2 equiv), PhMe:DMF (2.5 mL, 95:5, 0.2M) 2,6-Me₂PhSH (6.7 μL, 0.05 mmol, 0.1 equiv). Purified over silica using 5 → 35% EtOAc in hexanes to afford the product as a colorless oil (27.5 mg, 40% yield). Run 2 afforded 31.8 mg, 47% yield. **¹H NMR (500 MHz, CDCl₃)**: δ 10.00 (s, 1H), 7.88 (d, *J* = 8.2 Hz, 2H), 7.53 (d, *J* = 7.9 Hz, 2H), 4.81 (s, 2H). **¹³C NMR (126 MHz, CDCl₃)**: δ 192.17, 147.87, 135.81, 130.17, 127.09, 64.73.

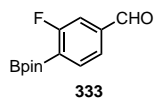


According to general procedure **A**, 3-trifluoromethoxybenzoic acid (103.1 mg, 0.5 mmol), **290** (5.1 mg, 0.005 mmol, 0.01 equiv), PPh₃ (157.4 mg, 0.6 mmol, 1.2

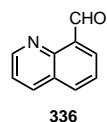
equiv), (*p*-OMeC₆H₄)₂S₂ (13.9 mg, 0.05 mmol, 0.10 equiv), 2,6-lutidine (57.9 μ L, 0.5 mmol, 1.0 equiv), PhMe (5.0 mL, 0.1M). ¹⁹F NMR yield v. 1-fluoronaphthalene as an external standard (81% yield). Run 2 afforded 78% yield. **¹⁹F NMR (282 MHz, CDCl₃):** δ -57.57.



According to general procedure A, 4-((trifluoromethyl)thio)benzoic acid (111.1 mg, 0.5 mmol), **290** (5.1 mg, 0.005 mmol, 0.01 equiv), PPh₃ (157.4 mg, 0.6 mmol, 1.2 equiv), (*p*-OMeC₆H₄)₂S₂ (13.9 mg, 0.05 mmol, 0.10 equiv), 2,6-lutidine (57.9 μ L, 0.5 mmol, 1.0 equiv), PhMe (5.0 mL, 0.1M). ¹⁹F NMR yield v. 1-fluoronaphthalene as an external standard (77% yield). Run 2 afforded 72% yield. **¹⁹F NMR (282 MHz, CDCl₃):** δ -41.21.

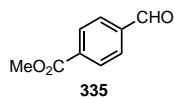


According to general procedure A, benzoic acid (133.0 mg, 0.5 mmol), **290** (5.1 mg, 0.005 mmol, 0.01 equiv), PPh₃ (157.4 mg, 0.6 mmol, 1.2 equiv), (*p*-OMeC₆H₄)₂S₂ (13.9 mg, 0.05 mmol, 0.10 equiv), 2,6-lutidine (57.9 μ L, 0.5 mmol, 1.0 equiv), PhMe (5.0 mL, 0.1M). Purified over silica using 5 \rightarrow 20% EtOAc in hexanes to afford **333** as a colorless oil (47.5 mg, 38% yield) and benzyl alcohol (12.1 mg, 10% yield). Run 2 afforded 45.6 mg, 36% yield and benzyl alcohol (9.8 mg, 8% yield). **¹H NMR (500 MHz, CDCl₃):** δ 10.01 (d, *J* = 1.7 Hz, 1H), 7.91 (dd, *J* = 7.6, 5.5 Hz, 1H), 7.65 (dd, *J* = 7.5, 1.3 Hz, 1H), 7.52 (dd, *J* = 8.9, 1.4 Hz, 1H), 1.38 (s, 12H). **¹³C NMR (126 MHz, CDCl₃):** δ 191.25, 167.40 (d, *J* = 253.7 Hz), 140.56 (d, *J* = 7.1 Hz), 137.77 (d, *J* = 7.9 Hz), 136.67, 124.99 (d, *J* = 3.2 Hz), 115.42 (d, *J* = 24.9 Hz), 84.60, 24.97. **¹⁹F NMR (282 MHz, CDCl₃):** δ -101.42 (ddd, *J* = 8.4, 5.4, 1.3 Hz). **¹¹B NMR (96 MHz, CDCl₃):** δ 29.83. **HRMS:** (ESI-TOF) calculated for ([C₁₃H₁₆FO₃B + H]⁺): 251.1249, found 251.1258. **IR (ATR, cm⁻¹):** 2981, 1701, 1566, 1498, 1421, 1383, 1353, 1231, 1141, 1064, 855, 753

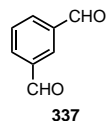


According to general procedure A, benzoic acid (86.6 mg, 0.5 mmol), **290** (5.1 mg, 0.005 mmol, 0.01 equiv), PPh₃ (157.4 mg, 0.6 mmol, 1.2 equiv), (*p*-OMeC₆H₄)₂S₂ (13.9 mg, 0.05 mmol, 0.10 equiv), 2,6-lutidine (57.9 μ L, 0.5 mmol, 1.0 equiv), PhMe (5.0 mL, 0.1M).

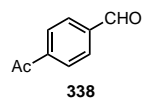
Purified over silica using 5 → 25% EtOAc in hexanes to afford **336** as a white solid (38.4 mg, 49% yield). Run 2 afforded 39.7 mg, 51% yield. **¹H NMR (500 MHz, CDCl₃):** δ 11.46 (s, 1H), 9.05 (dd, *J* = 4.2, 1.8 Hz, 1H), 8.33 (dd, *J* = 7.2, 1.5 Hz, 1H), 8.25 (dd, *J* = 8.3, 1.8 Hz, 1H), 8.09 (dd, *J* = 8.1, 1.4 Hz, 1H), 7.68 (t, *J* = 7.7 Hz, 1H), 7.52 (dd, *J* = 8.3, 4.2 Hz, 1H). **¹³C NMR (126 MHz, CDCl₃):** δ 192.77 (d, *J* = 1.8 Hz), 151.46, 147.72, 136.45, 134.37, 131.81, 129.45, 128.43, 126.36, 121.94.



According to general procedure **A**, benzoic acid (90.1 mg, 0.5 mmol), **290** (5.1 mg, 0.005 mmol, 0.01 equiv), PPh₃ (157.4 mg, 0.6 mmol, 1.2 equiv), (*p*-OMeC₆H₄)₂S₂ (13.9 mg, 0.05 mmol, 0.10 equiv), 2,6-lutidine (57.9 μL, 0.5 mmol, 1.0 equiv), PhMe (5.0 mL, 0.1M). Purified over silica using 5 → 15% EtOAc in hexanes to afford **335** as a waxy solid (64.5 mg, 79% yield). Run 2 afforded 66.3 mg, 81% yield. **¹H NMR (500 MHz, CDCl₃):** δ 10.11 (s, 1H), 8.20 (d, *J* = 8.1 Hz, 2H), 7.96 (d, *J* = 8.3 Hz, 2H), 3.97 (s, 3H). **¹³C NMR (126 MHz, CDCl₃):** δ 191.80, 166.21, 139.27, 135.23, 130.34, 129.67, 52.75.

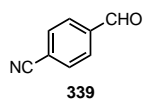


According to general procedure **A**, benzoic acid (75.1 mg, 0.5 mmol), **290** (5.1 mg, 0.005 mmol, 0.01 equiv), PPh₃ (157.4 mg, 0.6 mmol, 1.2 equiv), (*p*-OMeC₆H₄)₂S₂ (13.9 mg, 0.05 mmol, 0.10 equiv), 2,6-lutidine (57.9 μL, 0.5 mmol, 1.0 equiv), PhMe (5.0 mL, 0.1M). Purified over silica using 0 → 20% EtOAc in hexanes to afford **337** as a waxy solid (53.1 mg, 79% yield). Run 2 afforded 51.8 mg, 77% yield. **¹H NMR (500 MHz, CDCl₃):** δ 10.11 (s, 2H), 8.38 (t, *J* = 1.7 Hz, 1H), 8.15 (dd, *J* = 7.6, 1.7 Hz, 2H), 7.73 (t, *J* = 7.6 Hz, 1H). **¹³C NMR (126 MHz, CDCl₃):** δ 191.18, 137.10, 134.76, 131.13, 130.04.

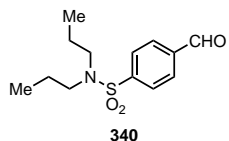


According to general procedure **A**, benzoic acid (82.1 mg, 0.5 mmol), **290** (5.1 mg, 0.005 mmol, 0.01 equiv), PPh₃ (157.4 mg, 0.6 mmol, 1.2 equiv), (*p*-OMeC₆H₄)₂S₂ (13.9 mg, 0.05 mmol, 0.10 equiv), 2,6-lutidine (57.9 μL, 0.5 mmol, 1.0 equiv), PhMe (5.0 mL,

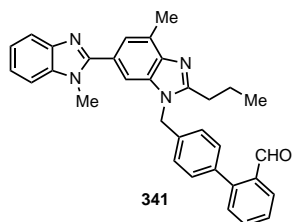
0.1M). Purified over silica using 5 → 20% EtOAc in hexanes to afford **338** as a waxy solid (54.6 mg, 74% yield). Run 2 afforded 49.5 mg, 67% yield. **¹H NMR (500 MHz, CDCl₃):** δ 10.10 (s, 1H), 8.09 (d, *J* = 8.1 Hz, 2H), 7.97 (d, *J* = 8.2 Hz, 2H), 2.65 (s, 3H). **¹³C NMR (126 MHz, CDCl₃):** δ 197.50, 191.72, 141.30, 139.14, 129.93, 128.93, 27.11.



According to general procedure **A**, benzoic acid (73.6 mg, 0.5 mmol), **290** (5.1 mg, 0.005 mmol, 0.01 equiv), PPh₃ (157.4 mg, 0.6 mmol, 1.2 equiv), (*p*-OMeC₆H₄)₂S₂ (13.9 mg, 0.05 mmol, 0.10 equiv), 2,6-lutidine (57.9 μL, 0.5 mmol, 1.0 equiv), PhMe (5.0 mL, 0.1M). Purified over silica using 5 → 35% EtOAc in hexanes to afford **339** as a yellow solid (22.4 mg, 34% yield). Run 2 afforded 27.6 mg, 42% yield. **¹H NMR (500 MHz, CDCl₃):** δ 10.10 (s, 1H), 8.00 (d, *J* = 8.4 Hz, 2H), 7.85 (d, *J* = 8.2 Hz, 2H). **¹³C NMR (126 MHz, CDCl₃):** δ 190.73, 138.86, 133.05, 130.04, 117.86, 117.77.

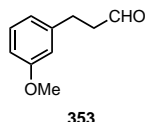


According to general procedure **A**, Probenecid (141.7 mg, 0.5 mmol), **290** (5.1 mg, 0.005 mmol, 0.01 equiv), PPh₃ (157.4 mg, 0.6 mmol, 1.2 equiv), (*p*-OMeC₆H₄)₂S₂ (13.9 mg, 0.05 mmol, 0.10 equiv), 2,6-lutidine (57.9 μL, 0.5 mmol, 1.0 equiv), PhMe (5.0 mL, 0.1M). Purified over silica using 5 → 20% EtOAc in hexanes to afford **340** as a white solid (93.9 mg, 70% yield). Run 2 afforded 87.7 mg, 65% yield. **¹H NMR (500 MHz, CDCl₃):** δ 10.09 (s, 1H), 8.03 – 7.93 (m, 4H), 3.15 – 3.06 (m, 4H), 1.55 (dq, *J* = 14.9, 7.4 Hz, 4H), 0.86 (t, *J* = 7.4 Hz, 6H). **¹³C NMR (126 MHz, CDCl₃):** δ 191.06, 145.61, 138.62, 130.27, 127.74, 50.04, 22.06, 11.27. **HRMS:** (ESI-TOF) calculated for ([C₁₃H₁₉NO₃S + H]⁺): 270.1158, found 270.1149. **IR (ATR, cm⁻¹):** 2969, 2877, 1707, 1598, 1340, 1154, 732

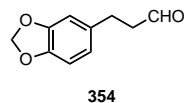


According to general procedure **A**, Telmisartan (257.3 mg, 0.5 mmol), **290** (5.1 mg, 0.005 mmol, 0.01 equiv), PPh₃ (157.4 mg, 0.6 mmol, 1.2 equiv), (*p*-OMeC₆H₄)₂S₂ (7.0 mg, 0.025 mmol, 0.05 equiv), PhMe:DMF

(95:5, 2.5 mL, 0.2M). Purified over silica using 40 → 100% EtOAc in hexanes to afford **341** as a yellow oil (198.3 mg, 80% yield) mixed with Ph₃P(O) (160.8 mg). Run 2 afforded 200.6 mg, 80% yield mixed with Ph₃P(O) (90.9 mg). Purified by prep plate to obtain a clean characterization sample. **¹H NMR (500 MHz, CDCl₃)**: δ 9.92 (s, 1H), 7.99 (dd, *J* = 7.8, 1.4 Hz, 1H), 7.83 – 7.78 (m, 1H), 7.61 (td, *J* = 7.6, 1.4 Hz, 1H), 7.55 (s, 1H), 7.49 (t, *J* = 7.5 Hz, 1H), 7.42 (s, 1H), 7.39 – 7.35 (m, 2H), 7.34 – 7.27 (m, 4H), 7.15 (d, *J* = 8.1 Hz, 2H), 5.49 (s, 2H), 3.83 (s, 3H), 2.97 – 2.88 (m, 2H), 2.78 (s, 3H), 1.88 (h, *J* = 7.4 Hz, 2H), 1.05 (t, *J* = 7.4 Hz, 3H). **¹³C NMR (126 MHz, CDCl₃)**: δ 192.18, 156.60, 154.73, 145.10, 143.29, 142.81, 137.66, 136.72, 136.06, 135.22, 133.79, 133.75, 130.84, 130.83, 129.63, 128.15, 127.91, 126.27, 124.06, 123.98, 122.75, 122.57, 119.63, 109.69, 109.05, 46.97, 32.00, 29.97, 22.03, 17.09, 14.25. **HRMS**: (ESI-TOF) calculated for ([C₃₃H₃₀N₄O + H]⁺): 499.2492, found 499.2489. **IR (ATR, cm⁻¹)**: 2947, 1739, 1691, 1596, 1437, 1194, 1119, 721, 695

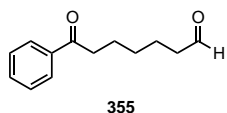


According to general procedure **B**, acid (90.1 mg, 0.5 mmol), PhMe (37.5 mL, 0.0133M). Purified over silica using 0 → 15% EtOAc in hexanes to afford **353** as a pale-yellow oil (47.9 mg, 58% yield). Run 2 afforded 50.8 mg, 62% yield. **¹H NMR (500 MHz, CDCl₃)**: δ 9.82 (s, 1H), 7.22 (td, *J* = 7.7, 0.8 Hz, 1H), 6.81 – 6.72 (m, 3H), 3.80 (s, 3H), 2.94 (t, *J* = 7.5 Hz, 2H), 2.81 – 2.75 (m, 2H). **¹³C NMR (126 MHz, CDCl₃)**: δ 201.67, 159.87, 142.06, 129.76, 129.72, 120.72, 114.26, 111.62, 55.28, 45.31, 28.27.

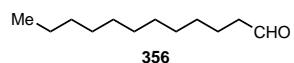


According to general procedure **B**, **404** (97.1 mg, 0.5 mmol), PhMe (37.5 mL, 0.0133M). Purified over silica using 0 → 12% EtOAc in hexanes to afford **354** as a colorless oil (50.7 mg, 57% yield). Run 2 afforded 49.1 mg, 55% yield. **¹H NMR (500 MHz, CDCl₃)**: δ 9.80 (s, 1H), 6.73 (d, *J* = 7.9 Hz, 1H), 6.68 (s, 1H), 6.64 (d, *J* = 7.9 Hz, 1H), 5.92 (s,

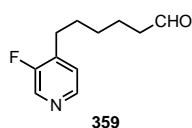
2H), 2.88 (t, $J = 7.5$ Hz, 2H), 2.73 (t, $J = 7.4$ Hz, 2H). **^{13}C NMR (126 MHz, CDCl_3)**: δ 201.70, 147.85, 146.09, 134.20, 121.20, 108.89, 108.44, 101.02, 45.69, 28.01.



According to general procedure **B**, acid (110.1 mg, 0.5 mmol), PhMe (37.5 mL, 0.0133M). Purified over silica using 0 \rightarrow 15% EtOAc in hexanes to afford **355** as a colorless oil (53.5 mg, 52% yield). Run 2 afforded 59.3 mg, 58% yield. **^1H NMR (300 MHz, CDCl_3)**: δ 9.79 (t, $J = 1.7$ Hz, 1H), 7.97 (dt, $J = 7.1, 1.4$ Hz, 2H), 7.62 – 7.53 (m, 1H), 7.48 (dd, $J = 8.2, 6.7$ Hz, 2H), 3.00 (t, $J = 7.3$ Hz, 2H), 2.48 (td, $J = 7.3, 1.7$ Hz, 2H), 1.87 – 1.64 (m, 4H), 1.53 – 1.38 (m, 2H). **^{13}C NMR (126 MHz, CDCl_3)**: δ 202.73, 200.26, 137.07, 133.13, 128.72, 128.15, 43.85, 38.35, 28.92, 24.03, 22.03.

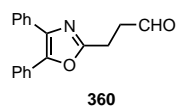


According to general procedure **B**, lauric acid (100.2 mg, 0.5 mmol), PhMe (37.5 mL, 0.0133M). Purified over silica using 0 \rightarrow 10% EtOAc in hexanes to afford **356** as a pale-yellow oil (33.3 mg, 36% yield). Run 2 afforded 36.3 mg, 38% yield. **^1H NMR (500 MHz, CDCl_3)**: δ 9.76 (s, 1H), 2.42 (td, $J = 7.4, 1.9$ Hz, 2H), 1.67 – 1.58 (m, 2H), 1.36 – 1.20 (m, 16H), 0.88 (t, $J = 6.9$ Hz, 3H). **^{13}C NMR (126 MHz, CDCl_3)**: δ 203.19, 44.07, 32.05, 29.74, 29.73, 29.58, 29.51, 29.48, 29.31, 22.83, 22.23, 14.27.

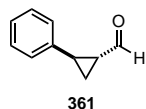


According to general procedure **B**, **405** (105.6 mg, 0.5 mmol), PhMe (37.5 mL, 0.0133M). ****Note****: Reaction was poured into brine with EtOAc and the organic layer dried and concentrated. Purified over silica using 10 \rightarrow 25% EtOAc in hexanes to afford **359** as a colorless oil (59.4 mg, 61% yield). Run 2 afforded 43.2 mg, 44% yield. Run 3 afforded 57.0 mg, 58% yield. **^1H NMR (500 MHz, CDCl_3)**: δ 9.75 (s, 1H), 8.35 (s, 1H), 8.28 (d, $J = 4.8$ Hz, 1H), 7.17 – 7.08 (m, 1H), 2.65 (t, $J = 7.8$ Hz, 2H), 2.43 (td, $J = 7.2, 1.7$ Hz, 2H), 1.65 (h, $J = 7.7$ Hz, 4H), 1.45 – 1.31 (m, 2H). **^{13}C NMR (126 MHz, CDCl_3)**: δ 202.47, 158.53 (d, $J = 254.5$ Hz), 145.63, 137.92 (d, $J = 13.6$ Hz), 137.79 (d, $J = 24.8$ Hz), 125.10, 43.79, 29.05, 28.75,

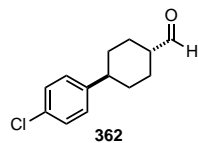
28.19, 21.77. **¹⁹F NMR (282 MHz, CDCl₃):** δ -133.38 (d, J = 6.3 Hz). **HRMS:** (ESI-TOF) calculated for ([C₁₁H₁₄FNO + H]⁺): 196.1132, found 196.1125. **IR (ATR, cm⁻¹):** 2934, 2862, 1719, 1614, 1493, 1415, 1243, 1197, 1052, 841



According to general procedure **B**, Oxaprozin (146.7 mg, 0.5 mmol), PhMe (25.0 mL, 0.02M). Purified over silica using 5 → 20% EtOAc in hexanes to afford **360** as a white solid (17.8 mg, 13% yield). Run 2 afforded 21.4 mg, 15% yield. **¹H NMR (500 MHz, CDCl₃):** δ 9.93 (s, 1H), 7.65 – 7.53 (m, 4H), 7.40 – 7.28 (m, 6H), 3.19 (t, J = 7.4 Hz, 2H), 3.09 (t, J = 7.1 Hz, 2H). **¹³C NMR (126 MHz, CDCl₃):** δ 200.05, 161.80, 145.66, 135.26, 132.50, 129.01, 128.79, 128.72, 128.63, 128.24, 128.03, 126.59, 40.46, 20.93. **HRMS:** (ESI-TOF) calculated for ([C₁₈H₁₅NO₂ + H]⁺): 278.1176, found 278.1165. **IR (ATR, cm⁻¹):** 3058, 2923, 2830, 1726, 1570, 1445, 1217, 1059, 962, 763, 694

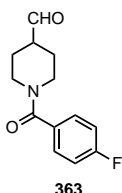


According to general procedure **B**, acid (81.1 mg, 0.5 mmol), PhMe (37.5 mL, 0.0133M). Purified over silica using 50 → 100% DCM in hexanes and the resulting mixture purified by prep TLC in DCM to afford **361** as a colorless oil (31.5 mg, 43% yield). Run 2 afforded 27.4 mg, 38% yield. **¹H NMR (500 MHz, CDCl₃):** δ 9.33 (d, J = 4.6 Hz, 1H), 7.33 – 7.27 (m, 2H), 7.26 – 7.20 (m, 1H), 7.14 – 7.09 (m, 2H), 2.64 (ddd, J = 9.3, 6.7, 4.0 Hz, 1H), 2.18 (dtd, J = 8.5, 5.0, 4.2 Hz, 1H), 1.74 (dt, J = 9.2, 5.1 Hz, 1H), 1.54 (ddd, J = 8.2, 6.7, 5.0 Hz, 1H). **¹³C NMR (126 MHz, CDCl₃):** δ 199.73, 138.97, 128.62, 126.86, 126.26, 33.84, 26.61, 16.49.

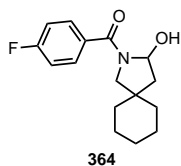


According to general procedure **B**, acid (119.4 mg, 0.5 mmol), PhMe (25.0 mL, 0.02M). Purified over silica using 0 → 15% EtOAc in hexanes to afford **362** as a waxy white solid (50.6 mg, 45% yield). Run 2 afforded 45.2 mg, 41% yield. **¹H NMR (500 MHz, CDCl₃):** δ 9.68 (d, J = 1.5 Hz, 1H), 7.26 (d, J = 8.4 Hz, 2H), 7.13 (d, J = 8.4 Hz, 2H), 2.52 – 2.43 (m, 1H), 2.34 – 2.24 (m, 1H), 2.13 (d, J = 11.9 Hz, 2H), 2.01 (d, J = 11.7 Hz, 2H), 1.59 –

1.37 (m, 4H). **¹³C NMR (126 MHz, CDCl₃):** δ 204.40, 145.18, 131.88, 128.64, 128.23, 49.96, 43.33, 33.04, 26.35.

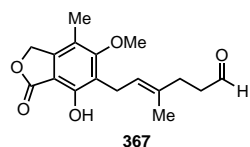


According to general procedure **B**, **406** (125.6 mg, 0.5 mmol), PhMe (25.0 mL, 0.02M). Purified over silica using 10 → 20% acetone in hexanes to afford **363** as a white solid (77.1 mg, 66% yield, mixed with 56.0 mg Ph₂P(O)OEt). Run 2 afforded 71.3 mg, 61% yield, (50.2 mg mixed with 4.8 mg Ph₂P(O)OEt, and 21.1 mg clean product). **¹H NMR (500 MHz, CDCl₃):** δ 9.69 (s, 1H), 7.40 (dd, *J* = 8.7, 5.3 Hz, 2H), 7.09 (t, *J* = 8.6 Hz, 2H), 4.55 – 4.18 (m, 1H), 3.93 – 3.54 (m, 1H), 3.16 (ddd, *J* = 13.6, 10.7, 3.2 Hz, 2H), 2.56 (tt, *J* = 10.2, 4.2 Hz, 1H), 2.19 – 1.50 (m, 4H). **¹³C NMR (126 MHz, CDCl₃):** δ 202.31, 169.67, 163.43 (d, *J* = 250.7 Hz), 131.73, 129.22, 129.15, 115.73, 115.56, 47.75, 40.50, 25.36. **¹⁹F NMR (282 MHz, CDCl₃):** δ -110.19 (tt, *J* = 8.5, 5.2 Hz). **HRMS:** (ESI-TOF) calculated for ([C₁₃H₁₄FNO₂ + H]⁺): 236.1081, found 236.1074. **IR (ATR, cm⁻¹):** 2933, 1711, 1604, 1441, 1365, 1282, 1222, 1096, 1008, 846, 760

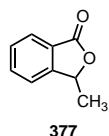


According to general procedure **B**, **407** (146.7 mg, 0.5 mmol) PhMe (37.5 mL, 0.0133M). Purified over silica using 10 → 30% EtOAc in hexanes to afford **364** as a sticky oil (109.9 mg, 79% yield). Run 2 afforded 79.9 mg, 58% yield. Run 3 afforded 110.0 mg, 79% yield. **¹H NMR (500 MHz, CDCl₃):** δ 7.56 (dd, *J* = 8.5, 5.4 Hz, 2H), 7.11 (t, *J* = 8.6 Hz, 2H), 5.81 (t, *J* = 7.2 Hz, 1H), 4.40 (d, *J* = 2.6 Hz, 1H), 3.38 (dd, *J* = 60.8, 10.5 Hz, 2H), 2.16 (dd, *J* = 13.4, 6.6 Hz, 1H), 1.84 – 1.69 (m, 1H), 1.63 – 1.23 (m, 10H). **¹³C NMR (126 MHz, CDCl₃):** δ 170.27, 163.95 (d, *J* = 250.7 Hz), 131.98, 129.80 (d, *J* = 6.3 Hz), 115.60 (d, *J* = 22.7 Hz), 82.64, 59.63, 43.20, 41.80, 36.07, 35.43, 26.00, 23.45, 23.05. **¹⁹F NMR (282 MHz, CDCl₃):** δ -109.12 (tt, *J* = 9.0, 5.3 Hz). **HRMS:** (ESI-TOF) calculated for ([C₁₆H₂₀FNO₂ + Na]⁺):

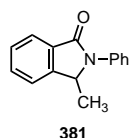
300.1370, found 300.1373. **IR (ATR, cm⁻¹):** 3409, 2926, 2855, 1701, 1603, 1425, 1245, 1158, 1076, 848, 763



According to general procedure **B**, Mycophenolic acid (160.2 mg, 0.5 mmol), PhMe (37.5 mL, 0.0133M). Purified over silica using 5 → 25% EtOAc in hexanes to afford **367** as a white solid (70.9 mg, 47% yield). Run 2 afforded 63.3 mg, 42% yield. **¹H NMR (500 MHz, CDCl₃):** δ 9.72 (t, *J* = 1.9 Hz, 1H), 7.67 (s, 1H), 5.23 (t, *J* = 6.9 Hz, 1H), 5.19 (s, 2H), 3.75 (s, 3H), 3.38 (d, *J* = 7.0 Hz, 2H), 2.54 – 2.46 (m, 2H), 2.31 (t, *J* = 7.5 Hz, 2H), 2.14 (s, 3H), 1.80 (s, 3H). **¹³C NMR (126 MHz, CDCl₃):** δ 202.62, 173.05, 163.75, 153.71, 144.18, 133.96, 123.02, 122.09, 116.88, 106.50, 70.19, 61.13, 42.16, 31.89, 22.71, 16.42, 11.71. **HRMS:** (ESI-TOF) calculated for ([C₁₇H₂₀O₅ + H]⁺): 305.1384, found 305.1378. **IR (ATR, cm⁻¹):** 3426, 2931, 1728, 1622, 1454, 1368, 1134, 1075, 1027, 968, 793

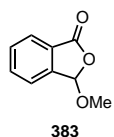


According to general procedure **C**, **376** (82.1 mg, 0.5 mmol), **290** (5.1 mg, 0.005 mmol, 0.01 equiv), PPh₃ (157.4 mg, 0.60 mmol, 1.2 equiv), Ph₂S₂ (5.5 mg, 0.025 mmol, 0.05 equiv), PhMe:DMF (95:5, 2.5 mL, 0.2M). Purified over silica using 5 → 25% EtOAc in hexanes to afford **377** as a pale-yellow oil (70.6 mg, 95% yield). Run 2 afforded 66.5 mg, 90% yield. **¹H NMR (500 MHz, CDCl₃):** δ 7.88 (dt, *J* = 7.7, 1.0 Hz, 1H), 7.67 (td, *J* = 7.5, 1.1 Hz, 1H), 7.52 (tt, *J* = 7.6, 0.8 Hz, 1H), 7.44 (dq, *J* = 7.7, 0.9 Hz, 1H), 5.56 (q, *J* = 6.7 Hz, 1H), 1.63 (d, *J* = 6.8 Hz, 3H). **¹³C NMR (126 MHz, CDCl₃):** δ 170.61, 151.31, 134.17, 129.19, 125.91, 125.84, 121.66, 77.87, 20.54.

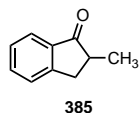


According to general procedure **C**, **380** (119.6 mg, 0.5 mmol), **290** (5.1 mg, 0.005 mmol, 0.01 equiv), PPh₃ (157.4 mg, 0.60 mmol, 1.2 equiv), **TRIP-SH** (11.8 μL, 0.05 mmol, 0.1 equiv), PhMe:DMF (95:5, 2.5 mL, 0.2M). Purified over silica using 5 → 15% EtOAc in hexanes to afford **381** as a pale-yellow oil (55.2 mg, 49% yield). Run 2 afforded 57.3 mg, 51%

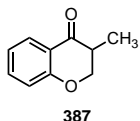
yield. **¹H NMR (500 MHz, CDCl₃):** δ 7.94 (d, *J* = 7.5 Hz, 1H), 7.65 – 7.57 (m, 3H), 7.55 – 7.42 (m, 4H), 7.26 – 7.21 (m, 1H), 5.22 (q, *J* = 6.7 Hz, 1H), 1.46 (d, *J* = 6.7 Hz, 3H). **¹³C NMR (126 MHz, CDCl₃):** δ 167.02, 146.40, 137.21, 132.19, 131.92, 129.24, 128.53, 125.50, 124.28, 123.51, 122.10, 57.03, 18.91.



According to general procedure **C**, **382** (90.0 mg, 0.5 mmol), **290** (5.1 mg, 0.005 mmol, 0.01 equiv), PPh₃ (157.4 mg, 0.60 mmol, 1.2 equiv), 2,6-Me₂PhSH (6.7 μL, 0.05 mmol, 0.1 equiv), PhMe:DMF (95:5, 2.5 mL, 0.2M). Purified over silica using 5 → 20% EtOAc in hexanes to afford **383** as a pale-yellow oil (68.2 mg, 83% yield). Run 2 afforded 69.6 mg, 85% yield **¹H NMR (500 MHz, CDCl₃):** δ 7.88 (d, *J* = 7.6 Hz, 1H), 7.71 (t, *J* = 7.5 Hz, 1H), 7.63 – 7.55 (m, 2H), 6.30 (s, 1H), 3.63 (s, 3H). **¹³C NMR (126 MHz, CDCl₃):** δ 168.72, 144.78, 134.53, 130.99, 127.26, 125.54, 123.52, 103.21, 56.92.

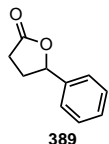


According to general procedure **C**, **384** (81.1 mg, 0.5 mmol), **290** (5.1 mg, 0.005 mmol, 0.01 equiv), PPh₃ (144.3 mg, 0.55 mmol, 1.1 equiv), **TRIP-SH** (11.8 μL, 0.05 mmol, 0.1 equiv), PhMe (2.5 mL, 0.2M). Purified over silica using 0 → 10% EtOAc in hexanes to afford **385** as a pale-yellow oil (40.4 mg, 55% yield). Run 2 afforded 37.5 mg, 51% yield. **¹H NMR (500 MHz, CDCl₃):** δ 7.75 (d, *J* = 7.6 Hz, 1H), 7.58 (t, *J* = 7.4 Hz, 1H), 7.45 (d, *J* = 7.6 Hz, 1H), 7.36 (t, *J* = 7.4 Hz, 1H), 3.44 – 3.35 (m, 1H), 2.72 (td, *J* = 11.3, 10.2, 4.2 Hz, 2H), 1.31 (d, *J* = 7.2 Hz, 3H). **¹³C NMR (126 MHz, CDCl₃):** δ 209.64, 153.61, 136.49, 134.81, 127.48, 126.67, 124.11, 42.12, 35.09, 16.43.

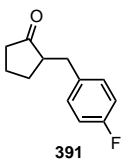


According to general procedure **C**, **386** (89.1 mg, 0.5 mmol), **290** (5.1 mg, 0.005 mmol, 0.01 equiv), PPh₃ (144.3 mg, 0.55 mmol, 1.1 equiv), **TRIP-SH** (11.8 μL, 0.05 mmol, 0.1 equiv), PhMe (2.5 mL, 0.2M). Purified over silica using 0 → 10% EtOAc in hexanes to afford **387** as a pale-yellow oil (51.4 mg, 63% yield). Run 2 afforded 43.2 mg, 53% yield. **¹H**

NMR (500 MHz, CDCl₃): δ 7.90 (dd, J = 7.9, 1.7 Hz, 1H), 7.46 (ddd, J = 8.5, 7.2, 1.8 Hz, 1H), 7.01 (ddd, J = 8.0, 7.1, 1.1 Hz, 1H), 6.96 (dd, J = 8.3, 1.0 Hz, 1H), 4.50 (dd, J = 11.3, 5.1 Hz, 1H), 4.15 (t, J = 11.1 Hz, 1H), 2.86 (dq, J = 11.0, 7.0, 5.0 Hz, 1H), 1.22 (d, J = 7.0 Hz, 3H). **¹³C NMR (126 MHz, CDCl₃):** δ 194.97, 161.83, 135.83, 127.47, 121.47, 120.66, 117.86, 72.34, 40.85, 10.83.



According to general procedure **B**, **388** (89.1 mg, 0.5 mmol), PhMe (25.0 mL, 0.02M). Purified over silica using 5 \rightarrow 25% EtOAc in hexanes to afford **389** as a colorless oil (32.9 mg, 41% yield). Run 2 afforded 35.9 mg, 44% yield. **¹H NMR (500 MHz, CDCl₃):** δ 7.42 – 7.32 (m, 5H), 5.52 (dd, J = 8.0, 6.1 Hz, 1H), 2.71 – 2.61 (m, 3H), 2.27 – 2.14 (m, 1H). **¹³C NMR (126 MHz, CDCl₃):** δ 177.04, 139.48, 128.89, 128.57, 125.39, 81.36, 31.12, 29.09.



According to general procedure **B**, **390** (104.1 mg, 0.5 mmol), PhMe (25.0 mL, 0.02M). Purified over silica using 0 \rightarrow 10% EtOAc in hexanes to afford **391** as a colorless oil (45.0 mg, 52% yield). Run 2 afforded 37.9 mg, 39% yield with 6.2 mg of the aldehyde, 6% yield. Run 3 afforded 39.9 mg, 42% yield, with 3.6 mg of the aldehyde, 4% yield. **¹H NMR (500 MHz, CDCl₃):** δ 7.15 – 7.06 (m, 2H), 6.96 (t, J = 8.7 Hz, 2H), 3.09 (dd, J = 14.0, 4.3 Hz, 1H), 2.54 (dd, J = 14.0, 9.2 Hz, 1H), 2.39 – 2.27 (m, 2H), 2.14 – 2.03 (m, 2H), 2.00 – 1.90 (m, 1H), 1.79 – 1.67 (m, 1H), 1.59 – 1.48 (m, 1H). **¹³C NMR (126 MHz, CDCl₃):** δ 220.18, 161.59 (d, J = 244.4 Hz), 135.69, 130.46, 115.40, 51.18, 38.36, 34.83, 29.16, 20.68. **¹⁹F NMR (282 MHz, CDCl₃):** δ -117.20 (ddd, J = 14.0, 8.7, 5.3 Hz). **HRMS:** (EI+) calculated for C₁₂H₁₃FO ([M]⁺): 192.0945, found 192.0944. **IR (ATR, cm⁻¹):** 2960, 1737, 1601, 1509, 1220, 1156, 1016, 824, 761

Stern-Volmer quenching studies:

Emission intensities were measured on a Perkin Elmer LS50 Luminescence spectrometer. All solutions and samples were prepared in an N₂-filled glovebox, sealed well with electrical tape and analyzed immediately. A stock solution of [Ir(dFMeppy)₂dtbbpy]PF₆ (4.1 mg in 2.0 mL DMF, 2.0 x 10⁻³M) was diluted 0.5 mL into DMF (2.0 mL) and PhMe (2.5 mL) (total volume 5.0 mL) for a final concentration of 2.0 x 10⁻⁴M. This final stock solution (0.2 mL) was added to each cuvette with total volume of 2.0 mL (active concentration of [Ir] = 2.0 x 10⁻⁵M). Stock solutions of each quencher PPh₃, TRIP-SH and *p*-toluic acid (**317**) were prepared with the final concentrations as denoted (0.04M, 0.02M, 0.008M, 0.004M). The reaction sample was prepared with all components at the specified concentrations.

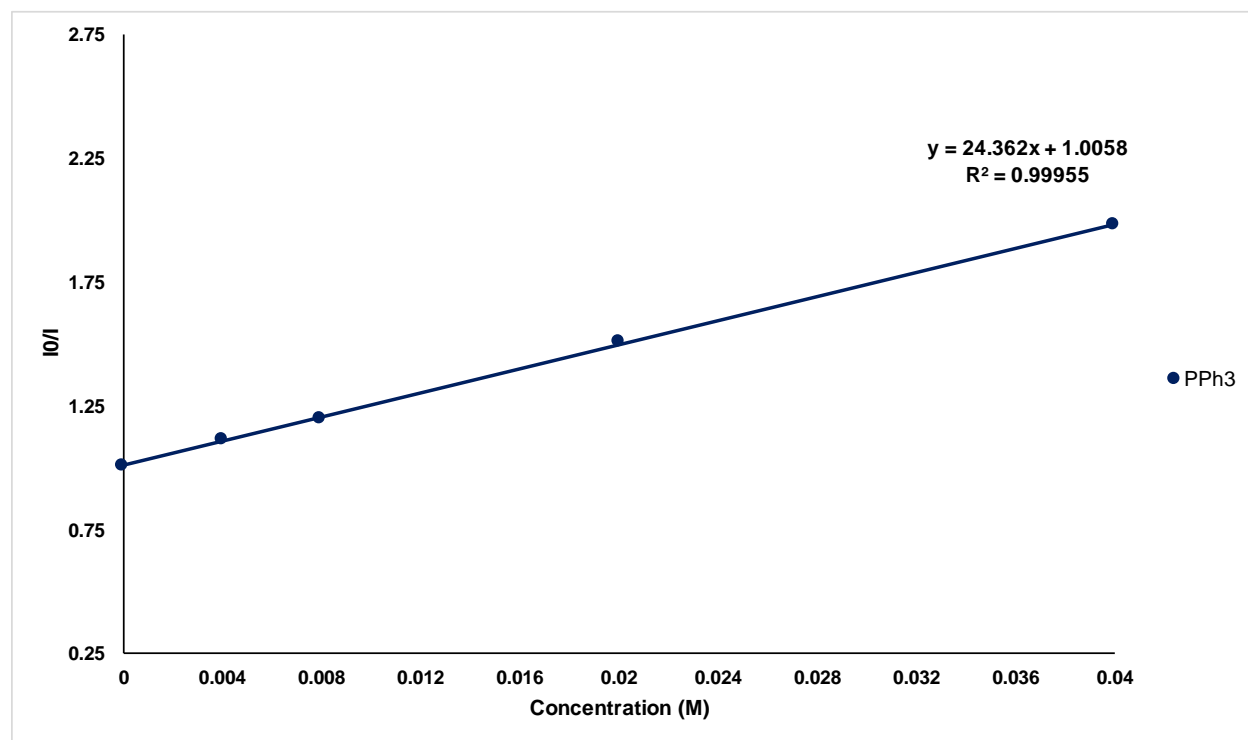


Figure A2.1 PPh₃

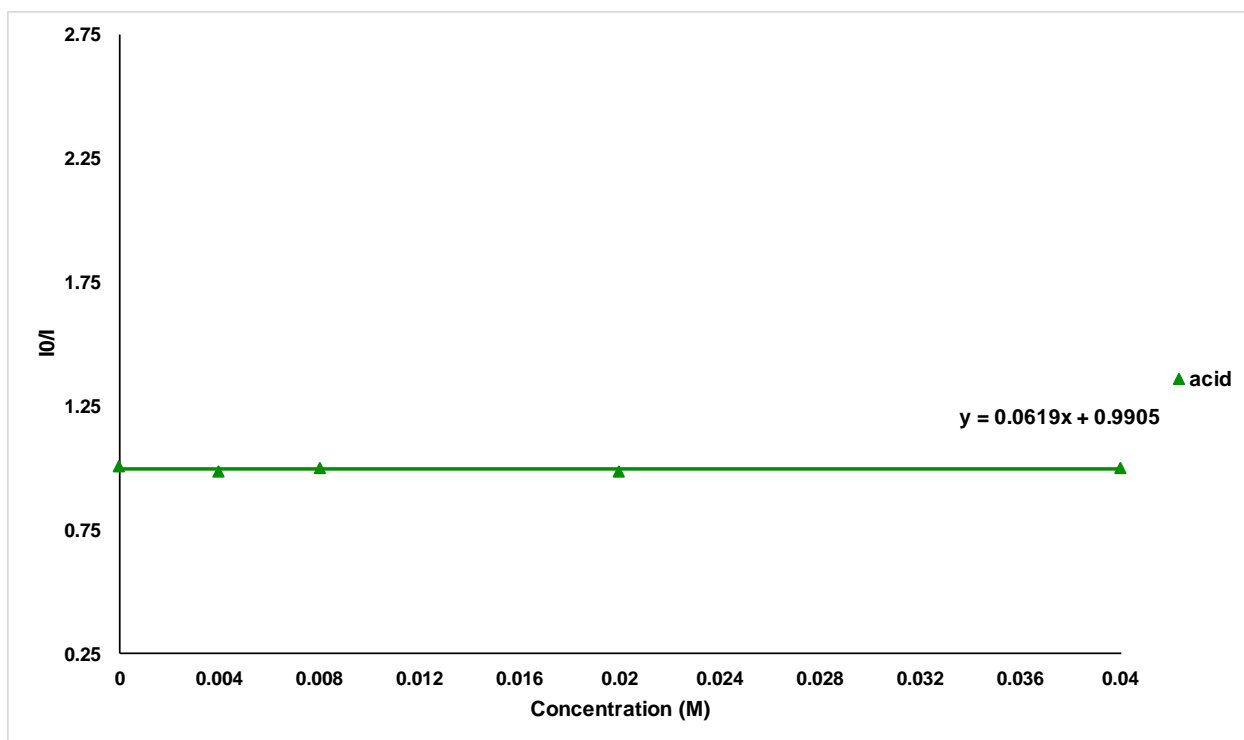


Figure A2.2. *p*-Toluic acid

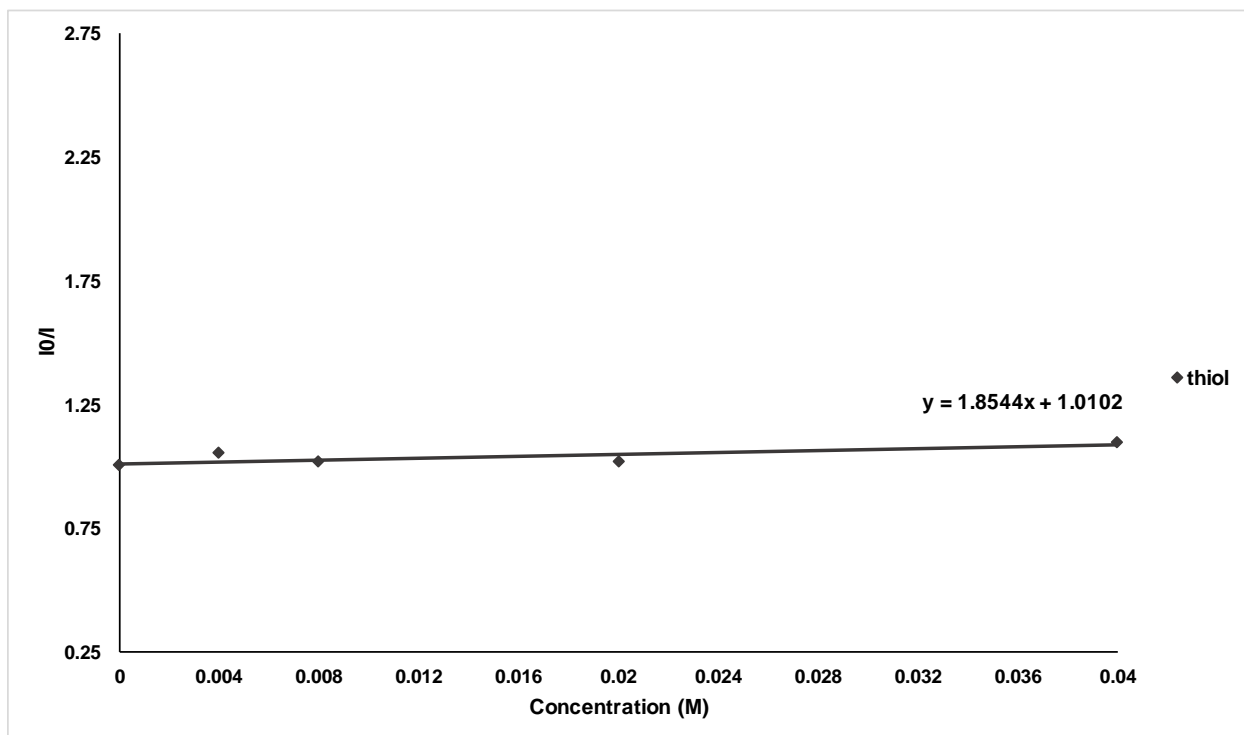


Figure A2.3. TRIP-SH

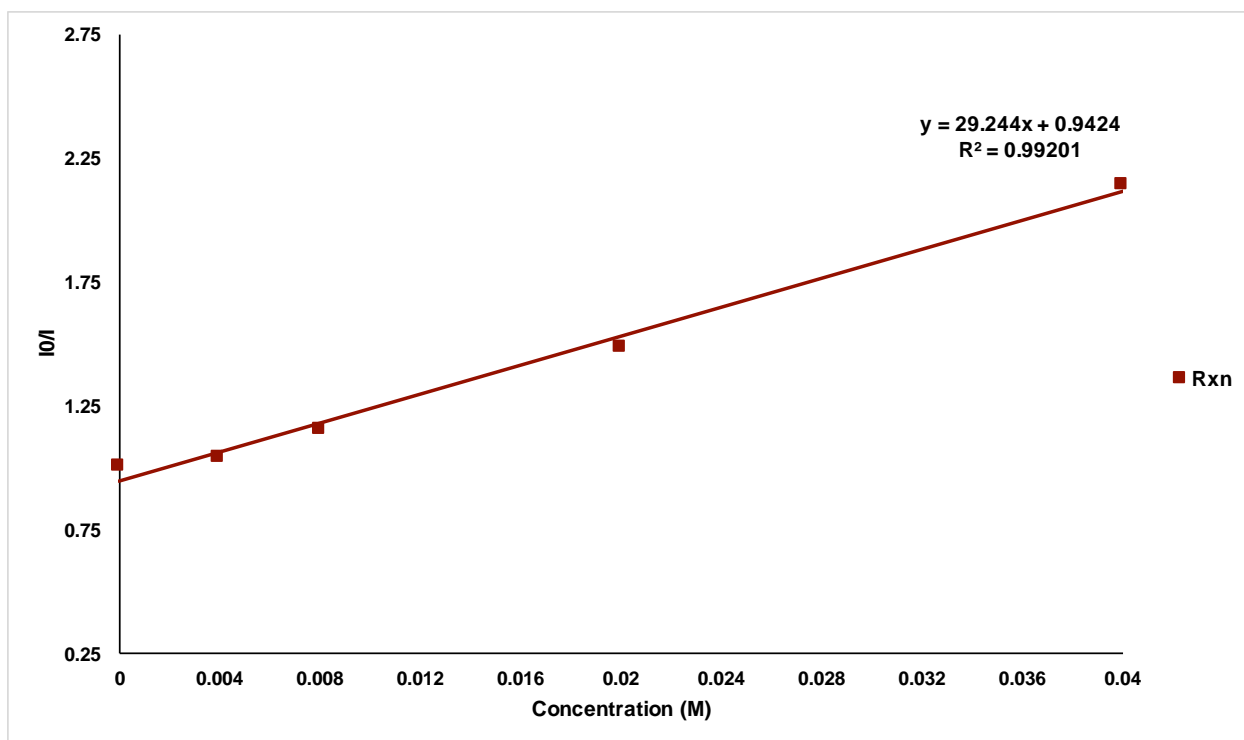


Figure A2.4. Reaction

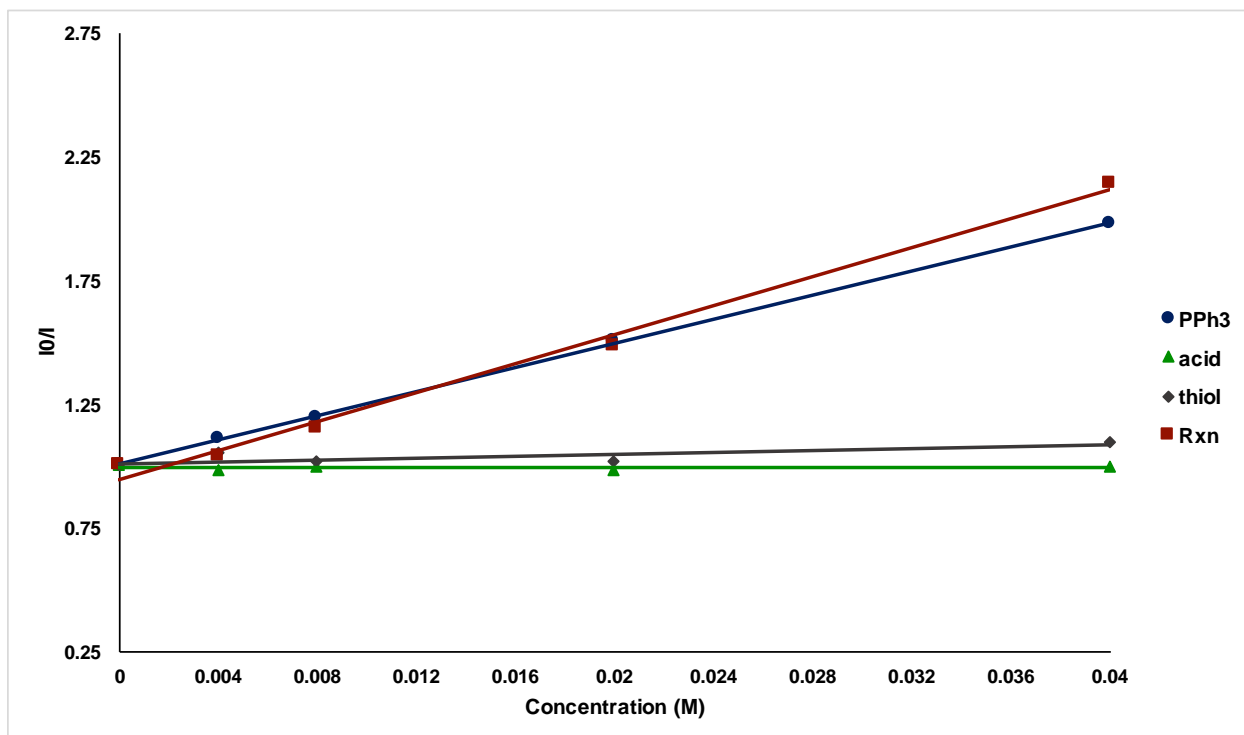
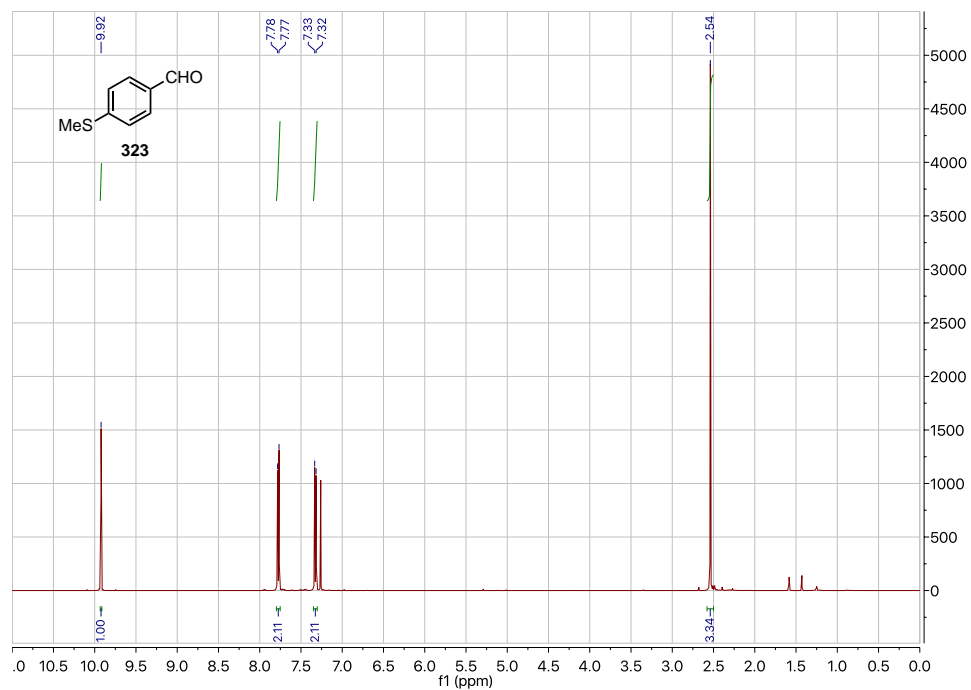
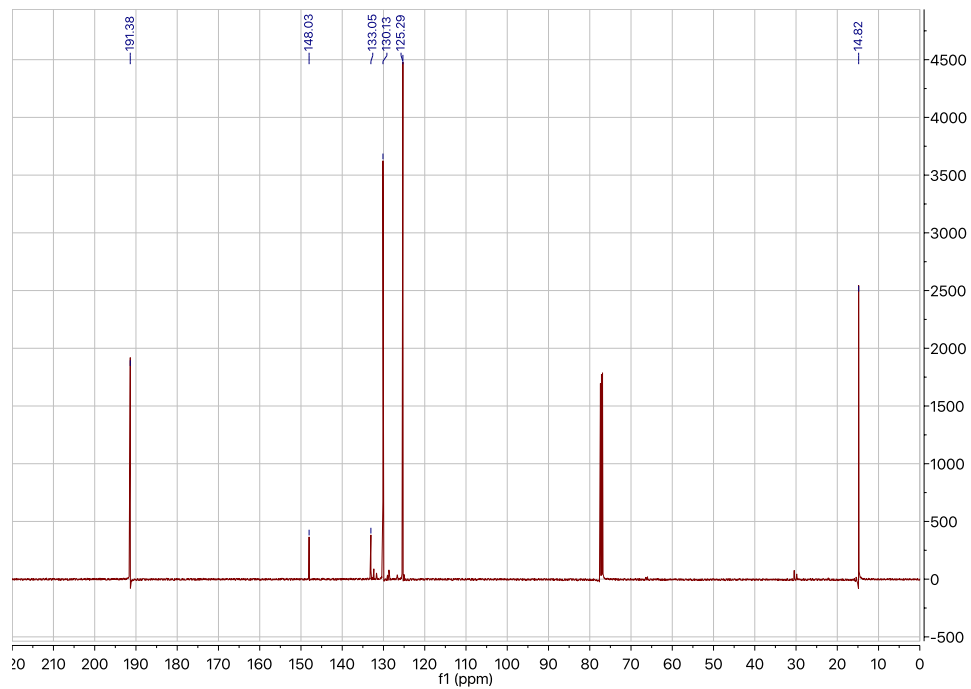


Figure A2.5. Overlay of all components

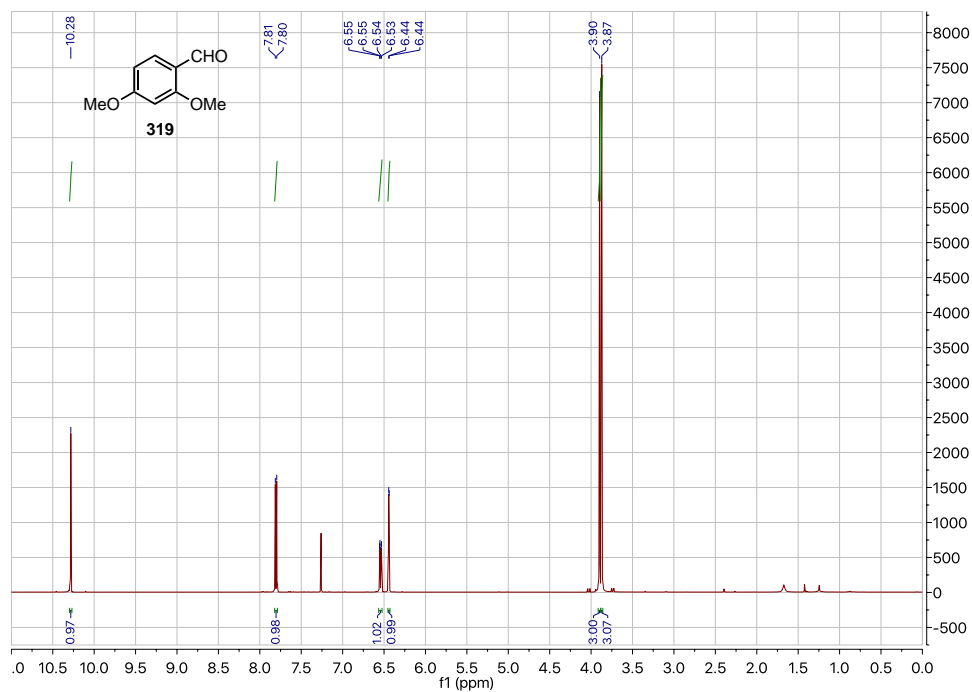
^1H NMR (500 MHz, CDCl_3): 4-(methylthio)benzaldehyde (323)



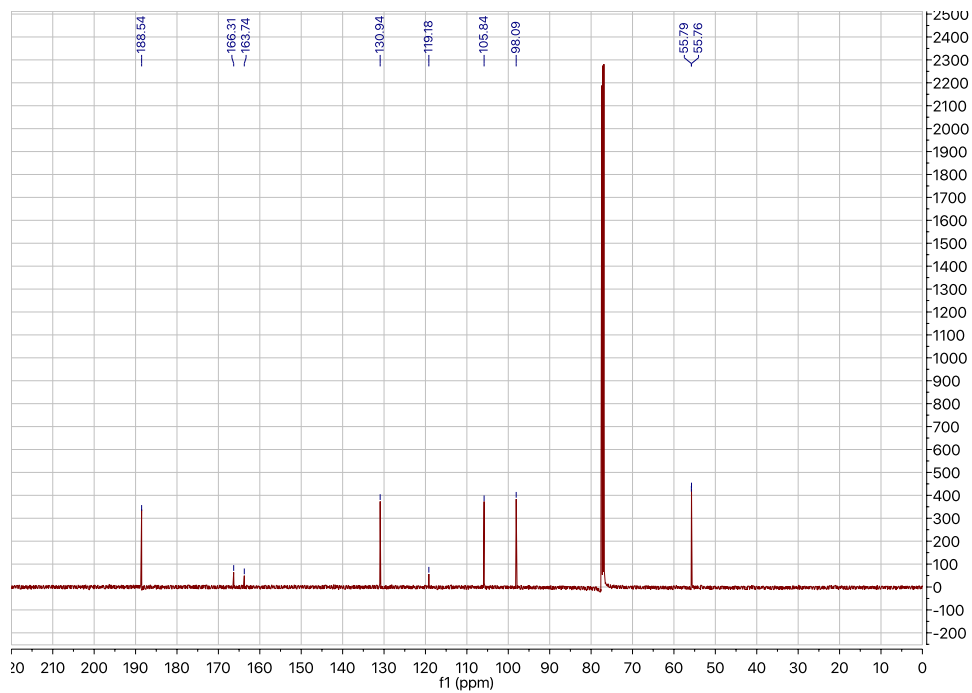
^{13}C NMR (126 MHz, CDCl_3): 4-(methylthio)benzaldehyde



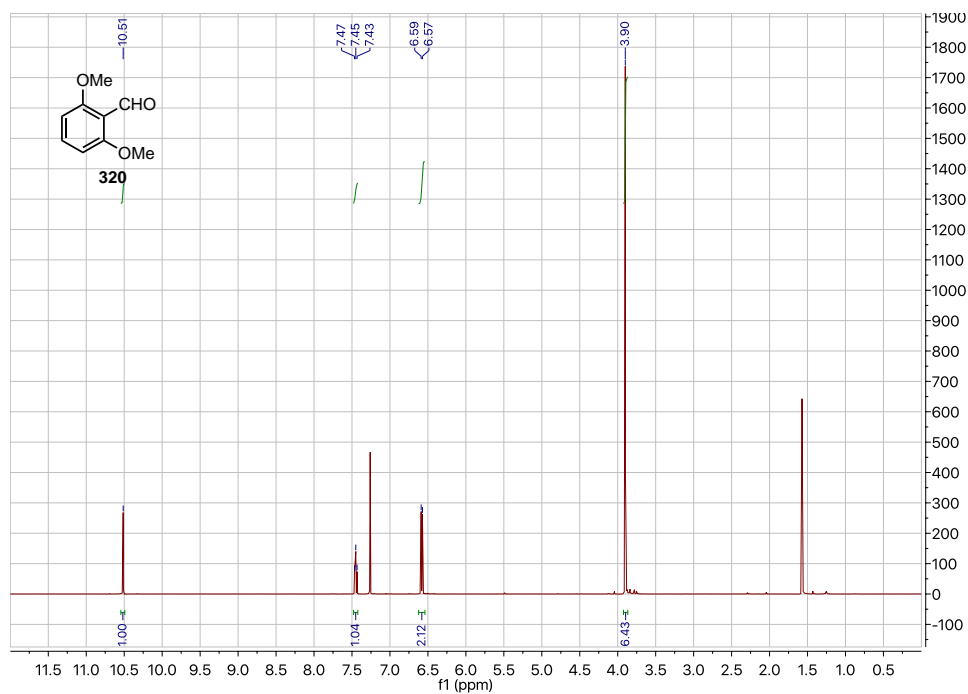
^1H NMR (500 MHz, CDCl_3): 2,4-dimethoxybenzaldehyde (319)



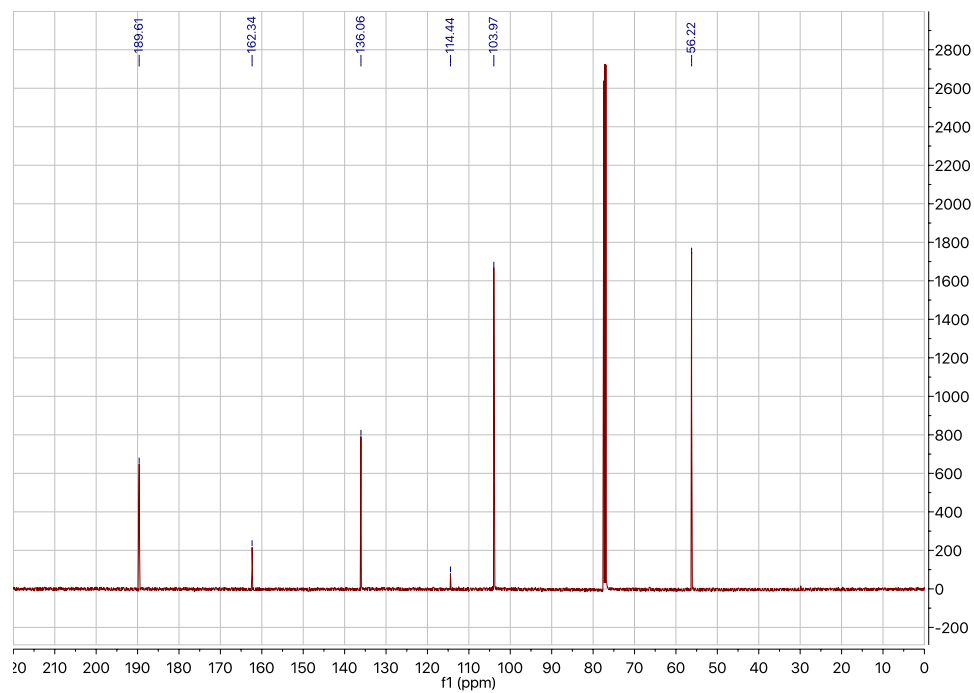
^{13}C NMR (126 MHz, CDCl_3): 2,4-dimethoxybenzaldehyde



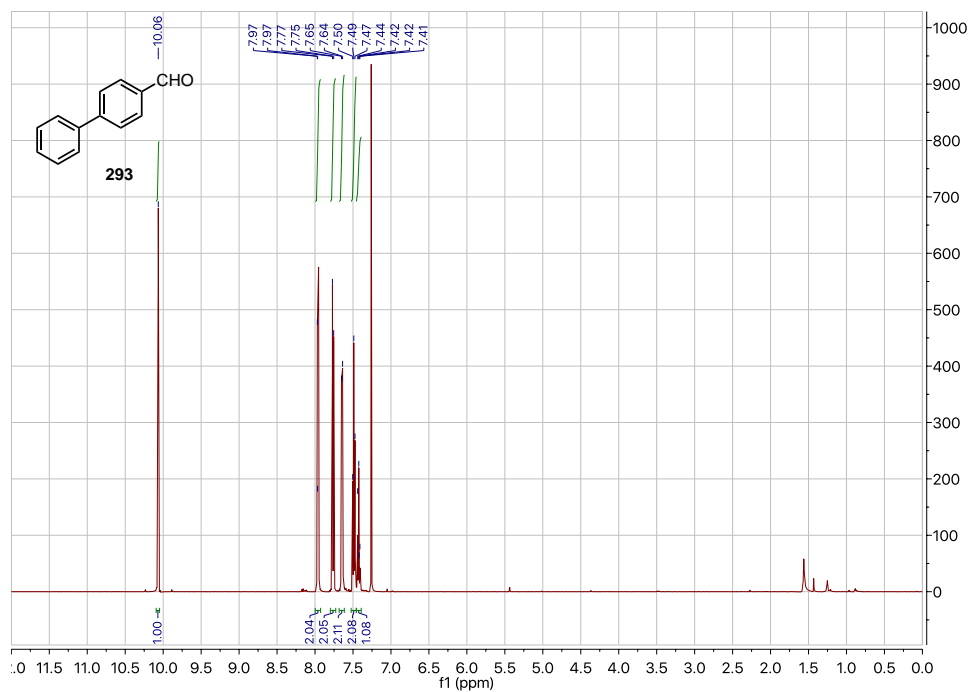
^1H NMR (500 MHz, CDCl_3): 2,6-dimethoxybenzaldehyde (320)



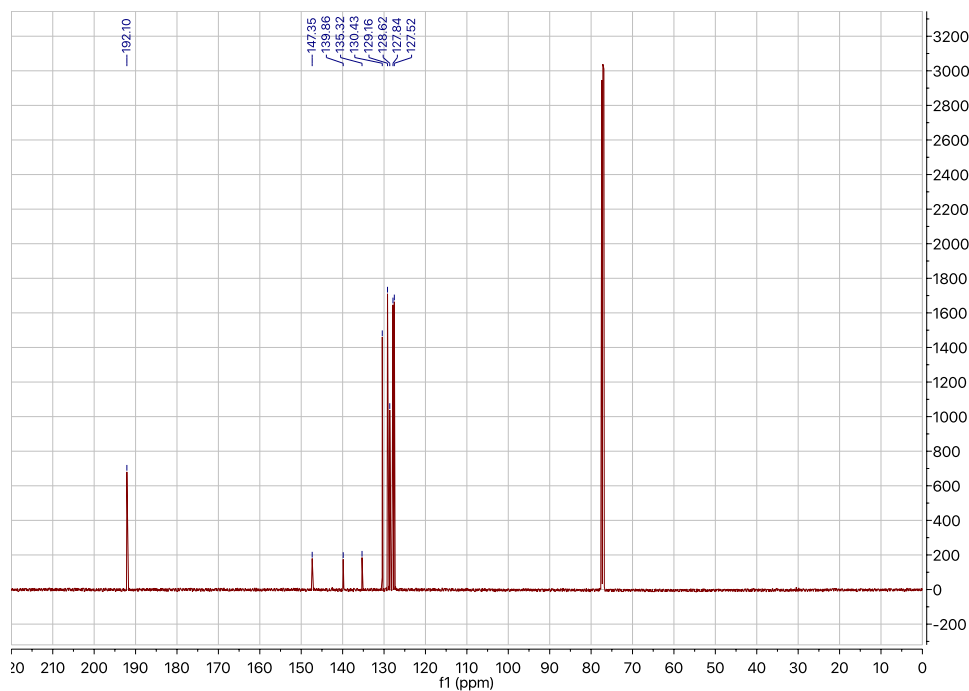
^{13}C NMR (126 MHz, CDCl_3): 2,6-dimethoxybenzaldehyde



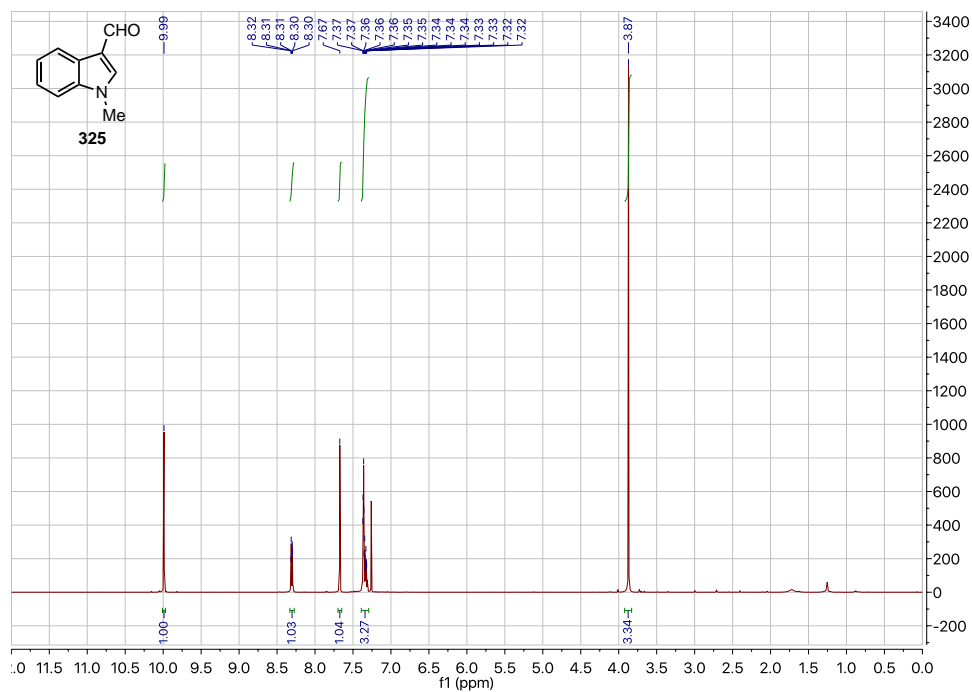
^1H NMR (500 MHz, CDCl_3): [1,1'-biphenyl]-4-carbaldehyde (293)



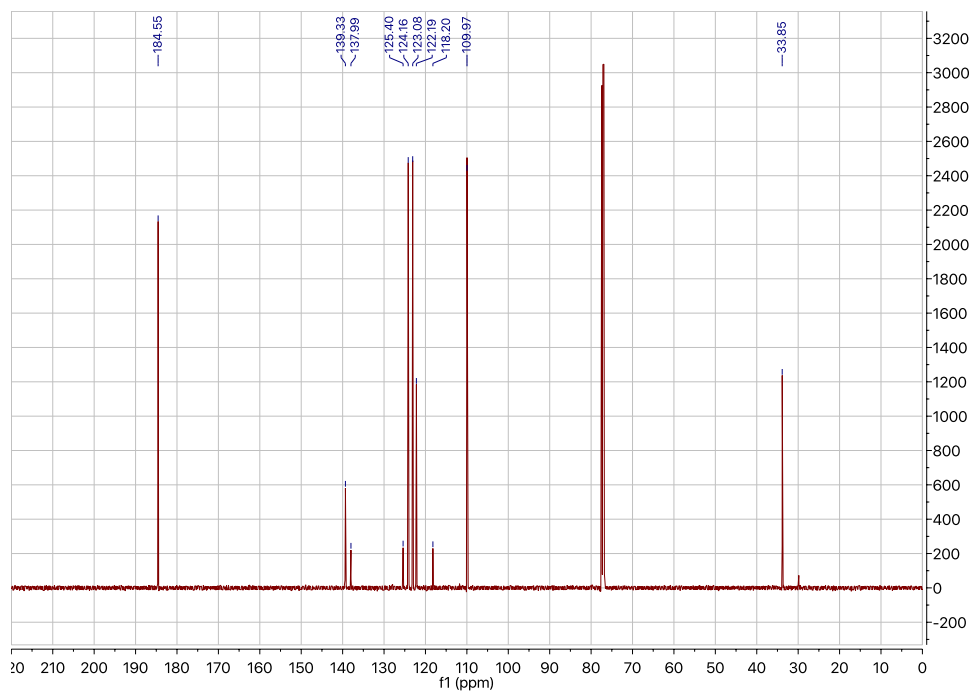
^{13}C NMR (126 MHz, CDCl_3): [1,1'-biphenyl]-4-carbaldehyde



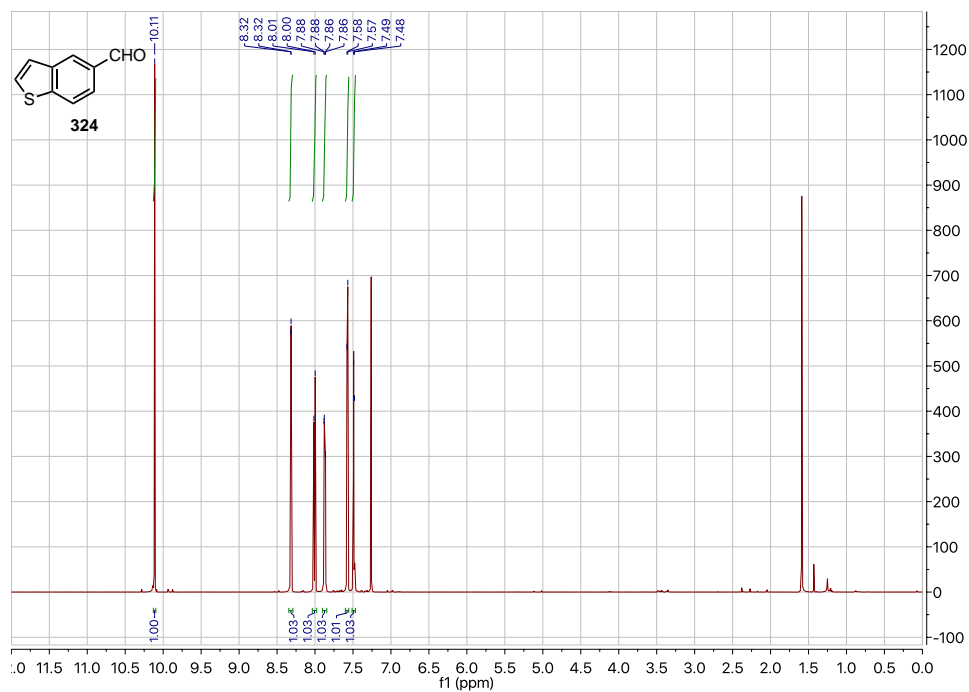
^1H NMR (500 MHz, CDCl_3): 1-methyl-1*H*-indole-3-carbaldehyde (325)



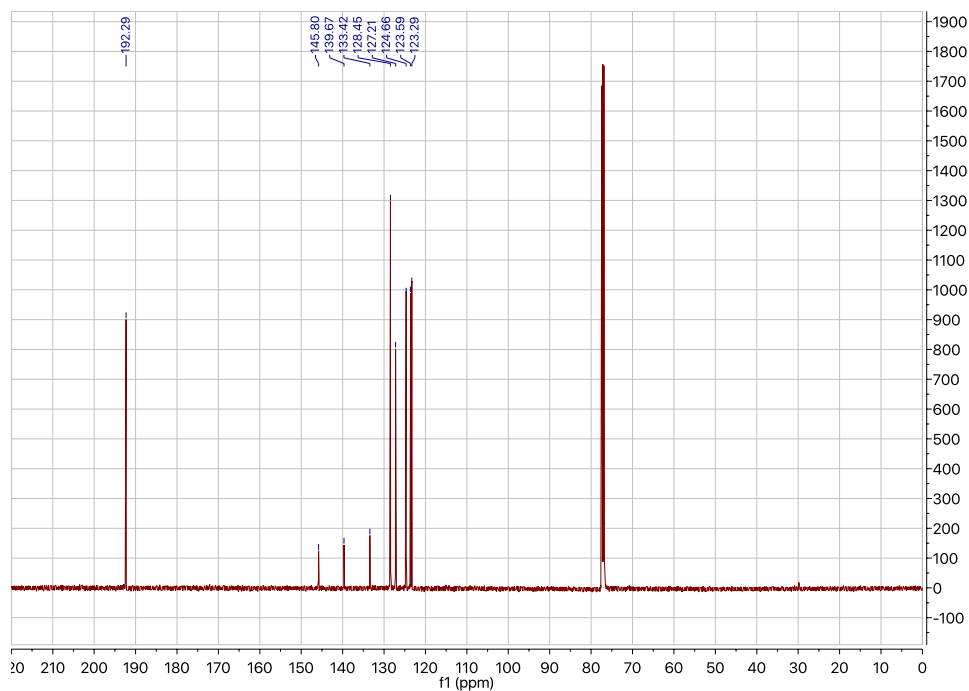
^{13}C NMR (126 MHz, CDCl_3): 1-methyl-1*H*-indole-3-carbaldehyde



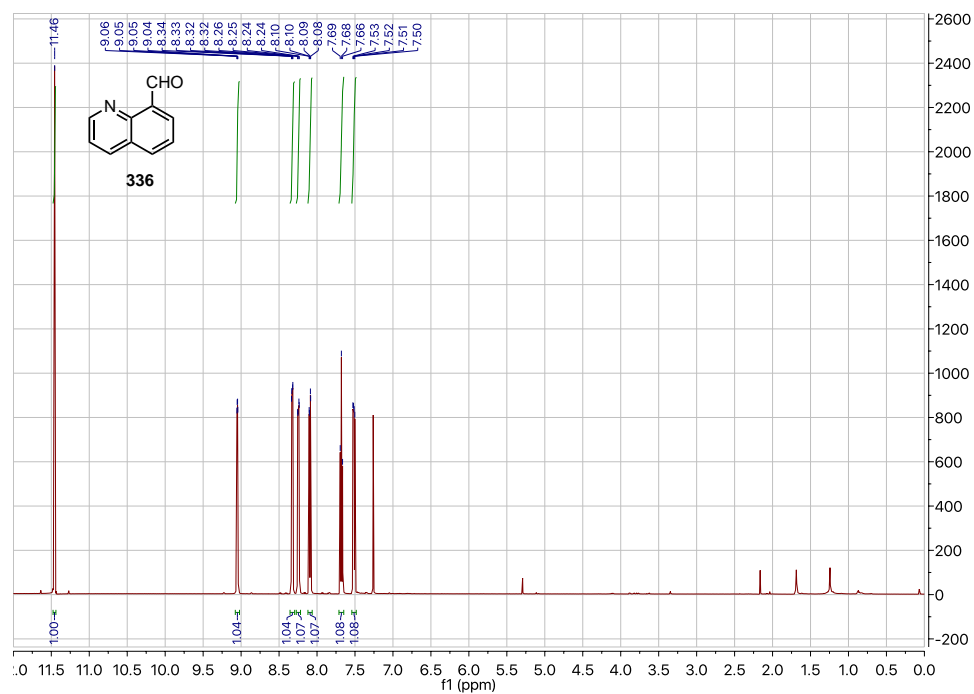
^1H NMR (500 MHz, CDCl_3): benzo[*b*]thiophene-5-carbaldehyde (324)



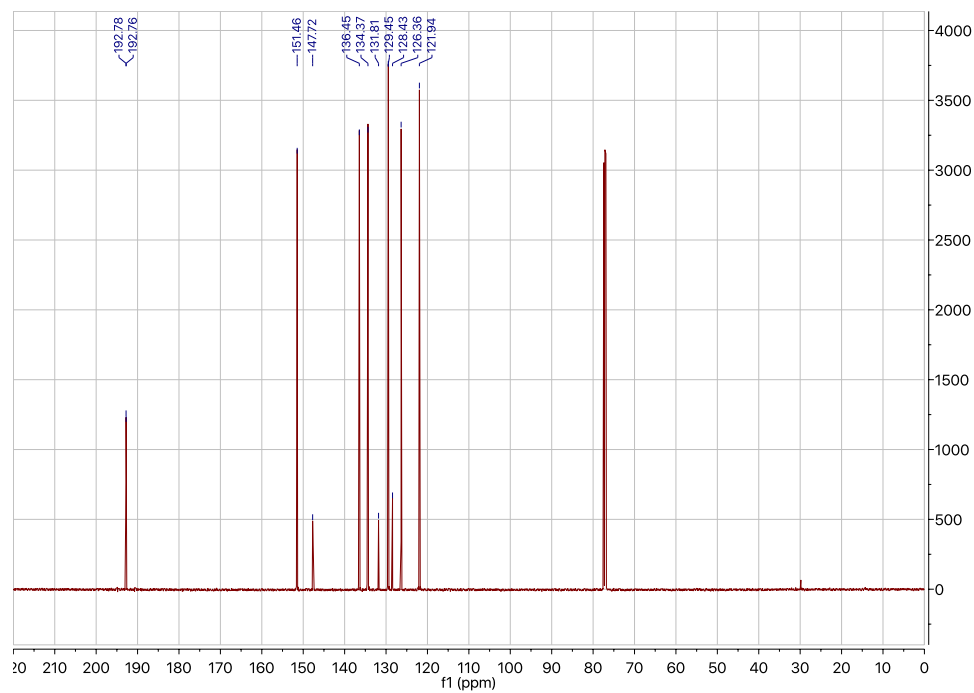
^{13}C NMR (126 MHz, CDCl_3): benzo[*b*]thiophene-5-carbaldehyde



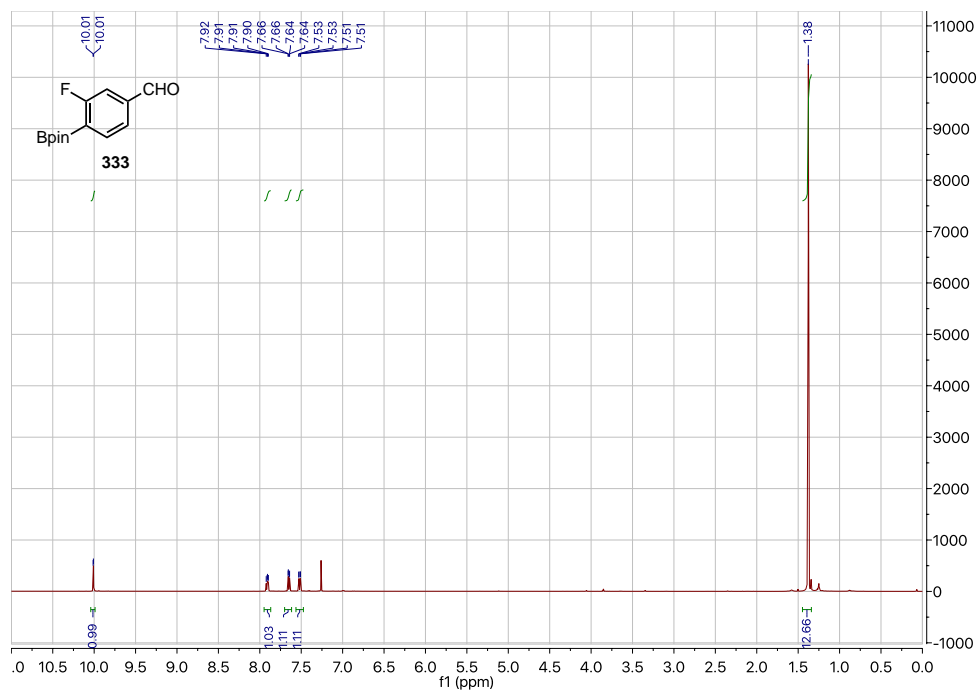
^1H NMR (500 MHz, CDCl_3): quinoline-8-carbaldehyde (336)



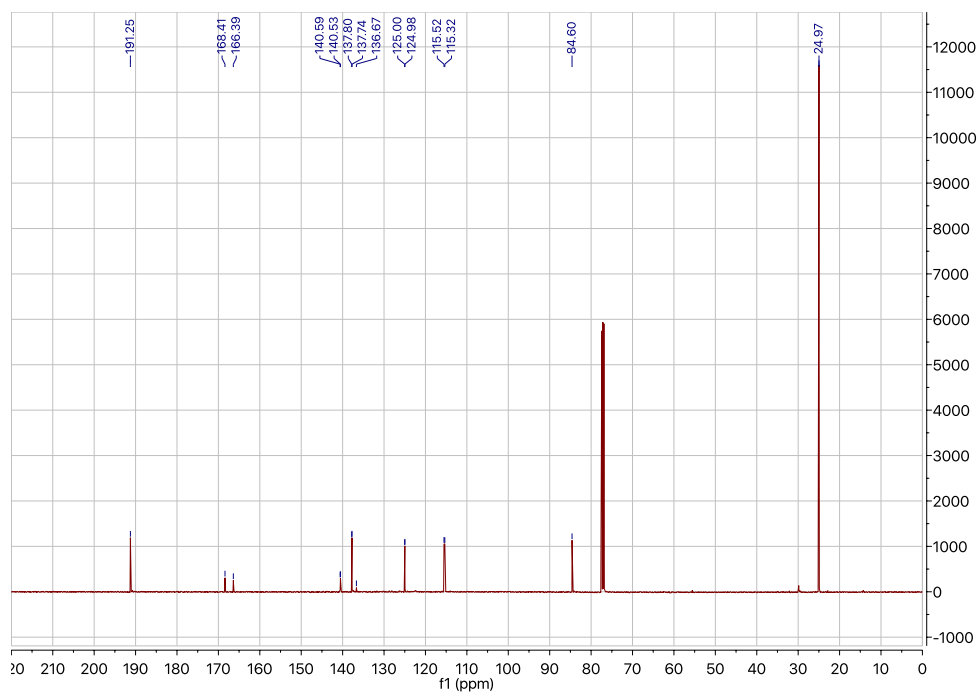
^{13}C NMR (126 MHz, CDCl_3): quinoline-8-carbaldehyde



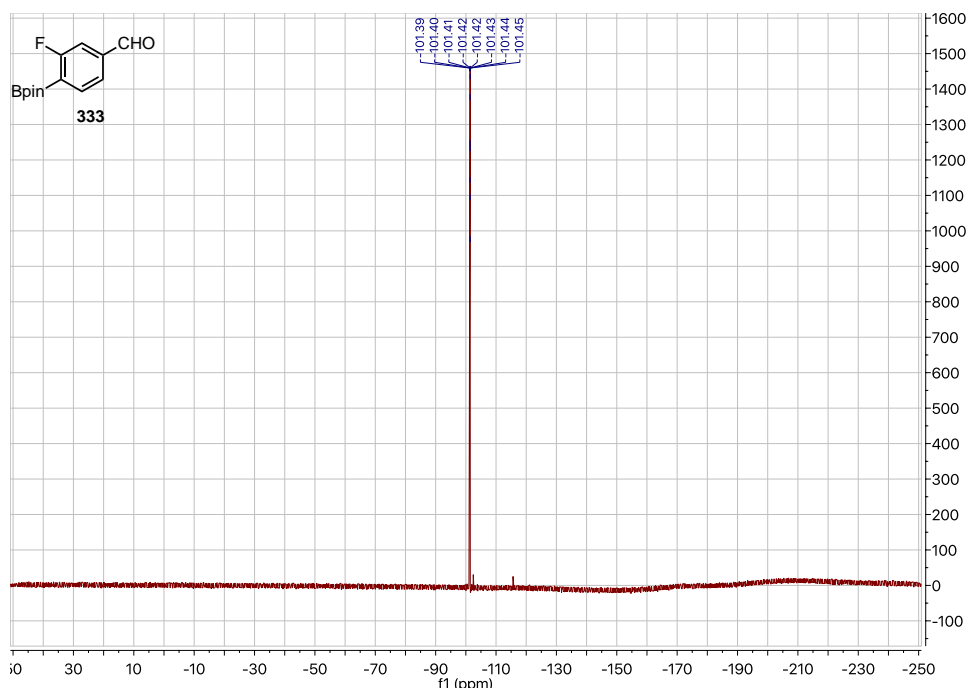
^1H NMR (500 MHz, CDCl_3): 3-fluoro-4-(4,4,5,5-tetramethyl-1,3,2-dioxaborolan-2-yl)benzaldehyde (333)



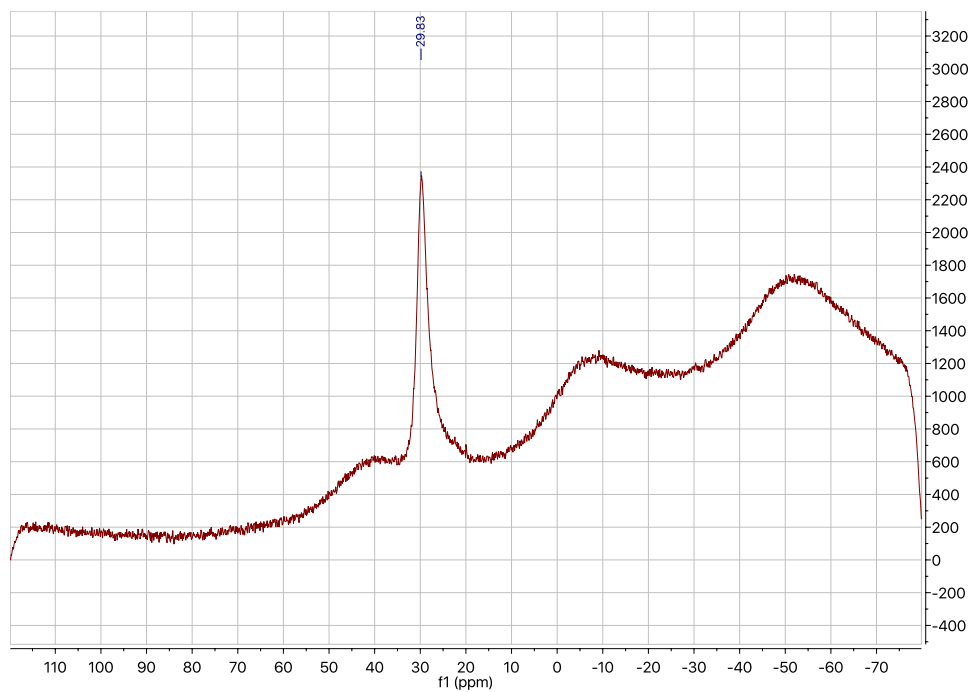
^{13}C NMR (126 MHz, CDCl_3): 3-fluoro-4-(4,4,5,5-tetramethyl-1,3,2-dioxaborolan-2-yl)benzaldehyde



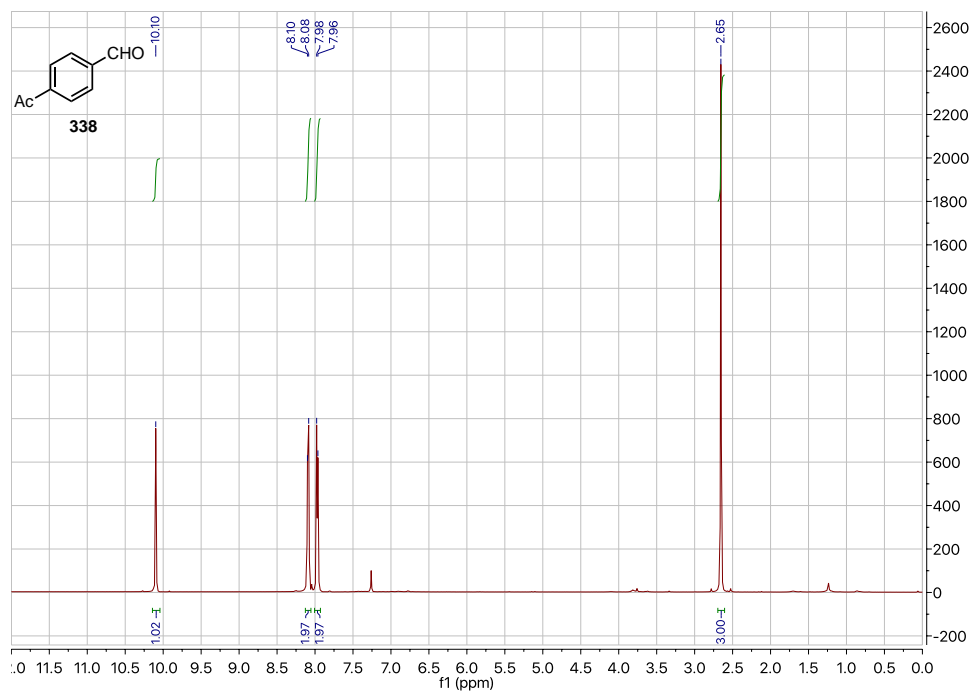
^{19}F NMR (282 MHz, CDCl_3): 3-fluoro-4-(4,4,5,5-tetramethyl-1,3,2-dioxaborolan-2-yl)benzaldehyde (333)



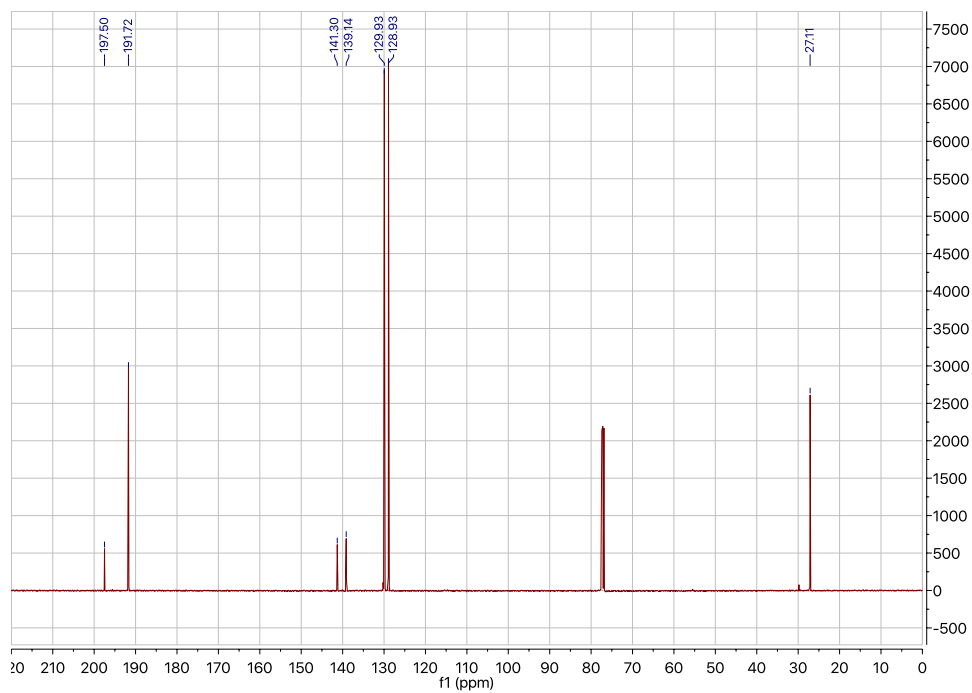
^{11}B NMR (96 MHz, CDCl_3): 3-fluoro-4-(4,4,5,5-tetramethyl-1,3,2-dioxaborolan-2-yl)benzaldehyde



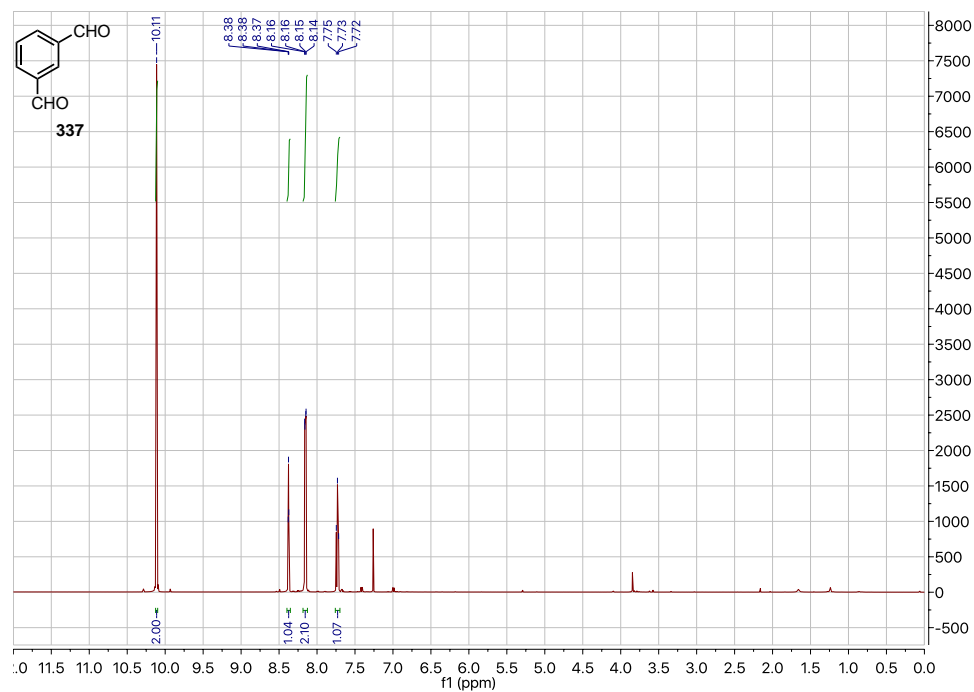
^1H NMR (500 MHz, CDCl_3): 4-acetylbenzaldehyde (338)



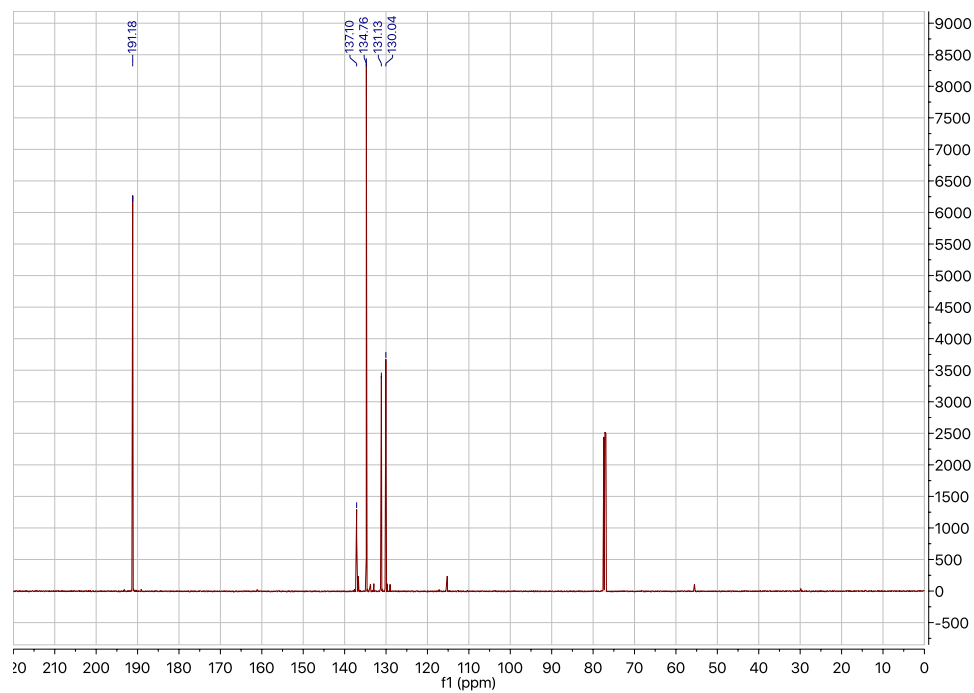
^{13}C NMR (126 MHz, CDCl_3): 4-acetylbenzaldehyde



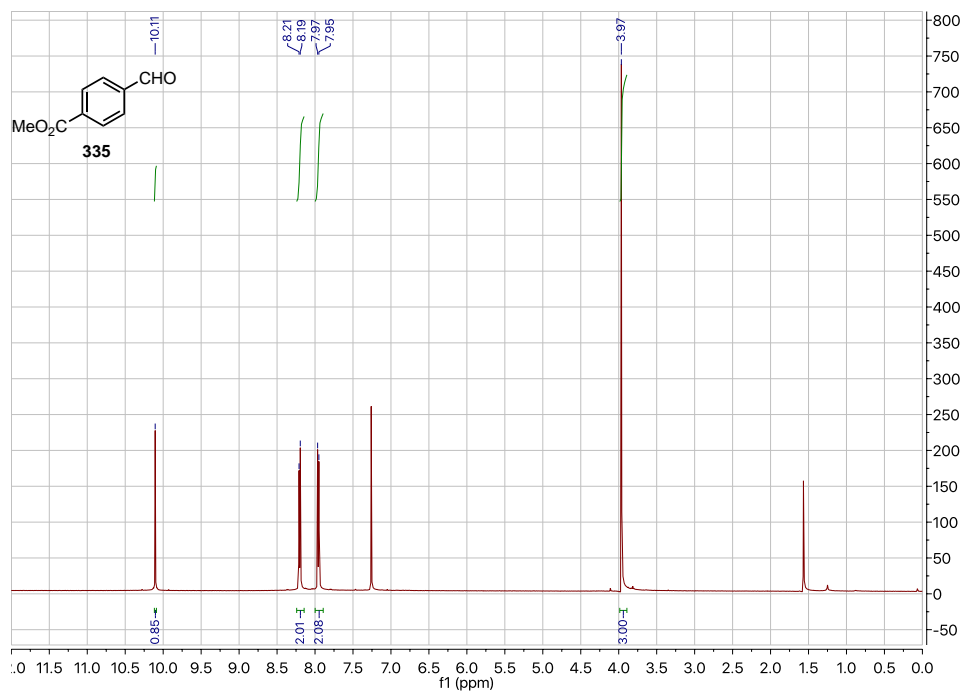
^1H NMR (500 MHz, CDCl_3): isophthalaldehyde (337)



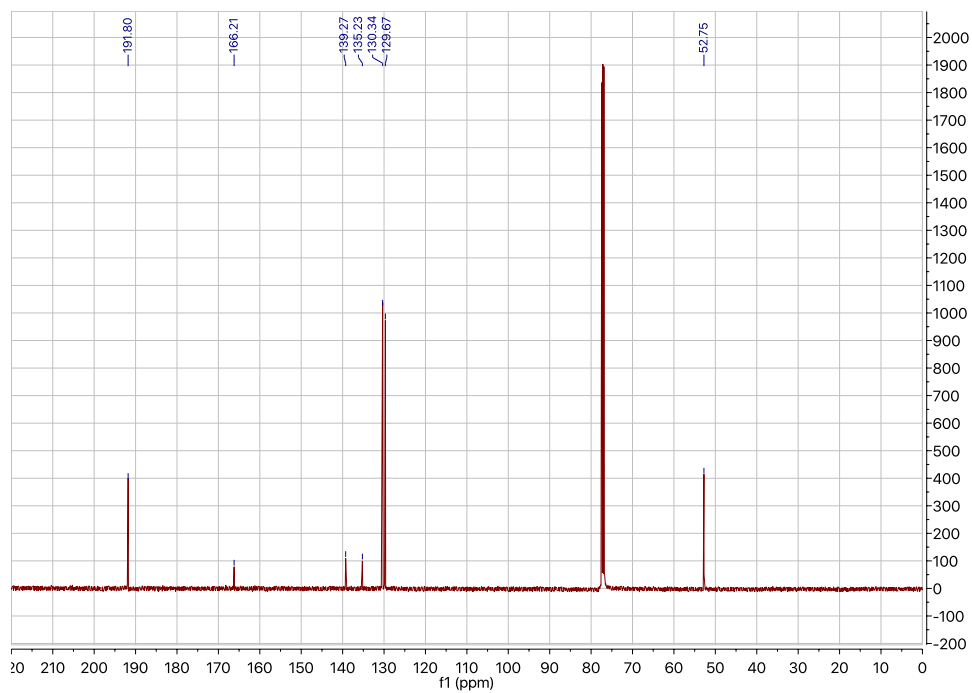
^{13}C NMR (126 MHz, CDCl_3): isophthalaldehyde



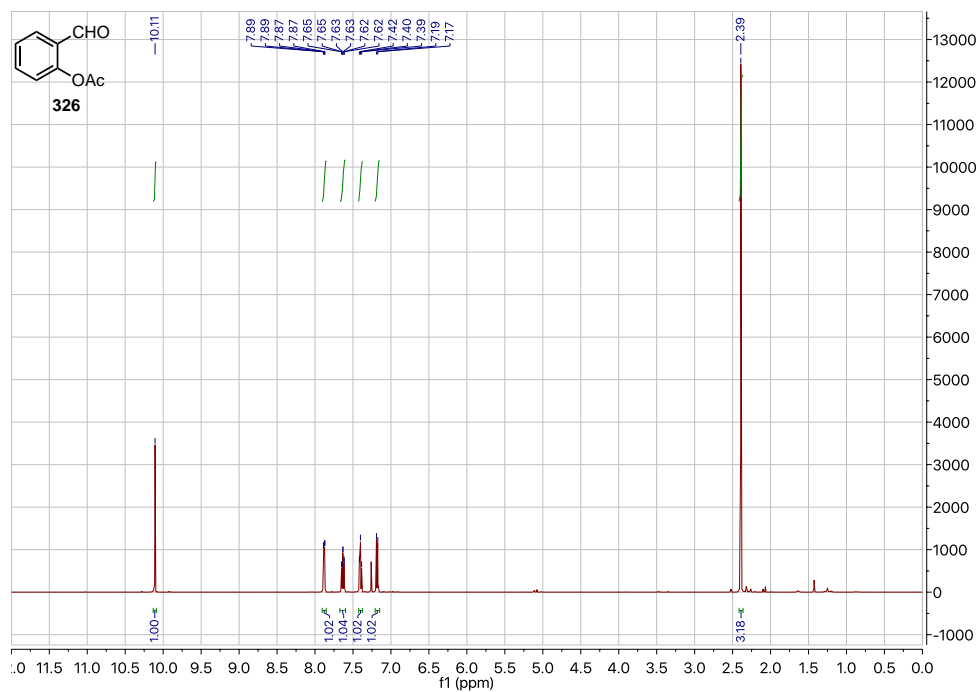
^1H NMR (500 MHz, CDCl_3): methyl 4-formylbenzoate (335)



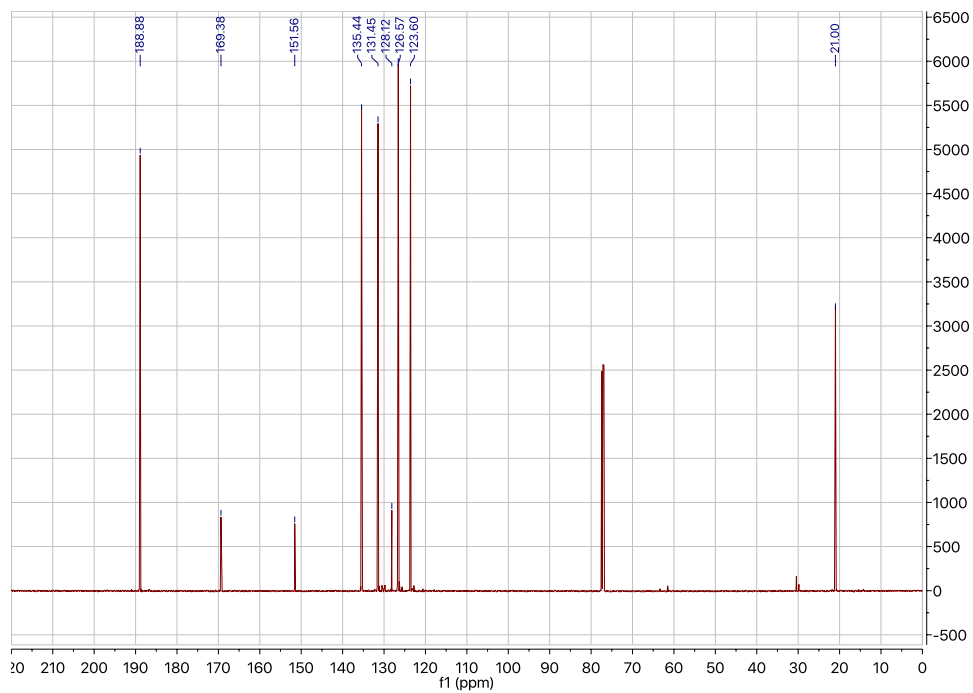
^{13}C NMR (126 MHz, CDCl_3): methyl 4-formylbenzoate



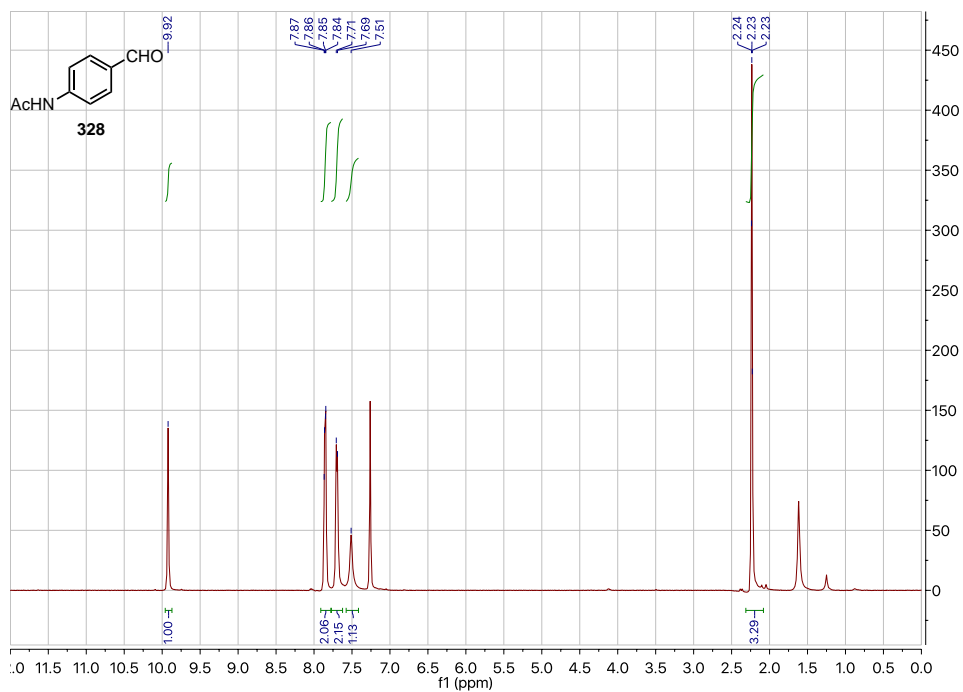
^1H NMR (500 MHz, CDCl_3): 2-formylphenyl acetate (326)



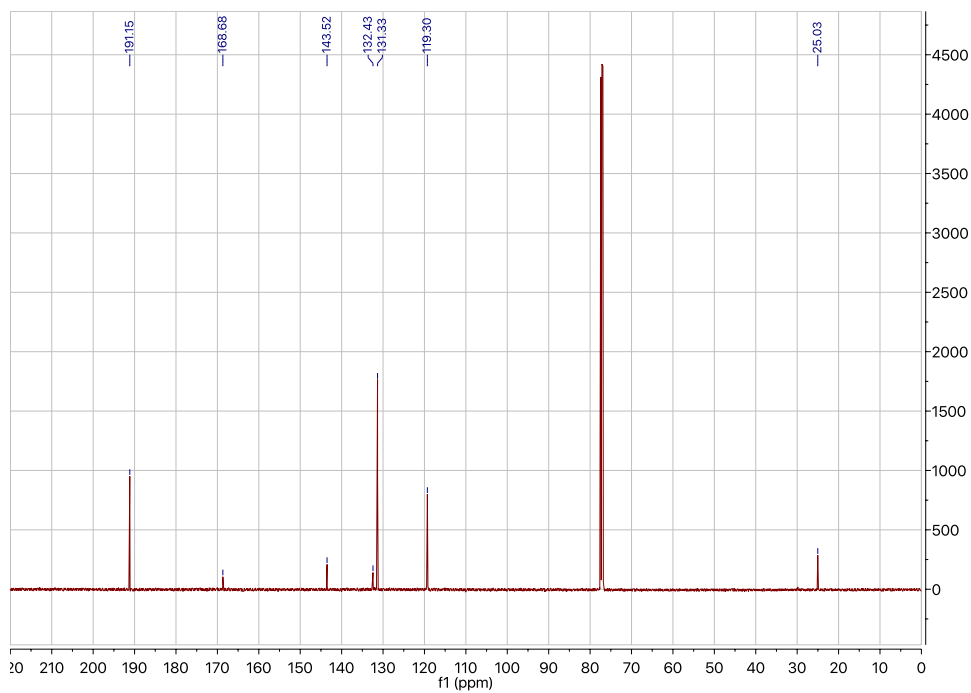
^{13}C NMR (126 MHz, CDCl_3): 2-formylphenyl acetate



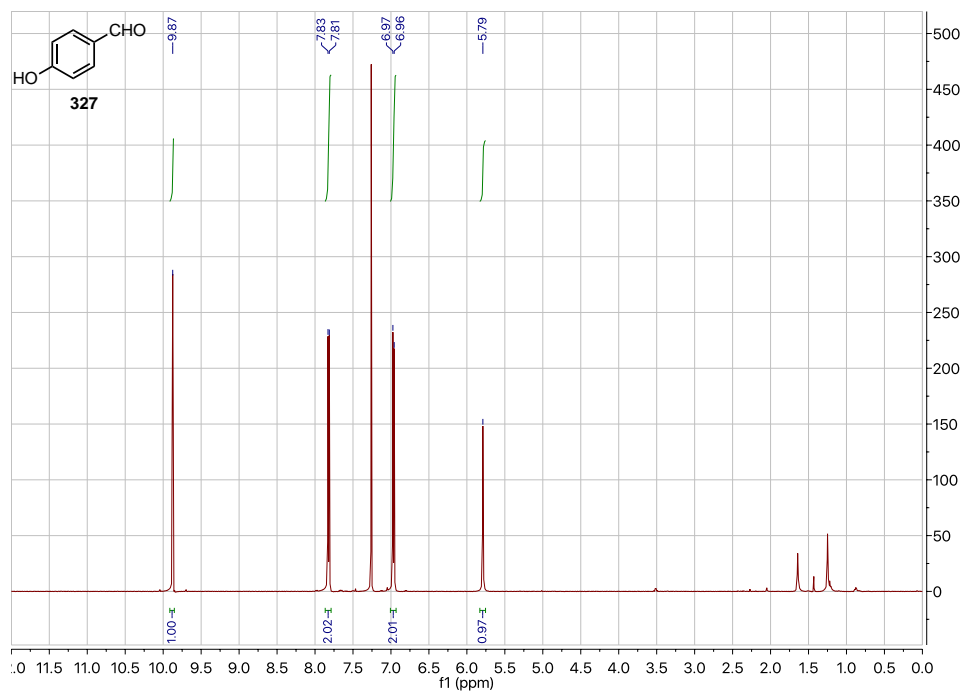
^1H NMR (500 MHz, CDCl_3): *N*-(4-formylphenyl)acetamide (328)



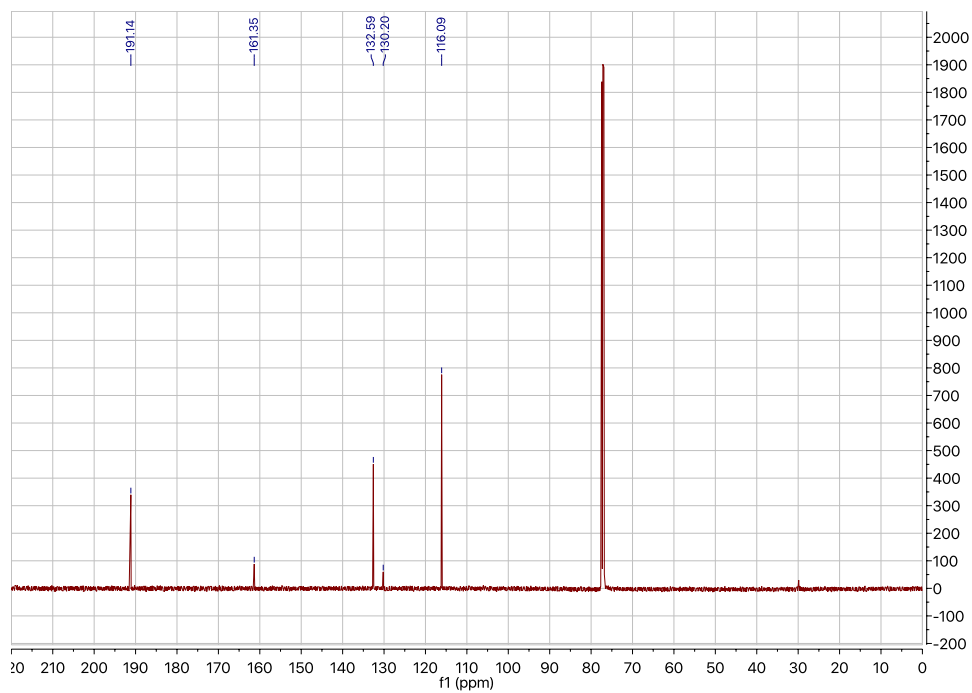
^{13}C NMR (126 MHz, CDCl_3): *N*-(4-formylphenyl)acetamide



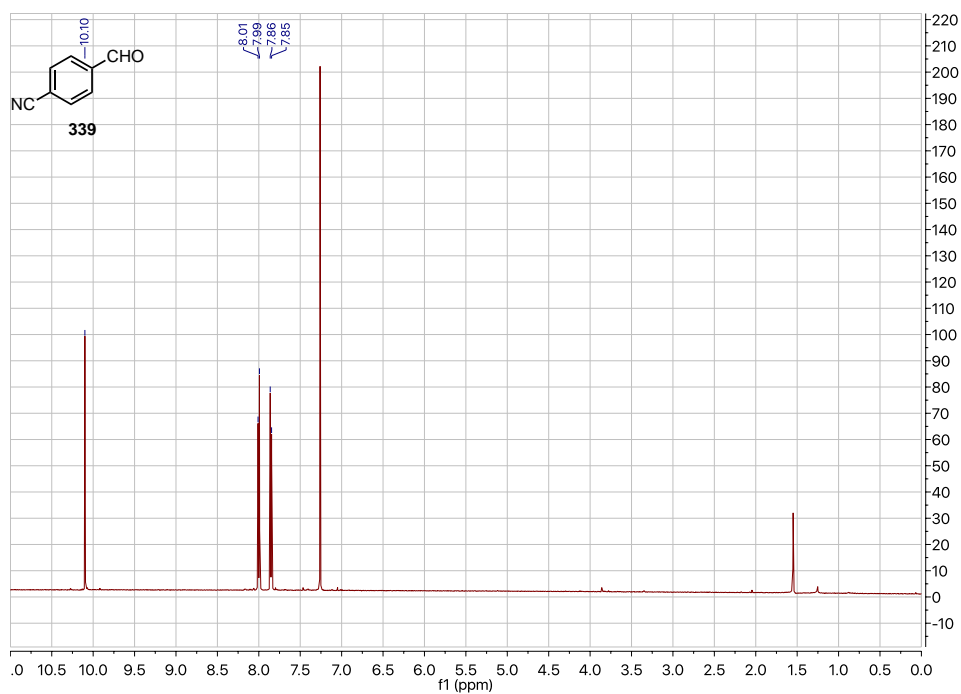
^1H NMR (500 MHz, CDCl_3): 4-hydroxybenzaldehyde (327)



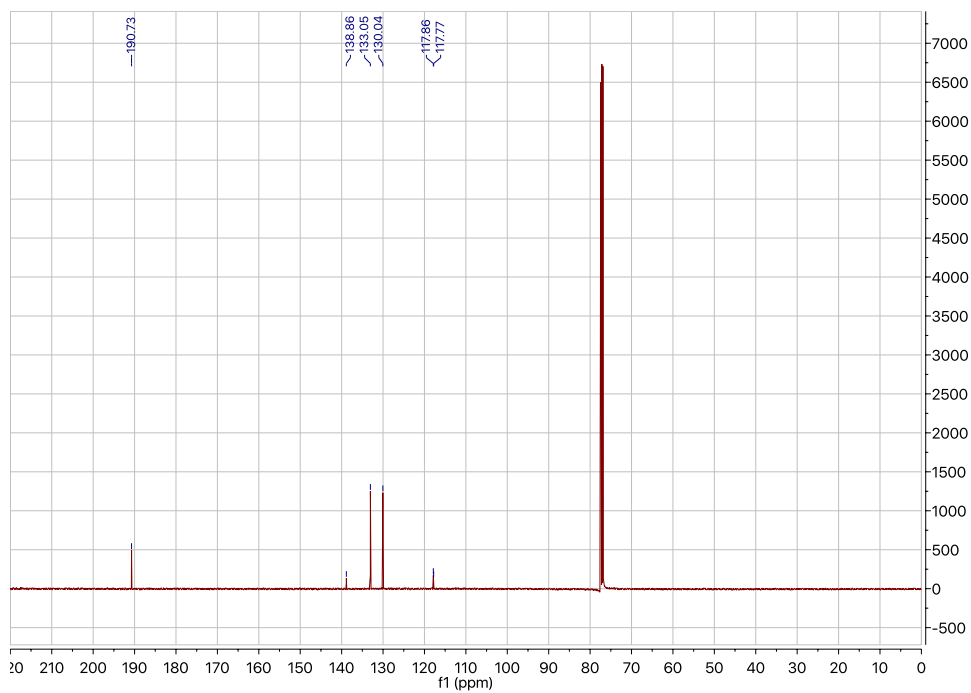
^{13}C NMR (126 MHz, CDCl_3): 4-hydroxybenzaldehyde



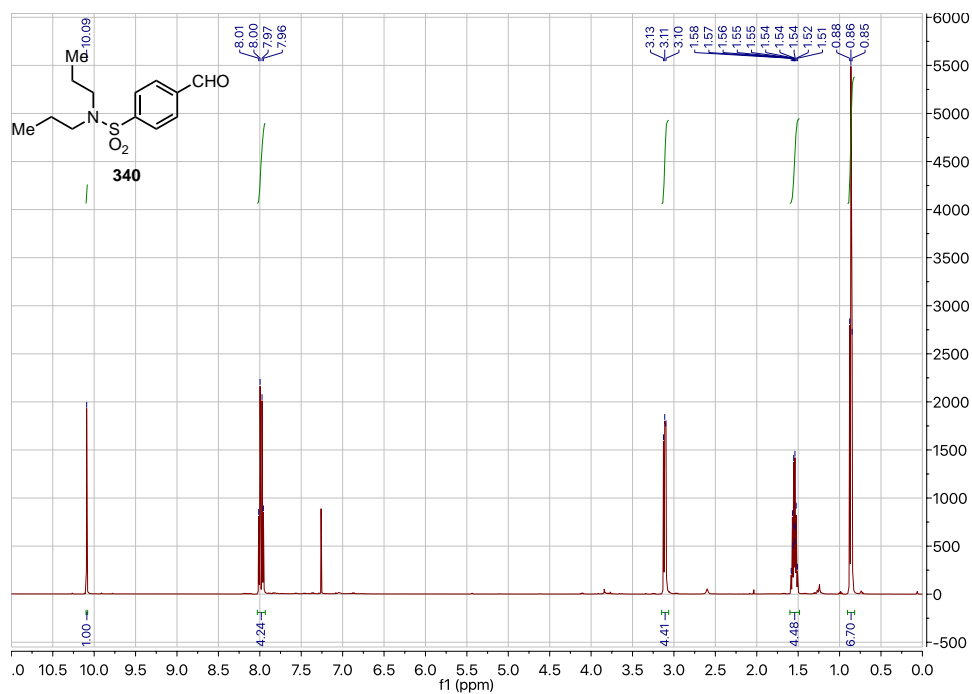
^1H NMR (500 MHz, CDCl_3): 4-formylbenzonitrile (339)



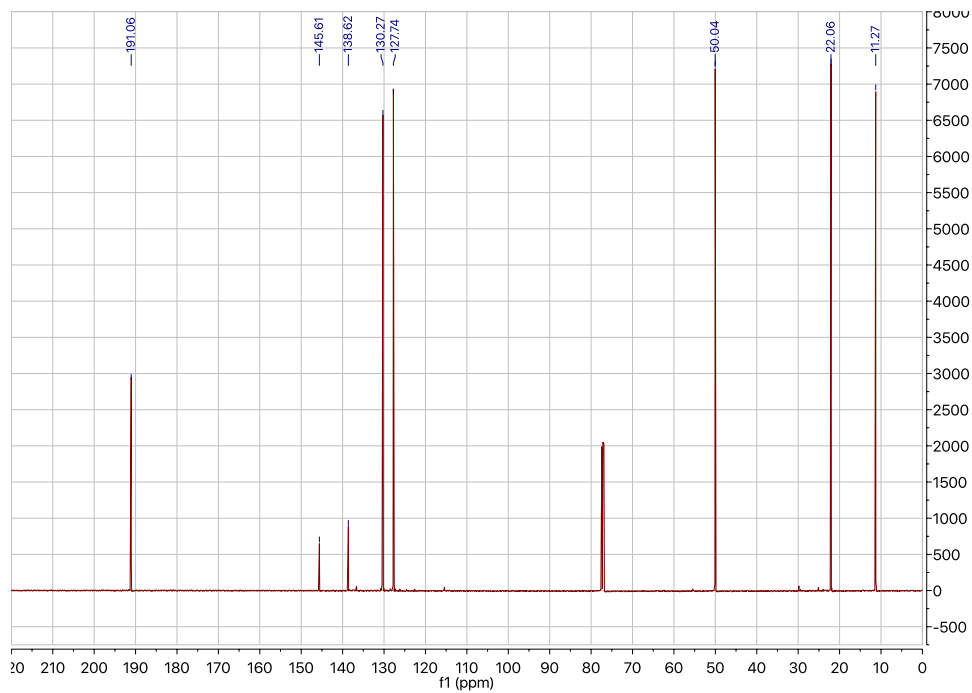
^{13}C NMR (126 MHz, CDCl_3): 4-formylbenzonitrile



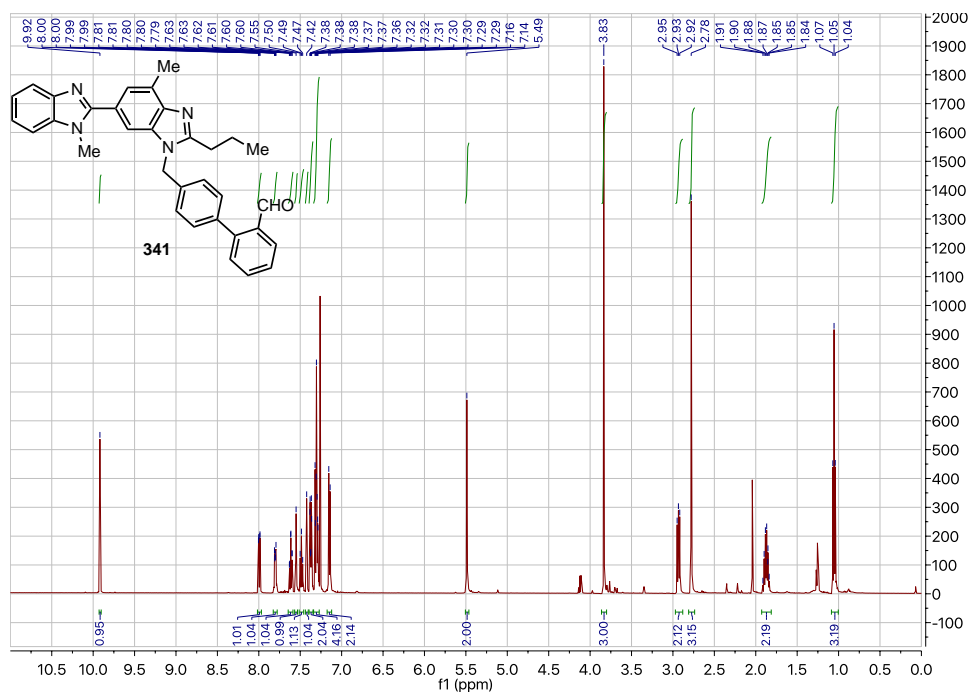
^1H NMR (500 MHz, CDCl_3): 4-formyl-*N,N*-dipropylbenzenesulfonamide (340)



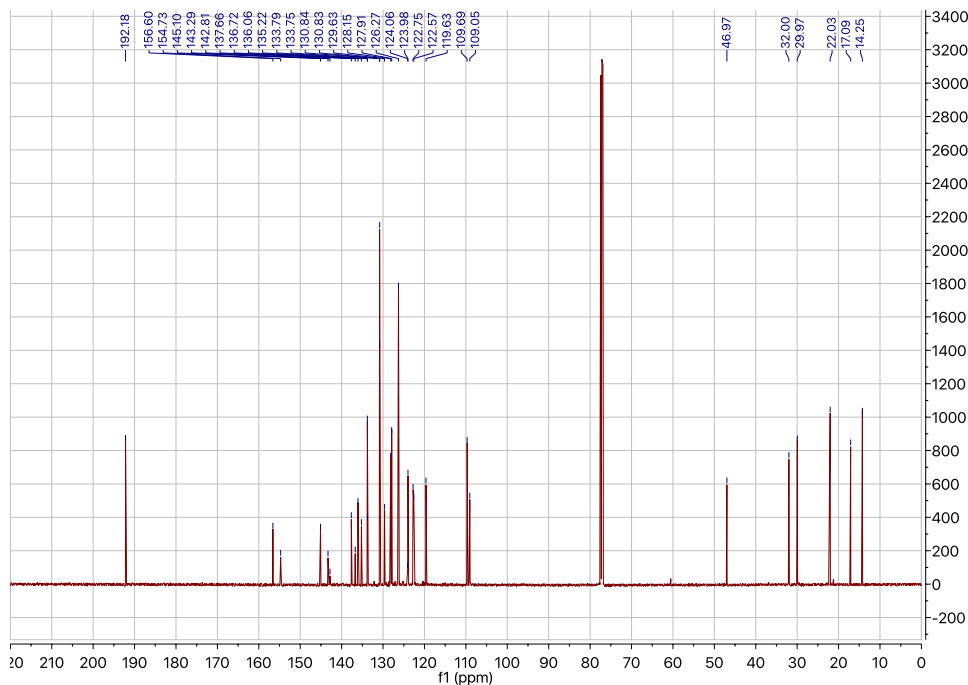
^{13}C NMR (126 MHz, CDCl_3): 4-formyl-*N,N*-dipropylbenzenesulfonamide



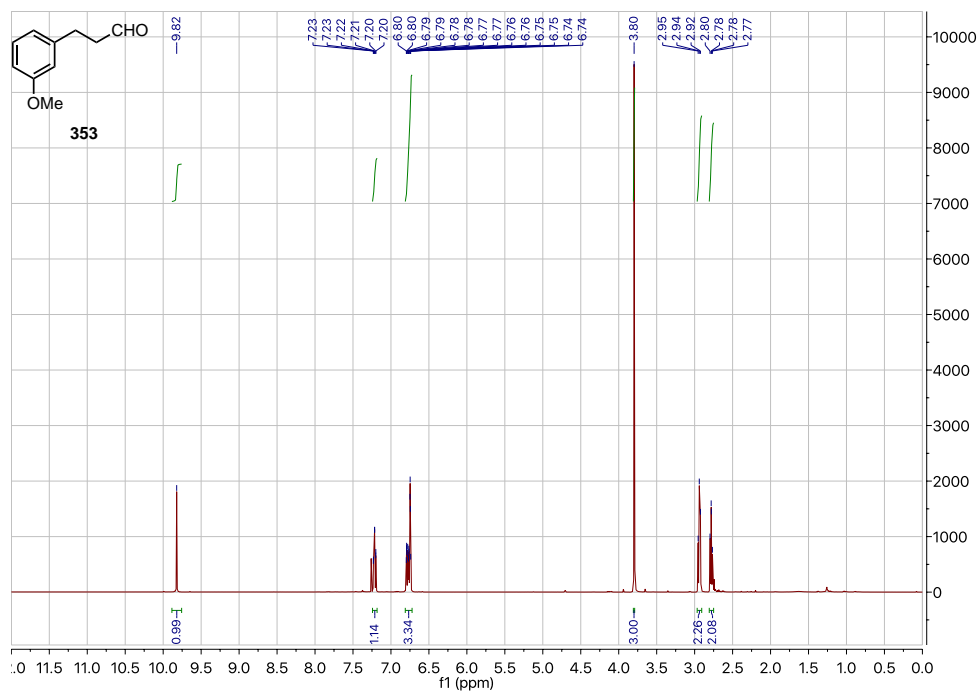
¹H NMR (500 MHz, CDCl₃): 4'-((1,7'-dimethyl-2'-propyl-1*H*,3'*H*-[2,5'-bibenzo[*d*]imidazol-3'-yl)methyl)-[1,1'-biphenyl]-2-carbaldehyde (341)



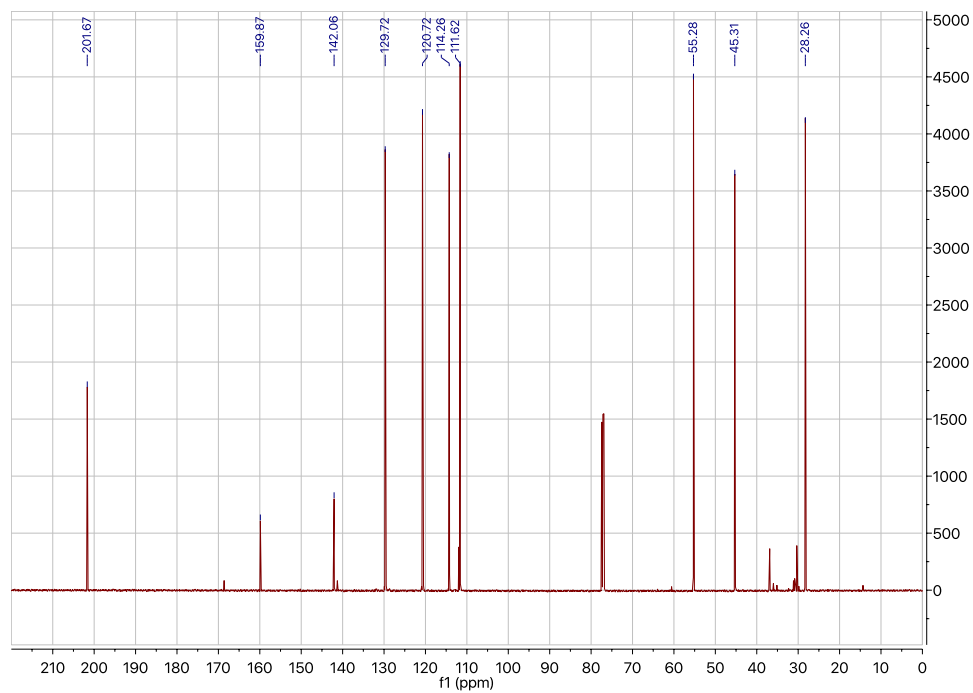
¹³C NMR (126 MHz, CDCl₃): 4'-((1,7'-dimethyl-2'-propyl-1*H*,3'*H*-[2,5'-bibenzo[*d*]imidazol-3'-yl)methyl)-[1,1'-biphenyl]-2-carbaldehyde



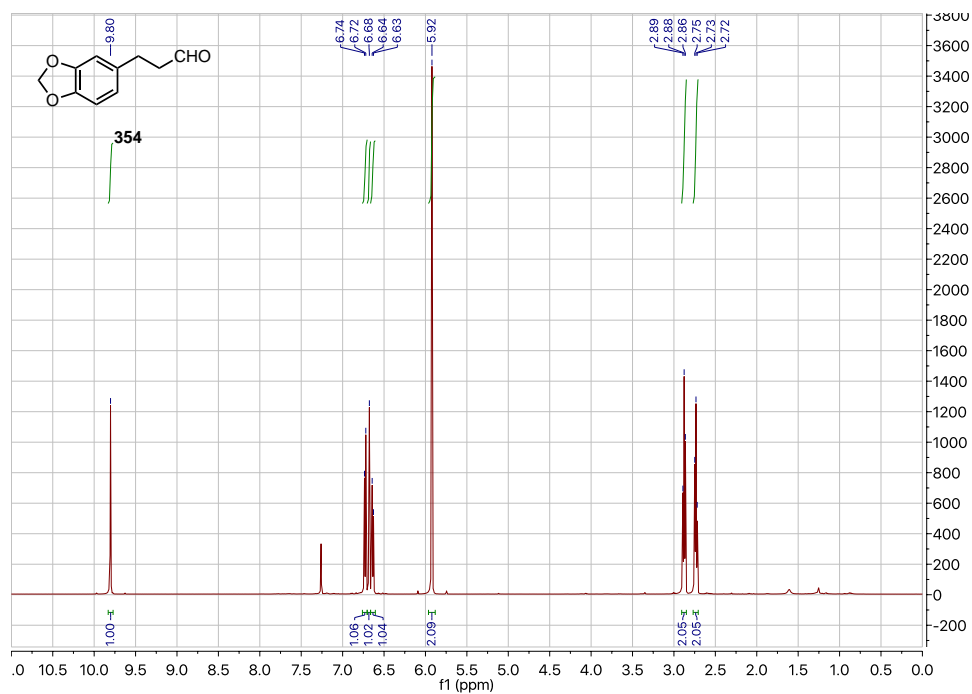
^1H NMR (500 MHz, CDCl_3): 3-(3-methoxyphenyl)propanal (353)



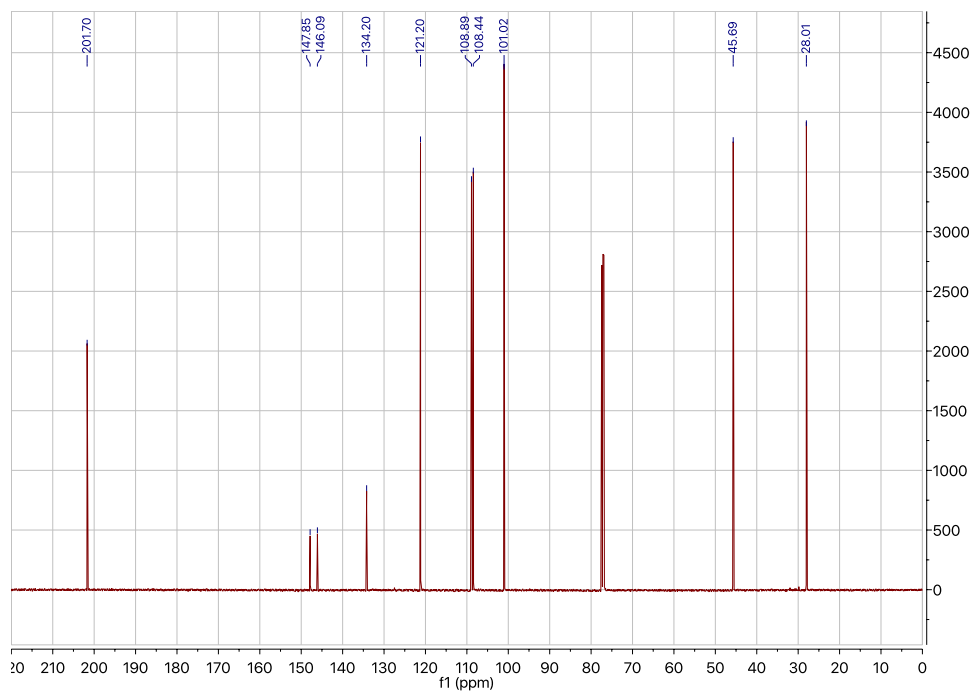
^{13}C NMR (126 MHz, CDCl_3): 3-(3-methoxyphenyl)propanal



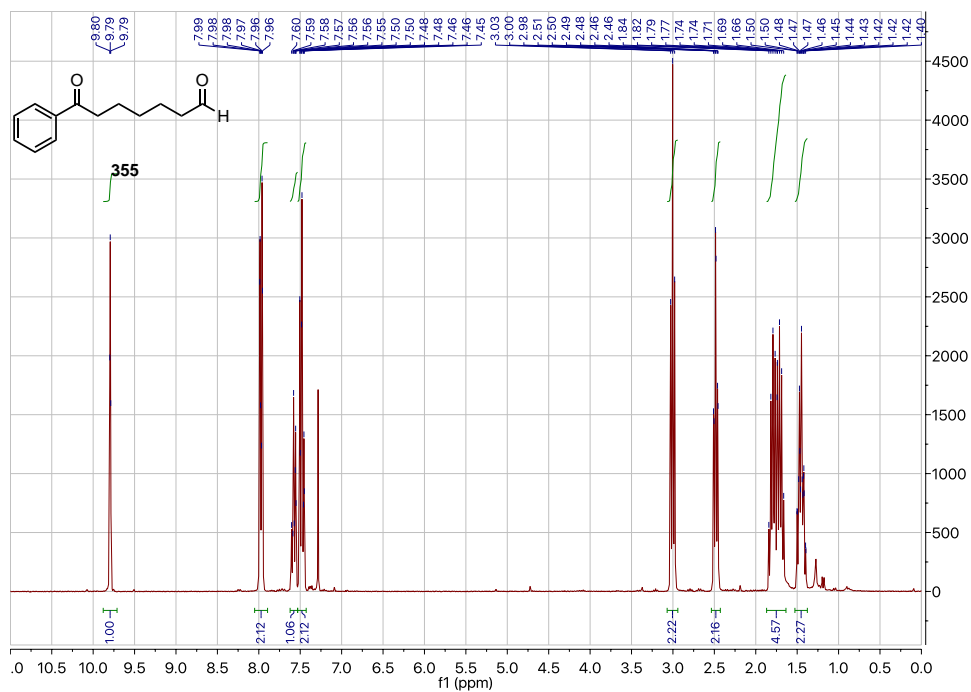
^1H NMR (500 MHz, CDCl_3): 3-(benzo[d][1,3]dioxol-5-yl)propanal (354)



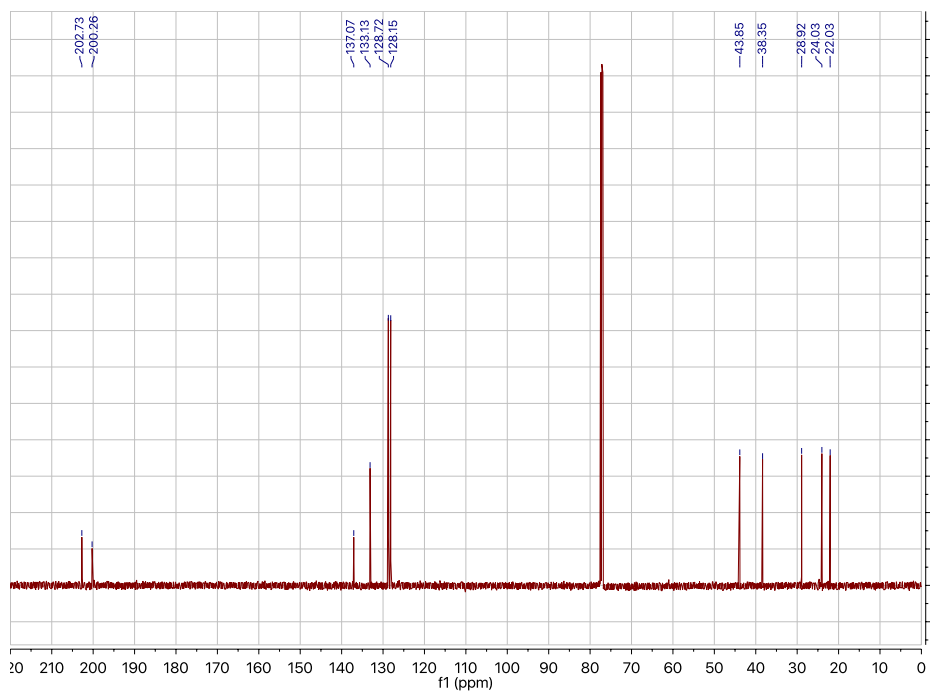
^{13}C NMR (126 MHz, CDCl_3): 3-(benzo[d][1,3]dioxol-5-yl)propanal



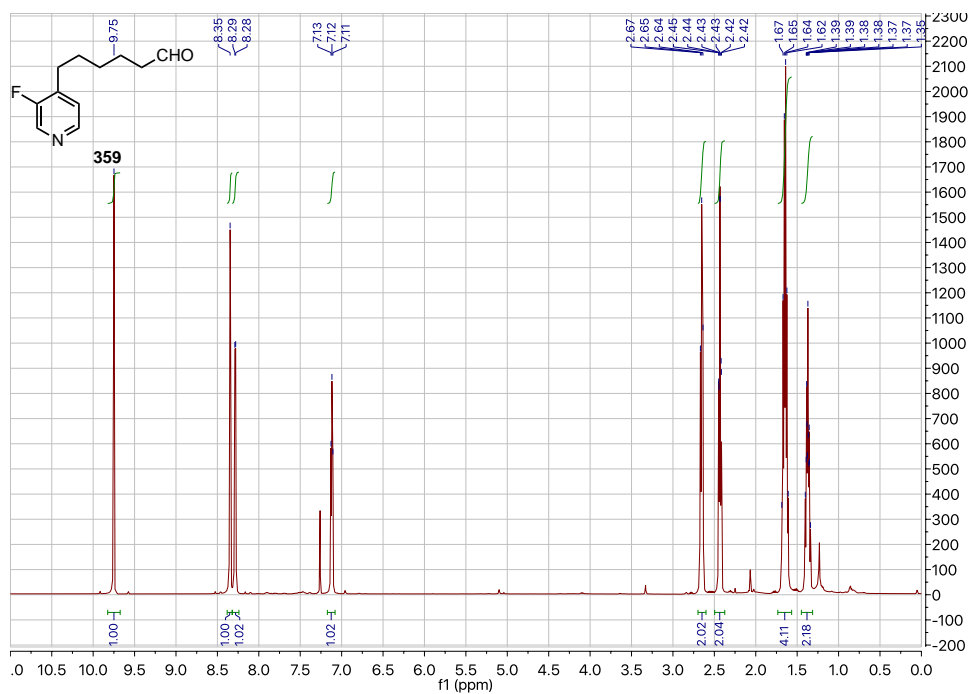
^1H NMR (300 MHz, CDCl_3): 7-oxo-7-phenylheptanal (355)



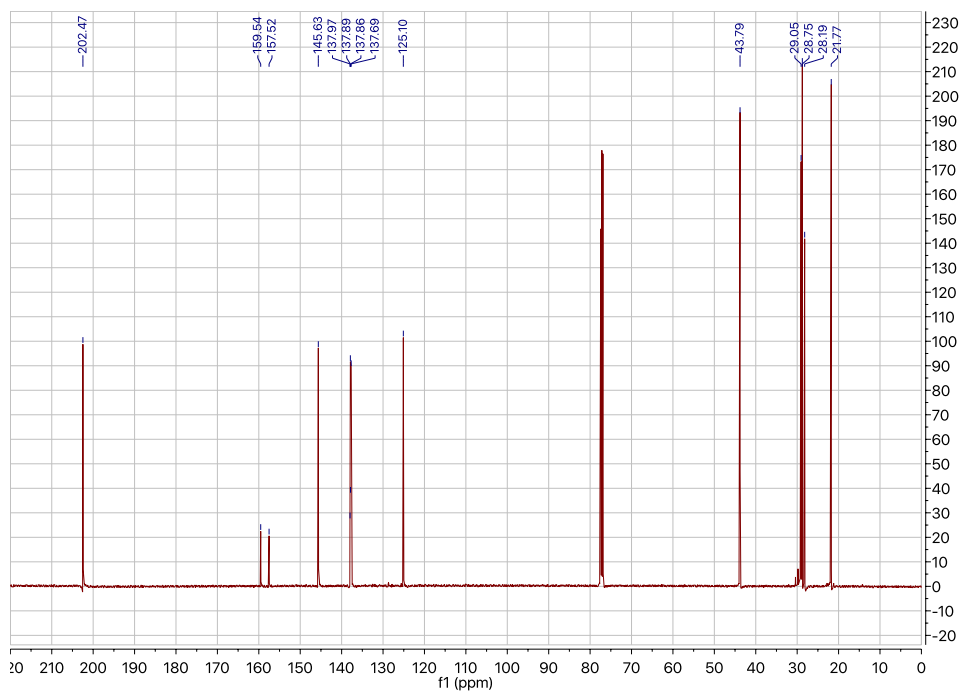
^1H NMR (500 MHz, CDCl_3): 7-oxo-7-phenylheptanal



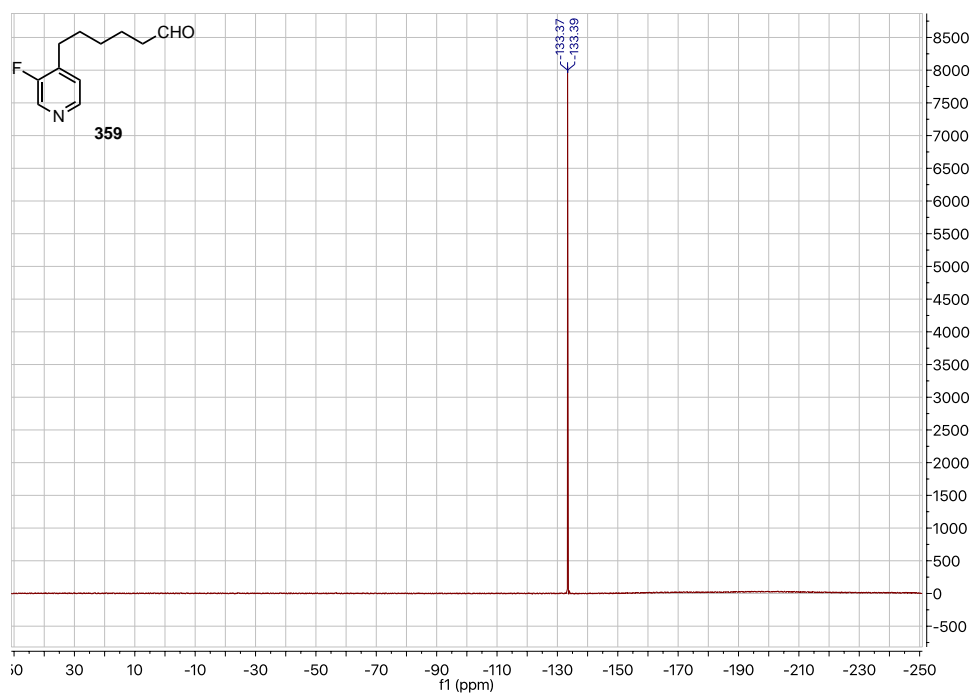
^1H NMR (500 MHz, CDCl_3): 6-(3-fluoropyridin-4-yl)hexanal (359)



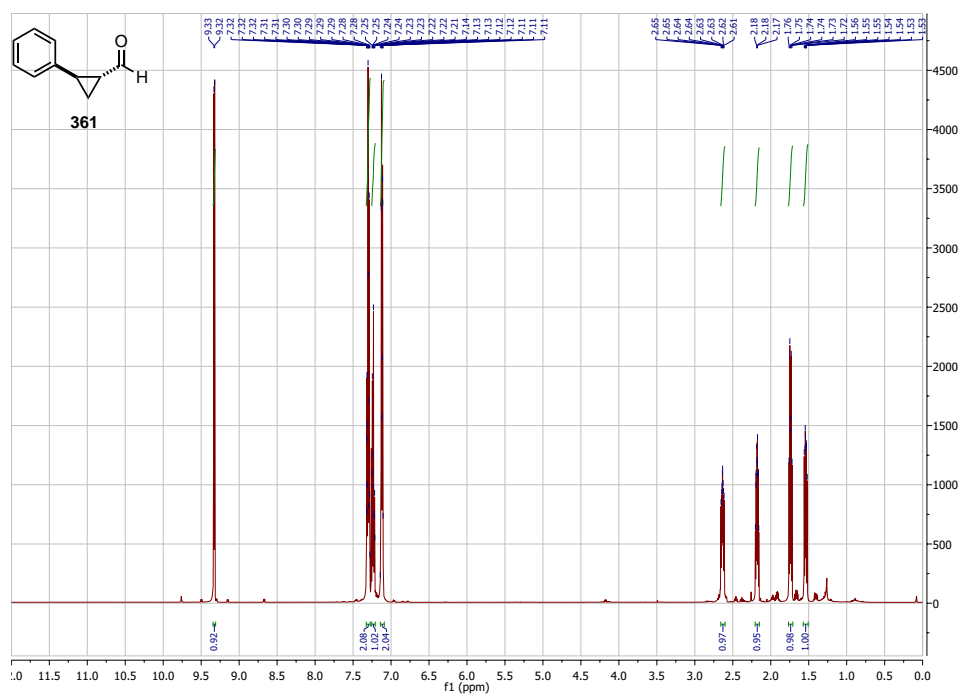
^{13}C NMR (126 MHz, CDCl_3): 6-(3-fluoropyridin-4-yl)hexanal



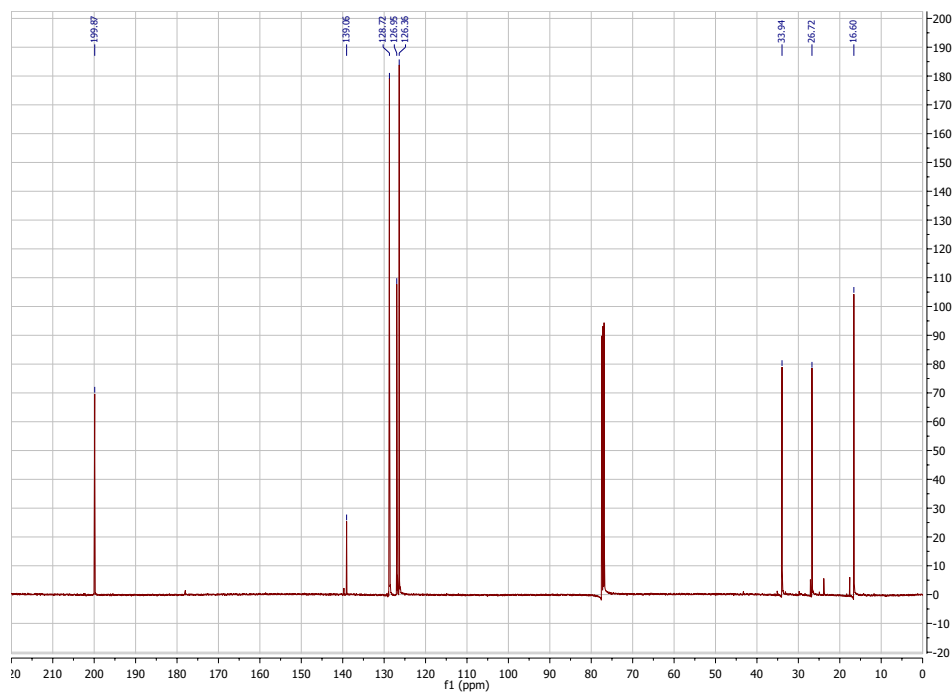
^{19}F NMR (282 MHz, CDCl_3): 6-(3-fluoropyridin-4-yl)hexanal (359)



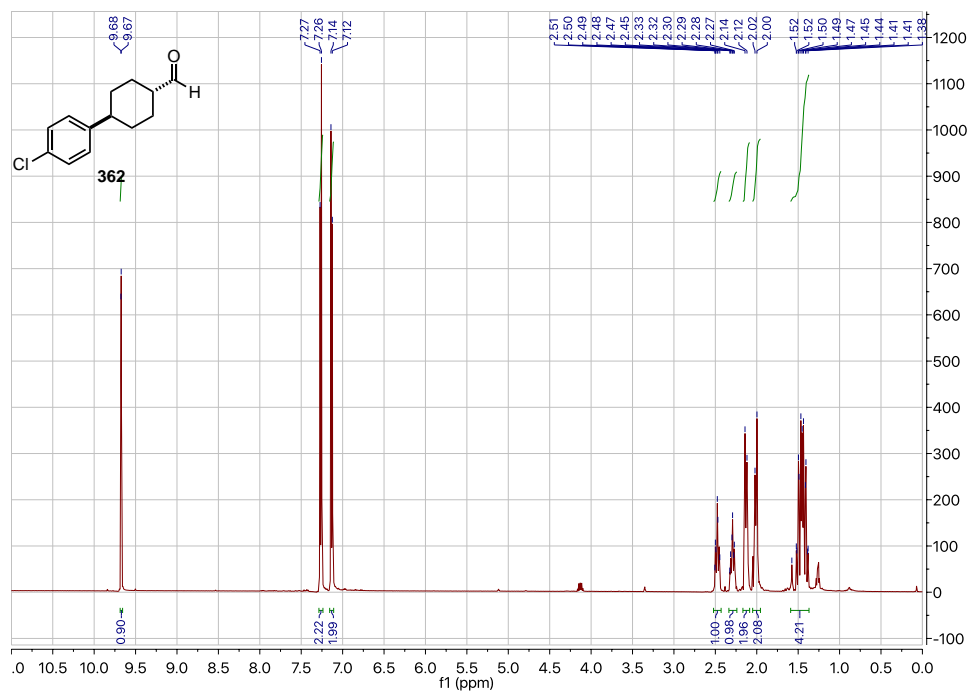
^1H NMR (500 MHz, CDCl_3): *Trans*-2-phenylcyclopropane-1-carbaldehyde (361)



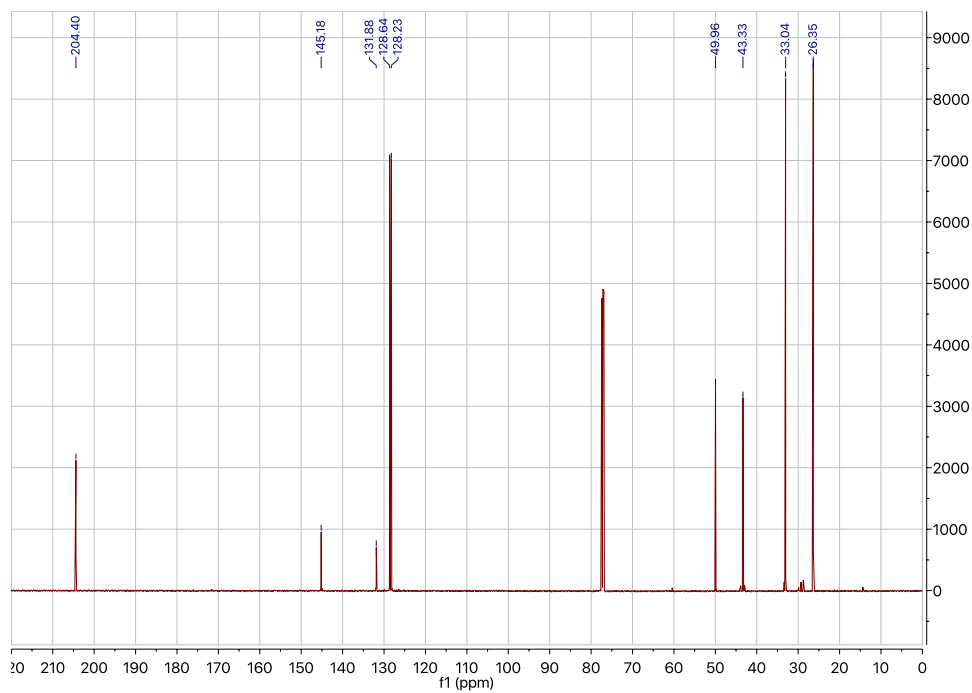
^{13}C NMR (126 MHz, CDCl_3): *Trans*-2-phenylcyclopropane-1-carbaldehyde



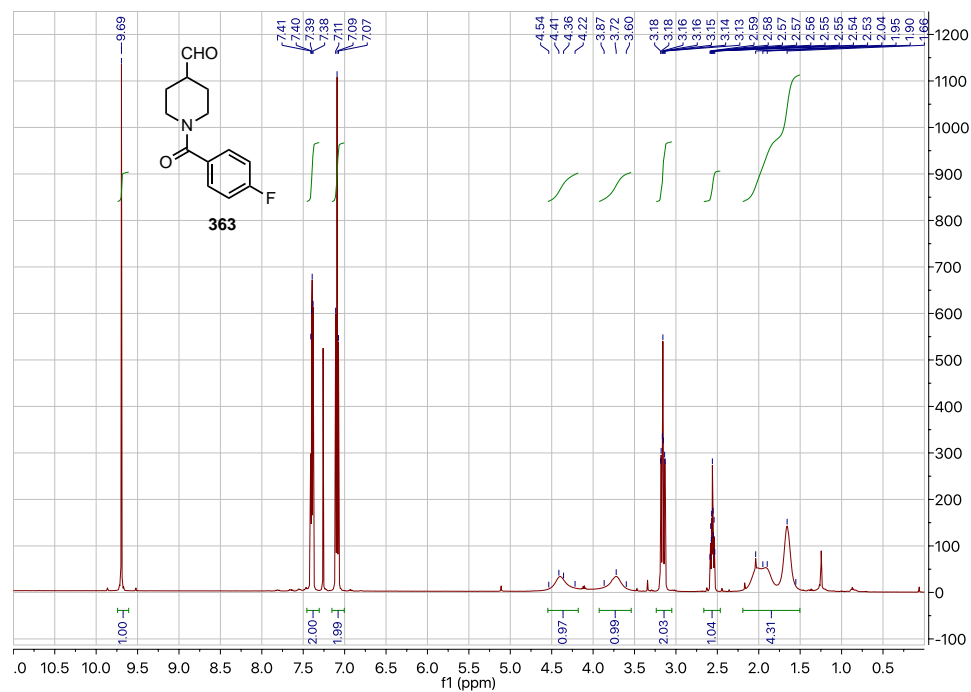
^1H NMR (500 MHz, CDCl_3): *Trans*-4-(4-chlorophenyl)cyclohexane-1-carbaldehyde (362)



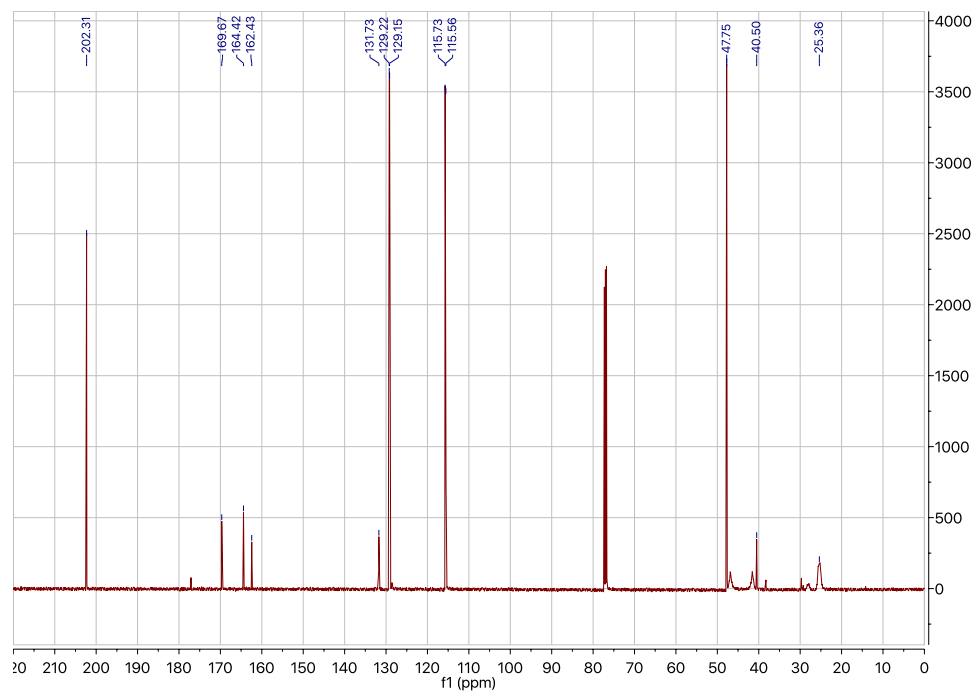
^{13}C NMR (126 MHz, CDCl_3): *Trans*-4-(4-chlorophenyl)cyclohexane-1-carbaldehyde



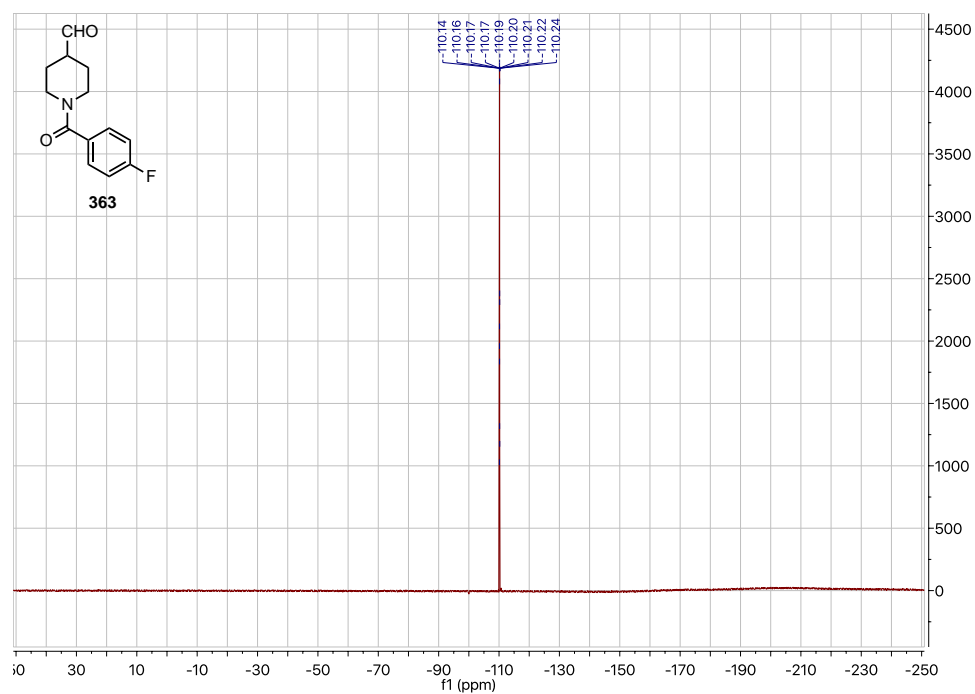
^1H NMR (500 MHz, CDCl_3): 1-(4-fluorobenzoyl)piperidine-4-carbaldehyde (363)



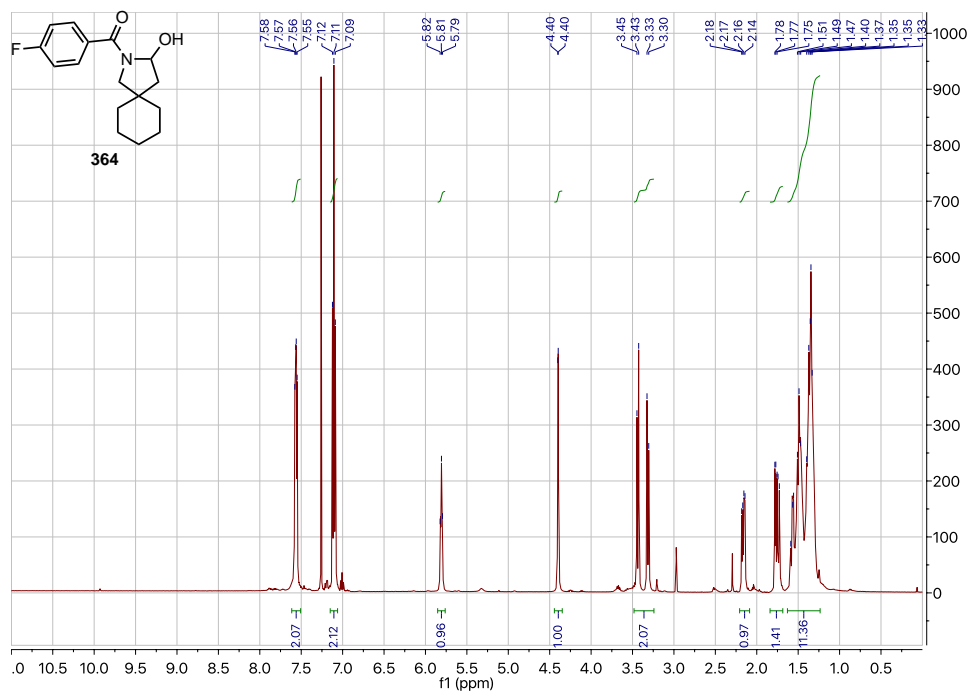
^{13}C NMR (126 MHz, CDCl_3): 1-(4-fluorobenzoyl)piperidine-4-carbaldehyde



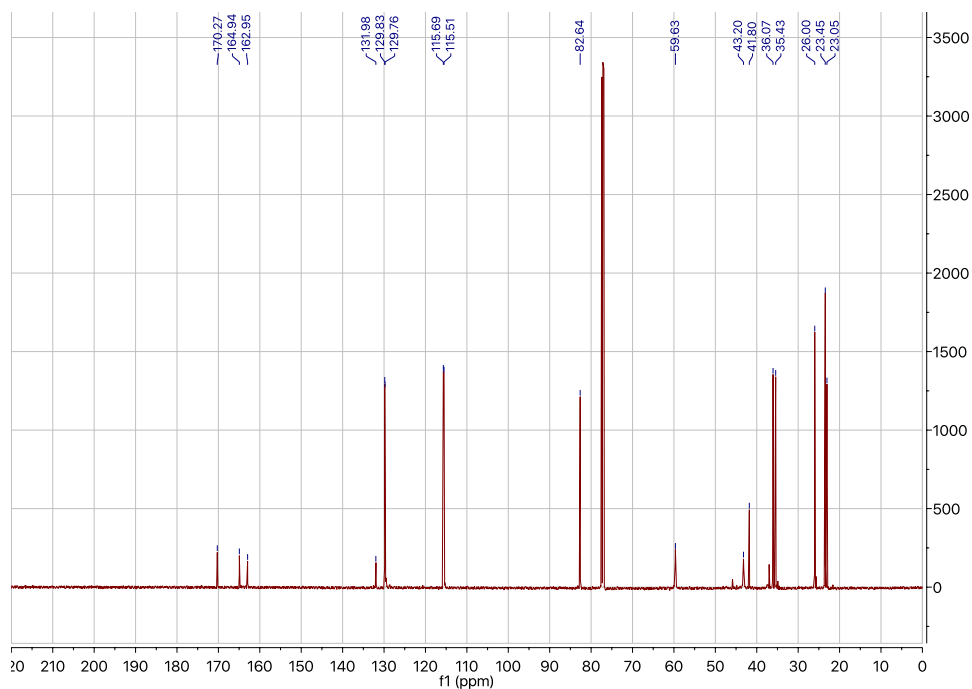
^{19}F NMR (282 MHz, CDCl_3): 1-(4-fluorobenzoyl)piperidine-4-carbaldehyde (363)



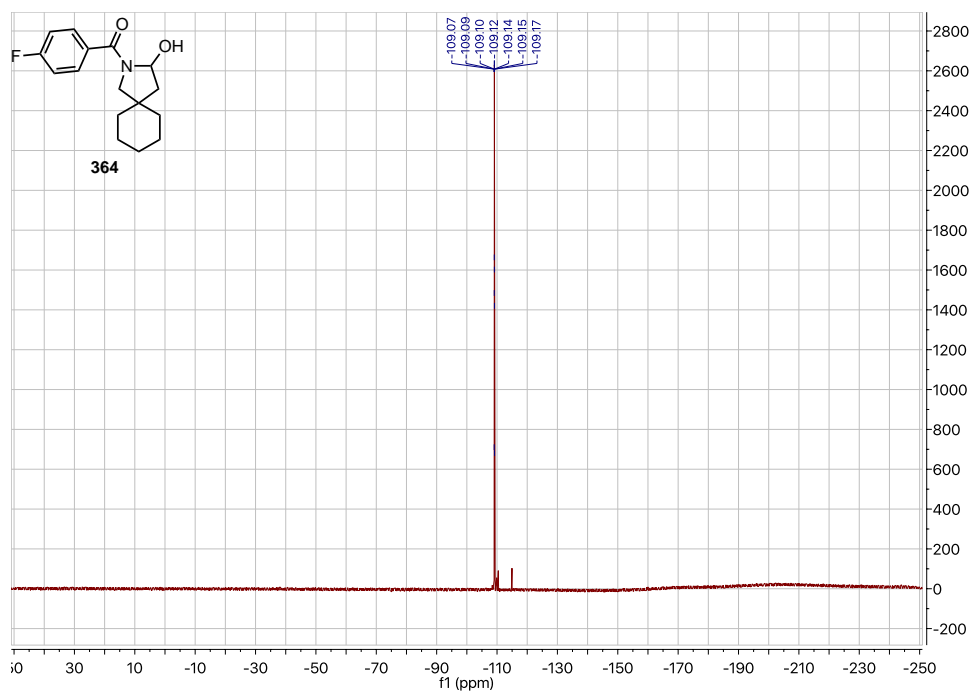
^1H NMR (500 MHz, CDCl_3): \pm (4-fluorophenyl)(3-hydroxy-2-azaspiro[4.5]decan-2-yl) methanone (364)



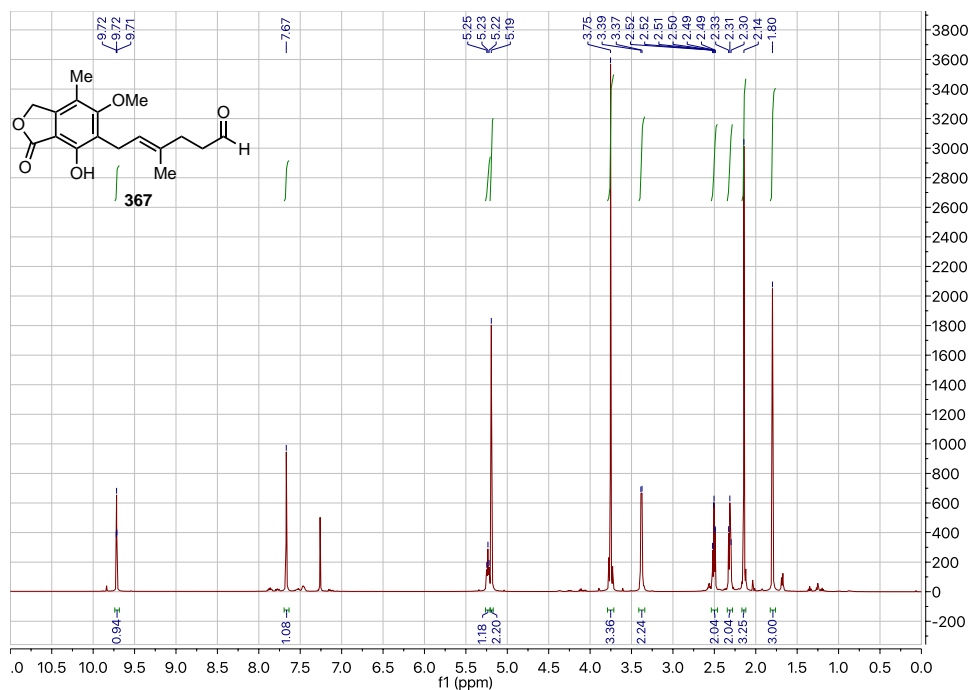
^{13}C NMR (126 MHz, CDCl_3): \pm (4-fluorophenyl)(3-hydroxy-2-azaspiro[4.5]decan-2-yl) methanone



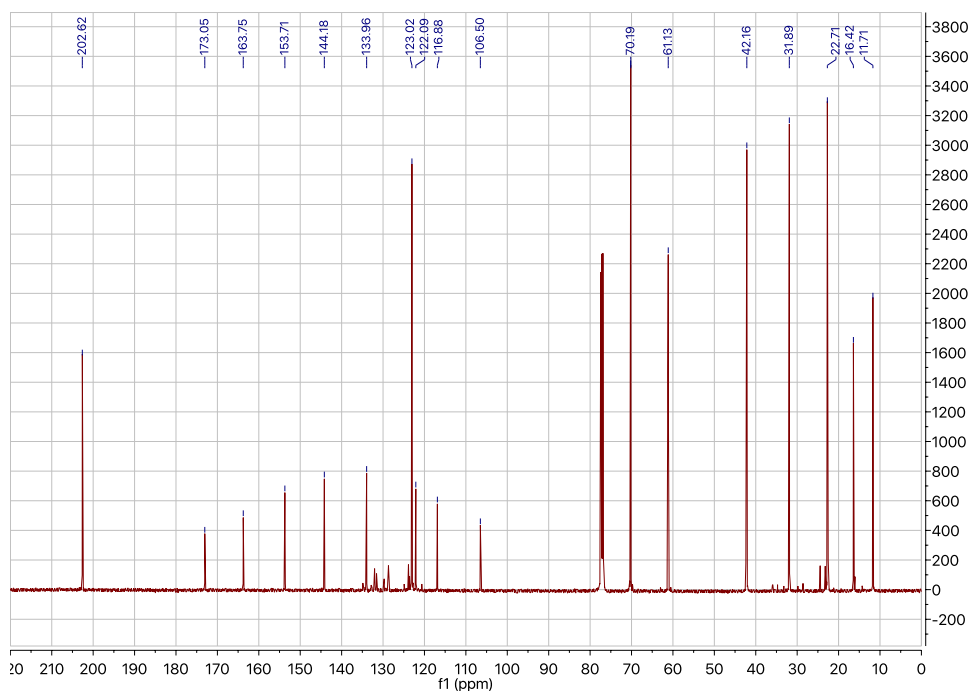
^{19}F NMR (282 MHz, CDCl_3): \pm (4-fluorophenyl)(3-hydroxy-2-azaspiro[4.5]decan-2-yl)methanone (364)



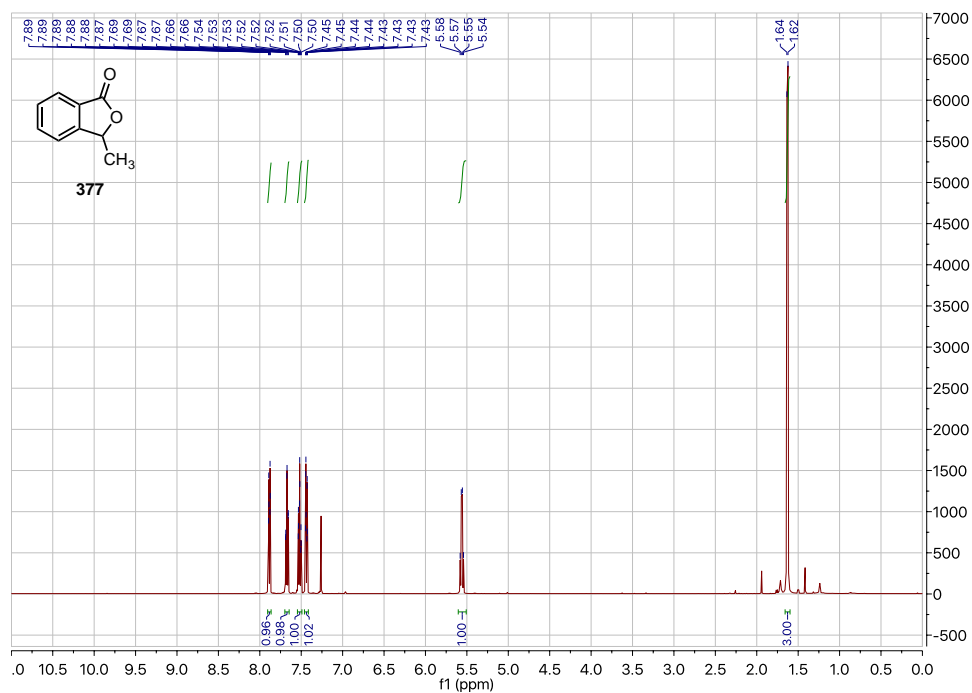
¹H NMR (500 MHz, CDCl₃): (*E*)-6-(4-hydroxy-6-methoxy-7-methyl-3-oxo-1,3-dihydroisobenzofuran-5-yl)-4-methylhex-4-enal (367)



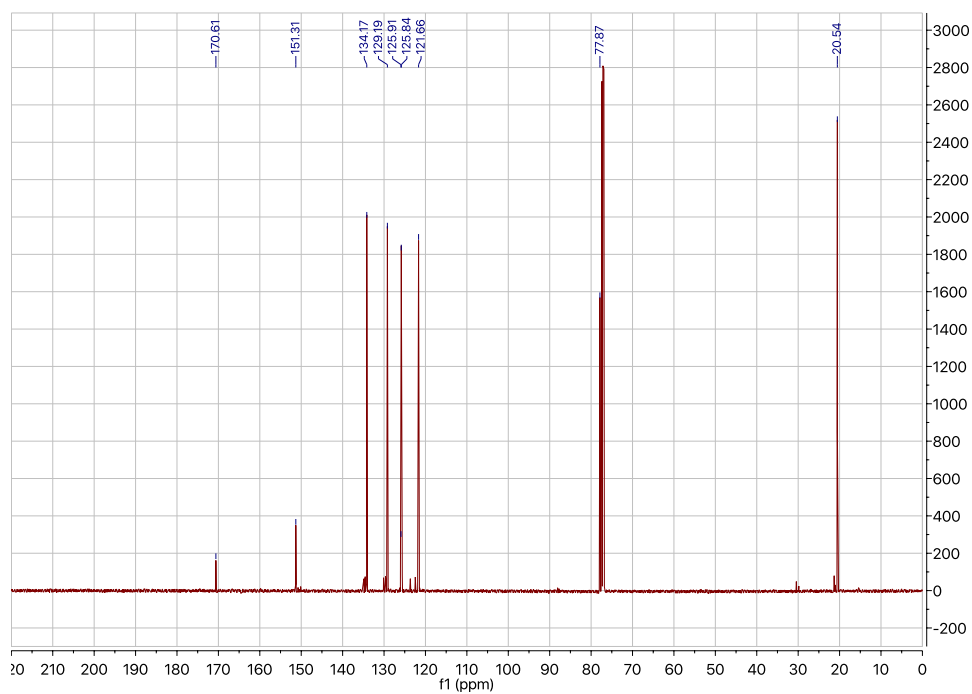
¹³C NMR (126 MHz, CDCl₃): ((*E*)-6-(4-hydroxy-6-methoxy-7-methyl-3-oxo-1,3-dihydroisobenzofuran-5-yl)-4-methylhex-4-enal



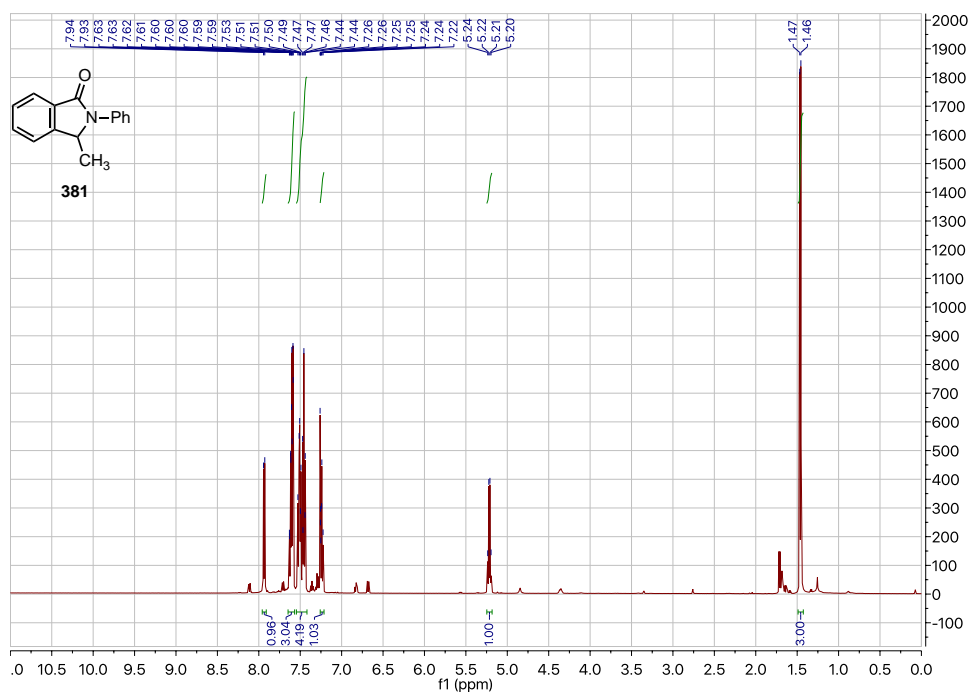
^1H NMR (500 MHz, CDCl_3): \pm 3-methylisobenzofuran-1(3*H*)-one (377)



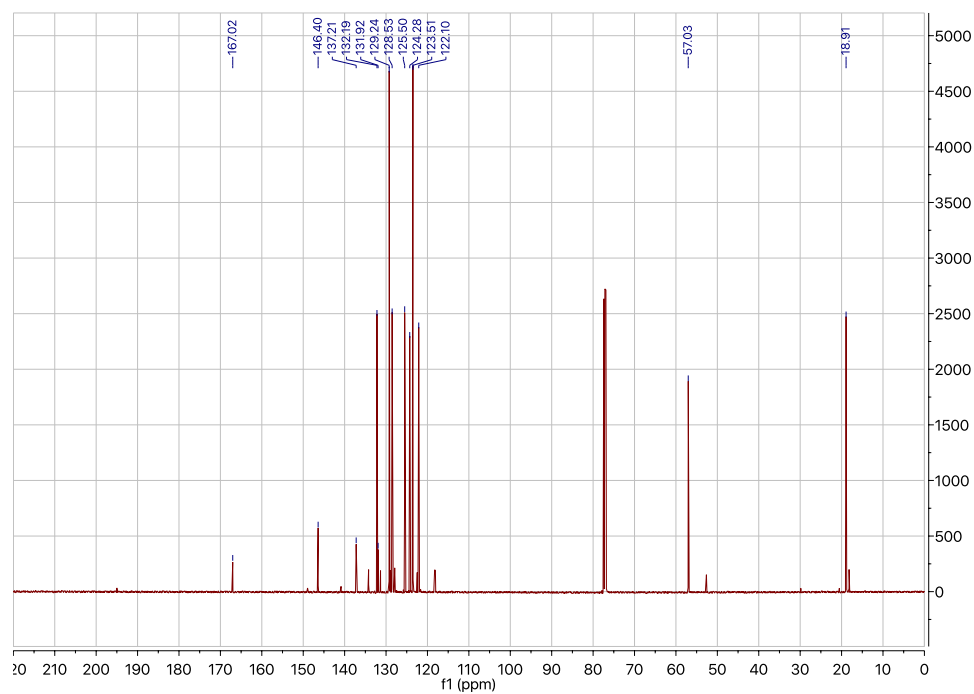
^{13}C NMR (126 MHz, CDCl_3): \pm 3-methylisobenzofuran-1(3*H*)-one



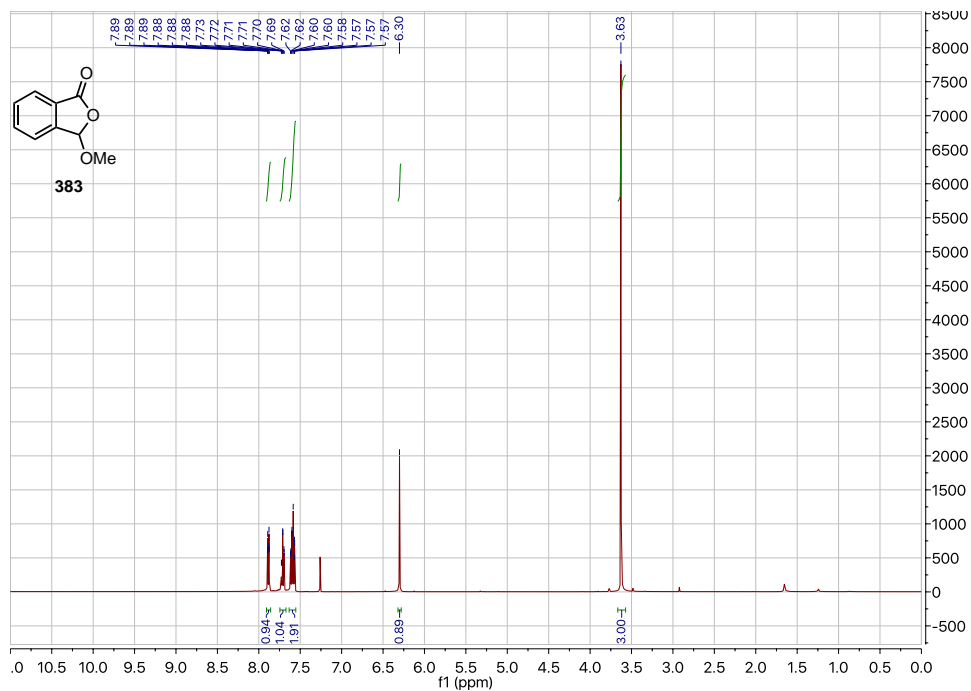
^1H NMR (500 MHz, CDCl_3): \pm 3-methyl-2-phenylisoindolin-1-one (381)



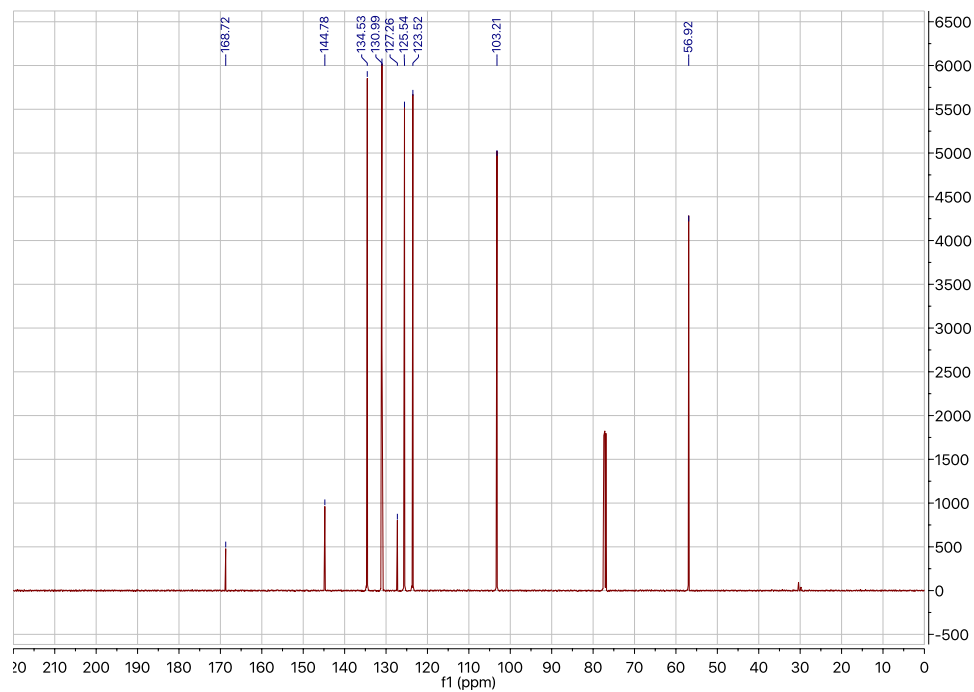
^{13}C NMR (126 MHz, CDCl_3): \pm 3-methyl-2-phenylisoindolin-1-one



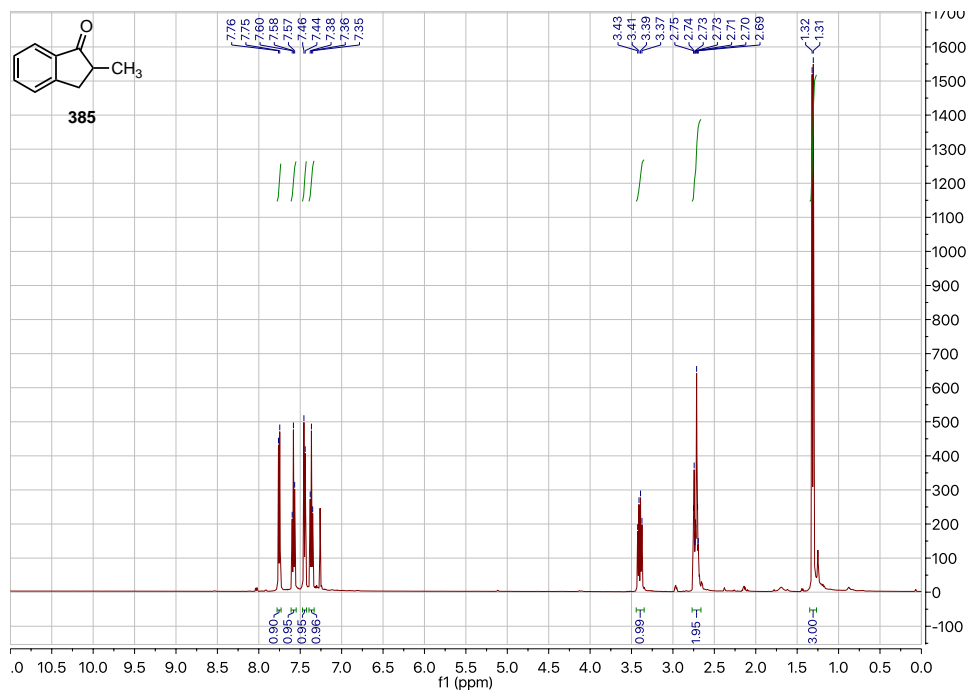
^1H NMR (500 MHz, CDCl_3): \pm 3-methoxyisobenzofuran-1(3*H*)-one (383)



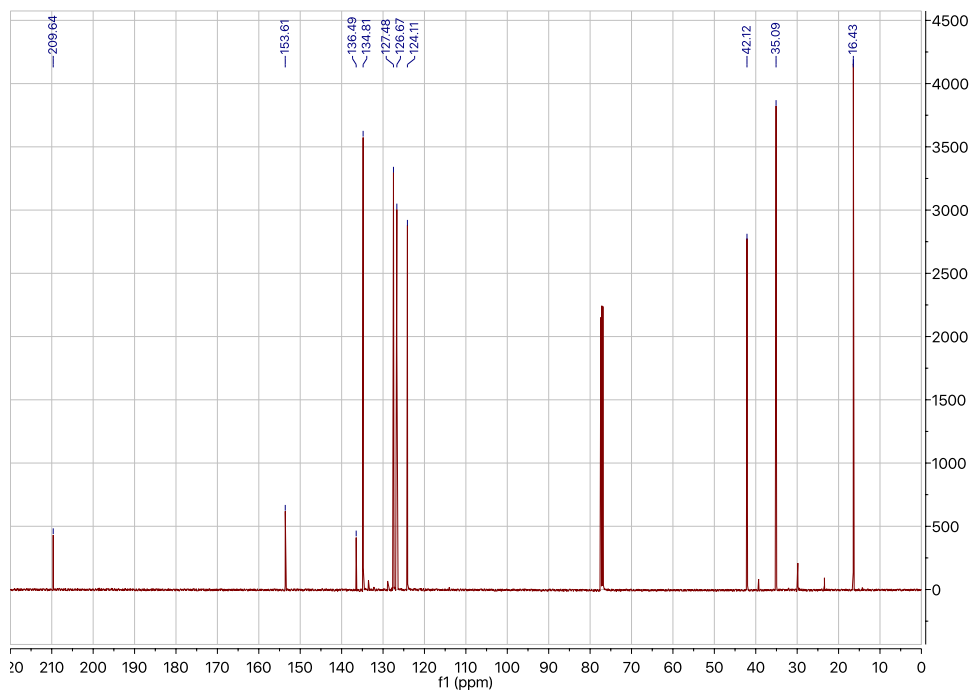
^{13}C NMR (126 MHz, CDCl_3): \pm 3-methoxyisobenzofuran-1(3*H*)-one



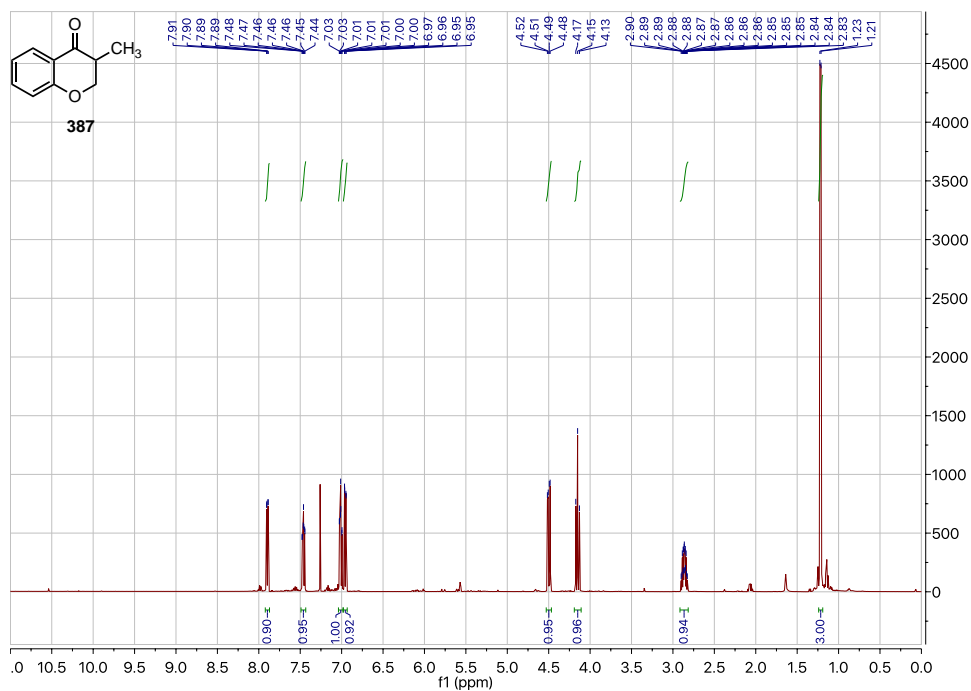
^1H NMR (500 MHz, CDCl_3): \pm 2-methyl-2,3-dihydro-1*H*-inden-1-one (385)



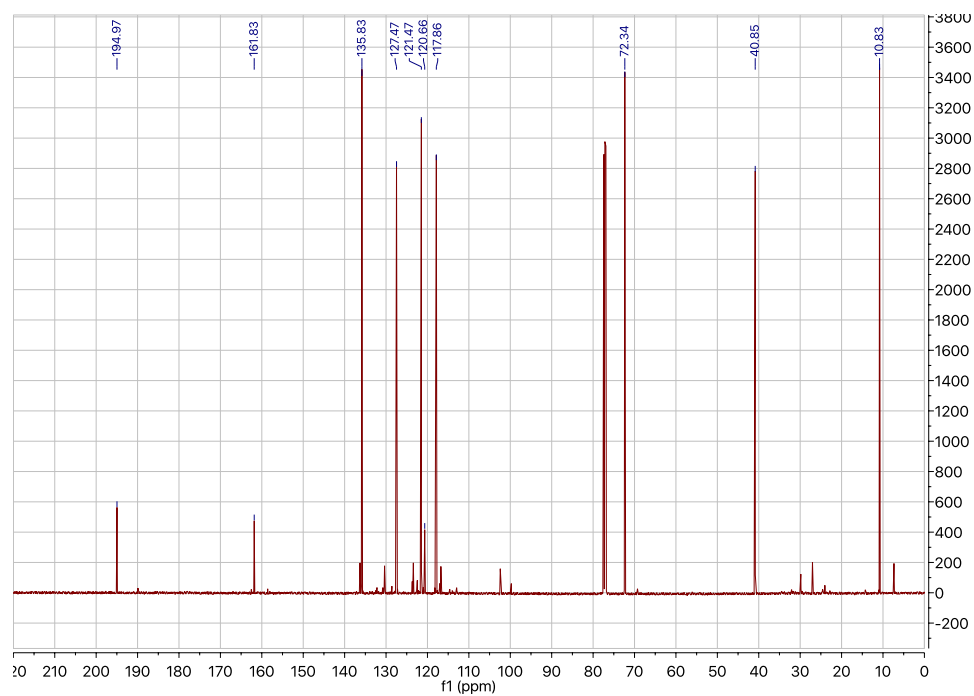
^{13}C NMR (126 MHz, CDCl_3): \pm 2-methyl-2,3-dihydro-1*H*-inden-1-one



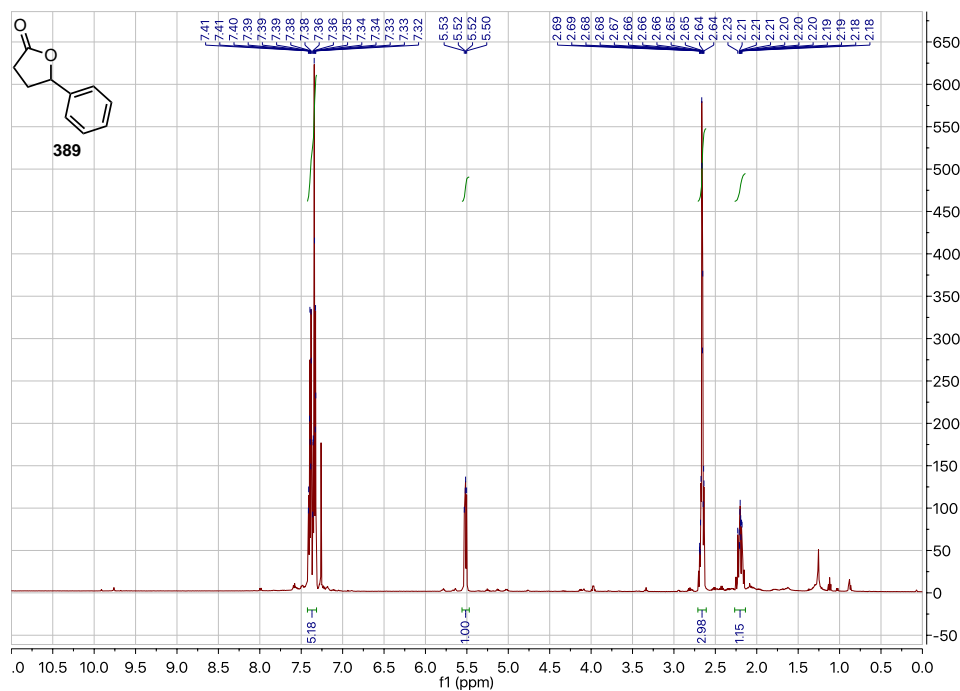
^1H NMR (500 MHz, CDCl_3): \pm 3-methylchroman-4-one (387)



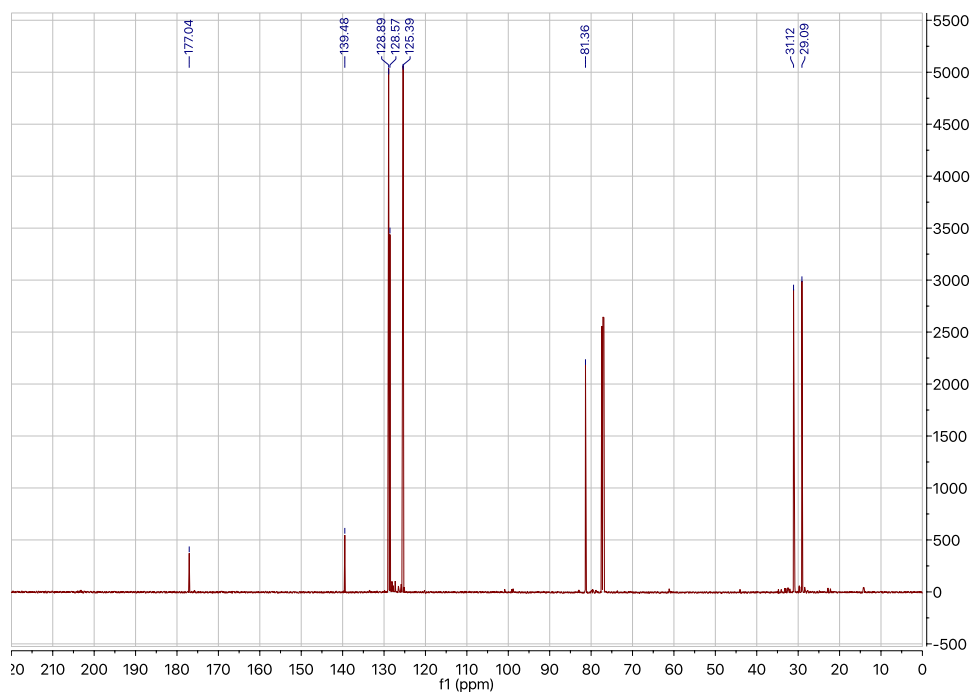
^{13}C NMR (126 MHz, CDCl_3): \pm 3-methylchroman-4-one



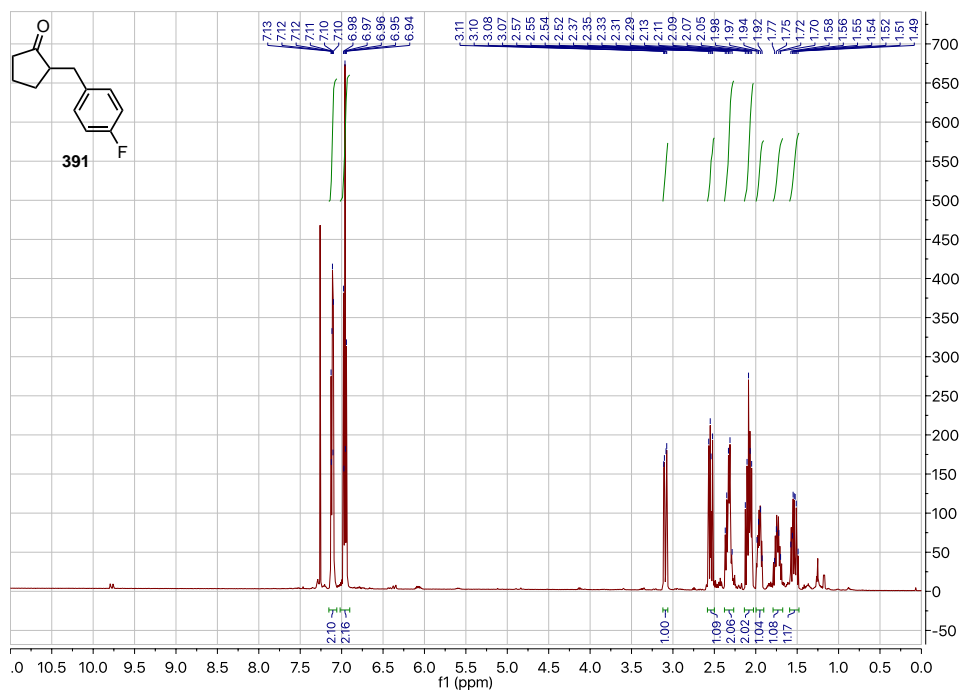
^1H NMR (500 MHz, CDCl_3): \pm 5-phenyldihydrofuran-2(3*H*)-one (389)



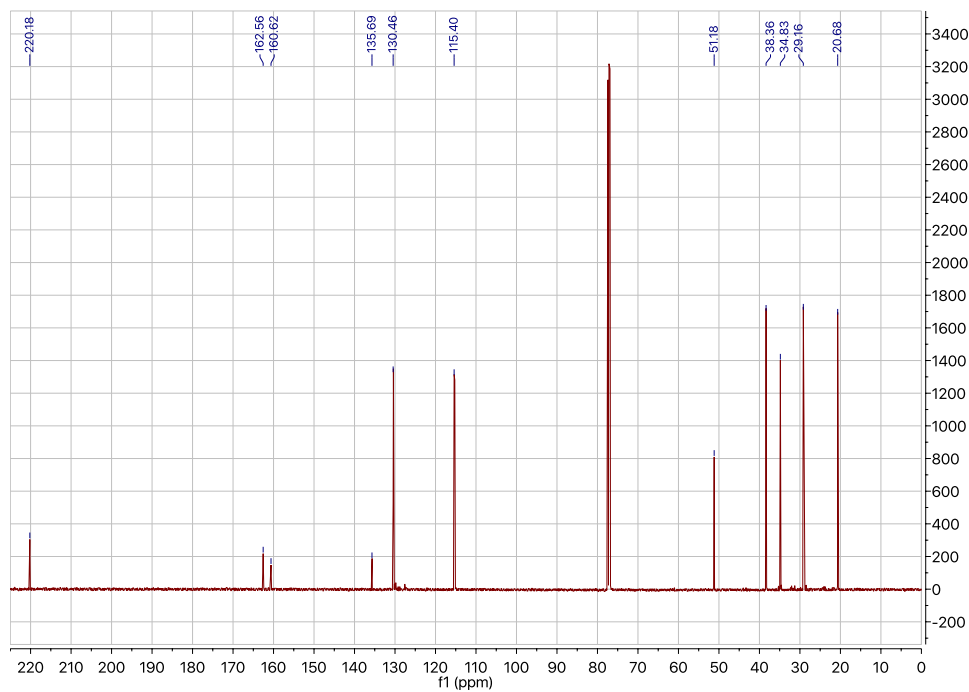
^{13}C NMR (126 MHz, CDCl_3): \pm 5-phenyldihydrofuran-2(3*H*)-one



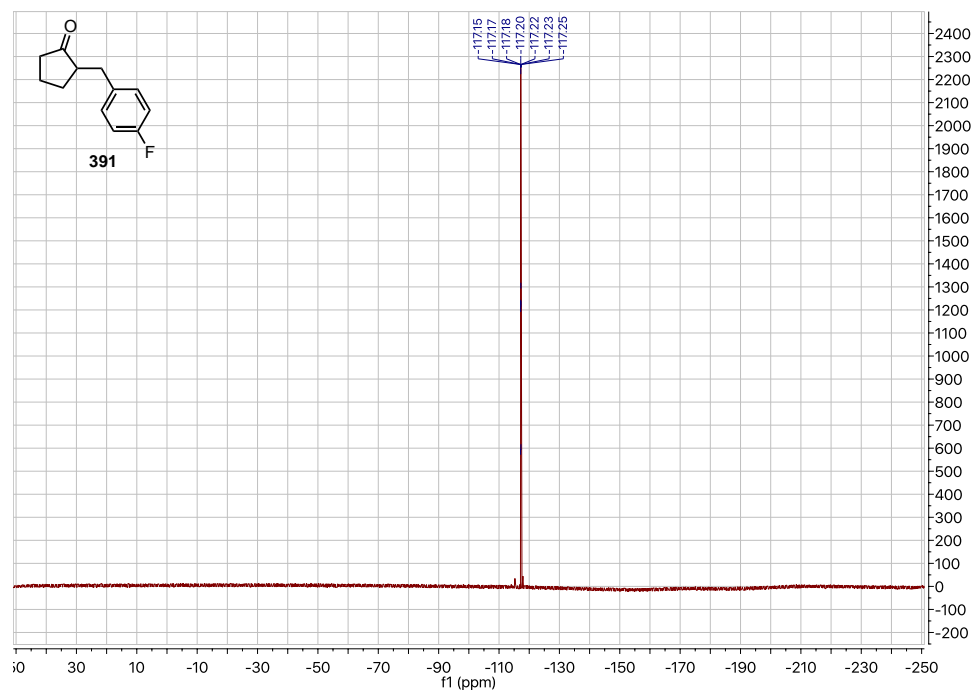
^1H NMR (500 MHz, CDCl_3): ± 2 -(4-fluorobenzyl)cyclopentan-1-one (391)



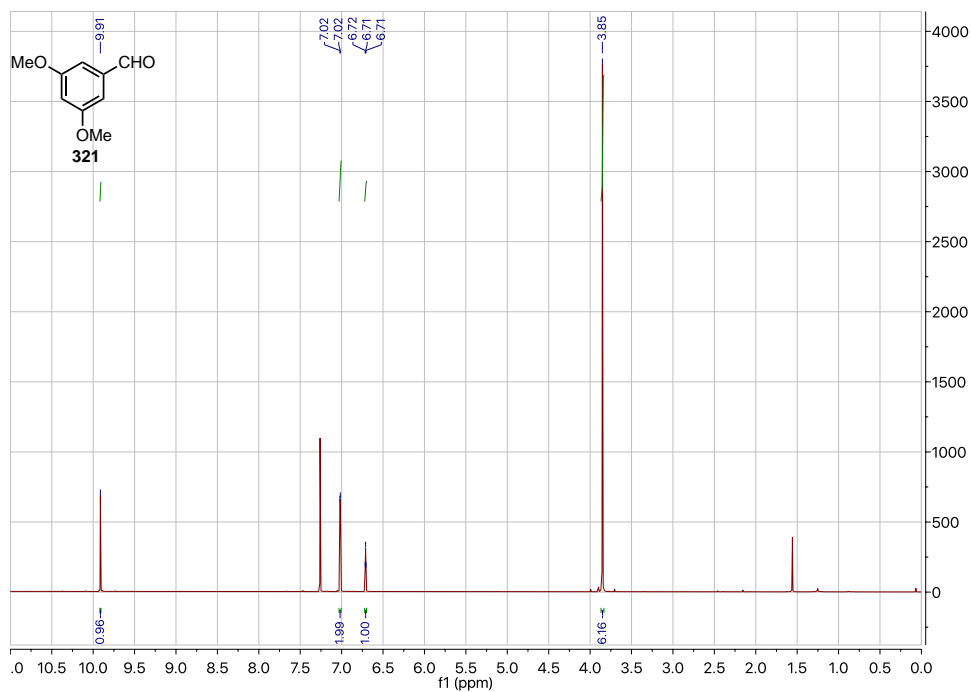
^{13}C NMR (126 MHz, CDCl_3): ± 2 -(4-fluorobenzyl)cyclopentan-1-one



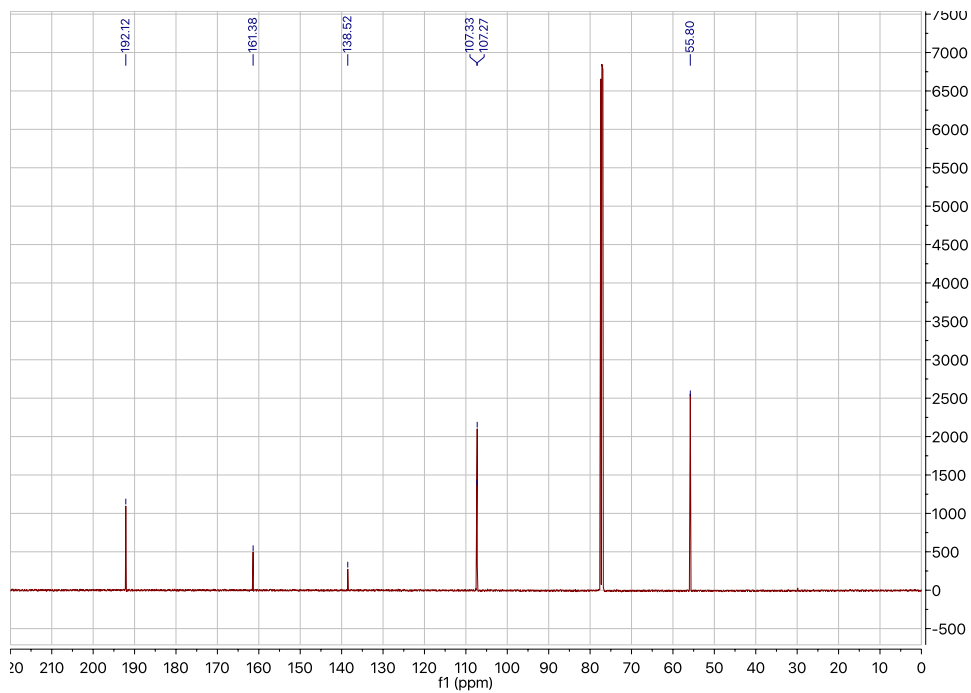
^{19}F NMR (126 MHz, CDCl_3): \pm 2-(4-fluorobenzyl)cyclopentan-1-one (391)



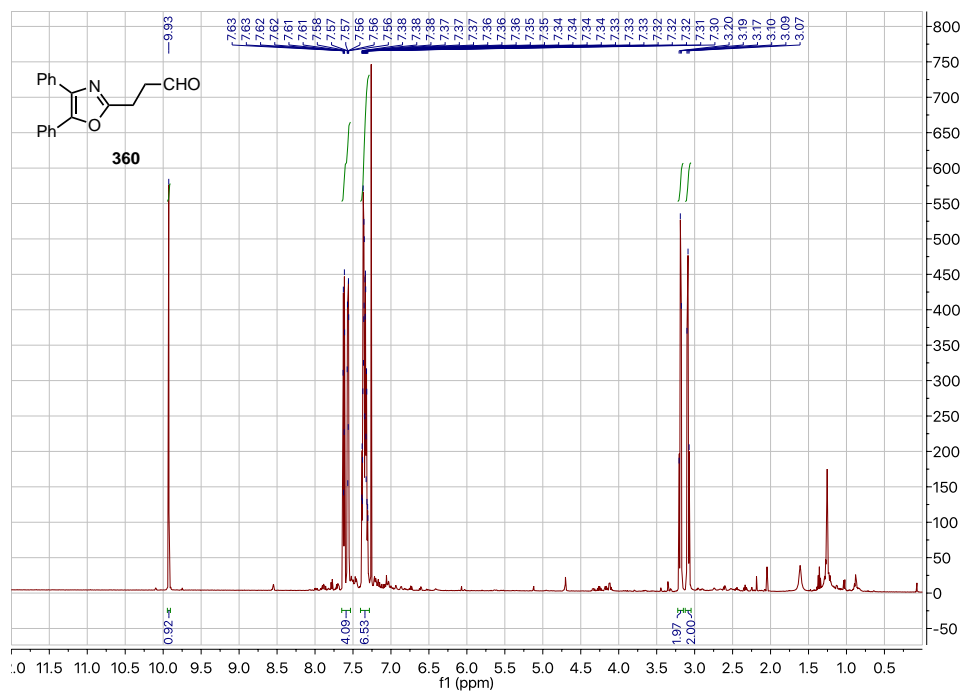
^1H NMR (500 MHz, CDCl_3): 3,5-dimethoxybenzaldehyde (321)



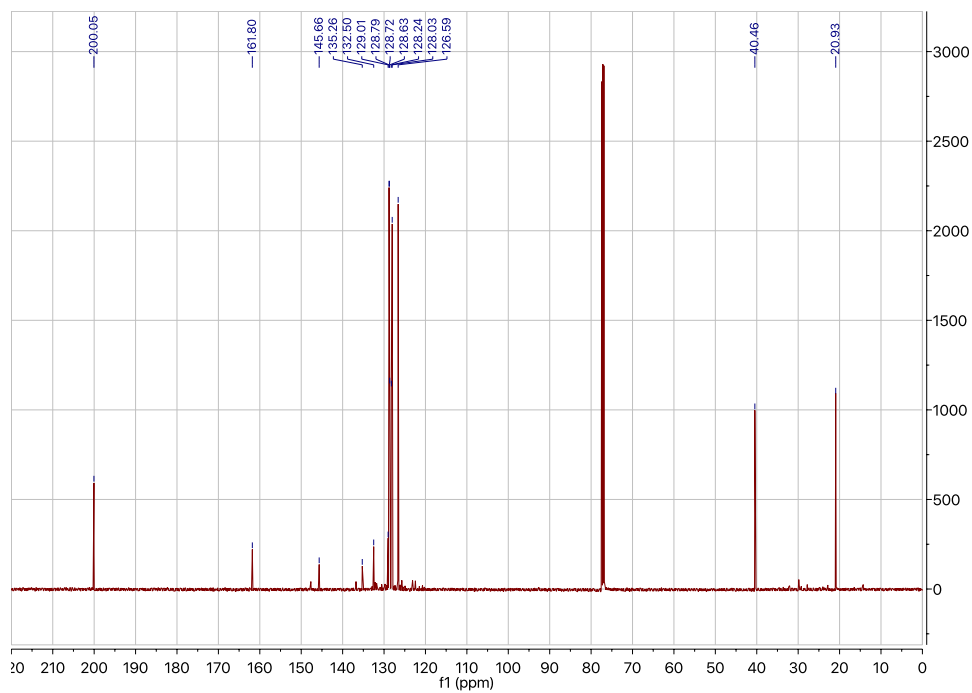
^{13}C NMR (126 MHz, CDCl_3): 3,5-dimethoxybenzaldehyde



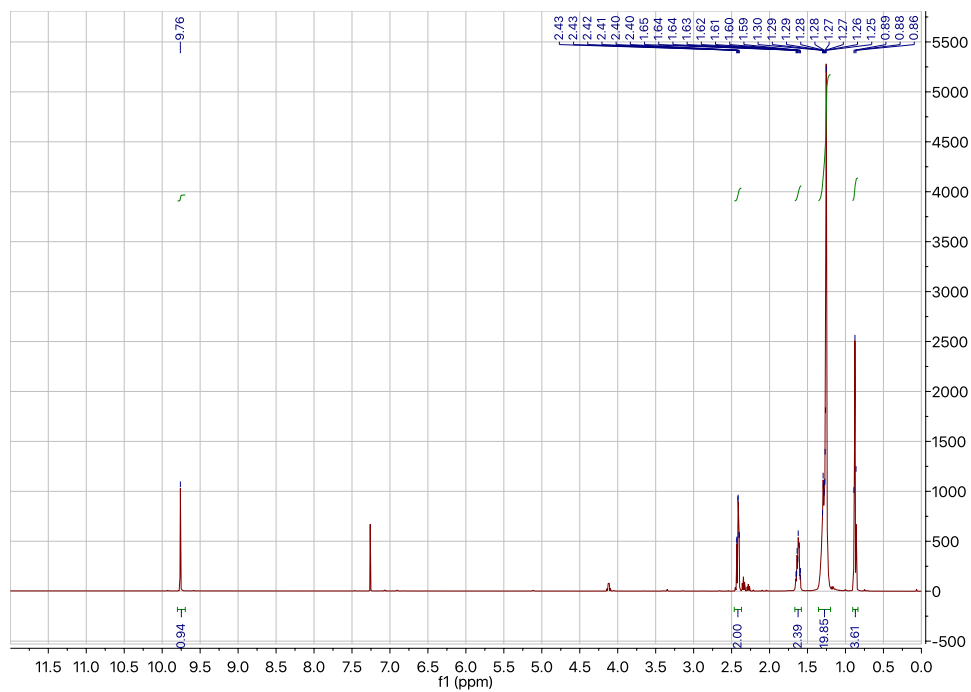
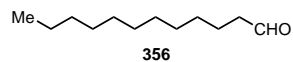
^1H NMR (500 MHz, CDCl_3): 3-(4,5-diphenyloxazol-2-yl)propanal (360)



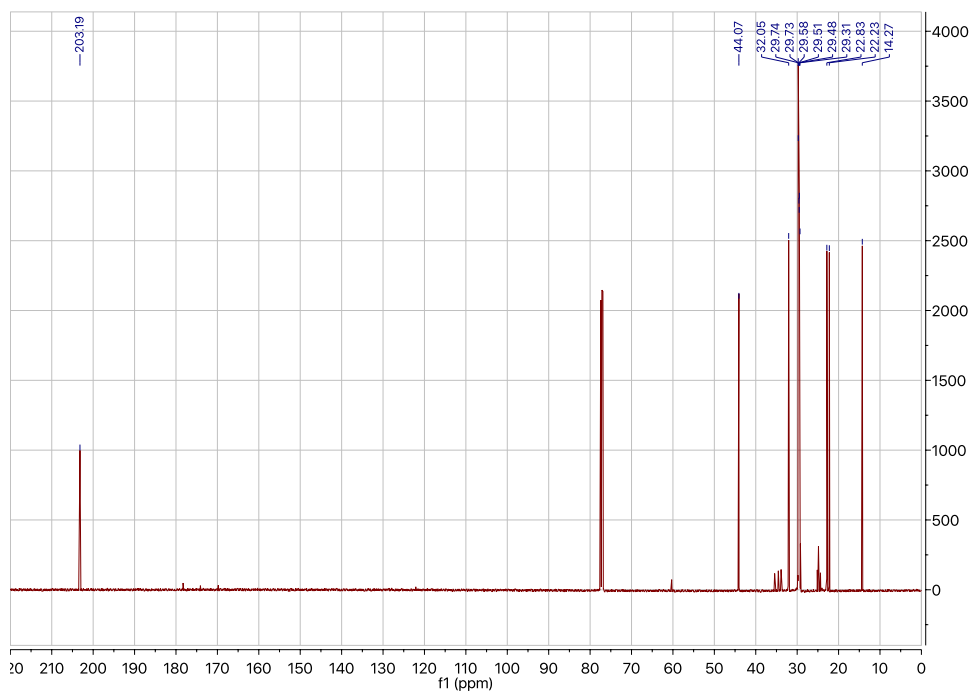
^{13}C NMR (126 MHz, CDCl_3): 3-(4,5-diphenyloxazol-2-yl)propanal



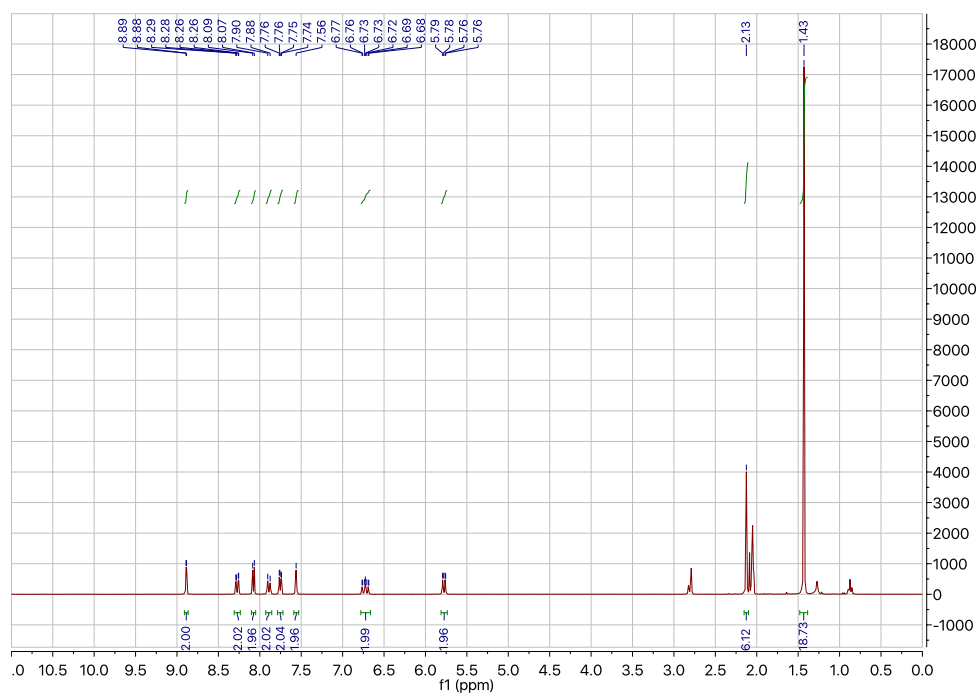
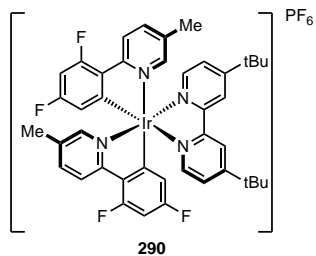
^1H NMR (500 MHz, CDCl_3): dodecanal (355)



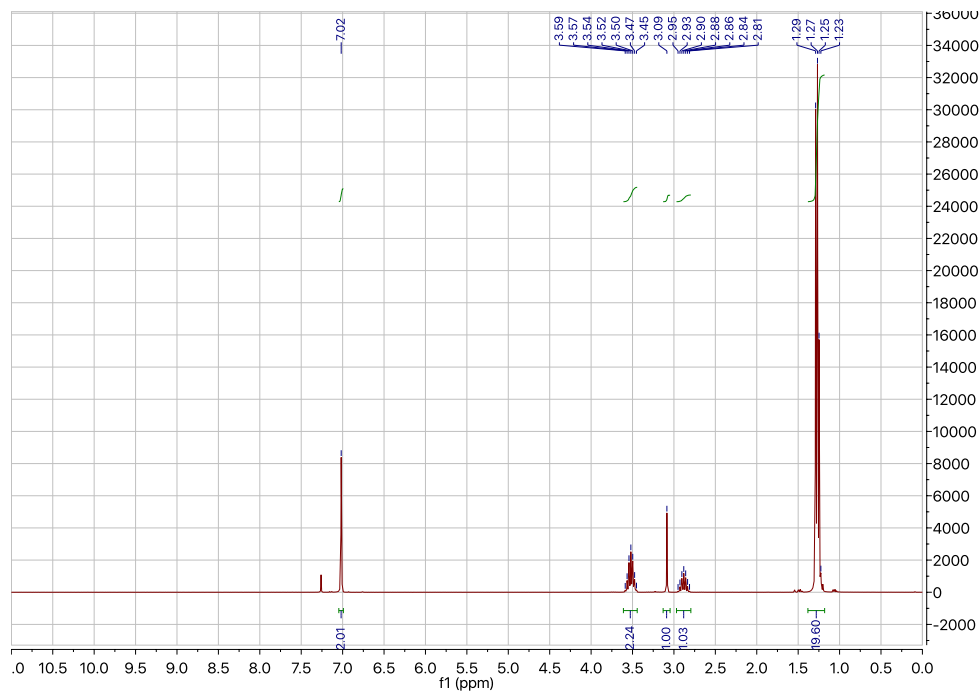
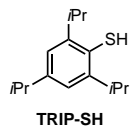
^{13}C NMR (126 MHz, CDCl_3): dodecanal



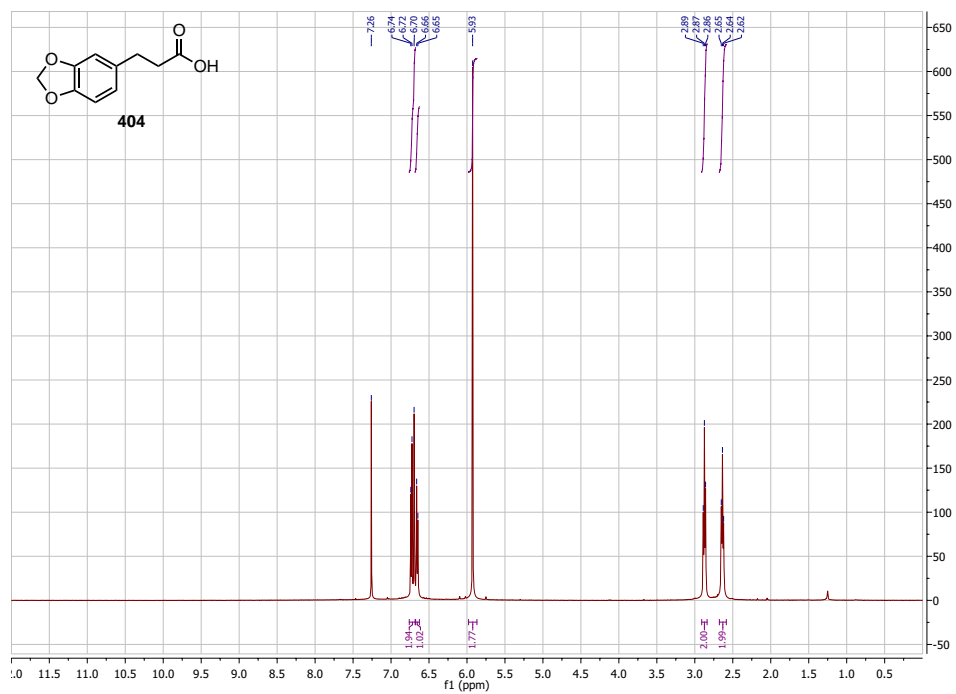
^1H NMR (500 MHz, $(\text{CD}_3)_2\text{CO}$): $[\text{Ir}(\text{dFMeppy})_2\text{dtbbpy}]\text{PF}_6$ (290)



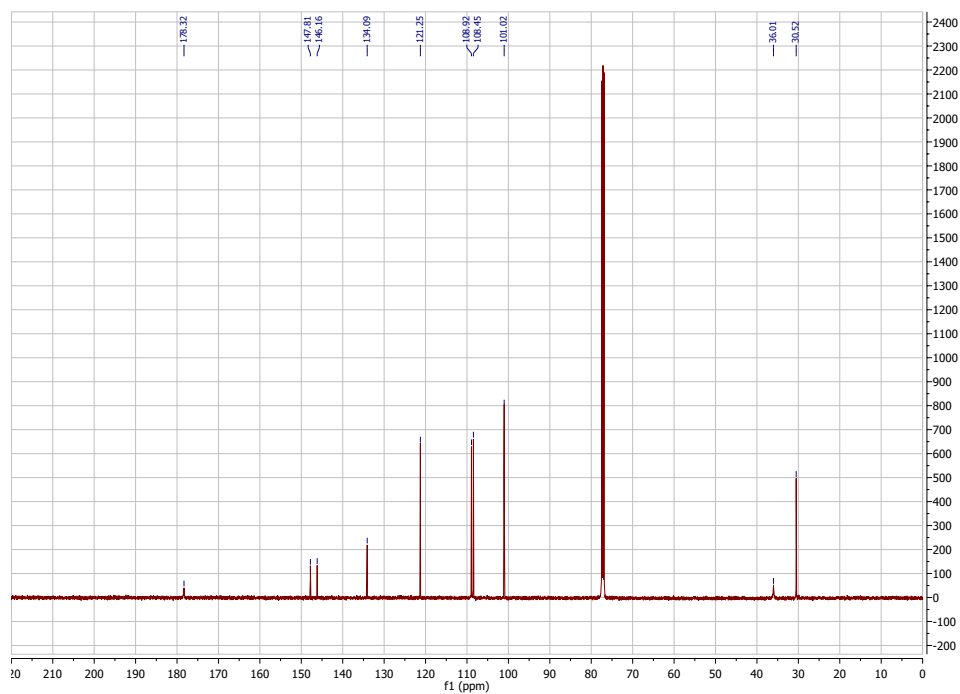
^1H NMR (500 MHz, CDCl_3): 2,4,6-triisopropylbenzenethiol (TRIP-SH)



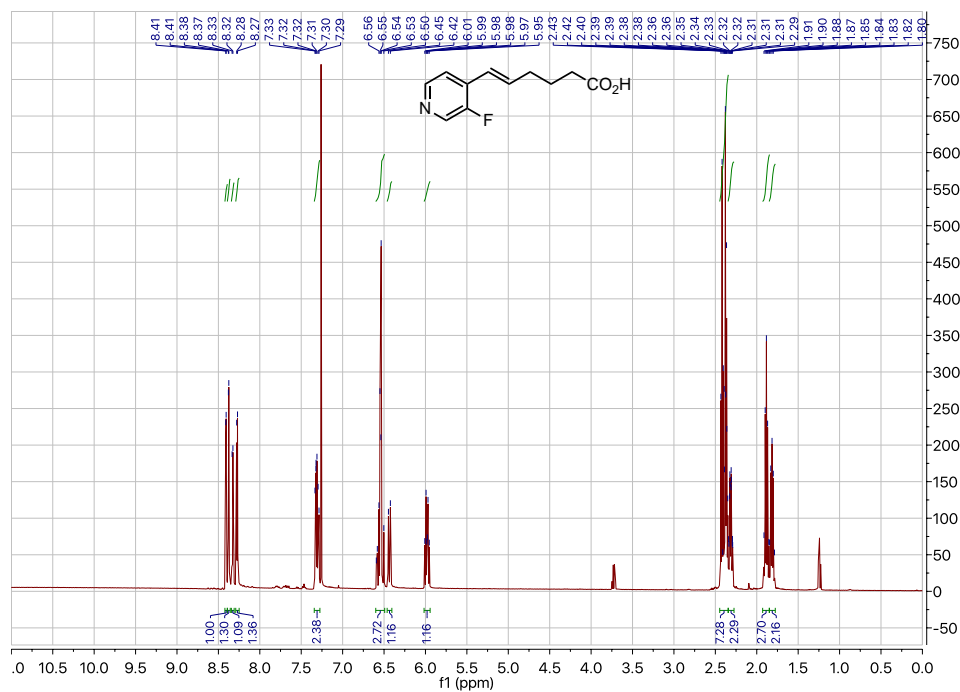
^1H NMR (500 MHz, CDCl_3): 3-(benzo[d][1,3]dioxol-5-yl)propanoic acid (404)



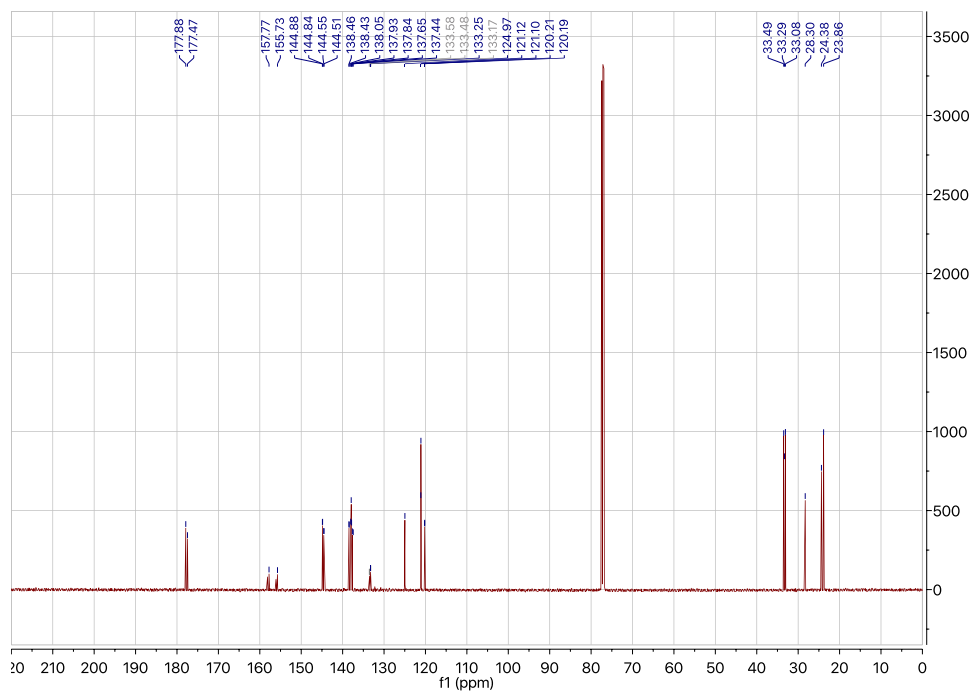
^{13}C NMR (126 MHz, CDCl_3): 3-(benzo[d][1,3]dioxol-5-yl)propanoic acid



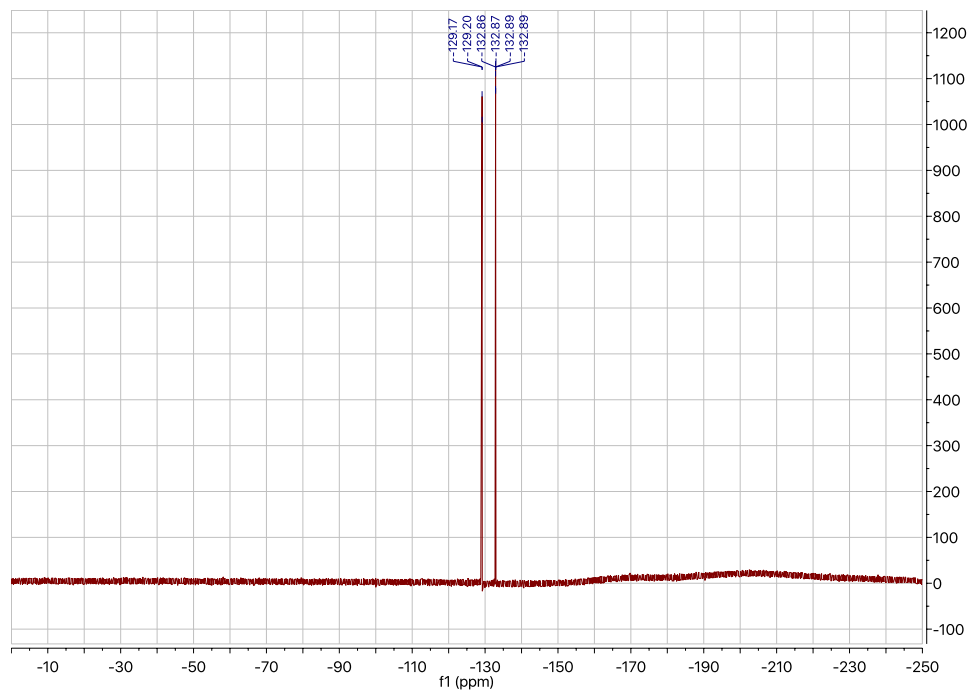
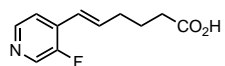
^1H NMR (500 MHz, CDCl_3): (E/Z)-6-(3-fluoropyridin-4-yl)hex-5-enoic acid



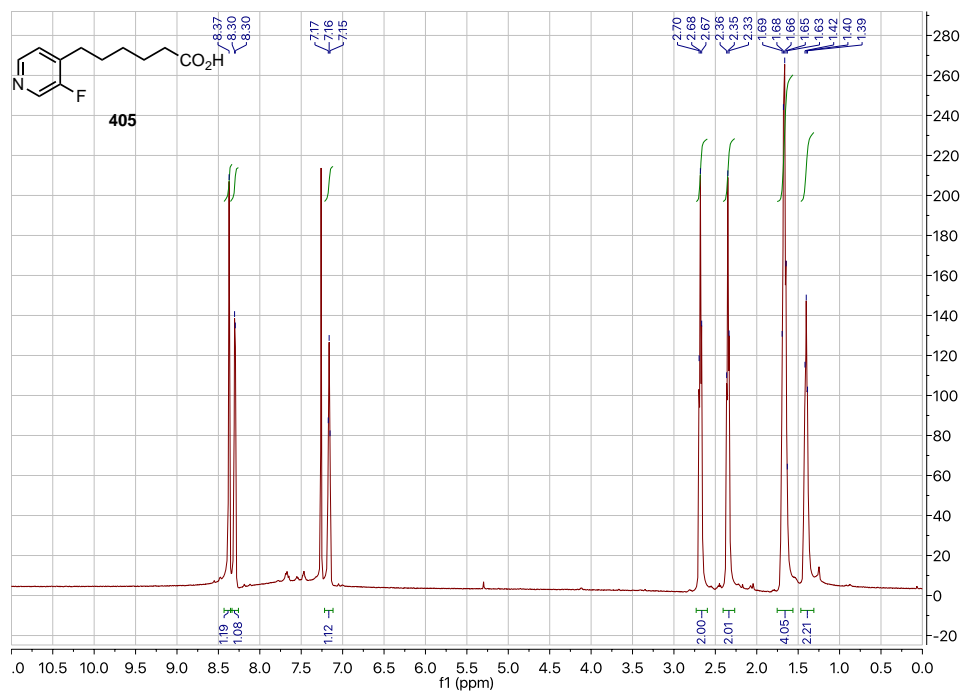
^{13}C NMR (126 MHz, CDCl_3): (E/Z)-6-(3-fluoropyridin-4-yl)hex-5-enoic acid



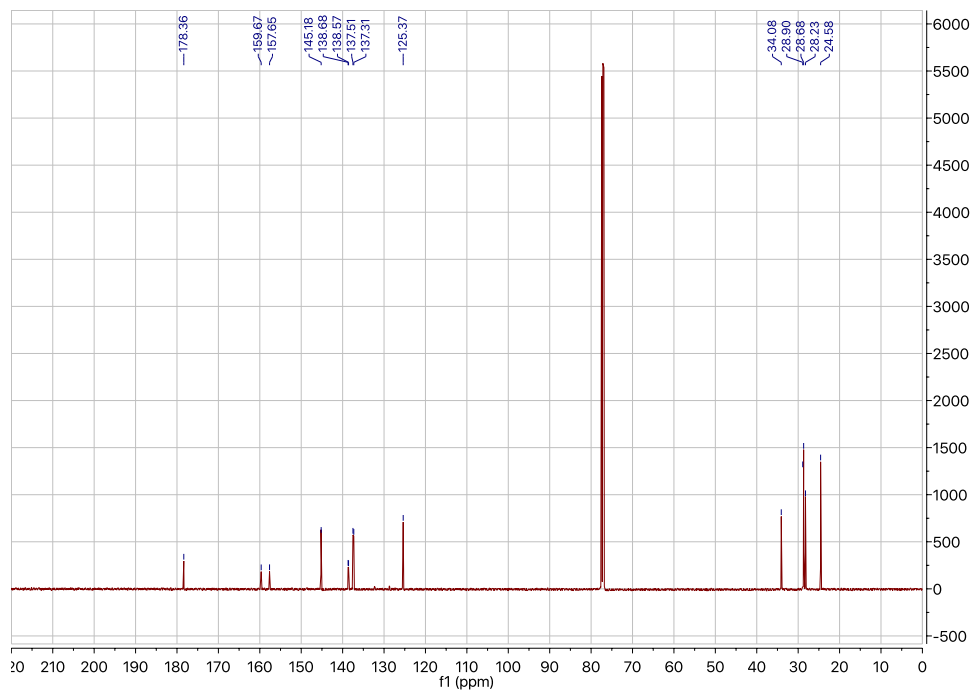
^{19}F NMR (282 MHz, CDCl_3): (E/Z)-6-(3-fluoropyridin-4-yl)hex-5-enoic acid



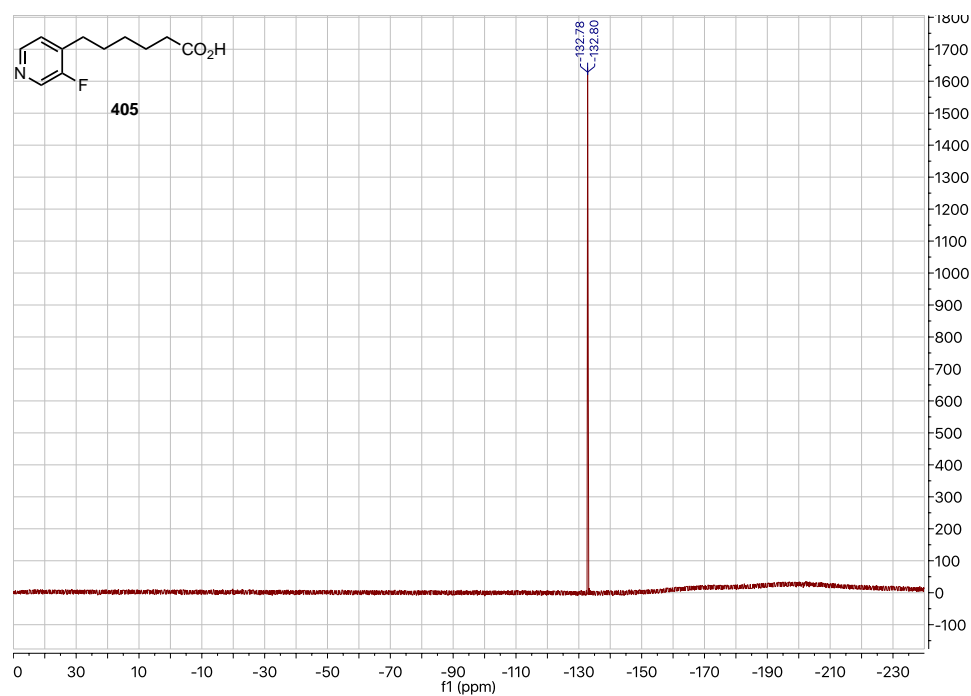
^1H NMR (500 MHz, CDCl_3): 6-(3-fluoropyridin-4-yl)hexanoic acid (405)



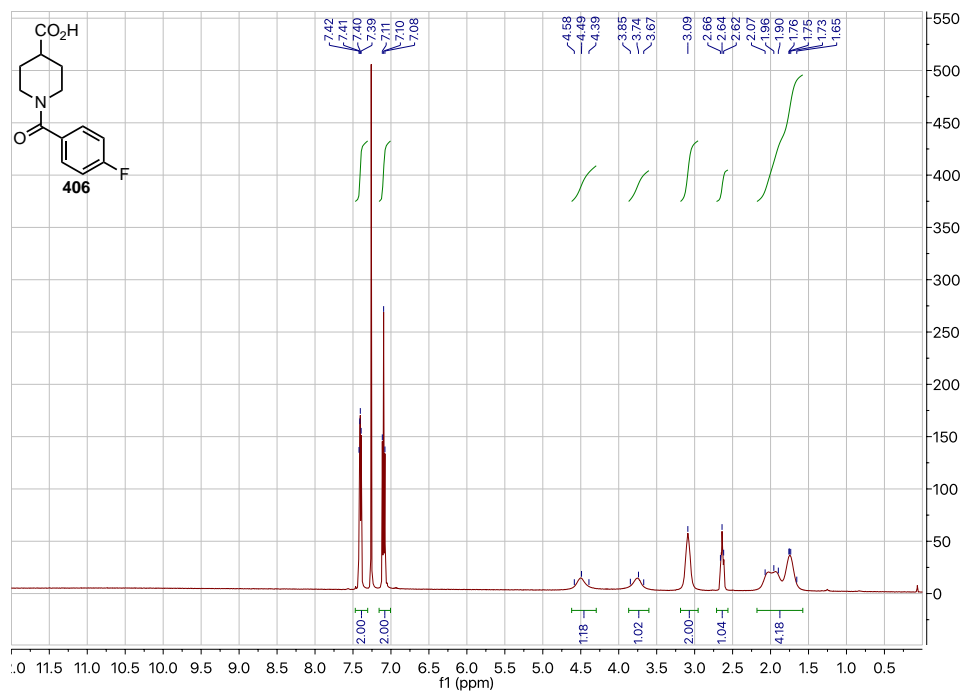
^{13}C NMR (126 MHz, CDCl_3): 6-(3-fluoropyridin-4-yl)hexanoic acid



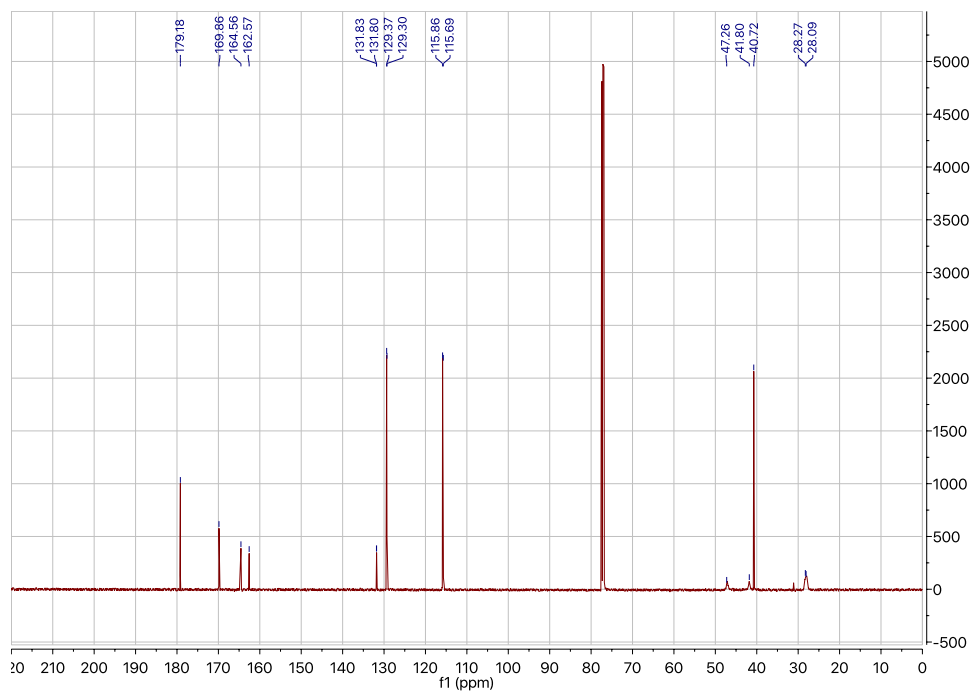
^{19}F NMR (282 MHz, CDCl_3): 6-(3-fluoropyridin-4-yl)hexanoic acid (405)



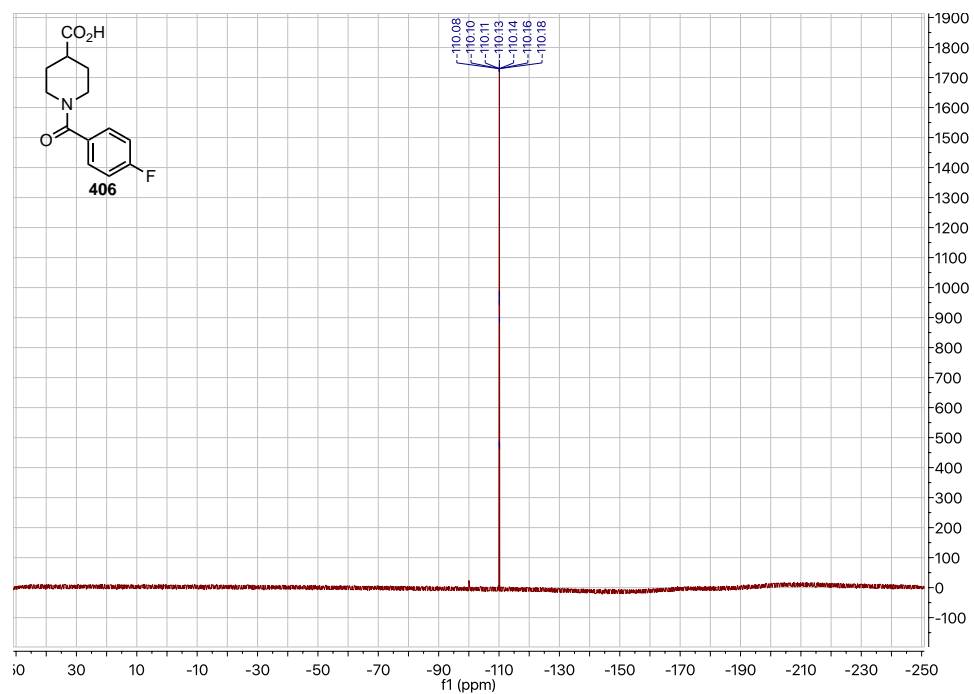
^1H NMR (500 MHz, CDCl_3): 1-(4-fluorobenzoyl)piperidine-4-carboxylic acid (406)



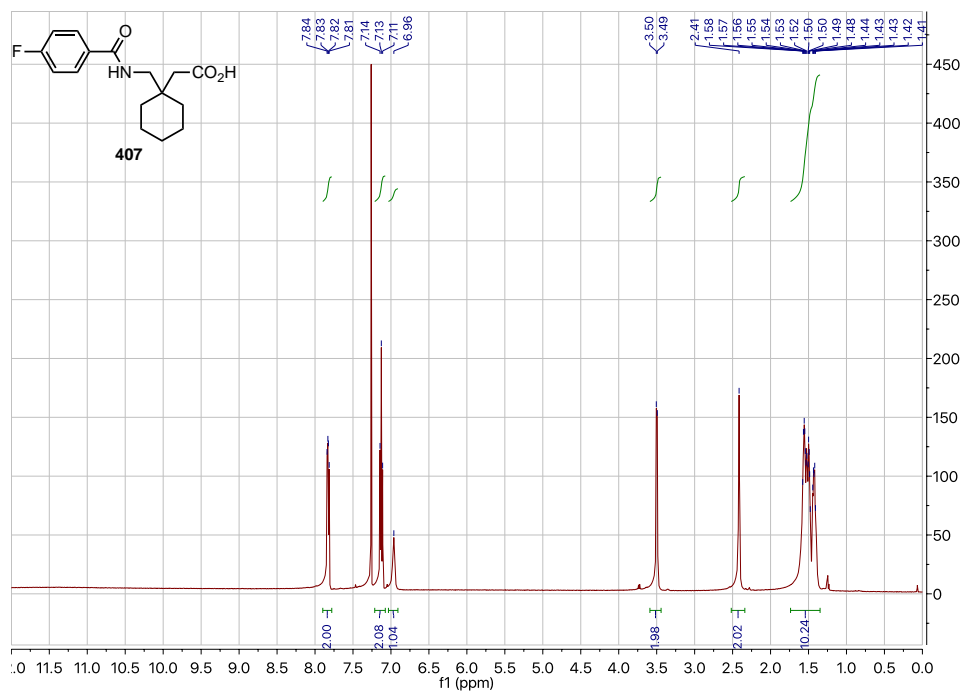
^{13}C NMR (126 MHz, CDCl_3): 1-(4-fluorobenzoyl)piperidine-4-carboxylic acid



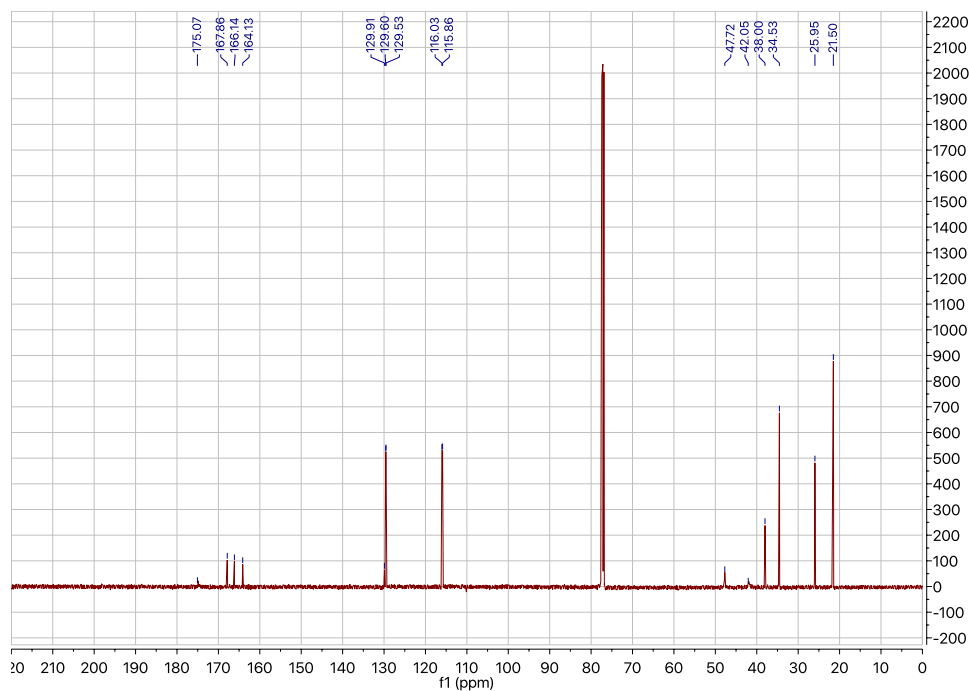
^{19}F NMR (282 MHz, CDCl_3): 1-(4-fluorobenzoyl)piperidine-4-carboxylic acid (406)



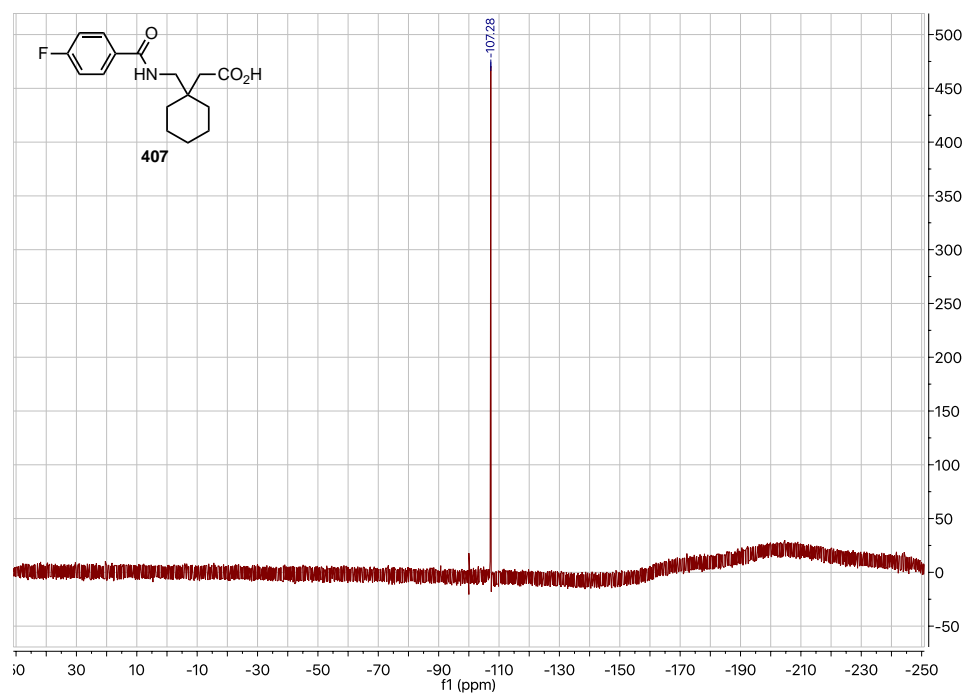
^1H NMR (500 MHz, CDCl_3): 2-(1-((4-fluorobenzamido)methyl)cyclohexyl)acetic acid (407)



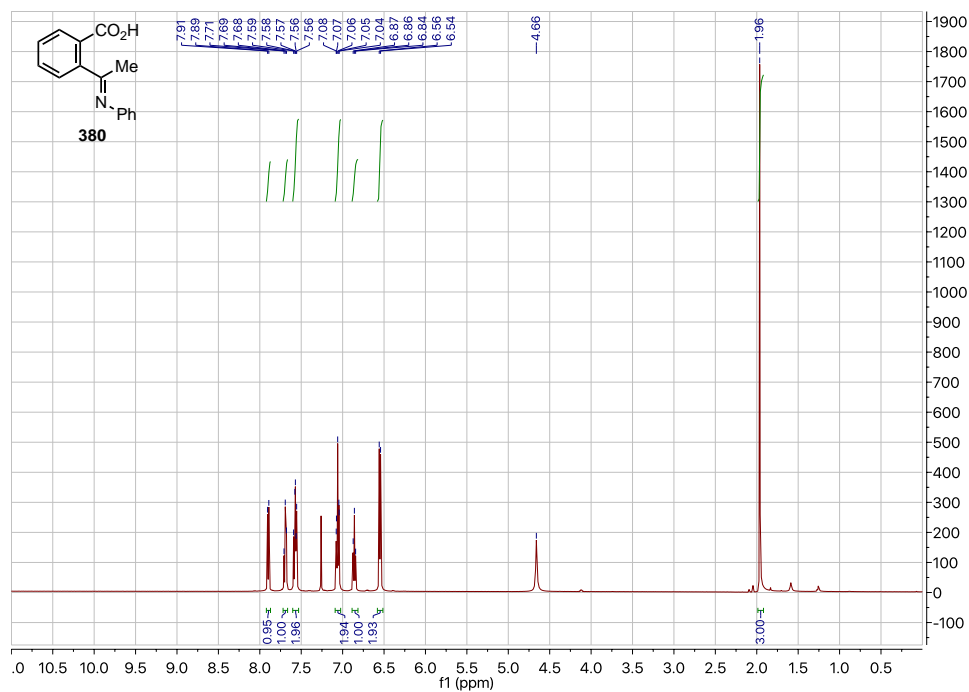
^{13}C NMR (126 MHz, CDCl_3): 2-(1-((4-fluorobenzamido)methyl)cyclohexyl)acetic acid



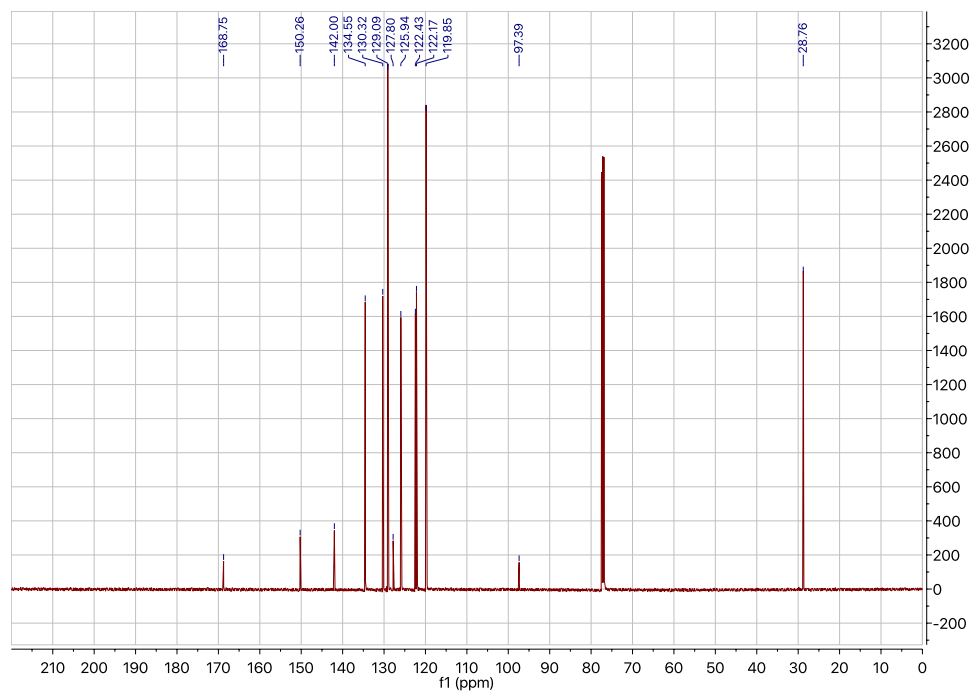
^{19}F NMR (282 MHz, CDCl_3): 2-(1-((4-fluorobenzamido)methyl)cyclohexyl)acetic acid (407)



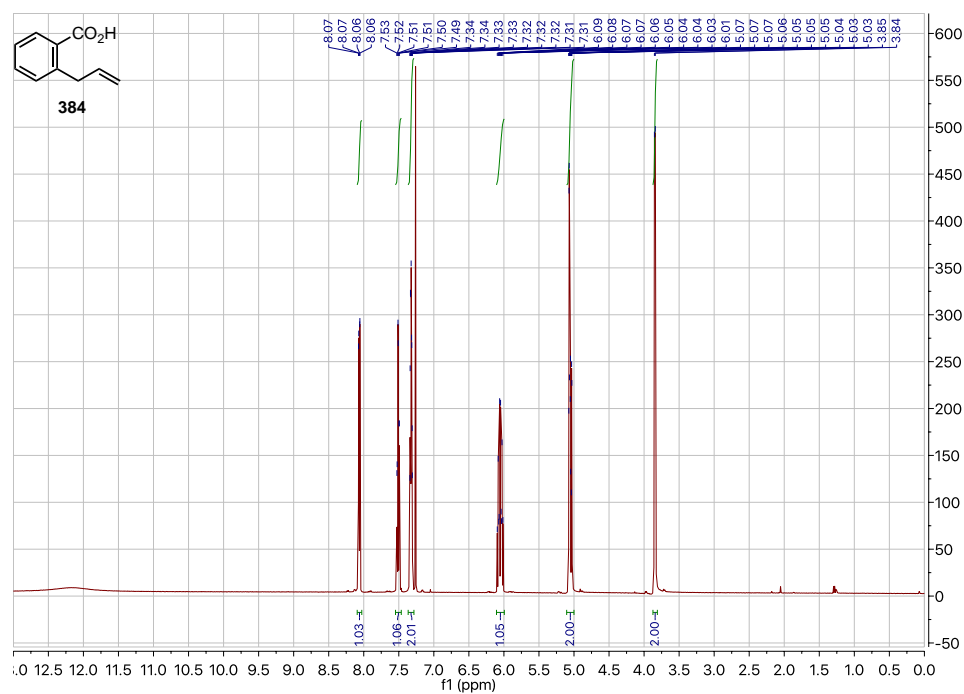
^1H NMR (500 MHz, CDCl_3): 2-(1-(phenylimino)ethyl)benzoic acid (380)



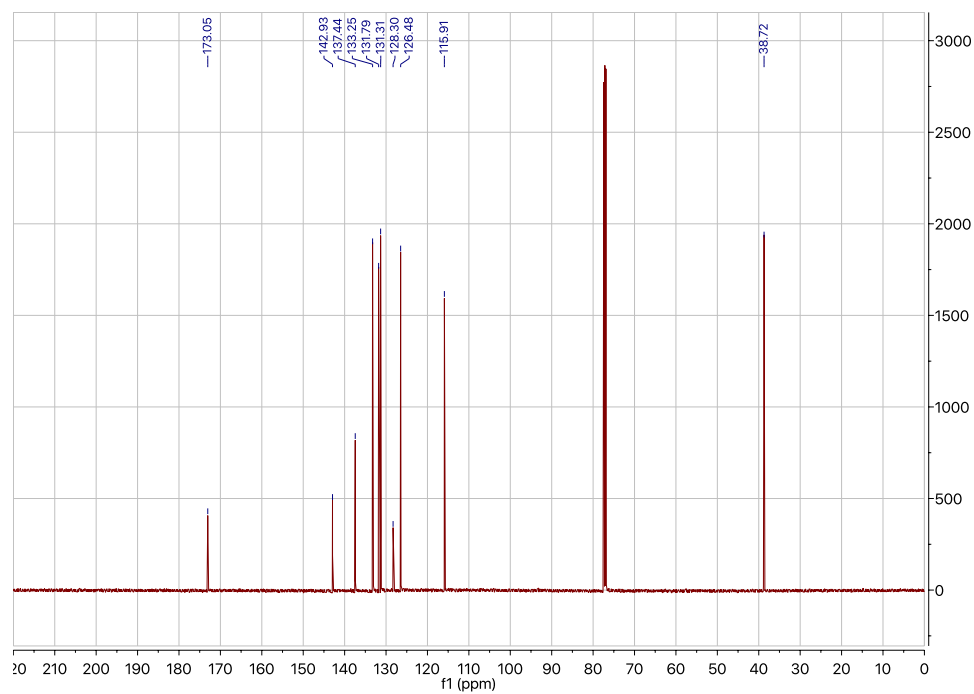
^{13}C NMR (126 MHz, CDCl_3): 2-(1-(phenylimino)ethyl)benzoic acid



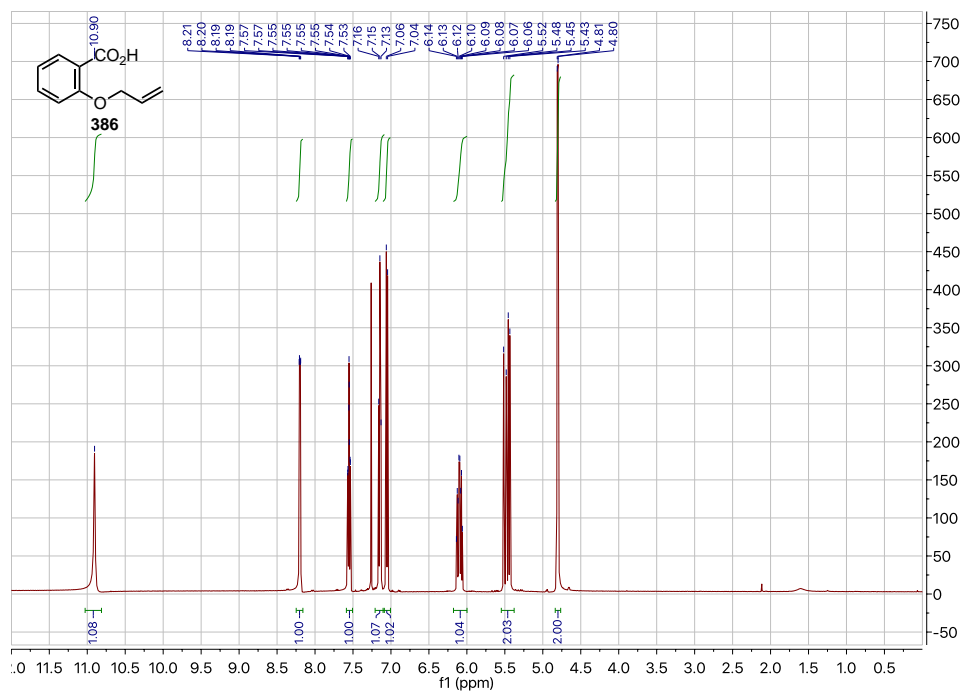
^1H NMR (500 MHz, CDCl_3): 2-allylbenzoic acid (384)



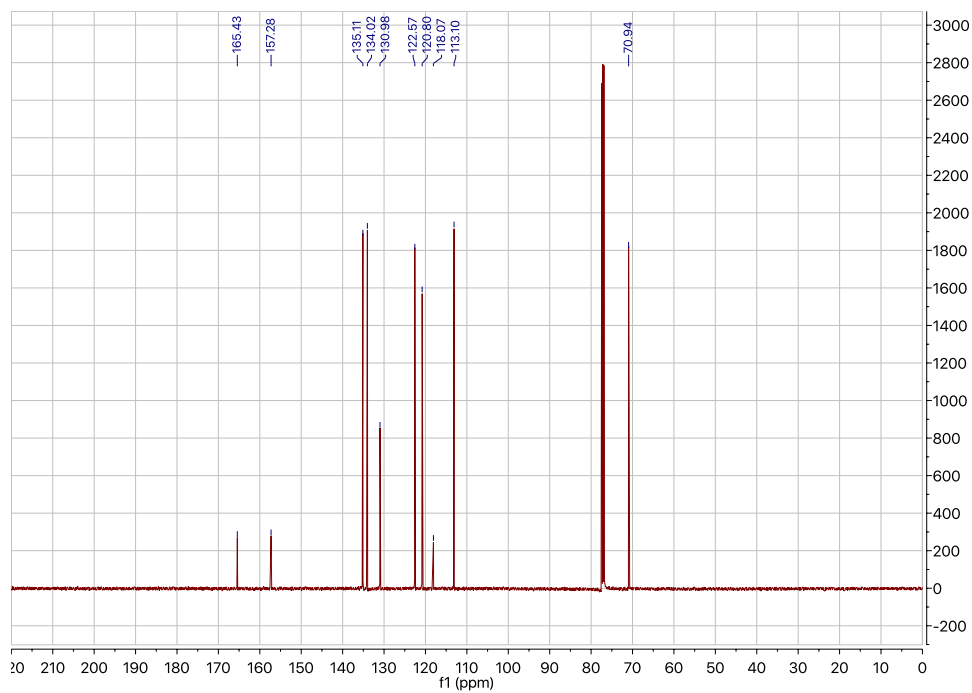
^{13}C NMR (126 MHz, CDCl_3): 2-allylbenzoic acid



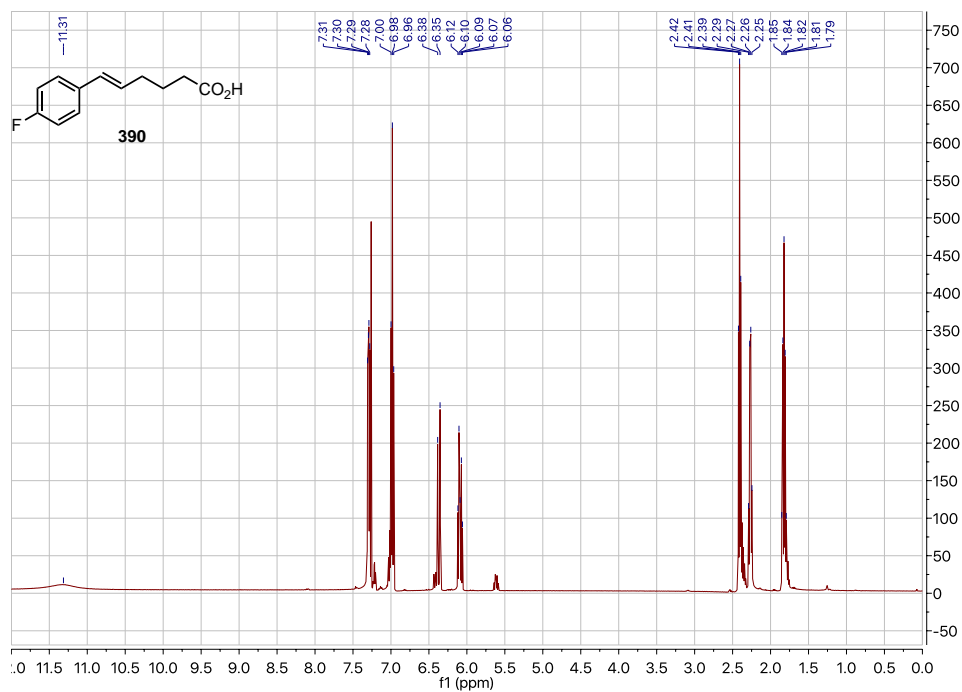
^1H NMR (500 MHz, CDCl_3): 2-(allyloxy)benzoic acid (386)



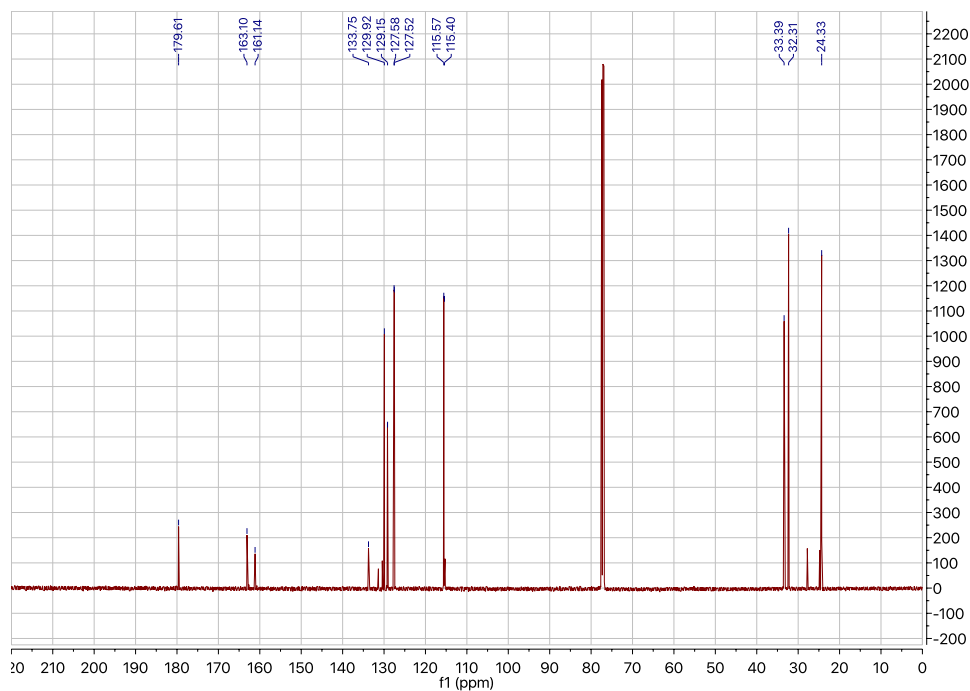
^{13}C NMR (126 MHz, CDCl_3): 2-(allyloxy)benzoic acid



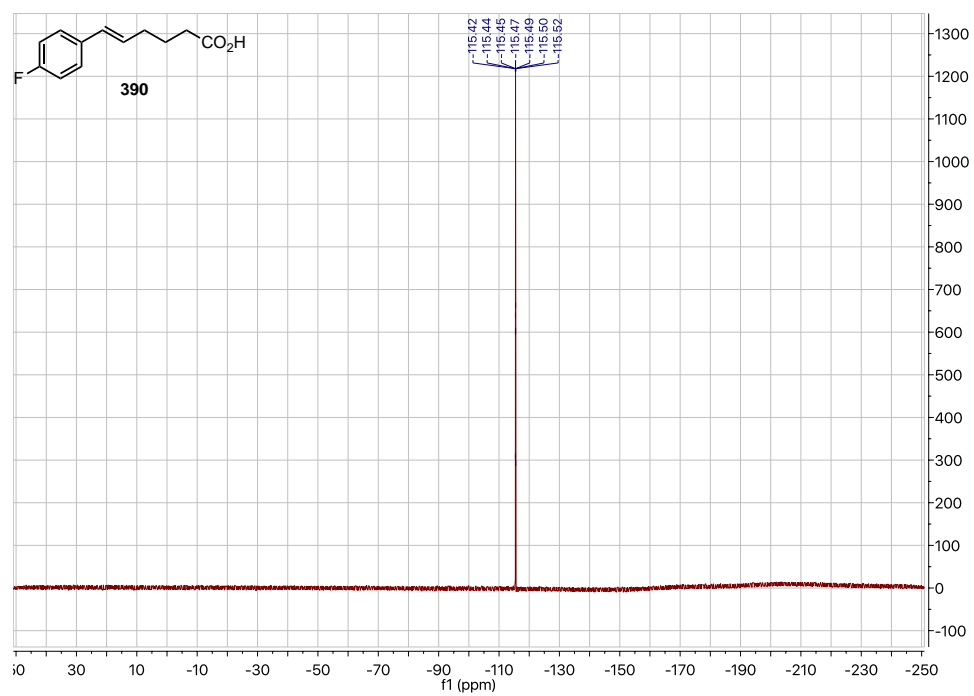
^1H NMR (500 MHz, CDCl_3): (*E*)-6-(4-fluorophenyl)hex-5-enoic acid (390)



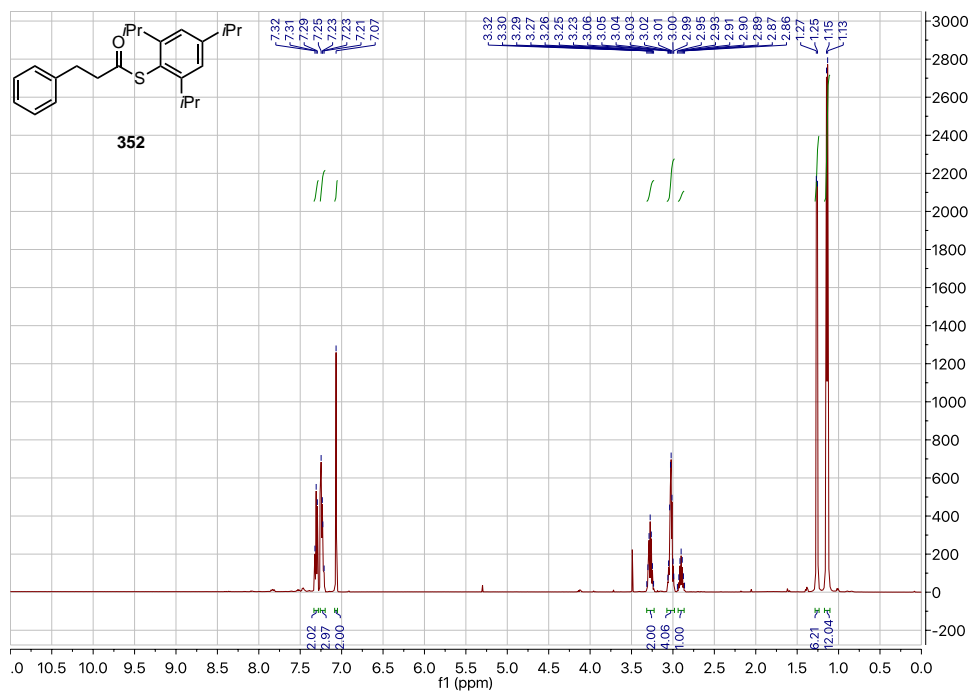
^{13}C NMR (126 MHz, CDCl_3): (*E*)-6-(4-fluorophenyl)hex-5-enoic acid



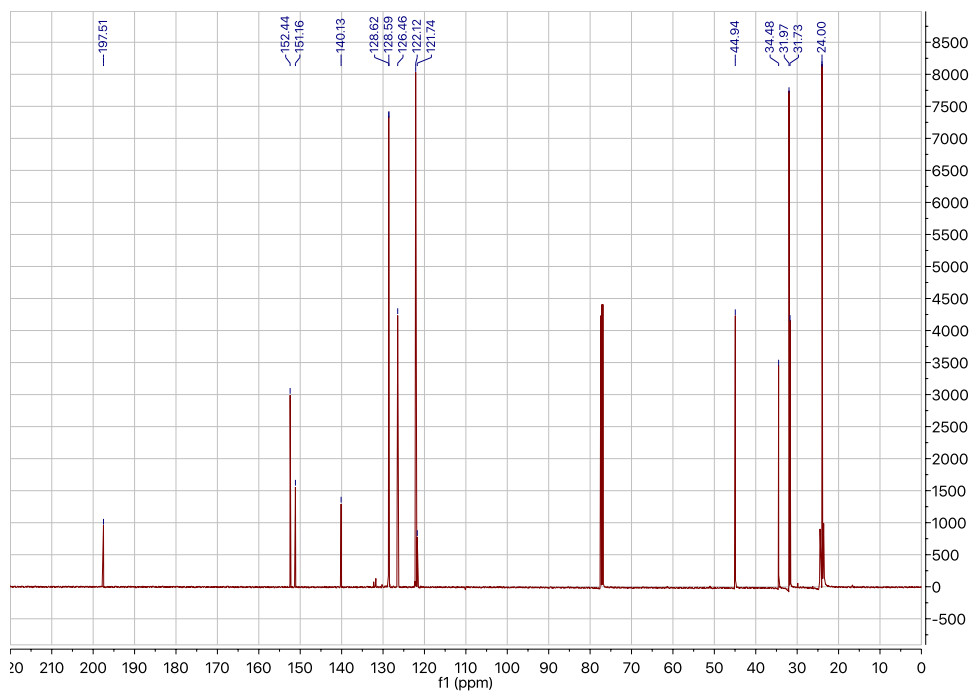
^{19}F NMR (282 MHz, CDCl_3): (*E*)-6-(4-fluorophenyl)hex-5-enoic acid (390)



^1H NMR (500 MHz, CDCl_3): (2,4,6-triisopropylphenyl) 3-phenylpropanethioate (352)



^{13}C NMR (126 MHz, CDCl_3): (2,4,6-triisopropylphenyl) 3-phenylpropanethioate



References

- (1) Singh, A.; Teegardin, K.; Kelly, M.; Prasad, K. S.; Krishnan, S.; Weaver, J. D. *J. Organomet. Chem.* **2015**, 776, 51.
- (2) Ladouceur, S.; Fortin, D.; Zysman-Colman, E. *Inorg. Chem.* **2011**, 50 (22), 11514.
- (3) Zhu, Q.; Graff, D. E.; Knowles, R. R. *J. Am. Chem. Soc.* **2018**, 140 (2), 741.
- (4) Allen, A. D.; Fenwick, M. F.; Henry-Riyad, H.; Tidwell, T. T. *J. Org. Chem.* **2001**, 66, 5759.
- (5) Miles, K. C.; Le, C. C.; Stambuli, J. P. *Chem. Eur. J.* **2014**, 20 (36), 11336.
- (6) Wakasugi, K.; Iida, A.; Misaki, T.; Nishii, Y.; Tanabe, Y. *Adv. Synth. Catal.* **2003**, 345, (11), 1209.

List of Abbreviations

OAc	Acetate
<i>t</i> -Bu	<i>tert</i> -butyl
DCM	dichloromethane
DMF	<i>N,N</i> -dimethylformamide
DMA	<i>N,N</i> -dimethylacetamide
NMP	<i>N</i> -methylpyrrolidinone
bpy	2,2'-bipyridine
dtbbpy	4,4'-di- <i>tert</i> -butyl-2,2'-bipyridine
cod	1,5-cyclooctadiene
Ni	nickel
THF	tetrahydrofuran
PHOX	phosphinooxazoline
equiv	equivalents
ee	enantiomeric excess
TMS	trimethylsilyl
acac	acetylacetonate
OTf	triflate
<i>i</i> -Pr	isopropyl
nbd	norbornadiene
Bn	benzyl
pin	pinacol
CFL	compact fluorescent light
ppy	phenylpyridine
DMSO	dimethylsulfoxide
DMPU	1,3-Dimethyl-3,4,5,6-tetrahydro-2-pyrimidinone
TRIP	2,4,6-triisopropylphenyl
er	enantiomeric ratio
dr	diastereomeric ratio
DIPEA	diisopropylethylamine (Hünigs base)
AIBN	